

PAPERS PRESENTED AT

MASS SPECTROMETRY CONFERENCE

JUNE 3-8, 1962

NEW ORLEANS, LA.

ASTM COMMITTEE E-14

PAPERS PRESENTED AT

**MASS
SPECTROMETRY
CONFERENCE**

JUNE 3-8, 1962

NEW ORLEANS, LA.

ASTM COMMITTEE E-14

P R E F A C E

This volume is a collection of papers presented at the Tenth Annual Meeting of ASTM Committee E-14 on Mass Spectrometry, held June 3 - June 8, 1962, in New Orleans, Louisiana.

It is intended that this volume be distributed only to members of ASTM Committee E-14, and therefore should not be considered as publication.

Program Committee

R. E. Fox, Chairman
R. A. Brown
A. G. Sharkey
W. M. Hickam

1962 Officers

V. H. Dibeler, Chairman
R. E. Fox, Vice-Chairman
R. A. Brown, Vice-Chairman
G. F. Crable, Secretary
J. H. Beynon, Member-at-Large
C. F. Robinson, Member-at-Large

TABLE OF CONTENTS

PROCEEDINGS OF THE ASTM COMMITTEE E-14 ON MASS SPECTROMETRY

New Orleans, Louisiana, June, 1962

Page
No.

HYDROCARBON STUDIES I

1. Mass Spectrometric Investigation of Thermally Treated Extracts from Coal, A. G. Sharkey, Jr., J. L. Shultz, and R. A. Friedel, Bureau of Mines, Bruceston, Pa.	1
2. Analysis of Saturated Hydrocarbons in Boiling Range 450-900°F, W. C. Ferguson and L. R. Snyder, Union Oil Company of California, Brea, California	11
3. Mass Spectrometric Analysis of Middle Distillate Saturated Hydrocarbons, A. Hood, P. R. Mommessin, and B. K. Fritts, Shell Development Company, Houston, Texas	12
4. Characterization of Aromatics in Light Catalytic Cycle Stock, K. W. Bartz, Thomas Aczel, H. E. Lumpkin, and F. C. Stehling, Humble Oil and Refining Company, Baytown, Texas	13
5. The Mass Spectra and Analytical Correlations of C ₅ Through C ₁₀ Coda Compounds, R. F. Kendall, F. O. Cotton, N. G. Foster, and B. H. Eccleston, Bureau of Mines, Bartlesville, Oklahoma	26
6. Determination of Hydrocarbon Types in Kerosene Range Distillates by Mass Spectrometry, (Withdrawn) L. R. Snyder, H. E. Howard, and W. C. Ferguson, Union Oil Company of California, Brea, California	27
7. Mass Spectrometry of Sulfur Compounds. IV. Studies of the Mass Spectra of 2-t-Butyl-, 3-t-Butyl-, and 2, 5, di-t-Butylthiophenes, N. G. Foster, D. E. Hirsch, R. F. Kendall, and B. H. Eccleston, Bureau of Mines, Bartlesville, Oklahoma	28
8. Appearance Potentials and Mass Spectra of Fluorinated Olefins, Chava Lifshitz and F. A. Long, Cornell University, Ithaca, New York	29
9. Mass Spectra of Terpene and Sesquiterpene Hydrocarbons, C. B. Koons and J. N. Mercer, Jersey Production Research Company, Tulsa, Oklahoma	37
10. Rearrangement Ions of Aliphatic Esters as Observed in the Mass Spectrometer, H. O. Colomb, Jr., B. D. Fuls, and V. A. Yarborough, Union Carbide Chemicals Company, South Charleston 3, West Virginia	41

HYDROCARBON STUDIES II

11. Mass Spectra of Trimethylsilyl Esters, R. H. Teeter, California Research Corporation, Richmond, California	51
---	----

(Continued on next page)

TABLE OF CONTENTS - Continued

HYDROCARBON STUDIES II - Continued

	Page No.
12. Information Regarding the Fragmentation of Long Chain Compounds Obtained from the Mass Spectra of Heavy Isotope-Labelled Molecules, Ng. Kinh-Nguyen, Ragnar Ryhage, Stina Stållberg-Stenhagen, and Einar Stenhagen, Institute of Medical Biochemistry, University of Göteborg, Mass Spectrometry Laboratory, Karolinska Institutet, Stockholm 60, Sweden	57
13. Detergent Alkylate Analysis by Mass Spectrometry, E. W. Foyer, H. C. Hamming, and H. T. Ford, Continental Oil Company, Ponca City, Oklahoma	58
14. Mass Spectra Correlations and Appearance Potentials of the Major Tobacco Alkaloids, W. F. Kuhn, C. J. Varsel, and W. A. Powell* Philip Morris Research Center, Richmond 6, Virginia *Department of Chemistry, University of Richmond, Virginia	67
15. Spectra of Compounds of Biological Interest, K. Biemann and J. A. McCloskey, Department of Chemistry, Massachusetts Institute of Technology, Cambridge, Massachusetts	78
16. Recent Studies of n-Paraffin Mass Spectra, John C. Schug, Gulf Research and Development Company, Pittsburgh, Pa.	81
17. Application of the Improved Quasi-Equilibrium Theory of Mass Spectra to Propane, Marvin L. Vestal and William H. Johnston, William H. Johnston Laboratories, Inc., Baltimore, Maryland, and Austin L. Wahrhaftig, University of Utah, Salt Lake City, Utah	94
18. Quantitative Observations of Metastable Ion Transitions with a 180° Mass Spectrometer, Norman D. Coggeshall, Gulf Research Research and Development Company, Pittsburgh 30, Pa.	100
19. The Chemistry of Unimolecular Ion Decompositions, Fred W. McLafferty and Roland S. Gohlke, Eastern Research Laboratory, The Dow Chemical Company, Framingham, Massachusetts	115
20. Mass Spectra of Organic Compounds Using a Radio Frequency Spark Source, Michel Desjardins, Neil Hodgson, and William Baun, Wright Patterson Air Force Base, Dayton, Ohio	123

ANALYTICAL TECHNIQUES I

21. Application of Time-of-Flight Mass Spectrometry and Gas Chromatography to Reaction Studies, E. J. Levy, E. D. Miller, and W. S. Beggs, Atlantic Refining Company, Philadelphia, Pennsylvania	131
--	-----

(Continued on next page)

TABLE OF CONTENTS - Continued

ANALYTICAL TECHNIQUES I - Continued		Page No.
22. Use of Capillary Gas Chromatography with a TOF Mass Spectrometer, W. H. McFadden, Roy Teranishi, D. R. Black, and J. C. Day, U. S. Dept. of Agriculture, Western Regional Research Laboratory, Albany, California		142
23. Uses of a Total Ionization Monitor for Time-of-Flight Mass Spectrometry, Roland S. Gohlke, ✓ The Dow Chemical Company, Eastern Research Laboratory, Framingham, Massachusetts		147
24. Copolymer Analysis by Pyrolysis and Mass Spectrometry, G. G. Wanless, Esso Research and Engineering Company, Linden, New Jersey		152
25. Mass Spectrometric Study on the Evaporation of Volatile Components in Commercial Polyethylene, Kisaku Nakagawa, Electrical Communication Laboratory, Nippon Telegraph and Telephone Public Corporation, Musashino-shi, Tokyo, Japan		159
26. A Mass Spectrometric Study of Phosgene and Its Intermediaries, H. R. Harless and C. M. Lovell, Research and Development Dept., Union Carbide Chemicals Company, South Charleston, West Virginia		166
27. Mass Spectrometric Study of Polymeric Ions, A. H. Turnbull, Atomic Energy Research Establishment, Harwell, Berkshire, England		170
28. Investigations of Azide Decomposition Reactions by Isotopic Tracer Technique, Donald P. Easter and Amos J. Coleman, USAERDL, Fort Belvoir, Virginia		174
29. An Isotope Dilution--Mass Spectrographic--Sealed Tube Microanalytical Method for Combined Oxygen Determination, R. N. Boos, A. Soha, and N. R. Trenner, Merck Sharp and Dohme Research Laboratories, Division of Merck and Co., Inc., Rahway, New Jersey		182
30. Approaches to Mass Spectrometer Gas Analysis Using Photographic Plate Ion Detection, James W. Guthrie, Sandia Corporation, Albuquerque, New Mexico		192
ANALYTICAL TECHNIQUES II		
31. Upper Atmospheric Ion Composition Measurements with Magnetic Mass Spectrometer, John H. Hoffman, Charles Y. Johnson, and Julian C. Holmes, U. S. Naval Research Laboratory, Washington 25, D. C.		197
32. Oxygen Outgassing Caused by Electron Bombardment of Glass, Jack L. Lineweaver, Corning Glass Works, Corning, New York		198

(Continued on next page)

TABLE OF CONTENTS - Continued

ANALYTICAL TECHNIQUES II - Continued		Page No.
33. Mass Spectrometric Investigation of Gas Evolution from Metals, John Roboz and Robert Wallace, General Telephone and Electronics Laboratories, Inc., Bayside 60, New York		199
34. The Effects of Surface Reactions on Mass Spectra, Dwight A. Hutchison, John W. Kraus*, and Louis G. Pobo, Argonne National Laboratory, Argonne, Illinois, *The M. W. Kellogg Company, Jersey City 3, New Jersey		209
35. The Analysis of Gases in Transistor Packages Using an Ultra High Vacuum Mass Spectrometer System, P. D. Davidse, Philco Scientific Laboratory, Blue Bell, Pa.		214
36. Analysis of Gas in Glass Diodes without Diode Destruction, R. A. Meyer, Atomics International, Canoga Park, California, and J. Brandewie, Autonetics, Downey, California		216
37. Residual Gases During Operation and Life-Testing of Power Klystrons, Lowell Noble and Robert K. Waits, Eitel-McCullough, Inc., San Carlos, California		218
38. Solution of Linear Simultaneous Equations, J. Leonard, Tidewater Oil Company, Martinez, California		219
39. Realization of an I.B.M. Punched Cards File for Identification of Chemical Compounds, A. Cornu, Centre D'Etudes Nucleaires De Grenoble, Grenoble, France		226
INSTRUMENTATION I		
40. A Mass Spectrometer for a Study of the Composition of the Upper Atmosphere, Alfred O. Nier, University of Minnesota, Minneapolis, Minnesota		231
41. A Quadrupole Spectrometer for Precision Mass Determinations, U. von Zahn, S. Gebauer, and W. Paul, Physikalisches Institut, Bonn, Germany		232
42. High Resolution Time-of-Flight Mass Spectrometer, D. B. Harrington, The Bendix Corporation, Cincinnati Division, Cincinnati, Ohio, and R. S. Gohkle, The Dow Chemical Company, Eastern Research Laboratories, Frammingham, Massachusetts		234

(Continued on next page)

TABLE OF CONTENTS - Continued

INSTRUMENTATION I - Continued

Page
No.

43. A Cascade Mass Spectrometer, F. A. White, J. C. Sheffield, and F. M. Rourke, General Electric Company, Knolls Atomic Power Laboratory, Schenectady, New York	244
44. An Experiment Involving the Numerical Determination of Ion Paths in Non-Homogeneous Magnetic Fields, A. C. Lilly, T. J. Weismann, and D. A. Lowitz, Gulf Research and Development Company Pittsburgh, Pa.	250
45. A High Sensitivity Mass Spectrometer Source, M. Doctoroff and S. S. Gossel, Vacuum Electronics Corp. Plainview, New York	261
46. Source Design Considerations for Sector Mass Spectrometers, George Salser and Yuji Tajima, Dept. of Chemical Engineering, New York University, New York, New York	263
47. Study of Resolving Power of a Single Focusing, 60°, 12 inch Radius Mass Spectrometer, Graham G. Wanless and George A. Glock, Jr. Esso Research and Engineering Company, Linden, New Jersey	269
48. Correction Coils for Second Order Focusing with the Argonne 100 Inch Radius Mass Spectrometer, C. M. Stevens, Argonne National Laboratory, Argonne, Illinois	279
49. Mechanical Modification of Two-Stage Mass Spectrometer at Vallecitos Atomic Laboratory, W. E. Duffy, General Electric Company, Atomic Power Equipment Department, Vallecitos Atomic Laboratory, Pleasanton, California	280

INSTRUMENTATION II

50. Some New Examples of Application of the Atlas Mass Spectrometer CH 4, Drs. Curt Brunnée, Ludolf Jenckel, Kurt Kronenberger Atlas Mess Und Analysetechnik, G.m.b.H., Bremen, Germany, and Dr. Gerhard Spittler Organisch-Chemisches Institut der Universität Wien Bremen, Germany	289
51. Application of Polyphenyl Ethers as Condensation Pump Fluids in Mass Spectrometry, F. G. Maseles, Mass Spectrometry Laboratory, University of Texas, Austin, Texas	295
52. Simultaneous Measurement of Two Ion Currents by Pulse Counting in a Mass Spectrometer, L. A. Dietz, General Electric Company, Knolls Atomic Power Laboratory, Schenectady, New York	300
53. Display System for Recording Rapid Changes in Gas Composition, B.R.F. Kendall, Nuclide Analysis Associates, Box 752, State College, Pa.	306

(Continued on next page)

TABLE OF CONTENTS - Continued

INSTRUMENTATION II - Continued

	Page No.
54. Modifications to the Inlet and Recording Systems of a C. E. C. 21-103C Mass Spectrometer to Enable Direct Gas Introduction for Dynamic Evolution Studies, J. D. Reynolds and P. C. Green, General Dynamics, Fort Worth, Texas	313
55. Improvement in Readout Accuracy of the CEC Mascot, H. M. Grubb and R. W. Vander Haar, Research and Development Dept., American Oil Company, Whiting, Indiana	317

NEGATIVE ION SYMPOSIUM

56. Negative Ion Formation in Various Gases at Pressures up to .5 mm Hg, R. K. Curran, Westinghouse Research Laboratories, Pittsburgh 35, Pa.	324
57. Electron Transfer in Collisions of Negative Ions with O ₂ Molecules, T. L. Bailey, College of Engineering and Dept. of Physics, University of Florida, Gainesville, Florida	333
58. Some Unique Applications of Negative Ion Mass Spectra, Russell Baldock, Chemistry Division, Oak Ridge National Laboratory, Oak Ridge, Tennessee	334
59. Electron Affinities of the Halogens, B. W. Steiner, M. L. Seman, and L. M. Branscomb, National Bureau of Standards, Washington 25, D. C. , and R. S. Berry, Yale University, New Haven, Connecticut	342
60. Measurement of Electron Capture Cross Sections Using Swarm Methods, G. S. Hurst, Health Physics Division, Oak Ridge National Laboratory, Oak Ridge, Tennessee	348

COLLISION PROCESSES

61A. A Mass Spectrometric Investigation of Secondary Reactions in Mixtures Containing Hg Vapour, V. Cermák and Z. Herman, Institute of Physical Chemistry, Czechoslovak Academy of Sciences, Prague, Czechoslovakia	358
61B. Rare Gas Molecule-Ion Formation by Mass Spectrometry. Kinetics of Ar ₂ ⁺ , Ne ₂ ⁺ , and He ₂ ⁺ Formation by Second and Third Order Processes, J. S. Dahler, J. L. Franklin, M. S. B. Munson, and F. H. Field, Humble Oil and Refining Company, Baytown, Texas	365
62. A High Pressure Mass Spectrometric Study of Reactions of Rare Gases with N ₂ and CO, M. S. B. Munson, F. H. Field, and J. L. Franklin, Research and Development, Humble Oil and Refining Company, Baytown, Texas	366

(Continued on next page)

TABLE OF CONTENTS - Continued

COLLISION PROCESSES - Continued

	<u>Page No.</u>
63. Observation of the Products of Collision Processes and Ion Decomposition in a Linear, Pulsed Time-of-Flight Mass Spectrometer, R. E. Ferguson, K. E. McCulloch, and H. M. Rosenstock, National Bureau of Standards, Washington, D. C.	367
64. Velocity Dependence of Ion-Molecule Reaction Cross Sections, D. A. Kubose and W. H. Hamill, Dept. of Chemistry and Radiation Laboratory, University of Notre Dame, South Bend, Indiana	368
65. Mass Spectrometric Observation of Electron and Proton Transfer in 'Cermak' Experiments, A. Henglein and G. A. Muccini, Mellon Institute, Pittsburgh, Pa.	379
66. The Effect of Pressure Scattering on High Precision Isotopic Abundance Measurements, K. A. Kaiser, University of Minnesota, Minneapolis, Minnesota (Present Address: Argonne National Laboratory, Argonne, Illinois)	391
67. Ions in the Carbon Dioxide Glow Discharge, P. H. Dawson and A. W. Tickner, National Research Council, Ottawa, Canada	392
68. Determination of Electronic Energy Levels of Molecules by Low Energy Electron Impact, Aron Kuppermann and Lionel M. Raff, Dept. of Chemistry, University of Illinois, Urbana, Illinois	395
69. Photoionization Processes Studied by Mass Spectrometry, (withdrawn) D. C. Frost, D. Mak, and C. A. McDowell, Dept. of Chemistry, University of British Columbia, Vancouver 8, British Columbia	396

SOLIDS TECHNIQUES

70. Study of Low Melting Metals by Spark Source Mass Spectrometry, W. A. Wolstenholme and J. D. Waldron, Associated Electrical Industries Limited, Instrumentation Division, Apparatus Dept. Barton Dock Road, Urmston, Manchester, England	397
71. Ion Charge Distribution in a R. F. Spark Ion Source and Its Effect on Quantitative Analysis, Edward B. Owens, Lincoln Laboratory, Massachusetts Institute of Technology, Lexington 73, Massachusetts	403
72. Photographic Quantitative Analysis with a Solids Spark Mass Spectrograph, Charles W. Hull, Consolidated Electrodynamics Corporation, Pasadena, California	404
73. Improved Accuracy in Solids Mass Spectrometry, (Withdrawn) G. D. Perkins and Charles F. Robinson, Bell and Howell Research Center, Pasadena, California	413

(Continued on next page)

TABLE OF CONTENTS - Continued

SOLIDS TECHNIQUES - Continued

	Page No.
74. Studies with Spark Source Mass Spectrometry, W. Fletcher, United Kingdom Atomic Energy Commission, Capenhurst, England	414
75. Ion Source for Solid Materials, (Withdrawn) Richard F. Herzog and Helmut J. Liebl, Geophysics Corporation, Bedford, Massachusetts	420
76. High Temperature Vaporization Studies, J. Drowart, Laboratoire de Chimie Physique I, University of Brussels, Brussels, Belgium	421
77. Thermodynamics of Dilute Solutions by Knudsen Cell Techniques, John H. Norman and Perrin Winchell, General Dynamics-General Atomic, San Diego, California	427
78. The Vaporization of Beryllium, Magnesium, and Aluminum Borates, Alfred Büchler and Joan B. Berkowitz-Mattuck, Arthur D. Little, Inc., Cambridge, Massachusetts	432
79. Mass Spectrometric Study of High Temperature Reactions of $\text{BF}_3(\text{g})$ with Oxides, William P. Sholette and Richard F. Porter, Dept. of Chemistry, Cornell University, Ithaca, New York	439
80. A New Method of Increasing the Efficiency of Surface Ionization Sources, N. R. Daly and N. C. Fenner, (Withdrawn) Atomic Weapons Research Establishment, Aldermaston, England	441

MASS SPECTROMETRIC INVESTIGATIONS OF THERMALLY TREATED EXTRACTS FROM COAL

by

A. G. Sharkey, Jr.,^a J. L. Shultz,^b and R. A. Friedel^c

ABSTRACT

As part of an investigation to obtain information on the chemical structure of coal, mass spectrometric techniques were used to study pyridine extracts. Materials extractable at room temperature from Pittsburgh seam (hvab), Wyoming subbituminous, and North Dakota lignite were examined before and after heating for 4 hours at 450° C. Changes were observed in the carbon number distribution for several aromatic structures.

INTRODUCTION

As part of a program at the Federal Bureau of Mines to obtain information on the structure of coal, mass spectrometric techniques were used to investigate coal and various materials derived from coal. The purpose of this investigation was to determine primary materials associated with the coal structure. H. W. Holden and J. C. Robb (6) pyrolyzed coal directly in a mass spectrometer ion source and R. I. Reed (11, 12) has applied mass spectrometric techniques to coal and coal extracts. Because of the complexity of the spectra obtained under normal operating conditions and the lack of calibration data, only qualitative interpretations were attempted in these preceding investigations.

While several investigators have noted the similarity in the infrared (i.r.) spectra of coal, various extracts of coal, and condensates obtained by the vacuum pyrolysis of coal, little has been reported concerning the constituents of these materials or the molecular weight distribution of these constituents (2, 10). In an investigation of pyridine extracts of various coals, H. N. M. Dormans and D. W. van Krevelen found average molecular weights of approximately 500 for extracts from coal with 80 and 91 percent carbon (3). The highest average molecular weight, near 1200, was reported for a pyridine extract from 87 percent carbon coal. J. K. Brown, in a summary of the i.r. results for extracts, noted that while the closest agreement between the i.r. spectra of extracts and the parent coals was shown for extracts obtained with good solvents, the major bands persisted even with the poor coal solvents (2). Similarly, in investigating condensates from the vacuum pyrolysis of coal to 550° C, A. A. Orning and B. Greifer reported that condensates constituting up to 10 percent of the coal had i.r. spectra very similar to the spectrum of the coal (10).

In the present mass spectrometric investigation, low-ionizing voltage techniques were used to produce a spectrum consisting primarily of molecular-ions (4, 13, 14). With this technique, many structural types associated with materials derived from coal can be identified and, in certain instances, carbon number distribution data can be obtained for the alkyl derivatives. The mass spectrometer is ideally suited for this type of investigation as (1) it is a highly sensitive analytical tool, (2) the equivalent of only 0.001 ml. of liquid sample is required for analysis, and (3) vacuum pyrolysis and similar investigations can be carried out directly in the instrument, thus reducing the possibility of secondary reactions.

One phase of this investigation was the determination of changes occurring in material extracted at room temperature, following heating to temperatures associated with low-temperature carbonization. By investigating the extracted material apart from the coal structure, it was hoped that changes occurring in the major hydro-

a. Supervisory physicist.

b. Mathematician.

c. Project coordinator.

All authors are with the Pittsburgh Coal Research Center, Bureau of Mines,
U. S. Department of the Interior, Pittsburgh, Pa.

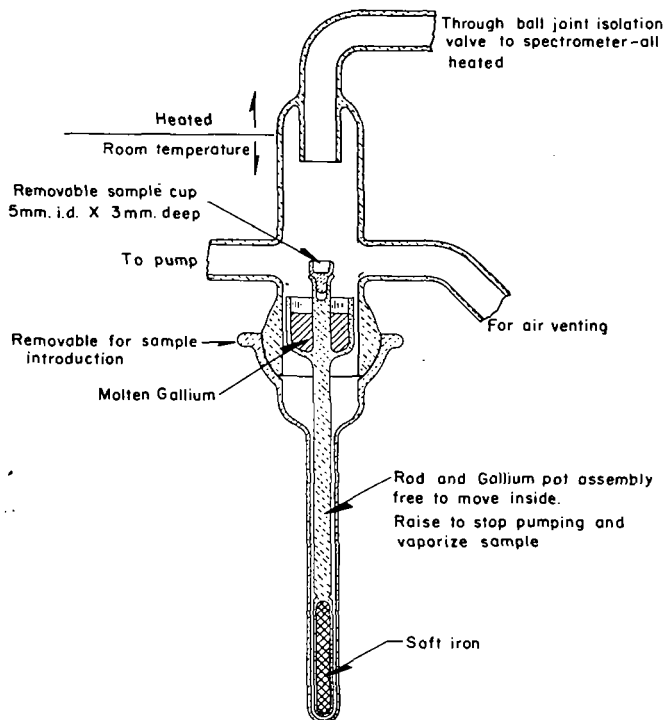


Figure 1. - Mass spectrometer heated inlet system for solids.
(Lumpkin - reference 8)

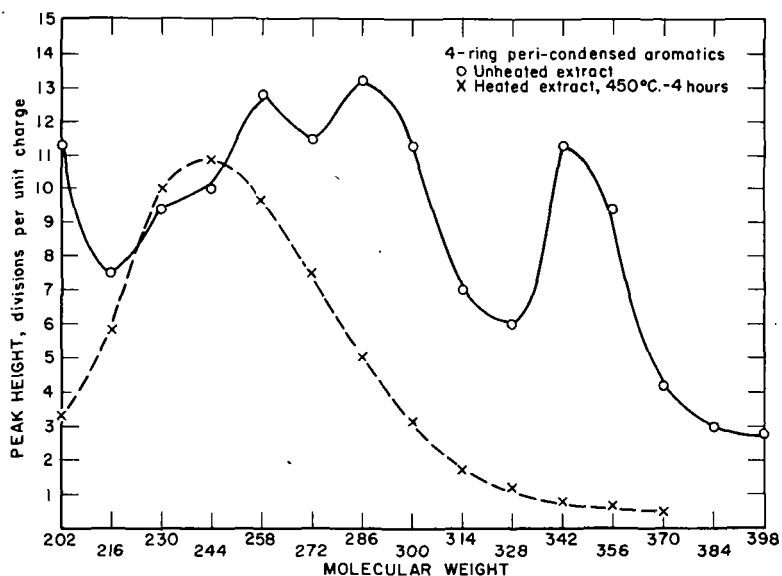


Figure 2. - Partial mass spectrum of pyridine extract from Wyoming subbituminous, 75.5 per cent carbon, coal.

carbon portion of coal could be determined independently of physical and geometrical features (such as pore structure of the particular coal). It has been established that primary tars and coal extracts contain similar components; however, it has not been determined how close is this relationship, or what differences do exist in the two materials (16).

EXTRACTION PROCEDURE AND RESULTS

For this investigation, it was desirable to obtain a maximum yield of extract at room temperature. Dormans and van Krevelen found that coals could be exhaustively extracted by shaking with pyridine at room temperature for about 17 hours (3). Yields and also average molecular weights for the extracted material compared favorably with those obtained using Soxhlet extraction methods. Pyridine extracts for this investigation were prepared following the general procedure outlined by Dormans and van Krevelen. A sample of dry, greater than 200-mesh coal was prepared from newly-mined lumps of Pittsburgh seam (hvab), 84 percent carbon coal. The coal was stored under nitrogen following preparation. Approximately 1 gram of the coal was extracted to exhaustion by shaking with 10 cm³ of pyridine for 17 hours. The extract was prepared and handled in an inert atmosphere, including introduction of the extract into the inlet system of the mass spectrometer. A Consolidated Electrodynamics Model 21-103C mass spectrometer, equipped with the solids inlet system shown in figure 1, was used for all determinations (8). Approximately 5-mg samples were introduced.

Ultimate analyses for the three coals investigated, Pittsburgh seam (hvab), Wyoming subbituminous, and North Dakota lignite (vitrain), and also the percent of material extracted with pyridine at 25° C, are given in table 1. The percentages of extracted material obtained are in agreement with results reported by Dormans and van Krevelen (3).

TABLE 1.- Carbon content and percent of coal extracted
with pyridine at 25° C

<u>Coal</u>	<u>Percent carbon</u>	<u>Percent extracted</u>
Bituminous, Pittsburgh seam (hvab)	84.0	21.2
Subbituminous, Nugget Mine, Wyoming	75.5	13.5
Lignite (vitrain), from Kincaid Mine, Burke Co. North Dakota	67.9	9.5

A major portion of each extract from the above coals was heated (under vacuum) for 4 hours at 450° C. Mass spectra to approximately mass 400 were obtained of the original extracts and the heated portion. To compare the major features in the spectra before and after heating, the spectra were tabulated on the basis of peak height (in chart divisions) per unit charge to the mass spectrometer (5 mg). Peak intensities at any given mass in the spectra are an indication of the relative concentrations of material having this molecular weight. Alkyl series corresponding to the following structural types are shown in figures 2-7: For Pittsburgh seam coal-- 4-ring, peri-condensed and fluorenes; subbituminous coal-- 4-ring, peri-condensed and acenaphthenes; lignite-- 4-ring, peri-condensed and anthracenes and/or phenanthrenes.

CHANGES IN SPECTRA FOLLOWING HEATING

Mass spectra of the extracts before and after heating show the following general features: The extract from the Pittsburgh seam coal shows one to three maxima for the various alkyl series. After heating, the alkyl series show only one or two maxima with the majority having a single, well-defined maximum. The unheated extract from subbituminous coal is the most complex, showing three to six maxima for most alkyl series. Following heating, the number of maxima is reduced to three or less. The alkyl series for the extract from lignite show the least complexity, having only one or two maxima, both before and after heating. In all these spectra a maximum indicates the presence of one (or more) structural type. While peak intensities for the extracts from Pittsburgh seam and subbituminous coals are comparable before and

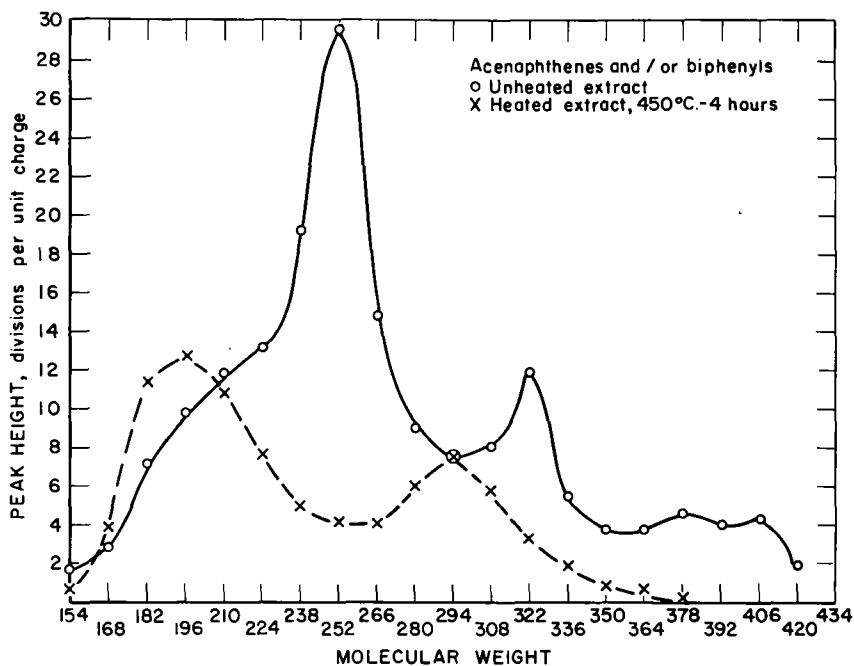


Figure 3. - Partial mass spectrum of pyridine extract from Wyoming subbituminous, 75.5 per cent carbon, coal.

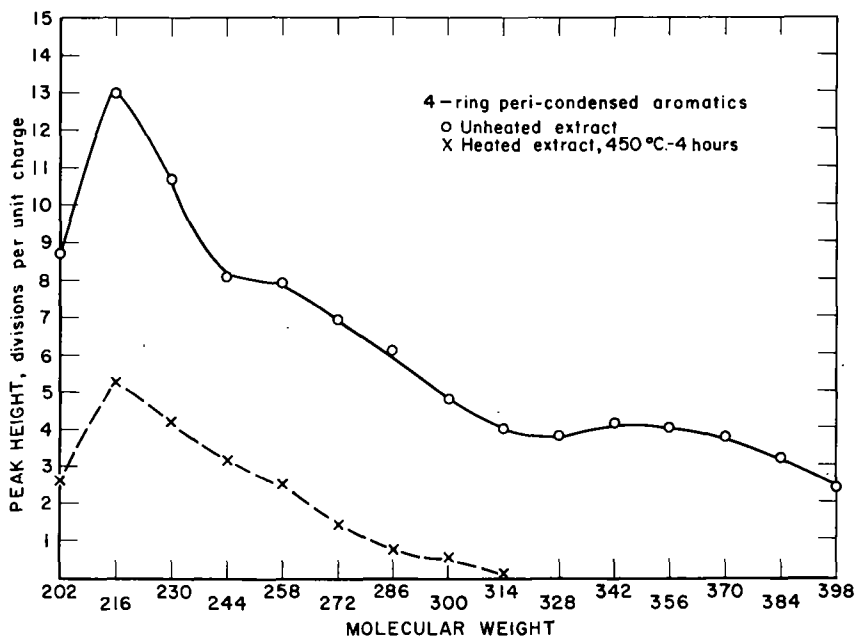


Figure 4. - Partial mass spectrum of pyridine extract from North Dakota lignite, 68 per cent carbon.

after heating, a major reduction (one-tenth to one-third of original intensity) is shown for all peaks in the pyridine extract from lignite following heating. Partial analyses of the gases produced during the four hours of heating at 450° C are shown in table 2.

TABLE 2.- Partial analysis of gas from vacuum pyrolysis of coal extracts heated to 450° C for 4 hours

Gas	Weight percent of coal extract		
	Bituminous	Subbituminous	Lignite
H ₂	.041	.083	.13
CH ₄	2.08	3.59	4.55
C ₂ H ₆	1.06	1.89	1.85
C ₃ H ₈	.61	1.31	1.26
CO ₂	.42	1.70	2.83
Total of above components	4.21	8.57	10.62

Mass spectra of thermally treated Pittsburgh seam and subbituminous coal extracts show many of the same features. Peak intensities for the various alkyl series in Pittsburgh seam and subbituminous coal extracts indicate considerable simplification of the mixture after heating. Peak distribution curves for the heated Pittsburgh seam extract, in general, show a single, well-defined maximum, and indicate a much lower average molecular weight for the alkyl derivatives. The mass spectrum of the heated extract of subbituminous coal also indicates a considerably less complex mixture after thermal treatment. This is illustrated by the peak distribution curve for 4-ring, peri-condensed compounds (figure 2). In this instance, a single, well-defined maximum is shown. Prior to heating six maxima were present, indicating a minimum of six different structural types having molecular weights in the same series of mass numbers. Other than an indication of a large reduction in the amount of material having molecular weight below 400, mass spectra of the pyridine extractable material from lignite show essentially the same features before and after heating (figures 4 and 5). The total quantity of gas produced by heating the extracts increases with decreasing rank of the coals, consistent with results obtained for the pyrolysis of whole coal. Gases from all three heated extracts indicate extensive dealkylation. The lignite extract produced the largest amount of CO₂ as expected from the higher oxygen content.

QUANTITATIVE ANALYSIS OF PYRIDINE EXTRACT FROM PITTSBURGH SEAM COAL

The largest amount of pyridine-extractable material was obtained from Pittsburgh seam coal and, following heating of this extractable material, the mass spectrum indicates the least complex mixture. For these reasons, the pyridine extract from Pittsburgh seam coal was chosen for an attempt at a quantitative analysis. A portion of the unheated material was analyzed by mass spectrometry without further treatment giving the results shown in table 3. The major portion of the sample (approximately .15 g) was transferred in an inert atmosphere to a sample tube, placed under vacuum, and heated to 450° C for 4 hours. Analysis of the solid residue from the heated extract is also given in table 3. The carbon number range for the unheated and heated extracts was approximately C₈ to C₃₀, with structures containing from one to six or more ring(s) indicated. Major constituents, having values from 9 to 18 percent, included the following compounds and their alkyl derivatives: Naphthalenes, acenaphthenes and/or biphenyls, acenaphthylenes and/or fluorenes, anthracenes and/or phenanthrenes, phenylnaphthalenes and/or methylenephenanthrenes, and 4-ring peri-condensed compounds. Minor constituents, having values from 1 to 7 percent, included: Benzenes, naphthols and/or indenenes, indans and/or tetralins, and 4-ring cata-condensed compounds. Molecular weight distribution data for homologous series corresponding to phenanthrenes and/or anthracenes, acenaphthylenes and/or fluorenes, and 4-ring cata-condensed structures are shown in figures 8, 9, and 10. Approximate values for contributions to the same homologous series by larger ring systems (indicated on figures) were calculated using average sensitivities for these higher molecular weight constituents.

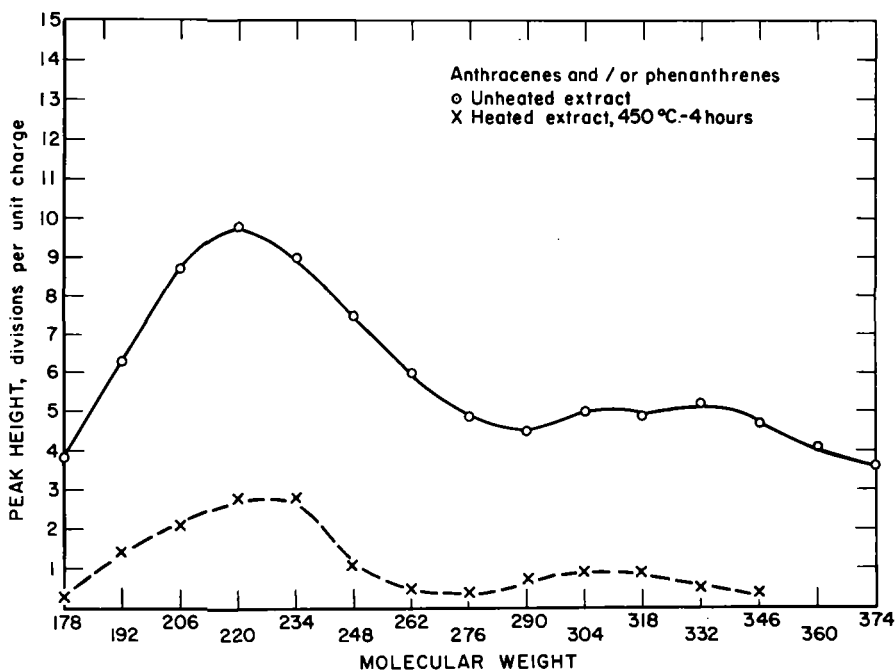


Figure 5. - Partial mass spectrum of pyridine extract from North Dakota lignite, 68 per cent carbon.

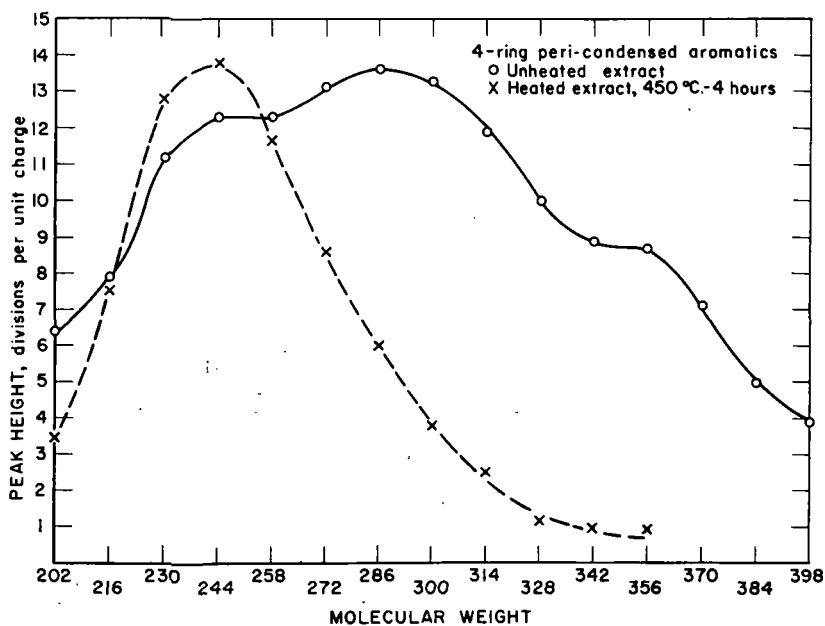


Figure 6. - Partial mass spectrum of pyridine extract from Pittsburgh seam (hvAb), 84 per cent carbon, coal.

TABLE 3.- Mass spectrometric analyses of pyridine extracts from
Pittsburgh seam (hvab), 84 percent carbon coal.

Compound types, including alkyl derivatives ^{1/}	Volume percent	
	Unheated	Solid residue from heating to 450° C
Benzenes	3.4	4.1
Indans, tetralins	0.8	1.3
Naphthalenes	17.8	14.9
Acenaphthenes, biphenyls	12.3	11.7
Acenaphthylenes, fluorenes	15.9	14.8
Anthracenes, phenanthrenes	9.1	13.4
Phenylnaphthalenes, methylenephenanthrenes	11.2	10.9
4-ring peri-condensed aromatics	11.1	8.9
4-ring cata-condensed aromatics	7.4	6.6
Naphthols, indenenes	1.0	3.4
Unknowns (estimated)	10.	10.

^{1/} Values include contributions to same homologous series by high molecular weight alkyl derivatives of five- and six-member ring systems.

An increase in the concentration of components in the mass 200-500 range was found for extracts heated to 450° C for 4 hours. For example, the 3-ring phenanthrene and/or anthracene alkyl derivatives in the mass range 178-304 (figure 8) increased by a factor of 2 during heating. Molecular weight distribution data for other compound types (figures 9 and 10) indicate dealkylation. In addition, the high concentration of methane relative to hydrogen observed in the gases produced during the heating of the extract suggests the decomposition of alkyl substituents (9). There was also a decrease in the concentration of 4- and larger ring systems in the heated extract.

Accompanying the dealkylation was a tendency for the maximum concentration in any homologous series to occur 28 to 56 mass units higher, that is, after the addition of alkyl groups containing two to four carbon atoms. This distribution is similar to that observed in low-temperature carbonization products and also other materials derived from coal and processed at temperatures below 500° C.

A small percentage of residue, corresponding to an estimated 10 percent of the total sample introduced, remained following the mass spectrometric analysis. As indicated in table 3, very little low molecular-weight (m.w. < 150) phenolic material was found in the pyridine extract prepared under essentially oxygen-free conditions.

From this investigation it appears doubtful that vacuum pyrolysis products reported by previous investigators actually represent primary decomposition material. Holden and Robb, in their mass spectrometric investigation, heated the coal for days at temperatures up to 420° C (7). Sun, Ruof, and Howard used an average temperature of 550° C for 4 hours (15); Greifer used temperatures over 500° C for from 1 to 3 hours (5); Batchelder considered low-temperature tar closely related to primary material (1). Techniques for pyrolyzing the coal rapidly are perhaps the only valid methods for studying the primary thermal decomposition products.

The fact that the extractable material changed when heated to temperatures slightly above the plastic range for coal is of considerable interest and can possibly give an insight into the role played by these materials during coal decomposition and coking. Results obtained in this preliminary investigation possibly support a theory that materials derived from coal decrease in complexity in the order (1) extractable material, (2) low-temperature carbonization product, and (3) high-temperature carbonization product. While the step from low- to high-temperature carbonization is well established, the role played by the extract in this series is not as well known and will bear further investigation by this technique.

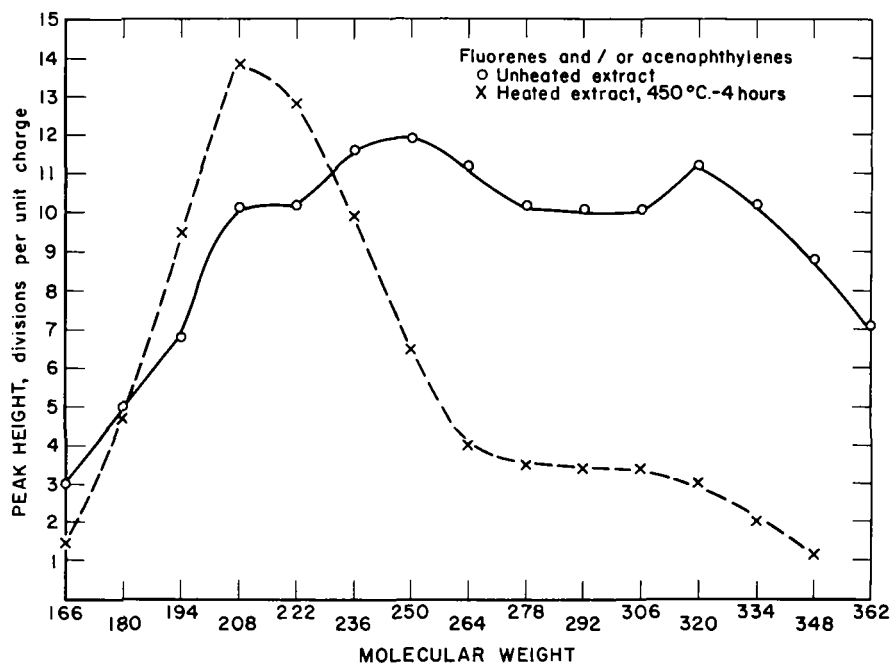


Figure 7. - Partial mass spectrum of pyridine extract from Pittsburgh seam (hvAb), 84 per cent carbon, coal.

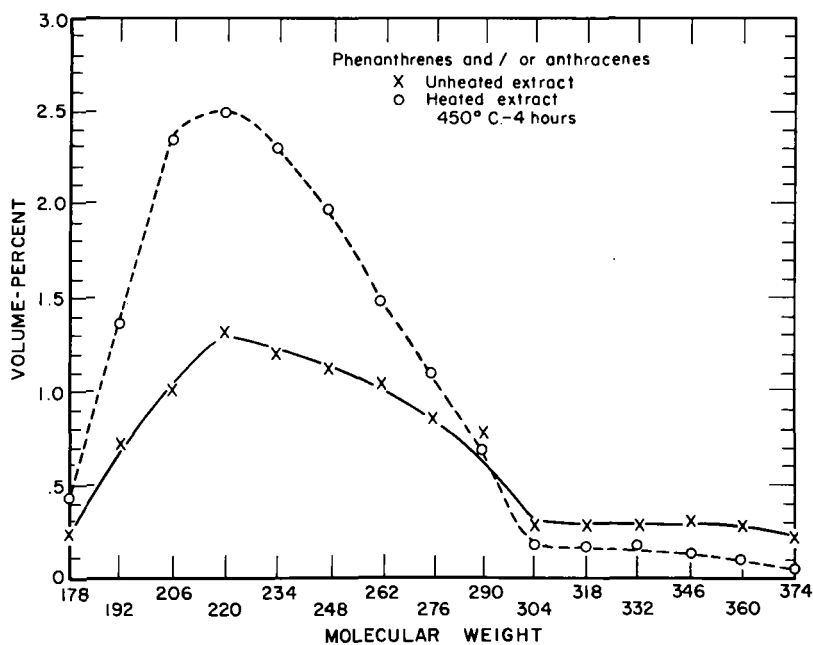


Figure 8. - Mass spectrometer analyses of pyridine extract of Pittsburgh seam (hvAb), 84 per cent carbon, coal.

REFERENCES

1. Batchelder, H. R., R. B. Filbert, Jr., and W. H. Mink. Ind. Eng. Chem. v. 52, 1960, pp. 131-136.
2. Brown, J. K. Fuel (London), v. 38, 1959, pp. 55-63.
3. Dormans, H. N. M. and D. W. van Krevelen. Fuel (London), v. 39, 1960, p. 273.
4. Field, F. H. and S. H. Hastings. Anal. Chem. v. 28, 1956, pp. 1248-1255.
5. Greifer, Bernard. Thesis, Dept. of Chemistry, Carnegie Inst. of Technol., Pittsburgh, Pa., 1958.
6. Holden, H. W. and J. C. Robb. Nature, v. 182, 1958, p. 340.
7. Holden, H. W. and J. C. Robb. Fuel (London), v. 39, 1960, pp. 39-46.
8. Lumpkin, H. E. and G. R. Taylor. Anal. Chem. v. 33, pp. 476-477, 1961.
9. Madison, J. J. and R. M. Roberts. Ind. Eng. Chem., v. 50, 1958, pp. 237-250.
10. Orning, A. A. and B. B. Greifer. Fuel (London), v. 35, 1956, p. 381.
11. Reed, R. I. and W. Snedden. Third International Conference on Coal Science, Valkenburg, Netherlands, April 27-30, 1959.
12. Reed, R. I. Fuel (London), v. 39, 1960, p. 341.
13. Sharkey, A. G. Jr., G. Wood, J. L. Shultz, I. Wender, and R. A. Friedel. Fuel (London), v. 38, 1959, p. 315.
14. Sharkey, A. G. Jr. Encyclopedia of Spectroscopy, ed. G. L. Clark, Reinhold Publishing Corp., New York, 1960, pp. 607-613.
15. Sun, Bozen, C. H. Ruof, and H. C. Howard. Fuel (London), v. 37, 1958, pp. 299-308.
16. Vahrman, M. Nature, v. 189, 1961, pp. 136-137.

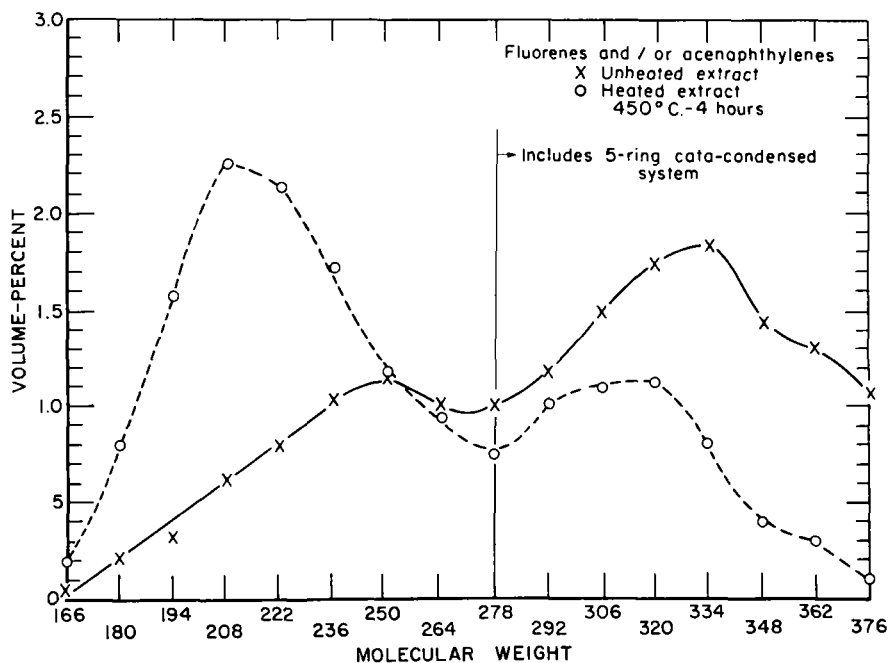


Figure 9. - Mass spectrometer analyses of pyridine extract of Pittsburgh seam (hvAb), 84 per cent carbon coal.

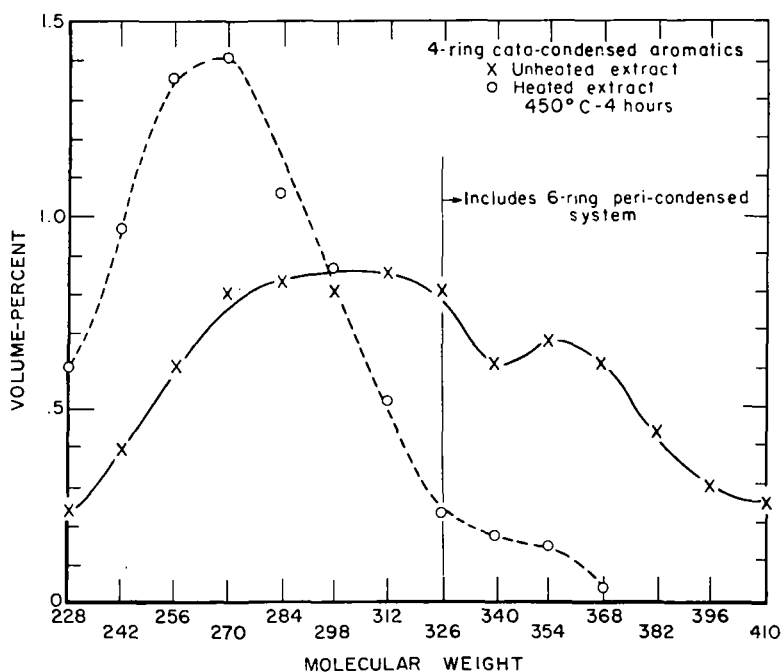


Figure 10. - Mass spectrometer analyses of pyridine extract of Pittsburgh seam (hvAb), 84 per cent carbon coal.

ANALYSIS OF SATURATED HYDROCARBONS
IN BOILING RANGE 450-900°F

W. C. Ferguson and L. R. Snyder
Union Oil Company of California
Brea, California

Abstract

A method for the determination of six compound classes in saturated hydrocarbon samples has been developed. These classes include paraffins and mono-, di-, tri-, tetra- and pentanaphthenes. The method is applicable to saturate fractions extracted from both straightrun and cracked stocks in the carbon number range from about 12 through 35 (450°-900°F). Data on which the method is based will be presented, together with some typical analytical results.

MASS SPECTROMETRIC ANALYSIS OF MIDDLE DISTILLATE
SATURATED HYDROCARBONS

A. Hood, P. R. Mommessin, and B. K. Fritts
Shell Development Company
Houston, Texas

Abstract

A mass spectrometric method is described for the analysis of mixtures of saturated hydrocarbons containing 11 to 18 carbon atoms per molecule. It is based on polyisotopic fragment ions and provides volume percentages of n-alkanes plus isoalkanes, monocycloalkanes, dicycloalkanes, tricycloalkanes, tetracycloalkanes, and monoaromatics. The significant advantages of this method are (1) that it has been developed specifically for the C_{11} to C_{18} range of petroleum saturates and (2) that it has been based primarily on hydrocarbon-type concentrates and therefore, for the most part, is not limited by the assumptions associated with pure compound calibrations.

Characterization of Aromatics in Light Catalytic Cycle Stock

by

Thomas Aczel, K. W. Bartz, H. E. Lumpkin and F. C. Stehling

Humble Oil & Refining Company
Research and Development
Baytown, Texas

Abstract

This paper describes the identification of aromatic compound types in a narrow fraction of a Light Catalytic Cycle Stock. Particular emphasis is given to the part of the investigation concerned with the analysis of compounds in the C_nH_{2n-14} series. The data obtained indicate that these compounds are naphthenonaphthalenes, such as tetrahydroanthracenes, tetrahydrophenanthrenes and benzindanes, and the corresponding ketones.

Analytical evidence in support of the conclusions reported is discussed in detail. The investigation was carried out on sharp chromatographic fractions obtained by alumina gel percolation of the aromatic portion of a narrow distillate (622-625°F). Individual fractions were examined mainly by MS, but UV, NMR, IR, and catalytic microdehydrogenation techniques were also employed.

Introduction

Interest in the composition of light cycle stocks from catalytic cracking stems from the possibility of using this material as a source of higher valued products. As reported in a previous paper (1), an extensive program for the characterization of the major components contained in this refinery stream has been carried out in our Laboratories. The investigation was conducted on a narrow boiling (622-625°F) distillate fraction, which was previously shown to contain the maximum concentration in the compounds hitherto characterized as acenaphthenes and acenaphthylenes, respectively. One of the aims of this study was in fact to prove or disprove the presence of these compound types.

The general approach to the problem consisted in the examination, by MS, UV, NMR, IR and microdehydrogenation techniques, of sharply separated chromatographic fractions obtained by repetitive alumina gel percolations of the aromatic portion of the material under investigation.

Details on the separation technique used and other experimental conditions are reported in the above mentioned work. In brief, the former consisted of an initial separation on alumina gel and repercolation on the same media of blends of adjacent cuts which appeared to be of interest. Thus cuts number 10, 11, 12, 13 and 14, 16, 17, 18 obtained in the first step became the feed for percolations A and B, respectively. The degree of separation achieved is illustrated in Figure 1, in which summations by series of low voltage parent peak intensities are plotted versus weight per cent of sample off the chromatographic column. The overlap noted between the terminal part of percolation A and the first of percolation B is due to the contiguity of the cuts selected for repercolation.

The identification of the compound types belonging respectively to the C_nH_{2n-6} , C_nH_{2n-8} , C_nH_{2n-10} , C_nH_{2n-16} and C_nH_{2n-18} series, i.e. alkylbenzenes and benzothiophenes, indanes and tetralins, indenes, dihydroanthracenes and fluorenes, phenanthrenes and anthracenes, is discussed in our previous communication.

This paper deals with the characterization of the compound types found in the C_nH_{2n-12} and C_nH_{2n-14} series.

Discussion

C_nH_{2n-12} Series

As expected, this series consists of two compound types, naphthalenes and dibenzothiophenes (6). The bimodal distribution of the parent peak intensities, plotted against cumulative weight per cent of the chromatographic fractions, in the -12 series is shown in both Figures 1 and 2. The separation between the C_{15} naphthalenes and the C_{13} dibenzothiophenes of the same molecular weight is particularly evident in Figure 2, as well as the carbon number separation, in order of decreasing molecular weight, achieved

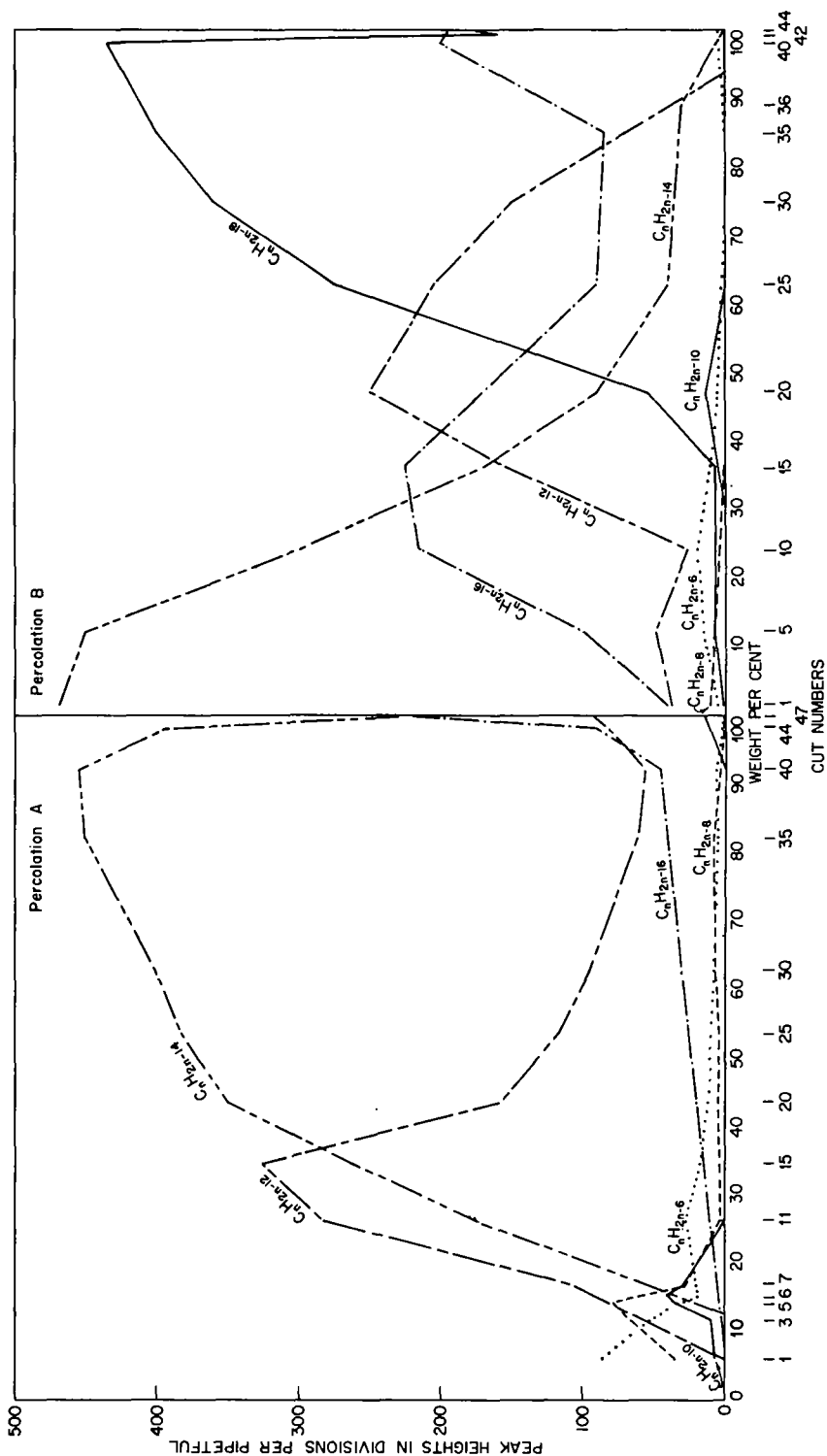


Fig. 1. Low Voltage Parent Peaks Summed by Series.

for the naphthalenes in percolation A. These identifications are substantiated by the data shown in Figure 3, in which the characteristic fragment peaks are plotted. Fragment peaks characteristic of alkyl naphthalenes are predominant in percolation A, coinciding with the first maximum in the parent peak plot, while the intense peak at m/e 197, attributed to dibenzothiophenes, coincides with the maximum in percolation B. Further evidence for these identifications is furnished by the large size of the peaks at m/e 141 and at m/e 197 compared to those at m/e 127 and at m/e 183.

The presence of a compound of molecular formula $C_{13}H_{10}S$ is proved also by the low voltage isotopic ratios reported below:

Cut No. (Percolation B)	Experimental					Theoretical	
	15	20	25	30	35	$C_{15}H_{18}$	$C_{13}H_{10}S$
Peak height 199 $\frac{1}{2}$							
Peak height 198 $\frac{1}{2}$	15.29	15.12	15.44	15.21	15.30	16.49	15.00

Heteroatoms can be detected from isotopic ratios because of the relatively more abundant C^{13} carbon isotope (8).

The difference between the average isotopic value found and the theoretical value for $C_{13}H_{10}S$ of +0.27% is higher than expected, and is probably due to the recording system rather than to a mixture of the hydrocarbon and sulfur compound, as high isotope ratios are also observed in other series.

UV spectra obtained on the above listed fractions contain characteristic dibenzothiophene absorption bands.

C_nH_{2n-14} Series

Mass spectral data indicate the presence of at least two and possibly three compound types in this series, revealed by the maxima in the plots of concentrations of individual carbon numbers versus weight per cent sample off the chromatographic column (Figure 4). It must be noted that concentrations were determined by low voltage analysis (7). Since only approximate calibration data were available, these should be regarded only as indicative of trends.

The first compound type is concentrated in fractions A-7 through A-40. The maxima for the individual carbon numbers appear again in order of decreasing molecular weight. The appearance of a second compound type is indicated by a second series of strong maxima in the C_{17} and C_{16} curves, respectively at A-44 and B-5 and at B-10.

Fractions A-44 and B-5 are equivalent because of the overlap in percolations A and B as mentioned in the introduction.

Indication of a third class of compounds belonging to the C_nH_{2n-14} series is given by another maximum in the C_{16} curve at cuts B-35 and B-40. No identification of this type has been attempted because of the extremely small amount present in the distillate under examination.

The high voltage fragmentation pattern (Figure 5) offers sparse clues for the identification and differentiation of the two compound types. The most abundant peaks can be attributed to a loss of a methyl group from the molecule ion, indicating the presence of at least two methyl substituents on the nucleus and possible nuclear molecular weights of 168 and 182.

Identifications for the two major compound types were carried out by using auxiliary spectral techniques. The investigation was focused primarily on the fractions in which maximum concentrations of the C_nH_{2n-14} compound types were indicated by mass spectral data.

The conclusions reached and the supporting evidence are discussed below in separate sections.

First Compound Type

Examination of the high and low voltage mass spectra and precise isotope ratio measurements (Table I) indicated that this compound type is a hydrocarbon of molecular formula C_nH_{2n-14} , as expected, with a nuclear molecular weight of 168 or 182.

NMR spectra obtained on fractions A-25 and A-35 contain absorption bands at

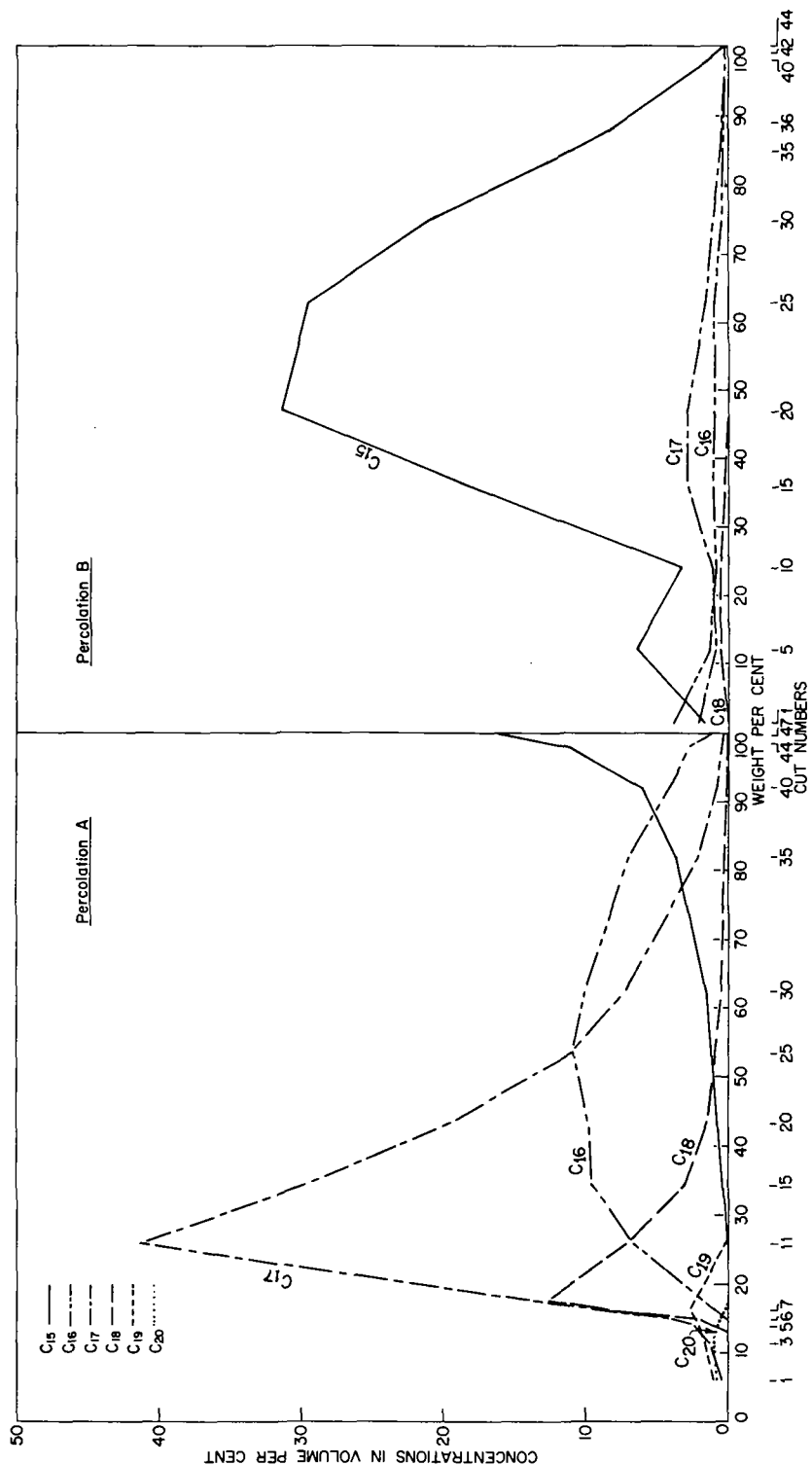
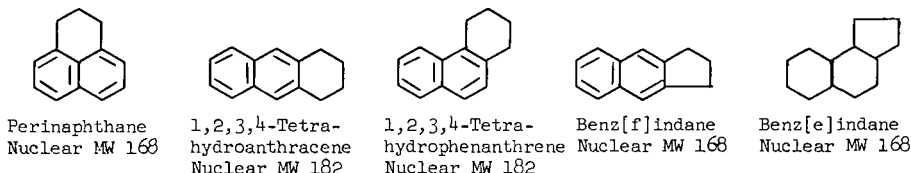


Fig. 2. C_nH_{2n-12} Series. Low Voltage Analysis.

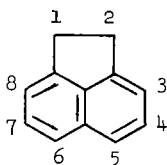
chemical shifts characteristic of

- (1) Aromatic H,
- (2) CH_2 α to an aromatic ring,
- (3) CH_3 α to an aromatic ring,
- (4) CH_2 β or β^2 to an aromatic ring,
- (5) CH_3 attached to an alicyclic ring.

This evidence is compatible with the following nuclear structures:



NMR data definitely exclude the presence of acenaphthenes



although this compound type has been considered to be one of the major components in middle distillates. This contention is based on the fact that neither fraction A-25 nor A-35 has an NMR absorption band at about 6.8 to 7.0 τ (tetramethylsilane standard = 10.0 ppm). The methylene groups in acenaphthene absorb at 6.85 τ , and methyl substitution in the 3 or 8 position would be expected to cause the ortho methylene resonance to shift upfield from this value by about 0.15 ppm. The NMR spectrum of A-35 given in Figure 6 shows no significant absorption in this range. It might be proposed that if the 1 and 2 carbon atoms in acenaphthene were each substituted with two methyl groups that no resonance at 6.85 τ would be obtained. Assuming that the $\text{C}_{17}\text{H}_{2n-14}$ species in A-35 are acenaphthenes, then the MS data indicate an average of 3.8 carbon atoms in side chains, predominantly as methyl groups. The intense absorption between 7.5 to 8.0 τ indicates that the substituents are largely attached to aromatic rings, hence the 1 and 2 carbon atoms of acenaphthene could not be exhaustively methylated.

The NMR spectrum of A-25 is very similar to that of A-35, except that the band assigned to CH_3 's attached to alicyclic ring is relatively more intense in the former fraction. This indicates that the decrease in the average carbon number observed by MS in proceeding from A-25 to A-35 is caused primarily by a decrease in the number of alicyclic methyl groups, the aromatic methyl content remaining approximately constant.

UV spectra obtained on fractions A-25, A-35 and A-40 (Figure 7) are broadly compatible with those published (3) for the five compounds depicted above. They are consistent with a perinaphthanic type structure with the exception of an absorption band at 255 millimicrons present in fractions A-35 and A-40 and a weak band at 326 millimicrons observed in all three fractions. The other suggested structures give rise to bands at 326 millimicrons, but not to the one at 255 millimicrons. In addition, they present weak bands in the 300-320 millimicrons region not detected in these fractions.

The intensities of the UV bands attributed with certainty to the first compound type (at 233 and at 326 millimicrons) follow the same variation pattern through the fractions examined as the corresponding MS parent peak intensities.

Since the absorption band at 255 millimicrons is increasing in intensity from fraction A-27 to fraction A-40 it can be ascribed to the second compound type in this series. The band at 282 millimicrons is probably common to both compound types.

The presence of moderate concentrations of tetrahydroanthracenes and tetrahydrophenanthrenes in the above fractions has been verified by catalytic microdehydrogenation techniques. This approach has been described by Keulemans and Voge (4), Rowan (9) and Cousins (2). The dehydrogenation is carried out in a stream of carrier gas and the effluent products are examined by GC. According to their data the compounds

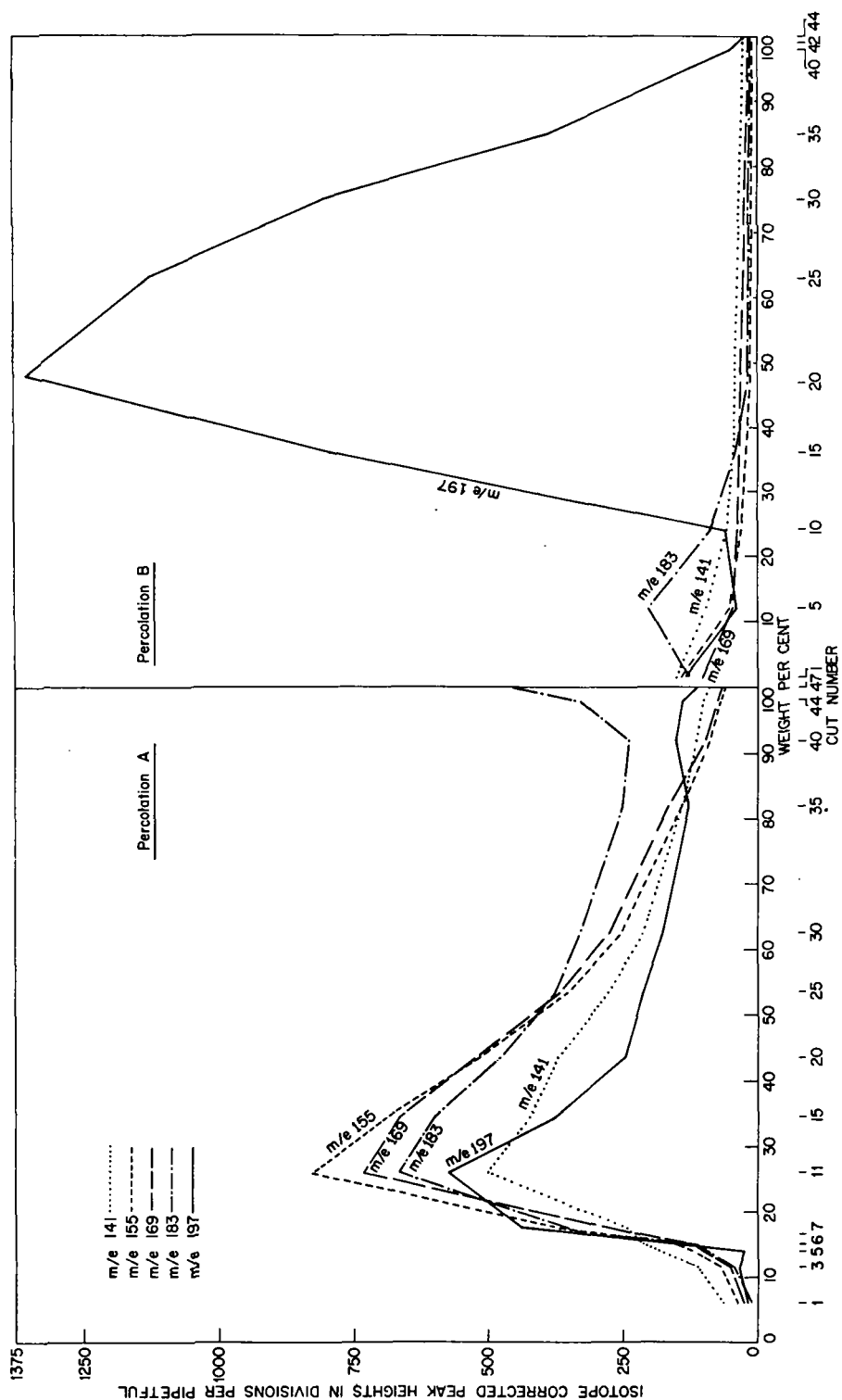


Fig. 3. C_nH_{2n-12} Series. Selected Fragment Peaks.

containing cyclohexyl rings are dehydrogenated to the corresponding aromatics, while the cyclopentyl rings remain essentially unaltered.

Slight modifications on the technique allowed its application to the problems encountered in this work. The equipment consisted essentially of a pyrex glass reaction tube heated at 700°F containing a platinum on Al_2O_3 catalyst, connected on one side to a supply of the carrier gas (helium) and on the other to a cold trap. Reaction products collected in the cold trap were transferred to the mass spectrometer for analysis and the data obtained compared with those recorded prior to dehydrogenation. The use of MS was warranted by the complexity of the materials under investigation.

Experiments with pure compounds and literature data indicated that tetrahydroanthracenes and tetrahydrophenanthrenes dehydrogenate to anthracenes and phenanthrenes belonging to the $C_{nH_{2n-18}}$ series, while benzindanes and perinaphthanes remain either unaffected or dehydrogenate at the most to compounds in the $C_{nH_{2n-16}}$ series.

The presence of anthracenes and phenanthrenes and the simultaneous decrease in the $C_{nH_{2n-14}}$ types detected by both MS and UV, as shown below, in the dehydrogenation products of cuts A-13 and of a blend of cuts A-27, -28, -29-31, indicates therefore that these fractions contain both tetrahydroanthracenes and tetrahydrophenanthrenes.

Dehydrogenation Data

A. MS Analysis by Low Voltage Method (wt. per cent)

Compound Type	Cut A-13			Cuts A-27, -28, -29, -31		
	Feed	Product	Δ	Feed	Product	Δ
$C_{nH_{2n-6}}$	10.9	12.8	+ 1.9	3.8	12.2	+ 8.4
$C_{nH_{2n-8}}$	2.8	-	- 2.8	1.8	2.5	+ 0.7
$C_{nH_{2n-10}}$	-	-	-	-	0.8	+ 0.8
$C_{nH_{2n-12}}$	45.5	50.6	+ 5.1	18.0	31.8	+13.8
$C_{nH_{2n-14}}$	36.6	22.4	-14.2	70.8	31.1	-39.7
$C_{nH_{2n-16}}$	4.2	7.1	+ 2.9	5.6	13.0	+ 7.4
$C_{nH_{2n-18}}$	-	7.1	+ 7.1	-	8.6	+ 8.6

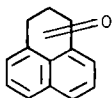
B. Differential UV Data (wt. per cent)

<u>Found after Dehydrogenation</u>	<u>Cut A-13</u>	<u>Cuts A-27, -28, -29, -31</u>
Anthracenes (at 377 $m\mu$)	1.5	3.3
Phenanthrenes (at 255 $m\mu$)	<u>7.2</u>	<u>13.1</u>
total $C_{nH_{2n-18}}$	8.7	16.4

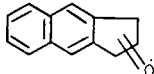
The MS data also show an increase in the -12 and -16 series. These may be attributed to craking of the -14 types to naphthalenes and to the dehydrogenation of perinaphthanes or benzindanes. The unreacted material in the $C_{nH_{2n-14}}$ series consists probably of benzindanes, although incomplete dehydrogenation of the other types cannot be excluded completely.

Second Compound Type

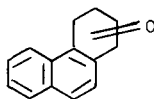
The material giving origin to the second series of maxima in Figures 4 and 5 is an oxygenated type, possibly one of the following structures, appropriately substituted with methyl groups to account for their molecular weights from 210 to 224.



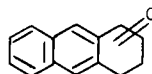
Perinaphthanone
Nuclear MW 182



Benzindanone
Nuclear MW 182



Tetrahydrophenanthrenone
Nuclear MW 196



Tetrahydroanthracenone
Nuclear MW 196

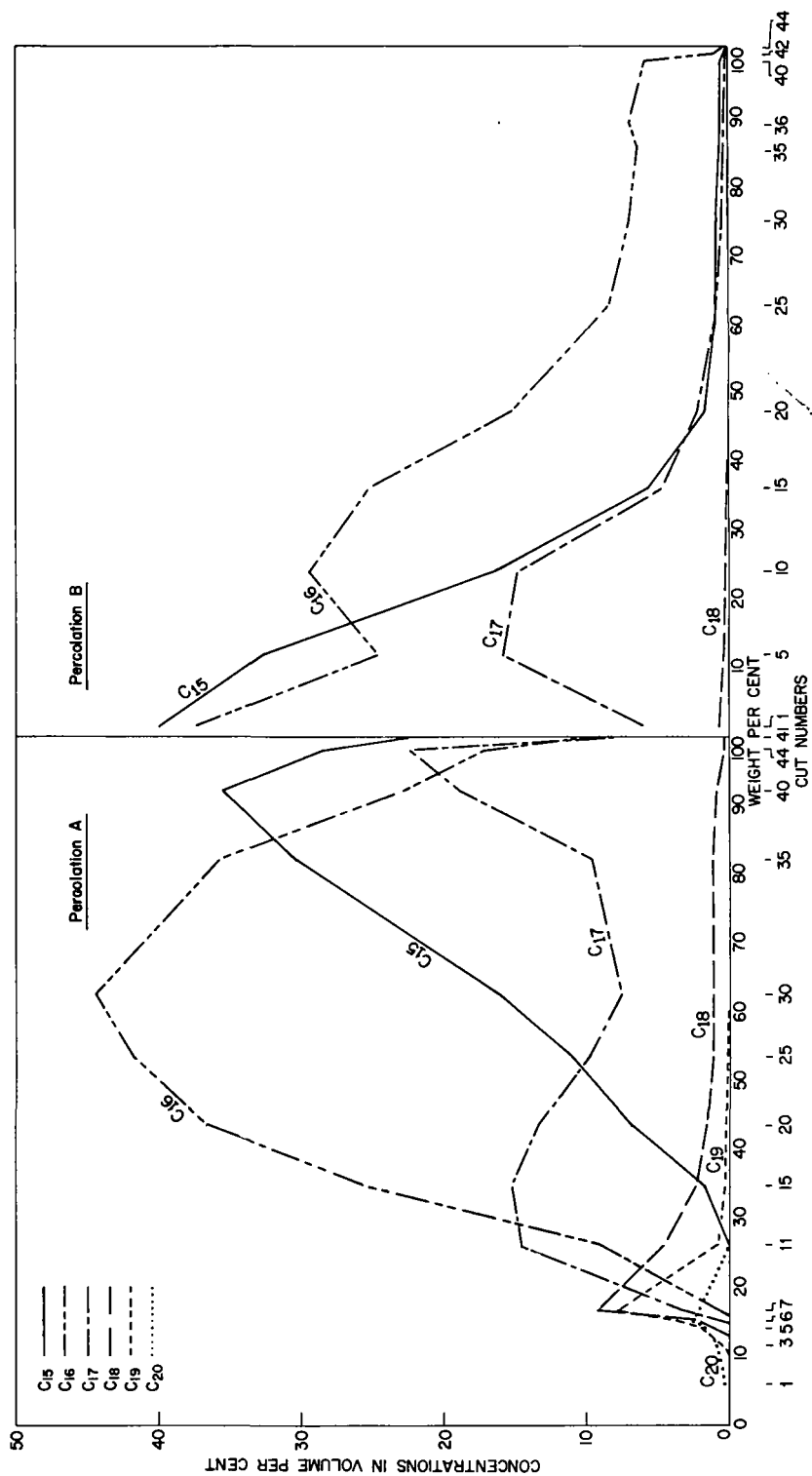


Fig. 4. $C_n H_{2n-14}$ Series. Low Voltage Analysis.

The experimental evidence in support of these structures furnished by exact MS isotopic data, high resolution mass measurements, IR and UV spectra, is discussed below. The presence of a similar class of compounds, fluorenones, in Wilmington petroleum has been reported recently by Latham et al. (5).

The measurement of isotope ratios from mass spectral data can be a very powerful technique in indicating the presence of a hetero-atom in a molecule. The first clue that the second peak in the C_nH_{2n-14} series was an oxygenated compound came from examining the ratios of the peak heights of masses 211 and 210 (C_{16}) in the fractions tabulated below:

	<u>B-1</u>	<u>B-5</u>	<u>B-10</u>	<u>B-15</u>	<u>$C_{16}H_{18}$</u>	<u>$C_{15}H_{14}O$</u>
Isotope, Ratio, %	17.69	17.01	16.48	16.58	17.57	16.47

The isotopic value at B-1 is in very good agreement with that expected for a $C_{16}H_{18}$ hydrocarbon; the value at B-5 is intermediate; those for B-10 and B-15 are much lower. The isotope ratios for the latter two fractions check extremely well with the theoretical value of 16.47 for an oxygenated compound, $C_{15}H_{14}O$. This material is thus believed to be an oxygenated compound. Fraction B-5 is a mixture of the hydrocarbon and the oxy-compound and the isotopic data is intermediate for this fraction, as would be expected for a mixture. The isotopic data mentioned above, together with similar data for other fractions, are given in Table I. In examining these data one should bear in mind that an unexplained bias of about + 0.1% to + 0.3% has been experienced recently in all of the isotopic data obtained on our instrument. This is exemplified by the measured isotopic values for the well identified C_{15} dibenzothiophene (C_nH_{2n-12} series).

Exact mass measurements, carried out on a CEC Model 21-110 high resolution mass spectrometer of the Mattauch design also confirmed the presence of oxygenated compounds in these fractions. Data obtained on fraction B-12 are reported below.

<u>Nominal Mass</u>	<u>Measured Mass</u>	<u>Theoretical Mass for</u>	
		<u>$C_{15}H_{14}O$</u>	<u>$C_{16}H_{18}$</u>
210	210.173	210.171	210.207
		<u>$C_{16}H_{16}O$</u>	<u>$C_{17}H_{20}$</u>
224	224.187	224.191	224.227

The infrared spectrum of fraction B-10 contains two sharp carbonyl bands. One at 1682 cm^{-1} is believed due to a conjugated carbonyl and the other at 1725 cm^{-1} is attributed to a non-conjugated carbonyl.

Examination of the UV spectra of several fractions containing the oxygenated material reveals that each has a weak, yet distinct maximum, at $255\text{ m}\mu$. This absorption band first appears in the UV spectrum of A-35 (shown in Figure 7), and is consistent with the appearance of the C_{17} oxygenated compound, shown by the MS data in Figure 4. The same $255\text{ m}\mu$ band also appears in A-40, and in the fractions of the B percolation through B-15, as shown in Figure 8. The initial appearance, general variation of intensity, and disappearance of the UV features in the chromatographic fractions agree well with the MS plots.

A complete interpretation of the data is hindered by the appearance in these fractions of two other compound types, dibenzothiophenes and dihydroanthracenes. Although not quite sufficient by themselves, the data obtained are consistent with the conclusions deduced from the MS and IR spectra, which clearly indicate that the second compound type found in the C_nH_{2n-14} series is an aromatic ketone. In addition to the evidence discussed above, the similarity of the high voltage mass spectrum to that of the first compound type indicates an analogous ring structure, i.e. the structures of ketonaphthenonaphthalenes shown at the beginning of this section.

Conclusion

The investigation discussed in this report, together with the data already published (1) has led to a radical change in our ideas of the nature of certain compound types in light catalytic cycle stocks. We deem particularly significant the proofs obtained on the absence of acenaphthenes, at least in the narrow distillate fraction studied. The discovery of an oxygenated compound type in relatively high concentration is also meaningful.

The gathering of the detailed information obtained in the course of this work was made possible by the sharp separations achieved and the integration of complementary

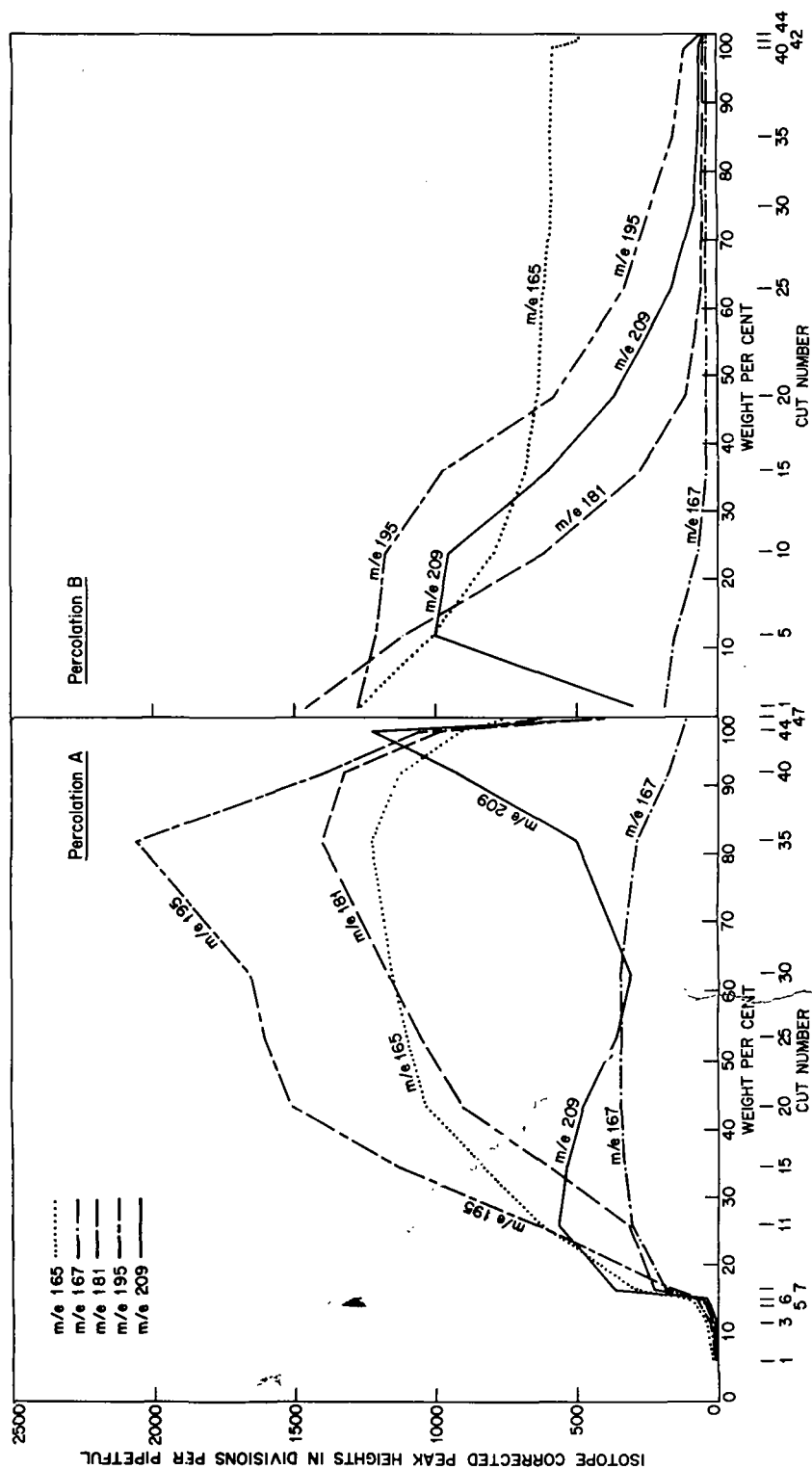


Fig. 5. C_nH_{2n-14} Series. Selected Fragment Peaks.

analytical techniques and tools. The role of mass spectrometry in particular was shown to be extremely valuable, both in indicating the presence of different compound types, and thus pinpointing the fractions to be subjected to further analysis, and in identifying the components contained in the same fractions. The data obtained by the use of high resolution mass spectrometry illustrate well the power of this technique.

Acknowledgement

We wish to thank Dr. P. J. Klaas, formerly of Esso Research and Engineering Company, for the precise mass measurements obtained on the high resolution mass spectrometer. We wish to thank also Mr. D. J. Krisher, Mr. J. L. Taylor, Mr. G. R. Taylor, Mr. R. K. Saunders, Mr. T. J. Denson, Mr. Theo Hines, and Mr. H. W. Kinsey for their valuable contributions to experimental phases of this work.

Literature Cited

- (1) Bartz, K. W., Aczel, T., Lumpkin, H. E., and Stehling, F. C., A.C.S., Div. of Petroleum Chem. Preprints, Vol. 7, No. 1, page 141.
- (2) Cousins, L. R., Clancy, D. J., and Crable, G. F., Anal. Chem., 33, 1875 (1961).
- (3) Friedel, R. A., Orchin, M., Catalog of Ultraviolet Spectra of Aromatic Compounds, John Wiley, Inc., New York, 1951, Nos. 213, 214, 215, 216.
- (4) Keulemans, A.J.M., Voge, H. H., J. Phys. Chem., 63, 476 (1959).
- (5) Latham, D. R., Ferrin, C. R., and Ball, J. S., Anal. Chem. 34, 311 (1962).
- (6) Lumpkin, H. E. and Johnson, B. H., Anal. Chem. 26, 1719 (1954).
- (7) Lumpkin, H. E., Anal. Chem., 30, 321 (1958).
- (8) Lumpkin, H. E., and Nicholson, D. E., Anal. Chem. 32, 74 (1960).
- (9) Rowan, Robert, Anal. Chem., 33, 658 (1961).

Table I

Isotope Ratios from MS Low Voltage Spectra
C_nH_{2n-14} Series

C No.	Experimental					Theoretical	
	Percolation A. Fractions					Hydrocarbon	Oxygenated Compd.
	<u>20</u>	<u>25</u>	<u>30</u>	<u>35</u>	<u>40</u>		
C ₁₅			16.72	16.67	16.92	<u>16.46</u>	15.36
C ₁₆	17.69	17.86	17.87	17.81	17.84	<u>17.57</u>	16.47
C ₁₇	19.07				18.03	<u>18.68</u>	<u>17.58</u>
	Percolation B. Fractions					Hydrocarbon	Oxygenated Compd.
	<u>1</u>	<u>5</u>	<u>10</u>	<u>15</u>			
C ₁₅	16.69	16.76	16.50			<u>16.46</u>	15.36
C ₁₆	17.69	17.01	16.48	16.58		<u>17.57</u>	<u>16.47</u>
C ₁₇		17.60				18.68	<u>17.58</u>

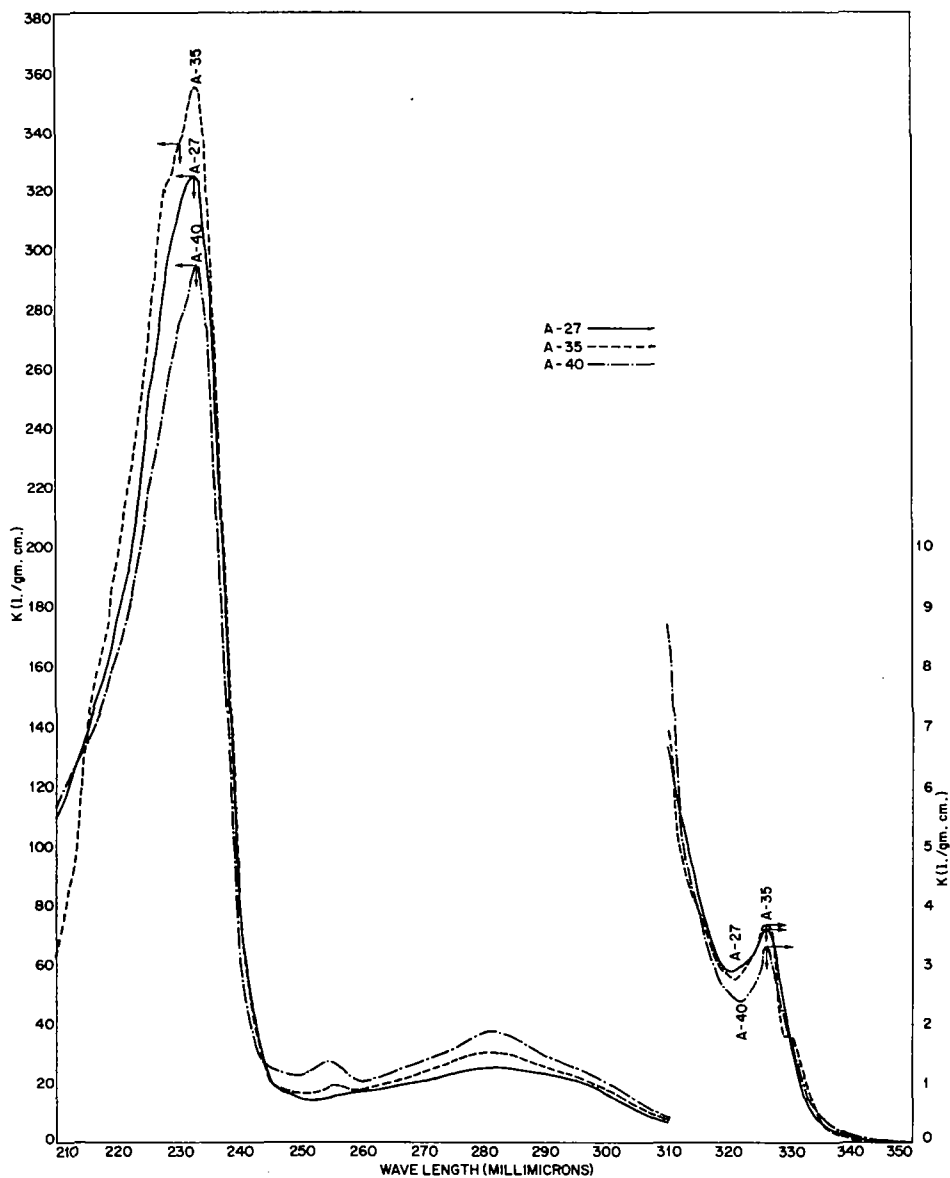


Fig. 7. Ultraviolet Spectra of Cuts A-27, A-35, and A-40 in Iso-octane.

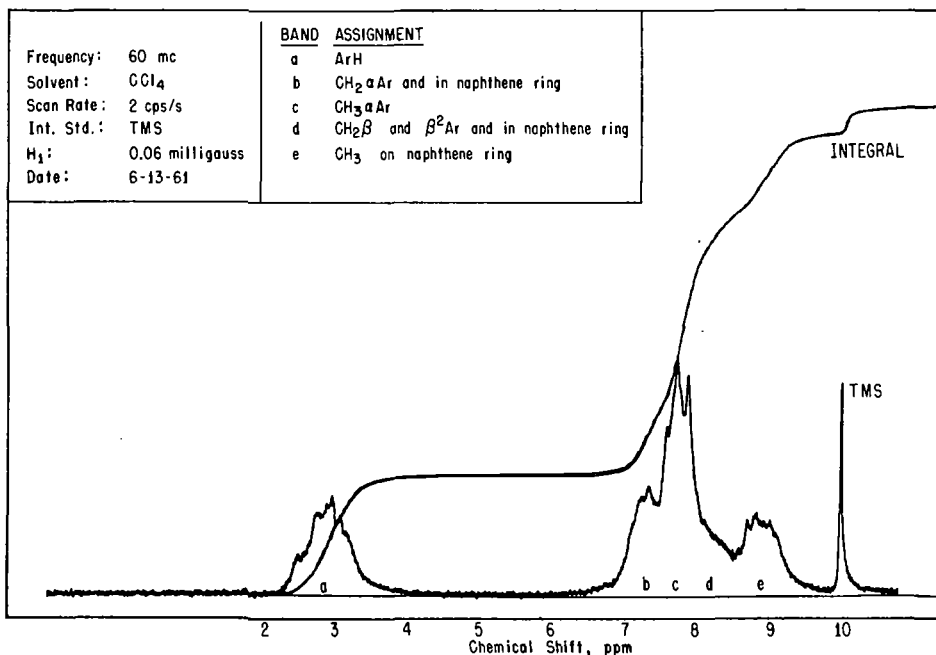


Fig. 6. NMR Spectrum of Cut A-35.

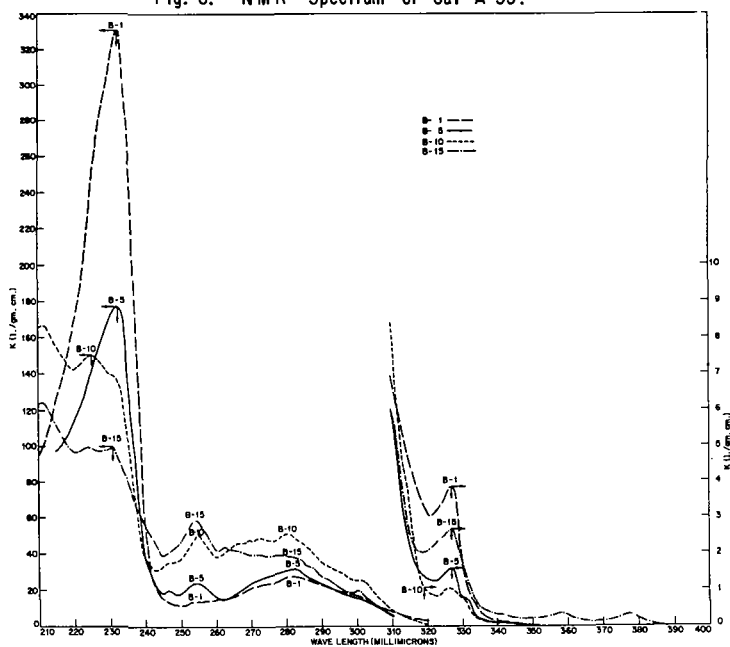


Fig. 8. Ultraviolet Spectra of Cuts B-1, B-5, B-10, and B-15 in Iso-octane.

THE MASS SPECTRA AND ANALYTICAL CORRELATIONS OF C₅ THROUGH C₁₀ CODA COMPOUNDS

by

R.F. Kendall, F.O. Cotton, N.G. Foster, and B.H. Eccleston
Bartlesville Petroleum Research Center, Bureau of Mines
U.S. Department of the Interior, Bartlesville, Okla.

SUMMARY

The problem of air pollution is of national interest, and as a part of the investigation of this problem the Bartlesville Petroleum Research Center is studying exhaust gases produced by automotive engines. These gases have been cited as contributors to the eye-irritating components of the smog that plagues urban areas throughout the country. Identifications of the hydrocarbons in automobile exhaust gases are hindered by the relative unavailability of pure mass spectra reference materials, especially of unsaturated hydrocarbons other than the simple alkenes.

The mass spectra and analytical correlations of over 30 cycloolefins, diolefins, and acetylenes (CODA compounds) are reported. Spectra correlations are supported by low voltage mass data. Methods utilizing gas-liquid chromatography for isolating high purity unsaturated reference compounds are described.

Particular emphasis is given to the mass fragmentation patterns of the acetylenes as compared to those of the cycloolefins and diolefins. Mass interpretation of mixtures containing such hydrocarbon types is frequently difficult because each type has the same empirical formula, C_nH_{2n-2}, and an abundance of rearrangement peaks.

Availability of spectra and correlations on pure CODA compounds should aid in future identification studies on exhaust gases.

DETERMINATION OF HYDROCARBON TYPES IN KEROSENE
RANGE DISTILLATES BY MASS SPECTROMETRY

L. R. Snyder, H. E. Howard, and W. C. Ferguson
Union Oil Company of California
Brea, California

Manuscript Withdrawn

MASS SPECTROMETRY OF SULFUR COMPOUNDS. IV. STUDIES OF THE
MASS SPECTRA OF 2-*t*-BUTYL-, 3-*t*-BUTYL-, AND 2,5-DI-*t*-BUTYLTHIOPHENES

by

N.G. Foster, D.E. Hirsch, R.F. Kendall, and B.H. Eccleston
Bartlesville Petroleum Research Center, Bureau of Mines
U.S. Department of the Interior, Bartlesville, Okla.

SUMMARY

The mass spectra of more than 50 alkylthiophenes have been reported in recent years, providing a better understanding of the processes of fragmentation in such molecules. Studies of mass spectra of the available tertiary butyl thiophenes have indicated a mechanism of fragmentation entirely different from that proposed for the bulk of the thiophenes. These data and similar results on closely related alkylbenzenes, observed by other workers, prompted the more detailed study of these types of alkylthiophenes reported here.

The mass spectra of 2-, 3-, and 2,5-di-*t*-butylthiophenes are presented and the possible paths of ion fragmentation discussed. Low voltage data will be used to support these suggested mechanisms. The fragmentation mechanisms will be compared with those existing for other alkylthiophenes and with those reported by other workers for analogous alkylbenzenes. The analytical consequences of fragmentations from these types of thiophenes will be discussed.

Knowledge of spectra of these types of compounds and of their fragmentation patterns will aid in interpreting mass spectra and in predicting basic mass spectral patterns for all alkylthiophenes.

Appearance Potentials and the Mass Spectra of
Fluorinated Olefins

Chava Lifshitz* and F. A. Long
Chemistry Department, Cornell University
Ithaca, New York

Abstract

Appearance potentials and mass spectra have been determined for a group of simple fluorinated olefins. In some respects the reactions of the positive ions are similar to those of the hydrocarbon analogues; for example there are frequent losses of H_2 or HF to form acetylene ions. Rearrangement processes, involving atom migration, occur more frequently in the more highly fluorinated compounds. For the most part the relative rates of the unimolecular decomposition processes vary with the energy demands, but frequency factors are occasionally quite low for rearrangements. The observed appearance potentials agree fairly well with values calculated from heats of formation of the species involved, but there are some exceptions. Ionization efficiency curves for some of the fragments from CF_2CFH and C_2F_4 show interesting features which are discussed.

Introduction

The mass spectra of fluorocarbons are usually quite different from those of the hydrocarbon analogues. For instance, several interesting rearrangements are observed, which are absent in the hydrocarbon spectra¹. The fluorinated olefins were chosen in the present study, because these compounds show considerable parent ion peaks in their spectra, contrary to the behavior of the fluorinated paraffins¹. Furthermore, the heats of formation of several of the fluoroethylenes have been determined experimentally by Neugebauer and Margrave², while others are known from estimations³. It is thus possible to gain further information from the appearance potentials of the different fragments about the thermochemistry of the radicals and ions involved.

Experimental

The data were taken on a C.E.C. mass spectrometer, model 21-401, which has been modified as described previously⁴.

Appearance potentials were determined by the vanishing current method, using argon or neon as calibrating gas, in the same way as has previously been discussed⁴.

The fluoro-ethylenes studied were all better than 99.8% pure.

Results and Discussion

75 volt spectra

Table I gives the spectra (in terms of percentage yields of the various ions) of several fluoroethylenes. These were obtained with 75 volt electrons, 10 μA current and an accelerating voltage of 210 v.

*On leave from the Israel Atomic Energy Commission

Table I
Mass Spectra of Fluoroethylenes

<u>Species</u>	<u>CH₂CH₂</u>	<u>CH₂CHF</u>	<u>CH₂CF₂</u>	<u>CHFCHF₂</u>	<u>CF₂CF₂</u>
CH ₂ ⁺	0.9	0.6	2.6		
CH ₃ ⁺	0.1	0.2			
C ₂ H ⁺	4.1	1.8			
C ₂ H ₂ ⁺	24.7	9.9	1.1		
C ₂ H ₃ ⁺	26.8	11.4			
C ₂ H ₄ ⁺	41.3 _p				
CF ⁺		2.8	13.1	15.2	28.6
CFH ⁺		0.9		5.7	
CFH ₂ ⁺		0.1	12.4		
C ₂ FH ⁺		10.4	9.2	1.8	
C ₂ FH ₂ ⁺		24.9	16.7		
C ₂ FH ₃ ⁺		34.5 _p			
CF ₂ ⁺			0.9	1.7	10.6
CF ₂ H ⁺			0.3	16.0	
C ₂ F ₂ ⁺				1.0	0.3
C ₂ F ₂ H ⁺			4.8	29.7	
C ₂ F ₂ H ₂ ⁺			35.4 _p		
CF ₃ ⁺					1.3
C ₂ F ₃ ⁺				0.4	37.3
C ₂ F ₃ H ⁺				26.2 _p	
C ₂ F ₄ ⁺					20.4 _p

Table II
Appearance Potentials for Fluoroethylenes in volts

<u>Species</u>	<u>CH₂CH₂</u>	<u>CH₂CHF</u>	<u>CH₂CF₂</u>	<u>CHFCHF₂</u>	<u>CF₂CF₂</u>
CH ₂ ⁺	19.0		17.8		
C ₂ H ₂ ⁺	13.2	13.7 ₃	19.7 ₈		
C ₂ H ₃ ⁺	14.0 ₈	14.3 ₈			
C ₂ H ₄ ⁺	10.6 ₈				
CF ⁺		15.4 ₃	15.2 ₃	15.2 ₂	14.0 ₈
CFH ⁺				15.3 ₈	
CFH ₂ ⁺			15.0 ₈		
C ₂ FH ⁺		14.0 ₄	14.4 ₄	20	
C ₂ FH ₂ ⁺		14.0 ₂	14.8 ₀		
C ₂ FH ₃ ⁺		10.4 ₅			
CF ₂ ⁺				19.2 ₈	15.1 ₃
CF ₂ H ⁺				14.2 ₂	
C ₂ F ₂ ⁺				14.8 ₃	
C ₂ F ₂ H ⁺			16.6 ₇	16.1 ₃	
C ₂ F ₂ H ₂ ⁺			10.4 ₅		
CF ₃ ⁺					13.5 ₄
C ₂ F ₃ ⁺					16.0 ₀
C ₂ F ₃ H ⁺				10.3 ₃	
C ₂ F ₄ ⁺					10.1 ₂

Intensities are rounded off to the nearest 0.1% and most of the peaks below this value are omitted. Doubly charged ions are not included. The agreement with previously published results on C_2H_4 , CH_2CF_2 and C_2F_4 is good, except for a generally smaller degree of reaction in the present case. This is especially apparent for C_2F_4 , where $C_2F_3^+$ is the highest peak in the spectrum whereas CF^+ is the highest according to Dibeler and coworkers⁵.

As one goes from ethylene to perfluoroethylene, successively substituting the hydrogens by fluorines, the general features are a gradual lowering of the yields of acetylene ions ($C_2H_2^+$, C_2HF^+ or $C_2F_2^+$) and an increase in the yields of the rearrangement products CH_3^+ , CH_2F^+ , CF_2H^+ , and CF_3^+ as well as CF^+ .

CH_2CF_2 and $CHFCF_2$ show low yields of the parent-minus-one-hydrogen-atom; a similar behavior has been observed in $C_6F_4H_2$ and C_6F_5H ¹. There is in this ethylene series also a gradual decrease in parent ion yield and an increase in the yields of ions of the type CH_2^+ , CHF^+ and CF_2^+ .

Appearance Potentials

Table II summarizes the appearance potentials observed for the main peaks of the fluoroethylenes. These data are averages of from 3 to 5 runs for each species. The standard deviations are in the order of from 0.05 to 0.10 e.v., for the more abundant ions.

The ionization potentials of these compounds have been previously determined. The values which were obtained are listed in Table III.

Table III
Comparison of Ionization Potentials

	<u>Present</u> <u>Electron Impact</u>	<u>Previous</u> <u>Electron Impact</u>	<u>Photo-</u> <u>ionization</u>	<u>Spectro-</u> <u>scopic</u>
C_2H_4	10.66	10.46-10.9 ⁸		10.51 ⁷
CH_2CHF	10.45		10.37 ⁸	
			10.36 ⁹	
CH_2CF_2	10.45		10.30 ⁸	
			10.33 ⁹	
$CHFCF_2$	10.33		10.14 ⁸	
C_2F_4	10.12	9.3 ¹⁰	10.12 ⁸	

The present electron impact ionization potentials are all 0.1-0.2 e.v. higher than the photoionization values^{8,9} except that for C_2F_4 . Other appearance potentials which have been measured previously are for the fragments from C_2H_4 ⁸ and for CF_2^+ from C_2F_4 ¹⁰ and the agreement is quite good.

The ions of lowest appearance potential for the "hydrogen" end of the series (Table II) are the acetylene ions, which are formed from the parent by an H_2 or HF split, while for the more fluorinated members the rearrangement ions CF_2H^+ , CF_3^+ and CF^+ lead to the lowest appearance potentials. The energy demand for the production of the CX_2^+ ions (CH_2^+ , CHF^+ and CF_2^+) decreases with fluorine content. On the other hand, the energy which is needed for the production of parent-minus-one-atom increases with fluorine content; this again is similar to the trend observed for fluorobenzenes¹. The next section illustrates these features further.

Breakdown Mechanisms

Figure 1 shows the proposed mechanism for the CH_2CHF spectrum. The numbers above the formulas are the percentage yields, while those above the arrows are the energy differences in going from parent ion to product ion. $C_2H_2^+$ is formed from the parent by an HF split, while C_2HF^+ is formed by an H_2 split. Although the acetylenic ions have lower appearance potentials than the parent-minus-one-F or one-H ions, their total yield is lower. This is indicative of unfavorable frequency factors. CF^+ is formed by direct rearrangement from the parent,

together with CH_3 and not with CH_2+H ; this will become evident in the forthcoming thermochemical calculations.

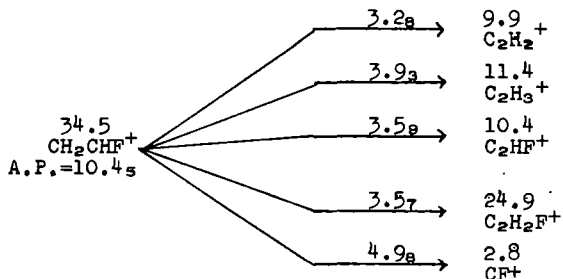


Fig. 1. Mechanism of CH_2CHF spectrum

Figure 2 shows the mechanism for the production of the CH_2CF_2 spectrum. Here already a greater contribution from rearrangement ions as compared to acetylenic ions is observed. That CH_2^+ is not a secondary (from $\text{C}_2\text{H}_2\text{F}^+$ or CH_2F^+) but formed directly by cleavage of the ethylenic bond, will be seen from the thermochemical calculations. Neutral radicals are assumed to be formed along with the different positive ions. Indeed no negative ions have been observed for $\text{CH}_2\text{CF}_2^{11}$.

Figure 3 shows the proposed mechanism for C_2F_4 . The possibility that CF^+ is a secondary as well as a primary is shown by the arrow in parenthesis. The value of 1.7 which is given beside the arrow will be discussed in the following section.

Ionization Efficiency Curves

It is seen that on the whole the energy demand is what determines the likelihood of a process, but there are some striking exceptions. In C_2F_4 (Fig. 3) for example, CF_3^+ has the lowest appearance potential other than the parent, yet comprises only 1.3 percent of the spectrum at 75 volts. Figure 4 shows the ionization efficiency curve for this ion; the striking feature is that there is almost no linear rising part.

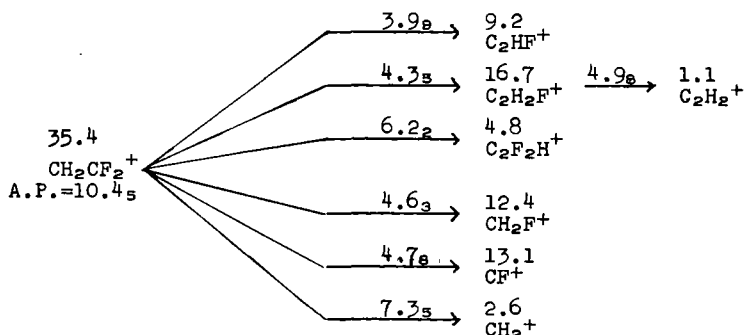


Fig. 2. Mechanism of CH_2CF_2 spectrum

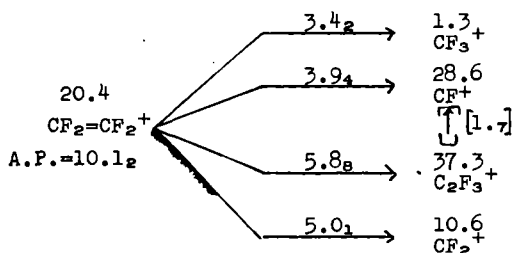


Fig. 3. Mechanism of CF_2CF_2 spectrum

In order to study this point further, the dependence of the percentage yields of the different fragments from C_2F_4 upon the ionizing voltage was determined. Figure 5 shows this dependence for several ions. $V_e - I^2$ is the ionizing voltage minus the ionization potential of the parent. CF_3^+ rises to a low maximum yield at a relatively low $V_e - I^2$ and then levels off. CF^+ shows a similar behavior to that of CF_3^+ at low voltages (see Figure 5) but at higher voltages the CF^+ yield rises very steeply.

The dependence of the percentage yields of the different fragments from CFHCF_2 on the ionizing voltage was also studied and the results are given in Figure 6 (the voltage scale was not calibrated in this case). Here, too, CF_2H^+ rises to a maximum but this is at a much higher yield than CF_3^+ in C_2F_4 and at a higher ionizing voltage.

Several ionization efficiency curves for CF^+ are shown in Figure 7. These were drawn so that the slopes of the linear parts are equal in all three cases. The CF^+ curve from CH_2CF_2 illustrates the expected behavior. The CF^+ curve from C_2F_4 shows a break, while the CF^+ curve from CHFCH_2 shows a long tail.

It is appropriate to point out at this point how appearance potentials were determined for CF^+ and CF_3^+ in C_2F_4 and for CF^+ from CFHCF_2 . In all of these cases the pressure of the gas studied and that of the argon were matched so that the first parts of the ionization efficiency curves for the ion and for Ar^+ coincided (contrary to the usual procedure⁴ of matching the linear parts). The values thus obtained are the ones given in Table II. A second appearance potential of 17.7 v was determined for CF^+ in C_2F_4 from the break in the ionization efficiency curve by adjusting the pressures of C_2F_4 and Ar so that the linear slopes were the same. If it is assumed that this higher appearance potential is the consequence of a secondary decomposition process one calculates the parenthetically noted value of 1.7 volts for going from C_2F_3^+ to CF^+ (Figure 3). Appearance potentials for these ions CF^+ and CF_3^+ are uncertain to a greater degree than is shown by the experimental spread because of the odd shapes of the ionization efficiency curves.

Thermochemical Calculations

Some thermochemical calculations were carried out based on the measured appearance potentials. Table IV shows some of the heats of formation which were used in these calculations, as well as the results obtained. The values for CH_2CHF and CF_2CFH are estimations by Maslov and Maslov³. The ΔH_f value for CH_2CHF is shown to be correct by the appearance potential of C_2H_3^+ from this compound; knowing the heat of formation of C_2H_3^+ from its appearance potential from C_2H_4 , the heat of formation of CH_2CHF is calculated to be -1.22 e.v.

The heats of formation of CH_2F^+ , CF_2H^+ and CF_3^+ given in Table IV are from their respective appearance potentials in CH_2CF_2 , CHFCH_2 and CF_2CF_2 . The listed heat of formation of CF was used in these calculations. These results are based on two assumptions, namely that neutral CF is formed in the processes forming these three ions and that excess rearrangement activation energy is negligible.

Fig. 4.

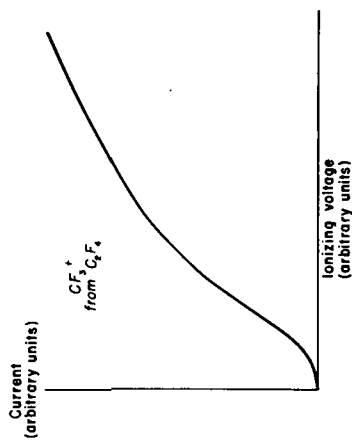
Ionization efficiency curve of CF_3^+ from C_2F_4 .

Fig. 6.

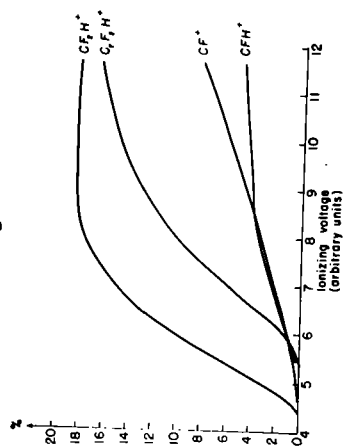
Dependence of fragment-ion yields on ionizing voltage in CHF_2 .

Fig. 5.

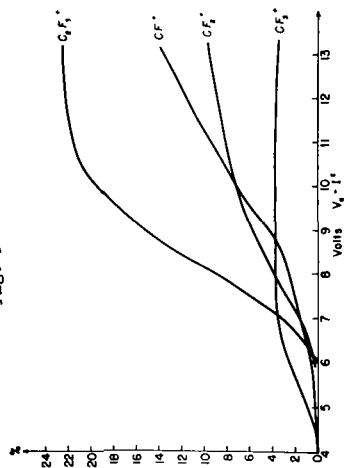
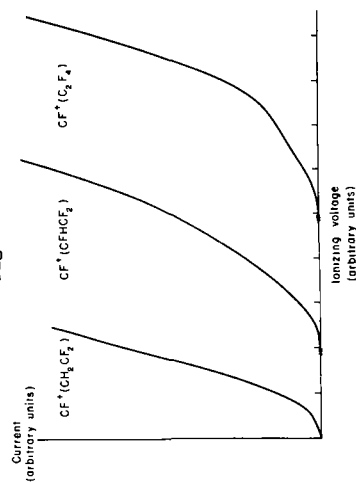
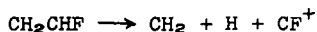
Dependence of fragment-ion yields on ionizing voltage in C_2F_4 .

Fig. 7.

Comparison of CF^+ ionization efficiency curves from different compounds.

The heat of formation of CF^+ given in Table IV is calculated from its appearance potential in CH_2CHF assuming the process: $CH_2CHF \rightarrow CH_3 + CF^+$. From the heats of formation of CF^+ and CF the ionization potential of CF is calculated to be 9.5 e.v. As any contribution from rearrangement energy was again neglected in this case $\Delta H_f(CF^+)$ as well as I.P. (CF) constitute upper limits. The latest spectroscopic ionization potential of CF is 8.9 volts¹⁵. The possibility that CF^+ is formed by the process:



instead of by direct rearrangement from the parent was considered but discarded, because this would give I.P. (CF) = 6.22 e.v., which is much lower than any of the previously reported results on CF .

Table IV
Heats of Formation and Ionization Potentials of Some Selected

Fluorocarbon Species

Species	ΔH_f , e.v.	
CH_2CHF^*	-1.22 ^a	
$CH_2CF_2^*$	-3.36 ^b	
$CHF CF_2^*$	-4.82 ^a	
$CF_2 CF_2^*$	-6.59 ^b	
$CF_3 CF=CF_2^*$	-11.22 ^c	
CH_2F^+	+8.4 ₈	
CF_2H^+	+6.1 ₇	
CF_3^+	+3.7 ₂	
CF^+	+12.8 ₂	
		<u>I.P., v</u>
CF^*	+3.23 ^d	9.5 ₈
CF_2	-1.6 ₀	
CH_2F		9.4 ₅
CF_3^*	-5.2 ^e	8.9

* Literature values which were used in our calculations

a. Ref. 3, these are estimations which are good to within 5-10%

b. Ref. 2, experimentally determined values

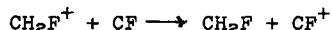
c. Ref. 12, an estimation based on $\Delta H_f(C_2F_4)$

d. Ref. 13, based on the spectroscopically determined C-F bond energy.

e. Ref. 14, from kinetic measurements of activation energies.

From the heats of formation of CF_3 and CF_3^+ (Table IV), the ionization potential of CF_3 is calculated to be 8.9 v, as compared to the direct electron impact value on the CF_3 radical, of 10.1 v¹⁶. The present value is in better agreement with the value based on CF_3^+ appearance potentials from trifluoromethyl halides¹⁷. The present low value may be the adiabatic ionization potential of the radical. On the other hand, the possibility of an ion-pair formation cannot be excluded, especially in view of the peculiar ionization efficiency curve of CF_3^+ from C_2F_4 .

If CF^+ and CH_2F^+ are both formed by similar rearrangements from the parent CH_2CF_2 , then the difference in their appearance potentials from this compound is equal to the difference in the ionization potentials of the respective radicals, because both of these differences are equal to the ΔH of the reaction:



Having obtained an independent value for the ionization potential of CF (Table IV) one may proceed to calculate the ionization potential of CH_2F . The value (9.4₅ v) thus obtained is in good agreement with the direct measurement on this radical (9.3₅ v), according to Lossing and coworkers¹⁸.

Attempts were made to calculate the ionization potentials of CHF and CF_2 from their appearance potentials in $CHF CF_2$ and C_2F_4 , respectively. In order to do this, the heat of formation of CF_2 had to be known. There

are several conflicting values for this in the literature. The value in Table IV of $\Delta H_f(\text{CF}_2) = -1.60$ is calculated from measurements on the appearance potential of C_2F_4^+ from C_3F_8 and is in good agreement with the value of Margrave and coworkers¹⁸. Even so it is an upper limit due to possible rearrangement energy. But the appearance potential of CH_2^+ in C_2H_4 is ~ 2.6 volts higher than the calculated value, if CH_2^+ is formed with CH_2 . The CH_2^+ appearance potential in CH_2CF_2 is ~ 1.6 volts higher than the calculated value, if CH_2^+ is formed with CF_2 . Yet both of these appearance potentials are several volts lower than the values calculated, if CH_2^+ is a secondary (in one case via C_2H_3^+ and in the other via $\text{C}_2\text{H}_2\text{F}^+$). It thus seems that excess energy is involved in the breakage of the ethylene bond and the CHF^+ and CF_2^+ appearance potentials cannot be used to calculate their ionization potentials.

References:

1. J. R. Majer, "Mass Spectrometry of Fluorine Compounds" in *Advances in Fluorine Chemistry*, M. Stacey, J. C. Tatlow and A. G. Sharpe, Editors, Vol. 2, pp. 55-103.
2. C. A. Neugebauer and J. L. Margrave, *J. Phys. Chem.*, **60**, 1318 (1956).
3. P. G. Maslov and Yo P. Maslov, *Khim. i. Tekhnol. Topliva i. Gaz*, No. 10, 50-5 (1958); *CA* **53**, p. 1910.
4. A. B. King and F. A. Long, *J. Chem. Phys.*, **29**, 374 (1958).
5. F. L. Mohler, V. H. Dibeler and R. M. Reese, *J. Res. Natl. Bur. Stand.* **49**, 343 (1952).
6. F. H. Field and J. L. Franklin, "Electron Impact Phenomena" pp. 248-253.
7. Price and Tutte, *Proc. Roy. Soc.* **A174** 207 (1940).
8. R. Bralsford, P. V. Harris and W. C. Price, *Proc. Roy. Soc.* **A258** 459 (1960).
9. Matsunaga and Watanabe, private communication.
10. J. L. Margrave, *J. Chem. Phys.*, **31**, 143 (1959).
11. R. M. Reese, V. H. Dibeler and F. L. Mohler, *J. Res. Natl. Bur. Stand.* **57**, 367 (1956).
12. H. C. Duus, *Ind. Eng. Chem.* **47**, 1445 (1955).
13. E. B. Andrews and R. F. Barrow, *Nature* **165**, 890 (1950), *Proc. Roy. Society (London)* **64A**, 681 (1951).
14. B. S. Rabinovitch and J. F. Reed, *J. Chem. Phys.*, **22**, 2092 (1954).
15. J. W. C. Johns and R. F. Barrow, *Proc. Roy. Soc.* **A71**, 476 (1958).
16. F. P. Lossing, P. Kebarle and J. B. Desousa, "Advances in Mass Spectrometry", Ed. J. D. Waldron, Pergamon Press, p. 439 (1959).
17. V. H. Dibeler, R. M. Reese and F. L. Mohler, *J. Res. Natl. Bur. Stand.* **57**, 367 (1956).
18. L. Brewer, J. L. Margrave, R. F. Porter and K. Wieland, *J. Phys. Chem.* **65**, 1913 (1961).

MASS SPECTRA OF TERPENE AND SESQUITERPENE HYDROCARBONS

C. B. Koons and J. N. Mercer
Jersey Production Research Company
Tulsa, Oklahoma

A study of the mass spectral - chemical structure correlations of fifteen terpene and sesquiterpene hydrocarbons will be presented. The presence of carbon-carbon double bonds in all of these hydrocarbons makes correlation difficult because of the abundance of rearrangement peaks. However, the fragmentations of these hydrocarbons on electron impact do seem to present certain patterns which may be useful to the analyst involved in either qualitative or quantitative analysis of these hydrocarbons. Some excellent mass spectral data and interpretations have been reported by Friedman and Wolf (1958) and Gilchrist and Reid (1960). This report will be concerned with five of the same hydrocarbons investigated by these workers as well as six terpenes and four sesquiterpenes not reported.

The mass spectra for these hydrocarbons were obtained on a Consolidated 21-103C mass spectrometer and recorded with the CEC Mascot peak digitizer. The mass spectra were taken with 70 volt ionizing electrons. Exhaust pumping was accomplished with a Varian 40/liter/sec. ion pump. Liquid and solid samples were introduced into the mass spectrometer through the Microtek Dry Orifice Inlet System, which was described in some detail by McAdams and Harris at the last ASTM 8-14 Meeting in Chicago. A double-ended-glass pipet was used for the liquid samples and a glass sample cup dipper for solids such as camphene. Standard deviation of sample size on multiple runs with the double-ended pipet was 2% and the solids dipper 3%. This heated inlet system is so constructed that the vaporized sample comes in contact only with glass. Metal surfaces, which are known to catalyze double bond migrations in hydrocarbons, are avoided. In order to determine if any appreciable double bond migrations and subsequent rearrangements were occurring in the heated inlet system at 150° C., spectra were obtained on several of the same terpenes investigated by Friedman and Wolf (1958). In their system, the samples were sealed directly to a tube going into the ionization chamber and were run from the vapor pressure of the sample at dry ice temperature. Spectra on four hydrocarbons were compared: camphene, dipentene, α -pinene, and β -pinene. Figure 1 shows comparisons of the more prominent spectral peaks for camphene, and Figure 2 the same for α -pinene. Dipentene and β -pinene gave similar results. It appears that similar spectra are obtained by the two methods, and that double bond migration is negligible in the heated inlet system. The inlet system was maintained at 150° C. for obtaining the mass spectra of the eleven terpene and four sesquiterpene hydrocarbons.

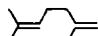
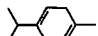
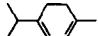
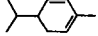
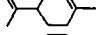
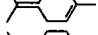
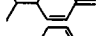




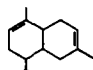
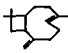


The investigated terpene and sesquiterpene hydrocarbons are listed in Table I. These hydrocarbons were obtained from commercial sources: Hercules Powder Co., Dodge and Oleott, Heyden Newport Chemical Corporation, and Fritzsche Bros. Included in the samples (Table I) is an acyclic terpene, six monocyclic terpenes of which three contain exocyclic double bonds and three do not, four bicyclic terpenes of which two contain an exocyclic double bond and two do not, and four sesquiterpene hydrocarbons of which two are bicyclic and two tricyclic.

Total ionization was obtained by the summation of peak heights from m/e 27 to m/e parent +2. The total ionization for the eleven $C_{10}H_{16}$ isomers was very similar, averaging 1.58 ± 0.08 relative to the total ionization of normal butane. The relative total ionization for the four sesquiterpenes was 1.92 ± 0.09 . The range is again quite small. These results seem to agree well with the work done by Mohler and coworkers where they found that the total ionization for C_{11} - C_{10} hydrocarbons to be essentially constant for isomers but proportional to molecular weight. Field and Franklin have later proposed that the lack of the dependence of the total ionization upon the structure of the individual isomers is evidence in favor of the molecular-ion intermediate theory. If the decomposition of the molecule occurred immediately upon ionization, larger variations in the amount of ionization occurring with the different isomers might be expected.

In the following discussion, the monoisotopic peak heights for the various hydrocarbon spectra are expressed in per cent of total ionization. Let us first look at the most prominent peaks for the acyclic and monocyclic terpenes listed in Table I. The base peaks are enclosed in rectangles. It is apparent that there is considerable variation of spectra with structure. The monocyclic terpenes because of the stability associated with the ring have much more intense parent peaks than does the acyclic terpene. It should also be noted that the parent peaks are more intense for the monocyclic terpenes with both double bonds in the ring than those with one double bond exocyclic. The myrcene spectrum shows many more C_2 , C_3 , and C_4 fragments, such as m/e 41, indicating more severe fragmentation in the absence of the ring. The two monocyclic terpenes with the larger minus - 15 peaks are α - and γ -terpinene which have two methyl groups allylic to a double bond in the ring. The minus - 43 peaks are quite large in all terpene

TABLE I

PROMINENT SPECTRAL PEAKS OF TERPENE AND SESQUITERPENE HYDROCARBONS

<u>Terpenes</u>							
<u>Name</u>	<u>Structure</u>	<u>Classification</u>	<u>Per Cent of Total Ionization</u>				
			<u>m/e</u>	<u>136</u>	<u>121</u>	<u>93</u>	<u>68</u>
Myrcene		Acyclic	1.1	1.3	15.5	2.7	<u>19.4</u>
γ -Terpinene		Monocyclic	6.9	6.4	<u>18.9</u>	0.2	4.3
α -Terpinene		Monocyclic	4.7	<u>10.6</u>	9.0	0.9	4.2
α -Phellandrene		Monocyclic	4.4	2.7	<u>19.8</u>	0.6	4.7
Dipentene		Monocyclic	2.5	2.6	7.5	<u>16.0</u>	5.2
Terpinolene		Monocyclic	3.1	5.3	<u>14.6</u>	2.6	5.5
β -Phellandrene		Monocyclic	3.7	1.8	<u>19.3</u>	7.2	4.9
α -Pinene		Bicyclic	2.4	4.8	<u>26.7</u>	1.5	6.9
3-Carene		Bicyclic	3.3	3.8	<u>16.9</u>	0.6	5.4
β -Pinene		Bicyclic	1.9	2.4	<u>19.4</u>	0.8	10.3
Camphene		Bicyclic	3.1	11.8	<u>19.0</u>	4.0	10.0
Sesquiterpenes							
<u>Name</u>	<u>Structure</u>	<u>Classification</u>	<u>Per Cent of Total Ionization</u>				
			<u>m/e</u>	<u>204</u>	<u>161</u>	<u>119</u>	<u>93</u>
Cadinene		Bicyclic	6.0	<u>8.8</u>	2.8	1.8	4.9
β -Caryophyllene		Bicyclic	0.6	1.6	1.8	6.1	<u>8.9</u>
α -Cedrene		Tricyclic	2.8	3.0	<u>13.2</u>	6.9	6.7
Longifolene		Tricyclic	1.8	3.8	2.4	<u>4.2</u>	3.9

spectra including those shown here. It is the base peak in four and the second largest in the other three. Friedman and Wolf have proposed a cyclic C_7H_9 ion intermediate for camphene fragmentation, which also could be formed from the terpenes shown here. The large 93 peak for myrcene may indicate ring closure after loss of a 3 carbon group. The two largest 93 peaks are formed from α - and β -phellandrene which contain the isopropyl group allylic to the double bond. Dipentene shows the smallest 93 peak, probably because of the preferred allylic bond rupture to form the prominent m/e 63 fragment. This hydrocarbon is the only one by which two allylic bond ruptures can occur simultaneously to produce C_5H_8 fragments.

Also shown in Table I is similar data for the bicyclic terpenes. The parent peak intensities are similar to those for the monocyclic terpenes with one double bond exocyclic. Ring strain no doubt accounts for the reduced parent peak intensities. Camphene shows the largest minus - 15 peak, probably due to allylic bond rupture. The other three bicyclic terpenes do not contain methyl groups allylic to a double bond. The minus - 43 peak is the base peak in the spectra of these four hydrocarbons. For the first three, the fragmentation likely involves the loss of the bridge structure C_3H_6 plus an additional hydrogen. For camphene, the rupture probably occurs at the bonds of the quaternary carbon. The largest minus - 43 peaks occur in the spectra of α - and β -pinene in which double bonds are allylic to the bridge structure. The hydrocarbons containing the double bond exocyclic show larger amounts of C_2 , C_3 , and C_4 fragments, such as m/e 41. Apparently the presence of double bonds in the ring increases the stability of the ring and prevents extensive fragmentation.

The spectra for the sesquiterpene hydrocarbons because of their more complicated structure show more complex fragmentation patterns. The prominent peaks for these hydrocarbons are also shown in Table I. Cadinene shows the largest parent ion, m/e 204, probably due to the comparative stability of the fused six carbon rings and the presence of both double bonds in the rings. α -cedrene contains the next largest parent ion, probably because of the absence of exocyclic double bonds. The other two possess more ring strain and exocyclic double bonds and the molecular ion is quite small. None of these hydrocarbons show very large minus - 15 peaks, and these are not listed in Table I. Longifolene shows the largest minus - 15 peak relative to the parent, probably because of the presence of the double bond allylic to the angular methyl group. Cadinene's base peak occurs at m/e 161, the loss of 43 mass units or the isopropyl group from the ring. The other three do not have large minus - 43 peaks or isopropyl groups attached to a ring. The base peak for α -cedrene occurs at m/e 119, a C_9H_{11} fragment. The fragmentation to form this ion no doubt involves several bond ruptures, either simultaneously or consecutively. One plausible simultaneous rupture could occur in the two cyclopentane rings adjacent to the two quaternary carbons. The base peak for longifolene occurs at m/e 93, a $C_7H_9^+$ fragment which was so prominent in the spectra of the terpene hydrocarbons. This same peak is also large for β -caryophyllene and α -cedrene, and may indicate that the sesquiterpene molecular ion, like the terpene counterpart, fragments to form a stable C_7H_9 cyclic intermediate ion of the form proposed by Wolf and Friedman. The base peak for β -caryophyllene occurs at m/e 41 along with a high concentration of C_2 , C_3 , and C_4 fragments. The instability of the fused four and nine carbon rings may account for the extensive fragmentation of this molecular ion.

From the data on these terpene and sesquiterpene hydrocarbons, it appears that the three structural characteristics which most greatly affect the mass spectral patterns of these hydrocarbons are (1) position of double bonds, either cyclic or exocyclic, (2) position of possible fragmentation allylic to a double bond, and (3) presence or absence of ring strains. Because of the evident differences in the spectra of these hydrocarbons, it is believed that effective qualitative or quantitative analysis by mass spectrometry is possible with these naturally-occurring hydrocarbons.

References

1. L. Friedman and A. P. Wolf, J. Am. Chem. Soc. **80**, 2424 (1958).
2. T. Gilchrist and R. I. Reed, *Experimentia* **16**, 134 (1960).
3. D. R. McAdams and R. J. Harris, A.S.T.M. E-14 Committee on Mass Spectrometry, June 1961.

PROMINENT PEAKS OF CAMPHENE

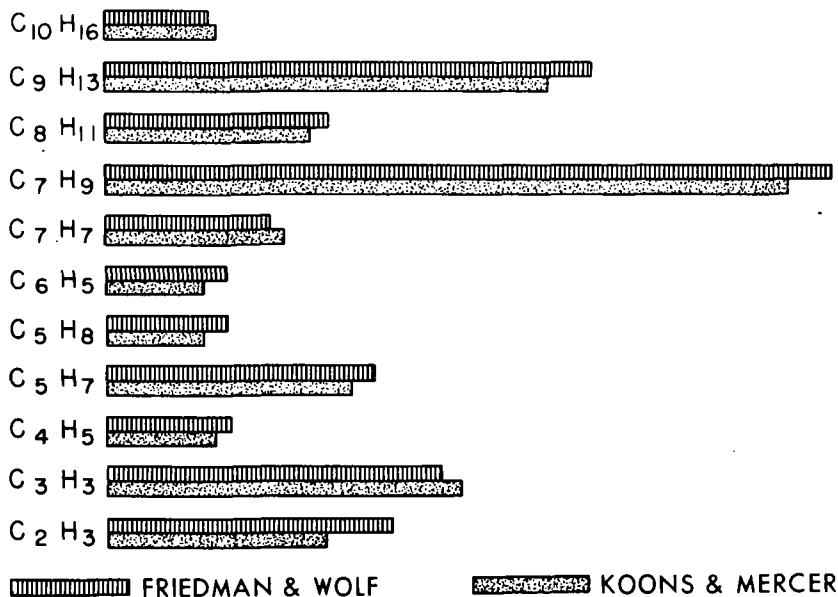


FIG. 1

PROMINENT PEAKS OF α -PINENE

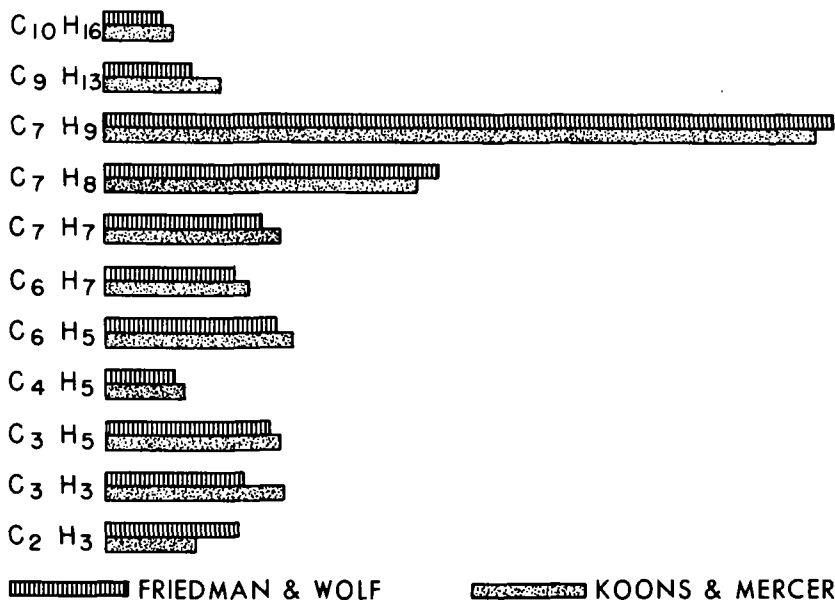


FIG. 2

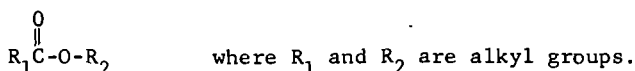
REARRANGEMENT IONS OF ALIPHATIC ESTERS AS OBSERVED IN THE MASS SPECTROMETER

H. O. Colomb, Jr., B. D. Fulks and V. A. Yarborough

The mass spectra of aliphatic esters have previously been correlated with their structure by Sharkey, Shultz and Friedel. The high resolution mass spectra of many of these esters as obtained by Beynon, Saunders and Williams have largely confirmed postulations concerning the fragmentation processes.

The determination of structure by mass spectrometry is made more difficult by molecular rearrangement. In the esters presented here, the major rearrangements are specific and may even aid in structure determination.

The first slide lists the most important rearrangement ions in the mass spectra of the formic acid esters and their abundance relative to the most intense peak in the spectrum which is called the base peak. The general formula for these esters may be written:



The R_1 group corresponds to the acid portion of the ester and the R_2 group to the alcohol portion.

The most important rearrangement peaks in the formic acid esters are the ions at m/e 31, 45 and the $[\text{R}_2\text{-H}]^+$ or olefin ion. The base peak is the same in these esters as it is in the corresponding alcohol for all except n -butyl, 3° -butyl, isoamyl and cyclohexyl, and in general the mass spectra resemble those of the alcohols, R_2OH . The peak at m/e 45 is the base peak in the formates of 2° alcohols as it is in the alcohol. Of all the esters, the olefin ion is largest in the formic acid esters where R_2 is butyl or less (except 2° -butyl).

The acetic acid esters are shown in Slide 2. Here the major rearrangement ions have the same type of structure as they do in all the esters studied above the formates. The base peak for all the acetates is the m/e 43, $([\text{CH}_3\text{CO}]^+)$ ion. The relative intensity of the olefin ion, $([\text{R}_2\text{-H}]^+)$, shows the same relationship as in the higher esters, that is, cyclohexyl gives the maximum olefin ion intensity and neopentyl gives the least. Also the n - and iso-alcohol esters give more olefin ion intensity than do the 2° -alcohol esters.

The $[\text{R}_1\text{COO} + 2\text{H}]^+$ or acid plus 2 hydrogen atoms peak at m/e 61 is not as intense in the acetates as it is in the other acid esters. The general trend, however, is evident in that n -alcohol esters give rise to more rearrangement than branched or 2° -alcohol esters. The $[\text{R}_1\text{COO} + 2\text{H}]^+$ peak is least for the ester from the most highly branched alcohol, neopentyl and 3° -butyl, as is the case in all the acid esters above the acetates.

SLIDE 1
REARRANGEMENT ION INTENSITY IN FORMIC ACID ESTERS

	Base Peak	$R_2\text{-H, \%}$	$M/e\ 31$	$M/e\ 45$
Ethyl ¹	31	71.3	100	32.6
Propyl	31	65.0	100	3.0
Isopropyl	45	30.0	6.0	100
n-Butyl	56	100	57.8	7.4
2°-Butyl	45	26.9	18.0	100
Isobutyl	43	80.6	64.5	2.6
3°-Butyl	41	39.2	18.1	8.4
n-Amyl	42	58.3	50.9	5.2
2°-Amyl	45	27.3	9.1	100
Isoamyl	55	74.0	42.7	10.0
Neopentyl	57	2.3	14.5	7.2
Cyclohexyl	67	17.1	10.0	3.5

¹Sharkey, A. G. Jr., et al., Anal. Chem. 31 87 (1959)

SLIDE 2
REARRANGEMENT ION INTENSITY IN ACETIC ACID ESTERS

	Base Peak	$R_2\text{-H, \%}$	$M/e\ 61\ [R_1\text{COO} + 2H]^+$
Ethyl ¹	43	5.0	10.5
Propyl ¹	43	10.6	20.4
Isopropyl ¹	43	7.6	14.2
n-Butyl	43	34.6	10.7
2°-Butyl ²	43	19.7	4.5
Isobutyl	43	22.9	2.5
3°-Butyl	43	35.4	1.6
n-Amyl ²	43	46.3	23.4
2°-Amyl	43	12.9	2.5
Isoamyl ²	43	39.7	12.3
Neopentyl	43	2.7	1.0
Cyclohexyl	43	55.0	5.6

¹Sharkey, A. G. Jr., et al., Anal. Chem. 31 87 (1959)

²Beynon, et al., Ibid. 33 221 (1961)

Slide 3 shows the relative abundance of the two types of rearrangement ions for propionic acid esters. The n-alcohol esters in this series give the largest $[R_1COO + 2H]^+$ ion intensity, and the esters from neopentyl and 3°-butyl alcohols give the least.

Slide 4 shows the relative abundance of the rearrangement ions in the butyric acid esters. Both the olefin ion and the $[R_1COO + 2H]^+$ ion are more intense than in the corresponding acetates and propionates. Also, in general the more stable the R_2^+ ion is the less will be the $[R_1COO + 2H]^+$ ion intensity. The base peak is usually the R_1CO^+ ion but depends more on the nature of the R_2 group than it does in the other esters except the valerates.

Slide 5 shows the relative abundance of the rearrangement ions in the isobutyric acid esters. Here the effect of chain branching in R_1 is evident and in most cases causes a decrease in the olefin ion and $[R_1COO + 2H]^+$ ion intensities from those in the unbranched acid esters. The isoamyl ester gives about as intense an olefin ion as does the cyclohexyl ester.

Slide 6 shows the rearrangement ion intensities for the valeric acid esters. The $[R_1COO + 2H]^+$ ion is maximum in intensity for all the esters except the ethyl and isobutyl compounds. The olefin ion is also at maximum intensity for R_2 n-amyl and higher. The intensity of the $[R_1CO]^+$ ion is more dependent on R_2 than any of the other acid esters studied.

Slide 7 gives the rearrangement ion intensities for the pivalic acid esters which are esters of acetic acid with all the hydrogens of the alkyl part of the acid group replaced by methyl groups. Because of the large amount of chain branching in R_1 the base peak is the m/e 57 which is probably the $C_4H_9^+$ ion. This peak is so intense as to be off scale in some of these ester spectra when run at normal pressure. The olefin ion is lowest in intensity and the $[R_1COO + 2H]^+$ ion intensity is much decreased over the corresponding valerate ester.

The effect of chain branching in R_1 , the alkyl portion of the acid group, is more clearly shown in Slide 8 which lists the rearrangement ion intensity for the cyclohexyl esters. The $[R_1COO + 2H]^+$ ion intensity increases as R_1 increases and decreases with increased chain branching.

The mechanism McLafferty proposed to explain the formation of the $[R_1COO + 2H]^+$ ion is shown in Slide 9. This concept involves a six membered ring-type intermediate with the shift of a hydrogen beta to the carbonyl carbon and one which is gamma. This gives an alkene radical and a positive ion which is stabilized by resonance. This mechanism requires both beta and gamma hydrogens in the alcohol portion of the ester; indeed, where there are no hydrogens beta to the carbonyl carbon as in the 3°-butyl esters, there is very little rearrangement; and, in the neopentyl esters where the gamma hydrogens are all replaced by methyl groups, there is even less rearrangement. In these later cases, it would seem more reasonable to expect a methyl shift, and Slide 10 shows the

SLIDE 3
REARRANGEMENT ION INTENSITY IN PROPIONIC ACID ESTERS

	Base Peak	$R_2\text{-H, \%}$	$M/e\ 75\ [R_1\text{COO} + 2H]^+$
Ethyl ¹	29	17.8	8.2
Propyl	57	10.9	34.7
Isopropyl	57	9.2	22.7
n-Butyl	57	32.4	23.7
2°-Butyl	57	14.3	7.2
Isobutyl	57	26.1	6.0
3°-Butyl	57	10.7	2.9
n-Amyl	57	37.2	34.3
2°-Amyl	57	16.6	6.9
Isoamyl	57	49.1	10.3
Neopentyl	57	4.0	0.9
Cyclohexyl	57	58.0	21.4

¹Sharkey, A. G. Jr., et al., Anal. Chem. 31 87 (1959)

SLIDE 4
REARRANGEMENT ION INTENSITY IN BUTYRIC ACID ESTERS

	Base Peak	$R_2\text{-H, \%}$	$M/e\ 89\ [R_1\text{COO} + 2H]^+$
Ethyl	71	7.0	13.0
Propyl	71	29.8	54.6
Isopropyl	43	13.9	18.9
n-Butyl	71	54.7	52.0
2°-Butyl	71	25.9	18.7
Isobutyl	71	42.3	14.8
3°-Butyl	43	35.8	7.8
n-Amyl	43	48.3	48.1
2°-Amyl	71	20.9	11.2
Isoamyl	71	72.2	12.2
Neopentyl	71	10.2	1.2
Cyclohexyl	71	83.2	60.2

intensity of the $[R_1COO + CH_4]^+$ ion in the neopentyl esters. This ion and the olefin ion are the most important rearrangement ions in these spectra.

This same mechanism, shown in Slide 11, has been applied to the rearrangement ion, $[CH_2COOR_2 + H]^+$, found in some methyl and ethyl esters. This rearrangement requires a hydrogen gamma to the carbonyl carbon and the only acids in this series that meet this requirement are butyric and valeric acids. In Slide 12, this is shown to be the case, only butyric and valeric esters having this peak in appreciable abundance.

To test the validity of the mechanism even further, cyclohexyl butyrate and valerate were synthesized with the alpha positions of the cyclohexyl group deuterated. The rearrangement peak, $[R_1COO + 2H]^+$, was found to be shifted, and the ratio of the intensities corresponding to the addition of two hydrogens, hydrogen-deuterium and two deuteriums was 1:2:1. This corresponds to an equal choice of hydrogen and deuterium for the rearrangement. This result seemed puzzling as all the hydrogens gamma to the carbonyl carbon had been replaced by deuterium. However, investigation of the molecular models (Figures 1 and 2) shows that when the cyclohexyl group is in the boat form all the hydrogens on the same side as the carbonyl group are accessible to the carbonyl oxygen by a cyclic mechanism like that previously outlined. The three hydrogens on the side of the cyclohexyl group opposite to the ester carbonyl group are not accessible to the carbonyl oxygen without bond breaking. Thus, in the rearrangement process, there is an equal choice among four hydrogen and four deuterium atoms for the two atoms shifted. The deuterated esters were checked by NMR and found to be essentially completely deuterated in the alpha positions of the cyclohexyl group and nowhere else. In conclusion, the experimental evidence is consistent with the cyclic mechanism and involves the concerted shift of a hydrogen beta to the carbonyl carbon and one further down the chain, the gamma one being favored, to form the $[R_1COO + 2H]^+$ rearrangement ion.

SLIDE 5

REARRANGEMENT ION INTENSITY IN ISOBUTYRIC ACID ESTERS

	<u>Base Peak</u>	<u>R₂-H, %</u>	<u>M/e 89 [R₁COO + 2H]⁺</u>
Ethyl	43	8.5	2.8
Propyl	43	12.7	30.9
Isopropyl	43	8.3	8.7
n-Butyl	43	40.0	52.8
2°-Butyl	43	25.3	20.0
Isobutyl	43	45.2	22.3
3°-Butyl	43	6.9	2.2
n-Amyl	43	27.5	35.9
2°-Amyl	43	14.1	9.4
Isoamyl	43	51.3	8.8
Neopentyl	43	13.0	1.2
Cyclohexyl	43	52.3	54.0

SLIDE 6

REARRANGEMENT ION INTENSITY IN VALERIC ACID ESTERS

	<u>Base Peak</u>	<u>R₂-H, %</u>	<u>M/e 103 [R₁COO + 2H]⁺</u>
Ethyl	29	22.8	5.3
Propyl	85	30.9	62.2
Isopropyl	43	16.1	25.3
n-Butyl	29,85	93.8	67.5
2°-Butyl	85	42.1	26.0
Isobutyl	85	62.4	19.7
3°-Butyl	60	20.3	7.9
n-Amyl	85	90.2	73.9
2°-Amyl	85	35.6	18.9
Isoamyl	70	100	12.8
Neopentyl	82	15.3	1.6
Cyclohexyl	85	100	84.8

SLIDE 7

REARRANGEMENT ION INTENSITY IN PIVALIC ACID ESTERS

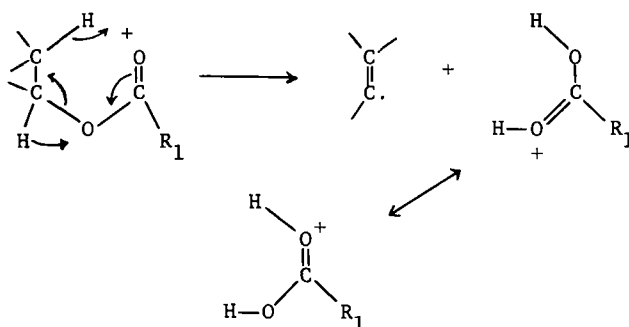
	<u>Base Peak</u>	<u>R₂-H, %</u>	<u>M/e 103 [R₁COO + 2H]⁺</u>
Ethyl	57	4.3	.2
Propyl	57	6.6	20.3
Isopropyl	57	5.8	4.8
n-Butyl	57	18.0	22.2
2°-Butyl	57	6.9	5.2
Isobutyl	57	21.2	14.4
3°-Butyl	57	3.8	.1
n-Amyl	57	15.5	28.2
2°-Amyl	57	6.2	6.8
Isoamyl	57	34.8	7.3
Neopentyl	57	8.8	.8
Cyclohexyl	57	15.6	25.1

SLIDE 8

REARRANGEMENT ION INTENSITY IN
CYCLOHEXYL ESTERS

<u>R₂-H</u> <u>Mass 82</u>	<u>Ester</u>	<u>[R₁COO + 2H]⁺</u>	<u>Mass</u>
17.2	Formate	.36	47
52.6	Acetate	5.7	61
58.0	Propionate	21.4	75
82.5	Butyrate	60.1	89
52.2	Isobutyrate	54.0	89
100	Valerate	84.8	103
15.6	Pivalate	25.2	103

SLIDE 9

REARRANGEMENT MECHANISM OF THE $[R_1COO + 2H]^+$ ION¹¹McLafferty, F. W., Anal. Chem. 31 85 (1959)

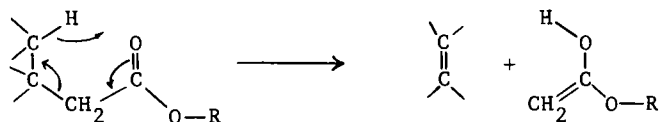
SLIDE 10

RELATIVE INTENSITY OF THE $[R_1COO + CH_4]^+$ REARRANGEMENT
ION IN THE NEOPENTYL ESTERS

Acid	Intensity, %
Formic	0.3
Acetic	16.2
Propionic	13.8
Butyric	14.9
Isobutyric	20.4
Valeric	15.2
Pivalic	5.2

SLIDE 11

REARRANGEMENT MECHANISM IN METHYL AND ETHYL ESTERS¹



R = -CH₃, -C₂H₅

¹McLafferty, F. W., Anal. Chem. 31, 82 (1959)

SLIDE 12

RELATIVE INTENSITY OF THE [CH₂COOR₂ + H]⁺

REARRANGEMENT ION

Acid	R ₂ Group	
	Methyl	Ethyl
Acetic	16.0* ⁺	3.9* ⁺
Propionic	0.2* ⁺	0.1*
Butyric	63.2	41.9*
Isobutyric	2.8	6.3
Valeric	100	50.2
Pivalic	0.6	0.5

*From Sharkey, et al., Anal. Chem. 31
88-9 (1959)

⁺Parent peak, not a rearrangement peak

Figure 2

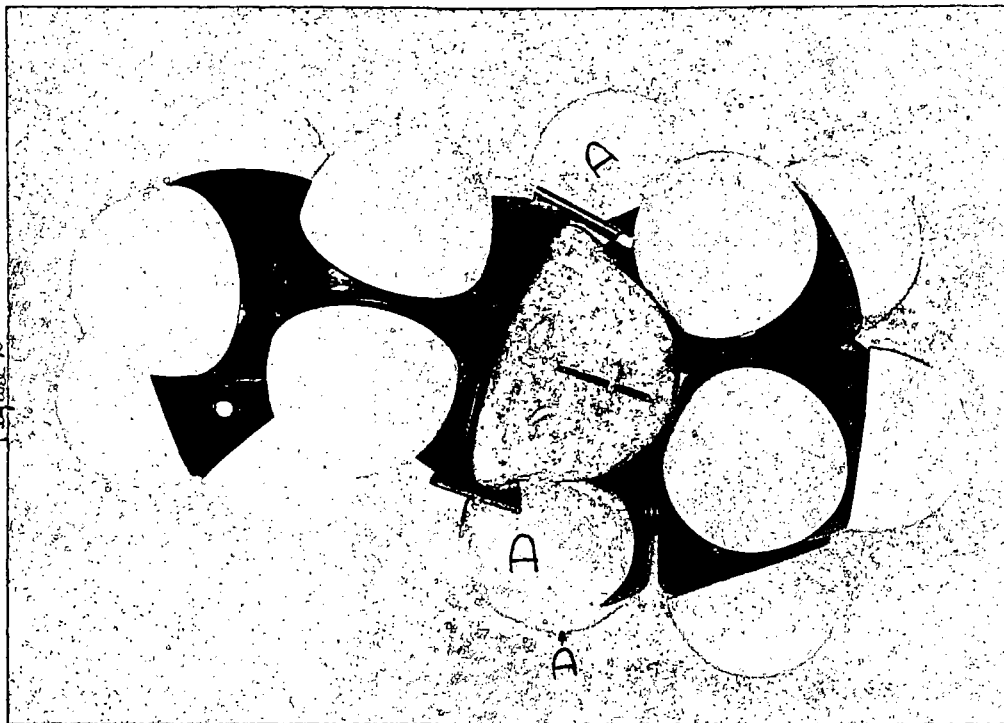
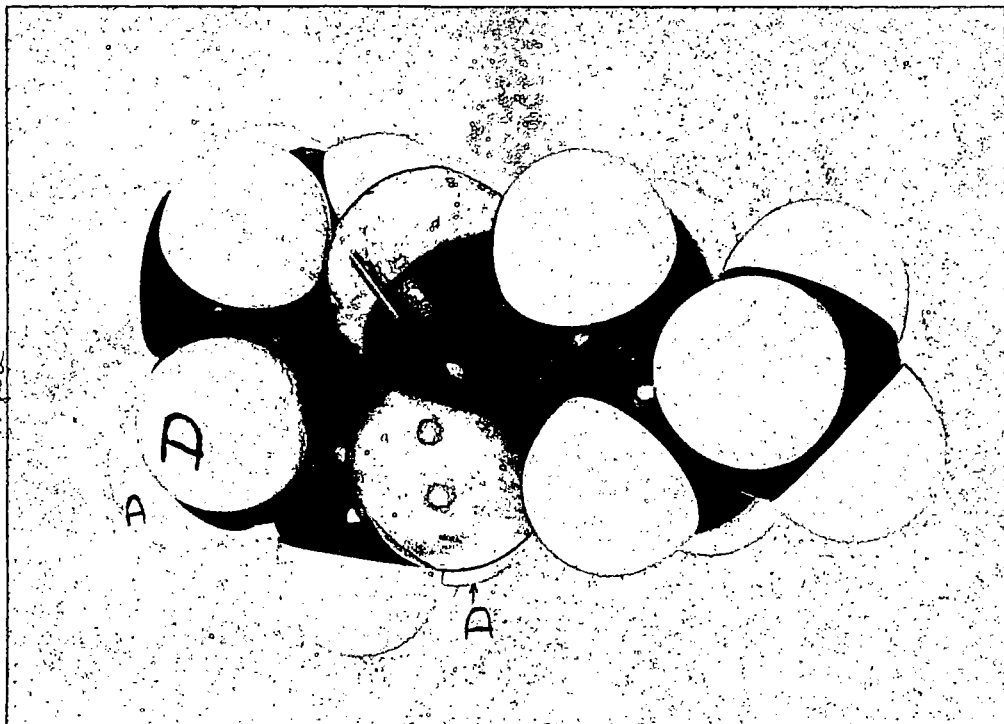


Figure 1



MASS SPECTRA OF TRIMETHYLSILYL ESTERS

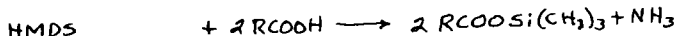
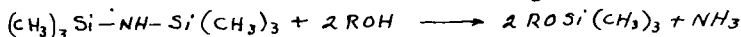
R. M. Teeter

California Research Corporation, Richmond, California

Hexamethyldisilazane (HMDS) was introduced as a reagent for the preparation of volatile derivatives for mass spectrometry in 1957 by Langer, Connell, and Wender (1) and by Sharkey, Friedel, and Langer. (2) The group from the Bureau of Mines has continued to use HMDS profitably for the preparation of ethers. (3,4)

Independently, Becke-Goehring and Wunsch (5) and Birkofer and Ritter (6) have treated acids with HMDS to form trimethylsilyl esters, but no mass spectra were reported. Ruhlmann and Giesecke (7) have used the esters, prepared by a different technique, to aid the gas chromatographic analysis of amino acids.

The reactions to be discussed are given below:



The principal advantage of trimethylsilyl (TMS) esters over other acid derivatives is the simplicity of preparation. In a typical preparation one places 2 or 3 mg of an acid or acid mixture in a small flask, adds a crystal of NH_4Cl and 8 or 10 drops of HMDS. The mixture is heated under reflux for 2 or 3 hours, and a 1- μ l sample is removed for mass spectral analysis. Usually, no isolation step is required since the molecular weights of most of the esters are higher than that of the HMDS. The flask is a special one consisting of a 10 mm diameter reflux condenser sealed off into a test tube end 1-2 cm below the water jacket. A standard taper joint at the top accepts a drying tube to protect from atmospheric moisture. Protection from moisture is important since hydrolysis occurs very readily. A drop of purified TMS benzoate exposed to air starts to deposit crystals of benzoic acid in about 10 minutes. Excess HMDS protects the esters.

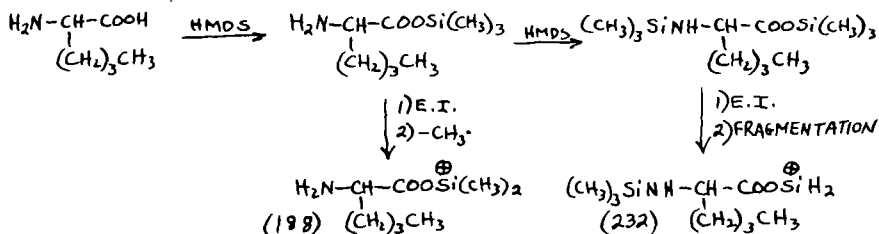
In the mass spectra of the esters, the loss of methyl is frequently the most favored process, with the resulting M-15 peak the largest in the spectrum. In the case of the benzoate ester, the m/e/179 from the loss of methyl is even larger than the very stable benzoyl ion at m/e 105. The spectrum of TMS octadecanoate shows an even larger M-15. It can be seen from this that the TMS group sometimes dominates the spectrum to the point where structural information is lost.

- (1) S. H. Langer, S. Connell, and I. Wender, J. Org. Chem. 23, 50 (1958).
- (2) A. G. Sharkey, Jr., R. A. Friedel, and S. H. Langer, Anal. Chem. 29, 770 (1957).
- (3) S. H. Langer, R. A. Friedel, I. Wender, and A. G. Sharkey, Jr., Anal. Chem. 30, 1353 (1958).
- (4) S. Friedman, M. L. Kaufman, and I. Wender, J. Org. Chem. 27, 664 (1962).
- (5) M. Becke-Goehring and G. Wunsch, Chem. Ber. 93, 326 (1960).
- (6) L. Birkofer and H. Ritter, Chem. Ber. 93, 424 (1960).
- (7) K. Ruhlmann and W. Giesecke, Angew. Chem. 73, 113 (1961).

Although the study of the effect of HMDS on other functional groups has been largely confined to hydroxy and amino substituents, it is worth noting that in the one case studied, ester interchange did not take place. The spectrum of the TMS ester from hydrogen methyl terephthalate has its largest peak at m/e 237, the M-15 fragment from methyl trimethylsilyl terephthalate. The M-15 fragment (at m/e 295) from bis(trimethylsilyl) terephthalate was present but corresponded roughly to the very small amount of free terephthalic acid in the original half-ester.

Reaction of HMDS with hydroxy and amino groups proceeds as described in the papers already cited; amino acids yield N-(trimethylsilyl) amino trimethylsilyl esters. In the spectrum of the product from norleucine, the M and M-15 peaks are present; and, in addition, peaks at m/e 188 and m/e 232 due respectively to the amino ester and silylamino ester are found. The reaction paths are shown in Figure 1.

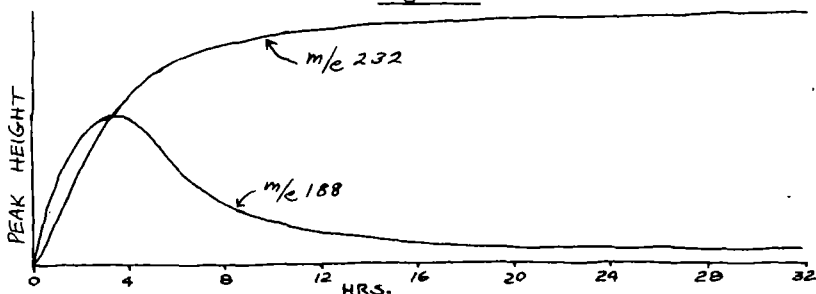
Figure 1



The structure of the m/e 232 ion will be discussed later.

In Figure 2 the heights of the 188 and 232 peaks are plotted as a function of time of reaction with HMDS.

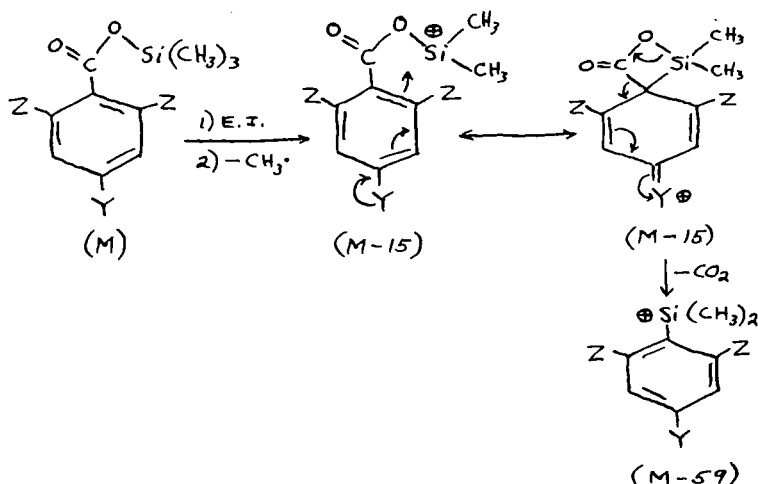
Figure 2



The m/e 188 peak shows the typical behavior of an intermediate that is consumed by a subsequent reaction. That it does not drop to zero is probably due to the presence of a small fragment of the same m/e from the final product.

Several esters undergo decarboxylation. An example is the fragmentation of the product from *p*-hydroxybenzoic acid. The M-15 fragment is at m/e 267. This ion loses CO_2 to form an ion at m/e 223. That 44 is lost in one unit is shown by a large metastable peak at m/e 186.3. A mechanism is proposed in Figure 3 for a generalized aromatic acid.

Figure 3



Ortho attack by the charged silicon atom is a possibility but is probably not the major route on the basis of the evidence in Table I.

Table I

Y	Z	Ht (M-59)/Ht (M-15)	m/e Metastable
-OH	-H	0.4	186.3
-NH ₂	-H	0.3	185.4
-NO ₂	-H	0.09	(144.7)*
-CH ₃	-CH ₃	0.02	(144.7)*
-COOCH ₃	-H	0.2	157.1
-COOSi(CH ₃) ₃	-H	0.07	(213.5)

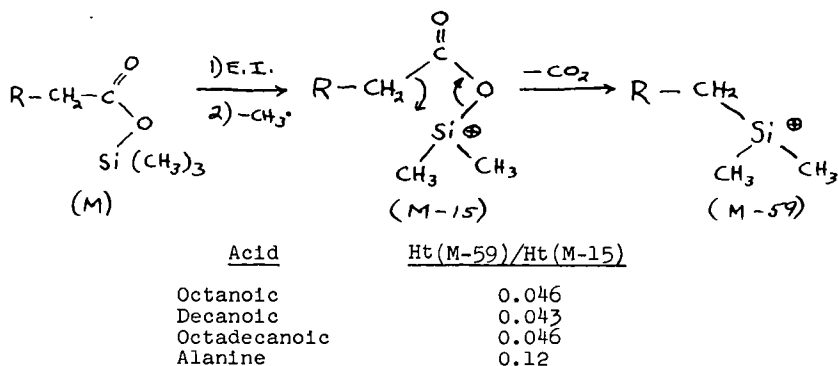
() Metastable ion not observed.

* Metastable ion lost in HMDS spectrum.

Note that in the case of the p-nitroester, where the nitro group cannot donate electrons, the extent of the reaction is decreased relative to that observed with hydroxy and amino substituents. Mesitoic acid, with both ortho positions blocked, still loses CO₂.

Further evidence in favor of attack on the carbon holding the carboxyl comes from the spectra of some aliphatic esters as shown in Figure 4.

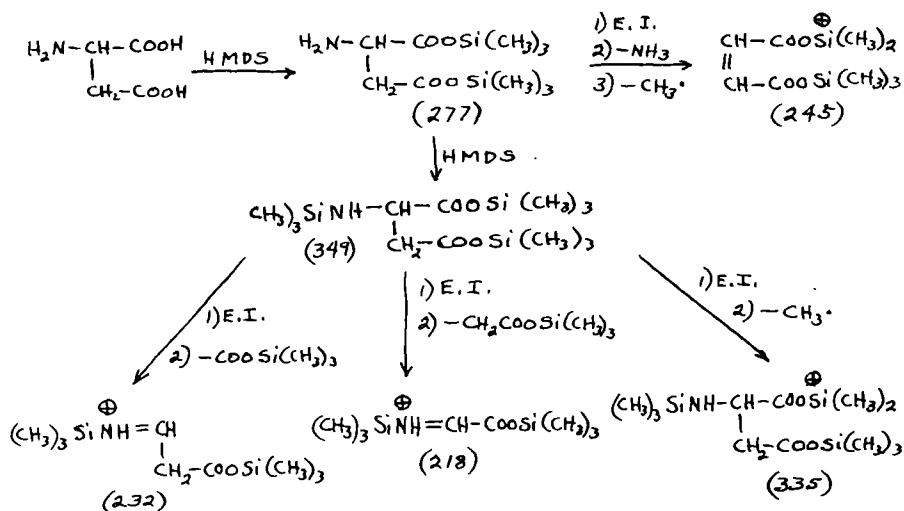
Figure 4



The first three esters show a small M-59/M-15 ratio, while in alanine this ratio is larger. This may reflect a change in mechanism with the nitrogen participating in the formation of a five-membered ring intermediate. Here we do not have the supporting evidence of metastable peaks.

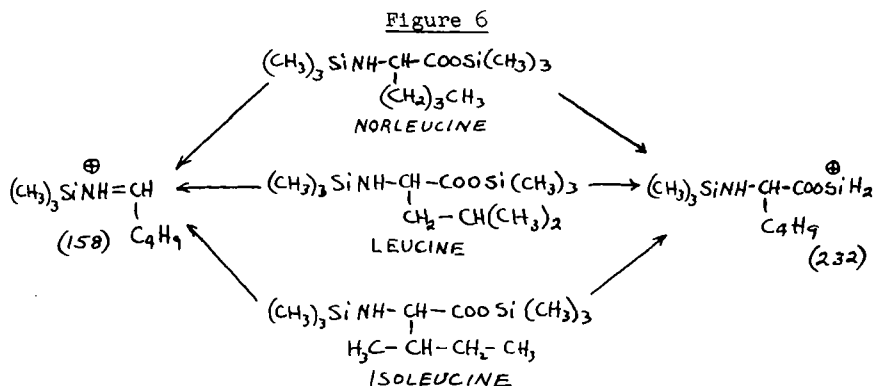
In the spectrum of the product from aspartic acid, we can see a peak which seems to be characteristic of most α -amino acids. The reactions are shown in Figure 5.

Figure 5



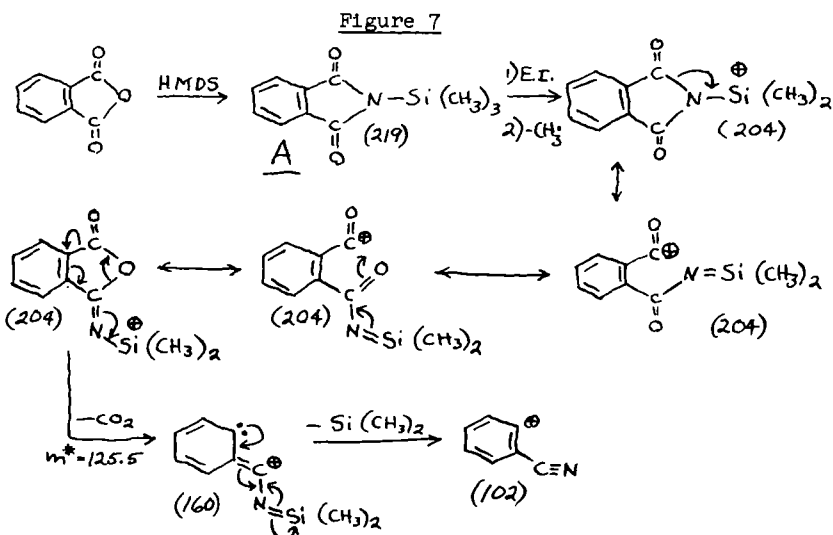
Apparently the diester is formed which then loses ammonia to give the maleate or fumarate product, characterized by its M-15 peak at m/e 245. The same ion is formed under the same conditions by dehydration of malic acid. The completely silylated material fragments to yield ions at 232 and 218, the latter is common to most amino acid esters except proline, which does not have a primary amino group.

An m/e 232 ion has already been mentioned as a fragment from the norleucine ester. In this case, and in that of leucine, mass 232 can be obtained by the loss of *n*-propyl or isopropyl, respectively, from the parent ion; but the isoleucine ester shows the same ion in the same abundance. Figure 6 shows the structures assigned on this basis.



Loss of C_3H_7 from the trimethylsilyl group, accompanied by rearrangement, seems a likely route, especially since $\text{M}-43$ ions are seen in other ester spectra where, in some cases, there is no other possible source. The reaction is probably loss of a methyl radical (to $\text{M}-15$) followed by loss of neutral ethylene. The 158 fragment ($\text{M}-117$) is also common to most amino acid ester spectra and is exactly analogous to the "amine fragment" that Biemann(8) reports in the spectra of the ethyl esters. In both types of esters, it is frequently the largest peak in the spectrum.

One reaction other than that of active hydrogen replacement was found in our survey. Reaction of HMDS with phthalic anhydride yields N-trimethylsilylphthalimide which undergoes an interesting series of reactions in the mass spectrometer. The sequence is shown in Figure 7.



(8) K. Biemann, JACS 83, 3795 (1961)

On electron impact a parent ion is formed (m/e 219) followed by loss of methyl to give the base peak at m/e 204. Migration of electrons yields the acylium ion. Rotation of the other carbonyl can then give the rearranged product containing a potential CO_2 group. Another electron shift can then lead to expulsion of CO_2 with a confirming metastable peak at 125.5. The resulting ion at m/e 160 subsequently fragments to the phenylene nitrile ion of m/e 102.

The critical point in this reaction sequence is the decarboxylation step, and it is tempting to postulate that the original reaction product might have the structure shown for the 204 ion just before decarboxylation. However, the structure of Compound A was verified by an independent synthesis from potassium phthalimide and chlorotrimethylsilane. The mass and infrared spectra of the substance prepared by the two routes were identical.

Table II is a list of the compounds which have yielded esters or other products on treatment with hexamethyldisilazane.

Table II

Phosphoric Acid	Malic Acid
Benzoic Acid	ϵ -Aminocaproic Acid
Terephthalic Acid	Caprolactam
Hydrogen Methyl Terephthalate	Alanine
Phthalic Anhydride	Serine
<i>p</i> -Hydroxybenzoic Acid	Aspartic Acid
<i>p</i> -Aminobenzoic Acid	Lysine
<i>p</i> -Nitrobenzoic Acid	Tryptophan
Mesitoic Acid	Proline
Octanoic Acid	Methionine
Decanoic Acid	Ethionine
Octadecanoic Acid	Phenylalanine
Maleic Acid	Glutamic Acid
Fumaric Acid	Leucine
Succinic Acid	Isoleucine
<i>p</i> -Toluenesulfonic Acid	Norleucine
	Heptafluorobutyric Acid

INFORMATION REGARDING THE FRAGMENTATION OF LONG CHAIN COMPOUNDS
OBTAINED FROM THE MASS SPECTRA OF HEAVY ISOTOPE-LABELLED MOLECULES

Ng. Dinh-Nguyen, Ragnar Ryhage,
Stina Stållberg-Stenhagen and Einar Stenhagen
Institute of Medical Biochemistry
University of Göteborg, and Mass Spectrometry Laboratory
Karolinska Institutet
Stockholm 60, Sweden

Abstract

A study of the mass spectra of a series of isomeric long chain methyl esters with a $-CD_2$ -group at different positions along the chain has given information about hydrogen—deuterium exchange—phenomena and the formation of ions through elimination—rearrangement and elimination—coupling reactions. Results obtained with ^{13}C and halogen-substituted esters have given further information on some of these processes.

DETERGENT ALKYLATE ANALYSIS BY MASS SPECTROMETRY

By

E. W. Boyer, M. C. Hamming, and H. T. Ford
Research and Development Department
Continental Oil Company
Ponca City, Oklahoma

ABSTRACT

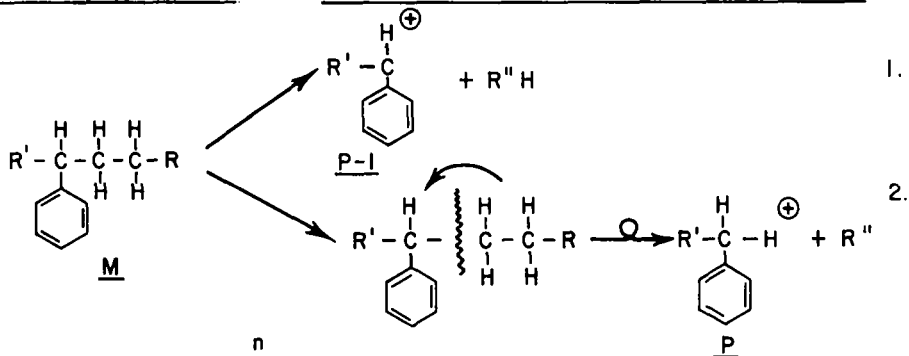
Analysis of detergent alkylate by mass spectrometry is conventionally based upon pattern coefficients obtained by examination of distillation fractions from crude alkylates. A new approach based on rearrangement phenomena and employing sensitivity data independent of volume or pressure measurements is described. The quantitative rearrangement technique reduces and simplifies computations. Calibration data presented should be directly applicable in other laboratories for molecular distribution analysis on a wide range of monoalkylbenzene systems.

INTRODUCTION

Analyses of alkylbenzenes in the detergent alkylate range are normally accomplished by the use of synthetic cracking patterns. These synthetic patterns are obtained by mass spectrometer examination of narrow fractions separated from crude alkylate by high efficiency distillation. Analytical techniques using this approach have been described by Brown et al (4). Modifications of this basic technique have been utilized in many laboratories concerned with the characterization of detergent alkylates by mass spectrometry. The basic concept in the synthetic cracking pattern method of calculation involves the use of mixed alkylbenzene isomers of essentially the same molecular weight to represent the fragmentation patterns of the mixed isomers in an alkylate to be examined. Although the technique is entirely satisfactory for determining molecular distribution of alkylate samples similar in chemical history to that from which the calibration fractions were separated, serious limitations are apparent when attempts are made to apply these patterns to alkylbenzenes of dissimilar structure. The work to be presented here describes a technique which, to a large extent, overcomes these limitations to conventional analytical methods. Analysis is based upon a sufficient consistency of the rearrangement ions (m/e 162 and above) relative to the C_nH_{2n-7} fragment ions (P-1). The rearrangement ions are equal in mass number to the molecular ions of lower homologs (P). Corrections to the polycomponent molecular ion are based on measurements of the parent minus one peak. Sensitivity data presented are based on total ionization studies of thirty-six known structure alkylbenzenes synthesized at Continental Oil Company or obtained from API Research Project 42.

PARENT MOLECULE

PSEUDO STRUCTURES OF FRAGMENT IONS



$$M_i = P_i - \sum_{j=i}^n a_{ij} x_j = P_i - k_{i-1} (P_i - 1)$$

M_i monocomponent peak, M , at m/e i

P_i polycomponent peak, P , at m/e i

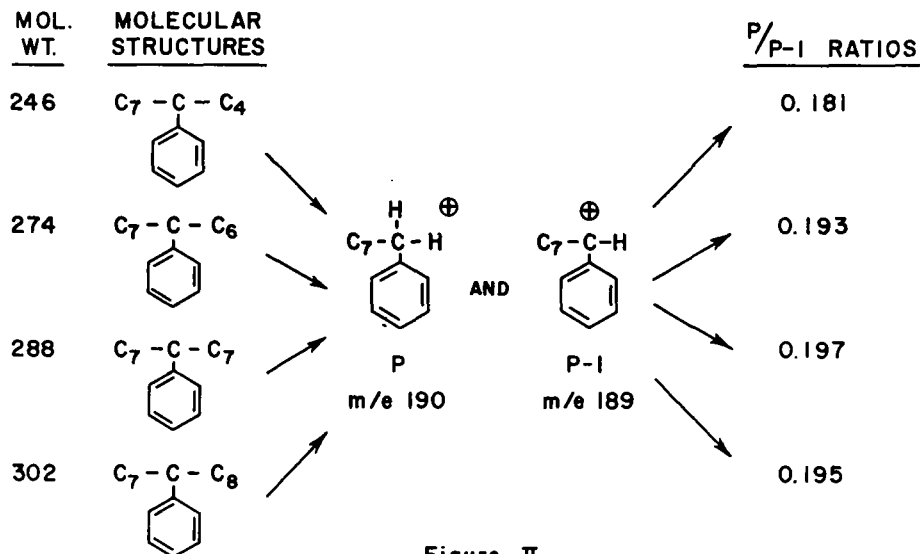
a_{ij} calibration coefficient, a , at $m/e = i$, for component j

x_j divisions of base peak, x , of component j appearing in mixture spectrum

k_{i-1} correction factor, k , at m/e $i-1$

Figure I

CONSISTENCY OF THE 190/189 RATIO AFTER β BOND CLEAVAGE



GENERAL THEORY

Alkylbenzenes cannot form, by simple bond cleavage under electron bombardment, fragment ions equal in mass to molecular ions of lower homologs. Theoretical considerations supporting the major premises of this analytical method can be simply stated. Molecular ions of alkylbenzenes in a mixture spectrum can occur by four processes: 1.) by a molecular specie actually present in the mixture, 2.) by concerted bond cleavage and rearrangement, 3.) by contributions from heavy isotopes, and 4.) by intermolecular processes. Considering these four possibilities for the formation of an alkylbenzene molecular ion, it is possible to eliminate intermolecular processes, since it has been shown (1) that contributions from such processes are negligible at the pressures normally employed in analytical mass spectrometers. Effects of contributions from heavy isotopes can be corrected by the use of standard tables of natural abundance such as that of McAdams (8). This leaves only two possibilities for the formation of a molecular ion in a mixture spectrum. Since the intensity of molecular ions in the mixture is desired, it is necessary only to correct this peak for contributions through rearrangement processes. Figure 1 shows the schematic arrangement of beta bond cleavage of the alkylbenzene under electron bombardment. It is important to emphasize that the ion structures shown are symbolic and are not intended to represent the true configuration. Skeletal rearrangements of the phenyl moiety of the molecule may take place. Evidence has been presented by Meyerson and his coworkers (12,13,14,16) and others (6) that the $C_7H_7^+$ ions are the symmetrical seven-member tropylium ion.

Mechanism 1 in figure 1, showing the formation of an ion one mass unit less than a molecular ion, results from the true heterolytic cleavage of the beta bond. Formation of a lower molecular weight parent ion, mechanism 2, demonstrates a typical beta bond cleavage (7,11) with simultaneous proton shift. These two processes are interdependent in a manner not yet completely understood. General considerations and mechanisms of rearrangements under electron bombardment have been adequately described by McLafferty (9,10). Studies in this laboratory under different pressures have shown that P is not second order dependent on P - 1 at reasonable pressures. No work has been done to establish the order of dependence of P - 1 on P, although it appears that low voltage appearance potential studies would elucidate this mechanism (5). Data presented later will show a remarkable resemblance in the relative abundances of these two ions formed from several different molecular species of monoalkyl substituted benzenes. The basic premise in this work will support the theory that the contribution from any molecular specie to a molecular ion of a lower homolog, P, can be calculated from the peak intensity at P - 1. From this consideration and data presented in subsequent tables, it will be shown that the following equation is valid.

$$M_1 = P_1 - \sum_{j=1}^n a_{1j} x_j = P_1 - k_{1-1} (P_{1-1})$$

M_1	Monocomponent peak, M, at m/e 1
P_1	Polycomponent peak, P, at m/e 1
a_{1j}	Calibration coefficient, a, at m/e = 1, for component j
x_j	Divisions of base peak, x, of component, j, appearing in mixture spectrum
k_{1-1}	Correction factor, k, at m/e 1-1

Intensity factors (I_f) are reciprocals of total intensity sensitivities relative to normal hexadecane calculated by the following formula:

$$I_f = \frac{(m/e \ 226)}{(\sum nC_{16})} \frac{(\sum A)}{(m/e \ A)}$$

where

m/e 226 = Peak height in division at m/e 226 for nC_{16}

$\sum nC_{16}$ = Total ionization of nC_{16} (25 to 228)

m/e A = Peak height in divisions at molecular ion for compound A

$\sum A$ = Total ionization of compound A (25 to molecular ion +2)

The products of $P - 1$ and the corresponding I_f yield the partial volume fractions (15) which are subsequently normalized to 100 per cent.

Relative sensitivities are, to an extent, dependent upon the method of reducing the polycomponent peak to a monocomponent peak. The correction factors "k" and the intensities factors " I_f " from Table I are dependent variables and should not be used separately.

RESULTS AND DISCUSSION

Figure 2 shows the data obtained by examination of fragment ion intensities from beta bond cleavage of four alkylbenzenes of different molecular weights, each having a C7 branch. The two ions formed corresponding to P and $P - 1$ are m/e 190 and m/e 189, respectively. The ratio $P/P - 1$ is shown to be useably consistent. A similar study of thirty-six alkylbenzene standards provided additional data for calculating the contribution to P as a function of $P - 1$, regardless of the precursor to $P - 1$. A summary of data for the calculation of alkylbenzenes by the rearrangement technique is given in Table I. Correction factors for rearrangement ions vary inversely with the molecular weight (above mass 190) and become quite small at higher masses, while the isotopic contributions become larger with increasing molecular weight. To simplify calculations, these two contributions are combined in the final correction factor "k"; therefore only one mathematical operation is necessary, based on the $P - 1$ peak, to calculate the contribution from any number of higher homologs to the ion intensity at mass P.

TABLE I
SUMMARY OF DATA FOR THE CALCULATION OF ALKYL BENZENES
BY THE REARRANGEMENT TECHNIQUE

<u>Carbon No. of Molecule</u>	<u>"k" Correction Factor (Applied to P from P-1)</u>	<u>"I_r" Intensity Factor (Reciprocal of Total Intensity Sensitivity)</u>
12	.1629	.1505
13(a)	.1795	.1584
14	.1944	.1664
15(a)	.2055	.2186
16	.2058	.2708
17(a)	.2100	.3144
18	.2191	.3581
19(a)	.2262	.3778
20	.2318	.4008
21	.2387	.4615
22	.2498	.4713
23(a)	.2545	.4791
24	.2656	.4869
25(a)	.2767	.4947
26	.2878	.5024
27(a)	.2989	.5103
28(a)	.3100	.5181
29(a)	.3212	.5259
30(a)	.3322	.5337
31	.3434	.5415
32(a)	.3545	.5493
33(a)	.3656	.5571
34(a)	.3767	.5649
35	.3879	.5727
36(a)	.3989	.5805
37(a)	.4101	.5883
38(a)	.4212	.5961
39(a)	.4323	.6039
40(a)	.4434	.6117
41(a)	.4545	.6195
42(a)	.4769	.6273

(a) Extrapolated values

Efforts to evaluate the absolute accuracy of this method face the same dilemma as efforts to evaluate accuracy of the synthetic cracking pattern technique. Because of the complexity of the mixture, a typical detergent alkylate cannot be blended from known compounds. Previous analytical methods were not amenable to component analysis of simple mixtures of single isomers; however the present technique is applicable to any alkylbenzene mixture above mass 162. To demonstrate this, a blend of seven different known structure alkylbenzenes was made and analyzed using the figures from Table I. Blend values and analytical results are shown in Table II. Average error of ± 0.5 per cent is not outstanding compared with results expected from component analysis; however, when compared with results obtained from typical detergent alkylate pattern coefficients (Table II), the accuracy and extended application of the rearrangement technique can be appreciated.

TABLE II

ANALYSIS OF SYNTHETIC MIXTURE
(Liquid Volume Per Cent)

<u>Blended Compounds</u>	<u>Method</u>	Calculated By	Calculated By
		Rearrangement <u>Method</u>	Synthetic Cracking Pattern Method
1-phenyloctane	5.2	4.9	1.9
5-phenyldecane	17.0	17.6	27.1
3-phenyldodecane	44.5	43.2	41.7
7-phenyltetradecane	13.8	13.8	12.2
6-phenylpentadecane	10.0	10.7	8.4
8-phenylhexadecane	6.0	6.3	4.8
2-phenyloctadecane	3.5	3.5	3.9

TABLE III

ANALYSIS OF DODECYLBENZENE

<u>Carbon No. of Alkyl Chain</u>	Continental's	Continental's	<u>Published Method(1)</u>
	Synthetic Cracking Pattern <u>Method</u>	Rearrange- ment <u>Method</u>	
8	-	0.3	-
9	1.6	0.8	1.1
10	9.6	8.7	7.6
11	28.0	27.9	25.8
12	47.2	47.8	49.5
13	8.7	9.4	10.2
14	2.6	2.6	2.9
15	1.4	1.3	1.4
16	0.6	0.8	0.8
17	0.3	0.4	0.5
Average Molecular Weight	242	242	243
Average Molecular Weight by the Mechrolab Osmometer - 237			

(1) Brown, R. A., Skahan, D. J., Cirillo, V. A., Melpolder, F. W.,
Anal. Chem. 31, 1531-8 (1959).

Results from analysis of a typical dodecylbenzene mixture by this technique, by the synthetic cracking pattern method used at Continental Oil Company, and by the only previously published method by Brown et al (4) are shown in Table III. It should be emphasized that Continental's synthetic pattern data were obtained by calibration on fractions separated from a mixture very similar to the dodecylbenzene analyzed here. The rearrangement method is based entirely upon studies of pure alkylbenzene different in structure from those typically present in the dodecyl type alkylate produced by phenylating polypropylenes. Even so, the analytical accuracy is completely acceptable when compared with results obtained by the other methods. Average molecular weights calculated from the distribution analysis compare favorably with those obtained on the Mechrolab osmometer showing an average difference of 5 amu. This difference may well result from the fact that the osmometer is measuring the true average molecular weight of the mixture, while the mass spectrometer values represent the average molecular weight of the alkylbenzenes only.

A more stringent test of the applicability of this new method to complex mixture analyses has been made. A heavy residual alkylate, C₂₂ to C₄₂, was fractionated into approximately nine 10 per cent cuts and a bottoms portion. Each fraction was analyzed, and data obtained are shown in Table IV. These data were calculated to original sample composition with results shown under composite analyses. Distribution data obtained by the new method are shown in the last column of Table IV. Although absolute agreement is not extremely flattering, when the mass range of the sample and the complexity of such mixtures are considered, these results are entirely acceptable. The average molecular weights calculated from distribution data, 399, agree very well with the osmometer molecular weight of 396. Agreement between molecular weights obtained by these methods is not offered as proof of accuracy but serves only as circumstantial evidence for reasonable accuracy and consistency of the analytical method.

Any component in the mixture, other than alkylbenzenes, which contributes to the P or P - 1 peak intensities will interfere with accurate analyses. Generally, such interference can be expected from indanols, condensed tetracyclonaphthenes, certain sulfur-containing compounds, many halogenated compounds, etc. The analytical method is intended for application to detergent alkylate systems where typical aromatic content is approximately 99 per cent with a small saturate or cycloparaffin content. The method has been successfully applied to complex systems containing as little as 10 per cent alkylbenzenes in a mixture composed primarily of saturates and olefins. Generally, the method is applicable to any system for which the synthetic cracking pattern method was useful and is far less sensitive to changes in branching of the alkyl substituent.

This analytical technique has been in use at Continental Oil Company for the past year. It has been used successfully on detergent alkylate mixtures ranging from C₉ through C₄₂. The data presented in Table I should be usable for analyses of similar mixtures from any mixture spectrum obtained on a CEC-103 or comparable mass spectrometer. Recent work, which will be the subject of later papers, has demonstrated a similar applicability to dialkylbenzenes.

TABLE IV

ANALYSIS OF HEAVY ALKYLATE AND DISTILLATION CUTS

Mol. Wt.	No. of Carbon Atoms	Cut 1	Cut 2	Cut 3	Cut 4	Cut 5	Cut 6	Cut 7	Cut 8	Cut 9	Bottoms	Com- posite Analysis	Direct Analysis
302	22	3.1	1.2									0.4	1.1
316	23	6.8	1.5	1.5								0.9	2.6
330	24	16.8	3.0	1.7	1.9	1.6						2.3	3.3
344	25	24.9	9.8	4.2	2.6	1.8						4.0	5.2
358	26	21.2	17.0	9.5	6.5	2.9	1.7	1.1				5.5	6.6
372	27	13.9	19.2	13.7	9.9	6.0	3.4	1.7	0.9	1.3		6.4	7.4
386	28	8.5	23.0	24.0	22.8	16.1	12.8	6.9	3.4	1.5		10.9	12.1
400	29	3.6	17.9	27.4	31.3	31.5	31.6	25.9	17.4	7.2	3.4	18.4	19.5
414	30	1.1	6.4	15.5	20.9	31.4	39.7	13.7	17.6	24.5	5.2	23.5	22.8
428	31		0.9	2.4	4.1	6.5	8.9	3.9	7.6	14.7	7.2	8.6	7.6
442	32					2.3	2.0	1.1	2.9	9.0	12.4	4.4	3.5
456	33								0.7	3.1	9.6	3.4	2.5
470	34									1.0	2.0	2.0	1.4
484	35										8.9	1.6	1.1
498	36										8.2	1.4	0.9
512	37										7.3	1.3	0.8
526	38										6.1	1.1	0.6
540	39										5.6	1.0	0.5
554	40										5.5	1.0	0.4
568	41										5.5	1.0	-
582	42										5.7	1.0	-
Per Cent of Cut		9.1	9.2	9.2	9.1	9.4	9.1	9.3	8.9	9.3	17.4	411	399
Average Molecular Weight by Mass Spectrometry													
Average Molecular Weight by Mechrolab Osmometer - 396													

ACKNOWLEDGMENTS

The authors wish to thank Mr. Alex Shadan for synthesizing many of the standards used in this work; also we thank Dr. Joseph A. Dixon for standards provided from API Research Project 42. Instrumental data were obtained by Messrs. C. F. Maddox, E. E. McKelvey, and W. K. Moore. Mrs. W. M. Wright contributed substantially by doing much of the detailed computation and organization of the data presented.

REFERENCES

1. Beynon, J. H., "Mass Spectrometry and Its Application to Organic Chemistry," pp. 275-277, Elsevier, Amsterdam 1960
2. Boyer, E. W., Users' Clinic, Consolidated Electrodynamics Corporation, E-14 Meeting on Mass Spectrometry, Los Angeles (1959)
3. Boyer, E. W., Users' Clinic, Consolidated Electrodynamics Corporation, E-14 Meeting on Mass Spectrometry, Atlantic City (1960)
4. Brown, R. A., Skahan, D. J., Cirillo, V. A., Mel-polder, F. W., Anal. Chem. 31, 1531 (1959)
5. Bryce, W. A., and Clarke, E. W. C., in "Advances in Mass Spectrometry" (J. D. Waldron, ed.) p. 392, Pergamon Press, London, 1959
6. Foster, N. G., Hirsch, D. E., Kendall, R. F., Eccleston, B. H., and Ward, C. C., A.S.T.M., E-14 Meeting on Mass Spectrometry, Atlantic City, N. J. (1960)
7. Kinney, I. W., Jr., and Cook, G. L., Anal. Chem. 24, 1991 (1952)
8. McAdams, R. D., "Isotope Correction Factors for Mass Spectra of Petroleum Fractions," Esso Research Laboratories, Baton Rouge, Louisiana, 1957
9. McLafferty, F. W., Anal. Chem. 31, 82 (1959)
10. McLafferty, F. W., "Mass Spectrometry," in "Determination of Organic Structures by Physical Methods," suppl. ed., ed. by F. C. Nachod and W. D. Phillips, p. 131, Academic Press, New York, 1961
11. Meyerson, S., Appl. Spect. 9, 120 (1955)
12. Meyerson, S., and Rylander, P. N., J. Chem. Phys. 27, 901 (1957)
13. Meyerson, S., and Rylander, P. N., J. Phys. Chem. 62, 2 (1958)
14. Meyerson, S., Rylander, P. N., Elser, E. L., and McCollum, J. D., J. Am. Chem. Soc. 81, 2606 (1959)
15. Otvos, J. W., Stevenson, D. P., J. Am. Chem. Soc. 78, 546 (1956)
16. Rylander, P. N., Meyerson, S., and Grubb, H. M., J. Am. Chem. Soc. 79, 842 (1957)

MASS SPECTRA CORRELATIONS AND APPEARANCE POTENTIALS OF THE MAJOR TOBACCO ALKALOIDS

William F. Kuhn and Charles J. Varsel
Philip Morris Research Center
Richmond 6, Virginia
W. A. Powell
Department of Chemistry
University of Richmond
Richmond, Virginia

ABSTRACT

The mass spectra of some major tobacco alkaloids have been determined and correlations between the spectra and structures of these alkaloids are discussed. The more abundant peaks in the spectra of the alkaloids result from the following mechanisms: (1) The ionization of the molecule, (2) loss of a hydrogen atom from the molecule, (3) bond rupture between the pyridyl nucleus and the nucleus of the cyclic amine, and (4) splitting out an empirically CH_2N neutral fragment. The molecular weights of these alkaloids are readily determined from their intense molecular ions.

The appearance potentials of the major ion species from these alkaloids were measured and probable modes of ion formation are discussed.

The design of a heated inlet operable at 200°C and 1×10^{-6} torr is presented.

INTRODUCTION

The main objectives of this project were three-fold: (1) to design and fabricate a heated inlet system for the mass spectrometer; (2) to analyze under normal operating conditions the major tobacco alkaloids; and (3) to determine the ionization potentials of the alkaloids as well as the appearance potentials of some of the major fragment ions derived from the alkaloids.

The tobacco alkaloids comprise a small fraction of the many organic compounds which cannot be analyzed mass spectrometrically at room temperature and pressure of 1×10^{-6} mm. of Hg. or higher. Since this is the case, a suitable heated inlet must be improvised in order to vaporize the alkaloids. From the mass spectrum of the alkaloid, it is then possible to arrive at a positive identification of said material if present in a sample of unknown composition.

The ionization potential of a molecule is simply an additional physical constant similar to a boiling point, melting point, etc. Generally speaking, it cannot be used as a direct method of identification, but it can serve as an additional parameter for substantiating the proposed structure of a compound. The appearance potential of a fragment ion may lend itself useful in determining such entities as bond energy and heat of formation.

EXPERIMENTAL

A Consolidated Electrodynamics Corporation (CEC) Model 21-103 C Mass Spectrometer was used in this study. The general features of the instrument have been previously described (1). The salient modification of the instrument is evident in the exhaust pumping system. The standard mercury diffusion pump was replaced

HEATED INLET FOR MASS SPECTROMETRY

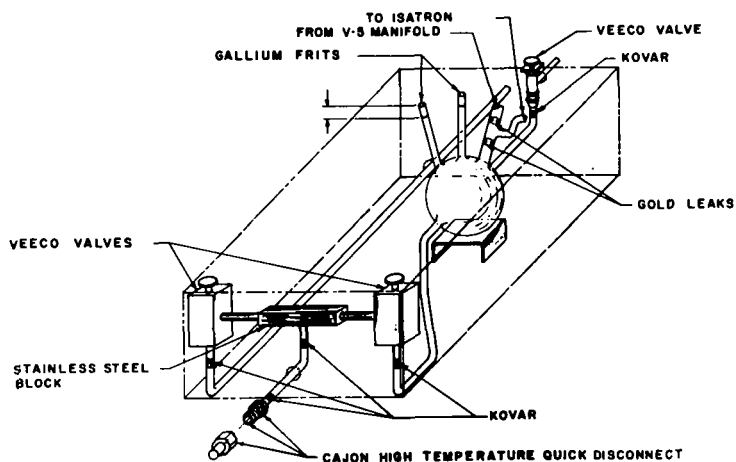


FIGURE 1

ALKALOID	m/e	APPEARANCE POTENTIAL (electron-volt)	RELATIVE INTENSITY (PERCENT)
NICOTINE	162	8.01 ± 0.06	19.2
	161	10.05 ± 0.06	17.6
	133	11.18 ± 0.09	26.6
	84	9.88 ± 0.03	100.0
ANABASINE	162	8.70 ± 0.08	30.9
	161	10.12 ± 0.07	21.5
	133	10.98 ± 0.08	42.3
	120	10.58 ± 0.04	16.3
	119	11.48 ± 0.09	32.1
	106	13.18 ± 0.06	45.4
	105	12.89 ± 0.04	57.8
	84	9.58 ± 0.02	100.0
NORNICOTINE	148	9.30 ± 0.06	23.1
	147	10.05 ± 0.03	34.1
	120	10.14 ± 0.02	32.5
	119	10.75 ± 0.05	100.0
	118	10.51 ± 0.06	22.1
	80	9.58 ± 0.09	21.5
	70	9.69 ± 0.05	80.4

APPEARANCE POTENTIALS and RELATIVE INTENSITIES of the
PRINCIPAL IONS from
NICOTINE, ANABASINE, and NORNICOTINE

Figure 2

by a Varian 8 l/sec. Vac-Ion pump with an argon stable cathode. The operating characteristics and the advantages of this pump have been described elsewhere (2).

The heated inlet system consists basically of three stainless steel valves to isolate the one-liter glass reservoir from the evacuation manifold. (see Figure 1) These valves are equipped with Viton seats and silicone rubber gaskets. The introduction of solid and viscous liquid samples is made possible by a Cajon vacuum coupling, fabricated into a sample holder, and positioned in the front of the heated inlet system between two of the valves described above. A silicone rubber gasket insures a vacuum seal between the body and the gland portions of this coupling. Graded seals (Kovar) are used to join the glass to metal portions of the inlet. This entire coupling is heated electrically. The introduction of non-viscous liquids of low vapor pressure can be accomplished through the use of this coupling or they can be charged through a gallium covered sintered disk as described by O'Neal and Weir (3).

The inlet line from the gas manifold system of the instrument is passed through the top of the oven and attached to one arm of a glass tee. The base of this tee is attached to the one-liter reservoir in the oven. Restricted orifices (gold leaks) are inserted in this arm of the tee and at the base of the tee. The orifice in the arm of the tee serves two purposes: (1) it restricts the flow of gases from the room temperature manifold to the ion source, and (2) it minimizes condensation of high boiling materials on the glass tubing outside the oven. The gold leak in the base of the glass tee restricts the flow of gaseous high boiling materials effusing toward the ion source. The sample exhaust valve, identical to those described above, is connected to the heated inlet reservoir. In operation, the residual air in the vacuum coupling is evacuated, after which the entire coupling is heated, and the sample in the vacuum coupling is vaporized. The vapors are expanded into the heated reservoir through the sample inlet valve. These vapors diffuse from the reservoir to the ion source (Isatron). The mass spectrum is then obtained in the usual manner.

The oven surrounding the heated inlet system is fabricated from asbestos board. An inner and outer casing are constructed of 0.25 inch asbestos board with a 1.5 inch Fiberglass bat between these two casings. A two kilowatt, two-coil, rectangular heater is used to provide a fast increase in temperature. Current for this heater is supplied from a two kilowatt Variac mounted above the oven. A Fenwal thermo-regulator is attached close to the heated sample reservoir to control the oven temperature. A thermocouple is used to monitor the temperature of the heated inlet system. The temperature of the oven may be varied from ambient to 300°C and controlled at less than 2% of the predetermined value.

The mass spectra of the alkaloids and their nuclear moieties were obtained at electron energies of seventy (70) volts and a magnet current of our hundred (400) milliamperes. The ion source was maintained at 250°C. The samples of pyridine, piperidine, pyrrolidine, and N-methylpyrrolidine were analyzed as received. The nicotine was freshly distilled prior to this study. Anabasine, obtained from Fluka A. G. (Switzerland) and estimated to be 95% pure by paper chromatography, was analyzed as received. Nor-nicotine was isolated in our laboratory from the dipicrate and analyzed without further purification. A search of the literature indicates that the mass spectral patterns of nicotine, anabasine, normicotine, and N-methylpyrrolidine have not been reported previously.

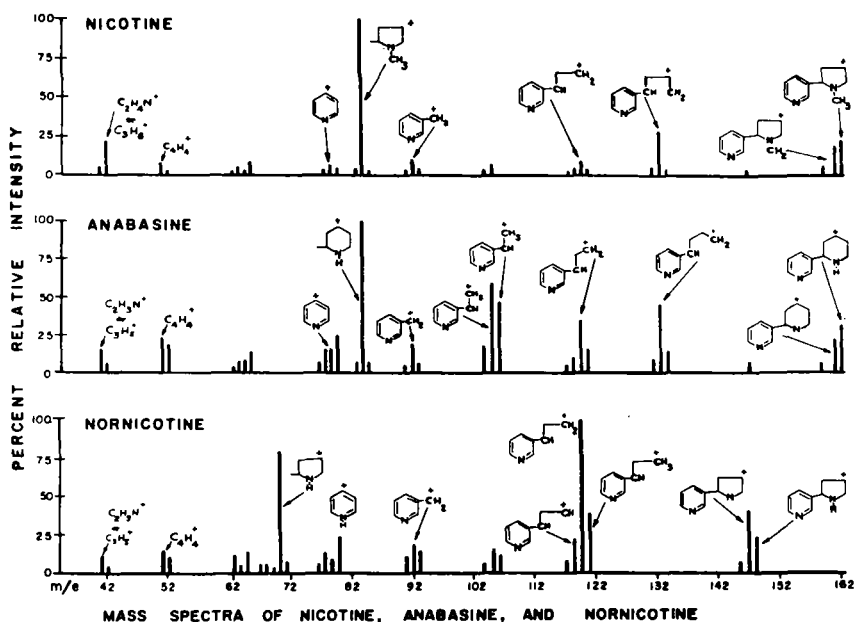


Figure 3

STRUCTURES, NAMES, AND IONIZATION POTENTIALS OF TOBACCO ALKALOIDS AND THEIR NUCLEAR MOIETIES

NUCLEAR MOIETIES



PYRIDINE

(9.98 ± 0.09 e.v.)
(9.8 ± 0.1 e.v.)^a



N-METHYLPYRROLIDINE

(8.06 ± 0.02 e.v.)



PIPERIDINE

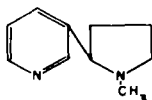
(8.49 ± 0.06 e.v.)
(9.2 ± 0.2 e.v.)^b
(8.47 e.v.)^b



PYRROLIDINE

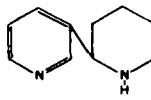
(8.60 ± 0.10 e.v.)
(9.2 ± 0.2 e.v.)^b
(8.55 e.v.)^b

TOBACCO ALKALOIDS



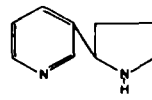
NICOTINE

(8.01 ± 0.06 e.v.)



ANABASINE

(8.70 ± 0.08 e.v.)



NORNICOTINE

(9.30 ± 0.06 e.v.)

^a FIELD & FRANKLIN

^b GALLEGOS & KISER

Figure 4

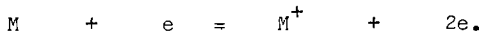
The mass spectra obtained for pyridine and piperidine compare favorably with those listed in the American Petroleum Institute tables of mass spectral data. The mass spectrum of pyrrolidine was reported by Gallegos and Kiser (4).

The ionization and appearance potentials were measured using the technique of Dibeler and Reese (5). The instrument modifications necessary to measure these potentials were described by Varsel and co-workers (6). In these studies, xenon was used as the calibrating gas. The ionization potential of xenon is 12.15 electron volts (7).

RESULTS AND DISCUSSION

A. High Voltage Mass Spectra

In the mass spectrometer which operates at low pressures (ca. 10^{-6} mm. Hg.) the molecules of the compound studied are bombarded in the gas phase with electrons of low energy (10 to 100 electron volts). The processes which result from the impact of electrons on organic molecules are exceedingly complex and are by no means fully understood (8,9, 10). If an impacting electron possesses energy greater than the ionization potential of the molecule, the most common primary process which results from this collision is the removal of one electron from the molecule:



The molecular ion, (M^+), may decompose into a positive ion and a neutral fragment. This process can occur repeatedly, thus leading to a stepwise multi-fragmentation. The nature of the ions and their relative abundances depend on the structure of the molecules which are bombarded. In general, two compounds that are structurally different will give different fragmentation patterns. Like the infrared spectrum, the mass spectrum can be considered as a fingerprint of the compound.

The partial mass spectra of nicotine, nornicotine, and anabasine obtained at a potential of 70 electron volts are shown in the accompanying figure. (Figure 3) Structures are included to coincide with the various ions which were detected. In all cases the molecular ion is one of the most abundant species noted.

The alkaloids are characterized by the following intense peaks: the molecular or parent, parent minus one (p-1), parent minus twenty-nine (p-29), and the parent minus seventy-eight (p78).

Although the empirical formulas of nicotine and anabasine are identical, the mass spectra of these compounds are quite different. The most outstanding difference is the relative intensity of the peaks in the m/e 104 to 106 region. These ions are quite abundant in the spectrum of anabasine, but are relatively small in the spectrum of nicotine.

Since the molecular weight of nornicotine is 148 as compared to 162 for nicotine and anabasine, there is no possibility of error in arriving at the identification of this compound whenever an unknown is suggested as being one of these three compounds.

B. Ionization and Appearance Potential Measurements

The ionization potentials of nicotine, anabasine, and nornicotine together with their nuclear moieties, pyridine, N-methylpyrrolidine, piperidine, and pyrrolidine, were determined. (Figure 4) Because of the good agreement between the ionization potentials of the alkaloids with those of the corresponding

cyclic amine, it is suggested that the electron removed from the alkaloid molecule comes from the cyclic amine portion of the alkaloid during the ionization process.

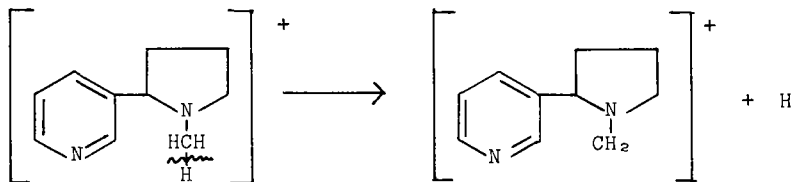
With pyridine, good agreement between the observed value (9.98 electron volts) and the literature values (9.8 electron volts) was obtained. Our observed ionization potential of pyrrolidine is about 0.6 electron volts lower than other reported experimental values, but it is in good agreement with the value calculated by the equivalent orbital method. Our precision for the ionization potential of pyrrolidine was quite good. The cause of the discrepancy between the observed value and the literature values is not known.

The ionization potential of N-methyl pyrrolidine has not been reported previously. One would perhaps expect the ionization potential of this compound to be lower than the ionization potential of pyrrolidine because of the electron donating capacity of the methyl group. The experimental data attest to this fact in that the ionization potential of N-methylpyrrolidine is 8.06 electron volts, as compared to 8.60 electron volts for pyrrolidine.

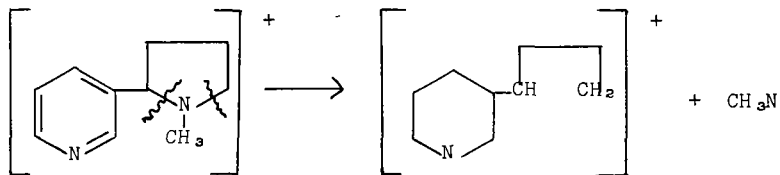
The ionization potential observed for piperidine is 8.49 electron volts. This value is about 0.7 electron volts lower than the literature value, but the observed value agrees well with that value calculated from the equivalent orbital method.

Nicotine (3'-pyridyl -2- (N-methyl)-pyrrolidine)

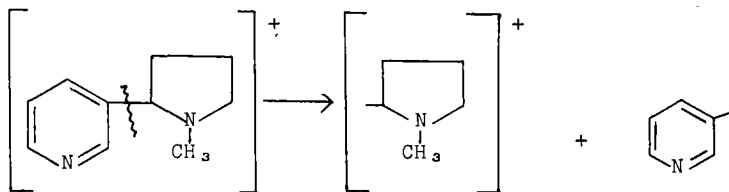
The ionization potential for nicotine is 8.01 ± 0.06 electron volts. The appearance potential of the m/e 161 ion (p-1) is 10.05 ± 0.06 electron volts. The hydrogen atom may be abstracted from the methyl group attached to the nitrogen atom of the N-methylpyrrolidinyl moiety. The proposed mechanism is:



The appearance potential of the m/e 133 ion (p-29) is 11.18 ± 0.09 electron volts. This ion is thought to be formed by rupture of both bonds alpha to the nitrogen atom of the N-methylpyrrolidinyl nucleus. The proposed mechanism is:



The appearance potential of the m/e 84 ion (p-78) is 9.88 ± 0.03 electron volts. This ion is formed by rupture of the carbon-carbon bond between the pyridyl and the N-methylpyrrolidinyl moieties. The proposed mechanism is:



These energies give insight to some of the bond energies of nicotine.

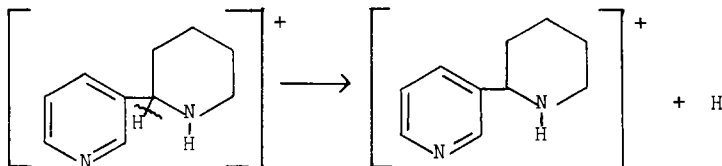
Since the appearance potential for the m/e 84 ion is less than that for the m/e 161 ion, it is probable that the carbon-carbon bond between the pyridyl and the N-methylpyrrolidynyl nuclei is weaker than the carbon-hydrogen bonds present in the N-methyl-pyrrolidynyl moiety. The difference in the appearance potentials of these two ions is 0.17 electron volts or 3.92 kcal (23.06 kcal/electron volt).

Since the m/e 133 ion is formed by breaking two bonds, one would expect that the appearance potential of this ion would be higher than those obtained when only one bond is broken. The experimental data support this premise.

Anabasine (3' pyridyl-2-piperidine)

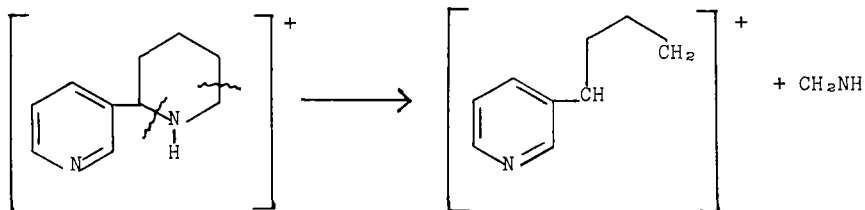
Since both individual moieties for anabasine are unsubstituted, one would expect the ionization potential of anabasine to be higher than that of nicotine. This was shown by experimental data to be the case. The ionization potential of anabasine is 8.70 ± 0.08 electron volts while that for nicotine is 8.01 ± 0.06 electron volts.

Since the bond dissociation energy required for the formation of the m/e 161 ion (p-1) from the molecular ion in anabasine (32.8 kcal) is less than that required for the formation of the same ion in nicotine (47.1 kcal), it is suggested that the hydrogen atom removed to form this ion comes from one of the carbon atoms of the piperidynyl nucleus. The proposed mechanism is:



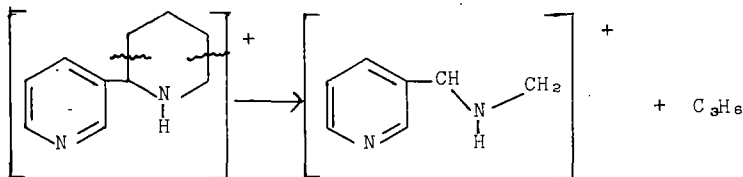
Since beta bond cleavage is preferred, it should be noted that in the proposed mechanism the hydrogen atom is beta not only to the pyridynyl moiety but also to the nitrogen atom of the piperidynyl moiety.

The appearance potential of the m/e 133 ion (p-29) is 10.98 ± 0.08 electron volts. This ion is thought to be formed by rupture of the bonds alpha and beta to the nitrogen atom of the piperidynyl nucleus. The mechanism may be as follows:



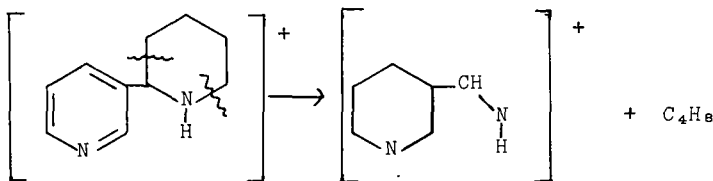
Since the m/e 119 ion is thought to be formed by splitting out a methylene group from the already formed m/e 133 ion, and additional bond must be broken and more energy is required. One would therefore, suspect that the appearance potential of the m/e 119 ion would be higher than that of the m/e 133 ion. The experimental data show that the appearance potential of the m/e 119 ion (11.49 ± 0.03 electron volts) is about 0.51 electron volt higher than that of the m/e 133 ion (10.98 ± 0.08 electron volt.)

The m/e 120 ion is possibly formed by bond rupture of the two bonds beta to the nitrogen atom in the piperidinyl nucleus. Since the appearance potential of this ion (10.58 electron volts) is less than that of the m/e 119 ion (11.49 electron volts), the author suggests that the bond dissociation energies of these bonds are less than the bonds alpha and gamma to the nitrogen atom. These latter bonds are thought broken to form the m/e 119 ion. The rupture of these latter bonds is postulated as the mode of formation for the m/e 119 ion. The proposed mechanism for the formation of the m/e 120 ion is:



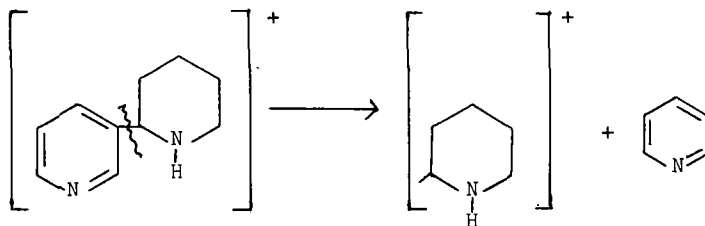
The m/e 105 ion is thought to be formed by removing an additional methylene group from the already formed m/e 119 ion. As stated previously, this process proceeds at the expense of energy; therefore, one would expect the m/e 105 ion to have a higher appearance potential than the m/e 119 ion. The observed values for the appearance potentials of the m/e 105 and 119 ions are 12.89 and 11.49 electron volts, respectively. The observed data are in good agreement with the proposed mechanism.

The experimental value for the appearance potential of the m/e 106 ion is 13.18 ± 0.06 electron volts. This ion could be formed by rupture of the bonds alpha and beta to the nitrogen atom of the piperidinyl nucleus according to the following mechanism:



Another possibility, although less favorable, for the formation of this ion is the rearrangement of a hydrogen atom to the already formed m/e 105 ion.

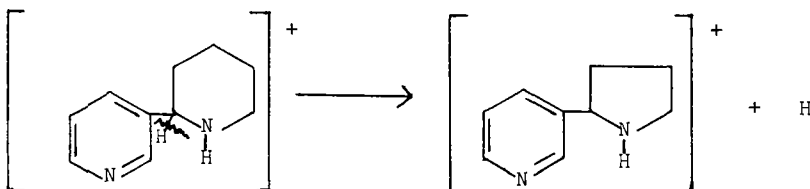
The base peak (m/e 84 ion) from anabasine is formed by breaking the bond between the pyridyl and the piperidinyl nuclei and imparting a positive charge to the piperidinyl nucleus. The observed value of 9.58 ± 0.02 electron volts for the appearance potential of this ion suggests, as in the case of nicotine, that the carbon - carbon bond between the two nuclei is weaker than any of the carbon-hydrogen bonds in the piperidinyl nucleus. The mechanism is:



Nornicotine (3'- pyridyl -2- pyrrolidine)

The observed ionization potential (9.30 electron volts) for nornicotine is somewhat higher than one would expect based upon the value obtained for pyrrolidine. (Recall that ionization potentials of nicotine and anabasine agree closely with those of N-methylpyrrolidine and piperidine, respectively). However, the ionization potential of nornicotine is lower than that of pyridine and the suggestion that the electron removed during the ionization process comes from the cyclic amine moiety is substantiated. Since all measurements were made at least in duplicate and the reproducibility within any given set of values was good, the apparent discrepancy is unexplainable at this time.

The appearance potential of the m/e 147 ion ($p-1$) from nornicotine is 10.05 ± 0.03 electron volts. The energy difference between this value and that observed for the ionization potential indicates that the hydrogen atom removed comes from one of the carbon atoms of the pyrrolidinyl nucleus. Since the appearance potential of this ion is in excellent agreement with that of the m/e 161 ion ($p-1$) from anabasine, it is suggested that the same process is occurring in both cases. The proposed mechanism is:



The splitting out of the neutral fragment, empirically CH_2N , forms the m/e 119 ion which is the base peak in the nornicotine spectrum. The appearance potential for this ion (10.75 ± 0.05 electron volts) is slightly lower than that for the formation of the m/e 133 ion formed by the removal of the same neutral fragment from nicotine and anabasine. Since a large amount of energy is required to ionize the nornicotine molecule, one would expect that the dissociation of the ionized molecule would proceed more readily than that observed for a molecule with a lower ionization potential if the same dissociation process is occurring. In this study, the observed data substantiate this postulation.

The observed appearance potential of the m/e 120 ion is 10.14 ± 0.02 electron volts. This ion can be formed either by the formation of C_2H_4 or CH_2N neutral fragment from the molecular ion. The formation of the latter fragment would require rearrangement of a hydrogen atom. Since this value is less than that observed for the m/e 119 ion, the data suggest that the C_2H_4 radical is the one actually formed. If the CH_2N radical were formed, the appearance potential of the m/e 120 ion should be greater than that of the m/e 119 ion because of the energy requirements of the rearrangement process.

The formation of the m/e 118 ion can occur if an additional hydrogen atom is removed from the m/e 119 ion. This process should proceed at the expense of energy and the appearance potential of the m/e 118 ion should be greater than the appearance potential of the m/e 119 ion. Experimentally this was not the case. The most probable mechanism for formation of the m/e 118 ion appears to be the splitting out of $C_2H_4 + 2H$ fragments from the molecular ion. In this case the appearance potential of the m/e 118 ion should be greater than that of the m/e 120 ion. The experimental data substantiate this proposal. The appearance potential of the m/e 118 ion (10.51 ± 0.06 electron volts) is greater by 0.37 electron volt than the appearance potential of the m/e 120 ion.

The m/e 80 ion in the nornicotine spectrum is one of the more abundant ions. The appearance potential of this ion is 9.58 ± 0.09 electron volts. This ion is not as intense in the mass spectra of nicotine and anabasine as it is in the nornicotine spectrum. This ion is thought to be formed by the rearrangement of two hydrogen atoms to the pyridyl moiety of the alkaloid.

The formation of the m/e 70 ion is attributed to the cleavage of the carbon-carbon bond between the pyridyl and pyrrolidinyl nuclei. The appearance potential of this ion is 9.69 ± 0.05 electron volts which is in reasonable agreement with the appearance potentials of the ions formed, via this mechanism, from nicotine (9.88 ± 0.03 electron volts) and anabasine (9.58 ± 0.02 electron volts).

In the accompanying table, the appearance potentials and the pattern coefficients are listed for the ions which were studied. The data demonstrate that there is not a definite correlation between the pattern coefficients and the appearance potentials.

SUMMARY

The mass spectra of nicotine, anabasine, nornicotine and their nuclear moieties (pyridine, N-methylpyrrolidine, piperidine, and pyrrolidine) were obtained at electron energies of 70 electron volts.

The mass spectra of the alkaloids are characterized by the intense peaks attributable to the following ions; the molecular or parent, the parent minus one (p-1), the parent minus twenty-nine (p-29), and the parent minus seventy-eight, (p-78). This latter ion is formed by the rupture of the bond between the pyridyl and the respective cyclic aminyl nuclei. The intensity of this ion in the spectra of all the alkaloids indicates the ease with which this bond is ruptured. Appearance potential data substantiate the weakness of this bond.

The ionization potentials of the alkaloids agree very closely with those of the respective cyclic amines. This indicates that the electron removed from the alkaloid during the ionization process comes from the cyclic amine moiety.

Appearance potential data show that the carbon-carbon bond between the pyridyl and the cyclic aminyl moieties is the weakest bond in all of the alkaloids studied. These data further indicate that the hydrogen atom removed to form the parent minus one ion comes from the N-methyl group in nicotine, and from the cyclic aminyl nitrogen in anabasine and nornicotine.

The heats of formation of the fragment ion and some of the bond dissociation energies may be determined from the data presented.

The studies presented herein were made possible by the design and fabrication of a suitable heated inlet system for

mass spectrometer. The outstanding feature of this inlet is that it permits the direct introduction of solids and viscous liquids into the instrument.

LITERATURE CITED

1. D. J. Fraade, and R. F. Howard, Instruments and Control Systems, 34, 2272 (1961).
2. R. D. High, and R. W. Schede, "The Use of an Electronic High Vacuum Pump on Various Types of Mass Spectrometers," AEC Report No. KD-1591, Oct., (1959).
3. M. J. O'Neal, Jr., and T. P. Weir, Anal. Chem., 22, 830 (1951).
4. E. J. Gallegos and R. W. Kiser, J. Phys. Chem., 66, 136 (1962).
5. V. H. Dibeler, and R. M. Reese, J. Res. Natl. Bur. Std., 54, 127 (1955).
6. C. J. Varsel, F. A. Morrell, F. E. Resnik, and W. A. Powell, Anal. Chem., 32, 182, (1960).
7. F. H. Field and J. L. Franklin, "Electron Impact Phenomena and the Properties of Gaseous Ions," p. 246, Academic Press, New York, N. Y., 1957.
8. A. J. B. Robertson, "Mass Spectrometry," Methuen, London, 1954.
9. F. H. Field and J. L. Franklin, op. cit, p. 166.
10. A. L. Wahrhaftig, Advances in Mass Spectrometry, ed. J. D. Waldron, Pergamon Press, London, 1959.

SPECTRA OF COMPOUNDS OF BIOLOGICAL INTEREST *

K. Biemann and James A. McCloskey
Department of Chemistry, Massachusetts Institute of Technology,
Cambridge, Mass.

Many of the organic compounds which are of importance in biochemistry are of rather low volatility, because of the number of polar groups present. Frequently these substances are encountered in rather small amounts thus making it difficult or impossible to employ chemical conversion into more volatile derivatives, an approach which we have used extensively in the past.

To obtain usable mass spectra of such compounds, such as nucleosides, free amino acids and peptides, etc., we have sublimed or distilled the samples directly into the ionizing electron beam, *a*, of a Bendix TOF mass spectrometer using a tiny oven assembly (Fig. 1) which enters the source region through a vacuum lock, *b*, (lock and piston are from a Bendix Model 843 Hot Filament Sample System). To avoid accidental pyrolysis of the sample, catalytic effects of the filament material, and contamination of consecutive samples, the substance, *c*, is placed into a disposable glass cup, *d*, (short piece of melting point capillary). By passing current through the helix of resistance wire, *e*, the cup is heated to a temperature at which the compound has sufficient vapor pressure to give a good spectrum (for example, 80 - 200° for various amino acids). Care has to be taken not to apply too much heat which leads to too fast an evaporation.

The spectra are scanned within a few seconds or as slowly as 1 - 2 minutes, using a Honeywell-Visicorder No. 1508.

Mass spectra of a number of nucleosides have been obtained ¹. They permit identification of the base, which gives rise to rearrangement peaks involving the abstraction of one and two hydrogen atoms (*m/e* 112 and 113 in Figs. 2a and b). The sugar moiety also gives rise to a significant peak (*m/e* 117 in the deoxypentosides shown in Figs. 2a and b, while it is at 133 in pentosides). Isomers such as 2' - deoxyuridine (Fig. 2a) and 5' - deoxylyxosyluracil (Fig. 2b) can be distinguished and the differences interpreted in terms of the structures.

With this technique it is quite easy to obtain the mass spectra of compounds deuterated on O, N or S by simply evaporating in a dessicator a drop of a solution of the sample in D₂O placed into the sample cup. Fig. 2c shows the spectrum of 5' - deoxylyxosyluracil so treated. The shifts of the peaks are in agreement with the assignments mentioned above. Furthermore, it indicates, for example, the structure of the fragment of mass 57 which cannot contain -OH because its mass remains unchanged.

The mass spectra of a considerable number of free amino acids have been obtained ². All exhibit a fragmentation pattern closely related to the spectra of amino acid ethyl esters ³ and can, therefore, be interpreted along the same lines. Differences in mass (28 m.u.) are observed with those fragments that contain the -COOH group (instead of -COOC₂H₅). In addition, the rearrangement of one hydrogen atom during the cleavage of the C_α² - C_β bond is observed to a certain extent.

To illustrate the extreme sensitivity of this method, a spectrum obtained with 0.25 microgram of phenylalanine is shown in Fig. 3.

* This work was supported by the National Institutes of Health (RG 5472) and the National Aeronautics and Space Administration (NsG 211 - 62).

- 1) For a more detailed discussion see K. Biemann and J. A. McCloskey, J. Am. Chem. Soc., **84**, 2005 (1962).
- 2) For a more detailed discussion see *ibid.*, August, 1962.
- 3) K. Biemann, J. Seibl and F. Gapp, J. Am. Chem. Soc., **82**, 3795 (1961).

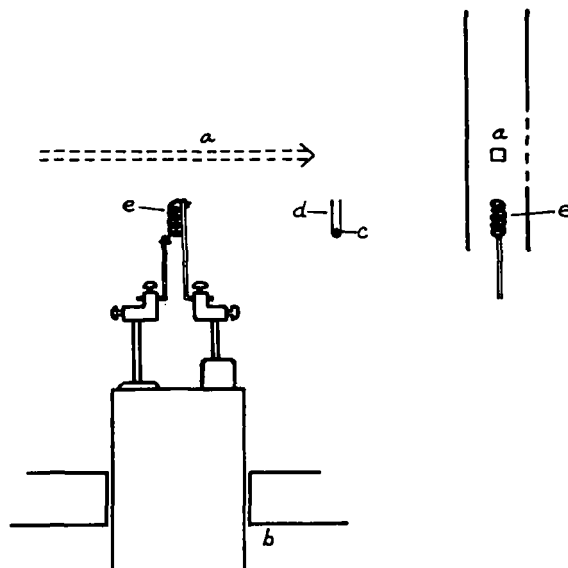


Fig. 1. Sample system for introduction into the ion source of a Bendix TOF Mass Spectrometer. For details see text.

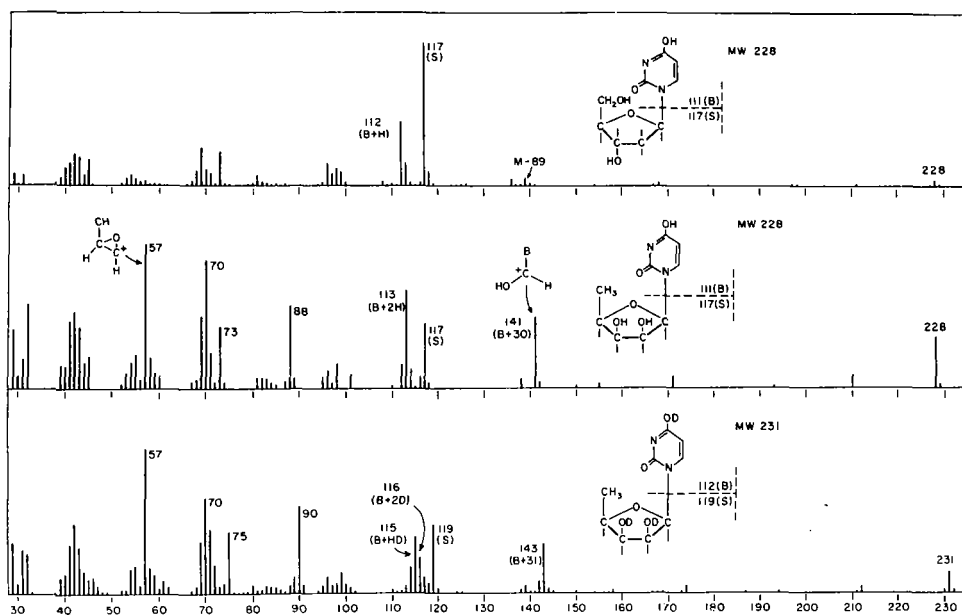


Fig. 2. Mass spectra of (a) 2' - deoxyuridine, (b) 5' - deoxyribose and (c) same as (b), but treated with D_2O .

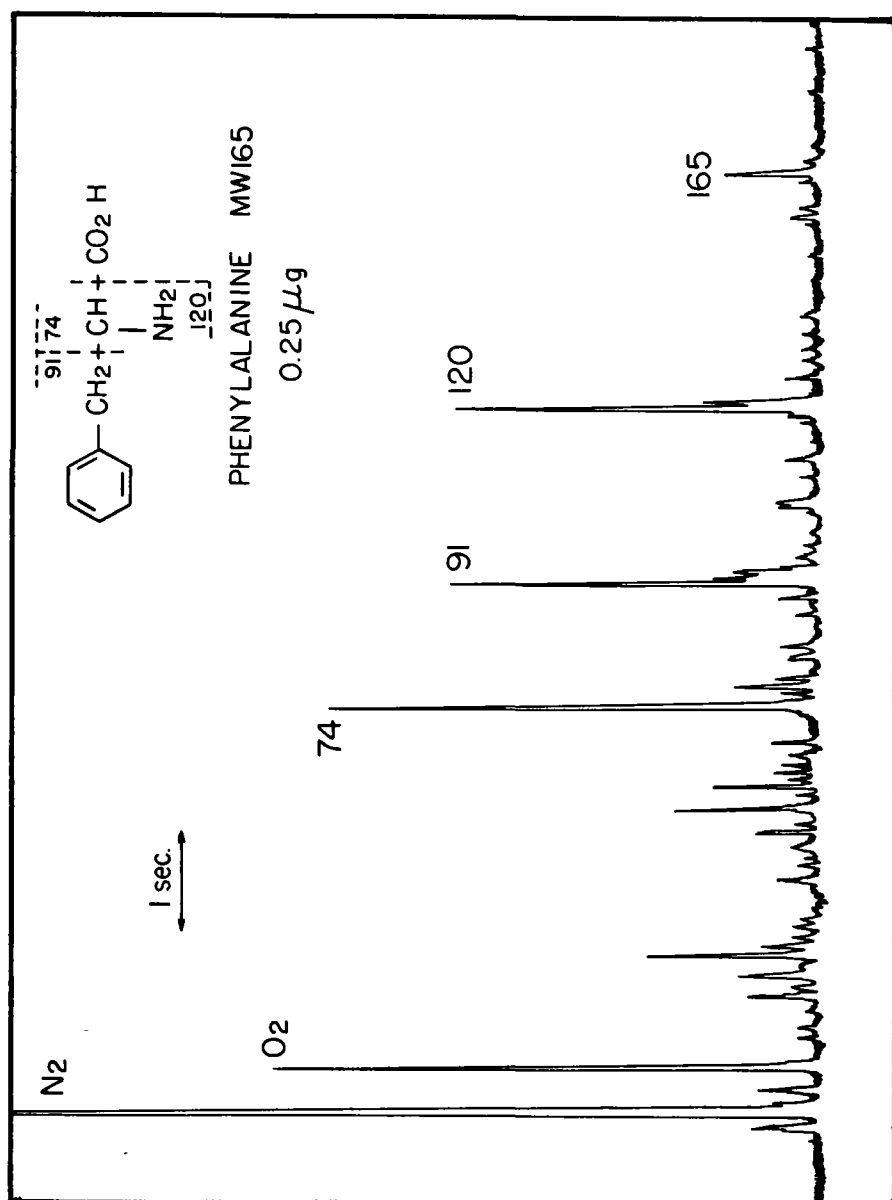


Fig. 3. Mass spectrum of 0.25 µg phenylalanine.

A FRAGMENTATION MODEL FOR n-PARAFFINS

John C. Schug
Gulf Research & Development Company
Pittsburgh, Pennsylvania

ABSTRACT

A tentative model is described to interpret the mass spectra of n-paraffins. In this model, it is assumed that parent molecule ions dissociate to produce primary fragments which contain at least half the total number of carbon atoms available. If the fragment ions retain sufficient excitation energy, they may dissociate further, with the same requirement that any products are at least half as large as the decaying species. At each step, all possible dissociations are assumed to be in competition. Rate constants are calculated by the latest version of the statistical theory. Breakdown curves are given for n-decane and described for other cases.

The assumed model is capable of explaining the dependence of the fragmentation patterns on the ionizing voltage, the relative abundances of numerous fragment ions, and the observation of several metastable ion peaks. However, other expected metastables do not appear, and in addition it is impossible to reconcile the computed breakdown curves with the observed mass spectra by the use of a presently acceptable internal energy distribution function. The need for further experiments and calculations is pointed out.

I. INTRODUCTION

Very little is actually known about the dissociation processes that are responsible for the mass spectra of large molecules. The fragmentation patterns of long-chain n-paraffin molecules have long been familiar, and have been thoroughly characterized¹, but no interpretation has been given for them. The recent studies by Beynon and coworkers² on C¹³-labeled molecules have definitely proved that these patterns result from a series of consecutive dissociations. If, as in the present work, the statistical theory of mass spectra³ be accepted, the same deduction can be drawn on the basis of the numerous metastable ion peaks that are observed⁴ in the spectra.

With the available data as a basis, it is possible to construct a number of reasonable dissociation mechanisms. In this paper, one such model is investigated. A tentative dissociation scheme for n-paraffin molecule-ions is postulated, and its predictions are compared with some experimental observations.

It is assumed that the breaking of carbon-carbon bonds is the controlling process and, therefore, simple dissociations of the paraffinic chain are the only steps that are considered in this work. Finer details, such as atomic rearrangement during dissociations and the loss of hydrogens, are left for future considerations. For the present, then, any fragment ions encountered will be characterized as C_n⁺, and the number of hydrogens contained in them will not be a point of concern. Whenever it becomes necessary to specify the fragment ions more completely, as in estimating activation energies and calculating dissociation rate constants, it will be assumed that all fragment ions observed are of n-alkyl stoichiometry (C_nH_{2n+1}).

The postulated dissociation scheme considered in this work is as follows:

a) By virtue of their excess internal energies³, parent molecule-ions, C_NH_{2N+2}⁺, undergo primary dissociations to fragments C_n⁺, where $n \geq N/2$.

b) During the primary, as well as any successive dissociations, it is assumed that the excess internal energy is equipartitioned between the fragment ion and its complementary neutral fragment. This is expressed by

$$E' = n_I(E - \epsilon_0) / (n_I + n_N), \quad (1)$$

where E is the excess energy of the initial ion, ϵ_0 is the activation energy for the reaction, n_I and n_N are the numbers of degrees of freedom in the ionic and neutral products, respectively, and E' is the excess energy found in the resulting ionic species.

c) Independent of its origin, any fragment ion, C_m⁺, that possesses sufficient energy may dissociate to smaller fragments, C_n⁺, with the stipulation that $m \geq n/2$.

Table I.

ESTIMATED ACTIVATION ENERGIES FOR
C-C BOND DISSOCIATIONS

Fragment Ion	Activation Energy (ev)	
	n-Decane	n-Eicosane
CH_3^+	3.6	3.6
C_2H_5^+	1.8	1.8
C_3H_7^+	0.9	0.9
C_4H_9^+	0.7	0.7
$\text{C}_5\text{H}_{11}^+$	0.6	0.6
$\text{C}_6\text{H}_{13}^+$	0.5	0.5
$\text{C}_7\text{H}_{15}^+$	0.5	0.5
$\text{C}_8\text{H}_{17}^+$	0.5	0.5
$\text{C}_9\text{H}_{19}^+$	0.8	0.5
$\text{C}_{10}\text{H}_{21}^+$	---	0.5
$\text{C}_{11}\text{H}_{23}^+$	---	0.5
$\text{C}_{12}\text{H}_{25}^+$	---	0.5
$\text{C}_{13}\text{H}_{27}^+$	---	0.5
$\text{C}_{14}\text{H}_{29}^+$	---	0.5
$\text{C}_{15}\text{H}_{31}^+$	---	0.5
$\text{C}_{16}\text{H}_{33}^+$	---	0.5
$\text{C}_{17}\text{H}_{35}^+$	---	0.5
$\text{C}_{18}\text{H}_{37}^+$	---	0.5
$\text{C}_{19}\text{H}_{39}^+$	---	0.8

Table II.

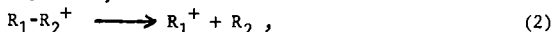
NORMAL MODE FREQUENCIES ASSUMED

FOR $\text{C}_N\text{H}_{2N+2}^+$ MOLECULE ION

Mode	Number	Frequency
C-C Stretching	N-1	1000 cm^{-1}
C-C-C Bending	N-2	500
C-H Stretching	2N+2	3000
CH_3 Deformation	6	1400
CH_2 Deformation	2N-4	1400
CH_2 Rocking	2N-4	1200
CH_3 Rocking	4	1000
Torsions	N-1	100

II. IMPLICATIONS OF THE MODEL

For a typical dissociation process,



the activation energy, ϵ_0 , may be estimated by the relation,

$$\epsilon_0 = D(R_1-R_2) + I(R_1) - I(R_1-R_2), \quad (3)$$

where D is the bond dissociation energy in the neutral species and I denotes ionization potential. In Table I are listed the activation energies obtained from this expression for the scission of all possible C-C bonds in *n*-decane and *n*-eicosane molecule-ions. (Only the lower halves of columns 2 and 3 are important in this treatment.) Bond dissociation energies were taken as 3.4 and 3.7 eV⁶, respectively, for interior and end bonds of the chains. The ionization potential of each molecule was taken as 10.2 eV⁷. The values used for the ionization potentials of *n*-alkyl radicals were determined by Clancy and Crable⁸. The data of the latter investigations showed that $I(C_nH_{2n+1})$ decreases as n increases, but that the changes are very small for $n > 6$. In Table I, it is apparent that zero increments were assumed here for $n > 6$. It might be noted that if the increments are in fact different from zero, then the first feature (a) of the dissociation scheme (preceding section) is compatible with the various empirical observations⁹ which are usually referred to as "Stevenson's Rule".

For dissociations other than the primary ones, the necessary data for estimating ϵ_0 are not presently available. For the lower molecular weight species, Eq. (3) generally leads to values of about 1 eV. In the present work, values of 1.2 and 1.0 eV were used for all subsequent reactions; the former quantity was applied to all losses of neutral C_1 fragments, and the latter to all other processes.

Earlier work^{10,11} has shown that the original version of the statistical theory³ gave poor results for the low-voltage mass spectra of *n*-paraffins. Consequently, in the present work, the improved expression for the rate constant given by Vestal et al¹² has been used:

$$k(E) = \frac{\sum_{Q=1}^L \binom{N-1}{Q} \frac{1}{Q!} \left[\frac{(E-\epsilon_0) \sigma_Q^+}{h \bar{\nu}^+} - \frac{Q-1}{2} \right]^Q}{\sum_{P=1}^K \binom{N}{P} \frac{\sigma_P}{(P-1)!} \left[\frac{E \sigma_P}{h \bar{\nu}} - \frac{P-1}{2} \right]^{P-1}}, \quad (4)$$

where N is the number of oscillators in the decaying ion; $\bar{\nu}$ and $\bar{\nu}^+$ are the geometric mean frequencies of the normal ion and the transition complex; each term in the denominator (numerator) corresponds to a state of the normal ion (transition complex) in which P (Q) of the oscillators are excited and the remaining ones unexcited;

$$\sigma_P = \left[\left(\frac{\bar{\nu}}{\nu_1} \frac{\bar{\nu}}{\nu_2} \cdots \frac{\bar{\nu}}{\nu_P} \right) \right]^{1/P} \quad (5)$$

where $\nu_1, \nu_2, \dots, \nu_P$ are the P excited oscillators, the bar indicates the arithmetic mean of all such possible terms, and a similar expression holds for σ_Q^+ ; and each series terminates with the last positive term, or with $K=N$ or $L=N-1$, whichever occurs first. Since Eq. (4) is so unwieldy, all the rate constants given in this paper have been evaluated with an IBM 7090 digital computer.

To evaluate rate constants, it is also necessary to specify frequency distributions for parent ions, decaying fragment ions, and the transition complexes of all reactions. An approximate frequency distribution for a C_nH_{2n+2} molecule-ion was obtained by generalizing the vibrational assignments made by Herzberg for ethane and propane¹³, and is given in Table II. For the transition complex of a primary reaction, this distribution was changed by deleting one C-C stretching mode (this corresponds to the reaction coordinate), and decreasing by a factor of ten each of: two C-C-C bending frequencies, four C-H stretching frequencies, four CH_2 deformation frequencies, and four CH_2 rocking frequencies. For fragment ions undergoing further dissociations, frequency distributions were obtained by simply choosing the appropriate number of each vibrational mode from Table II. These were then modified for the corresponding transition complexes in the same manner as described above for the primary reactions. These assumptions are highly arbitrary and, therefore, the dissociation rate constants calculated here may be in considerable error; however, fragmentation patterns are determined by the relative rate constants of competing processes, and in this sense the results should be reasonable.

Table III.

COMPARISON OF RELATIVE ABUNDANCE CURVES
FOR THREE n-PARAFFINS

Feature	Ionizing Voltage		
	n-Decane	n-Pentadecane	n-Eicosane
$C_2H_5^+$ Appearance	~ 17 volts	~ 20 volts	~ 24 volts
$C_5H_{11}^+$ Maximum	13	17	22
$C_4H_9^+$ Maximum	18	27	32
$C_3H_7^+$ Plateau	28	46	>60

Table IV.

SOME OBSERVED METASTABLE PEAKS IN MASS
SPECTRUM OF n-NONANE

m*	Dissociation
76.6	$C_9H_{20}^+ (128) \rightarrow C_7H_{15}^+ (99) + C_2H_5$
56.4	$C_9H_{20}^+ (128) \rightarrow C_6H_{13}^+ (85) + C_3H_7$
40.5	$C_9H_{20}^+ (128) \rightarrow C_5H_{12}^+ (72) + C_4H_8$
48.6	$C_7H_{14}^+ (98) \rightarrow C_5H_9^+ (69) + C_2H_5$
33.6	$C_7H_{13}^+ (97) \rightarrow C_4H_9^+ (57) + C_3H_4$
32.8	$C_7H_{15}^+ (99) \rightarrow C_4H_9^+ (57) + C_3H_6$
38.2	$C_6H_{13}^+ (85) \rightarrow C_4H_9^+ (57) + C_2H_4$
36.5	$C_6H_{14}^+ (86) \rightarrow C_4H_8^+ (56) + C_2H_6$
21.6	$C_6H_{13}^+ (85) \rightarrow C_3H_7^+ (43) + C_3H_6$
26.1	$C_5H_{11}^+ (71) \rightarrow C_3H_7^+ (43) + C_2H_4$
24.5	$C_5H_{12}^+ (72) \rightarrow C_3H_6^+ (42) + C_2H_6$
29.5	$C_4H_9^+ (57) \rightarrow C_3H_5^+ (41) + CH_4$
15.3	$C_4H_7^+ (55) \rightarrow C_2H_5^+ (29) + C_2H_2$

Figures 1 and 2 show some rate constants calculated as a function of excess energy from Eq. (4) and the assumptions outlined above. In Fig. 1 are shown rate constants for the primary C-C bond scissions of the n-decane molecule-ion; each curve corresponds to a different activation energy. Fig. 2 gives rate constants for dissociation of a C-C bond in several different n-alkyl radical ions, in each case for $\epsilon_0 = 1.0$ ev. The rate constants shown in the figures attain unreasonably high values, probably because of a poor choice of frequencies for the transition complexes. In the present work, the curves are not too important because the assumed model does not, in general differentiate the scission of various bonds in an ion, either in activation energies or in frequency distributions; in more refined treatments, their details will be much more important.

The method of calculating breakdown curves³ is well-known, and therefore is not repeated here; the procedure is laborious, but quite straightforward. In this work, an additional assumption has been made, viz., that the fragmentation of any species is an all or nothing proposition. If the sum of the rate constants for all considered dissociations of an ion is less than 10^6 sec^{-1} , it was assumed that no fragmentation occurs. For rate constant sums greater than this value, fragmentation was assumed to be complete, with each of the possible fragments being obtained in proportion to the corresponding rate constant.

The breakdown curves calculated for n-decane are shown in Fig. 3, where every aspect of the postulated model is apparent. Analogous breakdown curves can be constructed for all n-paraffins. The essential features of all such curves are equivalent, and the only differences lie in the energies that are of interest. For example, in n-decane C_3^+ ions predominate in the region of 4-5 ev. Calculations of n-eicosane show that about 10 ev is required for an equivalent result in that case. The greater energy spread for larger molecules is primarily caused by the fact that a greater number of consecutive reactions is required to cause the appearance of particular small fragment ions.

From the breakdown curves, denoted by $f_i(E)$, the fractional abundance of each ion in a mass spectrum can be calculated by

$$F_i = \int_0^{\infty} f_i(E) P(E) dE, \quad (6)$$

where $P(E)$, a normalized distribution of internal energies, is a function of the ionizing voltage. Chupka and Kaminsky¹⁴ have recently measured the $P(E)$ functions for propane and n-butane, but is not yet possible to generalize their results for larger molecules.

Even without knowledge of the $P(E)$ functions, though, the preceding considerations and results lead to a number of predictions regarding the mass spectra:

1. At low ionizing voltages, the mass spectra will be dominated by C_n^+ ions, where $N/2 \leq n \leq N-2$.
2. At all ionizing voltages, the smaller ions in this range should be more abundant than the larger ones; i.e., $F_{N-2} < F_{N-3} < F_{N-4} \dots < F_{N/2}$, where F is as defined in Eq. (6) and the subscripts refer to carbon numbers.
3. Fragment ions having $N-1$ carbon atoms should at all voltages constitute a negligible part of the spectrum.
4. Regarding the energy dependence of the spectra, it is predicted that the larger the molecule, the greater the ionizing voltage required before the pattern becomes independent of voltage.
5. The presence of numerous metastable ion peaks is predicted. For example, in n-decane, insofar as the activation energies and frequency distributions applicable to the primary formation of C_6^+ , C_7^+ , and C_8^+ ions are equivalent as assumed here, a metastable ion peak for each of these primary reactions is expected.

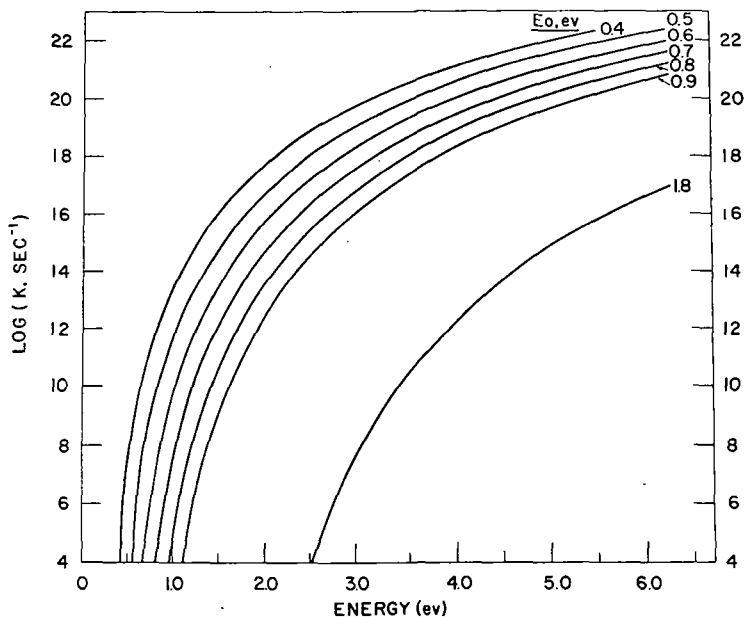


Figure 1. Rate constants calculated for primary dissociations of n-decane, for several different activation energies.

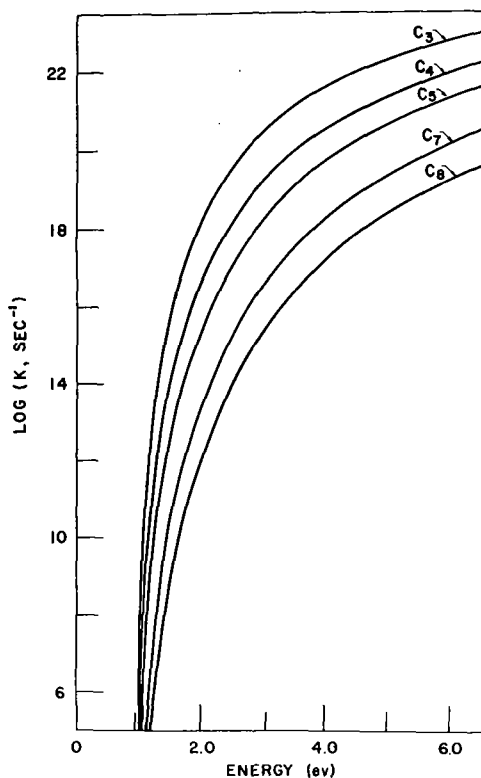


Figure 2. Rate constants calculated for dissociation of several different n-alkyl ions, with an activation energy of 1.0ev.

III. COMPARISON WITH EXPERIMENT

In the present work, two types of experimental data were examined. These are (a) the variation of mass spectra with ionizing voltage and (b) the occurrence of metastable ion peaks. All of the data presented here were obtained with Consolidated Electrodynamics Corporation 21-103 standard mass spectrometers.

A. Patterns

The fragmentation patterns of n-decane, n-pentadecane, and n-eicosane were studied as a function of ionizing voltage, from below the initial onset of ionization up to seventy volts. Some of the data are given in Figs. 4, 5, and 6, where the relative abundances of typical ions (given as per cent of the total observed ion current) are plotted against the ionizing voltage. Throughout the entire voltage range, the relative abundances of different classes of ions are much the same as at seventy volts⁺. The C_nH_{2n+1} ions are always most abundant, but the general behavior is similar for all ions of the same carbon number. Where some carbon numbers have been left off the figures entirely, the curve shapes of the omitted ions do show continuous gradations between the curves that are plotted.

It seems to be a general result that in the spectrum of C_nH_{2n+2} , the curves for C_n^+ ions can be divided into two classes, depending on whether n is greater or less than $N/2$. When $n > N/2$, the relative abundance begins at a maximal value, but decreases rapidly as the ionizing voltage is increased. When $n < N/2$, the curves begin at minimal values, pass through maxima, and attain plateaus. For smaller values of n , the maxima become broader and shift toward higher voltages, until finally, for C_1^+ , C_2^+ , and C_3^+ , the curves do not pass through maxima but just increase over the entire voltage range.

In terms of the postulated model, the gradual changes noted in the curve shapes of Figs. 4-6 can be correlated with the numbers of consecutive dissociations needed to form each species and the number of different paths that result in it. As regards the specific predictions listed at the end of the preceding section, each one may be examined in turn:

1. The first prediction is borne out. The data obtained at very low ionizing voltages are inaccurate, but the curves extrapolate in such a manner that at the onset, the spectra are dominated by ions in the range $N/2 \leq n \leq N-2$.
2. It is obvious that the second expectation is fulfilled.
3. The third prediction is also accurate, as the C_{N-1}^+ ions never account for more than a few hundredths of a per cent of the total ion current.
4. Table III contains a comparison of the curves for several specific fragment ions in Figs. 4-6. Clearly, prediction (4) holds true also.

B. Metastables

When an ion of mass m_1 dissociates to yield an ion of mass m_2 , and the rate constant is in the range of 10^6 sec^{-1} , a "metastable ion peak" is often observed in the spectrum at an apparent mass value of

$$m^* = m_2^2 / m_1. \quad (7)$$

Bloom and coworkers⁴ have already listed numerous observable metastables in the mass spectra of n-paraffins. In the present work, in addition to observing the m^* values, attempts were made to measure the ratio m_2/m_1 , as well, by using a metastable suppressor as a retarding device; this experiment is similar to some measurements described by Hipple et al.¹⁵ Since the available instrument with a heated inlet system does not contain a metastable suppressor, no compounds larger than n-decane have yet been studied. The results obtained for n-nonane and n-decane are shown in Tables IV and V, respectively. In general, the observations and results are the same as those reported by Bloom et al; however, the metastables corresponding to loss of hydrogen alone are not shown in the tables because these reactions are not considered in the present work.

Every assignment made in Tables IV and V corresponds to the loss of a neutral fragment which contains at most half the total number of carbon atoms in the decaying species. This is clearly not in disagreement with the reactions postulated in the assumed model and employed in the sample calculations. It is equally clear, though,

Table V.

SOME OBSERVED METASTABLE PEAKS IN MASS
SPECTRUM OF n-DECANE

m*	Dissociation
89.9	$C_{10}H_{22}^+ (142) \longrightarrow C_8H_{17}^+ (113) + C_2H_5$
70.4	$C_{10}H_{22}^+ (142) \longrightarrow C_7H_{16}^+ (100) + C_3H_6$
63.4	$C_8H_{18}^+ (114) \longrightarrow C_6H_{13}^+ (85) + C_2H_5$
61.6	$C_8H_{16}^+ (112) \longrightarrow C_6H_{11}^+ (83) + C_2H_5$
44.7	$C_8H_{17}^+ (113) \longrightarrow C_5H_{11}^+ (71) + C_3H_6$
50.4	$C_7H_{16}^+ (100) \longrightarrow C_5H_{11}^+ (71) + C_2H_5$
48.6	$C_7H_{14}^+ (98) \longrightarrow C_5H_9^+ (69) + C_2H_5$
33.6	$C_7H_{13}^+ (97) \longrightarrow C_4H_9^+ (57) + C_3H_4$
32.8	$C_7H_{15}^+ (99) \longrightarrow C_4H_9^+ (57) + C_3H_6$
38.3	$C_6H_{13}^+ (85) \longrightarrow C_4H_9^+ (57) + C_2H_4$
36.5	$C_6H_{14}^+ (86) \longrightarrow C_4H_8^+ (56) + C_2H_6$
21.8	$C_6H_{13}^+ (85) \longrightarrow C_3H_7^+ (43) + C_3H_6$
26.0	$C_5H_{11}^+ (71) \longrightarrow C_3H_7^+ (43) + C_2H_4$
24.5	$C_5H_{12}^+ (72) \longrightarrow C_3H_6^+ (42) + C_2H_6$
29.5	$C_4H_9^+ (57) \longrightarrow C_3H_5^+ (41) + CH_4$
27.7	$C_4H_7^+ (55) \longrightarrow C_3H_3^+ (39) + CH_4$
15.3	$C_4H_7^+ (55) \longrightarrow C_2H_5^+ (29) + C_2H_2$

that a metastable peak is not observed for every postulated reaction. One possible reason for the absence of some expected metastables is that in the region of $k \sim 10^6$ sec^{-1} , the rate constants vary extremely rapidly with the excess energy (see Figs. 1 and 2). It is quite possible that, for several competing reactions, extremely small differences in the activation energies and/or transition-complex frequency distributions would cause the relative yields in this energy range to be very unequal, while for larger energies, they would be essentially equal. Additional calculations must be made to confirm or deny this possibility.

IV. DISCUSSION

It has already been mentioned that Chupka and Kaminsky¹⁴ have experimentally measured the $P(E)$ functions [see Eq. (6)] for propane and n-butane molecule-ions. Since they found that these functions could be approximated on the basis of simple molecular orbital treatments, it is instructive to consider the required $P(E)$ functions for some larger molecules.

In the seventy-volt spectrum of n-decane, the experimental yields of C_8 , C_7 , C_6 , C_5 , C_4 , and C_3 ions are in the ratios¹ of 0.051:0.091:0.266:0.407:1.0:1.55. On comparing these numbers with the breakdown curves of Fig. 3, it is seen that the energy distribution function is required to have a maximum in the region of 3-4 ev, and also it must decrease quite rapidly at both higher and lower energies. In the case of n-eicosane, it is estimated that the corresponding maximum must occur in the region of 10 ev.

The molecular orbitals employed by Chupka and Kaminsky were linear combinations of equivalent bond orbitals, as originally derived by Lennard-Jones and Hall. It is recalled that the latter authors made several attempts to calculate the ionization potentials of n-paraffins, and found it was impossible to decide whether the first ionization occurs from a "symmetric" or an "antisymmetric" molecular orbital¹⁶⁻¹⁸. Whichever was assumed to be the case, it was possible to evaluate certain of the equivalent orbital interaction parameters by fitting a set of observed ionization potentials; however, an additional number of parameters were completely undetermined. One set of molecular orbital energy levels can be calculated from the determined parameters, but the other energy levels are not known.

In Figs. 7 and 8 are shown the energy levels calculated according to the two alternative assumptions for n-butane, n-decane, and n-eicosane ions. Fig. 7 is based on the assumption that the lowest ionization potential is for a symmetric molecular orbital, and Fig. 8 corresponds to the other case. In both figures, the energies shown are those above the minimum ionization potential, and the height of each line is proportional to the effective degeneracy of the energy level. In the former case, the quantity (a-b) is undetermined. The value indicated for it is a maximum, and the energies of the antisymmetric molecular orbitals are shown as degenerate on the figure. When the other assumption is made, both (a+b) and c, are unknown. The value shown for (a+b) is a minimum value, and that of c is the one found most appropriate for propane and butane by Chupka and Kaminsky. Here, the undetermined energy levels are shown as two groups of degenerate ones centered at (a+b) and c. In both figures, the quantity X is undetermined; it is responsible for two states that are neglected in the equivalent orbital treatment; and again, the value shown for it is that recommended by Chupka and Kaminsky. In both cases, the values used for the "known" parameters are the same ones found appropriate by Lennard-Jones and Hall, and employed by Chupka and Kaminsky.

It is tempting to try to relate the requisite maxima in the $P(E)$ functions to the high level density evident for the symmetric molecular orbitals in Fig. 7. However, neither Fig. 7 nor Fig. 8 provides an energy level distribution that is compatible with the required $P(E)$ functions for decane and eicosane. If a choice must be made between the "symmetric" and "antisymmetric" assumptions, the latter must be preferred in the present case. It is quite possible here that the undetermined energies of the symmetric molecular orbitals could bunch together at an energy considerably higher than the 1.6-1.7 ev obtained in Fig. 7. Thus, the situation for n-decane looks very reasonable. On the other hand, this high level density will definitely not shift from 3-4 ev in decane to 10 ev in n-eicosane.

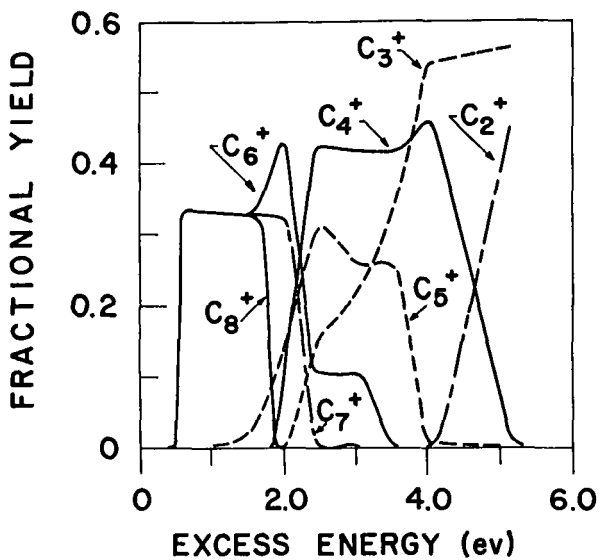


Figure 3. Breakdown curves calculated for n-decane.

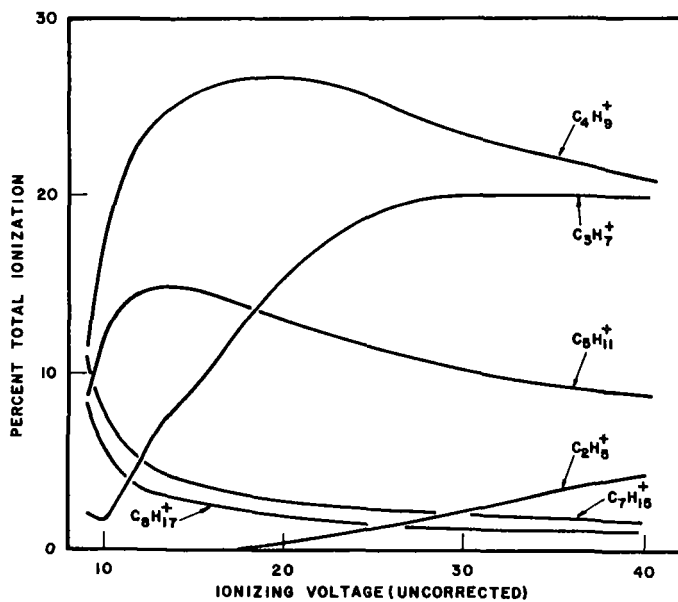


Figure 4. Typical data showing the variation of the fragmentation pattern with ionizing voltage for n-decane.

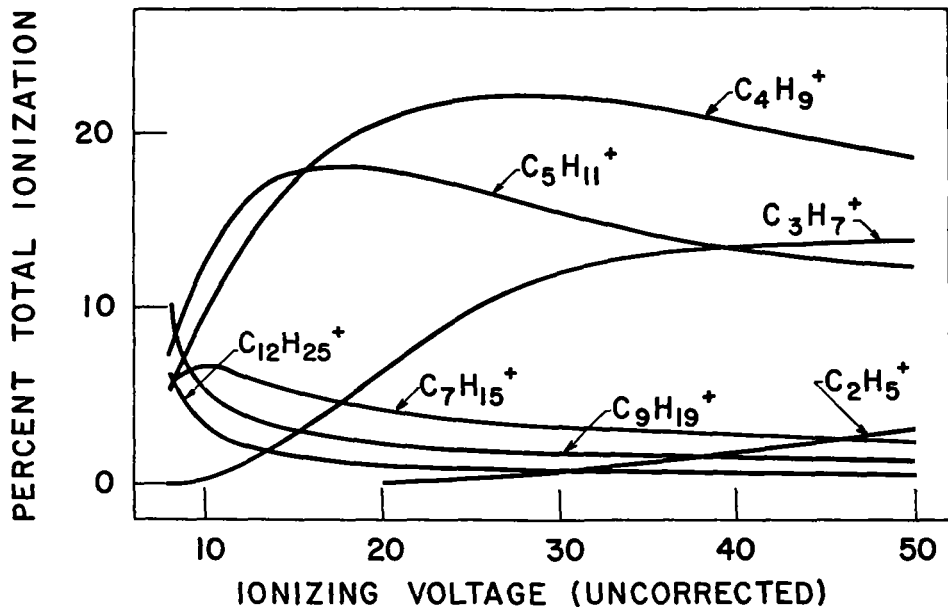


Figure 5. Typical data showing the variation of the fragmentation pattern with ionizing voltage for n-pentadecane.

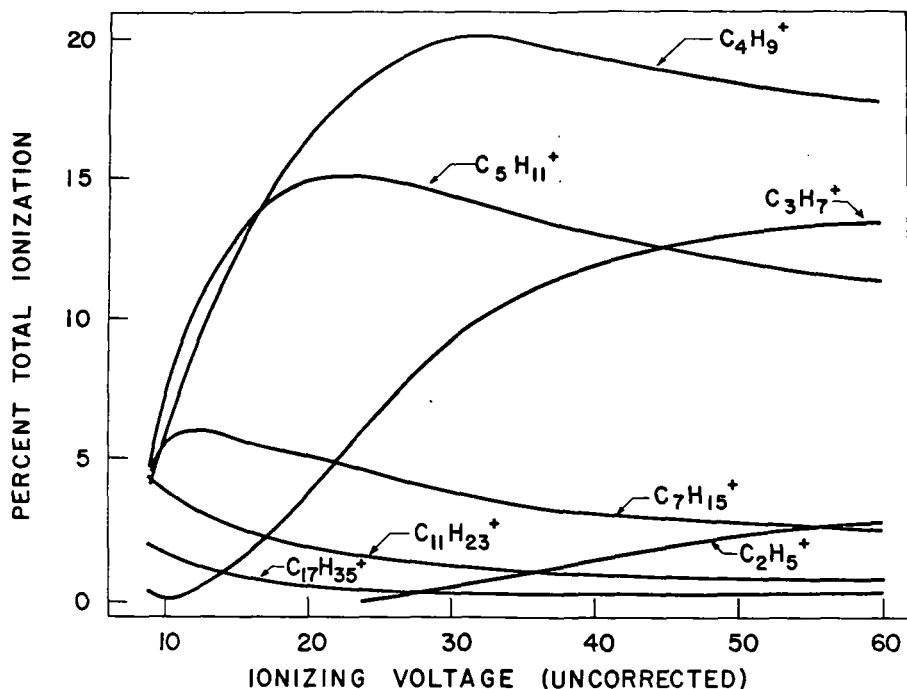


Figure 6. Typical data showing the variation of the fragmentation pattern with ionizing voltage for n-eicosane.

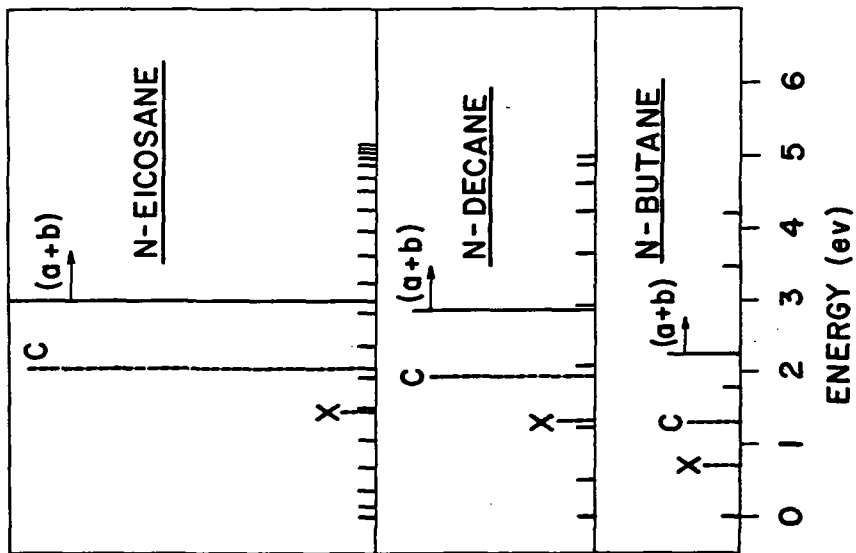


Figure 8. The energy levels of the antisymmetric molecular orbitals for several paraffins. The undetermined symmetric levels are shown as two groups of degenerate ones at $(a+b)$ and c .

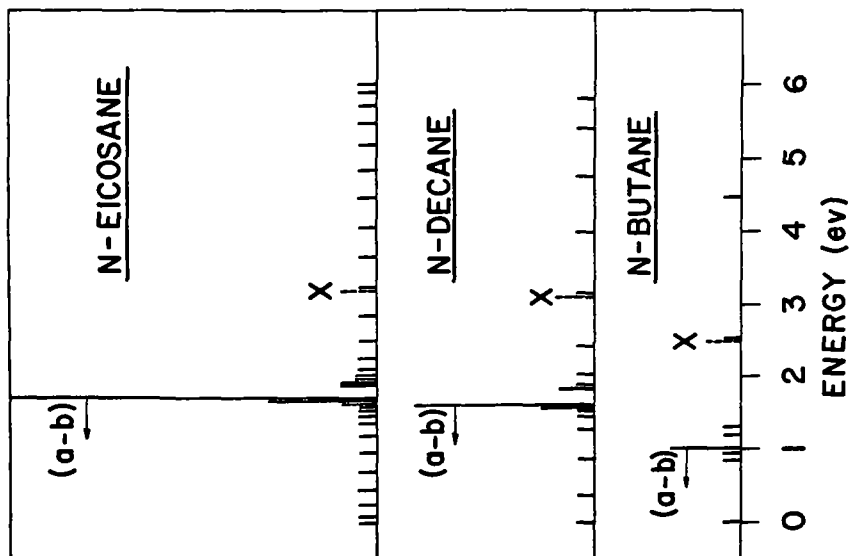


Figure 7. The energy levels of the symmetric molecular orbitals for several paraffins. The undetermined antisymmetric levels are shown as degenerate at $(a-b)$.

Some of the possible reasons for the discrepancies found here are:
(a) the Lennard-Jones and Hall energy levels are not appropriate; (b) the activation energies employed in the calculations are too high; and (c) the whole model applied here is in error. None of these possibilities can presently be singled out as the correct one.

Another difficulty arises when one considers the data of Beynon *et al.*² on ¹³C-labeled molecules. Inasmuch as nothing was said to the contrary, it was tacitly assumed in the above treatment that during each dissociation an ion may lose a neutral fragment from either of its ends with equal facility. However, such a picture is not capable of explaining the results of Beynon *et al.*². Although it presently appears that agreement can be obtained by slightly modifying the model, this problem will not be considered in detail at this time.

Future work to either confirm or deny the appropriateness of the model suggested here must include: further experimental and computational study of metastable peak intensities; experimental determinations of internal energy distributions in larger molecules; and inclusion of rearrangement processes in the calculations. Based on the necessarily qualitative considerations given in this paper, it can be concluded that the proposed model is reasonable in many respects. It is at least clear that the statistical theory is capable of interpreting the mass spectra of n-paraffins.

V. ACKNOWLEDGMENTS

The author is grateful to Dr. N. D. Coggeshall for numerous discussions, to Mr. J. P. Klems and Mr. H. T. Best for their experimental assistance, and to Professor A. L. Wahrhaftig for sending a preprint.

REFERENCES

1. N. D. Coggeshall, J. CHEM. PHYS. **33**, 1247 (1960).
2. J. H. Beynon, R. A. Saunders, A. Topham, and A. E. Williams, J. PHYS. CHEM. **65**, 114 (1961).
3. H. M. Rosenstock, M. B. Wallenstein, A. L. Wahrhaftig, and H. Eyring, PROC. NATL. ACAD. SCI. U.S. **38**, 667 (1952).
4. E. G. Bloom, F. L. Mohler, J. H. Lengel, and C. E. Wise, J. RES. NATL. BUR. STDS. **40**, 437 (1948); E. G. Bloom, F. L. Mohler, C. E. Wise, and E. J. Wells, *ibid.* **43**, 65 (1949).
5. R. D. Brown, J. CHEM. SOC. **1953**, 2615.
6. T. L. Cottrell, The Strengths of Chemical Bonds (Academic Press, Inc., New York, 1954).
7. R. E. Honig, J. CHEM. PHYS. **16**, 105 (1948).
8. D. J. Clancy and G. F. Crable, Personal communication.
9. D. P. Stevenson, DISC. FARADAY SOC. **10**, 35 (1951); TRANS. FARADAY SOC. **49**, 867 (1953).
10. B. Steiner, C. F. Giese, and M. G. Inghram, J. CHEM. PHYS. **34**, 189 (1961).
11. J. C. Schug and N. D. Coggeshall, J. CHEM. PHYS. **35**, 1146 (1961).
12. M. Vestal, A. L. Wahrhaftig, and W. H. Johnston, Paper No. 19 at the meeting of ASTM E-14, Mass Spectrometry, at Chicago, Ill. (June 1961).
13. G. Herzberg, Infra-red and Raman Spectra (D. VanNostrand Book Co., New York, 1945), pp. 344, 361.
14. W. A. Chupka and M. Kaminsky, J. CHEM. PHYS. **35**, 1991 (1961).
15. J. A. Hipple, R. E. Fox, and E. W. Condon, PHYS. REV. **69**, 347 (1946).
16. G. G. Hall, PROC. ROY. SOC. (London) **A205**, 541 (1951).
17. J. Lennard-Jones and G. G. Hall, TRANS. FARADAY SOC. **48**, 581 (1952).
18. G. G. Hall, TRANS. FARADAY SOC. **50**, 319 (1954).

APPLICATION OF THE IMPROVED QUASI-EQUILIBRIUM THEORY TO PROPANE⁽¹⁾

Marvin L. Vestal
Austin L. Wahrhaftig⁽²⁾
Wm. H. Johnston

We have recently completed some extensive calculations on the unimolecular decomposition of propane. These calculations were based on the quasi-equilibrium theory originally developed by Rosenstock, et al (1) but used the improved method for counting the states of a collection of harmonic oscillators which we presented at the E-14 Committee Meeting last year in Chicago (2, 3). The calculations were done on the IBM 7090 at Wright-Patterson AFB. We wish to express our appreciation to the Air Force Aeronautical Research Laboratory for support of this work and to Dr. Jean Futrell for his assistance in running the computer calculations.

The rate equation derived in the original development of the quasi-equilibrium theory using the classical approximation, is given by

$$k(E) = Z \left(\frac{E - \epsilon_0}{E} \right)^{N-1} \quad (1)$$

where E is the total energy in the molecule ion, ϵ_0 the activation energy, N the number of oscillators, and Z the frequency factor. Since the original development of this rate equation, a number of investigators have found serious quantitative disagreement between the prediction of the theory, using equation (1), and experiment. We recently developed a more accurate method for enumerating the states of a collection of non-identical harmonic oscillators, which when used in the quasi-equilibrium theory, results in equation (2) as the rate expression.

$$k(E) = \tilde{\nu} \frac{\sum_{Q=1}^{N-1} \binom{N-1}{Q} \frac{1}{Q!} \left[\frac{E - \epsilon_0}{h\tilde{\nu}^\ddagger} \sigma_Q^\ddagger - \frac{Q-1}{2} \right]^Q}{\sum_{P=1}^N \binom{N}{P} \frac{\sigma_P}{(P-1)!} \left[\frac{E}{h\tilde{\nu}} \sigma_P - \frac{P-1}{2} \right]^{P-1}} \quad (2)$$

$$\sigma_P = \left[\prod_{i=1}^P \frac{\tilde{\nu}}{\nu_i} \frac{\tilde{\nu}}{\nu_j} \dots \frac{\tilde{\nu}}{\nu_m} \right]^{1/P}$$

Here E , ϵ_0 , and N are the same as before and $\tilde{\nu}$ is the geometric mean frequency. σ_P , a dimensionless factor of order unity, is the ratio of the mean frequency to the arithmetic mean of the products of the reciprocals of the molecular frequencies taken P at a time. The daggers (\ddagger) denote similar quantities for the activated complex configuration.

For these calculations we have considered activated complex configuration in which some of the degrees of freedom are represented as free rotors. For these cases, the improved rate expression takes the form

(1) Work performed at the William H. Johnston Laboratories, Inc., Baltimore, Md., and was supported by U. S. Air Force Contract AF 33(616)-7638.

(2) University of Utah and William H. Johnston Laboratories, Inc.

TABLE I. ACTIVATION ENERGIES

Reaction	ϵ_0	Δ A. P.
$C_3H_8^+ \longrightarrow C_2H_5^+$	0.79	$1.0 \pm .3$
$C_3H_8^+ \longrightarrow C_2H_4^+$	0.58	$0.5 \pm .3$
$C_3H_8^+ \longrightarrow n-C_3H_7^+$	1.34	$1.4 \pm .2$
$C_3H_8^+ \longrightarrow s-C_3H_7^+$	0.52	$0.5 \pm .2$
$C_3H_8^+ \longrightarrow C_3H_6^+$	0.60	$1.0 \pm .2$
$C_2H_5^+ \longrightarrow C_2H_3^+$	3.5	$4.0 \pm .4$
$C_2H_4^+ \longrightarrow C_2H_2^+$	3.3	$3.3 \pm .4$
$C_3H_7^+ \longrightarrow C_3H_5^+$	2.7	$2.8 \pm .3$
$C_3H_6^+ \longrightarrow C_3H_4^+$	4.0	$3.6 \pm .3$
$C_3H_5^+ \longrightarrow C_3H_3^+$	6.0	—

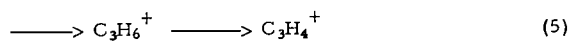
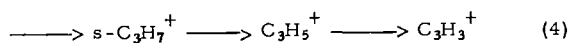
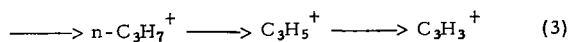
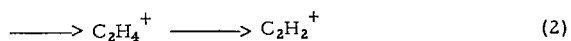
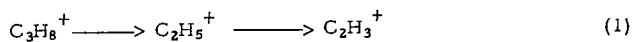


Figure 1. Simplified Reaction Scheme Used For Propane Calculation.

$$K(E) = \tilde{\nu} \left(\frac{\pi h \tilde{\nu}^\ddagger}{\tilde{B}^\ddagger} \right)^{\frac{L^\ddagger}{2}} \frac{\sum_{Q=1}^{\infty} \binom{N-L^\ddagger-1}{Q} \frac{1}{Q} \Gamma(Q + \frac{L^\ddagger}{2} + 1) \left[\frac{E - \epsilon_0}{h \tilde{\nu}^\ddagger} \sigma_Q^\ddagger - \frac{Q-1}{2} \right]^{Q + \frac{L^\ddagger}{2}}}{\sum_{P=1}^{\infty} \binom{N}{P} \frac{\sigma_P}{(P-1)!} \left[\frac{E}{h \tilde{\nu}} \sigma_P - \frac{P-1}{2} \right]^{P-1}} \quad (3)$$

where L^\ddagger is the number of free rotors in the activated complex configuration, N is the total number of degrees of freedom, and \tilde{B}^\ddagger is the geometric mean rotational energy constant.

For applying the theory to subsequent fragmentation of the primary ionic fragments, it is necessary to consider the distribution of the initial excitation energy between charged and neutral fragments. If we assume that all states within an energy shell between E and $E + dE$ are equally probable, then the probability that sufficient energy is contained in the charged fragment for the secondary fragmentation to occur is given by

$$P(E) = \frac{\int_{\epsilon_2}^{E-\epsilon_1} \rho_1(\epsilon) \rho_2(E - \epsilon_1 - \epsilon) d\epsilon}{\int_0^{E-\epsilon_1} \rho_1(\epsilon) \rho_2(E - \epsilon_1 - \epsilon) d\epsilon} \quad (4)$$

where E is the total excitation of the parent molecule-ion, ϵ_1 is the activation energy for the primary reaction, ϵ_2 is the minimum energy required in the charged fragment for the secondary reaction to be observable, $\rho_1(\epsilon) d\epsilon$ is the number of states of the charged fragment with energy between ϵ and $\epsilon + d\epsilon$, and $\rho_2(\epsilon) d\epsilon$ is the corresponding number of states for the neutral fragment. The minimum energy ϵ_2 for the secondary reaction to be observed is found by calculating the rate for the reaction as a function of energy using the improved rate equation and finding the energy at which this rate exceeds some selected minimum. For these calculations, we used 10^6 sec^{-1} as the minimum observable rate.

In these calculations we have also considered the effects of the temperature in the ion source on the fragmentation pattern. In these calculations we have made the following assumptions:

1. The internal energy of the molecule-ion is the sum of the internal thermal energy of the molecule and the energy added by the ionization process.
2. The probability of adding a given energy by the ionization process is independent of the thermal energy of the molecule.

This is equivalent to assuming that the ionization potential is unaffected by the temperature of the molecule, and that the probability of forming an ion with less vibrational excitation than the molecule from which it was formed is zero. It is well-known that the situation is really much more complex than this and these assumptions are certainly not valid for electron energies near threshold.

The simplified reaction scheme used for these calculations is shown in Figure 1. This is essentially the same reaction scheme used in previous calculations on propane by Wahrhaftig and co-workers (4). The activation energies assumed for these reactions

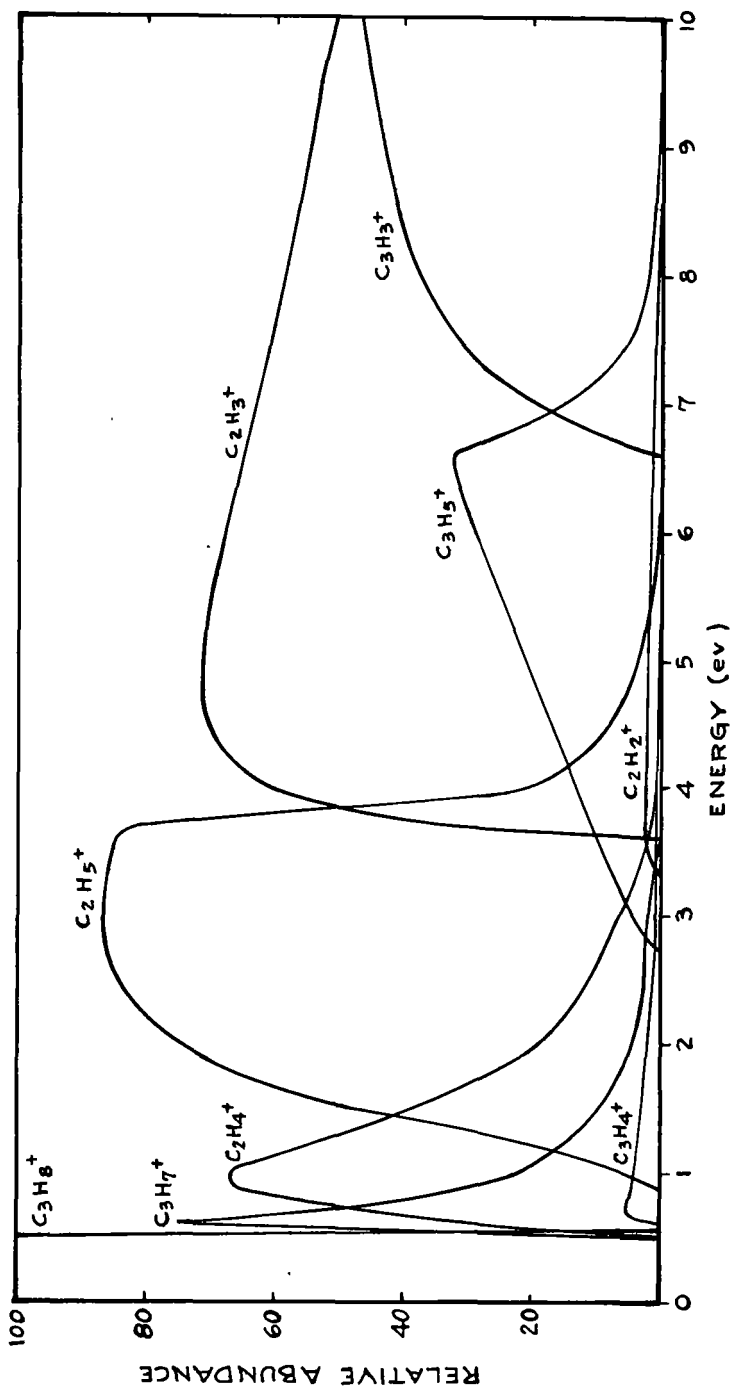


FIG.2 - CALCULATED BREAKDOWN GRAPH FOR PROPANE

are shown in Table I where they are compared with differences in appearance potentials as given in Field and Franklin (5). For all of the more abundant reactions, the appearance potentials used are within the range of error of the experimental values as determined from differences in appearance potentials. The activated complex configurations used in the calculations were similar to those used by Kropf, Eyring, Wahrhaftig, and Eyring (4) except that: no free rotations were assumed for the normal state, two free rotations for the activated complexes leading to the formation of $C_2H_5^+$ and $n-C_3H_7^+$, one free rotation for $C_2H_4^+$, and none for $S-C_3H_7^+$ and $C_3H_6^+$.

The calculated breakdown graph for propane is shown in Figure 2. Here we have plotted calculated relative abundance of the ions versus internal energy in the parent molecule ion. The rather long tails on some of the decaying fragment ions is a result of the fluctuation of energy between charged and neutral fragments. We are fortunate in having the breakdown curves of Chupka and Kaminsky (6) with which to compare these results. The experimental measurement is slightly smeared as a result of the energy spread in the electron beam and the thermal energy of the molecule. In order to have a more direct comparison of the calculated results with the experimental curves, it is necessary to include these effects in the calculations by averaging the calculated curves over suitable energy distributions. For the electron energy distribution we assumed a $2500^\circ K$ Boltzmann distribution. The effect of temperature was included by averaging the calculated distribution over the internal thermal energy distribution for the molecules at $600^\circ K$. The breakdown curves resulting from averaging over both the electron energy distribution and the internal thermal energy distribution are shown in Figure 3. At the top are Chupka and Kaminsky's experimental breakdown curves and at the bottom our calculated breakdown curves.

Overall the agreement between the two results is quite acceptable. Small discrepancies, such as the lower abundance of $C_2H_2^+$ ion in the calculations, probably result from the use of the simplified reaction scheme.

One difference which appears significant, however, is the rather long tail on the parent ion curve in the experimental result. There seems to be no way to account for this tail on the basis of direct ionization and complete energy randomization. Thus, it appears that this discrepancy may indicate either autoionization, in which case the second derivative curve would be distorted due to a different threshold law for this process, or it may indicate incomplete vibrational energy randomization in which case all of the energy is not available to the fragmentation process. This point should be investigated further.

Calculations on the variation of the propane mass spectrum with electron energy and with temperature have also been completed. The results of these calculations together with a more detailed discussion of the methods employed will be published elsewhere.

REFERENCES

1. Rosenstock, Wallenstein, Wahrhaftig, and Eyring, Proc. Nat. Acad. Sci. U.S. **38**, 667 (1952).
2. Vestal, Wahrhaftig, and Johnston, "An Improved Integral Approximation in the Quasi-Equilibrium Theory of Mass Spectra", presented at the ninth annual meeting of the ASTM Committee E-14 on Mass Spectrometry, June 6, 1961.
3. Wahrhaftig, Vestal, and Johnston, "The Application of the Improved Integral Approximation to the Quasi-Equilibrium Theory of Mass Spectra", presented at ninth annual meeting of the ASTM Committee E-14 on Mass Spectrometry, June 6, 1961.
4. Kropf, Eyring, Wahrhaftig, and Eyring, J. Chem. Phys. **32**, 149 (1960).
5. Field and Franklin, Electron Impact Phenomena, Academic Press, New York, 1957.
6. Chupka and Kaminsky, J. Chem. Phys. **35**, 1991 (1961).

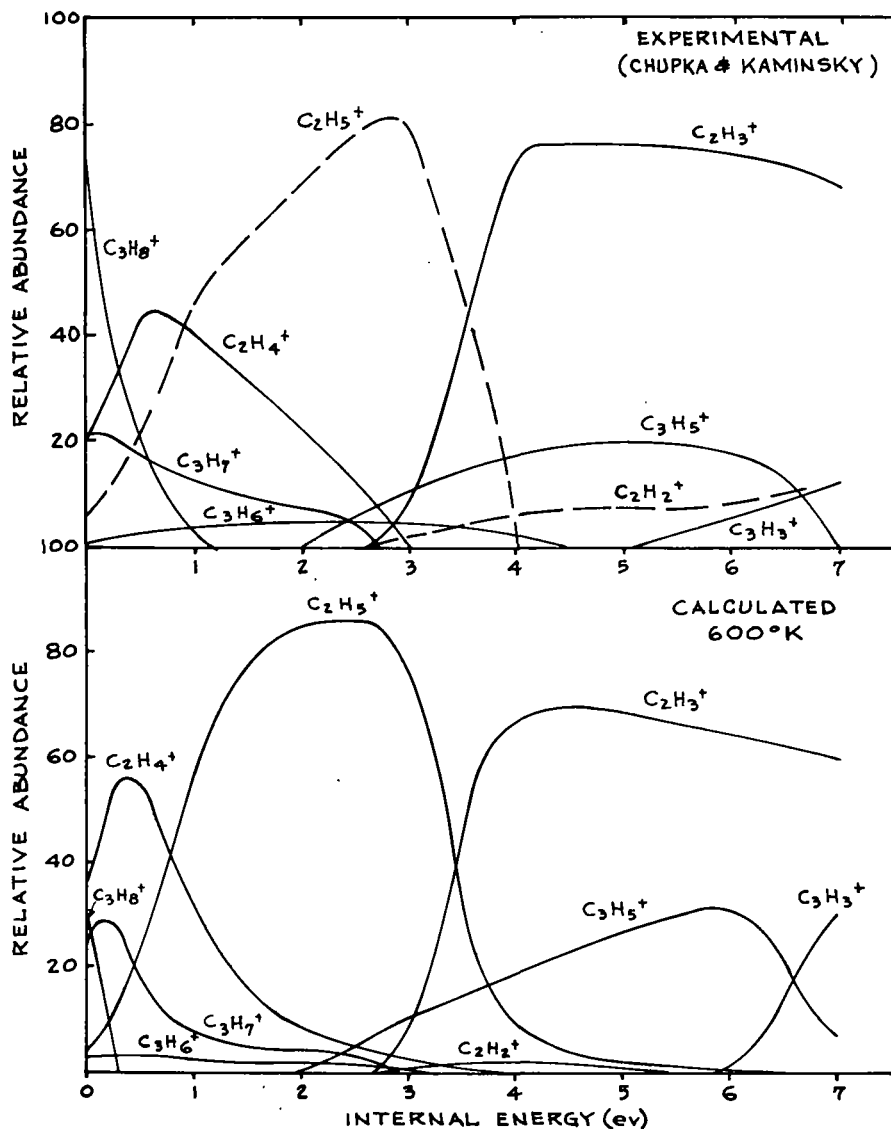


FIG. 3 COMPARISON OF EXPERIMENTAL AND CALCULATED PROPANE BREAKDOWN GRAPHS.

STUDIES OF METASTABLE ION TRANSITIONS WITH A 180° MASS SPECTROMETER

Norman D. Coggeshall
Gulf Research & Development Co.
Pittsburgh 30, Pa.

Abstract

The decay of metastable ions through transitions giving an ionized fragment and a neutral radical has been investigated with a 180° mass spectrometer. Four aspects of the main problem have been studied. These are: a) the decay of metastable ions within the ion source to produce a continuous distribution of "metastable ions"; b) an examination of the mathematical conditions relating dissociation beyond the ion source exit slit to the formation of a "metastable" peak, to the shape of such a peak, to the cut-off imposed by the analyzer walls and to the length of travel during which detectable dissociation may occur; c) an examination of the conditions for determining lifetimes with a 180° instrument and d) a consideration of the elements leading to the broadness of metastable peaks.

The distribution function resulting from dissociation within the source drops very rapidly and is ordinarily hidden within the peak due to the daughter ion. The formation of a metastable peak in a 180° instrument results from a low-order dependence of where the ion fragment resulting from dissociation hits the focal plane on the position of dissociation beyond the exit slit. The cut-off mass due to ions striking the walls of the analyzer tube may be readily calculated. In a CEC Model 21-103 instrument there is adequate distance of free travel beyond the exit slit to allow the instrument to be used for lifetime measurements. Using repeller voltages up to 120 volts, shorter lifetimes than those previously reported have been observed. For the $m^* = 31.9$ metastable peak from n-butane, for example, there is evidence that the metastable ions are created in at least three classes, each with its own lifetime. The shortest lifetime observed was of the order of 9×10^{-8} second. Evidence has been obtained to indicate that the broadness of the observed metastable peaks is probably the result of the perturbation of focussing conditions by the increased angular spread in the ion beam.

Introduction

The existence and interpretation of ions arising from the dissociation of metastable ions are of great importance in constructing a theory of mass spectra. The present report gives some results from a quantitative examination of metastable transition ions as observed in a 180° mass spectrometer. The ions resulting from the dissociation of metastable ions are usually observed at non-integral mass units. For simplicity these peaks will be referred to as metastable ion peaks and the mass in each case will be referred to as the metastable mass. The relationship between the metastable mass, the mass of the metastable ion from which it originates, and the mass of the dissociation fragment bearing the charge was first given by Hipple and Condon¹.

Unless otherwise stated, all data examined were determined with Consolidated Electrodynamics Corporation Model No. 180° mass spectrometers, equipped with Isatron ion sources. In some cases, a metastable suppressor was used. Slit widths and electrode separations utilized were those normally used and recommended by the manufacturer.

Dissociation of Metastable Ions Within the Ion Source

Let us denote by n_0 the total number of ions of mass m created per unit area in the electron beam. We shall assume that a fraction of these are created in a metastable state with a decay constant λ . We denote by m_1 the mass of the charged fragment resulting from dissociation. The apparent mass possessed by these ions when collected at the detector, otherwise referred to as the metastable mass, is denoted by m^* . The geometry and symbols used for the ion source are given in Fig. 1. Here, the electron beam passes through the ionization region approximately one-half way between the repeller and the first slit. Ions will reach the first slit at a time t_1 after being formed and with a potential of V_1 . Ions will reach the second slit at a time t_2 after passing through the first slit and with a total potential of $V = V_1 + V_2$.

¹J. A. Hipple and E. U. Condon, Phys. Rev. 68, 54 (1945).

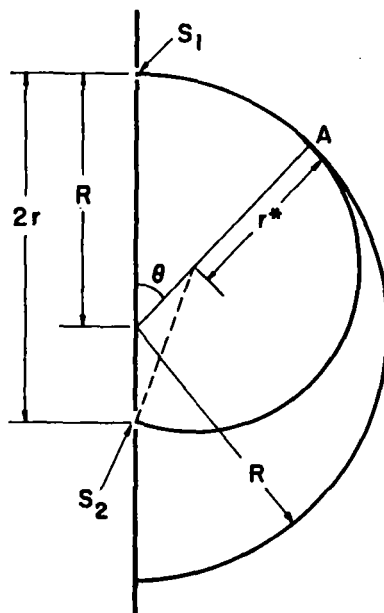


FIG. 2. Geometrical conditions required for a fragment ion to be collected at the detector.

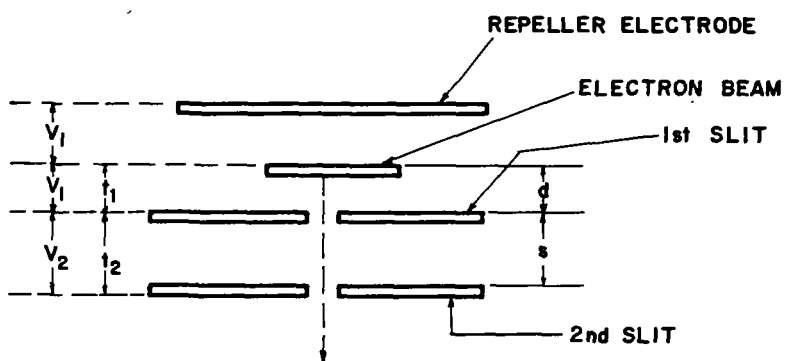


FIG. 1. Schematic ion source geometry and symbols.

The focussing conditions in a 180° instrument are given by

$$mV = r^2 eH^2 / (2c^2) \quad (1)$$

where r is the radius of curvature in cm., e is the charge of the electron in e.s.u., H is the magnetic field in gauss, and c is the velocity of light in cm./sec. The potentials used in Eq. (1) must be in e.s.u. The apparent mass of a metastable ion is calculated by inserting in Eq. (1) the value of V at which it is observed and calculating for m^* .

Metastable ions which dissociate immediately upon creation will yield normal ions of mass m_1 . Metastable ions which dissociate at the exit slit will yield ions of the usual apparent mass m^* given by

$$m^* = m_1^2 / m \quad (2)$$

Metastable ions dissociating between the plane of the electron beam and the exit slit will appear at apparent masses lying between m_1 and the m^* of Eq. (2). It is the purpose of this section to derive the distribution function for these metastable ions as a function of m^* .

Let us consider a metastable ion created at $t=0$ in the electron beam. Let us further consider the case wherein this ion dissociates at a time t before the ion has passed out of the source. The m_1^+ ion emerging from the exit slit will have an equivalent potential V_e which will be less than the instrument potential $V = V_1 + V_2$. When V_e is equal to the potential which normally focusses normal ions of mass m_1 , the m_1^+ ion resulting from dissociation of a metastable ion will be collected and will have an apparent mass m^* derived from Eq. (1). As will be seen later, we may calculate V_e as a function of t and invert the function to evaluate t in terms of V_e . This, in turn, may be transformed to provide t as a function of m^* , i.e., $t = t(m^*)$.

The number of metastable ions which dissociate in the interval between t and $t + \Delta t$ and which can be collected by the detector will be given by

$$f(m^*) dm^* = \lambda A n_0 e^{-\lambda t} dt \quad (3)$$

where $f(m^*)$ is the intensity distribution function for the number of ions from metastable transitions as a function of m^* , and A is a collection and transmission factor which relates the number of ions issuing from the exit slit to the internal geometry and discrimination of the source.

Using $t = t(m^*)$ we transform Eq. (3) to

$$f(m^*) dm^* = \lambda A n_0 e^{-\lambda t(m^*)} \frac{dt}{dm^*} dm^*$$

from which we may express $f(m^*)$ as

$$f(m^*) = - \frac{d}{dm^*} A n_0 e^{-\lambda t(m^*)} \quad (4)$$

The exact evaluation of $t(m^*)$ for a 180° instrument would be based on the equations of cycloidal motion.² However, for the sake of tractability we shall ignore the magnetic field. For large values of V_1 (one-half the repeller voltage) this will be a good approximation, whereas for low values of V_1 , it will be very poor. We shall also assume uniform electric fields between the repeller electrode and the first slit and between the first and second slits. This ignores the field penetration through the first slit but it would be impossible to account for it in a simple analytical treatment. The above approximations dictate that numerical results calculated from the following treatment should only be used to establish the qualitative and semi-quantitative nature of the behavior.

Let us first consider a metastable ion which dissociates before the first slit at time t ($0 \leq t \leq t_1$) where t_1 is the time it takes an ion of mass m to reach the first slit. We shall use the common operating conditions such that V_1/V_2 is constant so that $V_1 = d_1 V$ and $V_2 = d_2 V$, $d_1 + d_2 = 1$. Applying the equations of motion to a charge particle in a uniform field, we find

²N. D. Coggeshall, Phys. Rev. 70, 270 (1946).

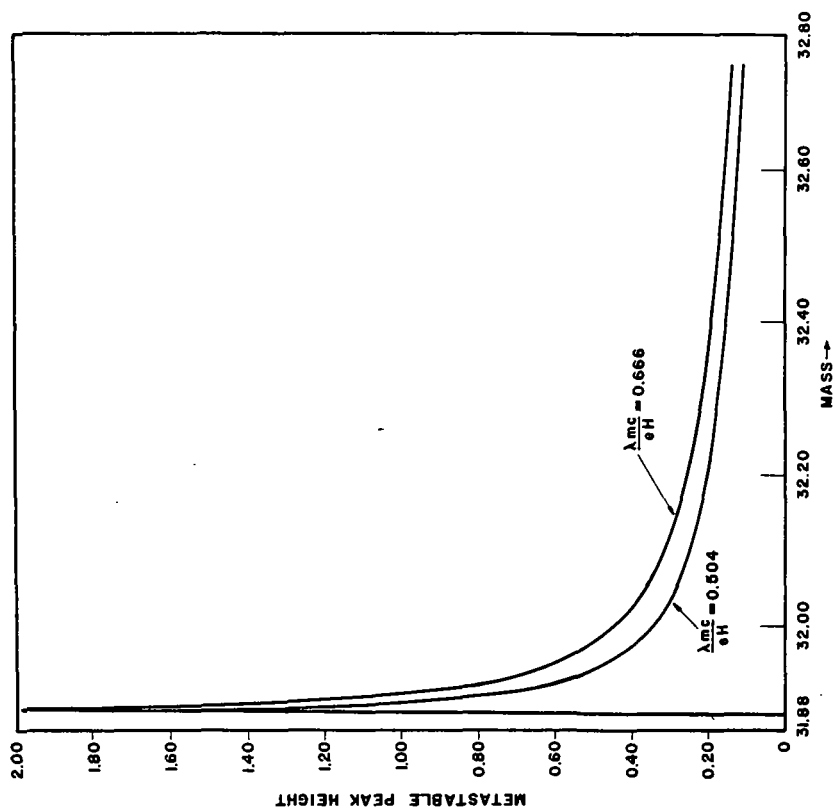


FIG. 3. Computed shapes of the peaks from metastable ions for $m^* = 31.9$ shown for two different parameter values.

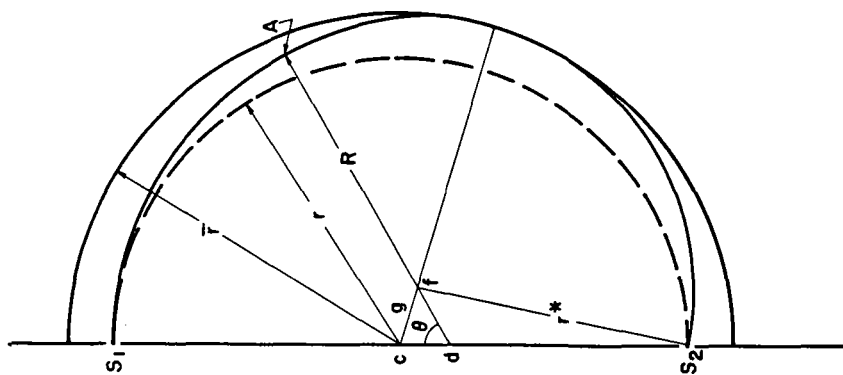


FIG. 4. Geometrical conditions representing cut-off conditions for fragment ions reaching the detector.

$$\frac{m_1 v^2(2)}{2} = e \left\{ V - \left(\frac{m-m_1}{m} \right) \frac{e d_1^2}{2m d^2} v^2 t^2 \right\} \quad (5)$$

where $v(2)$ is the velocity of the charged fragment resulting from the dissociation as it emerges from the second slit. If this ion is collected at the detector, it will appear at a mass m calculated from Eq. (1) by inserting the total instrument accelerating voltage V . We may use this with Eq. (1) to get

$$m^* V = \frac{H^2 e r^2}{2c^2} = \frac{m_1}{e} \left(\frac{m_1 v^2(2)}{2} \right) \quad (6)$$

This allows us to replace the $m_1 v^2(2)/2$ term and the V and v^2 terms in Eq. (5) as functions of m^* . When this is done and the resulting equation solved for t , we get

$$t = \left\{ (m_1 m^* - m^{*2}) / a_1 a_2 m_1 d_1^2 \right\}^{1/2} \quad (7)$$

where $a_1 = H^2 e r^2 / 2c^2$ and $a_2 = \left(\frac{e}{2m d^2} \right) \left(\frac{m-m_1}{m} \right)$

We may evaluate t_1 as

$$t_1 = d \sqrt{\frac{2m}{e d_1 v}}$$

When this is inserted in Eq. (7), we may solve for the m^* (1) which applies to ions dissociating at the first slit. This is given by

$$m^*(1) = m_1 \left\{ 1 - \left(\frac{m-m_1}{m} \right) d_1 \right\} \quad (8)$$

Utilizing Eq. (4), we may then evaluate $f(m^*)$ between m_1 and m^* (1) as

$$f(m^*) = A a n_0 \frac{d}{dm^*} \exp - \lambda \left\{ (m_1 m^* - m^{*2}) / a_1 a_2 m_1 d_1^2 \right\}^{1/2} \quad (9)$$

For the evaluation of $f(m^*)$ corresponding to the dissociation time occurring between t_1 and $t_1 + t_2$, let us denote $t' = t - t_1$. When this is done, we find for $0 \leq t' \leq t_2$ that

$$\frac{m_1 v^2(2)}{2} = \left[\frac{m_1}{m} e V_1 + e V_2 - \frac{e V_2}{s} \left(\frac{m-m_1}{m} \right) \left\{ v(1) t' + \frac{e V_2}{2ms} t'^2 \right\} \right] \quad (10)$$

where $v(1)$ is the velocity of the undissociated metastable ion as it passes through the first slit. We may proceed through the same type steps as used above to transform Eq. (5) to derive an expression relating m^* and t . This is

$$\frac{m^*}{m_1} = \left\{ a_3 - \frac{a_4}{\sqrt{m^*}} - a_5 t^2 - a_6 t \sqrt{m^*} + a_7 m^* \right\} \quad (11)$$

where a_3, a_4, a_5, a_6 and a_7 are constants which may be evaluated in terms of $m, m_1, d, s, d_1, d_2, a$, and a_2 . Eq. (11) is quadratic in t so that it may be solved explicitly in terms of m^* to obtain the $t(m^*)$ function to use in Eq. (4). Using this and Eq. (9), the complete $f(m^*)$ function may be evaluated for the distribution between m_1 and $m_1^{1/2}/m$, of the ions resulting from dissociation within the source.

The $f(m^*)$ function discussed above drops very rapidly in progressing from m_1 to lower masses. When observable at all it is in the form of an asymmetric tailing on the low mass side of the normal fragment peak. This tailing is normally not seen in the peaks from CEC Model 21 instruments used without metastable suppressors. In these the ion source dimensions and normally used values of the d_1/d_2 ratio favor a very sharp drop of the $f(m^*)$ function. However, the ion source geometry and d_1/d_2 ratios effective in the sector type instrument, employed by Hipple, Fox and Condon³, favor a less steep descent of $f(m^*)$ and the low mass asymmetric tailing may be observed in Figs. 1 and 8 of their article.

³J. A. Hipple, R. E. Fox and E. U. Condon, Phys. Rev. 69, 347 (1946).

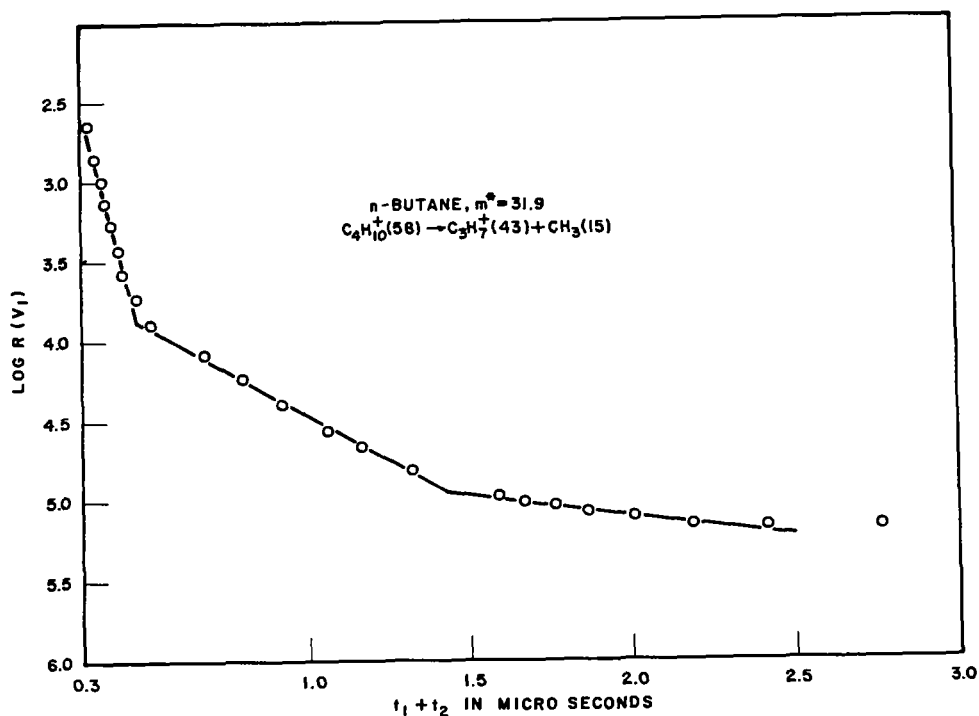


FIG. 5. Data used to determine the lifetimes for the metastable ion transition giving $m^* = 31.9$ for n-butane.

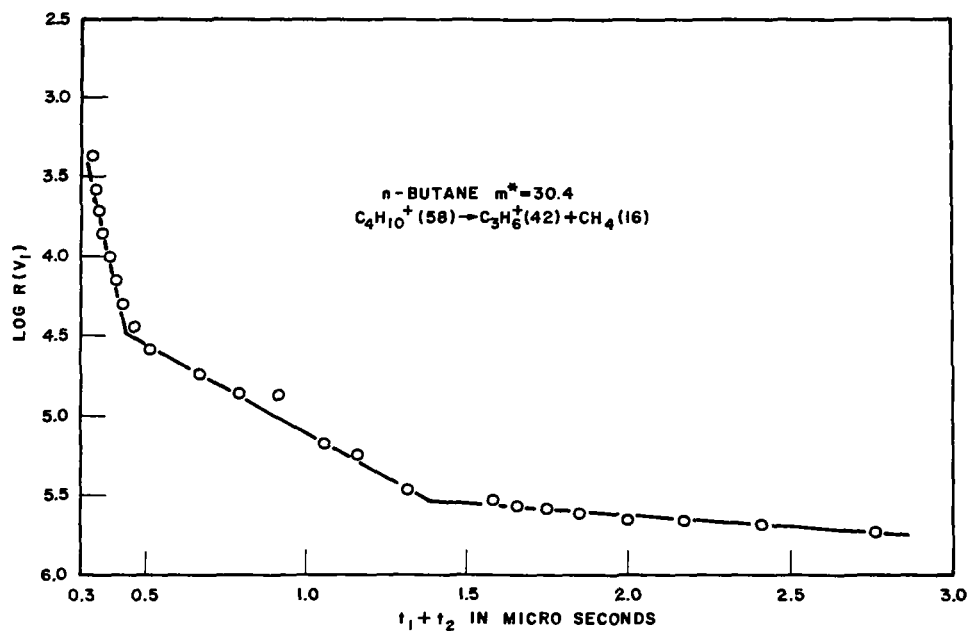


FIG. 6. Data used to determine the lifetimes for the metastable ion transition giving $m^* = 30.4$ for n-butane.

The reason $f(m^*)$ drops so fast is that the metastable ion spends most of its residence time in the ion source in the initial stages of its acceleration and, hence, most of the fragment ions from dissociation of metastable ions in the source will have m^* values so close to m_1 that their contribution cannot be detected. The $f(m^*)$ function cannot be graphically displayed without an arbitrary normalization at some mass value lower than m_1 . This is because the $f(m^*)$ function possesses a singularity at $m^* = m_1$. To appreciate how the major contribution from $f(m^*)$ is hidden within the experimental peak width of the m_1^+ peak, let us consider $C_3H_7^+ (58) \longrightarrow C_3H_7^+ (43) + 15$; $m^* = 31.9$ where m^* designates the normally observed metastable peak mass. We use the representative operating conditions of $V = 1610$ volts, $V_1 = 2$ volts. For these conditions $t_1 = 1.01 \times 10^{-6}$ seconds and $t_1 + t_2 = 1.17 \times 10^{-6}$ seconds. Assuming the metastable ion to have a half life of 2×10^{-6} seconds, we find that 34% of the metastable ions dissociate within the source but that 30% dissociate by the time they reach the first slit. Using the above relation for $m^*(1)$ we therefore find that of the total area under the $f(m^*)$ curve, 88% of it lies within the extremely narrow mass interval (unobservable) between $m_1(43)$ and $0.99996 m_1(43)$.

It would be of value to achieve experimental conditions such that the $f(m^*)$ curve could be unambiguously recognized and measured on the low mass side of the m_1^+ peaks. This could provide further information as to the approximate lifetimes of the metastable states dissociating to particular ions. We may obtain guidance on the physical conditions required by examining the above equations. Since the observations will be in the immediate neighborhood of m_1 , we may express $m^* = m_1 - \Delta m_1$. Ions dissociating as they pass through the first slit will give $\Delta m_1(1)$ calculated from Eq. (8) as

$$\Delta m_1(1) = m_1 d_1 (m - m_1) / m$$

The fraction of the total accelerating voltage, represented by d_1 , which operates behind the first slit, may thus be adjusted to make those ions dissociating at the first slit appear at a Δm_1 value outside the natural width of the m_1^+ peak. If we neglect Δm_1^2 relative to $m_1 \Delta m_1$, we may simplify Eq. (7) to

$$t = (\sqrt{\Delta m_1} / d_1 \sqrt{a_1 a_2})$$

The area under the $f(m^*)$ curve appearing between $\Delta m_1'$ and $\Delta m_1''$ when both are smaller than $\Delta m(1)$ but preferably lying outside the natural peak width will be

$$\int_{\Delta m_1'}^{\Delta m_1''} f(m^*) dm^* = A a n_0 \left\{ \exp - \lambda \left(\sqrt{\Delta m_1'} / d_1 \sqrt{a_1 a_2} \right) - \exp - \lambda \left(\sqrt{\Delta m_1''} / d_1 \sqrt{a_1 a_2} \right) \right\} \quad (12)$$

This area will be increased by decreasing the numerical values of a_1 and a_2 which correspond to reducing the value of $(H^2 r^2)$ and increasing the value of d (see Fig. 1), respectively. It should be remembered that the above derivations are based on the assumption of uniform electric fields, of no magnetic field, and of no field penetration. The latter effect, particularly, will make the above relations useful only for qualitative guidance.

An experimental difficulty that may negate the effects of increasing d_1 is the broadening of the m_1^+ peak as the repeller voltage is increased. This may occur if the effect of increasing repeller voltage is to thicken the electron beam so that ions may be created at points of different potential. The m_1^+ peak may also broaden due to changes in focus conditions. This broadening of the m_1^+ peak may, therefore, completely obscure the $f(m^*)$ contribution.

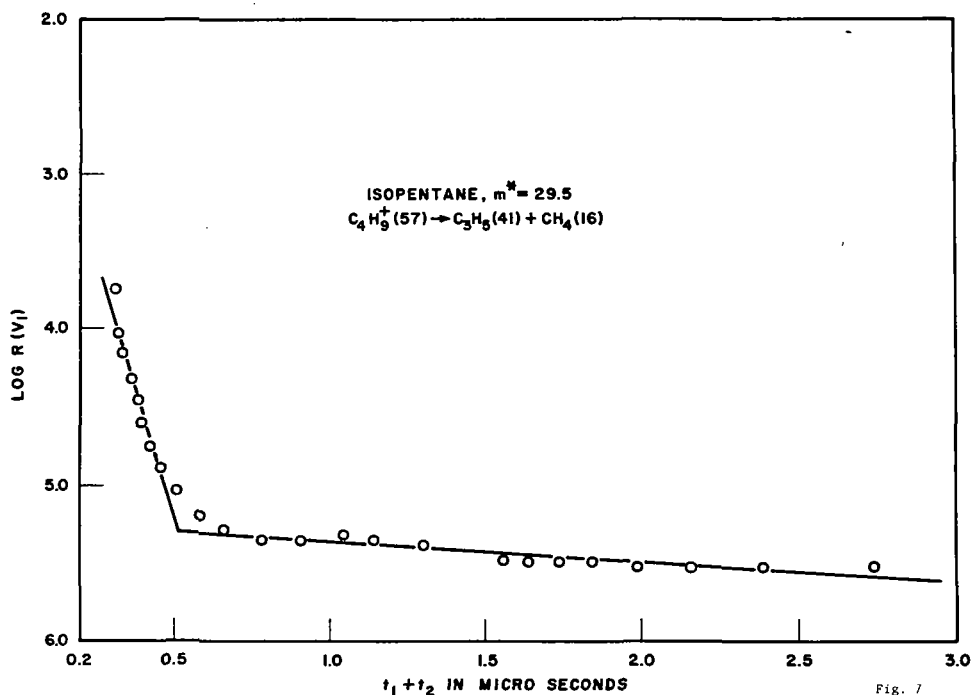


FIG. 7. Data used to determine the lifetimes for the metastable ion transition giving $m^* = 29.5$ for isopentane.

Fig. 7

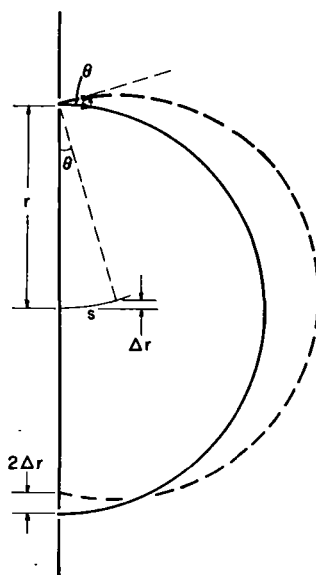


FIG. 8. Schematic diagram of the incremental velocity effect in metastable ion peak broadening.

Dissociation of Metastable Ions Beyond the Ion Source

Ion peaks resulting from the dissociation of metastable ions within the magnetic analyzer region of a 180° instrument would not appear if it were not for a fortuitous mathematical relationship. This is that the lateral displacement with which the fragment ions strike the focal plane has a low order dependence upon the position at which the metastable ion dissociates for some distance beyond the exit slit. This is inherent in the derivation made by Hipple who showed that such a peak should be observed in a 180° instrument.

We may derive, in the same manner as Hipple⁴, the $f(m^*)$ curve for ions resulting from the dissociation of metastable ions past the exit slit in the same general procedure as before. We let $t = 0$ at the exit slit and derive $t = t(m^*)$ for substitution in Eq. (4). Let us refer to Fig. 2 which refers to a 180° instrument. Here, S_1 refers to the exit slit of the ion source and S_2 refers to the entrance slit to the detector. Here, an m^+ ion path has a radius R , the m_1^+ fragment path has a radius r^* , and r is the radius for the paths of ions normally focussed. From the geometry, we see that when a metastable ion dissociates after traversing an angle θ , the conditions for the fragment to be collected dictate that:

$$r^{*2} = (R-r^*)^2 + (2r-R)^2 + 2(R-r^*)(2r-R)\cos\theta \quad (13)$$

To simplify this we may use (from Eq. 1):

$$\frac{m_1^2}{m} \frac{V}{r^{*2}} = \frac{mV}{R^2} = \frac{m^*V}{r^2} = \frac{H^2 e}{2c^2} \quad (14)$$

Denoting $m-m_1 = \Delta m$, this leads to:

$$\cos\theta = \frac{(2\sqrt{m^*}\sqrt{m-2m^*} - \Delta m)}{(2\sqrt{m^*} - \sqrt{m})(\Delta m/\sqrt{m})} \quad (15)$$

We may combine Eq. (15) with results from Eq. (14) to obtain

$$t(m^*) = (mc/eH)\cos^{-1} \frac{2\sqrt{m^*}\sqrt{m-2m^*} - \Delta m}{(2\sqrt{m^*} - \sqrt{m})(\Delta m/\sqrt{m})} \quad (16)$$

Using various results from above we, therefore, have for the distribution function of apparent metastable mass:

$$f(m^*) = Aa n_0 e^{-\lambda(t_1 + t_2)} \frac{d \exp -\lambda \frac{mc}{eH} \cos^{-1} \left\{ \frac{2\sqrt{m^*}\sqrt{m-2m^*} - \Delta m}{(2\sqrt{m^*} - \sqrt{m})(\Delta m/\sqrt{m})} \right\}}{dm^*} \quad (17)$$

In Eq. (17) only the derivative portion of the right-hand side need be considered to define the shape of $f(m^*)$. This is plotted in Fig. 3 for two cases: for $(\lambda mc/eH) = 0.666$ and 0.504 . These correspond to $m^+(58)$ dissociating to $m^+(43) + m(15)$ with half life of 1.5×10^{-6} sec and an impressed magnetic field of 4600 gauss for the first case and with half life of 2.5×10^{-6} sec and an impressed magnetic field of 3300 gauss for the second case. These curves were determined by machine calculation. The calculations thus predict a sharp asymmetric peak which tails off towards higher mass.

Hipple⁴ determined the same type of results to explain the existence of a metastable peak in a 180° instrument. He discussed the effect of baffles, sometimes used in a 180° instrument, which would cut out those ions which are not displaced very far from m_1^2/m . In the CEC instruments used here, there are no baffles between the exit slit of the source and the detector slit. It is, therefore, possible to calculate at what mass there would be a cut-off due to the ions hitting the walls of the analyzer tube. When we examine in detail how this cut-off operates, we find it does so for the ions resulting from dissociation of metastables rather than on the metastable ions before dissociation.

⁴J. A. Hipple, Phys. Rev. 71, 594 (1947).

Referring to Fig. 4, \bar{r} is the radius of the outer inside wall of the analyzer tube and we consider a metastable ion progressing on a circle of radius R until it dissociates at point A. Ordinarily, it would then progress in a circular path of radius r^* unless it encounters interference from the wall. This first occurs for the fragment paths that tangentially encounter the wall. In the figure c is the center of the tube, d is the center of the circle of radius R and f is the center of the circle of radius r^* . Interference occurs when the distance g between points c and f is such that

$$r^* + g = \bar{r}$$

We may evaluate g from the relation

$$g^2 = (R-r^*)^2 + (R-r)^2 - 2(R-r^*)(R-r) \cos \theta \quad (18)$$

Let us denote the ratio \bar{r}/r as h . Then using the relationships in Eq. (14) we transform Eq. (18) to

$$\frac{(h \sqrt{m^*m-m_1})^2}{m} = (\sqrt{m}-\sqrt{m^*})^2 + \frac{\Delta m^2}{m} - 2(\sqrt{m}-\sqrt{m^*}) \frac{\Delta m}{\sqrt{m}} \cos \theta \quad (19)$$

We may find the effective m^* at which wall interference occurs by inserting the appropriate value of h in Eq. (19) and find the proper values of m^* and $\cos \theta$ from the use of Eq. (15). In our instruments h was approximately 1.1⁵. For the mass 58 ion from *n*-butane, for example, decaying through a metastable transition to a mass 43 ion to give the mass 31.9 metastable peak, the predicted cut-off is calculated by the above procedure as mass 32.23. This corresponds to a limiting θ of 0.310 radians and an allowable travel distance in the analyzer tube of 3.94 cm. The quantities evaluated for this particular metastable transition will, in general, not be exactly applicable to other transitions. However, they will serve adequate order-of-magnitude values.

The upper mass limit of the 31.9 peak from *n*-butane was experimentally evaluated by extrapolating the high mass side of the peak to the base line. This gave an upper limit to the metastable peak of 32.27 which is in good agreement with the value predicted above of 32.23.

Lifetime Measurements with 180° Instrument

We shall show here that lifetime measurements may be made with a 180° machine and we shall provide several examples.

Let us assume that ions of mass m are formed in the electron beam at a density of n_0 per unit area. Let us assume as in Eq. (3) that a fraction a of them are in the metastable state at the instant of formation. The number of ions of apparent mass $m^* = m_1^2/m$ will be given by the following equation:

$$I(m^*) = a n_0 A(V_1, V_2, V) e^{-\lambda(t_1+t_2)} (1-e^{-\lambda s/v}) D_v(V) D_s \quad (20)$$

Here, $A(V_1, V_2, V)$ represents a collection-transmission factor, dependent on the potentials, which relates the number of metastable ions which emerge from the exit slit, available for dissociation, to the number created per unit area in the electron beam. Here, s is the distance such ions may travel with velocity v in the analyzer tube before effective cut-off. $D_v(V)$ is a discrimination function which measures the beam attenuation due to initial kinetic energy components parallel to the magnetic field⁶. D_s is a discrimination function which measures the beam attenuation due to kinetic energy components which are imparted to the ions by the process of dissociation of metastable states. Similarly, the intensity of the m^+ ion peak will be given by:

$$I(m) = (1-a) n_0 A(V_1, V_2', V') D_v(V') \quad (21)$$

where V_2' and V' indicate the different voltages for focussing the m^+ ion than were used for the m^* ion. Here, we omit any contribution due to undissociated metastable ions reaching the collector. This is due to the facts that with the accelerating voltages used and with the analyzer radius used, the total transit time is of the order of ten microseconds. This is adequate for essentially complete dissociation for lifetimes of the order of 10^{-6} sec.

⁵Private communication from Dr. C. E. Berry.

⁶C. E. Berry, Phys. Rev. **78**, 597 (1950).

Let us denote the ratio of these peak intensities as $R(V_1)$ where

$$R(V_1) = I(m)/I(m^*) = Be^{(t_1+t_2)}$$

where

$$B = \frac{(1-a)A(V_1, V_2', V')D_V(V')}{a(1-e^{-\lambda s/v})D_V(V)D_3A(V_1, V_2, V)} \quad (22)$$

Consider a set of runs, using constant magnetic field, in each of which a different V_1 is used. The total accelerating voltages for parent ions and fragment ions from metastable transitions will always be the same and, hence, B will be essentially constant. All terms in B are constant under the conditions defined except the ratio $A(V_1, V_2', V')/A(V_1, V_2, V)$. This ratio is that of the collection-transmission factor for the undissociated ion for the values of V corresponding to m and m^* . Since the collection-transmission value will depend primarily on V_1 , which is the same in both terms of the ratio, we may treat the latter as constant. We may, therefore, plot $\log R(V_1)$ versus t_1+t_2 to obtain information on metastable lifetimes.

A number of such experiments have been run in our Laboratory and the results are plotted in Figures 5, 6, and 7. In these experiments, V_1 (one-half of repeller voltage) values up to 60 volts were used to reduce the total residence time t_1+t_2 to the submicrosecond values seen. The metastable peak intensities were taken from the maxima of the metastable peaks. With each successive increase of V_1 , the electron voltage (nominally 70 volts) was decreased a corresponding amount so that the ionizing electron energy would be essentially constant for all points. Straight lines may be drawn through different segments of the curve with the immediate interpretation that the metastable ions are distributed in different species characterized by different lifetimes. An examination of Hipple's measurement of the half life for one of the metastable transitions for *n*-butane shows that the shorter half lives were not found then as the residence times achieved were not short enough.

It could be argued that the data presented represent a continuous distribution of half lives. However, the straight-line portions are rather distinct. There is some evidence in these data to indicate that shorter half lives than those observed would be found with a further reduction of residence time. In Table I are given the half lives as calculated from the straight-line portions.

TABLE I
METASTABLE TRANSITION HALF-LIFE VALUES

<u>Compound</u>	<u>Transition</u>	<u>Half-Life Values</u>
n-butane	$C_4H_{10}(58) \rightarrow C_3H_7(43) + CH_3(15)$	8.9×10^{-8} sec.
		6.1×10^{-7} sec.
		2.7×10^{-6} sec.
n-butane	$C_4H_{10}^+(58) \rightarrow C_3H_6^+(42) + CH_4(16)$	8.1×10^{-8} sec.
		5.8×10^{-7} sec.
		4.8×10^{-6} sec.
isopentane	$C_4H_9^+(57) \rightarrow C_3H_5^+(41) + CH_4(16)$	1.03×10^{-7} sec.
		5.4×10^{-6} sec.

Considerations on Metastable Peak Shape

In many cases, the peaks resulting from a metastable ion transition occur so close to the normal ion peaks that the complete peak shape cannot be observed. An example, however, where the metastable peak lies apart from neighboring peaks is the $m^* = 31.9$ peak for *n*-butane. In examining such metastable peaks it is seen that there is tailing on the high mass side as predicted in Fig. 3. However, the peaks do not rise abruptly on the low mass side as predicted by Fig. 3, but show a surprising amount of tailing towards lower mass (see Fig. 9).

It is important to determine, if possible, the origin of the low mass tailing. Let us first consider the effects of the incremental velocity changes imparted to the fragment ion in the process of dissociation. We may consider two extremes: the one in which an increment of velocity Δv is imparted perpendicular to the velocity v of the parent ion, and the other in which the increment is added to or subtracted from the parent ion velocity. In Fig. 8 we have a diagram, with exaggerated conditions, which applies to the first case for an ion which dissociates just as it passes through the exit slit. Let us suppose that the angle between the new velocity after dissociation and the velocity before dissociation is θ . Then $\theta \approx \Delta v/v$.

For the purposes of this calculation we may neglect the change of absolute value of velocity. Using the same absolute value of v we may determine the center of the orbit of fragment ion after dissociation. This will be swung out from the focal plane by a distance s , where $\theta = s/r$. This center will be shifted parallel to the focal plane and relative to the original center by a distance Δr where $\theta = \Delta r/s$. This deflection of orbit is equivalent to an apparent change of mass by Δm . To determine Δm we use the relations above plus the relations

$$mV = Dr^2 \text{ where } D \text{ is constant}$$

$$\begin{aligned} |\Delta V/V| &= |\Delta m/m| \\ |\Delta V| &= 2V\Delta r/r \\ |(\Delta m/m)| &= 2(\Delta v/v)^2 \end{aligned}$$

to obtain

Dissociations with the incremental velocity change opposite to that shown will produce the same value of Δm .

For dissociations wherein the incremental velocity completely adds to or subtracts from the original velocity, we may use

$$m v = H e r / c$$

$$\begin{aligned} |\Delta v| &= v |\Delta r/r| \\ |(\Delta m/m)| &= 2(\Delta v/v) \end{aligned}$$

to obtain

Thus, we see that the spread of apparent mass due to velocity additions perpendicular to the original velocity depends upon the square of the small quantity $(\Delta v/v)$, whereas, the apparent mass spread due to additions or subtractions of the velocity increment to the original velocity depends upon the first power of $(\Delta v/v)$. Thus, if the broadening of the peak were due to velocity additions, it should be dominated by the latter type. However, this argument is based on the assumption that the perpendicular type of dissociations would not sufficiently alter the solid angle of the beam to disturb focussing conditions.

Let us assume, for the moment, that the broadening is due to dissociations of the latter type, wherein there is numerical addition or subtraction of the energy of dissociation to the kinetic energy of the fragment ion. Since the processes that produce the metastable ions are the same, by the statistical theory of mass spectra, then we should observe the same kinetic energy spread or equivalently, mass spread, in the normal m_1^+ ion peak.

A comparison was made between the observed $(\Delta m/m)$ for the $m^* = 31.9$ and the $m_1 = 43$ peaks for n-butane under a number of operating conditions. The $(\Delta m/m)$ values were obtained by making, for each run, a plot of m versus chart distance and determining the width of the base of each peak. The width of the metastable peak was determined in each case by linearly extrapolating the sides of the peak to the base line, as in Fig. 9. The results of these determinations are given in Table II.

TABLE II

($\Delta m/m$) Values for $m^* = 31.9$ and $m_1 = 43$ for n-butane

(V^* refers to the accelerating voltage for m^* and V refers to the accelerating voltage for $m_1 = 43$)

Repeller ($2V_1$)	V^*	($\Delta m^*/m^*$)	V	($\Delta m_1/m_1$)	($\Delta m^*/m^*$)/($\Delta m_1/m_1$)
1/2% of V^* or V	737	0.0256	547	0.0089	2.88
"	1180	0.0223	875	0.0049	4.55
"	1505	0.0200	1116	0.00473	4.23
"	1880	0.0198	1387	0.00393	4.00
"	2260	0.0181	1676	0.00366	4.95
"	2635	0.0177	1955	0.00340	5.21
30	737	0.0278	547	0.01325	2.10
30	1180	0.0202	875	0.00612	3.30
30	1880	0.0175	1387	0.00426	4.11
30	2635	0.0173	1955	0.00367	4.72

Examination of the conditions applied in Table II show that the observations were taken across a wide range of accelerating voltages with both small and large repeller voltages. The results show that the ($\Delta m/m$) values decrease with increased accelerating voltage as expected but not to changes in repeller voltage. In all cases, ($\Delta m/m$) for m^* is larger than ($\Delta m/m$) for m_1 , whereas, the relation would be reversed if the broadening were due only to the kinetic energy spread effective for the m_1^+ peak.

Let us assume that the dissociation of the metastable ions is of a different type than the one that produces the normal m_1^+ ions and that an extra increment of kinetic energy ΔV^* is imparted to the fragment ions. Let ΔV be the energy spread of the normal m_1^+ ions and assume that the energy spread of the metastable ions can be represented by $\Delta V + \Delta V^*$. Then

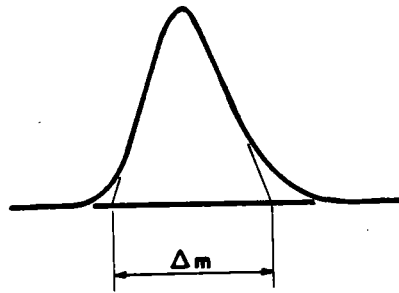
$$\left| (\Delta m^*/m^*) \right| = \left| (\Delta V + \Delta V^*)/V^* \right|$$

We may then derive the relation

$$\left| (\Delta m^*/m^*)/(\Delta m_1/m_1) \right| = \left| \Delta(m^*/m_1) + (m^*/m_1) (\Delta V^*/\Delta V) \right|$$

This predicts that the ratio ($\Delta m^*/m^*$)/($\Delta m_1/m_1$) should remain constant with increasing accelerating voltage. We see in Table II that rather than remain constant, the ratio changes by a factor of two over the range studied. We thus conclude that the abnormal broadening in the metastable peak is not due to an extra increment of energy ΔV^* imparted to the fragment ions during dissociation. Since we find no basis for an explanation based on incremental kinetic energy change, we conclude that the breadth of the metastable peak results from the details of the focussing action and its dependence on angular scatter, i.e., an instrumental effect.

In an earlier section it was shown that the metastable transitions studied exhibited species of different lifetimes. It is of interest to ascertain, if possible, if shape of the metastable peak depends upon the species making the major contribution to the metastable peak. When low repeller voltages are used so that the residence time in the ion source is long (of the order of 1.5 microseconds), the metastable peak is dominated by transitions of lifetimes of the order of 2 microseconds. If the repeller voltage is high so that the residence time is of the order of several tenths of a microsecond and if the short lifetime species predominate in the ion source (as was seen for the three cases studied), the metastable peak is dominated by transitions of lifetimes of the order of hundredths of microseconds. If the metastable transitions of short lifetime gave ions of a different kinetic energy spread, it would be expected that the shape of the metastable peak obtained with high repellers would be significantly different from the shape obtained with low repellers.



INCREASING MASS →

FIG. 9. Method of extrapolating the sides of the $m^* = 31.9$ peak to determine Δm^* .

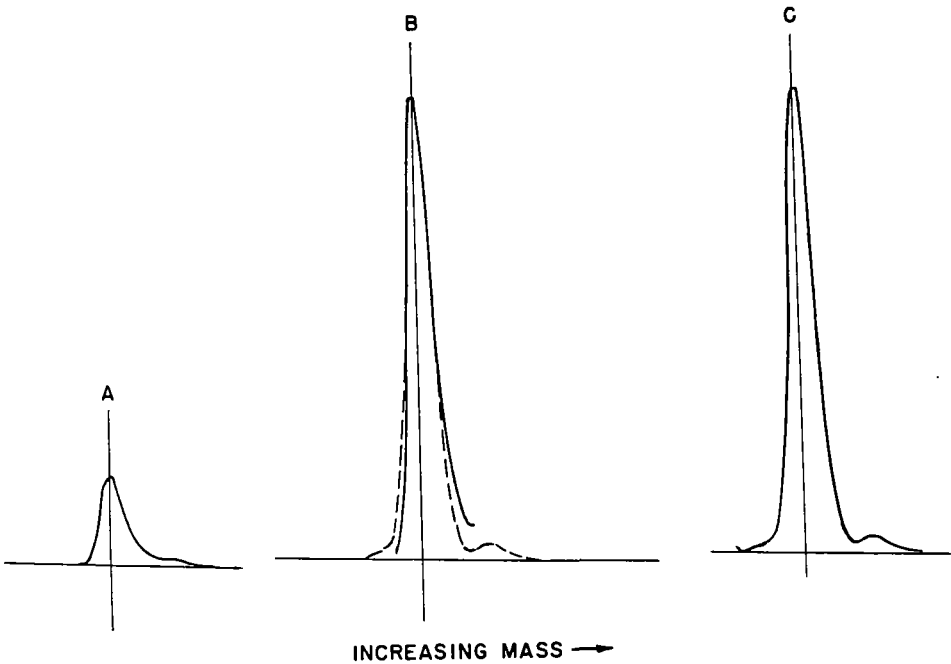


FIG. 10. Comparison of the shape of metastable peaks, $m^* = 31.9$, obtained at different repeller voltages. A is for a peak obtained at low repeller voltage. C is for a peak obtained with high repeller voltage. B is the superposition of curve A distended in the vertical direction to the same height as curve C onto curve C.

Fig. 10

In order to get information on this, a metastable peak obtained with low repeller voltage was graphically expanded to the same height as a peak obtained with high repeller voltage. The results are shown in Fig. 10. Here, A represents the $m^* = 31.9$ peak as observed with a repeller voltage of 3 volts and C is the same peak as observed with a repeller voltage of 120 volts. Curve B is that produced by the one-dimensional expansion of Curve A traced on top of Curve C. Here, the dashed portion at the bottom refers to lower portion from Curve C. On the whole, the curves are identical except for the departure as seen in the base. It is believed that this resulted from error in the expansion of the smaller portions of Curve A. This latter step was made by measuring peak to the nearest 0.001" at points separated by 1/64 inch and multiplying by a normalizing factor. Until this experiment can be done with greater accuracy, we must conclude that the factors affecting peak shape, such as kinetic energy, and angular spread, are the same for transitions of short and long half lives.

Acknowledgment

Appreciation is due to Dr. J. C. Schug for various discussions on these topics and to Messrs. J. P. Klems and H. T. Best for obtaining data and making calculations.

THE CHEMISTRY OF UNIMOLECULAR ION DECOMPOSITIONS

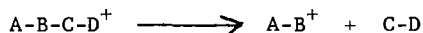
F. W. McLafferty and R. S. Gohlke
Eastern Research Laboratory
The Dow Chemical Company
Framingham, Massachusetts

Many correlations of mass spectra have been made in the last few years, and in most cases these have included some speculations on the mechanisms involved in formation of more abundant ions^{1,2}. At this time, it might be useful to attempt to set forth a more general picture of what is occurring during the unimolecular decomposition of organic ions caused by electron bombardment. The following picture is of necessity somewhat oversimplified, but the reader is referred to an amplified version which is in press³.

The title is meant to emphasize that these are types of chemical reactions. Despite the obvious differences between these and ordinary chemical systems, we find that emphasis on the similarities gives a useful framework for the understanding of the ion decomposition mechanisms. The major differences of these two chemical systems appear to be: (1) the effects of the extra energy imparted by the bombarding electrons, and (2) the effect of the removal of an electron on the stability of the positive ion as compared to its corresponding neutral entity.

Because any intermolecular reactions are ruled out by the low pressure in the ion source, there are relatively few modes of chemical reaction open to the molecular ion which is initially formed by electron impact. The most obvious of these is simple bond cleavage.

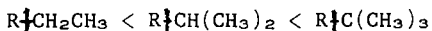
Simple Bond Cleavage. In



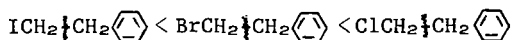
the B-C bond is cleaved to yield the ion $A-B^+$ plus neutral fragment C-D. The tendency for such a reaction to take place in general appears to be enhanced by

- (1) the lability of the particular bond
- (2) the stability of the ionic and neutral products

The factors in physical-organic chemistry which are found to affect ordinary chemical reactions appear applicable in general to these ionic systems also. Thus, the polarizability of the bonding electrons adjacent to an alkyl group increases in the order ethyl < isopropyl < tert-butyl, which fits in well with the known increased cleavage tendency at chain branchings in alkyl ions.

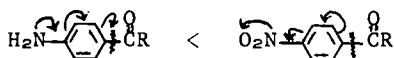


As will be seen later, the stability of the product ion can also be used as a strong driving force for this increased cleavage. The strong influence of the inductive effect is seen in the $C_7H_7^+$ ion abundance in the beta-haloethylbenzenes.



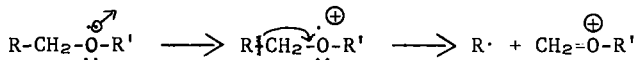
The abundance of the $C_7H_7^+$ ion is 8%, 37%, and 57% of the total ions for the iodo, bromo, and chloro compounds, respectively. Apparently, the electronegative halogen atom pulls electrons out of the beta bond, thus weakening it, as well as increasing the ionization potential of the methyl halo radical.

Bond lability is also affected in an expected manner by resonance. Thus, in a benzoyl compound the cleavage of the ϕ -carbonyl bond is reduced by an electron-supplying functional group in the para-position, and increased by an electron-withdrawing compound in the same location.



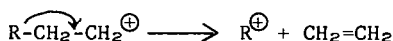
In fact, such effects can be correlated with the Hammett sigma constant⁴.

The electron removed in ionization may create a site of initial localized charge which effects the subsequent cleavage of a neighboring bond. Favored sites are atoms such as nitrogen, sulfur and oxygen, which contain non-bonding electrons which are easily donated, i.e., have a low ionization potential.



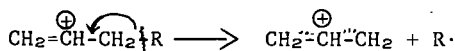
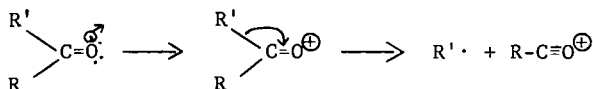
Electron transfer to neutralize this localized charge, as first proposed by Cummings and Bleakney⁵, will explain the well known beta bond cleavage in ethers, amines, sulfides, etc. Undoubtedly, the stable oxonium ion thus formed is a major driving force in this cleavage (it contains a new bond to compensate for the one cleaved) and could thus be viewed as the cause rather than the result of the mechanism shown. However, this concept of electron transfer to the site of initial localized charge has proved useful as a convention for such mechanisms.

This concept can also be applied to "even-electron" fragment ions such as

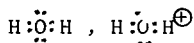


Here the radical ion structure of the fragment dictates a localized charge, which can be neutralized by the transfer of a pair of electrons, resulting in the new alkyl positive ion and neutral olefin molecule. Here again, the stability of the products could be viewed as the cause as well as the result of this localized charge mechanism.

This mechanism can also be successfully applied to common unsaturated functional groups, e.g., aldehyde, ketone, acid, ester, olefin, phosphate, sulfonyl, etc. Initial ionization from the oxygen atom of a carbonyl group or from the π -electrons of an unsaturated linkage can also cause transfer of electrons from an adjacent bond



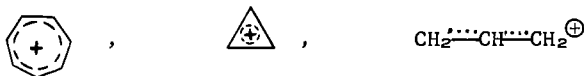
Product Stabilities. As outlined initially, the other major factor effecting the bond cleavage tendency is the stability of the ionic and neutral products produced. Here the significance of the electron removed in ionization should be reemphasized. This destroys the stability of the electron octet in producing the molecule ion, thus changing the stable "even-electron" molecule into an unstable "odd-electron". In the same way, a



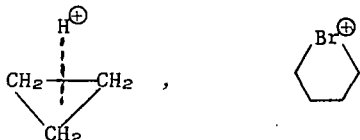
neutral "odd-electron" radical is less stable than its "even-electron" ion counterpart, as the latter does not contain the unpaired electron.



The stability of the neutral product from the ion degradation is analogous to the ordinary chemical case. For example, unsaturated molecules are generally more stable than saturated, thus the formation of such molecules as olefins, H_2O , HCN , CO , ROH , RCOOH , etc. can provide a major driving force for a particular decomposition. Product ion stabilities also parallel chemical experience. As predicted by the Hückel rule for $4n + 2$ π electrons, the tropylium⁸ and cyclopropenium ions ($n=1$ and 0 , respectively) are classic examples which provide strong driving forces,

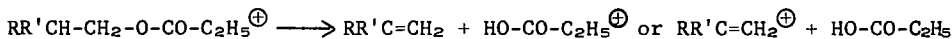


and the stability of the allyl ion is well known. Non-classical ions such as the "protonated cyclopropane"⁷ and cyclic bromonium⁹ structures have been postulated to explain unusual fragment ion intensities.



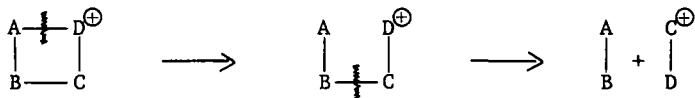
The unusual chemical stability found for difluoro carbene, CF_2 , as compared to CH_2 , can account for the surprising loss of CF_2 from the molecular ions of aromatic fluorocarbons^{2,9}. As mentioned above, a series of oxonium (e.g., $\text{RCH}_2\text{-OH}_2^+$, RCH=OH^+ , RC=O^+), quaternary ammonium, and similar ions containing hetero atoms are unusually abundant, corresponding to their well known chemical stability.

The relative stabilities of the products will also determine which of the two fragments resulting from the cleavage of the particular bond will hold the positive charge. This is known as "Stevenson's rule".¹¹ For example, in the prominent beta cleavage rearrangement of propionate esters,



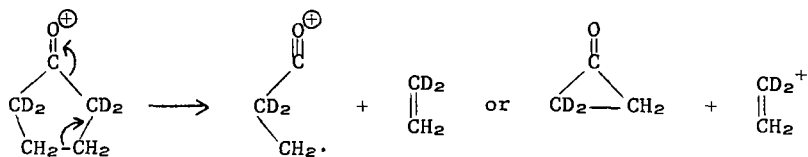
the propionic acid fragment has an ionization potential of 10.5 e.v. In the mass spectra of the ethyl ($\text{R}=\text{R}'=\text{H}$), n-butyl, ($\text{R}=\text{C}_2\text{H}_5$, $\text{R}'=\text{H}$) and isobutyl ($\text{R}=\text{R}'=\text{CH}_3$) esters, the respective olefin ions increase markedly in abundance through the series, in line with the respective ionization potentials of C_2H_4 , 10.5 e.v.; $\text{CH}_3\text{CH}_2\text{CH=CH}_2$, 9.70 e.v.; and $(\text{CH}_3)_2\text{C=CH}_2$, 9.3 e.v. Similarly, beta-phenethyl esters give C_6H_5^+ as the most abundant ion in their spectra^{12,13} in line with the 8.9 e.v. ionization potential of styrene.

Cyclic Compounds. Multiple cleavage of ring bonds is necessary to produce fragment ions in cyclic compounds. Thus, the cleavage of the AD bond as shown does not change the mass of the molecular ion, and further cleavage



such as a bond BC is necessary to produce a fragment ion.

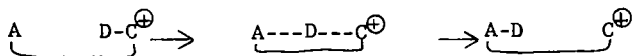
Thus, major ions from the 2,2,5,5-d₄-cyclopentanone¹⁰ might be explained by²



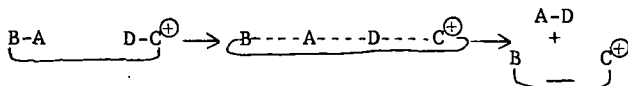
After the initial cleavage at the carbonyl group, loss of the stable ethylene molecule from the opposite end of the resulting open chain fragment ion would yield the abundant odd-electron oxonium ion. The fact that the corresponding CD_2CH_2^+ olefin ion is also abundant suggests that the accompanying carbonyl neutral fragment has the stable cyclopropanone structure instead of the diradical initially formed. The spectrum also exhibits major even-electron ions formed through rearrangements.

Decomposition Through a Cyclic Transition State (Rearrangements). One of the most fascinating aspects of the chemistry of the unimolecular decomposition of these energetic ions is the high tendency to produce rearranged products, often through a specific and favored mechanism. In retrospect, this is not so surprising if one considers a number of features of this unique system of chemistry. Ordinary chemical reactions, e.g., substitution, usually involve the formation of a new bond at the same time a bond is ruptured, thus lowering the energy requirements. For unimolecular ion decompositions, rearrangement can similarly provide a mechanism for formation of a new bond to offset the bond cleaved.

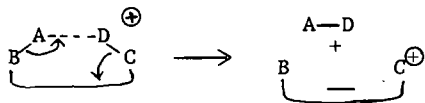
To make this new bond through the simple reaction of two active centers such as



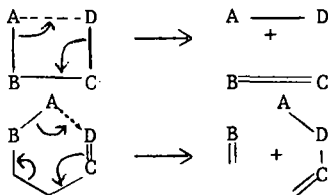
would not be generally feasible because of the marked change in the bonding orbital required in A and C. Actually, because of the cyclic transition state, there must be two bonds cleaved, and thus a compensating formation of two new bonds. This can be achieved by



involving a concerted shift of electrons. This can be rewritten as shifts of pairs of electrons.

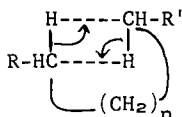


The most favored configurations of the cyclic transition state are those in which a concerted shift of electron pairs is possible. These are a four-membered ring, or a six-membered ring containing one double bond²



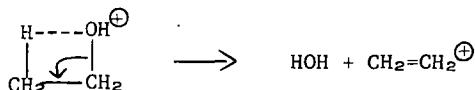
The tendency for an ion to undergo a particular rearrangement decomposition depends mainly on the relative probability of the transition state and the relative stabilities of the products. Where there is a strong tendency for one such rearrangement path is termed a "specific" rearrangement, or if there are quite a number of probable paths of similar energy requirements, the rearrangement is called "random".¹⁴

Typical "random" rearrangements are the formation of ions such as $C_3H_8D^+$, $C_3H_5D_2^+$, $C_2H_4D^+$, etc. in the spectrum of $CD_3CH_2CH_2CH_3$ ¹⁵ in competition with the expected major ions $C_3H_7^+$, $C_3H_4D_3^+$, $C_2H_5^+$, etc. All of the bonds in such a hydrocarbon are similar in requiring a relative high amount of energy for their decomposition, so that this randomizing process can be viewed as a competing exchange of the hydrogen atoms in the excited molecular ion, possibly through four-membered transition states².

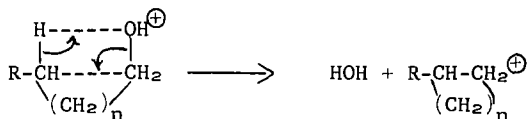


The presence of a polar functional group in the molecule usually lowers the energy required to cleave one or more of its bonds, decreasing the opportunity for such randomization. The hetero atoms of such functional groups can also provide a site for localization of the initial charge on molecular ion, which has been viewed as a driving force for such "specific" rearrangements¹⁴. Actually, there are a number of close analogs to such rearrangements, especially in high energy radiation, photochemical, and thermal reactions.

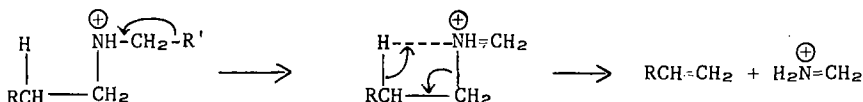
The four-membered ring transition state appears to be a logical explanation of a number of rearrangements, although one cannot generalize in its application to similar types of compounds. Thus, the large C_2H_4 ion in the spectrum of ethanol should appear to arise from the loss of a

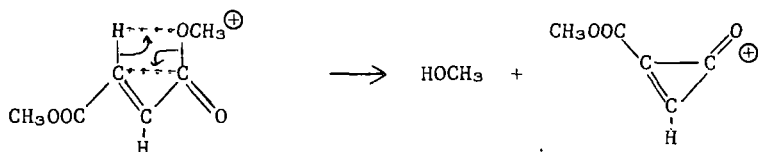


molecule of water through such a transition state, a low energy process with a high entropy of activation¹⁶. However, it has been shown that the mass spectra of deuterated *n*-butanols¹⁷ do not show specific loss of a beta hydrogen atom with the ejected H_2O molecule. This still might involve a four-membered ring intermediate with formation of a cyclic production³.

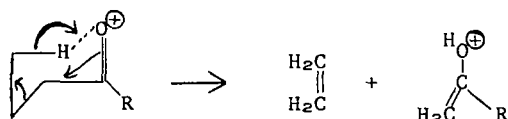


Quite a wide variety of rearrangements appear to go through a four-membered ring transition state², such as³

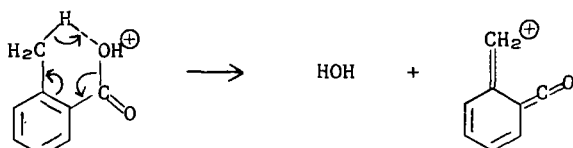




Probably the most well-defined general type of rearrangement is that of molecules containing unsaturated functional groups, involving a six-membered ring transition state^{14,18}.



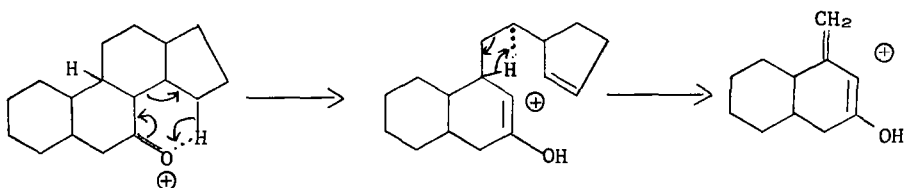
This class of rearrangement is prominent for carbonyl compounds (ketones, aldehydes, esters, acids, amides, and carbonates), olefins, vinyl and phenyl ethers, *n*-alkyl benzenes, phosphates, sulfites, etc. The spectra of labelled compounds have shown^{19,20,21} that almost all of the migrating hydrogen comes from the gamma-position as shown. A wide variety of rearrangements have been reported which evidently go through such a six-membered ring transition state, such as



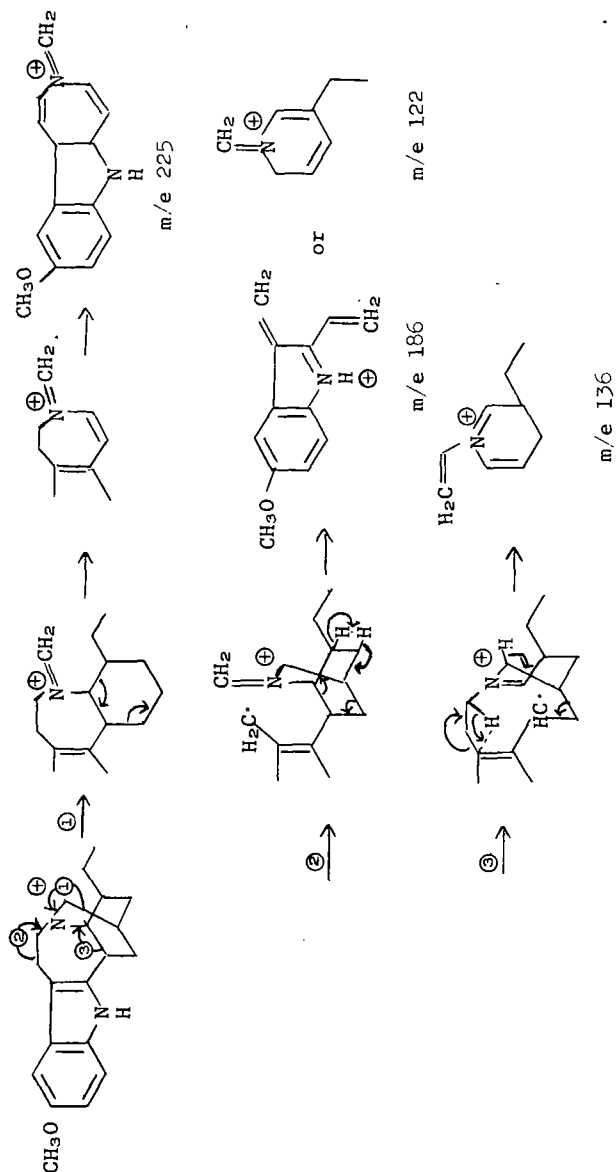
which has its unsaturation situated differently in the ring¹³, or the abundant $\text{CH}_2=\text{CHCH}_2\text{OH}^+$ ion from 1,2-epoxypentane²².

Additionally, there are examples of ion rearrangements in which a three-membered ring transition state seems to be involved². The best established case is the elimination of carbon monoxide from carbonyl compounds, which has been described in detail by Beynon and co-workers²³.

In recent studies of the mass spectra of complex fused ring compounds the major cleavage paths seem to involve combinations of the principles outlined above. A major ion of keto steroids described by Budzikiewicz and Djerassi²⁴ can be formulated as



while Biemann and co-workers²⁵ postulate an interesting series of degradations for the formation of major ions in the spectrum of ibogaine²⁵.



Although the mechanisms summarized hopefully show some progress towards our understanding of the chemistry of such excited organic ions, the mass spectra of many compounds still cannot be predicted in even a qualitative fashion. Excellent recent research from a number of laboratories involving labelled compounds promises that progress in the field should be much more rapid in the immediate future, however.

REFERENCES

1. J. H. Beynon, "Mass Spectrometry and Its Applications to Organic Chemistry", Elsevier, Amsterdam, 1960.
2. F. W. McLafferty, "Mass Spectrometry" in "Determination of Organic Structures by Physical Methods", F. C. Nachod and W. D. Phillips, Editors, Academic Press, 1962.
3. F. W. McLafferty, "Decomposition and Rearrangements of Organic Ions" in "Mass Spectrometry of Organic Ions", F. W. McLafferty, Editor, Academic Press, 1962.
4. F. W. McLafferty, *Anal. Chem.*, 31, 477 (1959).
5. C. S. Cummings and Walker Bleakney, *Phys. Rev.*, 58, 77 (1940).
6. P. N. Rylander, Seymour Meyerson and Henry Grubb, *J. Am. Chem. Soc.*, 79, 842 (1957).
7. P. N. Rylander, Seymour Meyerson, *J. Am. Chem. Soc.*, 78, 5799 (1956).
8. F. W. McLafferty, et al, *Anal. Chem.*, 34, 2 (1962).
9. J. R. Majer, *J. Appl. Chem.*, 11 141 (1961).
10. Paul Natalis, *Bull. Soc. Chem. Belg.*, 67, 599 (1958).
11. D. P. Stevenson, *Disc. Far. Soc.*, 10, 35 (1951).
12. E. M. Emery, *Anal. Chem.*, 32, 1495 (1960).
13. F. W. McLafferty and R. S. Gohlke, *Anal. Chem.*, 31, 2076 (1959).
14. F. W. McLafferty, *Anal. Chem.*, 31, 82 (1959).
15. W. H. McFadden and A. L. Wahrhaftig, *J. Am. Chem. Soc.*, 78, 1572 (1956).
16. Lewis Friedman, F. A. Long, Max Wolfsburg, *J. Chem. Phys.*, 27, 613 (1957).
17. W. H. McFadden, M. Lounsbury, and A. L. Wahrhaftig, *Can. J. Chem.*, 36, 990 (1958).
18. F. W. McLafferty, *Anal. Chem.*, 28, 306 (1956).
19. Ng. Dinh-Nguyen, Ragnar Ryahge, Stina Stallberg-Stenhagen, and Einar Stenhagen, *Arkiv. for Kemi*, 18, 393 (1961).
20. Henry Grubb and Seymour Meyerson, in "Mass Spectrometry of Organic Ions", F. W. McLafferty, Editor, Academic Press, New York, 1962.
21. F. W. McLafferty and M.C. Hamming, *Chem. and Ind.*, 1950, 1366.
22. Einar Stenhagen, Private Communication, 1960, Goteborgs University, Goteborgs, Sweden.
23. J. H. Beynon, G. R. Lester and A. W. Williams, *J. Phys. Chem.*, 63, 1861 (1959).
24. Herbert Budzikiewicz and Carl Djerassi, *J. Am. Chem. Soc.*, 84, 1430 (1962).
25. Klaus Biemann and M. Friedmann-Spiteller, *J. Am. Chem. Soc.*, 84, (1962).

MASS SPECTRA OF ORGANIC COMPOUNDS
OBTAINED USING A RADIO FREQUENCY SPARK SOURCE

Michel Desjardins	University of Cincinnati
F. Neil Hodgson	Monsanto Research Corporation
William Baun	Materials Central, Aeronautical Systems Division

ABSTRACT

Mass spectra of organic compounds were obtained, using the C.E.C. Field Evaluation Unit Double Focusing Mass Spectrograph, equipped with a radio frequency spark source.

Spectra were obtained for fused aromatic hydrocarbons, metal phenyl compounds, amino acids, and heterocyclics. In addition to showing a parent ion, the spectra show characteristic fragmentation which permits in many cases, elucidation of molecular structure. Techniques are discussed and data are presented for compounds such as coronene, anthracene, tetraphenylgermane, arginine, and thianthrene.

INTRODUCTION

The use of spark source mass spectrometry for organic materials has little precedent in the scientific literature. Indeed, it has been reported⁽¹⁾ that organic solids have been found to break up completely in the spark gap to yield the mass spectrum of the individual elements involved.

As reported previously by Baun and Fischer⁽²⁾ of this laboratory, with amino acids it is possible to obtain fragmentation with masses up to and above the molecular weight by using the spark source.

It will be shown that characteristic fragmentation can be obtained with many organic compounds and in some cases the data are not unlike those which are obtained with the conventional electron impact ion source.

INSTRUMENT

The instrument used for this work was the prototype of the C.E.C. 21-110, a double focusing instrument of the Mattauch-Herzog type.⁽³⁾

Figure 1 shows schematically the mass resolving system, which includes the source region, the electrostatic sector, the magnetic sector, and the photo box.

Figure 2 shows the instrument with the spark source in place. The electrode arrangement for the spark source is shown in Figure 3. The radio frequency spark source is supplied with 100-150 KV of rf voltage to the sample electrodes. Repetition rates of 1 to 10,000 pulses per second are available and the pulse length can be varied from 5 to 50 microseconds.

TECHNIQUE

In working with organic materials, conventional spark methods for nonconducting materials were tried. The most suitable was found to be one in which the samples were packed into hollow aluminum electrodes. These were then used as sparking electrodes. For this reason aluminum lines of mass 13.5, 27, etc., appear in all the spectra.

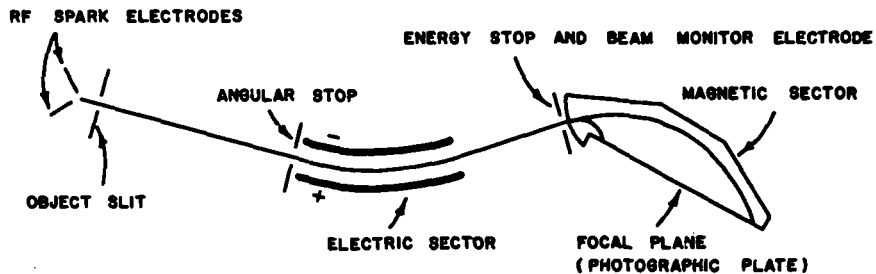


Figure 1 Mass Resolving System

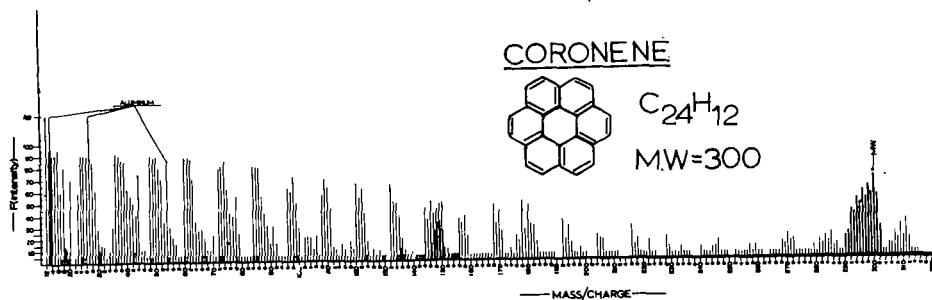


Figure 4 Spark Mass Spectrum of Coronene

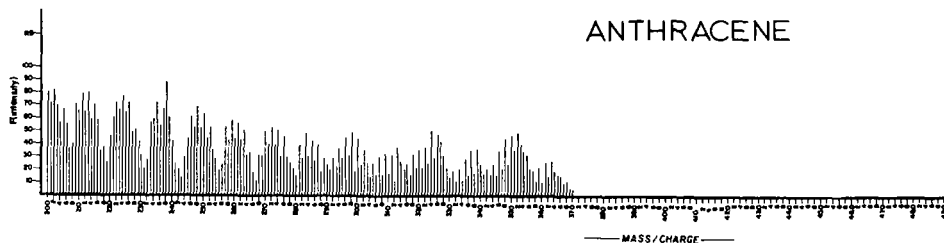
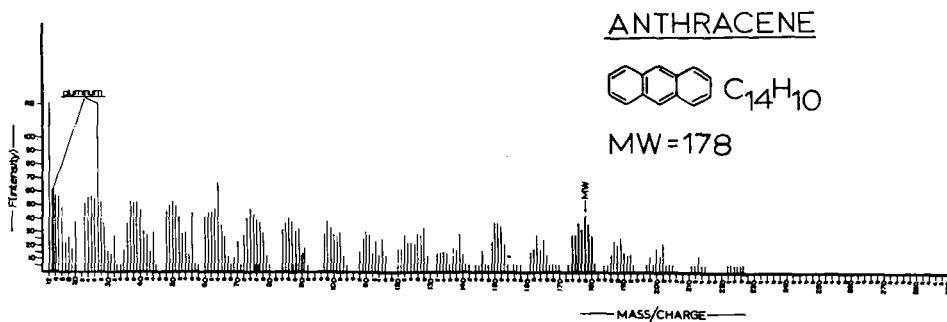


Figure 5 Spark Mass Spectrum of Anthracene

The spectra were recorded on Ilford Q-2 plates. Exposures were measured in coulombs by the integrating beam monitor. The photographic plates were then read on a microphotometer and values for per cent transmission were obtained. All the spectra shown have been plotted using 100 minus % transmission as a function of the intensity of the ion beams. In most spectra obtained, it was possible to observe one or more lines which showed photographic reversal due to very high intensity ion beams. The value for the per cent transmission of these lines has been reported as R.B.; i.e., reverse blackening.

DATA

In Figures 4 through 10, the data from the photographic plates have been plotted in a concise form, in order to easily observe the characteristics of all of the following spectra.

Coronene The spectrum of coronene as illustrated in Figure 4, represents an almost ideal case since it is one of the most stable of the fused aromatic hydrocarbons. Hence a good vacuum can be easily maintained while spark ionization takes place. Several interesting points are apparent in the spectrum of this compound.

1. A parent ion can be easily recognized. Examination of the photographic plate would reveal that the strong lines in the high mass region are, in addition to being darker, greatly broadened. This is true with most parent ions. Since only transmission measurements were made, we are justified in showing these lines heavier than others.
2. Masses corresponding to a doubly charged molecular ion group are to be observed at $m/e = 147.5$ to 150.5 .
3. It will be noted that this spectrum bears many similarities to the characteristic spectra of fused aromatic hydrocarbons as obtained by conventional electron-impact ionization. One such similarity is the grouping of lines, the number of which corresponds to the number of carbon atoms in the molecule.
4. Although a large portion of the ions produced are in the low mass range, one can see that masses even greater than the molecular weight occur. This is apparent also in the spectrum of anthracene, Figure 5.

Anthracene In the spectrum of anthracene, Figure 5a, one again observes the characteristic fragmentation that occurred with coronene. However, with a 20-fold increase in exposure, as shown in Figure 5b, lines are detected up to the mass of a dimer and above. These lines also occur in groups and are due to rearrangement and addition processes.

Mixture The spectrum of chrysene, Figure 6a, is another example of a spark ionized fused aromatic. Again the same characteristics are shown.

Triphenylsilane, the spectrum of which is shown in Figure 6b, is interesting in that several definite ions can be identified. For example, at mass number 77 a group of lines is seen which corresponds to a single phenyl group with varying numbers of protons. The line at mass number 105 corresponds to a silicon atom with a single phenyl group. At mass 154 we observe a rearrangement whereby two phenyl groups are associated. Mass 183 represents the parent molecule with a phenyl group removed. The parent ion is observed at 260, but a line at 259 representing the removal of the proton, probably from

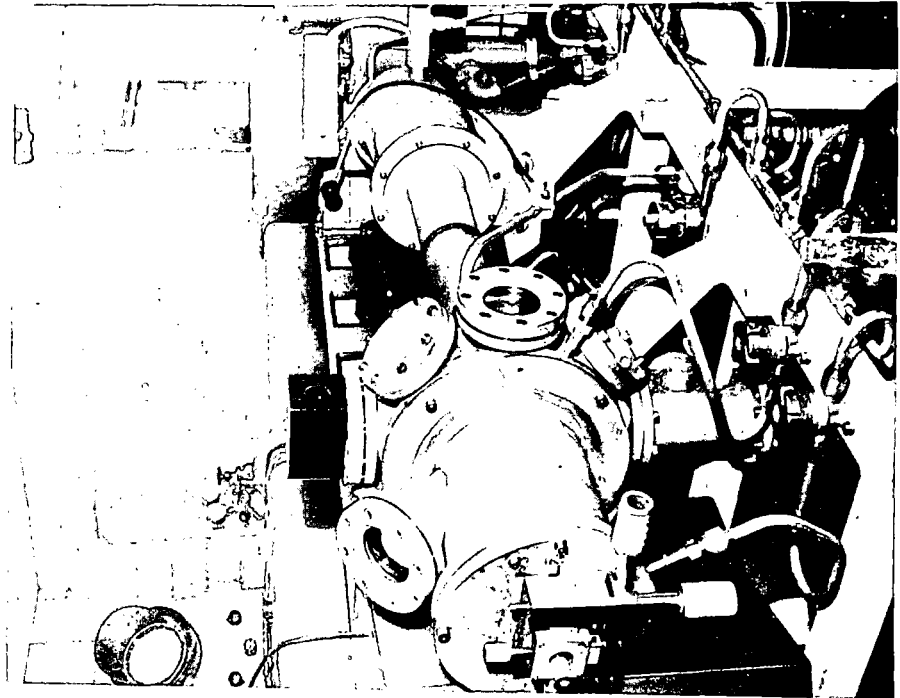


Figure 2 View of the Instrument

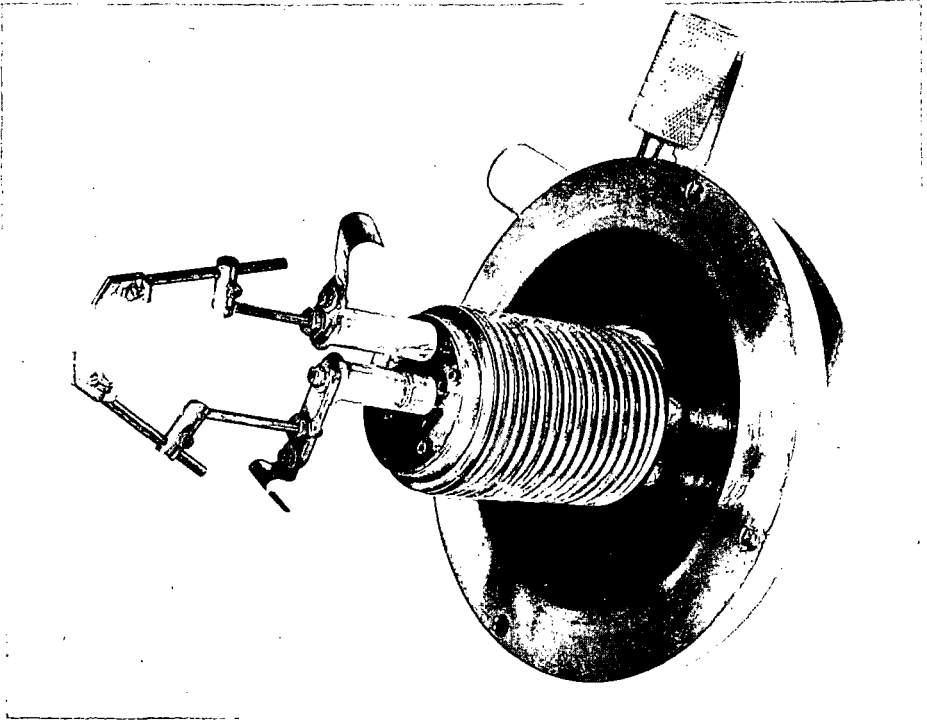


Figure 3 Electrode Assembly

the silicon, is more intense. Also a doubly charged parent ion is observed at mass 130. At mass 287 an additional ion corresponding to the parent ion plus aluminum (from the electrodes) can be observed.

The mixture spectrum of these compounds in approximately 50/50 proportion by weight is shown in Figure 6c. The characteristic features of the individual spectra are retained in the mixture spectrum. No attempt has yet been made to make a quantitative measure of mixtures.

Thianthrene The spectrum of thianthrene, a compound of a somewhat different nature is shown in Figure 7. Ions of special significance are, of course, the parent ion at mass number 216 and the doubly charged parent group observed at 107.5 to 108.5. Mass number 184 is the diphenyl-monosulfur ion.

Removal of one C and one H from the parent ion gives a strong peak at mass number 171. The peak 152 results from the rearrangement ion formed by the removal of both sulfur atoms from the molecule. Again the combination of aluminum with the organic molecule yields the ion at mass number 243.

Triphenylphosphine The spectrum of triphenylphosphine, illustrated in Figure 8a, shows similarities to that of triphenylsilane. A phosphorus-phenyl ion is observed at mass 107. At mass number 154, once again the rearrangement ion of two associated phenyl groups is observed. At mass number 183 an ion corresponding to the molecular weight minus one phenyl group occurs. The last strong mass observed is the parent peak. However, again by increasing the exposure, many additions and rearrangements can be observed as shown in Figure 8b.

Tetraphenylgermane Figure 9 illustrates the spectrum of tetraphenylgermane, a relatively high molecular weight compound. It is interesting because of the multiplicity of lines due to isotopes of germanium. At the molecular weight no one strong peak is observed, but three moderately intense peaks, which are due to the more abundant isotopes of germanium, can be seen. In the same fashion, the fragment ion, triphenylgermanium, shows three strong lines at masses 301, 303 and 305 for each of these isotopes.

Again the biphenyl metal ions at masses 224, 226 and 228 are seen. The monophenyl metal ions at masses 147, 149 and 151, and also the metal isotopes at mass number 70, 72, 73, 74 and 76 can be observed.

Arginine One advantage of the spark ionization technique for organic compounds lies in the fact that compounds which cannot be ionized by conventional means can be spark ionized. For example, in the case of amino acids, structural information can frequently only be obtained by analyzing derivatives if a conventional ion source is used. Free amino acids, because of their zwitter ion character, have very low vapor pressures and frequently decompose if heated to the temperatures required for vaporization.⁽⁴⁾ By using spark ionization, amino acids can be ionized as such.

Figure 10 shows the mass spectrum of arginine, an amino acid which gives some characteristic fragmentation by spark ionization. It has been noticed consistently that a proton can add to the amine group, giving rise to a parent plus one ion, usually stronger than the parent ion. This observation has been made using a conventional ion source for such compounds as peptides⁽⁵⁾ and esters of amino acids.⁽⁴⁾ In the arginine mass spectrum, two lines can be observed one and two mass units greater than the molecular weight. Both are stronger than the parent ion. These two lines can be explained by the presence of the two amine groups to which a proton may add.

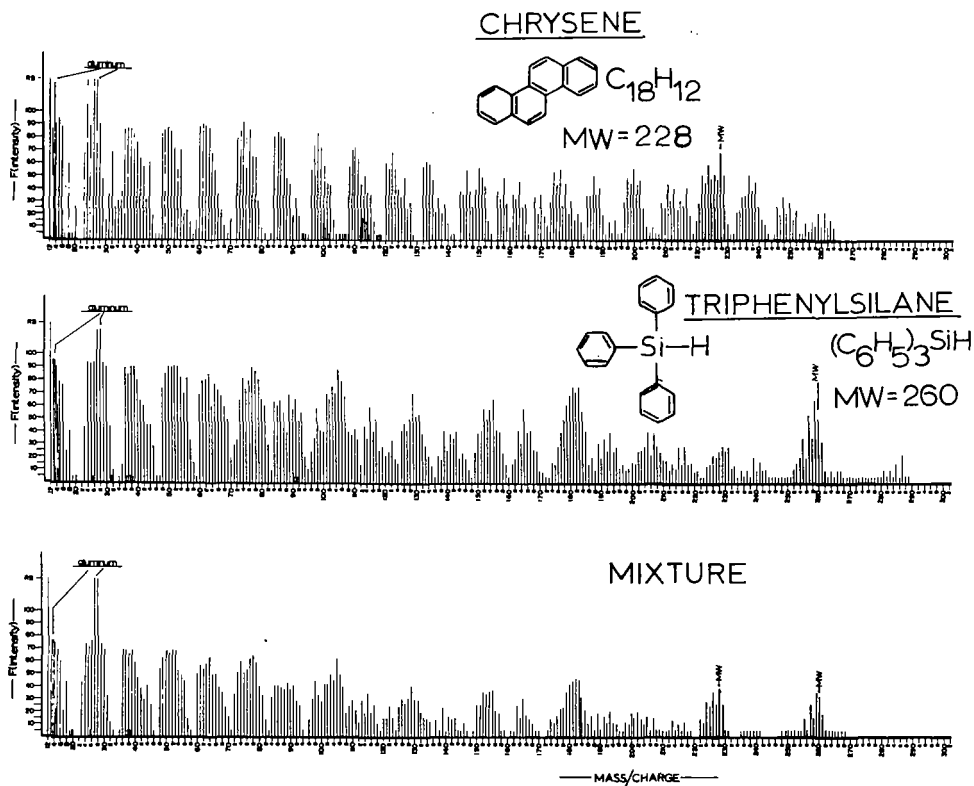


Figure 6 Spark Mass Spectrum of (a) Chrysene

(b) Triphenylsilane

(c) Mixture of (a) and (b)

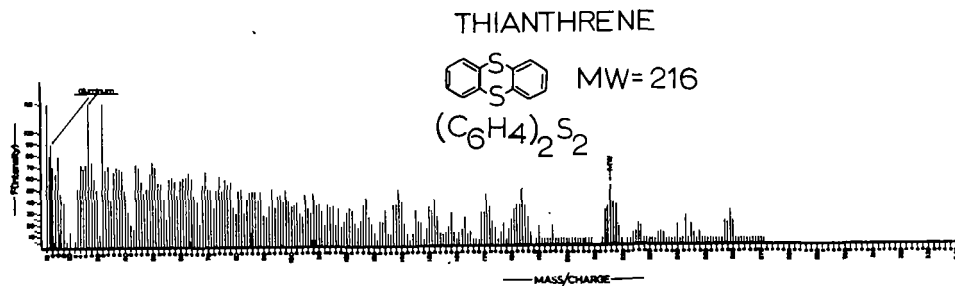


Figure 7 Spark Mass Spectrum of Thianthrene

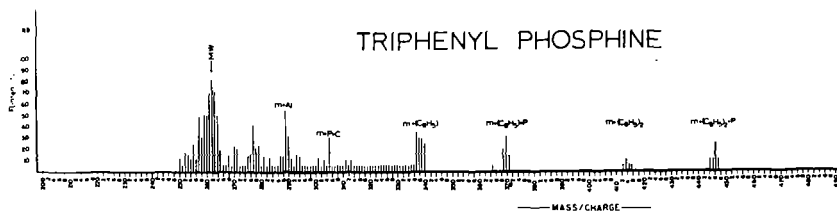
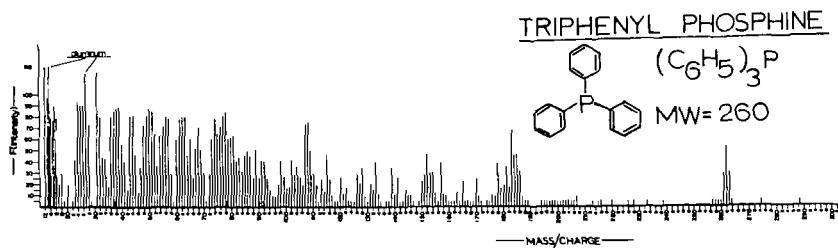


Figure 8 Spark Mass Spectrum of Triphenyl Phosphine

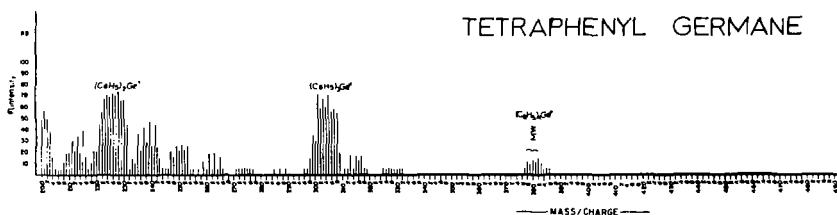
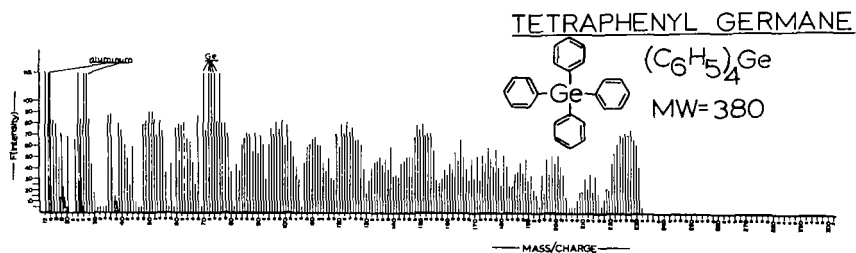


Figure 9 Spark Mass Spectrum of Tetraphenyl Germane

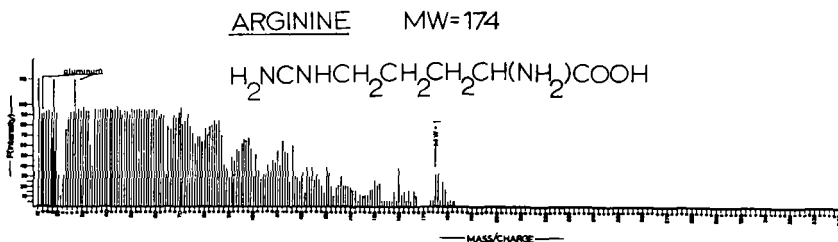


Figure 10 Spark Mass Spectrum of Arginine

Several characteristic lines in this spectrum may be observed. At mass 160 the parent-plus-one mass minus fifteen (or minus the NH group) occurs. The lines at masses 130 and 131 correspond to the parent-plus-one and the parent-plus-two masses minus 45 (or minus a carboxyl group).

SUMMARY

Certain difficulties are encountered in spark ionization of organic compounds which are not met when using the conventional ion source. The greatest of these is that intensity measurements made from photographic plate blackening cannot, at this time, be considered as accurate or reproducible from plate to plate as measurements made by electrical means. The erratic nature of the spark precludes use of non-integrating electrical measurements of intensity. Also the spark mass spectrum is frequently much more difficult to interpret than the conventional mass spectrum due to the large number of recombination and rearrangement ions which occur.

Some of the advantages of spark ionization might now be considered. Compounds of low vapor pressure, which are troublesome for conventional ionization, can be easily ionized by the spark. The problem of thermal degradation, sometimes encountered in electron-impact ionization, can many times be avoided in spark ionization.

For example, the conventional mass spectra of phthalic acid and phthalic anhydride are identical due to the thermal conversion of the acid to anhydride.⁽⁶⁾ By spark ionization, different spectra are obtained for these compounds, each being characteristic of the starting material.

From this short presentation one can recognize that the application of spark ionization mass spectrometry will have its place, along with conventional mass spectrometry, among the tools available for molecular structure studies.

BIBLIOGRAPHY

1. Craig, R. D., Errock, G. A. and Waldron, J. D., Advances in Mass Spectrometry, Session B, Pergamon Press, London, 1959.
2. Baun, W. L. and Fischer, D. W., Anal. Chem. 34, 294 (1962).
3. Mattauach, J. and Herzog, R., Z. phys. 89, 447 (1934).
4. Biemann, K., Seible, J. and Gapp, F., J. Am. Chem. Soc. 83, 3795 (1961).
5. Biemann, K., Gapp, F. and Seible, J., J. Am. Chem. Soc. 81, 2274 (1959).
6. Gohlke, R. S. and McLafferty, F. W., 4th Annual Meeting A.S.T.M. Committee E-14, San Francisco, 1955.

APPLICATION OF TIME OF FLIGHT MASS SPECTROMETRY AND GAS CHROMATOGRAPHY TO REACTION STUDIES

E. J. Levy, E. D. Miller and W. S. Beggs
The Atlantic Refining Company
Philadelphia, Pa.

Introduction:

The work to be described represents an application of time of flight mass spectrometry and gas chromatography to the study of the changes in product distribution, as a function of cracking cycle time⁽¹⁾, during the cracking of n-nonane over a silica alumina catalyst. Cracking cycle time may be defined as the period that a catalyst is exposed to "feed" before it is regenerated. This paper will describe the experimental techniques and some of the initial results.

In the usual microcatalytic studies a hydrocarbon feed is allowed to pass over a catalyst for a given period of time, e.g. 15 minutes and then the products are collected and analyzed and the % conversion for the 15 minute period determined. The percent conversion determined in this way is an integral conversion and represents the total conversion for the 15 minute period.

In the present investigation, the cracking period was directed into short intervals of approximately 28 seconds (corresponding to one slug of feed) and then the conversion and product distribution for each 28 second period was determined separately.

Apparatus and Experimental Procedures:

The equipment used in this investigation is shown schematically in Fig. 1 and consists of:

- 1) a Fisher introduction valve
- 2) a temperature controlled reactor containing 5 grams of silica-alumina catalyst
- 3) an indicating sampling system including a two position six ported aerograph valve, a sampling loop, and a Gow-Mac thermal conductivity cell
- 4) an F&M Model 500 gas chromatograph
- 5) a Bendex Model-14 Time of Flight mass spectrometer

In a typical run, a slug of 50 microliters (.05 ml) of n-nonane is introduced with a Fisher pipet through a Fisher introduction valve into a stream of preheated helium flowing at 30 ml/min. and is carried over a catalyst bed maintained at 950°F. The n-nonane is partially cracked over the silica alumina catalyst and passes as a slug through the reference side of the thermal conductivity cell. In one position of the Aerograph valve the slug goes from the reference side of the thermal conductivity cell through the sample loop and out through the detector side of the thermal conductivity cell. As can be seen from figure 2, with the valve in the position described, a positive and then a negative deflection was obtained from a recording potentiometer connected to the thermal conductivity cell. To transfer the product slug to the gas chromatography unit the above sequence is repeated except that when the positive deflection from the reference side of the thermal conductivity cell returns to the base line the Aerograph valve is switched and the sample is carried to the gas chromatographic inlet line. As may be noted in figure 2, no negative deflection was obtained indicating that the product slug was completely transferred to the gas chromatography unit.

The product slug was then separated by gas chromatography into some 35 peaks. The gas chromatographic column used for this separation was a 1/4 inch 50 foot length of 20% silicone grease in series with a 4 foot section of 15% Carbowax 20M on 42-60 mesh Chromosorb-W. The column temperature was maintained at 40°C. for the first 20 minutes and then programmed at the rate of 5.6°C./minute up to 200°C. It was then held at 200°C. until all the gas chromatographic peaks emerged. The total running time for a chromatogram was approximately 90 minutes. Slugs 1,2,3,4,9,14,24,34 and 44 were analyzed for each series before regeneration. Slug 45 would be equivalent to a slug 1 for a series using a catalyst after regeneration.

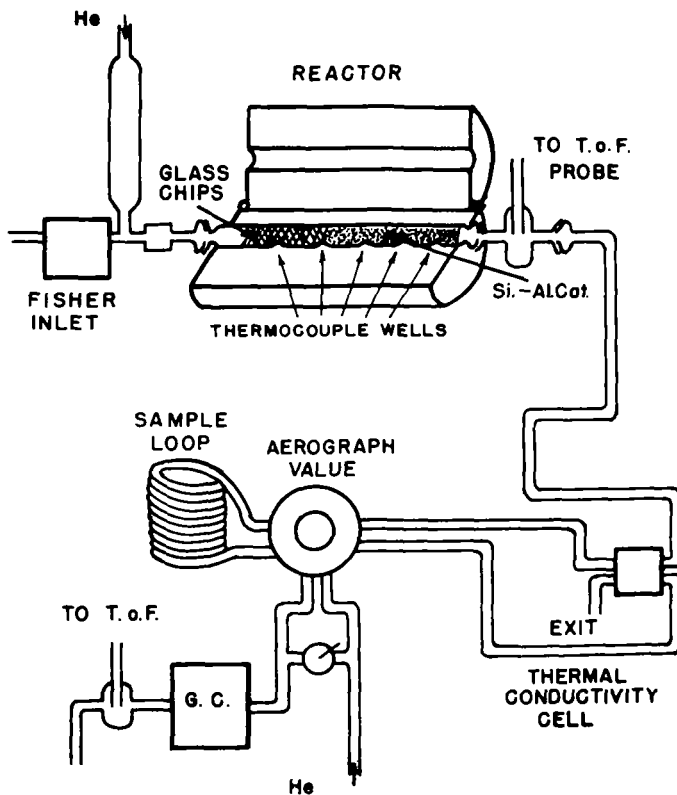


Figure 1
Schematics of Equipment

SAMPLE TRAPPING

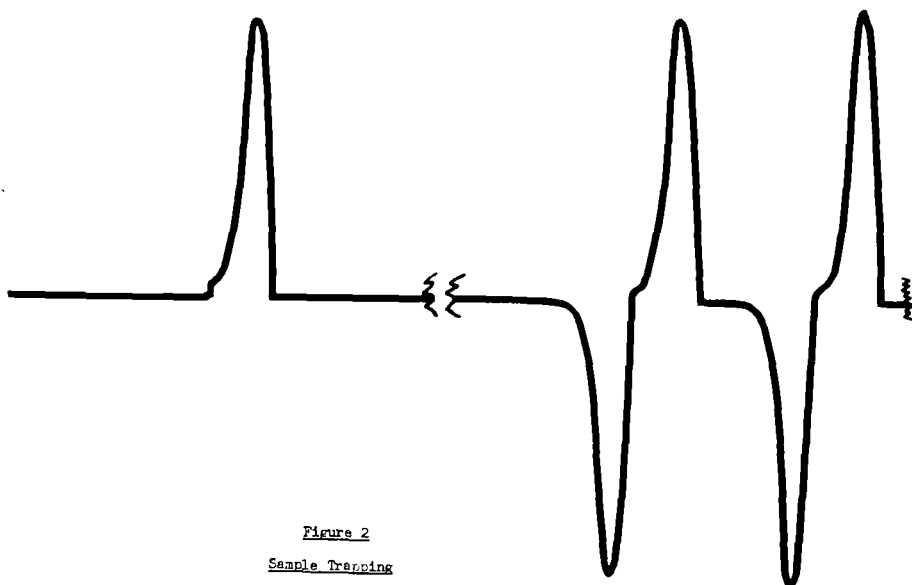


Figure 2
Sample Trapping

Figures 3 and 4 are photographs of the catalytic cracking reactor, the vacuum manifold connecting the 9 micron leak from the gas chromatograph unit to the spectrometer, and the Bendex Time of Flight Mass Spectrometer. The vacuum manifold enables the line between the leak, figure 5, which is located at the exit of the chromatographic unit to be evacuated before the valve to the spectrometer is opened. Once helium fills this line, little or no auxiliary pumping is required to maintain a pressure of 5×10^{-6} mm. in the spectrometer.

There are three modifications of the spectrometer that should be mentioned because they aided in obtaining useable mass spectra under the conditions of rapid variation of sample size over several orders of magnitude. The first is a voltage selector switch which reproducibly changed the potential applied to the ion multiplier. It consisted of a high voltage rotary selector switch with neon bulbs connected in series between the selector positions. By turning the selector switch the gain of the ion multiplier can be changed rapidly and reproducibly to match the size of the sample being observed. The second modification is a total ionization switch which applies a -150 volt potential to the analog controller gate, thereby collecting the secondary electrons produced by ions at all masses present. This device is a very convenient method for determining the time delay between the maximum of the peak on the gas chromatographic thermal conductivity cell and the maximum intensity of the sample in the spectrometer. The ions produced by the helium carrier gas are gated out by setting the analog scanner at Mass 4. The third modification is an electrical connection between the scanner and the controller so that the scan generator for the scanner will also drive the controller and thereby record another complete mass spectrum separated by a small time interval as shown in figure 6. The dual spectra permit detection of composition changes within a single gas chromatographic peak and help in making an accurate determination of the components contained within a single gas chromatographic peak.

Analysis of Spectra

The confidence that one can have in the reproducibility of the mass spectra under various conditions are shown in Tables I, II, III. Hexene-1 was selected as the test compound because it appeared to show a greater variability in pattern than the equivalent saturated hydrocarbon. In Table I, a pattern study is shown for hexene-1 introduced through a standard molecular leak inlet system. The first column lists the masses of the major ions observed. The second column contains the mean values for the patterns based on m/e 56=100%. The third column lists the standard deviations for the patterns. The next two columns are the high and low range from the mean. The last column is the confidence that one can have that any other pattern obtained will fall within the ranges defined. In Table II, the pattern data for 1-hexene introduced through the inlet system while helium is entering the spectrometer through the 9 micron glass leak from the gas chromatographic exit line, is treated in a similar fashion. This condition is equivalent to the isolation of a gas chromatographic peak plus carrier gas with a valve system as described by Ebert(2). In Table III hexene-1 was introduced through the gas chromatographic leak and the data tested as before.

From this study it can be concluded that the conditions in Tables I and II produced mass spectral patterns with a range of plus or minus 5-10%, approximately 70% of the time. With the conditions shown in Table III, the variability in % pattern is considerably greater so that the spectra obtained have to be treated very cautiously. The repeated spectra as shown in figure 6 helped considerably in establishing confidence in the patterns.

Results and Discussion

A typical gas chromatogram obtained for the cracked products of n-nonane is shown in figure 7. The identifications of the peaks in figure 7 and the product distributions by weight % are shown in Table IV.

When percent conversion was plotted against slug number as shown in figure 8 an initial conversion of 32% was obtained with the fresh silica alumina (90 Atlantic D+L) catalyst and 23% with the steam deactivated catalyst (60 Atlantic D+L). The values dropped sharply after a few slugs and leveled off at 20% and 9% respectively.

Table I

Pattern Study of hexene-1 Through Inlet System**Hexene-1 - Inlet System**

<u>m/e</u>	<u>% \bar{M}</u>	<u>σ</u>	<u>Range</u>		<u>% TA</u>
			<u>H-M</u>	<u>M-L</u>	
84	46.7	2.88	2.7	4.1	75.3
69	30.9	1.37	1.0	2.0	69.2
56	100				
55	64.8	0.87	1.1	1.0	77.6
43	65.4	1.95	1.6	2.7	71.2
42	78.5	1.78	1.5	2.2	69.1
41	96.3	3.61	3.7	3.2	65.5
39	48.7	1.65	2.4	1.3	74.1
27	53.4	3.05	2.9	2.9	65.8

Table II

Pattern Study of Hexene-1 Through Inlet System and Helium**Hexene-1 - Inlet System + Helium**

<u>m/e</u>	<u>% \bar{M}</u>	<u>σ</u>	<u>Range</u>		<u>% TA</u>
			<u>H-M</u>	<u>M-L</u>	
84	44.5	1.29	1.3	1.5	71.8
69	31.6	2.38	2.9	2.8	77.0
56	100.0				
55	65.1	4.47	5.1	4.2	69.9
43	66.8	3.96	4.6	3.9	71.2
42	78.4	1.55	1.0	2.3	67.4
41	97.1	3.98	4.1	3.6	66.4
39	48.0	0.90	0.9	1.1	79.7
27	54.6	0.32	0.3	0.3	64.8

Table III

Pattern Study of Hexene-1 Through Gas Chromatographic Inlet

Hexene-1 - Through G.C.

<u>m/e</u>	<u>% \bar{M}</u>	<u>σ</u>	<u>Range</u>		<u>M-L</u>	<u>% TA</u>
			<u>H-M</u>			
84	42.9	1.30	1.8		1.2	73.7
69	27.4	1.28	1.2		1.8	74.5
56	100					
55	65.7	2.98	3.7		2.9	72.6
43	68.1	9.10	12.4		8.7	74.2
42	78.6	8.85	7.5		10.5	68.5
41	94.4	10.05	13.9		9.3	74.2
39	48.8	8.00	8.3		9.9	74.4
27	51.3	13.22	18.1		13.0	75.7

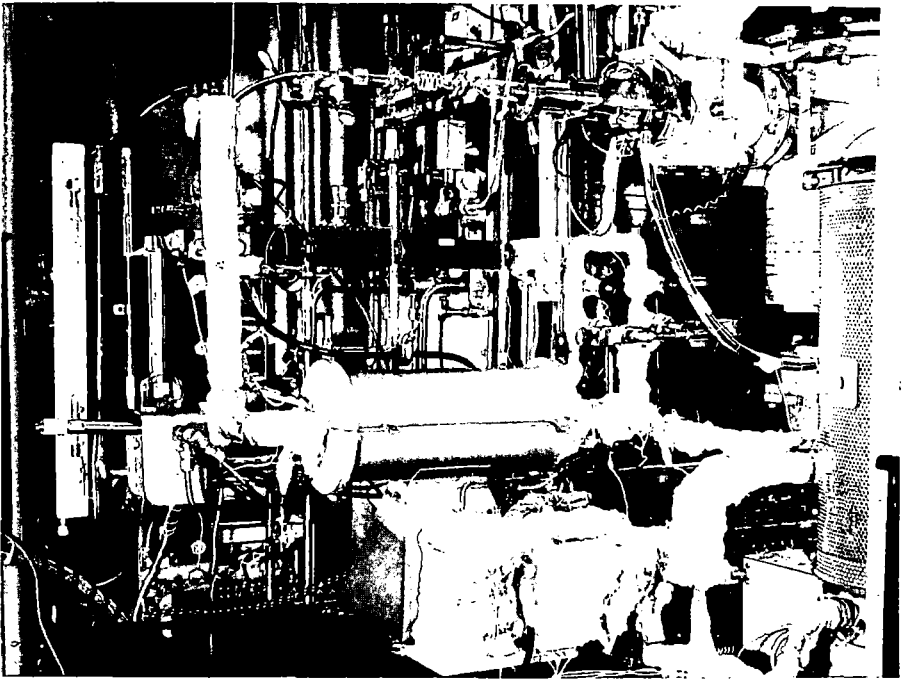


Figure 3

Photograph of Catalytic Reactor

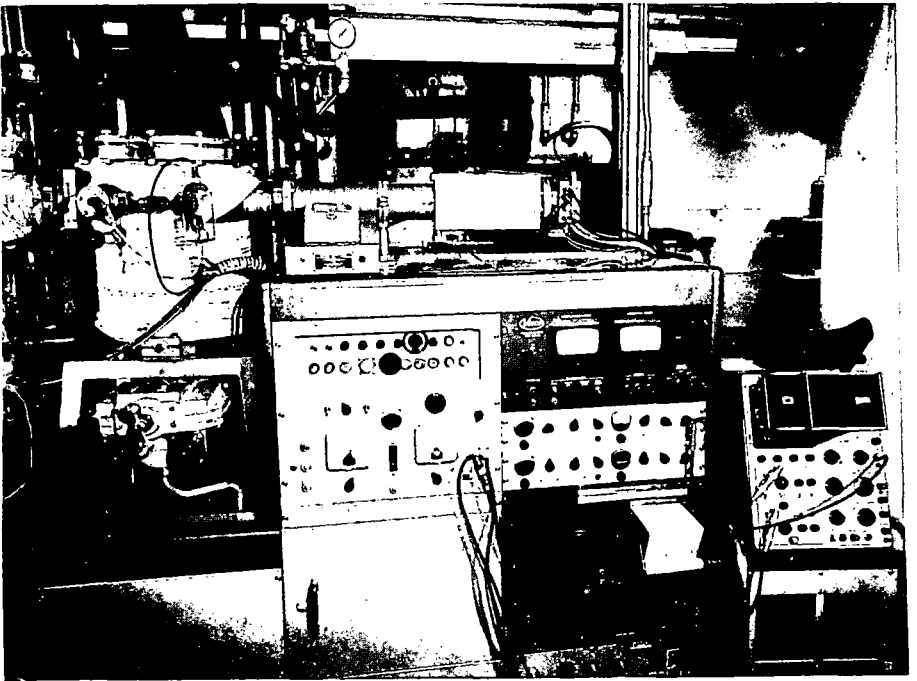


Figure 4

Photograph of Time of Flight Mass Spectrometer

Table IVIdentification of Gas Chromatographic Peaks and Product Distribution

<u>Gas Chrom.</u> <u>Peak #</u>	<u>Identification</u>	<u>Weight Percent</u>
1	Hydrogen	} 2.4
2	methane	
3	ethylene	0.920
4	ethane	0.895
5	propene	0.793
	propylene	3.172
6	isobutane	0.633
7	1-butene	} 2.148
	isobutylene	
8	n-butane	0.716
9	trans butene-2	0.964
10	cis butene-2	0.663
11	3 me butene-1	0.110
12	isopentane	1.060
12A	pentene-1	0.220
13	n-pentane	1.069
14	pentene-2	0.542
15	2 me butene-2	1.409
15A	3 me pentene-1	0.031
16	2 me pentane	} 0.277
	cyclopentane	
	4 me pentene-2	} 0.165
17	3 me pentene	
18	n-hexene	} 0.403
	3 me pentene-2 trans	
	3 ethyl butene-1	} 0.128
19	3 me pentene-2 cis	
20	me cyclopentane	0.081
21	2 me 1,3 pentadiene	0.041
22	benzene	} 0.186
	n heptane	
23	heptanes	0.077
24	toluene	0.288
25	unidentified C ₉ ?	0.045
26	nonane	78.395
26A	xylene M+P	0.305
27	xylene O	0.110
28	me. et. benzene	0.801
29	tri. me. benzene	0.550
30	tri. me. benzene	0.178
30A	C ₁₀ aromatics	0.083
31	C ₁₀ aromatics	0.124

Product distributions by carbon number for an initial slug of n-nonane over a fresh and a steam deactivated catalyst are shown in figure 9. Analysis of succeeding slugs indicated that the product distribution by carbon number remained approximately constant as a function of slug number or cracking cycle time. As can be seen in figure 10 when the ratios of isoC₄ to nC₄ are plotted against slug number there does not appear to be a significant change in ratio with slug number. When the ratios of C₄ olefin to C₄ paraffin are plotted against slug numbers (figure 11), there does appear to be a significant increase in ratio with increase in slug number.

Conclusions

The general techniques described here can be applied to any reaction that can be carried out in a flow system. When applied to the study of the product distribution from the catalytic cracking of n-nonane over a silica alumina catalyst as a function of cycle time it was found that the product distribution by carbon number was relatively independent of cycle time, however, the hydrocarbon type within a carbon number changed as a function of cracking cycle time.

References

- (1) Blending, F.H., Ind. Eng. Chem. 45 1186 (1953)
- (2) Ebert, A. A. Jr., Anal. Chem. 33 1865 (1961).

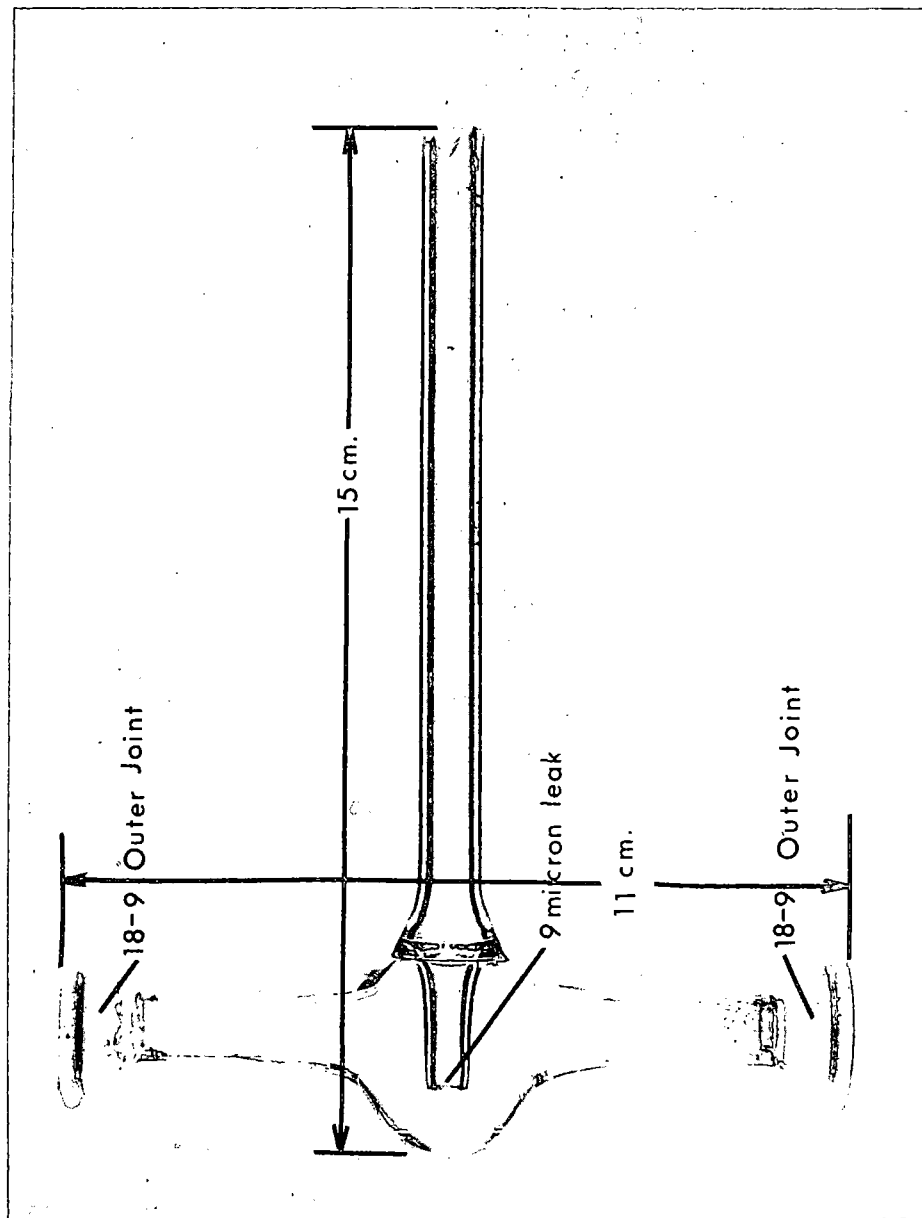


Figure 5

Photograph of Glass Leak

n-NONANE

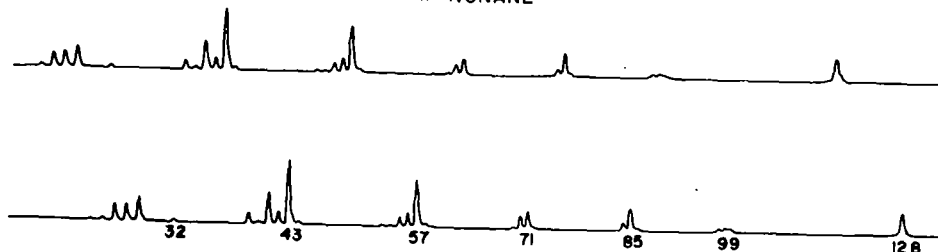


Figure 6

n-Nonane Mass Spectrum

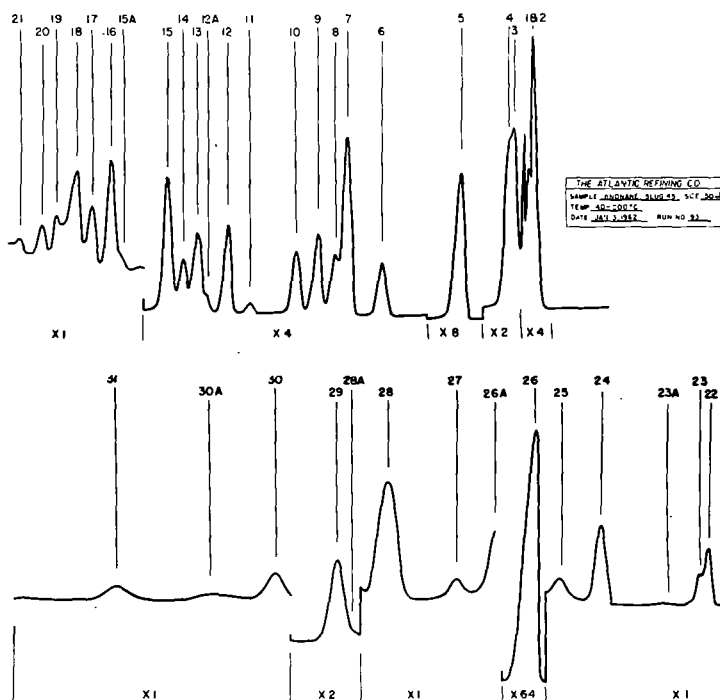


Figure 7

Gas Chromatogram of Cracked Products

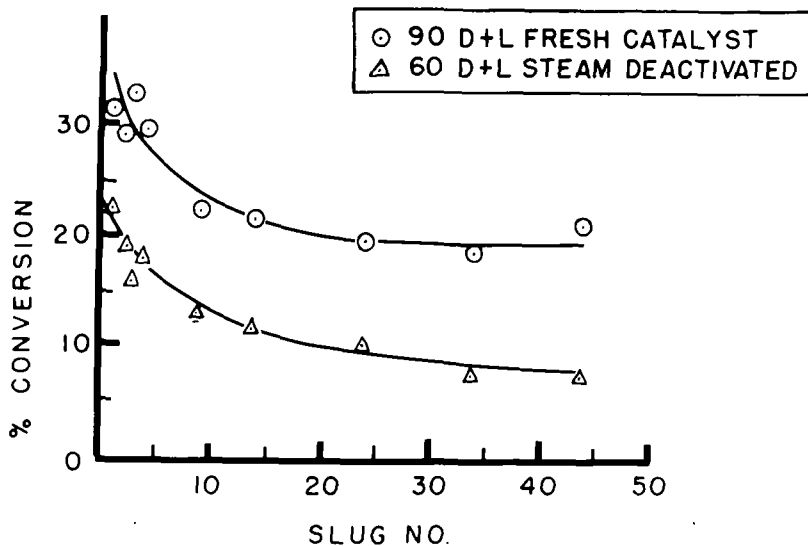


Figure 8

Percent Conversion vs. Slug Number

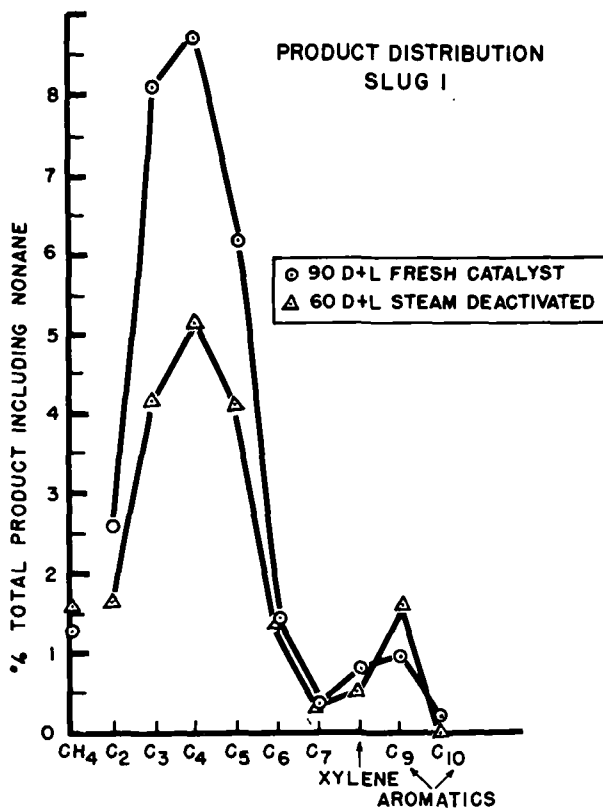


Figure 9

Product Distribution by Carbon Number

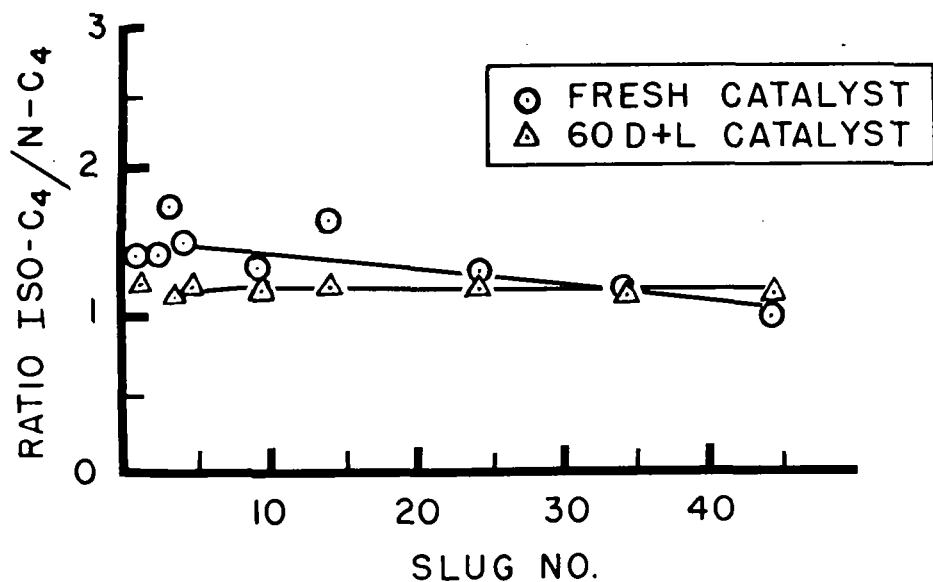


Figure 10
Iso C₄/n C₄ vs. Slug Number

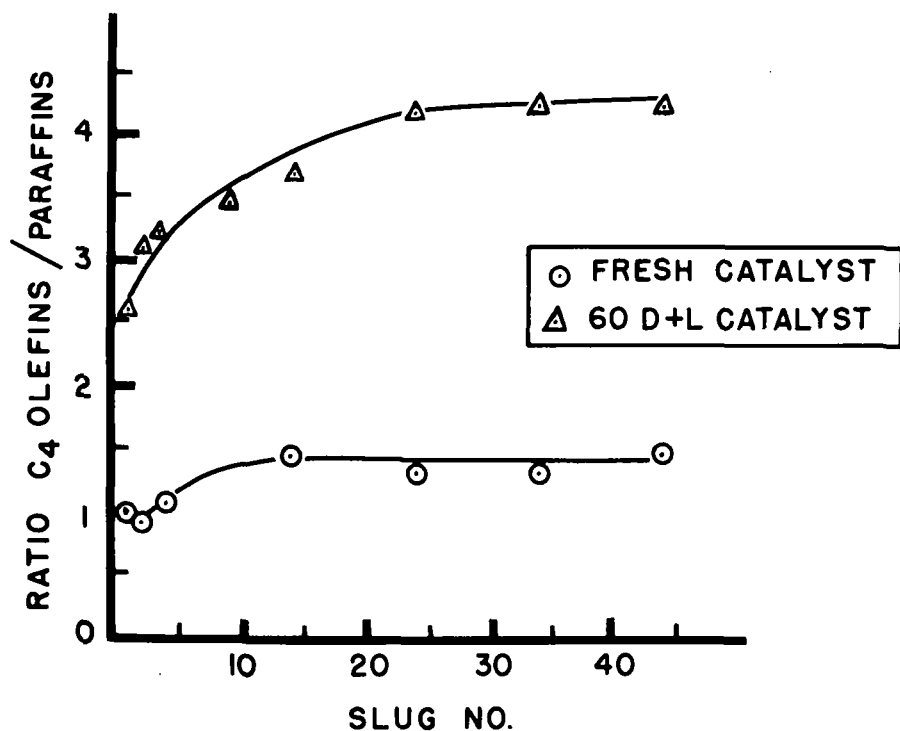


Figure 11
C₄ Olefin/C₄ Paraffin vs. Slug Number

USE OF CAPILLARY GAS CHROMATOGRAPHY WITH
A TOF MASS SPECTROMETER

W. H. McFadden, Roy Teranishi, D. R. Black, and J. C. Day

Western Regional Research Laboratory, Albany 10, California

In recent years considerable attention has been given to the direct introduction into a rapid scan mass spectrometer of eluents emerging from a gas chromatographic column (1,2,3). This technique is of value when it is not possible or convenient to collect the eluent and perform the analysis by means of a conventional inlet system. Such can occur when the unknown chemical may be unstable and polymerize or oxidize before the operator can perform the mass analysis. Frequently, the eluent contains only a few micrograms of material and subsequent transfer to the mass spectrometer may be difficult or inconvenient. Often these small amounts of material are collected with very low efficiency, primarily due to aerosol effects, and direct introduction becomes desirable.

Previous work has been done with packed chromatographic columns by diverting approximately 1% of the total eluent into the mass spectrometer. With capillary chromatograms the total gas flow is normally about 1% of that used in packed column chromatographs so it seemed logical to consider the possibility of introducing the total eluent into the mass spectrometer. This simple extension of the existing technique is very desirable when analyzing complicated mixtures which can only be satisfactorily fractionated with a capillary chromatograph. Normally the capillary column can be expected to have 10 to 100 times the theoretical plates obtainable with a packed column and consequently will give separations not achieved by the latter. This is particularly necessary when the unresolved components have a similar mass spectral pattern such as occurs with meta and para xylenes.

The apparatus used in this work is shown schematically in Figure 1. The chromatographic equipment is operated in a conventional manner except that the exit pressure is reduced to vacuum. To compensate for this, the gauge pressure at the inlet is reduced by 15 lbs. and in this manner retention times are close to those observed with the same equipment operating under normal atmospheric outlet pressures. The auxiliary vacuum is used for preliminary evacuation of the chromatograph exit. Occasionally it is used to reduce by a factor of two to four the amount of eluent entering the mass spectrometer. In operation the micrometer valve is wide open.

The helium carrier gas from the chromatograph enters directly into the ionization chamber of a Bendix Time-of-Flight Mass Spectrometer. The mass spectrometer vacuum system maintains a pressure of about 10^{-5} Torr (estimated from an ion gauge calibrated for dry air). The presence of an organic compound in the eluent is determined by observing the mass spectral output on the oscilloscope. When an unknown appears, the mass spectrum is recorded on a Minneapolis-Honeywell Visacorder at a scan rate of m/e 24-200 in 8 seconds.

In this preliminary work a simultaneous chromatographic detector has not been used. Consequently, without a chromatographic record, it is not possible to compare directly chromatograms obtained under vacuum with those obtained under normal operating conditions. However, reconstructed chromatograms have been obtained by plotting the intensity of the base peak recorded on the mass spectrum versus retention time. Although this does not give an exact measure of the amount of material, it enables the placement of the observed compounds and hence gives a general estimation of the chromatographic efficiency. Results have indicated this to be as good or better than that obtained by a similar column operating with a conventional ionization detector at atmospheric pressure. This is in accordance with currently accepted views on column operating efficiency (4).

In Figure 2, a typical chromatogram from a packed column is shown. The sample was a small fraction separated from an orange juice condensate oil. The column was a 1" preparatory column but the separation efficiency was essentially the same as can be obtained on a 1/8" column. The substrate used for this separation was neopentylglycol-succinate and is considered to be very favorable for compounds of the type present in this unknown. The chromatogram shows the presence of six compounds which were identified primarily by matching the RF values of classically known compounds.

In Figure 3, a capillary chromatogram of the same sample is shown. In spite of the fact that the Dow 710 silicone oil used in the column gives poorer separation than the neopentylglycol-succinate used in the packed column, the mixture is now resolved to show twelve compounds. Because the majority of these are $C_{10}H_{16}$ terpenes it is essential that they must be separated if any mass spectral identification is to be obtained. For example, the mass spectra of α -thujene and α -pinene are sufficiently similar that 1-5% impurity of α -thujene in α -pinene would go completely undetected. The pattern for

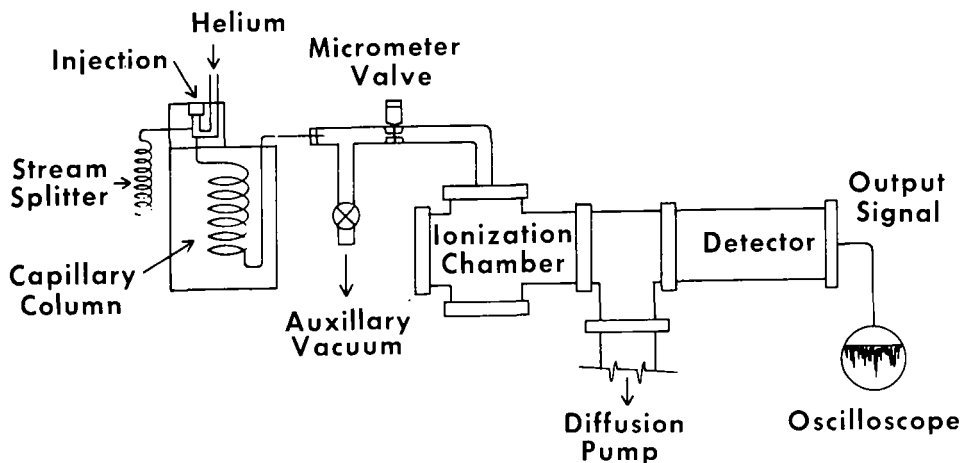


FIGURE 1

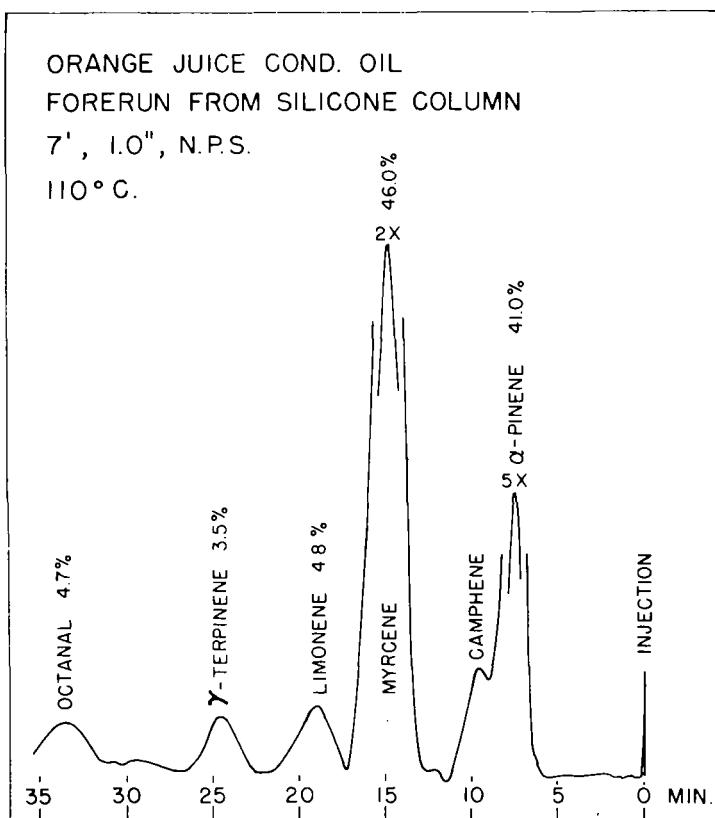


FIGURE 2

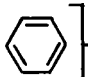

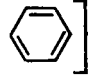
camphene differs considerably in the intensity of the base peak at m/e 93 (22% of the total ionization for α -pinene, 13% for camphene) but this difference is spread rather evenly throughout the other peaks so that 2% camphene in α -pinene might be interpreted as a small error in the base peak intensity. Clearly separation of these types of compounds is necessary. The two chromatographic peaks labeled $C_{10}H_{16}$ in Figure 3 have not yet been structurally identified but as impurities in the overwhelming myrcene fraction, their presence was not even detectable.

Another example that emphasizes the need for the utmost separating power in the chromatographic equipment is given by results obtained on a tiny sample of extract from peas. After a laborious series of chemical and extractive separations performed on 5000 lbs. of fresh peas, there was obtained, in addition to other fractions, about 3-4 microliters of a residual oil. This mixture gave 22 clear chromatographic peaks on a packed column. On a capillary column, 29 peaks were observed but this was not run with an optimum temperature program. With a lower temperature program the eluent from the capillary column was introduced into the mass spectrometer and 39 separate compounds were observed.

The class identity of these 39 compounds is shown in Table 1. Eighteen alkyl benzenes were observed. It is again emphasized that because many of these have similar mass spectral patterns the identification of one in the presence of an isomer is difficult even in relatively large amounts.

Table 1

COMPOUNDS OBSERVED IN EXTRACTANT
FROM BLANCHED FRESH PEAS

	Number of Compounds
 } C_2	3
 } C_3	6
 } C_4	9
Aliphatic Hydrocarbons above C_7 (Also possibly ketones)	12
Others: Terpenes, Indenes, Furans, etc.	9
Total	39

Although the presence of several aliphatic hydrocarbons was determined, the mass spectra of the many isomers of C_9H_{20} , $C_{10}H_{22}$, etc., are so similar that positive identification of such small quantities is almost impossible. It is of value however to get an estimate of how complex the mixture of this class of compound might be and again the combined capillary chromatography and mass spectrometry offers the most practical solution. Identification of some of the other compounds in this pea extract is still tentative and awaits further study.

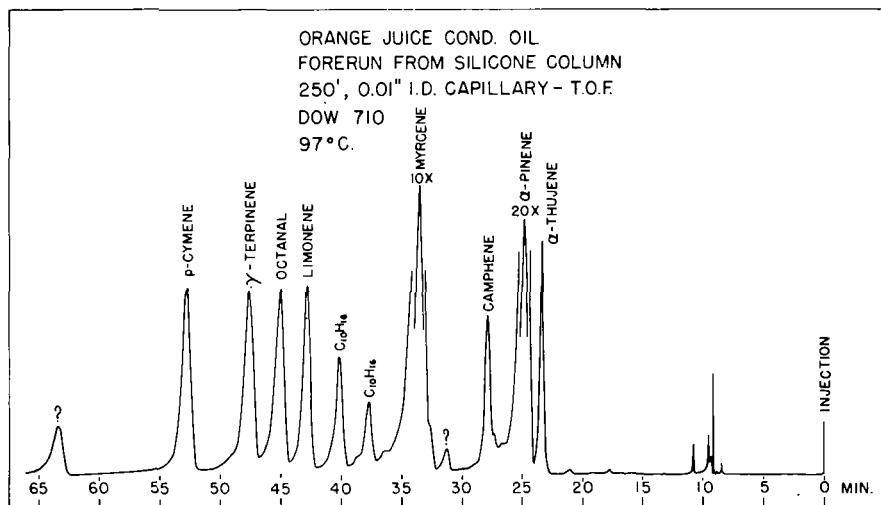


FIGURE 3

CAPILLARY-TOF APPLE JUICE EXTRACT

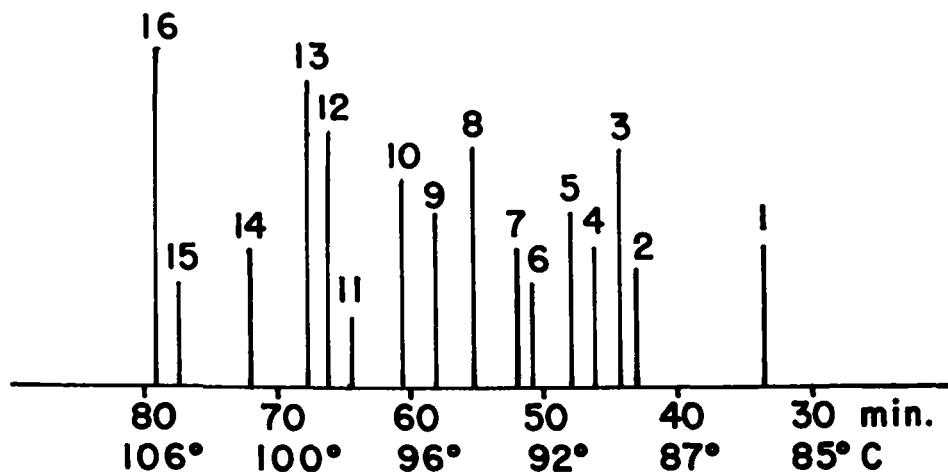


FIGURE 4

As a final example of the advantages of this technique, some of the data obtained on an apple juice extract are presented. Figure 4 is a synthetic chromatogram obtained by plotting the intensity of the base peak versus the retention time. Several of the peaks have been identified and, as would be expected, correspond to compounds established by classical identification methods. In addition, a pentenal and hexenal were tentatively identified. These compounds may have been missed in classical work because of the long, tedious extractive procedures in which such labile compounds were decomposed. In the present work, since only a few microliters were required, a quick extraction was performed on 1 liter of apple juice with a low-boiling solvent that was easily evaporated off. The total time from beginning to final analysis was only a few hours and the possibility of error due to decomposition or oxidation is considerably reduced.

Chromatographic peaks fifteen and sixteen have not yet been identified. A preliminary study indicates that each of these may be two uncatalogued compounds, possibly aldehydes or unsaturated esters or alcohols in the molecular weight range 114 to 128. If this work had been performed with a packed column, these two peaks would most likely have been one chromatographic peak and the hope of identifying four uncatalogued compounds of moderate complexity from the mass spectrum of their mixture would seem very unlikely. Indeed, it would not be easy to tell that four materials were present. Further work will be required, but the extra separation efficiency offered by the capillary column has in this case again given information not easily obtained.

In conclusion it is appropriate to note that this technique is only an extension of work pioneered and established by other workers (1,2,3). Because it makes possible separations and mass analysis not attained from previously described techniques, it is desirable to emphasize the simplicity with which capillary chromatography can be coupled to a rapid scan mass spectrometer.

We wish to acknowledge the contributions and encouragement of many other members of the Western Regional Laboratory staff, in particular, Dr. J. W. Ralls and Mr. R. M. Seifert who permitted us to use their work on pea extractant as an example.

References

1. Gohlke, R. C., Anal. Chem. 31, 535 (1959).
2. Lindeman, L. P., Annis, J. L., Anal. Chem. 32, 1742 (1960).
3. Ebert, A. A., Jr., Anal. Chem. 33, 1865 (1961).
4. Giddings, J. C., Nature 191, 1291 (1961).

Uses of a Total Ionization Monitor for Time-of-Flight Mass Spectrometry

Roland S. Gohlke
The Dow Chemical Company
Eastern Research Laboratory
Framingham, Massachusetts

Our laboratory has had a mass spectrometer, a time-of-flight instrument manufactured by Bendix, and has been modified to provide mass resolution which is considerably superior to time-of-flight instruments previously available. The mass spectrometer itself will be fully described in a paper to be given later in the week. One area we are going to investigate with the mass spectrometer is the study of chemical reactions occurring at near atmospheric pressure in a flowing system. For example, we might wish to examine, in a continuous manner, changes in the product distribution from cracking ethylbenzene to styrene as the temperature or pressure of the reaction were modified. To this end we have constructed a highly versatile, miniature reactor which essentially fits into the ion source of the mass spectrometer in such a manner that the reactor orifice is within 1 1/2 cm's of the ionizing electron beam. That's enough about the reactor - perhaps I'll describe it more fully at next year's meeting.

In preparing the mass spectrometer for its end use, it was desirable to incorporate several modifications into the mass spectrometer. One of these modifications appears to have a fairly wide area of application and this is what we wish to describe.

We have incorporated an electronic device into the mass spectrometer so that we have an option of two modes of operation. We can operate normally and obtain the usual 10,000 spectra per second from the instrument, or, we can obtain 5,000 spectra per second and a measurement of the total number of ions reaching the detector by switching in the circuitry shown in Fig. 1. This device functions as follows: on the first mass spectrometer cycle we are given the normal mass spectrum in the usual manner, to use as we see fit. On the second mass spectrometer cycle, however, -150 V is applied to one of the collectors in the multiplier within 0.5 microseconds and stays there for the entire duration of that instrument cycle, which is 100 microseconds. This has the effect of collecting the electrons provided by all the ions as they strike the collector and hence is a measure, or at least an indication of the total number of ions that strike the collector. On instrument cycles 1, 3, 5, 7, etc., we obtain the normal mass spectrum which can be viewed with the oscilloscope or which can be scanned in the usual manner. On cycles 2, 4, 6, 8, etc., we obtain a voltage which is a measure of the total ionization occurring. The total ionization measurement is monitored with the meter on the scanner chassis and also with a recorder. We do not observe it on the oscilloscope.

A separate, simple power supply is used to power this alternant cycle integrator, as we call it, and this is shown in Figure 2. The entire device was constructed by B-Line Electronics of Saxonville, Massachusetts and cost us \$350.00.

We use it for a number of different tasks. We might use it to check whether or not the trap current regulator is helping to stabilize the mass spectrometer output as shown in Figure 3, and we would see that the total ionization monitor tells us that the trap current regulator is helping to alleviate a downward drift in total ionization which is occurring from some unknown cause in the unregulated mode. The total ionization monitor also provides a rapid method of adjusting the various mass spectrometer controls such as the horizontal and vertical deflection to provide maximum output. These adjustments can be made with a higher degree of sensitivity than is possible to obtain by trying to visually observe slight peak height changes on the oscilloscope. Adjustment of the mass spectrometer's external magnets is also facilitated with the total ionization monitor.

We use it while we are obtaining spectra for analytical purposes as shown in Figure 4. Here we felt that the previous sample had been pumped out at this point so we injected a new sample of 1 μ l of acetone into the inlet system. When the total ionization monitor indicated that a reasonably

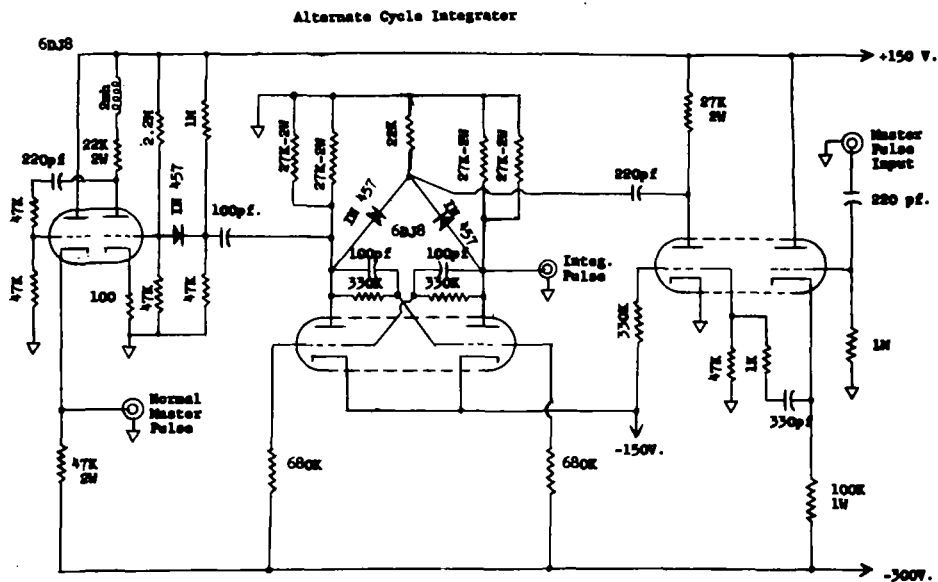


Figure 1

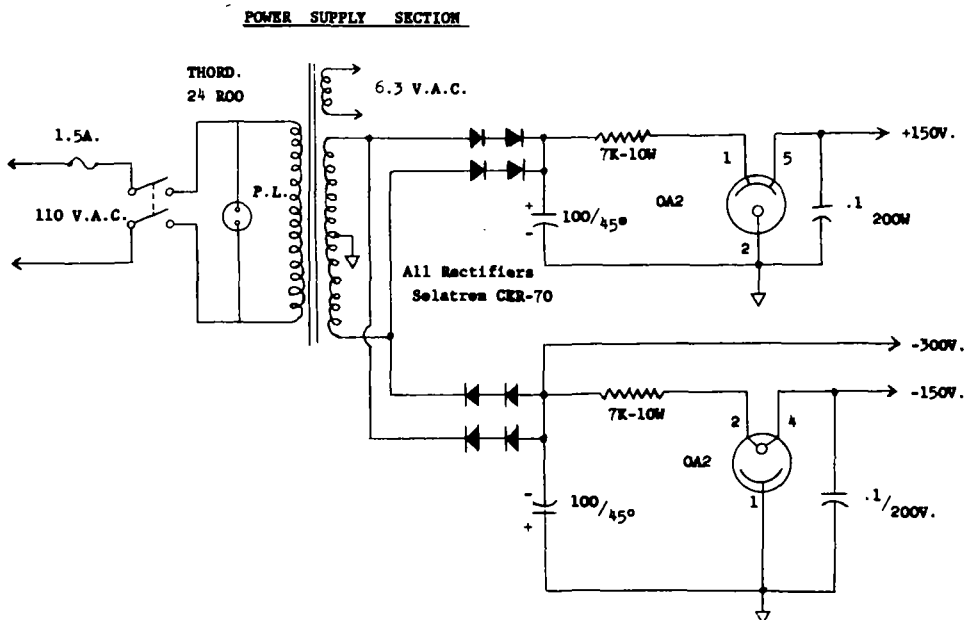


Figure 2

steady state existed, we scanned the acetone spectrum shown in the lower trace, while the monitor recorded an unusually rapid sample depletion. When we decided that a sufficient mass range had been scanned and opened the pump out valve, the total ionization monitor indicated a fairly slow pump out. The entire action shown on this slide required about three minutes.

Sometimes, not all goes well as shown in Figure 5. Here, in an extremely poor spectrum of an organo tin compound, the total ionization monitor indicated a series of rapid pressure fluctuations occurring at the low mass end, followed by a general withdrawal of the mass spectrometer from the field of battle as shown by this decline. In this manner, we have a very nice indication as to how much reliance we should place upon the spectrum. If we have to use a spectrum such as this, we can at least use the total ionization trace as a crude normalization base to adjust all the peak heights to constant pressure conditions.

Figure 6 shows another use. Here we wanted to know the identity of a solvent which had been used to crystallize a certain material. We heated a single crystal until it melted, whereupon a small amount of vapor was released. A glance at the oscilloscope revealed that this pressure surge was due to CH_2Cl_2 and this broader one was due to water. We could, of course, have scanned the spectra with one of the unused pens, if the identity had been in doubt (Recorder being used in a Minneapolis-Honeywell 12-channel Visicorder).

Figure 7 illustrates how well the total ionization monitor might demonstrate some unsuspected failure, such as a sudden leakage of the silicone rubber system through which liquid samples are injected into our inlet system. Unless the oscilloscope had been observed rather carefully, we would really have had no reason to suspect that the higher mass ions had been scanned under conditions quite different from the lower mass ions.

I should point out that one of the reasons the system failed so fortuitously is that it was being repeatedly pierced with a 20 ga hypodermic needle throughout the course of the scan. The sample was then pumped out as indicated.

We have also used the device to monitor the output from capillary gas chromatography columns, in which case the total ionization monitor responds to each component as it leaves the column. No other detector is necessary.

We have also used it in conjunction with our Knudsen Cell to indicate the changes in ionization as the effusion of a particular specie proceeds.

All in all, the device has been most useful to us and I am sure that additional applications or modifications of it have already suggested themselves to you.

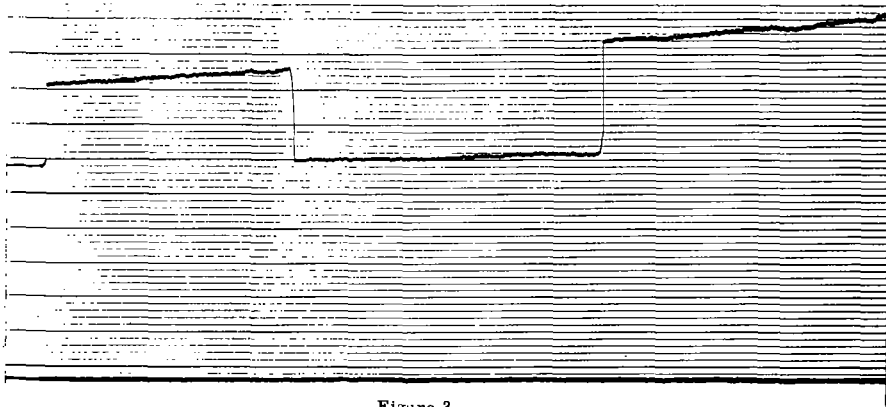


Figure 3

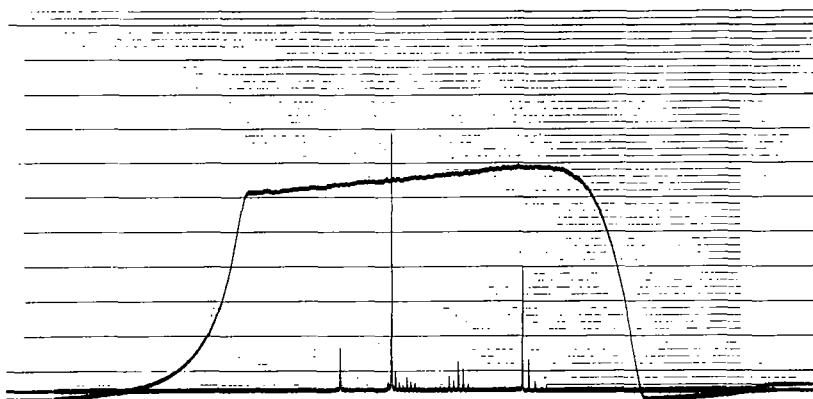


Figure 4



Figure 5

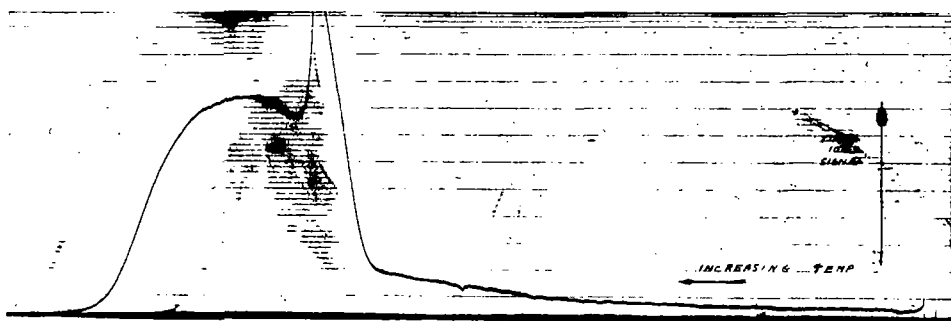


Figure 6

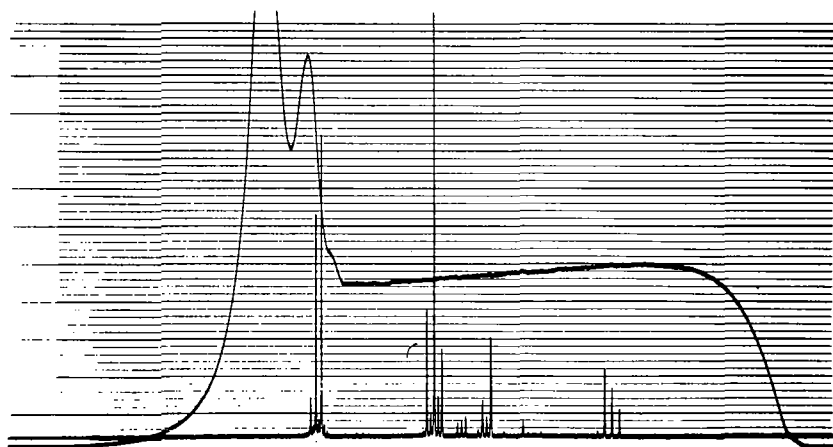


Figure 7

"ANALYSIS OF COPOLYMERS BY PYROLYSIS AND MASS SPECTROMETRY"

Graham G. Wanless
Esso Research & Engineering Company
Linden, New Jersey

The first slide⁽¹⁾, if you please, will show where this method fits in the polymer family. This tabulation shows skeletal parts of the Simha classification scale, which lists polymers according to the manner in which they come apart, on pyrolysis.

Slide 1

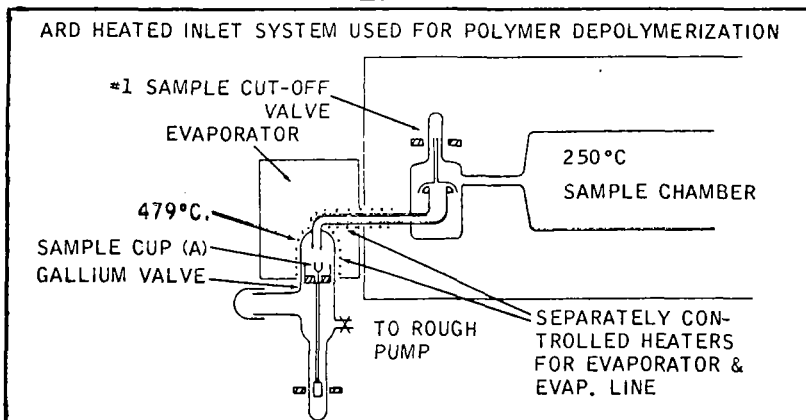
<u>Polymer Degradation Studies</u>	
<u>Polymer</u>	<u>Monomer Yield (Wt. %)</u>
Ethylene or Methylene	0.025 Wt. %
m-Methyl Styrene	45.
Methyl Methacrylate	>95.

Products which produce high yields of monomers can be dealt with easily by assaying the off-gases. There are published methods for this, for example, Strassburger, Brauer et al (1960). We are concerned principally with the other end of the Simha scale--that is, with those polymers which yield minor amounts of monomeric gases, decompose by random scission, and yield predominantly lube-oil-like fragments.

The objective of this work was to develop a rapid mass spectrometric method for analysis of copolymers--and the particular example of this paper is the copolymer of 1-pentene and 4 methyl 1-pentene.

Our best procedure consists of depolymerizing a portion of a milligram sample of a polymer in a device which is attached directly to the heated inlet system of the mass spectrometer. This equipment is sketched in the next slide⁽²⁾.

Slide 2



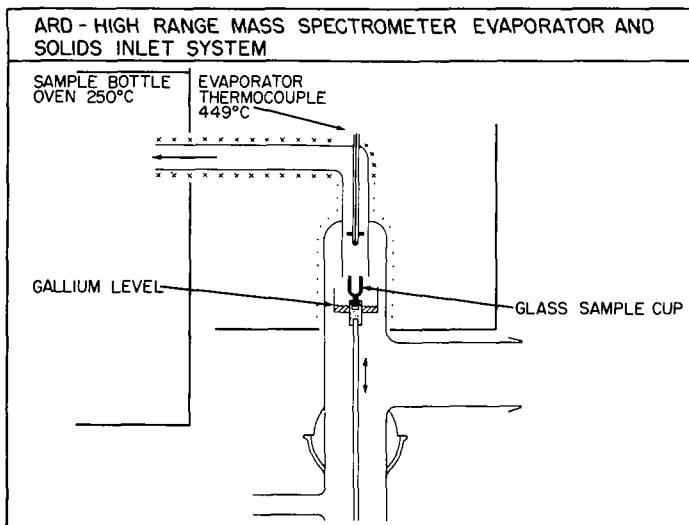
More detail of the sample cup is shown in Slide 2A, please. (Referring to the slide.....) This flange on the temperature probe forms a cover for the sample cup, after the latter has been raised up. Since the thermocouple bead is now inside the sample cup, we can know the polymer decomposition temperature rather exactly.

The mass spectrometer solids inlet system has two very special advantages for this type of work:

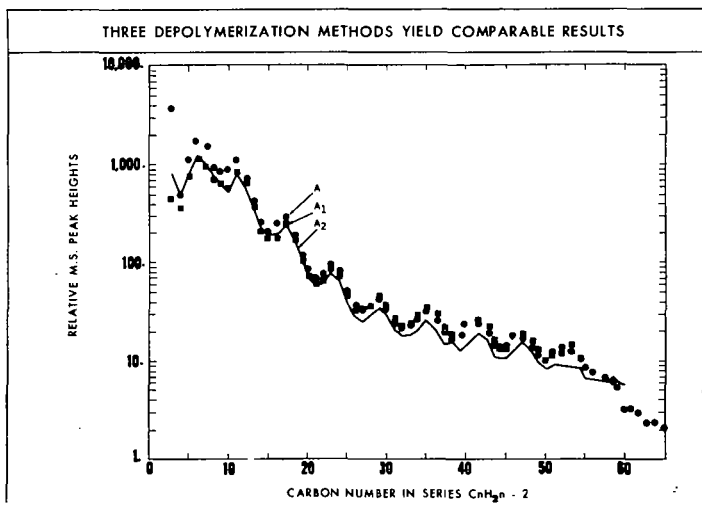
- (a) Rapid escape of the cracked fragments into the cooler high-vacuum sample system of the instrument, thus allowing minimum thermal abuse of these fragments.
- (b) The total ionization meter which permits us to control the quantity of cracked gases introduced into the instrument--without having to weigh out a sample.

It has been known already that the spectra which one can obtain from such depolymerizates are quite specific. I should make reference to an earlier paper in this committee by D. L. Cook in June 1959. An example of these spectral regularities are shown in Slide 3. You will note how these characteristics persist up to C_{60} at least, thus embracing a sequence of 9 or 10 monomer units. The slide shows only the series C_nH_{2n-2} , which we prefer for this work.

Slide 2A



Slide 3



Another objective of this slide is to show that essentially the same results can be obtained, with some variations in cracking severity. Slide 3 shows results from three different cracking procedures--two variations using the apparatus already described, and a third in an all glass vacuum apparatus comparable to that of D. L. Cook(1959). Some latitude is present and this is very satisfactory from an analytical standpoint.

The real problem is how to interpret such spectra. Our basis for doing so is the scheme shown in the next slide(4), please.

Thus, if the copolymer is made from two monomers A and B, one would expect by simple theory to obtain the products and cross products shown in this slide. Now if the copolymer is rich in B and poor in A, one would predict:

$$\begin{aligned} B &> A \\ 2B &> 2A \\ 1A2B &> 2A1B, \text{ etc.} \end{aligned}$$

Slide 4

Monomers	A	B
<u>Dimers</u>	2A	AB 2B
<u>Trimers</u>	3A	2A1B 1A2B 3B
<u>Tetramers</u>	4A	3A1B 2A2B 1A3B 4B
<u>Pentamers</u>	5A	4A1B 3A2B 2A3B 1A4B 5B
<u>Hexamers</u>	6A	5A1B 4A2B 3A3B 2A4B 1A5B 6B
<u>Heptamers</u>	7A	6A1B 5A2B 4A3B 3A4B 2A5B 1A6B 7B
<u>Octamers</u>	8A	7A1B 6A2B 5A3B 4A4B 3A5B 2A6B 1A7B 8B
<u>Nonamers</u>	9A	8A1B 7A2B 6A3B 5A4B 4A5B 3A6B 2A7B 1A8B 9B

This idea can be tested out by using a mass spectrum such as the one we have just shown in a previous slide. Let $B = C_6$ and $A = C_5$. Then the result of such a test is shown in the next slide(5).

You will note that the predictions hold perfectly up to hexamers. After this some superimposed complications set in, but the data can still be used for analytical purposes up to the nonamers.

Slide 5

MASS SPECTRAL ABUNDANCE RATIOS FOR COPOLYMER SAMPLE A

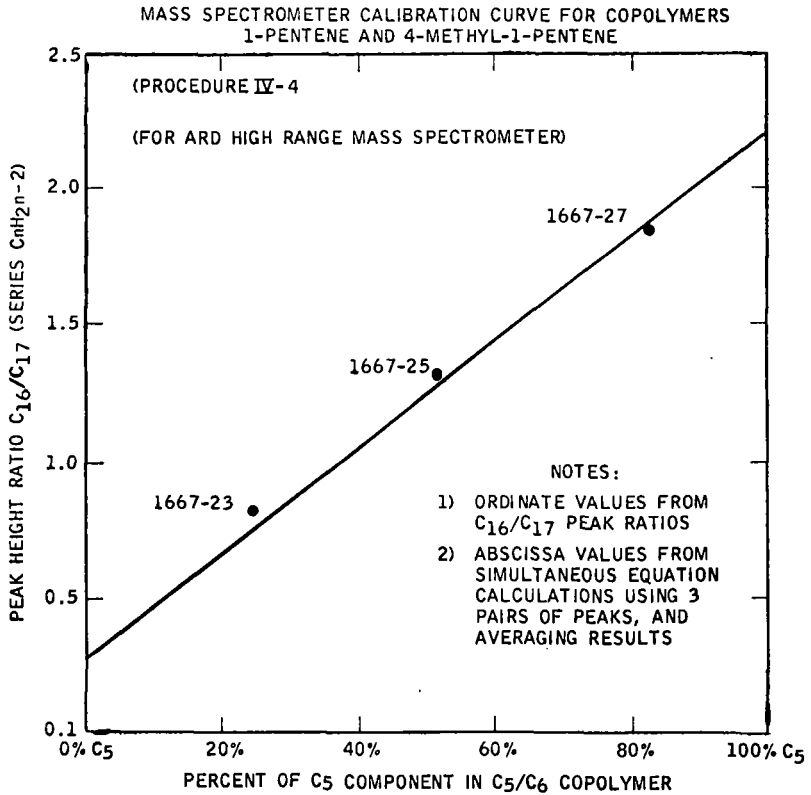
(Series C_nH_{2n-2} , Isotope Corrected Data)

<u>Fragment</u>	<u>Predicted Ratios</u>	<u>Predictions Confirmed or Not</u> (Fig. 2)
<u>Monomers</u>	$C_6 > C_5$	Yes
<u>Dimers</u>	$C_{12} > C_{10}$	Yes
<u>Trimers</u>	$C_{17} > C_{16}$	Yes
<u>Tetramers</u>	$C_{23} > C_{21}$	Yes
<u>Pentamers</u>	$C_{29} > C_{26}$	Yes
	$C_{28} > C_{27}$	Yes
<u>Hexamers</u>	$C_{35} > C_{31}$	Yes
	$C_{34} > C_{32}$	Yes
<u>Heptamers</u>	$C_{41} > C_{36}$	No
	$C_{40} > C_{37}$	No
	$C_{39} > C_{38}$	No but $C_{41} > C_{39}$ etc.
<u>Octamers</u>	$C_{47} > C_{41}$	No
	$C_{46} > C_{42}$	No
	$C_{45} > C_{43}$	Yes + No but $C_{47} > C_{45}$, etc.
<u>Nonamers</u>	$C_{53} > C_{46}$	No
	$C_{52} > C_{47}$	No
	$C_{51} > C_{48}$	No
	$C_{50} > C_{49}$	No but $C_{53} > C_{51}$, etc.

The theory says that we can carry out a one-step depolymerization and MS scanning operation, measure one or more pairs of peak ratios, and read the copolymer composition from a correlation plot. Slide 6 shows such a plot. This slide shows points for three unknown samples plotted about a two-point calibration curve. If one assumes that a linear calibration curve is a fact, then we have an absolute calibration. Rather than assuming this, it is much more satisfactory to correlate with an independent method. For this purpose we use NMR data, on the basis of the next slide(7). (Referring to this slide.....) The copolymers will have the ratio of $\frac{CH + CH_2}{CH_3}$ which will vary between these two extremes.

CH_3

Slide 6



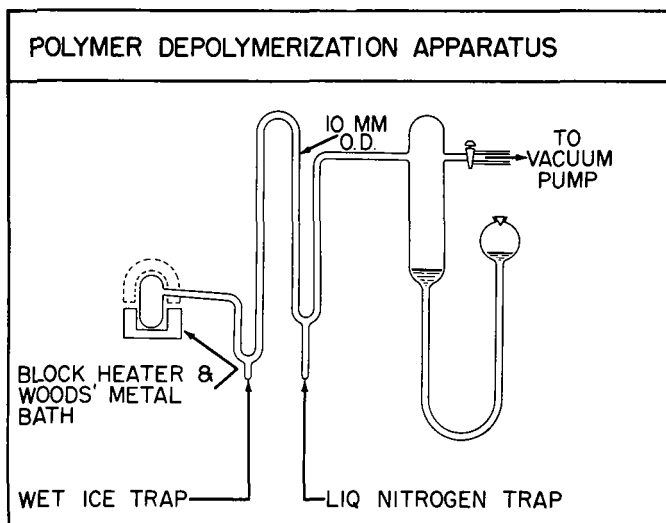
Slide 7

NMR ASSAY CAN REFLECT COPOLYMER COMPOSITION

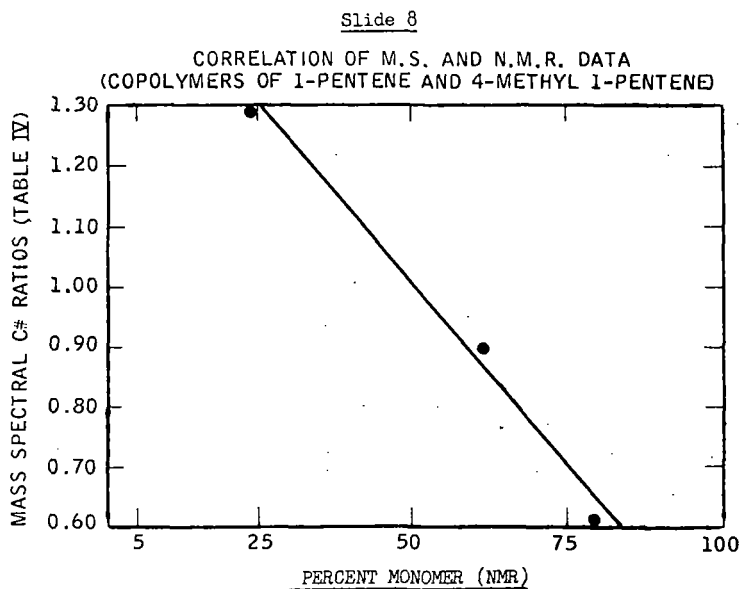
Polymer	Ratio $\frac{CH + CH_2}{CH_3}$
<u>1-Pentene:-</u> $ \begin{array}{c} CH_2 = C - \\ \\ CH_2 \\ \\ CH_2 \\ \\ CH_3 \end{array} $	$ \left[\begin{array}{c} H \\ \\ CH_2 - C - \\ \\ CH_2 \\ \\ CH_2 \\ \\ CH_3 \end{array} \right]_n $ 2.3
<u>4 Methyl-1-Pentene:-</u> $ \begin{array}{c} CH_2 = C - \\ \\ CH_2 \\ \\ C - H \\ / \quad \backslash \\ CH_3 \quad CH_3 \end{array} $	$ \left[\begin{array}{c} H \\ \\ CH_2 - C - \\ \\ CH_2 \\ \\ C - H \\ / \quad \backslash \\ CH_3 \quad CH_3 \end{array} \right]_n $ 1.0

However, these Zeigler-type copolymers are insufficiently soluble for conventional NMR analysis. The difficulty can be overcome by depolymerizing the polymers in an apparatus shown in Slide 7A. This equipment is comparable to that of D. L. Cook (1959). It gives products of about the same molecular weight distribution as does the direct mass spectrometric method.

Slide 7A



methods. The final slide(8) confirms the agreement between the MS and NMR



Mass Spectrometric Study on the Evaporation of Volatile
Components in Commercial Polyethylene

Kisaku Nakagawa

Electrical Communication Laboratory
Nippon Telegraph and Telephone Public Corporation
Musashino-shi, Tokyo, Japan

1. Introduction

Mass spectrometric method has been utilized successfully in analyzing the degradation products of high polymers. Extensive works have been conducted and excellent results have been reported.^(1,2,3)

The recent advances in the field of high molecular weight mass analysis^(4,5) has caused us to study the possibilities of the direct application of the mass spectrometric method to the analysis of the structures of macromolecules, especially for branching structures.

One of the purposes of this paper is to verify the presence of the light components which are vaporizable in a vacuum without being subjected to degradative reactions. The other purpose is to offer the typical mass spectra of the volatile components in commercial polyethylene, and to make comparisons with standard linear hydrocarbons.

2. Preliminary Experiments

2.1. Molecular Distillation of Polyethylene:

In order to confirm the existence of the light components which are volatile when the polyethylene is heated in a vacuum, a commercial high density sample (Marlex, made by Phillips Co. Nominal molecular weight: 70,000) was distilled as shown in Fig. 1. Distillations were performed over a temperature range of 150-400°C.

The molecular weight of the evaporation products condensed on the dry ice trap were estimated cryoscopically, and were on the order of 500-1,500. The results are illustrated in Fig. 2.

The variation in molecular weight of the residual polymer which remained in the bottom of the stills were estimated by means of limited viscosity measurements. The results shown in Fig. 3 indicate an increase in the relative molecular weight up to 250°C. By interpolating the curve in Fig. 3, the temperature at which the polymer sample begins to degrade can be estimated. Degradation reaction in Marlex appeared to predominate over the evaporation at about 280°C.

Finally, both the residues and products were examined by infrared absorption. In Fig. 4a and b, the relative optical density of the absorption due to vinyl, vinylene and vinylidene radicals of the residues and products are illustrated, respectively. Since the molecules of Marlex are believed to have a vinyl radical at each end, the spectrum shown in Fig. 4b could be taken as evidence of the general similarity of both molecules in the residue and product. Moreover, the opposite inclination in the relative optical density of vinyl (referred to the methylene rocking) against the distillation temperature could be regarded as evidence of the presence of evaporation stage prior to that of degradation.

Based on the results of this preliminary study, it would be reasonable to state the following conclusions:

- 1) In commercial polyethylene, there are components having a low molecular weight and can be vaporized at a certain temperature in a high vacuum.
- 2) The molecules in vaporized components have a similar terminal structure as those of molecules in the residue.

2.2. Determination of Ion Source Temperature:

The optimum condition of the mass spectrometer was determined by the following tests. Standard hydrocarbons (API), n-Hexadecane, 1-Hexadecene and 1-Pentadecene, were introduced into the spectrometer and analyzed. Both the ionic yield and the relative ion intensity in the spectra were found to be quite sensitive to the ion source temperature. These variations are shown in Fig. 5 and 6. The base peak was of $C_{16}H_{33}^+$ for three standard samples adopted and over the temperature range of 40-270°C. Most of the peaks belong to

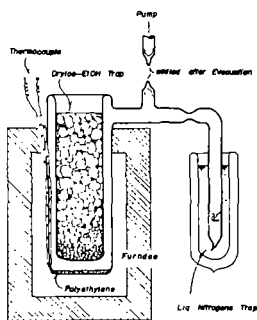


Fig 1 The molecular distillation of polyethylene

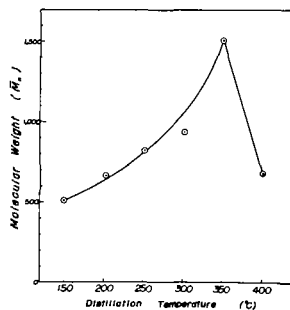


Fig 2 Molecular weight of evaporated product of Marlex

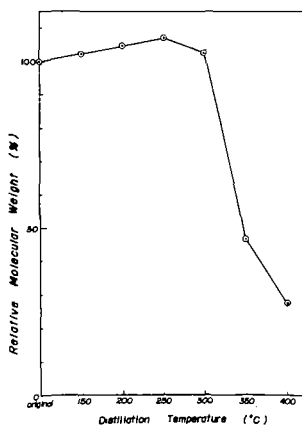


Fig. 3 Variation in average molecular weight of Marlex residue

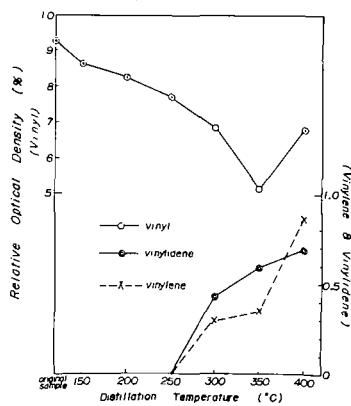


Fig 4 a) Relative optical density of Marlex residue ($D_{100} = 100$)

the $C_nH_{2n+1}^+$ sequence (abbreviated as $2n+1$, hereafter) displayed nearly similar variations to each other. Their intensity increased as the temperature was elevated up to about 200°C and turned to decrease for higher temperatures. The anomalous peaks in the $2n+1$ sequence are of C_{10} , C_{11} and C_{12} . These behaviors are found to have their maxima at about 120°C and minima at about 200°C.

Two species of ions, $C_2H_3^+$ and $C_3H_5^+$ in the $C_nH_{2n-1}^+$ sequence are observed to behave in nearly the same manner as those in the $2n+1$ sequence. Whereas, the peaks having more than 4 carbons belonging to this sequence are found to exhibit the similar variation of the anomalous peaks in $2n+1$ sequence.

The behavior of parent ions are unique to all others. Their decreases in intensity against the ion source temperature are observed to be almost linear up to 200°C. At higher temperatures they reduce their intensity to the amounts which are comparable to those of ions having 14 or more carbon atoms.

In view of the ionic yield and the stability against the temperature fluctuation, the ion source was kept constant at 200°C throughout the process.

3. Experiments on Polyethylene

3.1. Ion Source and the Instrument:

A conventional gas analysis ion source was modified slightly by winding a tungsten wire around the gas inlet glass pipe to serve as a simple furnace. Tungsten wire was 0.1 mm in diameter and the heating zone was 40 mm in length.

Sample polymers (re-precipitated powder) were placed in small vessel made of glass and placed in the furnace. Temperatures in the furnace were indicated by means of an Alumel-Chromel thermocouple enclosed in a glass tube. The modified ion source is illustrated in Fig. 7. The ion Acceleration was reduced to 1,000 v (normally 2,000 v) to extend the analyzable mass range to the C_{18} group or a little higher. The operation constants are listed in Table I.

Table I.
Operation Constants of the Instrument
(Hitachi Model RMU-5)

Ion Acceleration Voltage	1,000 v
Resolving Power (appro.)	170
Analyzable Range	below C_{18} group
Ionization Voltage	80 v
Ion Source Temperature	200°C

3.2. Operation:

When the instrument was evacuated to the order of 10^{-7} mm Hg, degassing was performed by maintaining the sample temperature at about 90°C. This condition was attained by only heating the ion source to 200°C.

It took about 15 minutes to scan from the C_1 to the C_{18} group. The repeated runs represented no marked decrease in ion intensity. Memory effect was examined by stopping the heating of the furnace before the elevation of temperature to a higher value. About half an hour was found to be sufficient to reduce the ion intensities to the amount corresponding to the initial temperature of 90°C. In conclusion, memories were observed to be not essential in this case.

4. Results and Discussion

4.1. Mass Spectra:

In addition to Marlex, Hostalen GD was subjected to the analysis. Hostalen is a polyethylene manufactured by the Ziegler-process. The nominal molecular weight is 70,000, the same as Marlex 50-15.

For both polyethylene samples, many peaks were observed in groups for every carbon number to the extend of our upper limit of mass range. An example of the spectra is shown in Fig. 8.

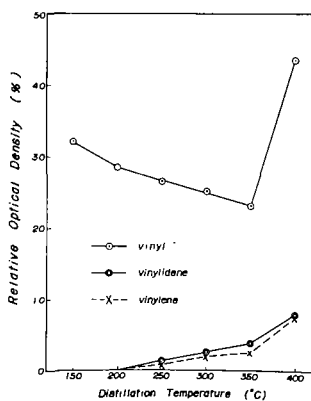


Fig. 4 b) Relative optical density of Marlex product ($D_{100} = 100$)

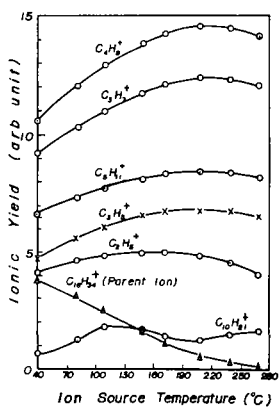


Fig. 5 Ionic yield versus ion source temperature

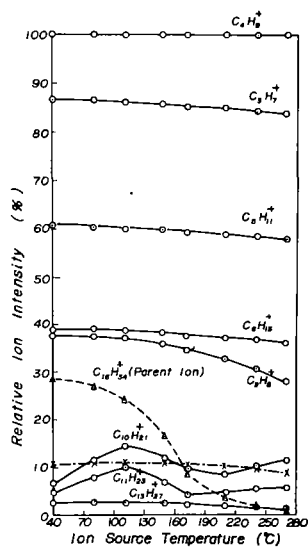


Fig. 6 Relative ion intensity versus ion source temperature

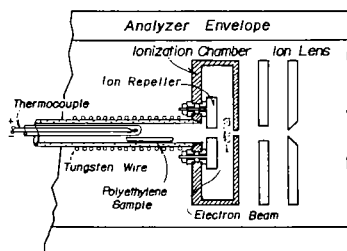


Fig. 7 The modified ion source

The characteristic features of these patterns are summarized as follows:

- 1) The peaks having the highest intensity is the $C_4H_9^+$ ion for both samples and over the entire range of temperature.
- 2) Peaks are distinctly divided into groups according to their number of carbon atoms.
- 3) Each group consists of $C_nH_{2n+1}^+$, $C_nH_{2n-1}^+$, $C_nH_{2n}^+$, $C_nH_{2n-2}^+$ and lower intensity ions. In all groups except C_6-C_9 , the $C_nH_{2n+1}^+$ have the largest and $C_nH_{2n-1}^+$ the next to the largest peak in their respective groups. In C_6-C_9 groups, the $C_nH_{2n-1}^+$ have the largest peaks.
- 4) Total ionization of groups is expressed in the descending intensity C_4 , C_3 , C_5 and the groups having more carbon atoms.

The percentage intensities of $C_nH_{2n+1}^+$ and $C_nH_{2n-1}^+$ relative to the base peak are illustrated in Fig. 9 and 10. The corresponding ions of the standard $n-C_{16}H_{34}$ and $1-C_{16}H_{32}$ are superimposed thereon. The anomalous peaks, of C_{10} and C_{11} , were found to be quite sensitive to the ion source temperature.

In comparing the $C_nH_{2n+1}^+$ patterns of standard normal paraffine with the corresponding patterns of both polyethylene samples a close similarity was observed. On the contrary the $C_nH_{2n-1}^+$ patterns were observed to come close to those of α -olefine.

4.2. Reactions at Temperature below 350°C:

In Fig. 11, temperature dependence of typical peaks of both samples were illustrated in Arrhenius plot. As shown in the figure, the processes of ion production, namely the production of vapor from the polymer sample, were found to consist of two stages: a gradual increase in intensity in the lower temperature range, and a following steeper increase at the higher temperatures. The former is named Process I, and the latter Process II.

Since, in this case, the peak height would be directly proportional to the rate of yield of vapor products, activation energies can be calculated from the figure directly.

For Process II, the activation energies are found to be 24.7 kcal/mol and 34.0 kcal/mol for Hostalen and Marlex, respectively. Two ionic species in each sample are regarded to behave similarly to each other. These activation energies are much lower than those presented by Jellinek, ⁽⁶⁾ who offered the values of 46-66 kcal/mol, and of Madorsky ⁽⁷⁾ of 71 kcal/mol. Both authors associated these values to the reaction of thermal degradation in polyethylene.

Although the details of the reactions occurring in these temperature regions are not obvious, it might be speculated that some degradative reactions are taking place. They might be caused by some other reasons than the simple C-C ruptures. Moreover, the temperatures corresponding to the nicks of the curves in the figure are found to be about 290°C and 210°C for Marlex and Hostalen, respectively. The former is in fair agreement to the molecular distillation mentioned previously in Sec. 2.1.

For Process I, activation energies are found to be 6.7 and 5.8 kcal/mol for $C_4H_9^+$ and $C_4H_7^+$ ions of Hostalen, and 7.6 and 6.5 kcal/mol for the corresponding ions of Marlex. Taking the mean values of all other ions belonging to each sequence, the value for Process I appeared to be 6.5 ± 1.2 kcal/mol. Taking into account the limited accuracy of the measurements, the whole ions which appeared at temperatures lower than the nick could be regarded to have been generated through a reaction.

In view of the low value in the activation energy, the rate determining step in this region can be attributed to evaporation or diffusion of the vapor molecules.

Employing the spin-echo technique, McCall et al ⁽⁸⁾ estimated the activation energy of the self-diffusion of low pressure polyethylene to be 5.3 kcal/mol. The same authors observed the levelling off in the activation energy at about $C_{20}-C_{30}$ in their experiment on standard hydrocarbons, and they correlated this phenomena with the segmental motion of molecular flow in polymers. On the other hand, Jensen ⁽⁹⁾ estimated the vapor pressure of polyethylene (details were not given) by evacuating an oven containing the polymer through an orifice. Jensen reported that the vapor pressure, P , for the temperature range of 30-180°C, was expressible as $\log P = 7.4 - 4,500/T$, which is the equivalent to an energy of activation of 8.9 kcal/mol.

Although both values are slightly different from the result obtained in this paper, McCall's value is rather close to ours. Taking into account the difference in the pump out speed between these two experimental conditions, it might be concluded that the reaction taking place during Process I is the evaporation of the lighter components included

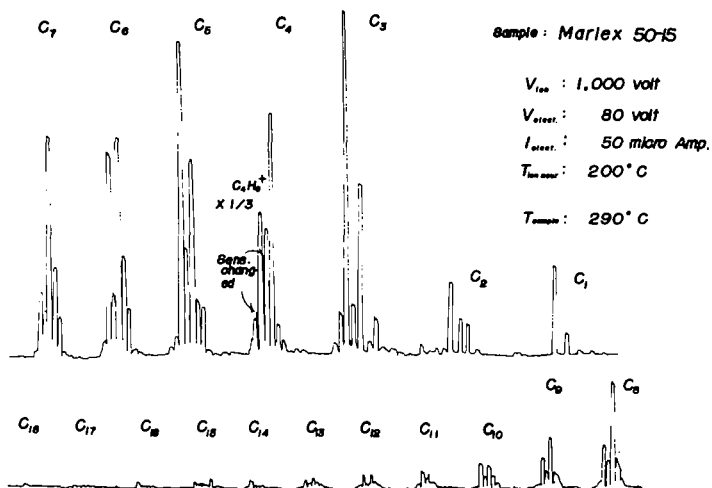


Fig. 8 A mass spectrum of polyethylene

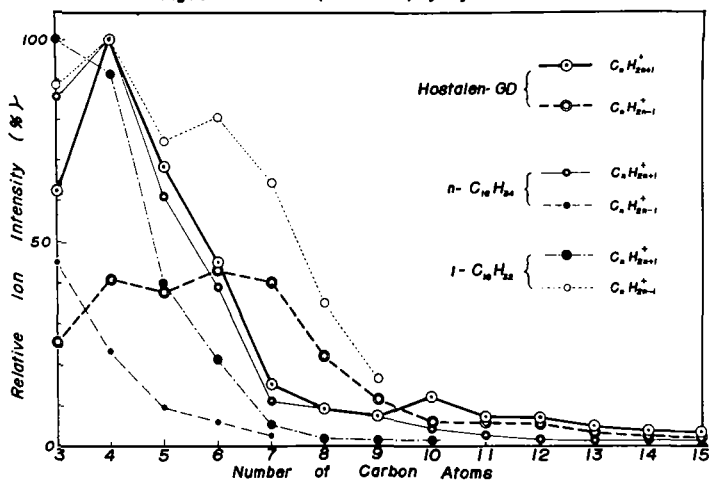


Fig. 9 Relative Intensity of $C_n H_{2n+1}^+$ and $C_n H_{2n+2}^+$ ions of Hostalen GD

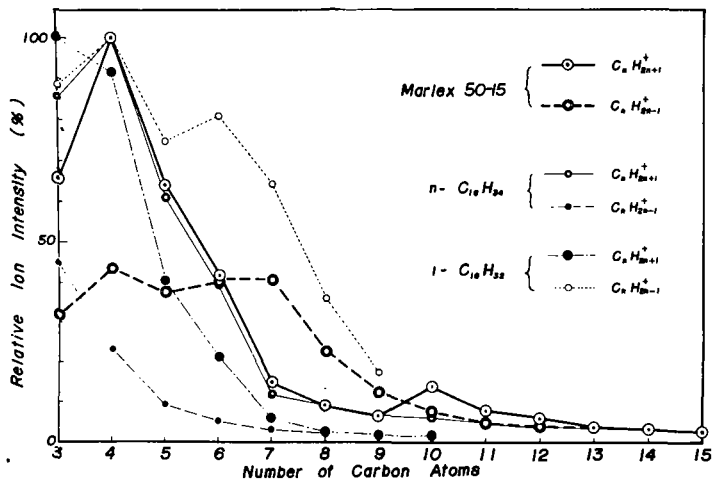


Fig. 10 Relative Intensity of $C_n H_{2n+1}^+$ and $C_n H_{2n+2}^+$ ions of Marlex 50-15

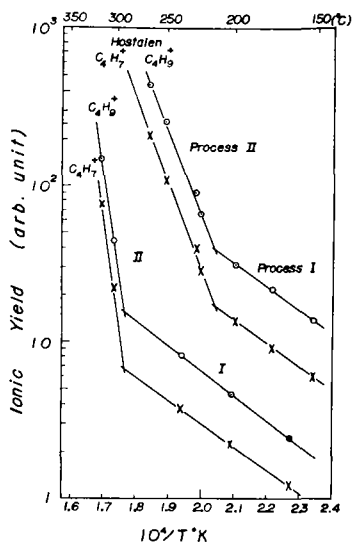


Fig. 11 Ionic yield versus reciprocal of evaporation temperature

originally in the polymer sample, and that the rate of the process is determined by the diffusion of these components through the sample.

Therefore, those ions which are detected at temperatures corresponding to Process I could be subjected to the mass analysis.

5. Summary

Two samples of commercial polyethylene were heated in the furnace prepared close by the ion source of a mass spectrometer. From the results obtained by this experiment and the preliminary works, the following conclusions are obtained:

- 1) Many ions were detected when the sample was heated up to about 150°C. These ions display a pattern which is characteristic to the chain hydrocarbons having carbon atoms more, at least, than 18. Cryoscopic determination indicated that the molecular weight of the Marlex product at that temperature to be about 500.
- 2) Arrhenius plot of the ion intensity indicates that the reactions taking place in the sample polymer consist of two stages: Process I and II.
- 3) Activation energies of two samples corresponding to Process I are appeared to be equal to each other, and to be 6.5 + 1.2 kcal/mol. This value might be correlated to the diffusion process of the volatile components through the sample polymers.
- 4) Process II would be associated to some reaction of degradation. Activation energies corresponding to this stage are appeared to be 34.0 and 24.7 kcal/mol for Marlex and Hostalen, respectively.
- 5) Transition temperatures from Process I to II indicate the point where the degradation in the polymer sample begins to predominate over the evaporation.
- 6) Thus, the peaks detected at temperatures in Process I are those of the ions of volatile components which evaporated out of polymer sample.

References

- 1) S. L. Madorsky and S. Straus, J. Res. NBS., **40**, 417 (1948).
- 2) S. L. Madorsky, S. Straus, D. Thompson and L. Williamson, *ibid.*, **42**, 499 (1949).
- 3) B. G. Achhammer, M. J. Reiney, L. A. Wall and F. W. Reinhart, J. Polymer Sci., **8**, 555 (1952).
- 4) M. J. O'Neal, "Mass Spectroscopy in Physical Research", NBS circular 522 (1953).
- 5) A. Hood and M. J. O'Neal, "Advances in Mass Spectrometry", Pergamon, pp. 175 (1959).
- 6) H. H. G. Jellinek, J. Polymer Sci., **3**, 859 (1948); **4**, 1; 13 (1949).
- 7) S. L. Madorsky, *ibid.*, **2**, 133 (1952).
- 8) D. W. McCall, D. C. Douglass and E. W. Anderson, J. Chem. Phys., **30**, 711 (1959).
- 9) Neals Jensen, J. Appl. Phys., **27**, 1460 (1948).

A MASS SPECTROMETRIC STUDY OF PHOSGENE AND ITS INTERMEDIARIES

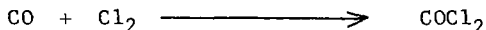
By: H. R. Harless
Research and Development Dept.
Union Carbide Chemicals Company
South Charleston, West Virginia

Phosgene (carbonyl chloride) is becoming more generally important as a commercial chemical. Due to recent added interest in this highly corrosive material it appeared imperative that crude product mixtures and refined batches of phosgene be subjected to extensive analytical rectification.

Phosgene is usually produced by the direct reaction of carbon monoxide and chlorine. Chlorine can be purchased from commercial suppliers in a relatively pure state. Carbon monoxide is ordinarily made according to the reaction shown on slide 1.



The carbon monoxide made from this reaction is combined with an equal amount of chlorine at elevated temperatures as illustrated in the lower equation of the first slide.



Analysis of phosgene had been accomplished, in the past, by wet-chemical methods using various techniques, many of which employed modified Orsat equipment. These procedures are lengthy and costly, therefore various instrumental methods of analysis were investigated. Infrared spectroscopy proved to be of value in identifying functional groups of contained impurities but was not amenable to the complete analysis of phosgene plus all impurities. Gas chromatography of commercial phosgene was explored but this method was also deficient due to the reactivity and corrosiveness of the material. The literature is essentially devoid of information about mass spectrometry and gas chromatography of phosgene.

At the Pittsburgh Conference on Analytical Chemistry and Applied Spectroscopy in March of this year W. H. Gunn and R. A. Murie, Diamond Alkali Research Center, Painesville, Ohio, noted that the reactivity and corrosiveness of hydrochloric acid, phosgene, and chlorine gases precluded their separation and determination via gas chromatography. A search of the literature by Gunn and Murie gave no information on this separation. Therefore, the development of columns for their separation was undertaken. A number of columns were investigated; some gave partial resolution, others resolved the component, but gave poor peaks. The substrate materials investigated included fluorocarbons, fluoro-silicone fluid, chlorowax, and other halogenated materials.

Also at the Pittsburgh meeting H. J. Hoenes, H. C. Proehl and Z. Nagy, Pittsburgh Plate Glass Company, Chemical Division, Barberton, Ohio, described a gas chromatographic method for the analysis of oxygen, nitrogen, carbon monoxide, carbon dioxide and chlorine in phosgene. Using a single chromatograph with two columns mounted on a four-way Teflon valve, their analysis was accomplished in about 30 minutes. With a four-meter column of Fluorolube and a one-meter column of 13X molecular sieve in series, oxygen, nitrogen, and carbon monoxide were eluted in time to turn the four-way valve causing phosgene to by-pass the molecular sieve column. A second sample, injected with the molecular sieve column in the by-pass position, gave a combined peak for oxygen, nitrogen, and carbon monoxide, but separated the carbon dioxide, chlorine, and phosgene. They noted that sample handling and peak height calibration were exceedingly delicate.

Since chemical methods are lengthy and expensive and other instrumental methods were not completely satisfactory, mass spectrometry was explored rigorously in this laboratory. Personal communications with commercial suppliers of phosgene indicated that they considered that it would be impossible to analyze this material with a mass spectrometer. Our study was undertaken as a last resort.

The most severe obstacles to a study of phosgene by mass spectrometry are, 1. the corrosive nature of phosgene toward the metals of the instrument, 2. the extreme dipole action upon the interior surfaces of the mass spectrometer, resulting in memory effects, and 3. the reaction of phosgene with residual micro amounts of water inside the instrument to form carbon dioxide and hydrogen chloride which is difficult to distinguish from that contained in the original phosgene. Any water is immediately consumed by the following reaction:



(As a sidelight I would like to suggest that if you wish to remove all traces of moisture from your mass spectrometers, merely inject a small sample of phosgene and pray for the life of your filament).

After many attempts to reconcile anomalous results, especially spurious concentrations of carbon dioxide and hydrogen chloride, a conditioning method was developed, wherein a large preliminary injection of phosgene was allowed to reach equilibrium inside the mass spectrometer. It is believed that this pretreatment will involve dipole dislodgement of prior residents, positioning of dipoles upon the interior surfaces, and the reaction of phosgene with residual water.

A period of five to seven minutes with 100 microns of phosgene appears sufficient for equilibrium to be achieved by this pre-treatment and subsequent evacuation of the mass spectrometer results in stable operating conditions. A rigorous program has been pursued which indicates that satisfactory analytical results, for product mixtures, can be attained.

A typical analysis of cylinder-grade phosgene lists eight components as follows:

Compound	Mole Per Cent
Carbon Monoxide	4.6
Carbon Dioxide	0.5
Hydrogen Chloride	0.2
Carbon Tetrachloride	0.1
Carbonyl Sulfide	0.1
Acetone	0.2
Sulfur Dioxide	0.1
Phosgene	94.2

In addition to these constituents, varying and sporadic amounts of nitrogen, chlorine, dichloroethane, and trichloropropene have been observed from time to time.

Carbon tetrachloride was considered an incongruous constituent until impurities present in the carbon monoxide from the modified water-gas reaction were resolved. Excess methane, one of the materials usually present in the carbon monoxide, is sometimes carried with product carbon monoxide and is chlorinated, primarily, to carbon tetrachloride. An extension of this reaction also leads to infrequent traces of the C-2 and C-3 halogenated hydrocarbons.

Mass spectrometry can be employed to resolve all of the listed impurities in phosgene. The easily predicted ionization modes of phosgene are seen in the monoisotopic mass spectrum shown in the next slide.

PHOSGENE MASS SPECTRUM (Monoisotopic)

M/E	R.I.	ION ⁺
12	0.3	C
16	0.1	O
28	2.3	CO
31.5	0.2	metastable
35	24.9	Cl
47	3.2	CCl
63	100.0	COC1
70	4.1	Cl ₂
82	0.6	CCl ₂
98	3.8	COC1 ₂

Additional demands were placed upon our technique due to the highly corrosive nature of chlorine which is detrimental to metallic parts of the inlet system and ionization chamber of a mass spectrometer. Free chlorine was eliminated by agitating product mixtures from the CO + Cl₂ reaction with mercury to form the non-volatile chlorides of mercury prior to injection of the gaseous products into the instrument. Estimates of the amounts of excess chlorine in certain mixtures were then made, independently, by gravimetric methods.

CONCLUSION

Mass spectrometry is amenable to analysis of phosgene in crude commercial product mixtures and in refined batches of high-purity material. Impurities inherent to the stepwise reactions leading to phosgene have been identified and resolved by applying unique conditioning methods. Adaptation of these methods to process control has been satisfactorily accomplished.

MASS SPECTROMETRIC STUDY OF POLYMERIC IONS, A.H. Turnbull,
Atomic Energy Research Establishment, Harwell, Berkshire,
England.

In the experiments described in this paper, gas was admitted to the mass spectrometer through a molecular beam system. Hence gas molecules reaching the ion chamber of the mass spectrometer had followed a collision-free path. The general layout of the apparatus is shown in Fig. 1, while the molecular beam system is shown in greater detail in Fig. 2.

Gas from a reservoir at pressures up to 6 atm. entered the first stage of the molecular beam system through a 0.6×10^{-5} inch diameter orifice. Some of the gas molecules then entered the second stage through a 0.05 inch diameter orifice. Gas-scattering of molecules from the beam was minimised by keeping the distance between the first and second orifices as short as possible. This was achieved, as shown in Fig. 2, by mounting the second orifice on a cone. The first stage bolted directly on to the mouth of a 4 inch oil diffusion pump (speed 300 litres/sec.), so that a pressure of about 1 torr was maintained within this stage for a reservoir pressure of about 5 atm. The second stage bolted directly on to a 2 inch oil diffusion pump (speed 70 litres/sec.) and was separated from the third stage by a slit 0.400 inch x 0.04 inch. The third stage was in turn separated from the mass spectrometer by a slit of the same size and was pumped by a 2 inch mercury diffusion pump with a liquid nitrogen trap (speed 30 litres/sec.).

This inlet system and the associated mass spectrometer (6 inch radius analyzer, 90° deflection in magnetic field) were designed and constructed in the Reactor Technology Branch of the U.K.A.E.A. Reactor Group. During experiments carried out there, using carbon dioxide as the sample gas, polymeric ions of the form $(\text{CO}_2)_n$ were reported by Bentley¹, who considered three possible sources.

(a) They are formed in the mass spectrometer itself, either by ion-molecule reaction or some other process. Experimental evidence seemed to rule out this possibility.

(b) Polymeric molecules are formed during the expansion of the gas from the reservoir into the molecular beam system. There was no evidence to show whether or not this was the cause. Bentley considered it unlikely on the grounds that an expansion involves, on average, the separation of adjacent molecules. Joule-Thomson cooling was calculated to be less than 6°C .

(c) Polymeric molecules are always present in carbon dioxide. Bentley considered that this was the most probable explanation "in the light of existing evidence".

The mass spectrometer and molecular beam inlet system were transferred from the U.K.A.E.A. Reactor Technology Branch to A.E.R.E., Harwell where, in the course of further work, the existence of these polymeric ions was confirmed. Their source, however, is still doubtful. The results of two experiments did not support the hypothesis that polymeric molecules are always present in carbon dioxide.

Experiment 1. Two baffle plates, each carrying a 5/16 inch diameter off-axis hole, were mounted inside the cone which carried the entrance orifice of the second stage of the molecular beam system, while the large end of the cone was closed by a plate carrying a 0.25 inch x 0.042 inch slit aligned with the entrance and exit slits of the third stage of the molecular beam system. Thus those gas molecules which reached the ion source of the mass spectrometer must have suffered several thousand wall collisions between entering and leaving the second stage of the molecular beam system. The effect of the baffles was to cause the complete disappearance of the ions $(\text{CO}_2)_n^+$ from the mass spectrum for $n > 1$. (The intensity of the CO_2^+ peak was about 1/5 of the value prior to the insertion of the baffles).

Experiment 2. The gas reservoir and the pipe leading from it to the entrance orifice of the molecular beam system were filled with 1/8 inch diameter lead shot, thus reducing the gas space to a large number of small volumes whose

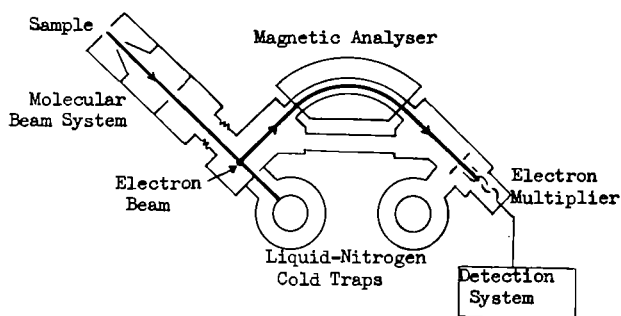


Fig. 1. Schematic Diagram of the Mass Spectrometer
and Molecular Beam Inlet System

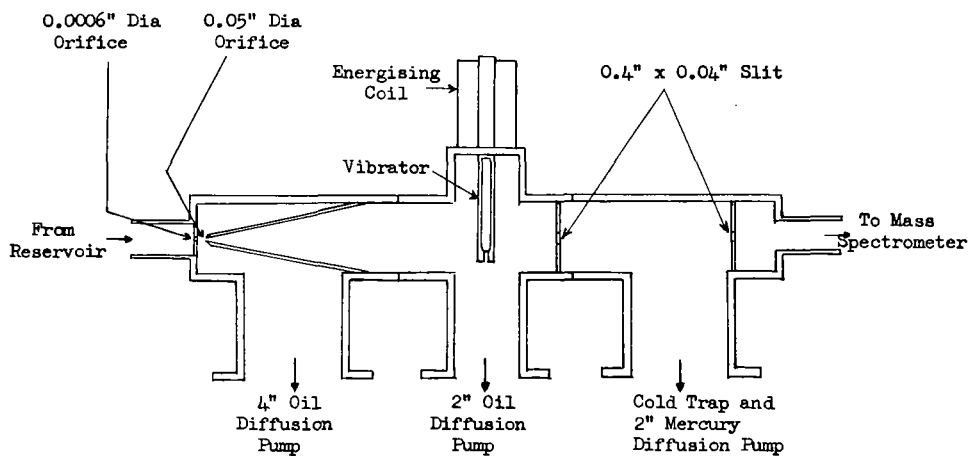


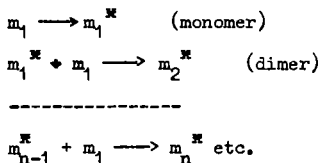
Fig. 2. Molecular Beam Inlet System.

wall-to-wall dimension was about 1/40 that of the empty reservoir. There was no resultant change in the relative intensities of the polymeric ions for a given carbon dioxide pressure in the reservoir.

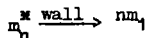
The results of Experiment 1 show that:

- (a) The polymeric ions are not formed in the mass spectrometer.
- (b) The polymers are destroyed by wall collisions.

On its way from the gas reservoir to the inlet of the molecular beam system, a molecule makes of the order of 10^4 wall collisions. Since polymers are in fact observed in the system (and are not formed in the mass spectrometer), they must if initially present in the reservoir, be reconstituted by gas collisions made on the way from the reservoir to the inlet of the molecular beam system. (It was calculated that gas collisions would be about 10^5 times as frequent as wall collisions). One therefore postulates an initiation process:-



and a chain termination process as follows:-



The equation governing the reaction may therefore be written:-

$$\frac{d[m_n^*]}{dt} = k_p [m_{n-1}^*][m_1] - k_p [m_n^*][m_1] - k_d [m_n^*]$$

where k_p and k_d are rate constants.

At equilibrium, $d[m_n^*]/dt = 0$

$$\text{whence } \frac{m_{n-1}^*}{m_n^*} = \frac{k_p [m_1] + k_d}{k_p [m_1]}$$

The rate of chain termination due to destruction at the wall is proportional to the rate of diffusion to the wall. According to the Einstein-Smoluchowski equation

$$k_d = \alpha \frac{2D_n}{\Delta^2}$$

where α = constant;

Δ = average distance to wall;

D_n = diffusion coefficient for m_n^*

Now D_n is inversely proportional to m_n^* and so one can write

$$k_d = K_n / \Delta^2 [m_n^*]$$

where K_n is a constant for a given value of n .

$$\text{Then } \frac{m_{n-1}^*}{m_n^*} = 1 + \frac{K_n}{k_p \Delta^2 [m_n^*][m_1]}$$

Thus a change in Δ should cause a change in $[m_{n-1}^*]/[m_n^*]$, which is at variance with the results of Experiment 2.

With the molecular beam system and reservoir in their initial condition, several other gases were examined in the mass spectrometer, with the following results.

He, O₂: No polymers seen.

N₂O: Polymers seen up to about (N₂O)₁₀⁺

N₂: A peak was seen at mass 56, i.e. (N₂)₂⁺, which was about 1/6 of the N₂ peak. No other polymers were visible at least up to (N₂)₆⁺. N₂ from the same gas cylinder was examined in a mass spectrometer with a conventional gas inlet system. No peak at mass 56 was visible.

SO₂: Polymers were seen up to (SO₂)₇⁺ at mass 448. Peaks were also present at masses 80, 112, 144, 176, 208 and 240, which correspond to (SO₂)_n⁺ + O. When examined in a conventional mass spectrometer, SO₂ from the same gas cylinder showed only the usual cracking pattern, with peaks at masses 32, 48 and 64.

It is considered possible that these polymers and complex molecules are created by a shock wave which forms in the molecular beam system, probably between the first and second orifices. By isolating the supply of gas to the reservoir and observing the rate of pressure drop in the latter as the gas passed into the molecular beam system, the mass flow rate of gas through the first orifice was determined, knowing the orifice area and the pressure on its downstream side, the gas velocity was calculated and found to be supersonic.

Experiments are in hand to test the shock wave hypothesis.

1. P.G. Bentley, Nature, 190, 432 (1961).

INVESTIGATIONS OF AZIDE DECOMPOSITION REACTIONS BY ISOTOPIC TRACER TECHNIQUE

Donald P. Easter and Amos J. Coleman

Basic Research Group
U. S. Army Engineer Research and Development Laboratories
Fort Belvoir, Virginia

The thermal and photolytic decomposition of the metal azides has been the subject of much study, particularly over the past ten years. However, no firm conclusions have been drawn regarding the reaction mechanism. The overall decomposition is usually represented by the equation:



where Me represents any metal. Since this must obviously be a step process we must consider the possible steps which can lead to this overall result. The formation of a neutral N_3 radical is generally accepted as the key to interpretations of decomposition of ionic azides.^{1, 2} Unimolecular breakdown of an azide radical to give a nitrogen molecule and an atom in their ground states requires only 7.5 kcal/mole but is forbidden by the correlation rules. Dissociation into excited products is permitted, but requires an additional 62 kcal/mole.

Unfortunately, the simple conclusion that the reaction must therefore be bimolecular is not borne out by kinetic studies. The evidence is not completely unequivocal, but a unimolecular process seems to be favored.³ Moreover, the products are not simply and invariably metal plus nitrogen. Depending upon the reaction conditions and the particular azide under study, varying amounts of nitrides and other products may be formed.

We have attacked this problem through the use of potassium azide labeled in a central or terminal position with nitrogen-15.^{4, 5, 6} (European and American usage differ with regard to the placing of the superscript numbers indicating atomic weights in formulae. In an effort to avoid any possible confusion in this regard, I have placed the superscript numbers directly over the symbol of the element). Figure 1 shows the two N-15 labeled forms of potassium azide. Since the compound is ionic, the two ends of the azide radical are indistinguishable. Below it are shown the three possible nitrogen molecules involving the mass 14 and 15 isotopes.

Two decomposition schemes will be considered, represented overall by the equations shown in Figure 2. Formation of potassium nitride indicated in the second equation may be considered to arise from the reaction of potassium metal with nascent nitrogen from decomposing azide around it, or by some stepwise process which does not involve the intermediate formation of free potassium. An alternative series of reactions in the presence of water can yield ammonia in the same overall stoichiometry without the intermediate formation of potassium nitride.

EXPERIMENTAL PART

The apparatus used in carrying out the decompositions is shown in Figure 3. The quartz reaction bulb is seen at the left of the figure. The gas handling system in which volatile reaction products were pumped off and measured consists of a recording manometer, cold trap, small diffusion pump, Toepler pump, gas burette, and McLeod gauge. A more detailed diagram of the reaction cell and recording manometer is shown in Figure 4. The pressure change produced by the decomposition reaction was followed by means of a single arm mercury manometer with a resistance wire sealed into the arm holding the moving mercury column. Any change in the mercury level resulted in a change in resistance which was measured and recorded by the circuit shown in Figure 5. This set-up permitted unattended operation of the apparatus for extended periods of time with continuous registration of the progress of the reaction. Figures 6, 7, and 8 show some typical time-pressure curves obtained in various modes of decomposition. In all cases the reaction was continued to virtual completion; that is, until no further pressure change was observed over an extended period of time. The gas was pumped over into the burette, measured, and transferred to a sample bulb for mass spectrometric analysis and determination of

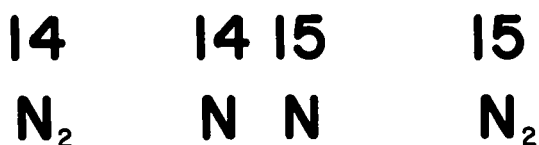


FIGURE 1

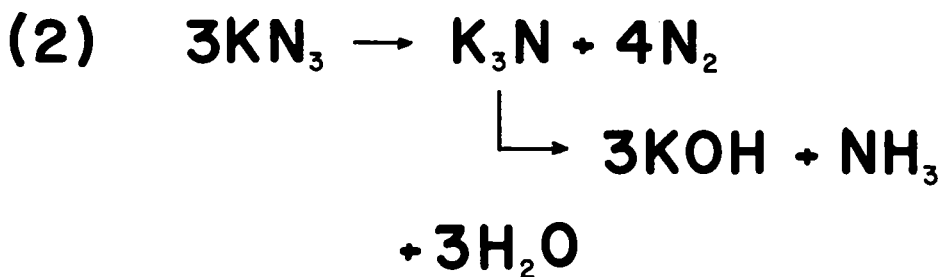
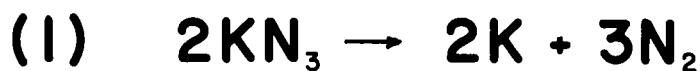


FIGURE 2

isotopic distribution. Water was added to the solid residue remaining in the bulb, resulting in a vigorous effervescent reaction. The solution was then cooled to liquid air temperature, and a second gas sample was taken.

An alternative procedure, used in the photolysis experiments, was to expose a water solution of the azide sample contained in a double walled quartz vessel to the light from a mercury lamp, GE UA-3. Cooling water circulating through the jacket held the temperature below 15°C during the reaction. After decomposition had apparently gone to completion, the solution was cooled to liquid air temperature and volatile products were pumped off and measured as described above.

Measurement of the isotopic distribution of nitrogen gas was made by standard mass spectrometric techniques. However, in order to make a similar determination on ammonia, it is essential to separate it quantitatively from water, since N-15 ammonia and H₂O coincide on the mass scale. This, unexpectedly, proved to be a formidable problem. There are a number of well known procedures for producing dry ammonia gas which are not particularly difficult. But the quantitative removal of a small concentration of ammonia in water solution to permit gas analysis and isotope determination has so far defied all efforts. Chemical drying agents capable under atmospheric pressure of reducing partial pressure of water in a gas stream to <0.001 mm are ineffective, since the traps must be evacuated to secure quantitative passage of NH₃. The gas chromatograph, using packing of polyethylene glycol on fluoropack, gave apparent separation, in that the detector trace indicated no overlap of the water and ammonia peaks, but mass spectrometric analysis of the trapped fractions showed that large amounts of water remained in the ammonia, even after a double pass through the column. By proper control of flow rate and column temperature, separation of the ammonia and water peaks on the detector trace could be extended to any desired time. Fraction cutting could be accomplished with assurance of no sample overlapping. The unheated parts of the apparatus were flamed for outgassing. Carrier gas was kept running continuously for weeks with liquid air trapping at the inlet and the whole system above atmospheric pressure. Even with all possible precautions that occurred to us, water contamination of the ammonia samples could not be eliminated.

Since isotopic distribution of the product ammonia is an important datum, we are now working on the chemical conversion of the ammonia to nitrogen to permit this determination.

Ammonia analyses to be reported here were made by titration following distillation from the basic solution remaining after the experimental procedure described above.

RESULTS

Our initial experimentation was done with terminally labeled compounds, simply because this was the material which was most readily available. The results, predictably, were inconclusive. It was found that the fraction of azide decomposing by the metal plus nitrogen route, as indicated by the amount of hydrogen liberated in the reaction with water, varied from a maximum of 11% in the rapid thermolysis runs down to a fraction of 1%. Isotopic distribution of the nitrogen gas obtained in decomposition reactions of terminally labeled potassium azide showed less than half the theoretically expected amount of N_2^{15} .

Similar experiments made with centrally labeled potassium azide yielded only a fraction of 1% N_2^{15} , whereas random recombination of nitrogen atoms should have been expected to give a mixture consisting of 44.4% N_2^{14} , 44.4% NN^{15} , and 11.1% N_2^{15} .

The results, in summary, are shown in Figure 9. The relative amounts of hydrogen and ammonia in the products were taken to indicate the percentage decomposition of the azides by the alternate routes. Isotopic distribution of nitrogen in each mode of decomposition for the two types of N-15 labeled potassium azide is shown at the right.

The results are consistent with the hypothesis of a unimolecular process. The formation of a free azide radical at some stage of the reactions is neither conclusively supported nor precluded by these findings. However, further studies⁷ are in progress in these laboratories which it is hoped will conclusively answer this question.

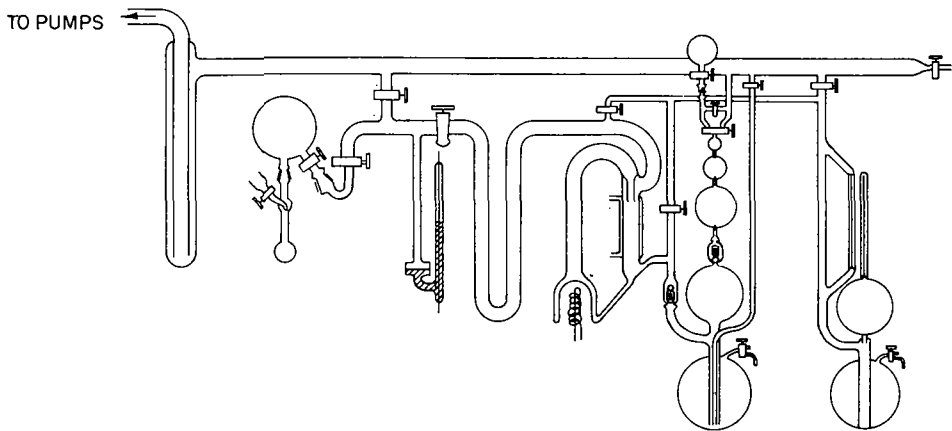


FIGURE 3

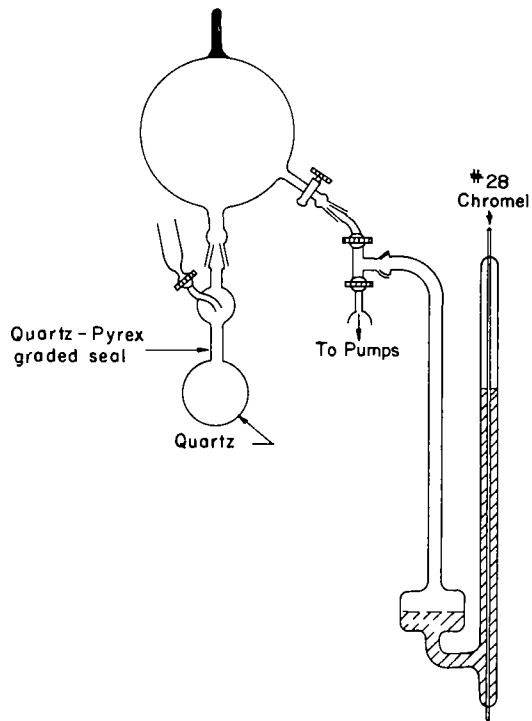
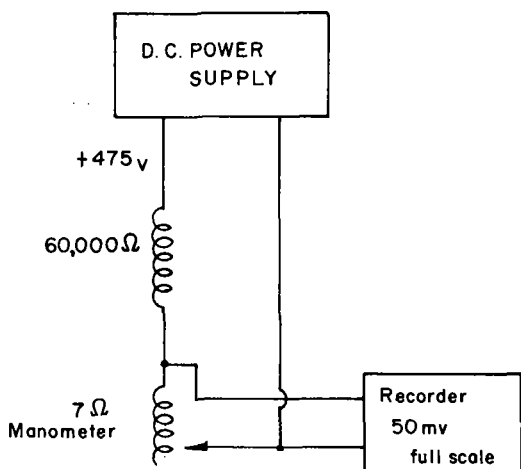


FIGURE 4

REFERENCES

1. Evans, B. L. and Yoffe, A. D. , Proc. Royal Soc. (London) A250, 346 (1959).
2. Gray, P. and Waddington, T. C. , Proc. Royal Soc. (London) A241, 110 (1957).
3. Jacobs, P. W. M. and Tompkins, F. C. , Proc. Royal Soc. (London) A215, 265 (1952).
4. Clusius, K. and Effenberger, E. , Helv. Chim. Acta 38, 1834, 1843 (1955).
5. Clusius, K. and Knopf, H. , Helv. Chim. Acta 39, 681 (1956).
6. Clusius, K. and Schumacher, H. , Helv. Chim. Acta 41, 972, 2265 (1958).
7. Easter, D. P. , Proc. 9th Annual Basic Research Contractors Conference and Symposium, USAERDL, 92-95 (1960).



CIRCUIT DIAGRAM OF RECORDING MANOMETER

FIGURE 5

PHOTOLYSIS OF KN_3 in AQUEOUS SOLUTION

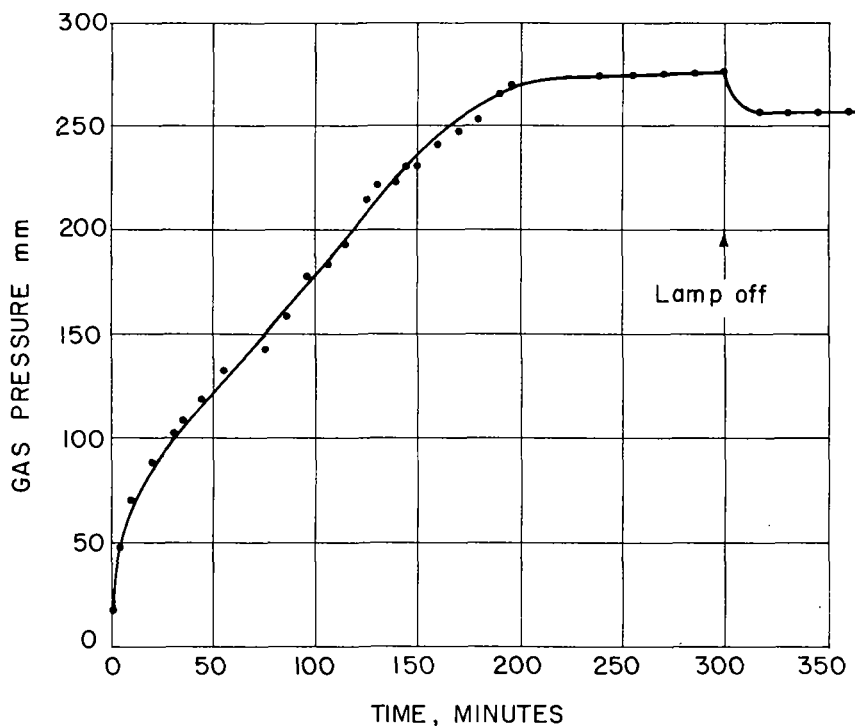


FIGURE 6

THERMOLYSIS OF KN_3 at 540°C

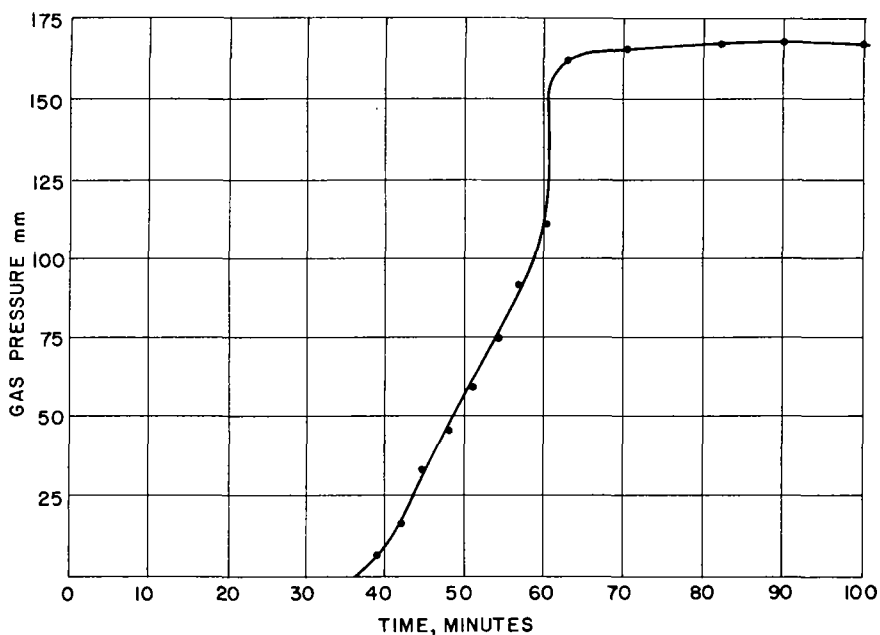


FIGURE 7

THERMOLYSIS OF KN_3 at 452°C

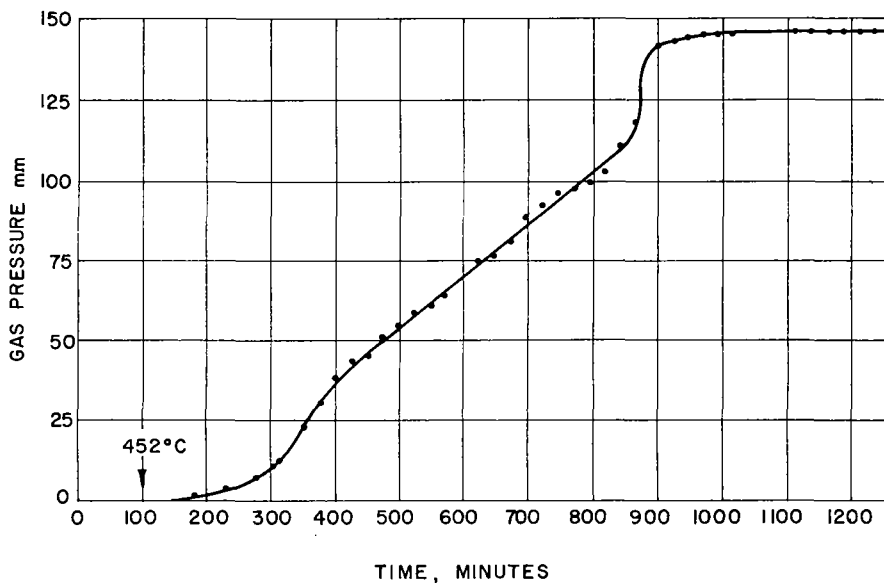
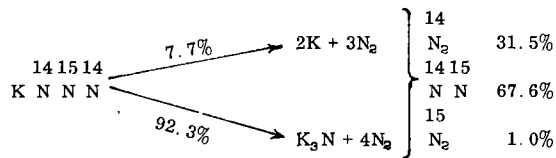
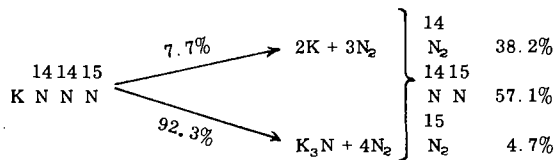
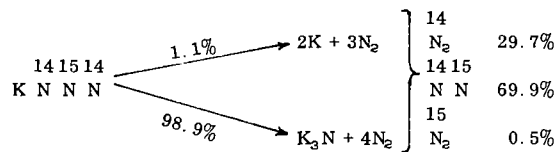
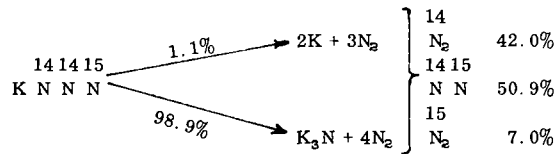


FIGURE 8

Photolysis
in water
solution



Slow
thermolysis



Deflagration

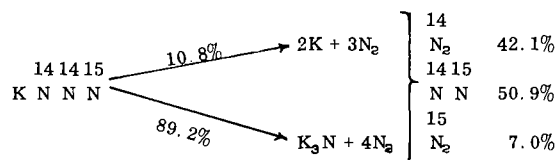


Figure 9

AN ISOTOPE DILUTION-MASS SPECTROGRAPHIC-SEALED TUBE MICROANALYTICAL

METHOD FOR COMBINED OXYGEN DETERMINATION

R. N. Boos, A. Soha, N. R. Trenner

Merck Sharp & Dohme Research Laboratories
Division of Merck & Co., Inc., Rahway, N. J.

One of the most difficult problems in elemental analysis has been the direct determination of oxygen. Elving and Ligett published a comprehensive review of the literature in 1944 including 99 references(7), concluding that the methods then available were not wholly satisfactory.

Many papers concerning the direct determination of oxygen have been published during the past two decades 1,2,6,11,15,16,18,19,20,21 giving improvements on or variations of the Schütze method(17). Zimmerman(21) adapted Schütze's procedure to the micro scale and Unterzaucher(19) vastly improved upon it. The voluminous literature is indicative of the difficulties encountered which included the elimination of air inclusion during the insertion of the sample into the tube, a study of the correct temperature required for the conversion of CO₂ to CO, the type of carbon essential to this conversion, the type of furnace that could withstand the extremely high temperature, the purification of the carrier gas, and the effects of the various pyrolytic gases such as hydrogen, ammonia, hydrogen sulfide, carbon disulfide, and carbonyl sulfide. Unterzaucher(20) found, too, that compounds containing phosphorus and fluorine not only produced high results but also had a harmful effect on the tube packing so that subsequent determinations were unsatisfactory.

With these difficulties in mind, it was deemed advisable to study an entirely different technique; one that required no carrier gas, nor an extremely high temperature, nor any added carbon which might contain adsorbed gases from the air, and yet would be specific for oxygen and thus unaffected by the pyrolytic gases evolved. An isotope dilution procedure similar to those developed for carbon(3) and nitrogen(12) but involving O¹⁸ seemed to offer an answer to these objectives, especially since this approach substitutes merely the attainment of total oxygen equilibration for the quantitative handling requirements of absolute methods.

Grosse, Hindin and Kirshenbaum(8,9) introduced an isotope dilution method for the direct determination of oxygen. They equilibrated a known weight of sample with a known volume of oxygen containing a known amount of O¹⁸ in excess of the natural abundance in a platinum tube at 600°-800°C. Grosse and Kirshenbaum(10) demonstrated an increased precision by using five to ten atom percent O¹⁸ enriched gas. Kirshenbaum, Streng and Grosse(13) extended the method to include fluorine compounds, and Kirshenbaum and Streng(14) used the procedure for the determination of oxygen in rubber. The Schütze-Unterzaucher procedure gave low oxygen values for compounds which form difficultly combustible carbon residues, whereas the isotope dilution method gave acceptable results.

The elaborate gas-handling system for accurately measuring and transferring the enriched oxygen to the sample tube required by the above procedure could be eliminated by substitution of a crystalline, nonhygroscopic, O¹⁸-enriched organic compound that could be readily prepared. It was found that O¹⁸-enriched succinic acid, meeting these requirements, could be prepared by simple exchange between succinic acid and O¹⁸-enriched water in a Carius tube at 145°C for 16 hours.

Preliminary experiments disclosed that, upon pyrolyzing an organic compound in a sealed, evacuated quartz tube at 800°C, a favorable equilibrium was established between CO₂ and CO in the presence of the carbon resulting from the pyrolysis of the organic material. Since nitrogen would undoubtedly be one of the pyrolytic products of nitrogen-containing compounds, it was necessary to measure, mass spectroscopically, the ratio of the 46 to 44 peaks (CO₂) rather than the 30 to 28 peaks (CO).

Initially temperatures ranging from 600°C to 900°C were used for the pyrolysis of mixtures of tracer and sample. The variable mass 46 to 44 ratios observed were attributed to the exchange of O¹⁸ with some 'background' source of O¹⁶ associated

Table I.

Temp. °C/16 Hrs.	W_o
400	0.04
500	0.20
600	0.54
700	0.90
800	1.40
800 a	0.035
600 b	0.280

Table II.

W_T	r_T
7.13	.779
4.65	.776
2.28	.771
1.95	.770
Average	.774

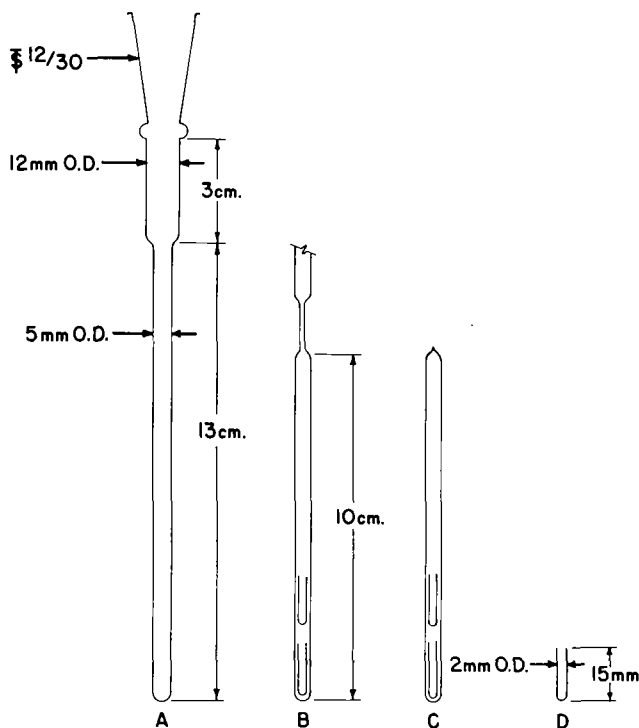
a - carbon coated tube.

b - outgassed at 900°C/16 hours.

Table III.

W_T	W_S	r_S	W_o
1.355	1.595	.290	.035
1.575	1.545	.322	.024
1.505	1.550	.309	.040
1.430	1.500	.298	.075
1.570	1.605	.310	.040
1.620	1.580	.318	.046
1.645	1.595	.319	.047
1.505	1.545	.310	.038
1.075	1.015	.323	.033

FIG. I



- A. QUARTZ PYROLYSIS TUBE PREPARED FOR CHARGING.
 B. CONSTRICTED AFTER CHARGING.
 C. SEALED UNDER VACUUM.
 D. PLATINUM WEIGHING-TUBE.

with the tube since they proved to be a function of the size of the tracer sample used. The quantity of oxygen exchanged varied from 0.5 mg to 1.5 mg depending upon the time and temperature of the pyrolysis. This prohibitively high blank was decreased to 0.05 mg to 0.1 mg of oxygen by utilizing a carbon-coated quartz tube prepared by the pyrolysis of acetone vapor at 1100°C. Unfortunately, however, the heavy deposit of carbon resulting from the pyrolysis of some organic compounds gave rise to a peeling away of the carbon coating from the wall of the tube resulting in recurrent high background values.

Dahn, Moll and Menassa(5) reported that water resulted from heating oxygen-containing compounds with o-phenylenediamine hydrochloride at 300°C. Boyer, Graves, Suelter and Dempsey recently found that CO₂ was obtained on heating water with guanidine hydrochloride in a sealed tube in a "soft gas flame"(4).

Since it had been observed that the amount of exchange of O¹⁸ with O¹⁶ was a function of the temperature, Table I, it seemed apparent that by adding a mixture of o-phenylenediamine hydrochloride and guanidine hydrochloride to the sample and tracer and pyrolyzing at 400°C, the blank would be smaller, less significant, and perhaps more reproducible. This proved to be the case and indeed the blank was experimentally determined as about 43 micrograms of oxygen, a more acceptable value.

Theory - Derivation and Definitions

The mass spectrometer measures:

$$\frac{N^{46}}{N^{44}} = r = \frac{\text{Relative numbers of } C^{12}O^{16}O^{18} \text{ molecules}}{\text{Relative numbers of } C^{12}O^{16}O^{16} \text{ molecules}} \quad (1)$$

$$\text{Now: } K_{eq.} = \frac{[N^{46}]^2}{[N^{44}][N^{48}]} = 4 \quad (2)$$

$$\text{Eqs. (1) \& (2) combined: } N^{48} = \frac{r^2 N^{44}}{4} \quad (3)$$

$$\text{but } N^{18} = N^{46} + 2N^{48}$$

$$N^{16} = N^{44} + 2N^{44}$$

$$\therefore \text{Eq. (3) becomes: } \frac{N^{18}}{N^{16}} = \frac{r}{2} \quad (4)$$

$$\text{By definition: } f_{18} = \frac{\frac{N^{18}}{N^{16}}}{\frac{N^{18}}{N^{16}} + \frac{N^{16}}{N^{16}}}$$

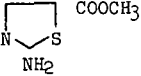
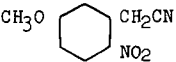

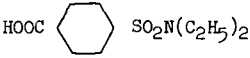
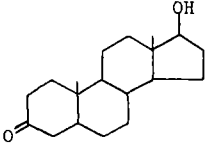
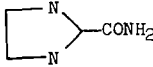
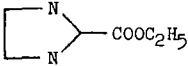
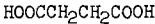
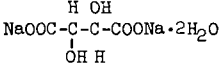
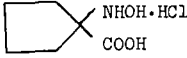
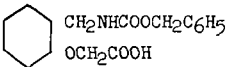
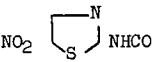
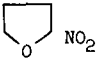
which by eq. (4) becomes:

$$f_{18} = \frac{r}{r+2} \quad (5)$$

$$\text{Similarly } f_{16} = \frac{2}{r+2} \quad (6)$$

A study of the O¹⁸ content of the succinic acid tracer carried out using varied specimen weights revealed that there was a significant O¹⁶ background (blank) contributed by the quartz ampule. The magnitude of this background effect was evaluated in the following manner.

Table IV.

	<u>% Oxygen</u>		<u>% Error</u>
	<u>C</u>	<u>F</u>	
	20.2	20.7	2
	25.0	24.4	3
	23.2	22.3	4
	25.0	26.0	4
	10.6	11.0	5
	14.4	14.2	1
	22.8	22.9	0.4
	54.2	54.4	0.4
	55.7	55.4	1
	26.6	26.9	1
	25.4	24.5	4
	33.8	32.7	3
	33.2	33.4	1

(Continued on next page)

Let the symbols T refer to the succinic acid tracer, S to the sample and O to the background, then the number of mole atoms of O^{18} is given by the following summations:

$$N^{18} = \underbrace{\frac{W_T}{M_T} n_T \left(\frac{r_T}{r_T + 2} \right)}_{\text{tracer}} + \underbrace{\frac{W_S}{M_S} n_S (2 \times 10^{-3})}_{\text{sample}} \quad (7)$$

$$+ \underbrace{\frac{W_O}{16} (2 \times 10^{-3})}_{\text{background}}$$

$$N^{16} = \frac{W_T}{M_T} n_T \left(\frac{2}{r_T + 2} \right) + \frac{W_S}{M_S} n_S (0.998) + \frac{W_O}{16} (0.998) \quad (8)$$

W = Weight of tracer or sample in system.

M = Molecular weight of tracer or sample.

n° = Number of O atoms per molecule of tracer or sample.

$$r_T = \frac{N^{16}}{N^{14}} \text{ for tracer only.}$$

W_O = Weight of oxygen contributed by background.

2×10^{-3} and 0.998 are natural abundances of O^{18} and O^{16} respectively.

The sought quantity is the weight fraction of oxygen in the

$$\text{sample defined as: } X_O = \frac{16 n_S}{M_S} \quad (9)$$

From combination of Eqs. (7), (8) and (9) and let

$$r_S = \frac{N^{16}}{N^{14}} \text{ for sample plus tracer pyrolysis:}$$


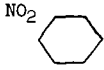
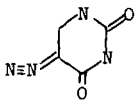
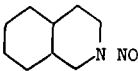
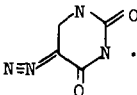

$$X_O = \frac{\frac{128 W_T}{M_T (r_T + 2)} (r_S - r_T) + (0.998 r_S - 4 \times 10^{-3}) W_O}{W_S (4 \times 10^{-3} - 0.998 r_S)} \quad (10)$$

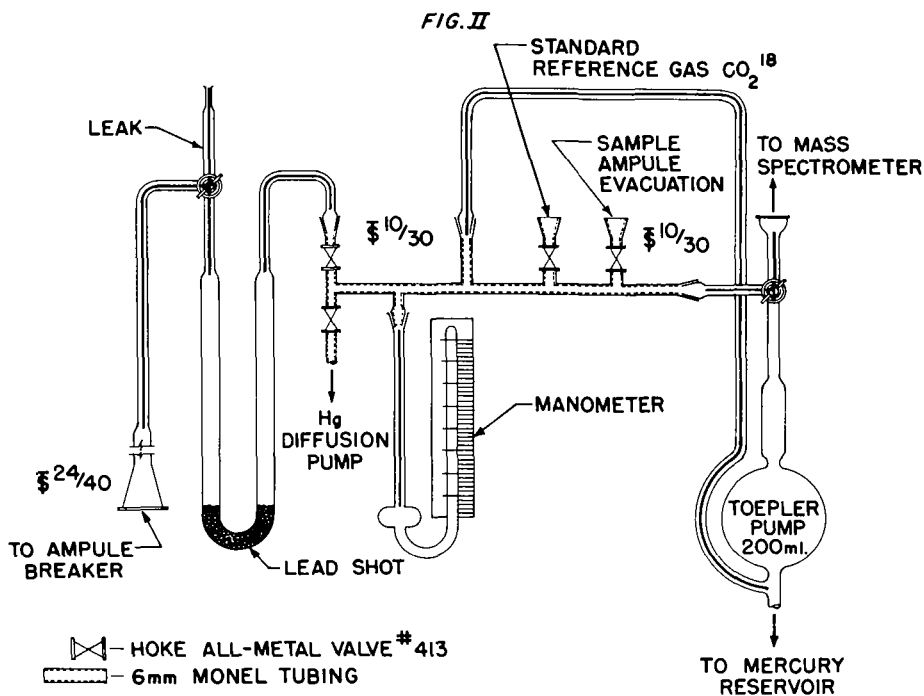
$$M_T = 18 n_O \left(\frac{r_T}{r_T + 2} \right) + 16 n_O \left(\frac{2}{r_T + 2} \right) + 1.008 n_H + 12.01 n_C$$

for succinic acid $n_O = 4$; $n_H = 6$, $n_C = 4$

In this work $r_T = 0.774$ & $W_O = 0.043$ then (10) reduces to:

Table IV.
(continued)

	% Oxygen		% Error
	C	F	
 $\text{SO}_2\text{N}(\text{CH}_3)_2$ $\text{SO}_2\text{N}(\text{CH}_3)_2$	21.9	23.0	4.5
 NO_2 SO_2NHCH_3	29.6	30.6	3
	23.0	23.3	1
 NO	9.8	10.3	5
 $\cdot \text{H}_2\text{O}$	30.6	29.9	2
	55.2	56.8	3



$$X_O = \frac{0.3834 W_T (r_S - 0.774) + (0.998 r_S - 4 \times 10^{-3}) W_O}{W_S (4 \times 10^{-3} - 0.998 r_S)} \quad (11)$$

$$X_O = \frac{0.383 W_T (0.774 - r_S) - 0.043 r_S}{W_S r_S} \quad (12)$$

$$W_O = \frac{0.383 W_T (r_T - r_S)}{r_S} \quad (13)$$

for case where $X_O = 1$ & $W_S = 0$

Method

Apparatus - Fig. I shows the quartz pyrolysis tube and the platinum weighing tubes. The latter were made by cutting lengths of 2 mm o.d. platinum tubing and sealing one end by fusing the platinum in an oxyhydrogen flame.

A pot furnace that can be maintained at 400°C.

Consolidated-Nier, Model 21-201, Mass Spectrometer equipped with a modified manifold system as shown in Fig. II.

A modified ampule breaker as shown in Fig. III.

Reagents -

Oxygen-18 enriched succinic acid: 1.6 grams of succinic acid and 1 ml of 65 atom percent O^{18} enriched water are sealed into an 11 mm o.d. heavy walled Carius tube and heated overnight at 145°C. After cooling, the tube is opened and the contents transferred to a 50 ml r.b. flask for lyophilization. When most of the water has been removed, the succinic acid is further dried to constant weight in a vacuum desiccator.

Guanidine hydrochloride.

o-Phenylenediamine hydrochloride.

Determination of r_T -

An approximate weight of between two and four milligrams of the tracer compound are transferred to the platinum weighing tube which is then inserted into a quartz pyrolysis tube. After adding approximately 8 mg of a 1:1 mixture of o-phenylenediamine hydrochloride and guanidine hydrochloride, the quartz tube is constricted in the oxyhydrogen flame as shown in Fig. I-B, evacuated to a few microns, and then sealed off as shown in Fig. I-C to form the pyrolysis ampule.

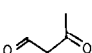
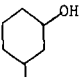

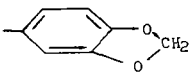

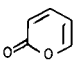

The sealed ampule is inserted into the electrically heated pot furnace and held at 400°C for 16 hours.

The ampule is put into the ampule breaker, the latter attached to the manifold of the mass spectrometer, Fig. II, and the system evacuated for ten minutes. The U tube is cooled in liquid nitrogen, the ampule broken and the non-condensable gases pumped off. After replacing the liquid nitrogen with a dry ice-acetone bath, the liberated CO_2 is transferred by the Toepler pump to the mass spectrometer for measurements of the 46 and 44 peak heights when succeeding set to fall on collector #2. In order to determine the peak heights more accurately, the read out devices originally provided with the mass spectrometer were replaced by a multirange Hewlett-Packard Model 412A vacuum tube voltmeter.

$$\text{Let: } r_T = \frac{V_{46}}{V_{44}}$$

Table II shows values found for r_T for various quantities of tracer.

Table V.

Oxygen Function	% Oxygen		% Relative Error
	Calc.	Found	
 , $\text{-}\overset{\text{O}}{\parallel}\text{C-NH-}$, NO_2	26.2	26.8	2
CH_3CO	15.6	15.4	1
NO_2 , $\text{-}\overset{\text{O}}{\parallel}\text{C-NH}_2$	16.9	16.6	2
	7.6	7.7	1
$\text{-}\overset{\text{O}}{\parallel}\text{C-NH}_2$	9.9	10.4	5
$\text{CH}_3\text{C-}\overset{\text{O}}{\parallel}$, $\text{-}\overset{\text{O}}{\parallel}\text{C-NH}_2$, NO_2	15.8	15.5 15.5	2
 $\text{-}\overset{\text{O}}{\parallel}\text{C-}$	23.4	23.2	1
$\text{O}=\text{C-N}<$	9.3	9.1	2
NO_2 , $\text{-}\overset{\text{O}}{\parallel}\text{C-NH}$	14.8	14.8	0
-NH-CO-NH-	6.6	6.9	4
CH_3O , $=\text{NOH}$, $\text{-COOC}_2\text{H}_5$	15.2	15.4	1
	13.5	13.3	1
 $\text{-CH}_2\text{-O-}$, $\text{CH}_3\text{-SO}_2\text{-O-}$ $>\text{C=O}$	33.7	33.6	1
	15.1	14.7	3
 $\text{-}\overset{\text{O}}{\parallel}\text{C-CH}_2\text{-O-}$, $\text{CH}_3\text{-}\overset{\text{O}}{\parallel}\text{C-O-}$	32.3	32.4	0
$\text{H}_2\text{PO}_3\text{-O-}$, -OH , $>\text{C=O}$	37.9	36.8	3
CH_3O , $(\text{CH}_3)_3\text{COO-}$, $\text{Cl C}_6\text{H}_4\text{-}\overset{\text{O}}{\parallel}\text{C-N=}$	14.8	15.2	3

Determination of r_S -

Since the accuracy of an isotope dilution method is highest when the amount of isotopically-labeled element approximately equals the unlabeled element content of the sample, the quantity of sample and tracer is so taken that $r_S = 1/2 r_T$.

An accurately weighed sample, W_S , of the compound in question is put into one of the platinum weighing tubes and an accurately weighed quantity of tracer, W_T , is put into a second one. The procedure is now exactly the same as that followed for the determination of r_T .

Determination of the Oxygen Background, W_O -

Having determined r_T for the tracer and r_S for a known compound, W_O can be calculated from equation (13). Table III represents the oxygen background effect for various values of W_T , W_S , and r_S when $r_T = 0.774$ and succinic acid containing only O^{16} was used as a standard.

Discussion of Results

As shown in Tables IV and V a wide variety of oxygen-containing organic compounds which included most of the common oxygen functions as well as the inclusion of elements, such as fluorine, sulfur, and phosphorus were used to test the subject method. It is worthy of note that fluorine, sulfur and phosphorus do not interfere.

Most of the compounds were prepared in our research laboratories and had been submitted for elemental analyses. Each compound had acceptable analyses for all of the elements present other than oxygen as well as having been characterized by a variety of appropriately critical physical measurements.

In Table V the compounds are listed only by their oxygen functions since they were compounds that might possibly have patent significance.

The only types of compounds thus far encountered which gave consistently unacceptable results were the coumarans and hydroxy benzoic acids yielding approximately 80 percent of the theoretical values.

References

1. Aluisse, V. A., Hall, R. T., Steats, F. C., Becker, W. W., Anal. Chem. 19, 347 (1947).
2. Aluisse, V. A., Alber, H. K., Conway, H. S., Harris, C. C., Jones, W. H., Smith, W. H., Ibid., 23, 530 (1951).
3. Boos, R. N., Jones, S. L., Trenner, N. R., Ibid., 28, 390 (1956).
4. Boyer, P. D., Graves, D. J., Suelter, C. H., Dempsey, M. E., Ibid., 33, 1906 (1961).
5. Dahn, W., Moll, H., Menassa, R., Helv. Chim. Acta 42, 1225 (1959).
6. Dundy, M., Stehr, E., Anal. Chem. 23, 1408 (1951).
7. Elving, P. J., Ligett, W. B., Chem. Revs. 34, 129 (1944).
8. Grosse, A. V., Hindin, S. G., Kirshenbaum, A. D., J. Am. Chem. Soc., 68, 2119 (1946).
9. Grosse, A. V., Hindin, S. G., Kirshenbaum, A. D., Anal. Chem. 21, 386 (1949).
10. Grosse, A. V., Kirshenbaum, A. D., Ibid., 24, 584 (1952).

(Continued on next page)

Technical drawing showing a cross-section of a device with various dimensions and labels:

- Overall width: 6"
- Top horizontal dimensions: $1\frac{1}{16}$ " and $\frac{7}{8}$ "
- Left vertical dimension: $5\frac{1}{2}$ "
- Internal vertical dimension: $1\frac{3}{4}$ "
- Right vertical dimension: $1\frac{1}{4}$ "
- Bottom horizontal dimension: $\frac{1}{4}$ "
- Labels:
 - BREATHER HOLE
 - $\text{Ø} 29/42$
 - METAL BELLOWS
 - CHISEL POINT
 - FOR TRUE ORIENTATION ROTATE 90°
 - $\text{Ø} 24/40$

References - Concluded

- 191

APPROACHES TO MASS-SPECTROMETER GAS ANALYSIS USING PHOTOGRAPHIC-PLATE ION DETECTION

J. W. Guthrie
Sandia Corporation
Albuquerque, New Mexico

INTRODUCTION

The analytical technique to be described was developed while investigating the possibility of using photographic-plate ion detection to measure semiquantitatively the normal methane and complex methane in certain gas mixtures. Methane occurs as an undesired impurity in sealed ion accelerating tubes where deuterium and tritium are also present. The complex methane resulted from exchange reactions between ordinary methane, protium, deuterium, and tritium. The samples of interest also contained helium 3 from tritium decay and helium 4 from leak detecting and atmospheric gases. The total pressure in the approximately 100-cc glass and metal sample containers ranged from tenths of microns to several torr. Helium 4 was selected as the single component for method development.

A CEC Model 21-110 mass spectrometer equipped with a room-temperature, glass-inlet system; an electron-bombardment type ion source; and a photographic-plate, ion-detection system were used. Usable resolution to an $M/\Delta M = 5000$ was available with a primary slit width of 0.002 inch. Ilford Q2 plates 15 x 2 x 1/32 inches were used.

Reasons for selecting photographic-plate ion detection were:

1. Sample size and the desire to cover a wide mass range (36:1 possible on one exposure).
2. High-resolution requirements involved in the complex-methane spectrum.
3. To gain experience with photographic plates for future use in solids analysis. (It has since been found that for solids-analysis work some of the problems involving photographic-plate ion detection might be more easily solved using the gas-source, photographic-plate combination.)

ANALYTICAL TECHNIQUE AND RESULTS

Figure 1 is a flow diagram of the mass-spectrometer, gas-handling system. Helium 4 calibration spectra were produced on the plate by the following procedure:

1. A calibration bulb, with volumes equal to the sample container and the special opening device, was attached to the inlet system at the same connection where the sample would subsequently be attached.
2. Helium was introduced to the manifold and calibration bulb. The helium pressure in the system was measured with a CEC micromanometer. Helium was then trapped by a stopcock (not shown in Figure 1) in the portion of the calibration bulb equal to the sample-container volume. The helium in the remainder of the system was then pumped out.
3. The manifold was isolated from the pumping system, and the trapped calibration gas was expanded to the stopcocks leading to the spectrometer ion source. Three paths, each with different leak rates, were available. A path having a leak rate of 0.2 cc/sec for air was usually used.

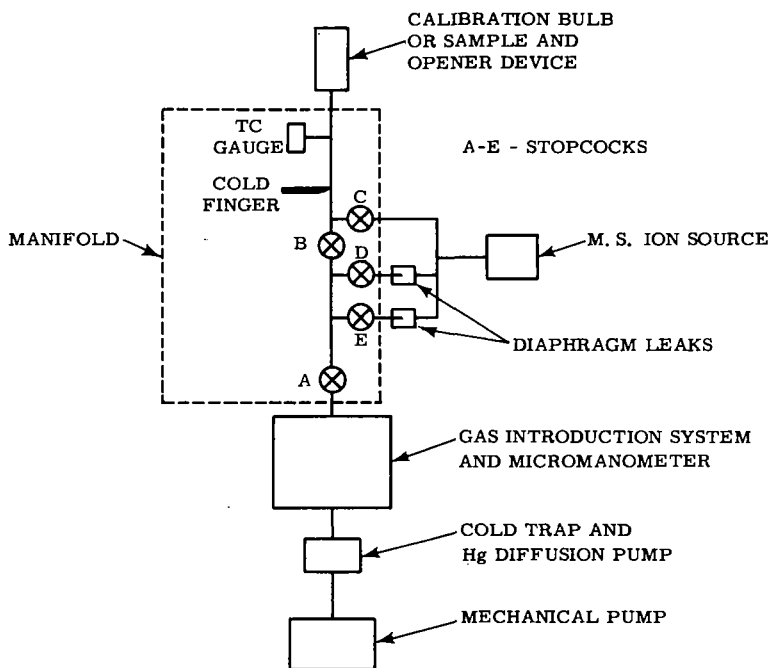


Figure 1. Mass-Spectrometer, Gas-Handling System

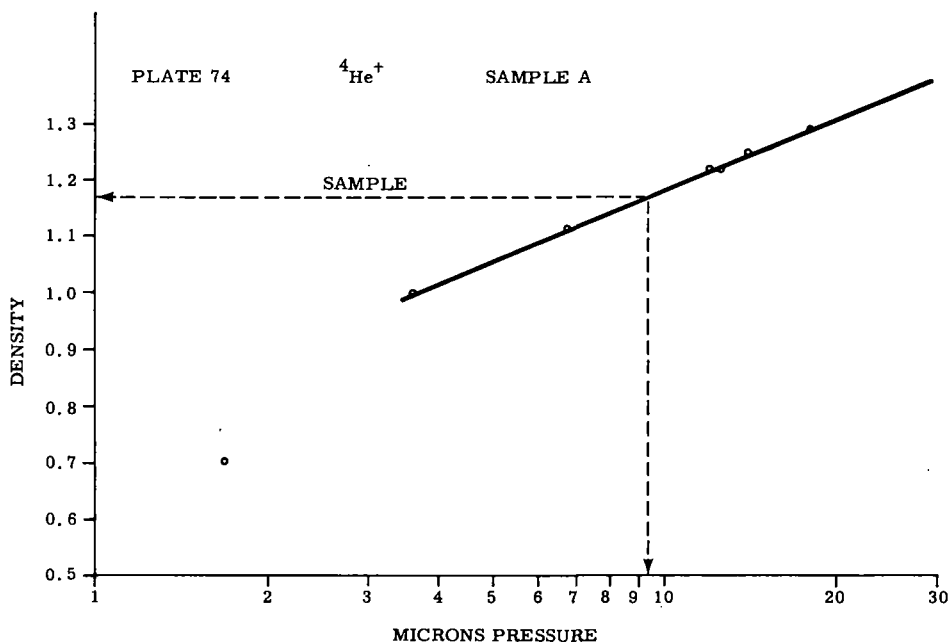


Figure 2. Calibration Curve for Sample A

4. The stopcock to the selected leak was opened, and after a 1-minute delay a timed exposure was made. After the first exposure, 5 seconds were allowed to position the plate for a second exposure of the same calibration sample. The second exposure was usually twice the length of the first. Two different exposure times provided some assurance that a usable line density would be obtained; however, for some calibrations and samples only one exposure time was used. Fifteen exposures could be made on each plate. The voltage selector for the electric sector was used to switch the beam off the photographic plate for exposure-time control.

This procedure was repeated with a range of pressures. The calibration bulb was then removed and replaced with a sample container and its opening device. The sample gas was expanded to the same volume and introduced to the ion source through the same leak used for the calibration gas. The same delay and exposure times used for calibration were used for the sample.

A recording microphotometer was used to obtain data from the photographic plate for line-density calculations. A calibration curve was made by plotting line density versus the helium pressure trapped in the calibration volume before expansion and introduction to the mass-spectrometer ion source. The partial pressure of helium in the sample was then obtained from the plot by using the density of the sample line.

Two typical results are given. Figure 2 shows a plot for Sample A where $^4\text{He}^+$ was the calibration line. Only one exposure per calibration pressure was used. Figure 3 shows plots for Sample B. $^4\text{He}^{++}$ was the calibration line, and two different exposure times were used for each calibration pressure and the sample. For Sample B, the line density was less than the desired level, and the sample helium pressure was not bracketed during calibration. The results for these typical samples compared favorably with results of similar samples analyzed by conventional mass-spectrometer gas-analysis techniques.

Figure 4 shows data from a single experiment to determine the argon content of air for a simple check on the method. $^{40}\text{Ar}^{++}$ was the calibration line, and two different exposure times were used for each calibration pressure and the air sample. Since the argon content in air was known to be about 0.93 mole percent, the range of argon pressures for calibration spectra was defined when the pressure of air to be introduced as the sample was chosen. The standard inlet system was used for this experiment. The mole fraction of argon in the air sample was calculated by reading the partial pressure of argon in the air sample from the calibration curves and dividing by the total air sample pressure measured with the micromanometer. Argon values of 0.98 and 1.00 mole fraction percent were calculated from the data. Again the recorded density range was somewhat lower than that of the desired straight-line portions of calibration curves. Also, the less than 1 micron values used for calibrations were in a difficult range for the micromanometer.

DISCUSSION

The technique described for helium 4 analysis depends somewhat upon previous knowledge of quantities expected or upon having sufficient similar samples for test runs. Preliminary tests are required to determine:

1. The most desirable spectrum line for calibration (whether it be a line produced by a singly or multiply charged ion or from a fragment or parent molecule ion in the case of methane).
2. Exposure times.
3. Best leak rate and ionizing current to use so that exposures of less than 10 seconds may be avoided.

Several changes could probably be made to speed up the analysis and include more data on each plate. These changes might include:

1. Narrowing the slit which defines the spectrum height so that more exposures per plate could be made.

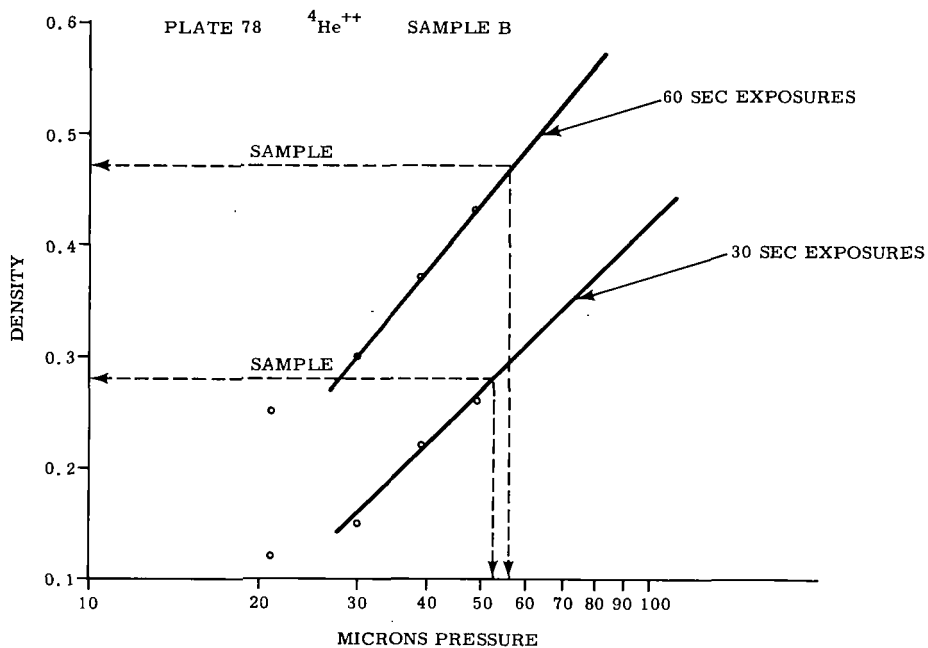


Figure 3. Calibration Curves for Sample B

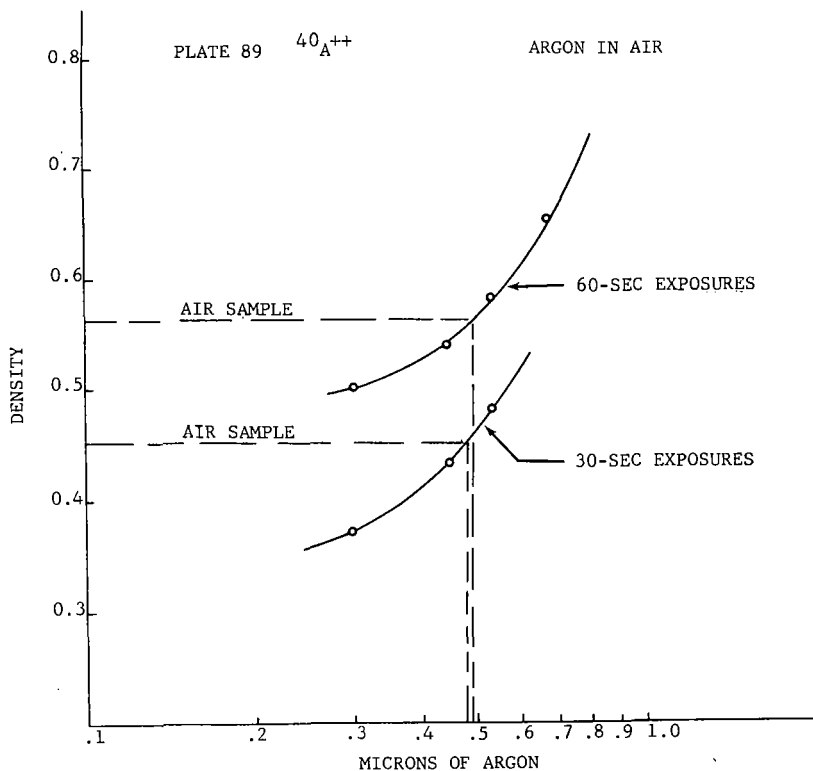


Figure 4. Calibration Curves for Argon in Air

2. Introducing calibration gas only one time and then plotting data relating line density with quantity of gas through the leak.
3. When the spectrum of interest is not crowded, such as in the ${}^4\text{He}^+$ and the ${}^4\text{He}^{++}$ regions, several rows of spectra could be recorded by a slight change in the magnetic field after the first 15 exposures. This method has been used in the helium experiment for some samples.

In any event, the method is not rapid; however, for the particular samples of interest the method could be expanded to include helium 3, the hydrogen isotopes, and related components such as HD, HT, and DT.

The method can also be applied to the normal-methane/complex-methane analysis, but a major difficulty is lack of resolution. Singly charged parent molecules and singly charged fragments produced in the mass-spectrometer ion source may produce 70 lines in the spectrum between m/e 12 and 25. Background components also add to the spectrum in the region of interest. A resolution of $M/\Delta M > 100,000$ is required to resolve all the normal- and complex-methane species. With a resolution of 5000 and assuming little contributions from fragments containing ${}^{12}\text{C}$ or parents and fragments containing ${}^{13}\text{C}$, then 13 of the 15 ${}^{12}\text{C}$ -containing, parent-molecule ions may be assigned for first approximations. However, concentration of the various species can greatly alter this approach. Calibration plots would be made from CH_4^+ lines. In the sample spectra observed to date, as many as 37 lines have been recorded between m/e 12 and 25. Twenty-nine of these lines have been assigned to the normal-methane and complex-methane spectra.

Our work on this project is incomplete and is likely to remain so for an indefinite time since solids analysis is presently of greater importance.

UPPER ATMOSPHERIC ION COMPOSITION MEASUREMENTS
WITH MAGNETIC MASS SPECTROMETER

John H. Hoffman, Charles Y. Johnson, and Julian C. Holmes
U. S. Naval Research Laboratory
Washington 25, D. C.

ABSTRACT

Measurements to date have shown that the most abundant ion in the F region of the ionosphere is O^+ . Theory predicts that the O^+ region yields to an He^+ region and finally to an H^+ region with increasing altitude. In order to provide direct experimental identification of these ions, and possibly of other minor constituents, and to demonstrate the relative importance of each as a function of altitude and solar activity, a magnetic mass spectrometer having a 60° sector field and 1-1/2-inch radius has been developed. This instrument, suitable for rocket or satellite experiments, has a resolving power of about twenty and is capable of measuring the energy distribution of ions from 0 to 2 kev/amu. Because the mass spectrometer has a sensitivity of the order of tens of ions per cc, depending on instrument orientation in the rocket and rocket velocity, it could be used to measure the ion composition of interplanetary space.

OXYGEN OUTGASSING CAUSED BY ELECTRON
BOMBARDMENT OF GLASS

Jack L. Lineweaver
Corning Glass Works
Corning, New York

Abstract

A flow system has been used to study the oxygen evolved, as a result of electron bombardment, from twelve commercial glasses. A small cathode ray tube, with the aluminum coated glass samples located near the face plate, is sealed directly to the source of a mass spectrometer. The samples are bombarded with a $3 \times 3/4$ inch television type raster using 150 microamperes of 20 kev electrons. It has been found that the outgassing, from all but two of the glasses, fits the empirical equation $Q = Q_{\infty} (1 - e^{-t/K})$. In this equation, Q is the sum of the oxygen released during the bombardment time, t , and that evolved during a subsequent thermal outgas. A mechanism for electron bombardment induced oxygen release is proposed.

MASS SPECTROMETRIC INVESTIGATION OF GAS EVOLUTION FROM METALS

John Roboz and Robert A. Wallace

General Telephone & Electronics Laboratories, Inc.
Bayside, N. Y.

The objective of this work was two fold: first, to extend analytical methods into the fractional ppm range; and second, to investigate the mechanism of the gas evolution from metals. The particular metal selected was nickel; the techniques developed, however, may easily be adapted to similar studies of other metals, or even non-metals.

The three major parts of the apparatus are: The extraction system, the gas transfer system, and the analytical system, which is a 21-620, cycloidal focusing mass spectrometer (Fig. 1).

Both fusion and hot extraction furnaces were used, and no significant changes were made on the more or less conventional designs, described in the literature (1). One minor modification is the simple elevator design in the hot extraction tube, shown in Fig. 2. It consists of a quartz platform, which can be moved up and down, making it possible to remove and re-introduce samples at any time.

In quantitative analytical work the major limitation of the vacuum fusion method is believed to be the blank; thus our first objective was to reduce its value. The total blank, obviously, represents the sum of the blanks of the various parts of the instrument. Since conventional furnaces were used, no reduction in the blank was expected from this part of the apparatus. Replacement of the chemical train by the mass spectrometer resulted in practically complete elimination of the blank contributed by the analytical system. Also, a very significant decrease in the blank was achieved through the design of the transfer system. Figure 3 shows a schematic drawing of the transfer system. A detailed description will be published elsewhere; only the more significant features will be discussed here. First, both stop-cocks and mercury cut-offs were completely eliminated by using stainless steel bellows seal valves. Second, the total pressure of the gases of interest in the system was kept at a level of $2-3 \times 10^{-7}$ Torr by means of the pumping system.

The most important component, D_1 , is a 3-stage mercury diffusion pump, which serves to remove the gases from the extraction system. Fast removal of all the evolved gases from the hot zone is one of the most significant factors in vacuum fusion and extraction analysis. The pumping speed of D_1 is 80 liters/sec, and its ultimate vacuum is 5×10^{-8} Torr. The fore-line of the transfer pump connects directly to the fine side of a second diffusion pump, D_2 , providing a straight path to transfer the removed gases into a storage place or directly into the mass spectrometer. The purpose of this second pump is to increase the accuracy of measuring the volume of the evolved gases. The pump was designed by Naughton and Uhlig (2) to have a constant volume fore-line. This was achieved by sealing an additional water-cooled tube into the condenser, so that mercury atoms with long mean free paths are condensed at a definite point. A third pump, D_3 , which is a standard pump, serves for evacuation and initial outgassing and for removal of residual sample gases.

In order to establish the accuracy of the gas transfer system, two different sets of experiments were performed. In Table 1 data for determining reproducibility are shown with a calibrated helium leak. From these data it may be concluded that the reproducibility of the gas transfer system is essentially limited by the signal-to-noise ratio of the detector system resulting in an accuracy within 4 to 6%.

In a second set of experiments, gas mixtures of similar quantity and composition to that expected from the nickel samples were prepared and transferred through the system. Results of a typical experiment are summarized in Table 2. The gas mixture was prepared right in the metal inlet system, and a known portion was taken out and re-introduced as an unknown sample. It can be seen that the transfer may be considered quantitative within about 5 to 6%, always negative. This is in agreement with results obtained using the helium leak. There was no change in composition and this was, in fact, the major significance of this test.

As mentioned previously, the principal objective was to obtain low blank values. In conventional vacuum-fusion instruments, according to an ASTM specification (3), a blank of about 0.2 micron-liter/min is necessary for quantitative determinations using standard operational procedure. Anyone with practical experience well knows how difficult it is to meet this requirement; in fact, the maintenance of low blanks is generally considered to be the major experimental problem in vacuum fusion analysis. With our equipment, it was possible to obtain blank values 5 to 20 times less than those

TABLE 1
- - - -

Reproducibility Experiments with Calibrated

		Helium Leak		
Collection time: 30 min				
Peak Height (m/e 4)				
	div			
	19.2			
	19.3	Average: 19.73 div		
	20.0	Standard Deviation: 0.47 div		
	19.9			
	19.0			
	21.0			

Collection time	Expected Value	Experimental Value	% Error
min	(based on average of 30 min collections)		
60	39.46 div	36.45 div	-10
90	59.19	57.50	-3
120	78.92	79.10	0.2

TABLE 2
- - - -

Accuracy Measurements on the Gas Transfer System

		Quantities expressed: microliter	
Introduced		11.63 Hydrogen	20.46 Carbon monoxide
Recovered		10.90 "	19.50 "
% difference		- 9.4 "	- 4.7 "

		Quantities expressed: mole per cent	
Introduced		36.42 Hydrogen	63.76 Carbon monoxide
Recovered		35.40 "	64.50 "

reported in the literature both for fusion and extraction experiments.

The high vacuum, low blank, gas transfer system, combined with the mass spectrometer could, in principle, be utilized to extend analytical methods into the fractional ppm range. In Table 3 calculated detectability limits are shown, corresponding to a reading of 3 divisions on the recorder.

As far as vacuum fusion techniques are concerned, the experimental results indicated, that in spite of the low blanks, and in spite of the use of the mass spectrometer, it was not possible to obtain better results than those using conventional methods. This indicates that the significance of the blank as a limiting factor is somewhat overestimated and directs attention to the problem of film formation during fusion analysis. Beach and Guldner (4) made an extensive study of the effect of evaporated films on the recovery of gases evolved from metals. Nickel exhibited the worst behavior, the limit of analysis being about 1-3 ppm. This is in agreement with our experiments. Our final conclusion is that mass spectrometric technique could be utilized to extend the vacuum fusion method into the fractional ppm range only if major modifications were also made on the furnace system, in order to eliminate or reduce film formation. This aspect of the problem was not pursued any further by us.

In the vacuum extraction type of analysis, the carbon film is totally absent, and the extraction is usually performed at temperatures at which the vapor pressure of the metals is relatively small. Therefore, the low blanks and the sensitivity of the mass spectrometer could be fully utilized. We were able to analyze very small gas quantities, originating either as impurities of very low concentration, such as in cathode studies where available samples are small, i.e., milligram size.

In Table 4 data are presented on the reproducibility of the determination of hydrogen in powder rolled nickel. Since the reproducibility of the transfer system has been determined previously (Table 1 and Table 2), the differences in the analyses made under identical conditions should provide information on the reproducibility of the outgassing. The analyses were made in a quartz tube, at 1200° C for 10 min. From these and similar experiments, we may conclude that our data are reproducible within a factor of about two in the fractional ppm region. The limiting factor is sample inhomogeneity.

In order to obtain information on the mechanism of the gas evolution, both static and dynamic type measurements were used. In the dynamic studies the mass spectrometer was continuously following the gas evolution.

In regard to the evolution of carbon monoxide, it is generally believed that it is a result of the reaction between the carbon and oxygen content, present as carbides and oxides; there is no carbon monoxide present as such (5). We have contributed support to this theory by showing that the total oxygen content may be recovered as carbon monoxide using only hot extraction techniques, provided there is a stoichiometric excess of carbon present in the nickel. This is usually the case in commercial nickel samples. Thus, in order to determine the total oxygen content, it is not necessary to fuse in graphite crucibles. If, however, the carbon content of the samples is insufficient to convert all the oxygen into carbon monoxide, the quantity of gas evolved is limited by the carbon content.

Experimental data are presented in Table 5 for the evolution of hydrogen from nickel at various temperatures. It can be clearly seen that while the total hydrogen obtainable was essentially the same in all the experiments, only a fraction of the total could be recovered at a given temperature, below 1200° C. A step-wise increase of temperature resulted in renewed gas evolution. These experimental data may be examined in view of the two main theories of the mechanism of the hydrogen containment in metals.

The process of the gas evolution from the metal into vacuum is dependent on the internal equilibrium pressure and the freedom of diffusion. The former is a function of the temperature, the quantity of the occluded gas and its mode of containment. The latter is characterized by the temperature and the activation energy. In a solution of the classical van't Hoff type, an interstitial solution, the equilibrium pressure of the solution must decrease with increasing solubility, as the temperature is raised, assuming a given concentration. This is a general characteristic of all endothermic occluders. Thus, the gas evolution should continue until all the gas is extracted into the external vacuum, and the rate of evolution should continuously decrease, in proportion to the decreasing concentration. This was obviously not the case in the present experiments.

Smith (6), on the other hand, has questioned the presence of any solid solution in

TABLE 3

-- -- --

Limits of Detectability for Various Gases

Values correspond to a 3 div reading (XI scale) on the recorder

<u>Gas</u>	<u>Pressure</u> (micron)	<u>Quantity</u> (micronliter)	<u>Mole</u> (STP) (1 g sample) $\times 10^{-9}$	<u>Weight %</u> $\times 10^{-4}$
Hydrogen	0.10	0.30	5.88	0.03
Methane	0.04	0.13	7.59	0.11
Water	0.03	0.09	5.12	0.08
Nitrogen	0.02	0.05	3.00	0.08
Carbon monoxide	0.02	0.05	2.82	0.07
Carbon dioxide	0.02	0.05	3.18	0.12

Limits of detectability for oxygen and carbon based on carbon monoxide and carbon dioxide evolution; expressed in ppm.

Oxygen from CO	0.04	Carbon from CO	0.03
Oxygen from CO ₂	0.09	Carbon from CO ₂	0.03

TABLE 4

Hydrogen Content of Powder Rolled Type Nickel Samples

<u>Sample Weight</u> g	<u>May, 1961</u> ppm	<u>August, 1961</u> ppm
1.3	2.45	3.45
	2.39	2.56
	1.64	3.15
	1.86	3.32
	2.23	2.15
0.9	2.88	3.20
	1.56	3.54
	1.48	2.68
0.4	1.56	3.50
	2.86	3.32
		4.02 *
		3.21
		3.83
		2.45
		2.11
		1.84
* Discarded		
	<u>Average:</u> 2.09	<u>Average:</u> 2.95
	<u>Range:</u> 1.40	<u>Range:</u> 2.00

the case of endothermic occluders, and has assumed that the absorbed hydrogen resides in lattice defects, so-called rifts or pockets. The opening and closing of these rifts, resulting from both mechanical and heat treatments, completely control the presence and distribution of the hydrogen. Our present experimental data appears to favor the rift-occlusion theory rather than the classical-type lattice solution, since complete outgassing could not be achieved at any given temperature, and an increase in temperature resulted in renewed hydrogen evolution. In addition, if samples were removed by means of the elevator, after extraction had been completed at a given temperature, and later introduced at the same temperature, additional hydrogen was released. Although the quantities involved were very small, hardly exceeding the limits of detectability, the trend is important. Again this can be explained by the rift-theory, assuming the opening of new rifts after the re-introduction of the samples.

In Fig. 4 dynamic measurements of the evolution of hydrogen are shown. It can be seen that after 2 min. the extraction is complete. The hydrogen peak actually starts to decrease, which is, of course, a consequence of the continuous pumping through the leak. The desorption of gases from thin plates can be treated mathematically as a special case of Fick's law, and the coefficient of diffusion may be evaluated from a plot of the logarithm of the rate of evolution against time, assuming that the physical dimensions are known. From such an analysis, it was shown that the mechanism of the hydrogen evolution at a given temperature is completely diffusion controlled.

It must be emphasized here that these samples were "taken from the shelves," i.e., the hydrogen content originated from the actual manufacturing process. In a series of experiments using the same nickel materials, all the hydrogen was removed by pumping at 1200° C for several hours, and hydrogen was introduced via diffusion, by simply heating the samples in a hydrogen atmosphere. In this way, we were able to introduce about the same quantity of hydrogen as the samples originally contained. Next we analyzed these samples to recover the hydrogen introduced and to observe whether the step-wise evolution also occurred. It was found that all the hydrogen introduced artificially could be removed at any desired temperature, and subsequent increase of the temperature did not result in additional hydrogen evolution. Experimental data are shown in Table 6. The total quantity of hydrogen can be seen to be the same, regardless of the temperature of the extraction. The mechanism of the release was found again to be controlled by diffusion. These experiments were also repeated using deuterium saturated samples, and the results were the same. Incidentally, use of deuterated samples enabled us to determine the diffusion coefficient of deuterium in nickel and its temperature dependence which has not been previously measured. These experiments will be published elsewhere.

In summarizing these experimental results, we may conclude that the characteristics of the thermal evolution of hydrogen in nickel are dependent on the mode of containment, which, in turn, is determined by the experimental conditions of the absorption of the gas. In cases where the gas absorption is purely diffusive in nature the containment is in interstitial solution, and the total quantity of gas can be released at a given temperature. However, in cases where the gas content originates during manufacturing of the material as a result of chemical reactions on the surface, probably involving water vapor, and where the metal is exposed to mechanical influence, the containment is in lattice defects and only portions of the total quantity can be released at a given temperature. The mechanism of the gas evolution in all cases is diffusion limited.

In the course of this work, it was observed that at 1200° C, after all the hydrogen was believed to be removed, a very slow hydrogen evolution persisted. At first this was considered to be due to an increase in the instrument background. Also the vacuum system as a whole and its various parts were accused of gettering and subsequently outgassing. This extraneous gas evolution, however, could be stopped easily by removing the samples from the hot zone by means of the elevator; this showed that the phenomenon was real. The quantity of this residual gas, in a 1 to 2 g sample, barely exceeded the limit of detectability. Although the gas increased with increasing sample size, the linear relationship found between the weight of samples and the partial pressures in the case of the readily diffusible hydrogen was not followed. An example of a dynamic measurement may be seen in Fig. 5. This clearly shows that while all the hydrogen evolves in a matter of minutes, the peak does not decrease the way one would expect as a consequence of the pumping out of the mass spectrometer reservoir. Here it appears that approximately the same quantity of gas was evolving as was being pumped out. From leak rate calculations the quantity turned out to be about 0.01 ppm/min, and the evolution continued for several hours, exhibiting a slow decreasing tendency. The study of the residual hydrogen involves experimental difficulties since it occurs at only higher temperatures, where the vapor pressure of nickel is already such that intensive film formation takes place. This makes quantitative determinations almost impossible.

TABLE 5

Temperature °C	Outgassing	Hydrogen					
		$\mu\text{-l/g}$	ppm	$\mu\text{-l/g}$	ppm	$\mu\text{-l/g}$	ppm
300	1st	5.6	0.6				
	2nd	3.6	0.4				
	3rd	1.7	0.2				
		10.9	1.2				
600	1st	8.0	0.9	22.1	2.4		
	2nd	*		*			
		8.0	0.9	22.1	2.4		
800	1st	3.0	0.3	0.6	0.06		
	2nd	*		*			
		3.0	0.3	0.6	0.06		
1000	1st	1.0	0.1	3.6	0.3		
	2nd	*		0.6	0.06		
		1.0	0.1	4.2	0.36		
1200	1st	2.0	0.2	2.0	0.2	25.6	2.8
	2nd	0.2	0.02	0.2	0.02	0.4	0.04
	3rd	0.2	0.02	0.2	0.02	0.2	0.02
	4th	0.2	0.02	0.2	0.02	0.2	0.02
		2.6	0.26	2.6	0.26	26.4	2.88
Total		25.5	2.76	29.5	3.08	26.4	2.88

*Below limit of detectability

The existence of this so-called residual hydrogen was previously observed in the outgassing of iron, and was considered as a unique phenomenon (7). It is apparent now, that the same phenomenon also occurs with nickel, except that the quantities involved are smaller, in fact so small, that only the mass spectrometric method makes it possible to detect them. It appears from the kinetics of the evolution, that in whatever form the residual hydrogen is contained, it must be firmly bound and the release must be controlled by factors other than diffusion. This suggests the presence of compounds such as water or a slowly decomposing hydride of an impurity. Finally it should be mentioned that in the experiments with charged samples, no increase of the residual hydrogen was observed, indicating that no hydrogen entering via diffusion forms residual hydrogen. Also, in the case of samples charged with deuterium, no residual deuterium was observable. Thus the residual hydrogen must be a consequence of the complex processes that take place during the absorption of hydrogen in the course of the manufacturing of the metal, resulting in a different mode of containment.

In summary, an experimental technique has been developed for studying gas evolution from metals using conventional extraction devices, an advanced gas transfer system and a mass spectrometer as the analytical tool. Experimental information was obtained regarding both the mode of containment of the gases in nickel and the mechanism of their release. In addition, quantitative methods for the determination of gas content by means of hot extraction techniques were extended into the fractional ppm range.

References:

- (1) Z. M. Turovtseva and L. L. Kunin, "Analysis of Gases in Metals", Consultants Bureau, New York, 1962.
- (2) J. J. Naughton and H. H. Uhlig, *Ind. and Eng. Chem., Anal. Ed.*, 15, 750 (1943).
- (3) "ASTM Standards on Electron-Tube Materials", ASTM, Philadelphia, Pa., 1957, p. 212.
- (4) A. L. Beach and W. G. Guldner, *Anal. Chem.*, 31, 1722 (1959).
- (5) C. J. Smithells and C. E. Ransley, *Proc. Roy. Soc. London, A*, 155, 195 (1936).
- (6) D. P. Smith, "Hydrogen in Metals", Univ. of Chicago Press, Chicago, 1948.
- (7) M. L. Hill, "Hydrogen Embrittlement in Metal Finishing", Reinhold, New York, 1961, p. 46.

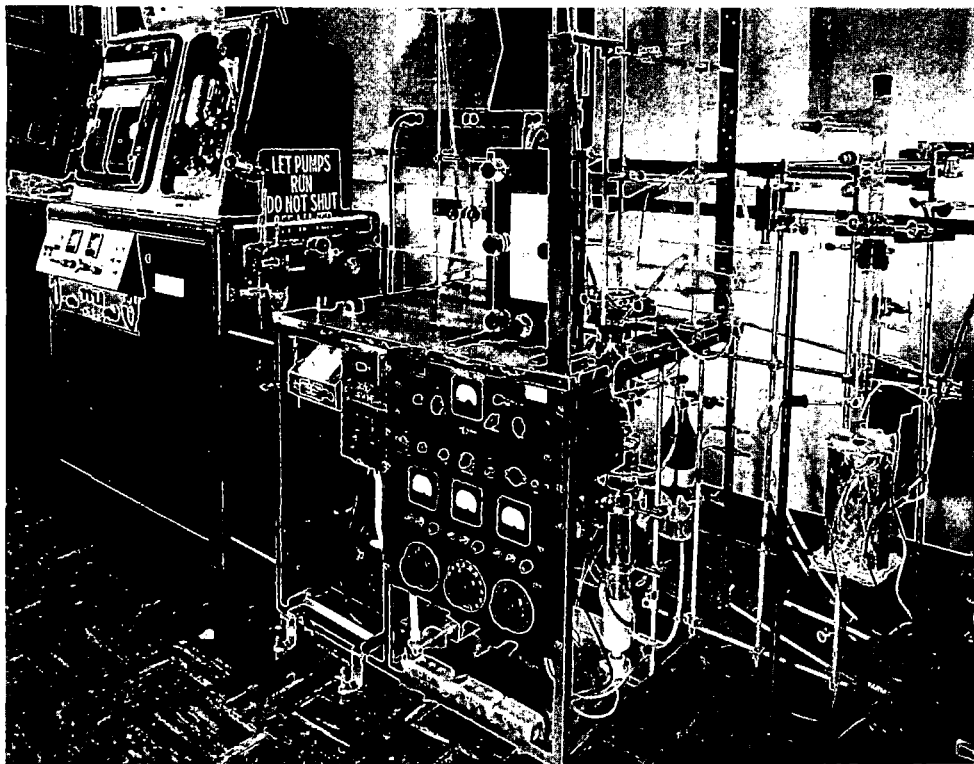


Fig. 1 - View of the Apparatus

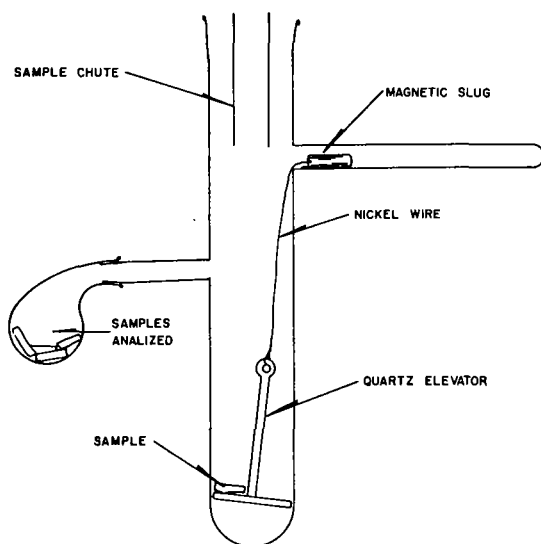


FIG. 2. QUARTZ TUBE WITH ELEVATOR.

FIG. 3.

SCHEMATIC DRAWING OF GAS TRANSFER SYSTEM.

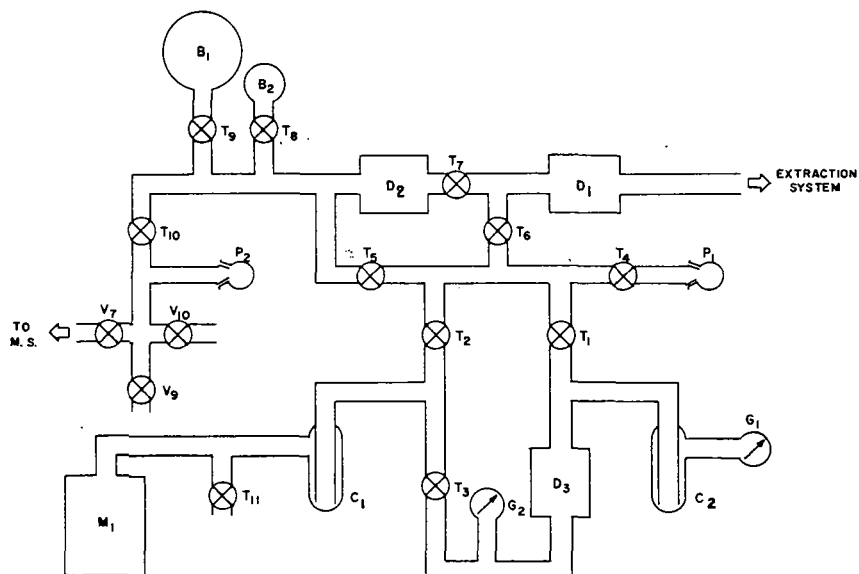


FIG. 4.

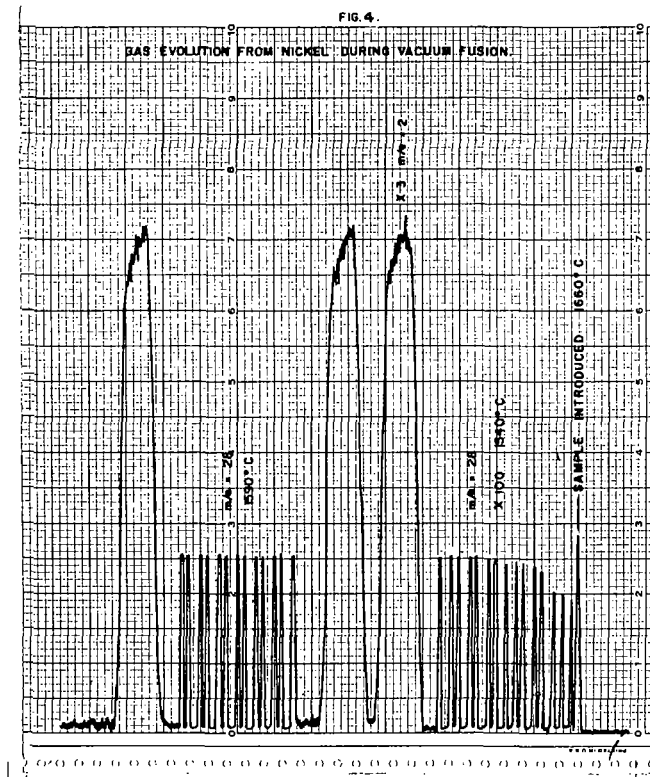
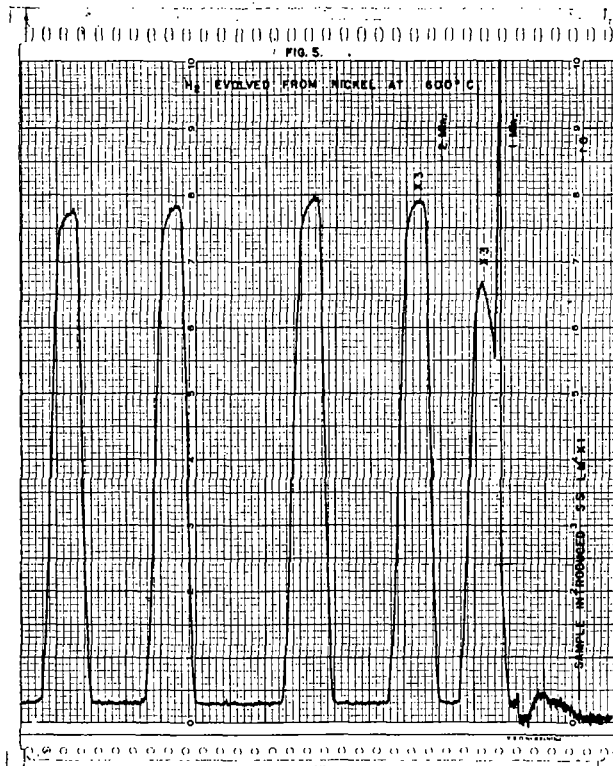


TABLE 6

Evolution of Hydrogen from Charged Samples

Temperature	Outgassing	#1	#2	#3	#4	#5
°C		Quantities expressed: $\mu\text{l/g}$				
400	1st	33.0				
	2nd	6.0				
	3rd	<0.2				
600	1st	<0.2	32.1			
	2nd		<0.2			
800	1st	<0.2	<0.2	30.6		
	2nd			<0.2		
1000	1st	<0.2	<0.2	<0.2	34.0	
	2nd				0.2	
1200	1st	0.4	0.6	<0.2	0.4	32.8
	2nd	0.4	0.2	<0.2	<0.2	0.2
	3rd	0.2	0.2	0.2		<0.2

Note: All 5 samples charged under identical conditions.



The Effects of Surface Reactions on Mass Spectra[†]

Dwight A. Hutchison, John W. Kraus,[‡] Louis G. Pobo

Argonne National Laboratory, Argonne, Illinois

Introduction

A number of effects called "memory effects" are well known to those concerned with mass spectrometric analyses, particularly where great precision of analyses is a matter of concern. If we eliminate electrical effects, e.g., polarization of input resistors to an electrometer, there still remain many disturbing "memory effects" with which to contend. It is well known that one must condition a mass spectrometer to obtain reproducible results. Baking at 250-300°C is a usual method of cleaning a vacuum system to rid it of adsorbed gases. Dependent on the gaseous adsorbing power of the metal from which the ion source box is constructed, varying amounts of gases introduced for analyses will be adsorbed. Before another sample can be analyzed, it is necessary to remove these gases so that they are not a source of interference to subsequent analyses. Methods used to eliminate these adsorbed gases consist of further baking, the introduction of a gas to be analyzed for a period of time necessary to displace the previously adsorbed sample, and the introduction of a gas which adsorbs more greatly than the previous sample yet has no ion peaks to interfere with the next sample to be analyzed.

As an example of the latter consider the isotopic analysis of carbon dioxide which is readily adsorbable on many metal surfaces, particularly Nichrome V or various steels from which most ion-source boxes are constructed. A technique of known practicability is to condition the ion-source with argon which apparently is more readily adsorbed than is carbon dioxide. In this manner the ion peaks due to m/e 40, 38, and 36 from argon do not interfere with the m/e 44, 45, and 46 peaks from carbon dioxide. It is commonly accepted that the reason for these procedures is to eliminate the isotopic exchange reactions occurring on the surfaces in the ion-source region.

Inasmuch as 10^{15} - 10^{16} collisions-cm⁻²-sec⁻¹ occur between the gas and the ionization-box walls under usual operating conditions, it is not surprising that surface reactions occur. Yet, the ideas expressed in many published papers appear to neglect the possibility that surface reactions may obscure the observed ion currents which are thought to be due wholly to gas phase processes. It is our purpose here to review possible tests for surface and gas phase reactions, and to present some illustrations of these tests wherein a typical electron-beam ion-source was employed.

Possible Tests for Surface Reactions

(a) Kinetic Order - The most definitive test as to whether a suspected secondary ion results from a surface or gas phase process is a determination of the kinetic order of the observed ionic current with respect to the various possible reactant molecular and ionic species. Since the composition of a gas is held constant during the course of observation, the kinetic order may be obtained from a record of ion current as a function of gas sample leak pressure if the leak is effusive. A log-log plot of the observed ion current versus leak pressure yields a straight line, the slope of which is numerically equal to the kinetic order with respect to the reactant species. If a first order plot is obtained for a secondary ion the atomic ion composition of which cannot have resulted from any one of the various possible reactant species, then there is evidence favoring a surface reaction for the formation of the secondary ion.

[‡]Post-Doctoral Research Fellow, 1957-58. Present address: The M. W. Kellogg Co., Jersey City 3, N. J.

[†]Based on work performed under the auspices of the U. S. Atomic Energy Commission.

Fig. 1. Log-log plot of $i_{D_2^+}$, $i_{N_2^+}$, and $i_{N_2D^+}$ versus leak-pressure.

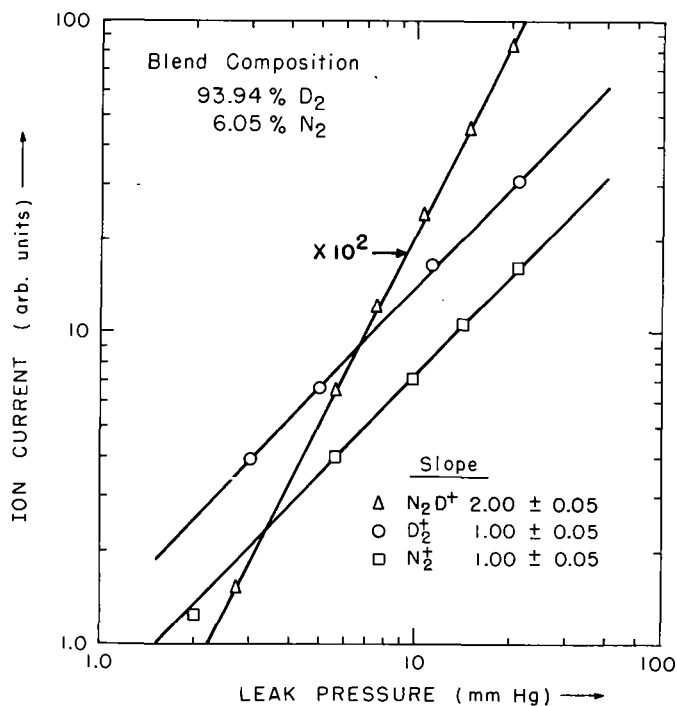
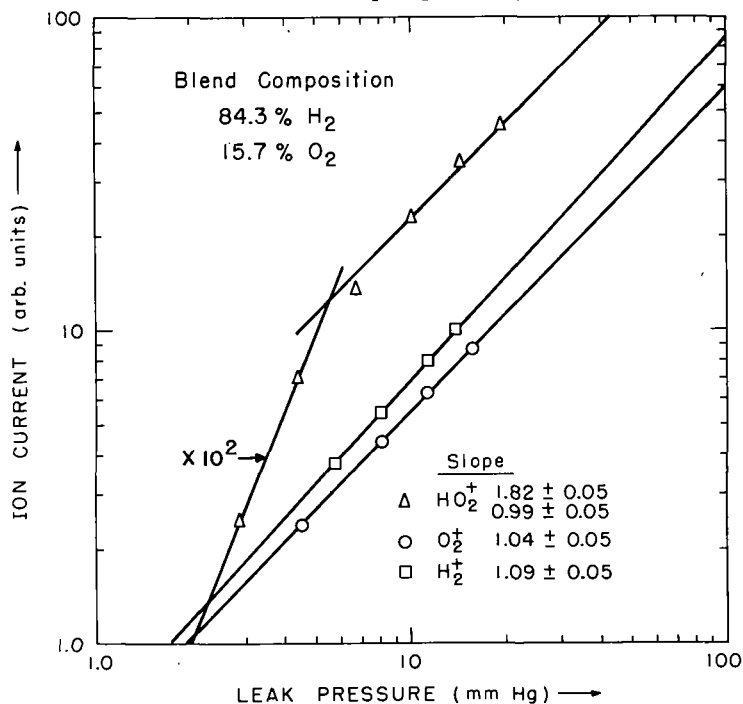


Fig. 2. Log-log plot of $i_{H_2^+}$, $i_{O_2^+}$, and $i_{HO_2^+}$ versus leak-pressure.



(b) Ion Current versus Time - If a gas leak which separates the sample container and ion-source region has been shown to exhibit effusive flow, then a linear relation between observed primary ion currents and gas sample pressure exists. Under these conditions a primary ion current will decrease exponentially with time. If two primary species react to form a secondary ion species in the gas phase, then plots of the logs of the primary and secondary ion currents versus time yield straight lines, the slopes of which are related by,

$$k_1 + k_2 = k_S \quad (1)$$

where k is a slope, and the subscripts 1, 2, and S refer to the reactant species M_1 , M_2 , and the secondary species S, respectively. Gutbier¹ has shown Eq. (1) to hold experimentally in the case of reactions between H_2 and H_2 , Ar, O_2 , N_2 , CO_2 . If relation (1) does not hold, then one may suspect the occurrence of a surface reaction.

(c) Ion Current versus Temperature of Ion-Source - It is well known that the density of adsorbed molecules on a surface depends exponentially on the reciprocal of the absolute temperature. Thus, the ratio $(i_1+i_2)/i_S$ where i is an ion current should remain essentially constant for a gas phase reaction and should vary considerably for a surface reaction. Under a given set of experimental conditions, one may record the various ion currents from the time when the electron beam filament is turned on until it has heated the ion-source to some equilibrium temperatures. If the above ion-current ratio varies greatly, we may conclude partial evidence for a surface reaction.

(d) Change of Kinetic Order with Ion-Box Surface - The change of the kinetic order of a reaction with a change in the material or surface from which a reaction vessel is made is well known. Thus, if the inner surface of an ionization-source is changed, we may obtain information as to how to produce a surface or gas phase reaction.

(e) Change of Kinetic Order with Gas Composition - If two reactant gases which adsorb differently on a given metal are introduced into an ion-source, then in principle the surface coverage of reactant species may be altered which may alter the kinetic order. The change of kinetic order with gas composition allows elucidation of the reaction mechanism.

(f) Ion Current versus Repeller Voltage or Electron Current - In principle, we might expect some differences of surface reactions from gas phase reactions in plots of ion current versus repeller voltage and in ion current versus electron current. It would appear, however, until the effects of changing space-charge are better explained, that these plots lend little practical value in distinguishing between gas and surface reactions.

Illustrations of Methods

We wish to illustrate the above listed tests from data which we have collected on the following reactions,



where the symbol (+) indicates that either of the reactant species may carry the positive charge.

In Figure 1 we have plotted the logs of $i_{N_2D^+}$, $i_{N_2^+}$, and $i_{D_2^+}$ versus the log of the leak pressure for reaction (2). The slopes for the reactant species are seen to be 1.00. The slope or kinetic order for the product N_2D^+ is 2.00. Thus, it would appear that reaction (2) occurs in the gas phase.

In Figure 2 we have made plots for reaction (3) similar to those in Figure 1. Again, the formation of reactant ions H_2^+ and O_2^+ is first

Fig. 3. Log-log plot of $i_{\text{CO}_2^+}$ versus leak-pressure.

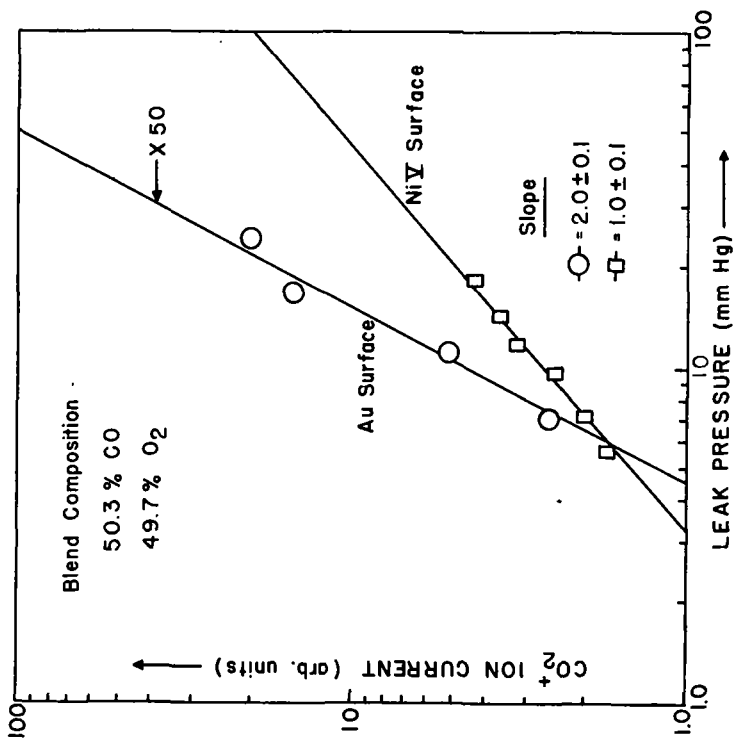


Fig. 4. Plot of log of $i_{\text{O}_2^+}$, $i_{\text{H}_2^+}$, and $i_{\text{HO}_2^+}$ versus time.

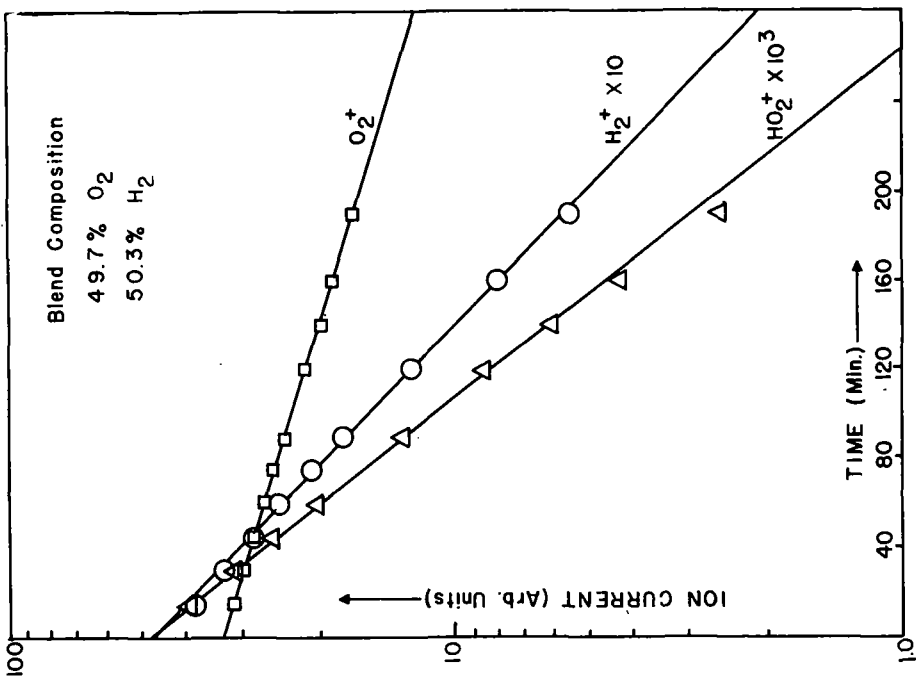


Table 1. Variation of pressure-order for formation of HO_2^+ from gases varying in $\text{H}_2\text{-O}_2$ composition.

PRESSURE DEPENDENCE OF HO_2^+ WITH
BLEND COMPOSITION IN $\text{H}_2\text{-O}_2$ MIXTURES.

Blend Composition (%)		Pressure Order
H_2	O_2	
84.3	15.7	1.82
64.2	35.8	1.42
50.3	49.7	1.18
38.6	61.4	0.99
19.6	80.4	0.97

order with respect to pressure. However, the formation of the secondary ion HO_2^+ changes from second order at the lower pressures to first order at the higher pressures. We may conclude that a gas phase reaction predominates at lower pressures and a surface reaction at higher pressures.

In both Figures 1 and 2 the data were collected with an ion-source constructed from Nichrome V metal. In Figure 3 we present data for reaction (4) for which a gold surface in the ionization box was used as well as a Nichrome V surface. It is seen that with the gold surface the formation of CO_2^+ is second order with pressure which indicates a gas phase reaction, whereas a surface reaction is indicated for the Nichrome V surface.

In Figure 4 we show a plot of the log of $i_{\text{O}_2^+}$, $i_{\text{H}_2^+}$, and $i_{\text{HO}_2^+}$ versus time for reaction (3) using a gold surface for the ion-source. We find that the sum of the slopes ($k_{\text{H}_2} + k_{\text{O}_2}$) is equal to $6.4 \times 10^{-3} \text{ min.}^{-1}$ while $k_{\text{HO}_2^+}$ is $6.5 \times 10^{-3} \text{ min.}^{-1}$. This confirms Eq. (1) and a similar plot given by Gutbier.¹ One may conclude that a gas phase reaction is occurring. However, it is seen from Table 1 that the kinetic order for formation of HO_2^+ on a Nichrome V surface from the same gas mixture is 1.18 which indicates a predominant surface reaction.

In Table 1 we show how the kinetic order for formation of HO_2^+ by reaction (3) changes with gas sample composition when an ion-source made from Nichrome V is used. The interpretation of these data follow closely the work of Langmuir² on platinum surfaces at higher temperatures where the oxygen is preferentially adsorbed instead of hydrogen. A similar explanation may account for our observed pressure-order changes.

We should like to mention that if two species react on the ion-box surface then we could obtain an experimental kinetic order of 2 even though a surface reaction were occurring. To eliminate such a case would require the variation of gas composition in conjunction with the other tests listed.

Conclusions

We have presented some methods for testing whether observed ion currents result from gas phase or surface reactions in the ion-source of a mass spectrometer. With these tests we have shown the existence of surface reactions occurring on the inner surfaces of the ionization box. These processes could easily have been interpreted as gas phase reactions if the tests had not been run. It is our hope that these tests will be utilized by those who appear to consider all ions of a mass spectrum to be formed by gas phase processes.

References

- ¹H. Gutbier, Zeit. f. Naturforschung 12a, 499 (1957).
- ²I. Langmuir, Trans. Faraday Soc. 17, 621 (1921-22).

(35) THE ANALYSIS OF GASES IN TRANSISTOR PACKAGES
USING AN ULTRA HIGH VACUUM MASS SPECTROMETER SYSTEM

P. D. Davidse

Philco Scientific Laboratory
Blue Bell, Pennsylvania

Extended Abstract

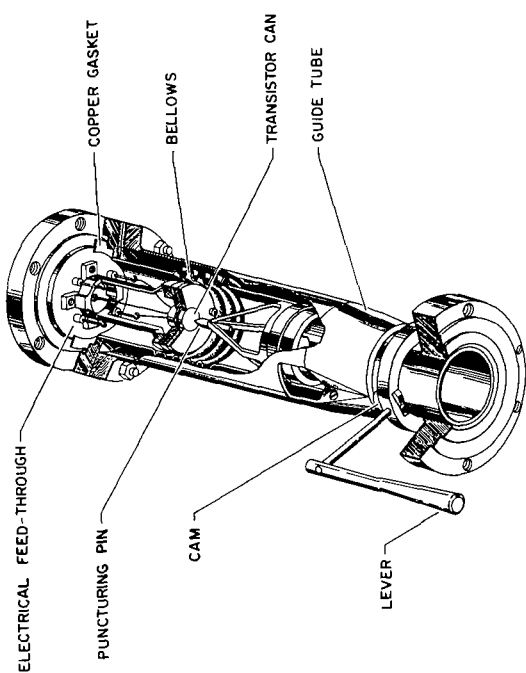
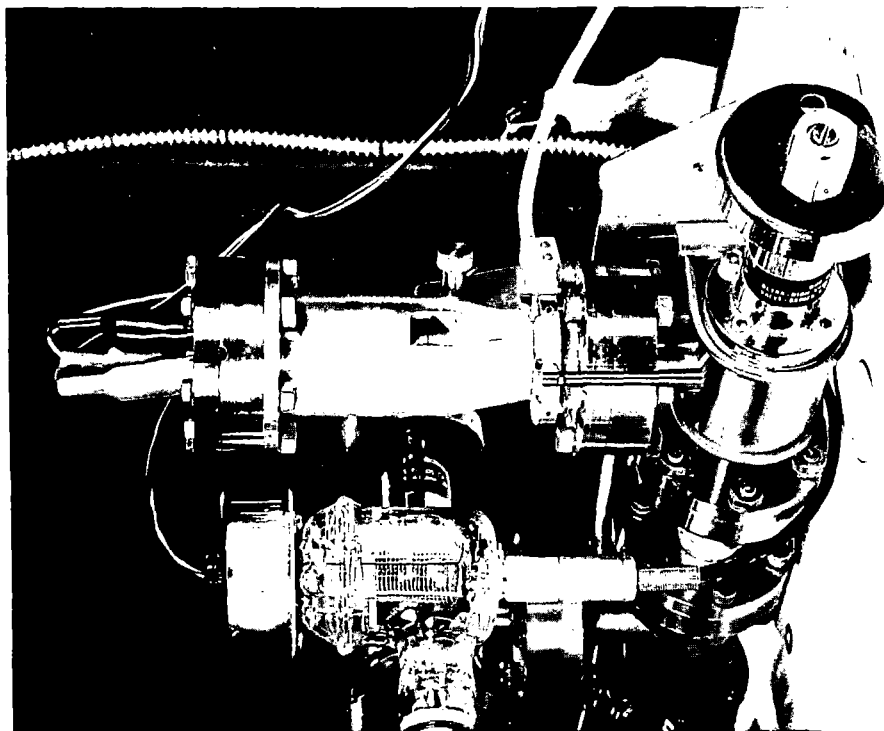
The work described is part of a study of the fundamental aspects of transistor failure. Some transistors that fail during aging tests show partial or complete restoration of their original characteristics following puncture of the transistor package. To further investigate this effect a device was constructed which would enable measurement of transistor properties during evacuation of the package, followed by the admission of another gas. A mass spectrometer was used to analyze the gas originally in the package.

The mass spectrometer used was a CEC 21-612 tube with an adsorption type forepump and a triode getter ion pump. The system was all metal (except for a Bayard-Alpert ionization gauge) and bakeable. Preliminary experiments carried out with a non-bakeable mass spectrometer (CEC 21-103C) have given inconclusive results, because of the elution of gases, notably water vapor, from the walls of the system during the analysis.

Figure 1 shows the gas sampling device. The transistor can is punctured by using the movement of metal bellows to drive the can against a metal pin. The package is supported by a holder mounted on a flange which has ceramic insulated feedthroughs for electrical connection to the transistor. The outside guide tube aligns the package during puncturing and carries a stop which keeps the bellows extended. On withdrawal of the stop by turning the lever to the "up" position the vacuum pulls in the bellows and forces the transistor can against the puncturing pin. By turning the lever another 180° to the original "down" position the transistor is moved up again. The whole operation may be performed with the index finger in about a second. The gas released is leaked into the mass spectrometer section of the system.

Figure 2 is a photograph of the transistor can puncher mounted in the vacuum system. In the photograph is shown attached to the guide tube a microswitch which makes contact with the ring holding the can when the transistor package is punctured. The switch closes a relay circuit which activates a camera mounted on the screen of a transistor curve tracer. This permits recording of transistor characteristics as a function of time during the puncturing operation. A similar arrangement serves for examination of the transistor characteristics during admission of other gases.

The analysis of the results is complicated by the large number of variables in transistor manufacture. As would be expected the detailed relationship between transistor characteristics and gas environment depends very much upon the particular type of transistor examined. The curves shown at the meeting illustrated some of the types of behavior seen, but the systematic investigation of these effects is, as yet, incomplete.



ULTRA-HIGH VACUUM TRANSISTOR CAN PUNCHER

FIGURE 1

Analysis of Gas in Glass Diodes Without Diode Destruction

K. A. Meyer, Atomics International, Canoga Park, Calif.

J. Brandewie, Autonetics, Downey, Calif.

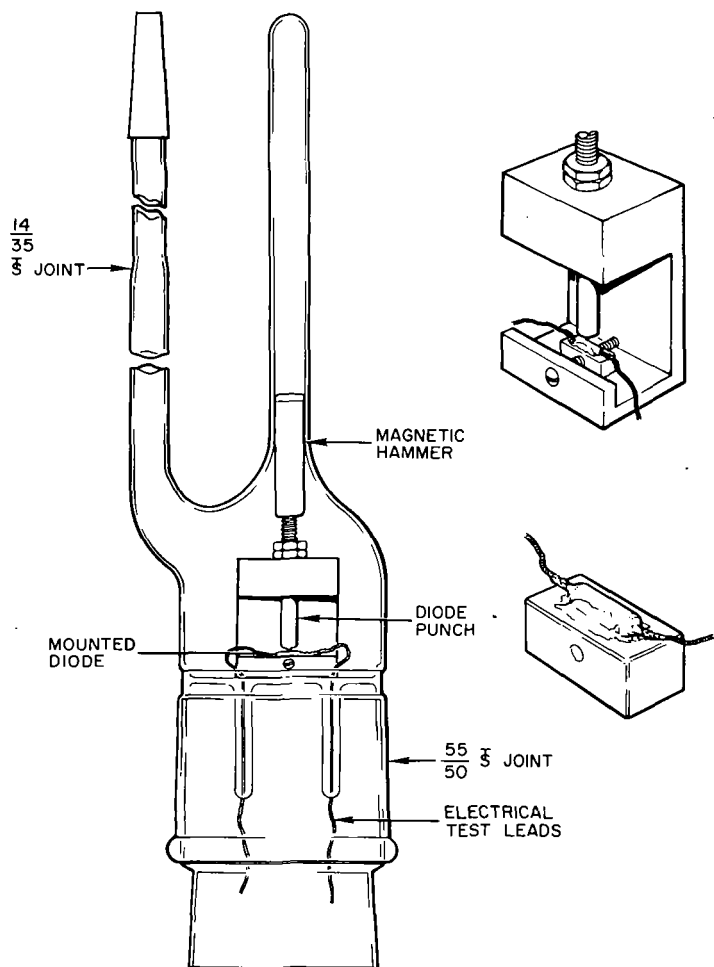
Persistent failure of several types of glass enclosed diodes to meet performance specifications led to a request for analysis of the gas contained within the envelope. It was further requested that the diode junction be preserved to allow electrical testing, etching, etc. after the gas had been removed. The second request precluded employment of standard vacuum crusher techniques and the apparatus shown in slide 1 was developed. This is of course a modification of the common magnetic hammer technique and provides a method for limiting the travel of the punch.

The glassware is based on a 55/50 standard taper joint. The punch and diode block holder shown in the slide detail was fabricated from brass. It provides opposing screws for holding the diode mounting blocks and also for centering the diodes under the punch. The top portion of the punch is threaded for the travel limiting nuts. The male member of the 55/50 joint was sealed, flattened and 2 electrical leads sealed through the edges of the section. The punch and diode block holder was then cemented to the flat section with epoxy cement. The design of the female part of the joint is obvious and contains the hammer guide and provision for connection to the mass spectrometer inlet system.

In operation the diode was mounted on a small steel block with epoxy cement as shown in the slide detail. Care was used to insure that the lead wire-glass junctions were covered and that envelope sides were well imbedded in the cement. R-313 bonding agent from the Carl H. Biggs Company, Santa Monica, California, was used throughout this work. It is a room temperature short cure time epoxy cement. After a 24 hour precautionary cure period, the diode and block were placed in the apparatus. The punch travel limiting nuts were adjusted so the point would just contact the diode when a 0.020" shim was placed between the nut and the top of the holder. Thus, when the shim was removed, the point could penetrate 0.020" into the diode envelope. The diode lead wires were soldered to the electrical test connections and the female part of the joint sealed on with apiezon W. The apparatus was then connected to the mass spectrometer inlet and evacuated. The hammer was lifted with an external magnet and dropped to drive the diode punch into the glass envelope thus releasing the gas for normal volume measurement and mass spectrometer analysis.

During the testing of a large number of diodes only one junction was broken when the glass envelope was opened.

The test results, while not germane to the paper title, are interesting and conclusive. For example, while one set of 5 good diodes averaged 5×10^{-3} standard cc of the typical nitrogen-argon carbon dioxide mixture of combustion gases, 4 out of 5 failing diodes contained 9×10^{-3} cc of air containing the normal amount of oxygen and up to 5% trichlorethylene. The increase in gas volume and the presence of both oxygen and trichlorethylene used as a cleaner after sealing were positive proof of leaks in the diode envelope.



5-14-62

9305-1833

RESIDUAL GASES DURING OPERATION AND
LIFE-TESTING OF POWER KLYSTRONS

Lowell Noble and Robert K. Waits
Eitel-McCullough, Inc.
San Carlos, Cal.

ABSTRACT

The gases present during exhaust processing, operation, and life testing of high-power klystrons were analyzed using a Diatron mass spectrometer. During bakeout at 500°C, hydrogen, water, carbon dioxide, and methane were evolved. Carbon dioxide, methane and carbon monoxide predominated during cathode conversion. Electron bombardment of internal tube parts released carbon monoxide. After seal-off, the pressure was 10^{-7} Torr (carbon monoxide, methane, hydrogen). One hundred hours of klystron operation reduced the pressure to 10^{-9} Torr (carbon monoxide, hydrogen). Microleaks in a sealed klystron resulted in the appearance of argon; neither oxygen nor a mass 28 increase were detected. The argon disappeared during klystron operation.

SOLUTION OF LINEAR SIMULTANEOUS EQUATIONS

by

J. Leonard

Tidewater Oil Company
Martinez, California

Abstract

A computer program for solving linear simultaneous equations is presented which works directly on a stored table of coefficients. No transfer matrix is required and the entire operation, including setting up the table of coefficients, can be handled by non-technical personnel. Input data and output printout orders are completely independent of each other and the arrangement within the computer storage. The program currently in use involves a 26×26 matrix with 9 items of supplementary information. It provides submatrix operations of any order and is completely stored within the drum capacity of an IBM 650 computer. Computing times vary but are generally comparable with square inverse calculations of the same order.

Introduction

The purpose of this program is to provide a system which:

- 1) Calculates mass spectrometer and other data related to the analysis of hydrocarbon and gaseous mixtures.
- 2) Is as secure as possible from operator or key punch confusion.
- 3) Can be maintained and operated entirely by non-technical personnel.
- 4) Requires as little knowledge of computers or computer programming for set up or operation as possible.

Three versions of the program have been prepared:

- 1) The original version which was written in September 1957 for use on a Burroughs E-101 computer.
- 2) A version for a basic IBM 650 computer with alphabetic feature which was written in 1959 and until recently was the version used.
- 3) An IBM 1620 version which is now in operation.

Some features of the original program were incorporated into a program described by J. M. Gillette of Tidewater's computer department.⁽¹⁾ This IBM 650 program preceded our own IBM 650 version but was not adaptable to our needs for several reasons, including limitations on available storage space.

The comments which follow apply particularly to both the IBM 650 and 1620 versions. Both versions use identical key punch forms for all constant and data inputs. The routines have the following features:

- 1) No transfer matrix of any kind is used.
- 2) Input, matrix and output can be independently altered.
- 3) The program instructions cannot be upset by any known key punch or data errors. Operations will either cease with an alarm or, in the case of improper data, will print out the defective case and then process correctly any following correct cases.
- 4) The program cannot be set up improperly on the computer.

Header Card

Except for columns 11-40 in the header card, all columns must be punched.

220

- 5) No case type identifications are required. There is only one very complicated case in the program. All real cases are simplifications of this complicated case. The input data are used by the routine to determine what skips of program instructions will take place to process a real case.
- 6) All card types are identified by their content. There are no extra punches required to identify card types. Header cards, for example, are identified as header cards because they contain alphabetic data.
- 7) The program is not committed to a particular mathematical procedure. Gauss-Seidel, square inverse, delta and successive subtraction methods can be used with little or no change in operating instructions.
- 8) All input data and all intermediate data of interest are included in the output.
- 9) A means of switching to other programs, including IBM library programs, is provided in both the program and the wiring.
- 10) No coded titles are used in the output.
- 11) Calculations are rapid. The time required, however, can vary considerably depending on several factors including matrix arrangement, mode of operation, and the leverage of the equations. In the Gauss-Seidel mode, an approximation is prepared by the program to reduce the number of cycles required for solution. The 1620 version, using Gauss-Seidel mode, often solves the equations in less time than that required to enter and punch out data.

The IBM 650 version has some unusual programming. There are no counters in the program. There are also no store data address or store instruction address instructions employed. The location of constant terms, including equation coefficients, is almost as important to the successful operation of the program as the instructions themselves.

The basic idea behind the original routine was to develop a case which was sufficiently complicated to cover all real cases. The developed case did not have to represent any real situation as all real cases would be merely simplifications of this complicated case. By this procedure, a minimum amount of storage would be required for instructions. Next was to try to develop an operating formula which could handle all of the principle mathematical problems to be encountered. No such formula exists but the following expression fulfilled our needs:

$$X' = \frac{m + bx - \sum ax}{c}$$

With such an expression and a means of locating individual terms, any of several mathematical processes can be used by simply eliminating selected steps in the operation. For example, eliminating all but the summation term provides the basic operation for square matrix calculation, eliminating the b and c terms provides an expression for calculating residuals, and using the expression as stated provides the expression for Gauss-Seidel operations. The basic expression for Gauss-Seidel operations is:

$$X_i' = \frac{m_i + a_{ii} x_i - \sum_{r=1}^n a_{ir} x_r}{a_{ii}}$$

The successive subtraction method uses the same operation steps as the Gauss-Seidel. The method is set up automatically whenever the matrix coefficients can be stated as a triangular matrix whose post diagonal terms are all zeros.

Although the Gauss-Seidel form arose from building up several mathematical models, it was a fortunate choice. Our operators were familiar with the system, having used it with a Consolidated Engineering Corporation Type 30-103 computer. They were already using the C. E. Berry ⁽²⁾ convergence criterion to set up matrices

for inversion by IBM library routines. (Using the largest or large terms for diagonal terms will not always produce satisfactory inverses for some of our matrices.) The Gauss-Seidel procedure also is one which could be used without a transfer matrix if an efficient selection method, cycling method and means of estimating could be found. The solution to these problems on the IBM 650 was as follows:

- 1) Set up the matrix as normally written using location 0051 for a_{ii} . This produces two desired results. The matrix is exceedingly simple to load and all coefficient terms are located prior to the punch band.
- 2) Convert the punch band into registers which will contain all input and output data. In this manner, all data which are variable will be in predictable locations.
- 3) Set all constants associated with the program in rows which are aligned with the appropriate coefficient columns.
- 4) Use the first digit of the first word of each punch band as a selecting switch and the next three digits as an index.
- 5) Disregard normal program languages in favor of a language which is geographically oriented.
- 6) Use remnants of the answers to the preceding case as an estimate for the present case.

Input, output and security problems were solved in the following manner:

Location zero always contains zero, location 1950 always contains 8000 and locations 0001 to 0036 contain the preferred order of output punching.

With this arrangement and the single read instruction calling for reading cards into band 1950, no card can enter without being subject to wiring and code checks except an IBM type load card. An IBM type load card, however, will cause a branch to the console switches to be executed and the console switch instruction will read in the next card. If this card is not a 5/card load card, both the 5/card load of the program and the program code will be destroyed. If a 5/card load program card is loaded, the program code will still be destroyed but alterations to the stored program can be made if cards of the proper format follow.

All input cards for cases contain the programs code. Therefore, the wrong code, the wrong wiring, the wrong program, or loss of cards from the correct program will result in a program stop.

The input cards are simple. Each card contains a seven-digit case identification number followed by a three-digit code. The header card which must be first of a set then contains an alphameric description of the case. The detail cards contain:

- 1) A three-digit index.
- 2) The data making up the constant term of the equations.
- 3) A ten-digit field consisting of background and/or combination analysis vector data.
- 4) A digit which shows whether the data are to be used to solve equations or to check equations solved by the use of other data.

The index in the case of mass spectrometer cases corresponds to the m/e data. Any three-digit index can be used except 000 and it is not necessary for each index to be a separate three-digit number. For example, 056 is used as the index for both grouped butylenes and a single butylene in the split butylene calculation. It is required, however, that there be a register for each index (two 056 registers in this case) and that the program properly set up switches and registers before solving the equations. A register with a zero index is not available. Therefore, the row, column, constants and register area associated with the zero index are free for storage of instructions.

The ten-digit field is a part of the vector used for combination analysis. The system used for combination analysis is similar to one described by James Weiss at an earlier ASTM E-14 meeting.⁽³⁾

On input, the program checks each card for suitability to the case being developed and the program being used. It then seeks out a register and stores the data. If required, it also turns on the switch for that register. The program senses the completion of case input by detecting the alphabetic information in the following header card.

Calculation proceeds as follows:

- 1) All switches are checked to see if a proper solution is set up. Switches and the location of data are altered as required.
- 2) In the Gauss-Seidel mode, an estimate is prepared.
- 3) The location of the first on switch is used to prepare a set of variable instructions. (A maximum of eight variable instructions are stored on the drum.)
- 4) The variable instructions and the location of the remaining switches determine the terms used in the calculation of an estimated root (Gauss-Seidel). The absolute difference between the absolute values of this term and the original estimate are added to the contents of a special accumulator and the new value stored.
- 5) Following switches are used in the same manner until all switches have been used to determine equations.
- 6) The sum of the absolute differences of the new and old estimates is compared against a standard. If within the standard, the program branches to post matrix calculations. If the standard is not met, the special register is reset to zero and a new cycle is started.
- 7) The post matrix calculations consist of calculations of all residuals (using modified instructions of the basic operating formula), and a series of normally programmed steps.

The printout is accomplished by printing a title card, followed by any special cards, and then going to a printout priority routine. This priority routine checks for "on" switches in the order determined by the data located in storage locations 0001 to 0036. When an "on" switch is found, the register associated with that switch is printed. When the complete list of priorities has been checked, an off switch variation is made in the punching routine and the list of priorities is again searched. This time the routine checks for "off" switches. Each time an "off" switch is located, the appropriate register data are punched providing input data entered that register. If the register was not used for either input or calculations, it is ignored.

Once set up, the operational part of the program does not have to be changed for handling a wide variety of problems involving the solution of simultaneous linear equations. Non-technical people set up their problems by writing the coefficient matrix on an IBM "Drum Storage Layout Form" (IBM Form No. 22-6283-1). The three-digit indexes are listed in the preferred order on locations 0001 to 0036 and the first word of each register. The IBM form can also be used as a key punch form. We do not permit different variations of the routine to use the same code. The code is selected by one person who keeps track of all codes used. Training time to set up and operate the routines is less than eight hours. This does not include the time required to learn what peaks are involved in a mass spectrometer calculation or any data on the internal operations of the routines. An experienced operator can set up the routine as fast as he can copy his data onto the form.

127150 733-88 FEED ALKY

2197

2036

LIQUID PCT

127150 733-PROPENE	65	72	1009	130	401	40	10	3480	8	42
PROPANE	92	102	483		680	83	1	797	8	44
BUTADIENE	1	1	26	10	360	83	1	267	8	54
ISOBUTENE	135	1149	2615	116	730	40	10	6784	8	39
BUTENE 1	120	133	2376	97	460	24	30	12983	8	41
BUTENE 2	184	182	3044					3440	8	56
ISOBUTANE	253	280	5973		1000	40	10	9600	8	43
N BUTANE	141	156	2928		570	83	1	487	8	58
PENTENES	12	13	13-	97	170	83	1	10-8	70	
ISOPENTANE	16	18	211		610	83	1	527	8	57
N PENTANE	1	1	35		98	83	1	15	8	72
			988					988	8300	
NITROGEN			12					12	8400	
ETHENE			613		573	40	10	4717	9	28
ETHANE			19		686	62	3	1855	9	26
BUTENES					284	83	1	201	9	30
					10	385	40	3440	9	56
RESID 27					97	750	40	7003	9	27
RESID 29					78	496	40	4482	9	29
ARGON						535	62	1419	9	40
										41

1000 1107

12

11

10

9

8

7

References

- (1) Mass Spectrometer Data Reduction Program for IBM 650, J. M. Gillette, Anal. Chem. 31, 1518 (1959).
- (2) A Criterion of Convergence for the Classical Iterative Method of Solving Linear Simultaneous Equations, C. E. Berry, Ann. Math. Stat. XVI, No. 4 (1945).
- (3) Analysis of Complex Hydrocarbon Mixtures: Maximum Utilization of Data from Combined Analytical Methods, James Wei, Charles D. Prater, Allan R. Emery, Am. Chem. Soc., Div. Petrol. Chem., Preprints 4 No. 3, 139-54 (1959).

CONSTRUCTION OF AN I. B. M. PUNCHED CARDS FILE FOR IDENTIFICATION
OF CHEMICAL COMPOUNDS BY THEIR MASS SPECTRA.- PAR Aymé CORNU -

After the spectrum of a given sample has been obtained, this spectrum is to be compared with all the pure compound spectra available in the laboratory, in order to find either an identical spectrum, or any similar ones.

At present, our own collection of mass spectra contains about three thousand three hundred spectra, and obviously, for each analysis it is practically impossible to go through the whole of these records, to find an answer to our problem. Therefore we have established an index system permitting a fast access to the greater part of the whole collection.

Our index system is composed of one set of handwritten matrix cards, destined to set up two collections of I. B. M. punched cards, nominative and analytical cards respectively.

I - MATRIX CARDS FILE -

Each of such card corresponds to a pure compound whose mass spectrum is filed in our collection.

On each matrix card is registered :

- 1°/ - The name of the compound ;
- 2°/ - Its reference, order number and collection number ;
- 3°/ - Its molecular formula ;
- 4°/ - Its molecular weight ;
- 5°/ - The list of masses of the ten strongest peaks, classified according to decreasing height ;
- 6°/ - The developed formula.

All these cards are gathered in a collection which includes to this day :

- 1 715 Cards from A. P. I. Collection ;
- 800 Cards from G. A. M. S. ;
- 700 Cards from Literature data.

TOTAL ... 3 215 ,

II - I. B. M. CARDS FILES -

Data registered on the matrix card are transcribed in perforations on I. B. M. punched cards, but this transcription is made in two stages.

.../

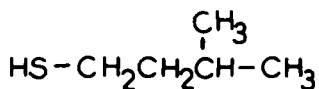
3-Methyl- 1-butanethiol
(Isopentyl mercaptan)

API 1718

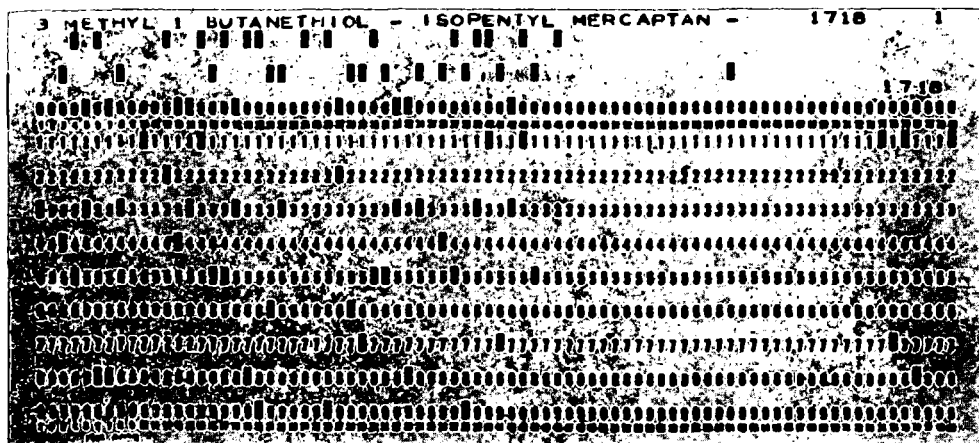
$C_5H_{12}S$

M 104,21

55 70 41 43 42 47 61 27 104 39



CARTE MATRICE



CARTE ALPHABETIQUE

A) - So-called "nominative" cards -

Nominative cards contain as perforations, the entire name of the compound, up to sixty types or signs, and the corresponding reference number (five figures, two letters and one figure).

Cards of this file do not contain any other scientific data and are exclusively destined to the clear interpretation of the compound name, on the analytical cards.

B) - So-called "analytical" cards -

Cards of this file contain :

- 1°/ - In columns number one to forty, the masses of the ten strongest peaks, following the order of decreasing peak height. Each peak is represented by four figures thus hundreds, tens, units, and tenths of mass. It is possible to put down in this list, peaks of double-charged ions, which are sometimes very strong in aromatic compound spectra.
- 2°/ - Molecular weight in columns number seventy to seventy two. Decimal part is neglected, and, for Br and Cl, molecular weight is computed for the lighter isotope only.
- 3°/ - Molecular formula are punched in columns number fifty two to sixty nine. Atom number of Carbon, Hydrogen, Bromine, Chlorine, Fluorine, Iodine, Nitrogen, Oxygen, Phosphorus, Sulphur, Silicon, are punched in predetermined columns, other eventually occurring elements are punched as "miscellaneous".
- 4°/ - Reference number is punched, as for nominative cards, in columns number seventy-three to eighty.

After punching, these cards are interpreted, i. e., on each card are automatically printed :

- 1°/ - The masses of the nine strongest peaks ;
- 2°/ - Molecular formula ;
- 3°/ - Reference number ;
- 4°/ - Molecular weight ;
- 5°/ - Complete clear name of the compound.

For this last interpretation, which is printed on a second row, the nominative cards file must be introduced, in connection with the analytical cards file, in an I. B. M. collator.

Three copies of this analytical file are made in different colours, blue, green and yellow.

Many tests are made for verification of punching ; wrong cards are eliminated and replaced by corrected ones.

.../

III - UTILIZATION OF THE ANALYTICAL FILES -

The first set of cards, (yellow coloured) is ranged according to molecular weights.

The second one (blue coloured) is filed according to reference numbers, and so, it forms a card copy of the spectral data lists.

The third one (green coloured) is filed according to the masses of the ten strongest peaks in decreasing order.

After filing, cards are tabulated, giving a list somewhat similar to the "spec finder" of infrared Sadlier spectra.

When the spectrum of the compound being investigated has been run, the strongest peaks are measured, and the list of the masses of the ten strongest peaks ; this list is immediately compared to the similar lists of the third cards file.

The order of masses of the ten strongest peaks seems to be a so characteristic value, for one compound, that it is almost certain that comparison of lists will permit identification of compound. If not, interversion of any peaks may be tried, for any differences may occur in spectral patterns due to instrumental peculiarities in ionization process.

If no similar list of peaks is found, it must be suspected that either the collection do not contain the true answer to the problem, or the compound is not a pure compound and must undergo further separation. Examination of spectra whose strongest peaks list is close to that of unknown compound can permit to obtain interesting data upon fragments or partial molecular structure of the analysed sample.

Practically, in the case of a pure compound whose spectrum is inside the collection, we do every time succeed in identification.

The yellow coloured file, classified according to molecular weight, is very useful in identifications based upon parent peak examination. The file, at the analyst's disposal gives him a complete list of the different atom combinations able to bring about any given molecular weight. Consideration of other strong peaks printed on the card give many valuable informations for identification.

Using an I. B. M. sorter it is possible to file the cards in any desired order, or to eliminate those of compounds with are obviously of no interest.

In conclusion, we think this punched card file solves with simplicity the difficult problem of a fast access to the principal data of the totality of our mass spectra collection.

N. B. - After this work was completed, we found out that F. W. McLafferty (Anal. Chem 31-1160-1959) and G.C. Doderer (Applied Spectroscopy 14 N° 15-139-1960) have studied the same subject, and created indices of rather different form.

A. CORNU.

A MASS SPECTROMETER FOR A STUDY OF THE
COMPOSITION OF THE UPPER ATMOSPHERE

Alfred O. Nier
University of Minnesota
Minneapolis, Minn.

ABSTRACT

A mass spectrometer suitable for installation in an Aerobee-Hi rocket has been constructed based on the prototype developed earlier¹. It will be used for a study of the composition of the atmosphere in the range 100-250 km. Two shots are scheduled for 1962 in a cooperative program with J. H. Hoffman, C. Y. Johnson and J. C. Holmes of the Naval Research Laboratory. Details of construction and operation will be discussed.

¹ Alfred O. Nier, Rev. Sci. Instr. 31, 1127 (1960).

A Quadrupole Spectrometer for Precision Mass Determinations

U. von Zahn, S. Gebauer and W. Paul

Physikalisches Institut, Bonn, Germany

The construction of a quadrupole spectrometer for precision mass determinations was stimulated by the fact that our knowledge about the accurate values of nuclidic masses is relatively poor in certain regions of the periodic table. Particularly, many of the elements between xenon and tungsten are known only to about one part in one million. Because of this situation, the layout of our quadrupole spectrometer is especially designed for heavy masses. The theory of the quadrupole spectrometer is given as reference 1.

To achieve a reasonable resolving power, the ions should stay a long time within the quadrupole field. In our case, we want to have the ions experience at least 500 periods of the Hf in the analyzing field. To reach this goal we built a long field-- it is about 6 m long, and second, we are using rather slow ions--ions with an energy between 10 and 30 eV. Figures of the spectrometer are:

Length of field	L = 5.82 m
Field radius	r ₀ = 3.5 cm
Frequency	ν = 471 kcps
Hf amplitude (for A = 200)	V = 3924 V
DC voltage	U = 658 V
Hf power	N = 290 W
Entrance diaphragm	Ø = 1 mm

Each electrode of the quadrupole field is made up of a group of 60 wires, which are stretched to 80% of their breaking load. The wires are fastened only at the ends of the field and in our opinion this is a fairly simple technique which gives us a rather constant field geometry. The ions are formed in a conventional electron impact source and detected by a 17 stage multiplier.

Mass scanning is achieved by simultaneous change of both the Hf voltage and the DC voltage with fixed frequency.

To compare an unknown mass with a reference mass, we make use of the linear relationship between focused mass and applied DC voltage. But this situation is complicated by the fact that the basic equation looks like this:

$$\frac{m_1}{m_2} = \frac{U_1}{U_2} \cdot \frac{a_2}{a_1} \quad a_i = \frac{8eU_i}{m_i \omega^2 r_0^2}$$

The mass ratio can be determined by the ratio of the applied DC voltages, but there appears the so-called Mathieu parameter "a" for both species of ions. These parameters determine the motion of the ions within the quadrupole field and the second equation gives the definition of "a". To derive the mass ratio from the voltage ratio alone, we need a criterion that a₁/a₂ equals exactly unity. For this the most sensitive test seems to be to look for the intensity of both peaks. Because the intensity ratio I₂/I₁ which one measures at the detector is proportional to the initial ratio I_{2,0}/I_{1,0} times a factor, which depends on both a values

$$\frac{I_2}{I_1} = \frac{I_{2,0}}{I_{1,0}} \cdot \frac{0.23699 - a_2}{0.23699 - a_1}$$

The number 0.23699 is a fundamental constant of Mathieu's differential equation; hence one gets the correct intensity ratio at the detector only when a₁ = a₂. Eliminating a₂ by means of the first equation gives the third expression

$$\frac{I_2}{I_1} = \frac{I_{2,0}}{I_{1,0}} \cdot \left[1 + \frac{a_1}{0.23699 - a_1} \left(1 - \frac{m_1}{m_2} \cdot \frac{U_2}{U_1} \right) \right]$$

The ratio U₂ over U₁ is given by a precision resistor divider. The circuit is such that always this equation is valid:

$$\frac{U_2}{U_1} = \frac{R}{R + \Delta R}$$

Therefore the intensity ratio as a function of ΔR is the following equation,

$$\frac{I_2}{I_1} = \frac{I_{2,0}}{I_{1,0}} \cdot \left[1 + \frac{a_1}{0.23699 - a_1} \left(1 - \frac{m_1}{m_2} \cdot \frac{R}{R + \Delta R} \right) \right]$$

Because ΔR is very small compared with R , we get a nearly straight line for the intensity ratio versus ΔR . The slope of this line depends on the factor with a_1 . All these curves with different a_1 should have a unique crossing point. This point then gives us both the true intensity ratio and the true ΔR . From that ΔR one can easily calculate the mass ratio.

To test this method and our apparatus we measured the well-known mass ratio of xenon isotopes. The results are:

Mass ratio:

$$\frac{^{132}\text{Xe}}{^{131}\text{Xe}} = 1.007\,632\,1 \pm 5 \quad \text{Quadrupole field}$$

$$1.007\,632\,06 \pm 8 \quad \text{Ries, Damerow and Johnson (1960)}$$

Intensity ratio:

$$\frac{^{131}\text{Xe}}{^{132}\text{Xe}} = (0.7902 \pm 0.0020) \times f$$

$$f = \sqrt{^{131}/^{132}}$$

$$= 0.7872 \quad \text{Quadrupole field}$$

$$0.7877 \pm 0.0027 \quad \text{Nier (1950)}$$

Mass ratio:

$$\frac{^{134}\text{Xe}}{^{132}\text{Xe}} = 1.015\,173\,0 \pm 10 \quad \text{Quadrupole field}$$

$$1.015\,171\,88 \pm 6 \quad \text{Damerow (1960)}$$

The mass ratio of 132 over 131 agrees very well with the much more precise value of the Minnesota group. The relative abundance ratio for the two isotopes is also quite good. The first value is the measured value. Because we are using a multiplier and the conversion factor from ions to electrons depends on the velocity of the incident ion, we applied a correction factor 0.9962 to get the final result. Although both values agree with that of Nier, the agreement of the corrected value is much better. It seems to be worthwhile to emphasize that this intensity measurement is done with a resolving power between 2,000 and 6,000.

To make further tests we compared two isotopes which are two mass units apart. In this case the agreement is not as good and there is no doubt that our measurement is in error. However, we now believe that we know the reason for this. There are indications that the intensity ratio is biased due to different time constants in the detection circuit for each peak, and this causes an error in the mass ratio also.

I should make a short remark on the resolving power of the instrument. As you saw, the accuracy of our measurements depends mainly on the sensitivity of the intensity versus DC voltage variations. Therefore the resolving power is of secondary importance but should be high enough to resolve impurities. Our measurements are normally made with resolution below 10,000 and the maximum resolving power was 16,000. This value is not high enough to resolve carbon 13 peaks which make it necessary to select the reference peaks very carefully.

References

1. W. Paul, H. P. Reinhard, U. von Zahn, Z. Physik 152, 143 (1958)
2. U. von Zahn, submitted to Z. Physik.

HIGH RESOLUTION TIME-OF-FLIGHT MASS SPECTROMETER

by

D. B. Harrington, Product Specialist,
The Bendix Corporation, Cincinnati Division
Cincinnati, Ohio

R. S. Gohlke, Research Chemist,
The Dow Chemical Company
Eastern Research Laboratories
Framingham, Massachusetts

A brief description of the operation of the time-of-flight mass spectrometer will be given, followed by a more detailed description of the factors affecting mass resolution. Following this, some examples will be given of improved mass resolution achieved with the high resolution time-of-flight mass spectrometer built by Bendix for The Dow Chemical Company.

The Bendix Mass Spectrometer produces from 10,000 to 100,000 complete mass spectra every second. (All instruments described in this paper operate at the more standard 10 KC frequency). The first event in the formation of each mass spectra is the creation of the ionizing electron beam in the ion source (Figure 1). This electron beam lasts approximately 0.3 microseconds, and ordinarily the ion accelerating pulse (ion focus pulse) occurs immediately after the shut-off of the electron beam. The ions which have just been created are thereby accelerated through the middle grid of the ion source and receive their final energy of 2,800 volts from the ion energy grid. All ions of the same mass to charge ratio receive the same energy, so that the lighter ions travel faster and reach the collector first. These separated mass bunches are amplified in the magnetic electron multiplier, whose output is presented to an oscilloscope synchronized with the operating frequency of the mass spectrometer. Simultaneously, individual mass signals as well as mass spectra can be recorded on a chart recorder, although the mechanism for this is not illustrated in Figure 1.

There are two major factors affecting mass resolution in a time-of-flight instrument, space focussing and energy focussing. Figure 2 illustrates space focussing. We take two ions with the same mass, the same charge, and zero initial velocity. The initial position of the white ion is slightly forward of the black ion's position, so that when the ion accelerating pulse is applied, the white ion finds itself at a -200 volt potential while the black ion is at a -190 volt potential. The white ion will leave the ion source well in advance of the black ion, but the black ion will have 10 volts more energy, so that eventually it will overtake and pass the white ion. The height of the ion accelerating pulse is chosen so that the black ion will just overtake the white ion at the collector.

Figure 3 illustrates energy focussing. We again have two ions with the same mass and the same charge, but this time their initial distances from the collector are identical, and their initial velocities are equal but in opposite directions. As soon as the ion accelerating pulse is applied, the white ion increases its speed towards the collector, while the black ion is brought to a stop and then returns to its initial position. From this time on, its subsequent history is identical to that followed previously by the white ion, since

the black ion velocity at this point is equal both in magnitude and direction to the initial velocity of the white ion. Therefore, the black ion will always trail the white ion, and will reach the collector after the white ion has already been detected. The difference in arrival times of these two ions will exactly equal, in this idealized case, the "turn-around time" of the black ion.

In practice, a pulse height for the ion accelerating pulse is chosen which will give the best compromise between space focussing and energy focussing. This best compromise is indicated by the sharpness of the mass spectrum presented to the oscilloscope or to the recorder.

Time-lag energy focussing is a device for overcoming the damaging effects which initial energies have on mass resolution. To help understand a later description of time-lag energy focussing, an inspection of Figure 4 may prove useful. This shows a graph of ion time-of-flight versus initial position in the ionization region. This graph is superimposed on a schematic of the ion source. One curve holds true for ions with the same mass, the same charge and the same initial velocity. If any of these three parameters is changed, a new curve is needed. To achieve best focussing for the white and black ion shown which have the same mass, charge and initial velocity, the height of the ion accelerating pulse would be adjusted so that the maximum of this curve coincided with the position of the ionizing electron beam within the ion source. This would result in the smallest flight time difference.

In Figure 5, a family of three curves is shown similar to the single one shown in Figure 4. The three ions in Figure 5 all have the same mass, the same charge, and they all are equally distant from the collector at the moment when the electron beam is turned off. The middle ion has zero initial velocity, while the white and the black ions have equal initial speed but opposite velocity. The white and black ions of Figure 5 correspond to the same two ions shown in Figure 3. In time-lag energy focussing, the beginning of the ion accelerating pulse is delayed, so that a time lag occurs between the end of the electron beam and the beginning of ion acceleration. During this lag, ions will move to new positions in the ionization region as a function of their initial velocities. In the case of the ions in Figure 5, the optimum lag is that which will permit the white and black ions to move to new positions in the ion source where their times of flight will be equal to each other as well as being equal to the flight time of the middle ion having zero initial velocity. Since we are still dealing with ions having the same mass and charge, time-lag energy focussing is mass dependent.

Theoretically, mass resolution in the time-of-flight mass spectrometer can be improved by increasing ion energy and increasing flight path, as well as by introducing time-lag energy focussing. In the latter half of 1961 the Cincinnati Division of The Bendix Corporation built a time-of-flight mass spectrometer for F. W. McLafferty and R. S. Gohlke of the Eastern Research Laboratory, The Dow Chemical Company, Framingham, Massachusetts. Gohlke specified that this instrument should include time-lag energy focussing, a flight path extended from the usual 100 centimeters to 167 centimeters, and an ion energy variable from 2,800 to 5,600 electron volts rather than the usual fixed energy of 2,800 volts. In practice, it was found that mass resolution was indeed improved markedly by time-lag energy focussing and by the increased flight path. However, increasing the ion energy gave indications of actually worsening mass resolution, so that

the energy now used with this instrument is approximately 3,000 electron volts. Subsequent theoretical and experimental work done by R. A. Fluegge at the Research Laboratories Division of Bendix in Detroit suggests strongly that increasing ion energy does actually improve the mass resolution occurring just before the multiplier anode, but that the output time constants of the readout circuitry more than off-set this improvement. As ion energy increases, these time constants become increasingly important because the time separation of adjacent masses gets smaller.

A photograph of a standard Bendix Mass Spectrometer utilizing a 100 centimeter flight path, 2,800 e.v. ion energy, and no time-lag energy focussing, is shown in Figure 6. This Model 12-101 Mass Spectrometer is also equipped with a Model 925 Knudsen Cell Sample Inlet System. Figure 7 is a photograph of the Dow instrument, which shows the obviously longer flight path. The heated molecular leak inlet system associated with this instrument was designed by Gohlke and built under his direction at Dow.

The harmful effect of large initial energies on mass resolution where no time-lag energy focussing is used can be seen by comparing Figures 8 and 10, which show spectra taken with a standard Model 12-101 (Figure 6). Figure 8 shows the recorded spectrum of mercury (there is an attenuation factor of 10 between the two traces) and Figure 10 shows the recorded spectrum of the CCl_3^+ ion from carbon tetrachloride. The oscilloscope presentation of this same carbon tetrachloride spectrum is shown in Figure 9. In each case, the masses, reading from left to right, are 117, 119, 121 and 123 a.m.u. Even though the carbon tetrachloride peaks are almost half the mass of the mercury peaks, the valley between peaks two mass units apart is certainly no lower for carbon tetrachloride than for mercury.

The mass resolution improvement made in this carbon tetrachloride spectrum by the longer flight path alone and by the combination of longer flight path and time-lag energy focussing can be seen in Figures 11 and 12. The same spectra are shown in both figures; Figure 11 shows the oscilloscope presentation and the oscillograph presentation is shown in Figure 12. The upper spectrum in each figure shows the resolution given by the longer flight path by itself, and the lower spectrum in each case shows the improvement given by combining the longer flight path with 2.6 microseconds of lag. Each spectra in Figure 12 is also divided into two attenuations, x1 and x5. In Figure 11, the peaks, reading left to right, are 117, 119 and 121 a.m.u., while in Figure 12 the order is reversed.

Summarizing our experience over the past 8 years as well as our future expectations, we arrive at Figure 13. We define unit resolution as that resolution which produces less than 1% peak height contribution. Good comparative figures for the resolution of various ion energy and flight path combinations using optimum values of time-lag energy focussing are not available, so the improvement in resolution given by time-lag energy focussing is not included in Figure 13.

An article by one of us which describes more fully the operation and application of the Bendix Time-of-Flight Mass Spectrometer is listed below. This article also contains a fairly complete bibliography.

Harrington, D. B., "Encyclopedia of Spectroscopy",
Reinhold Publishing Company, 1960, pp 628 - 647

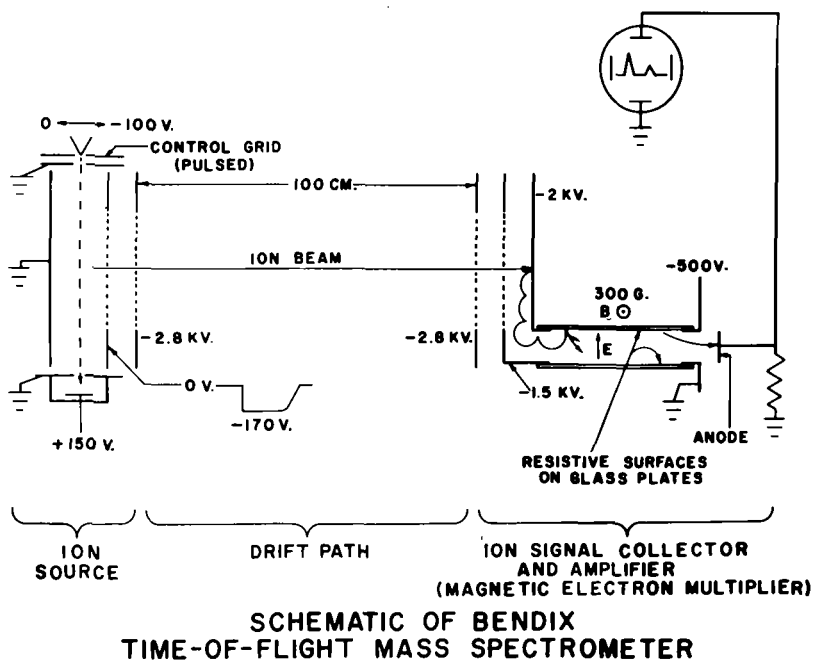
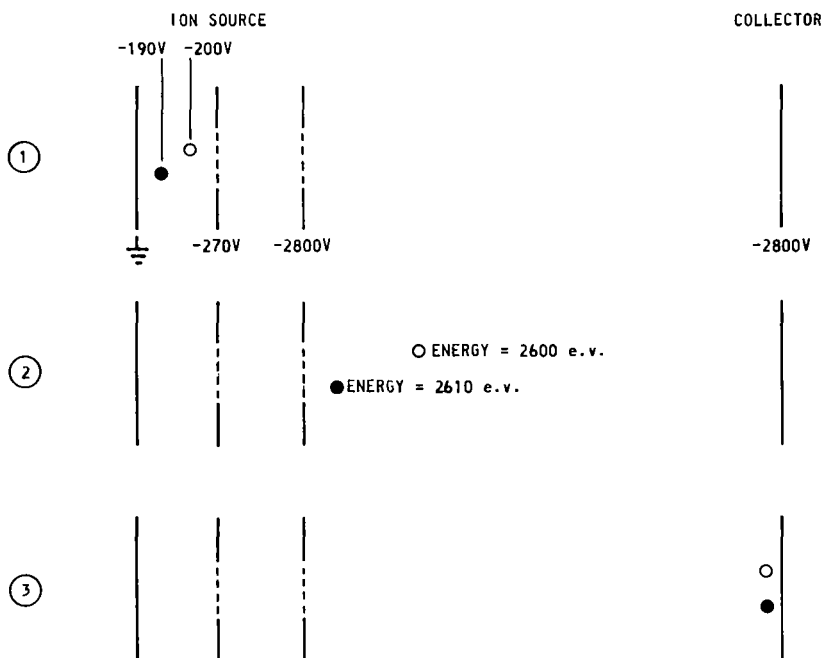
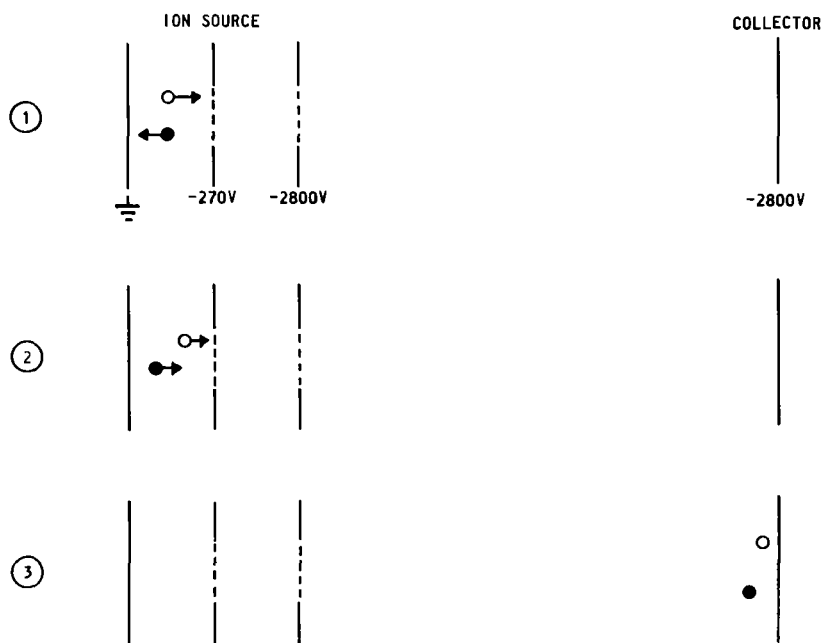


FIGURE 1



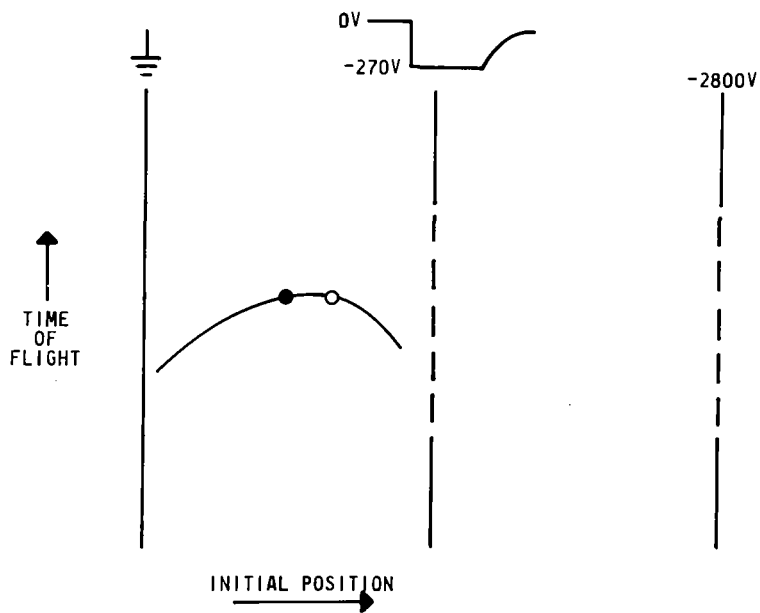
SPACE FOCUSING IN BENDIX T.O.F. MASS SPECTROMETER

FIGURE 2



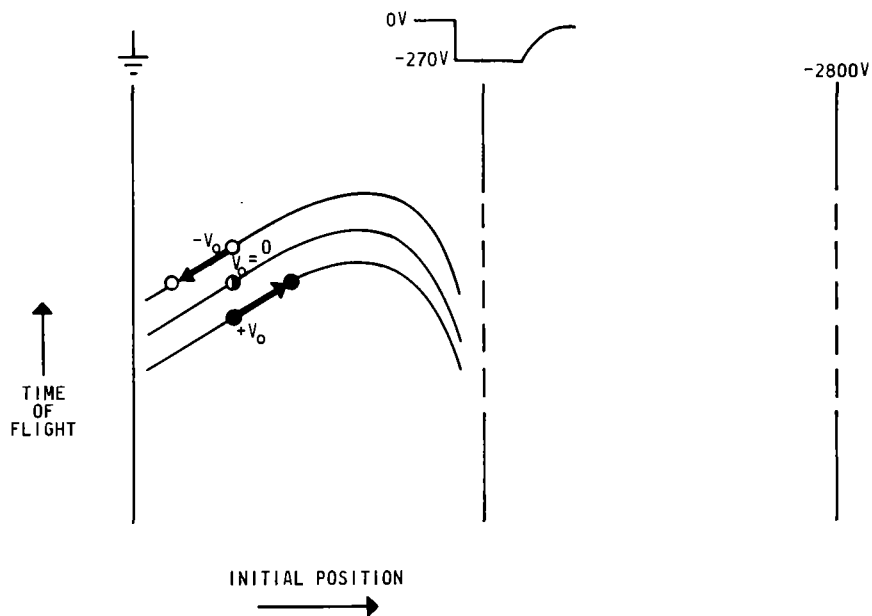
ENERGY FOCUSING IN BENDIX T.O.F. MASS SPECTROMETER

FIGURE 3



TIME-OF-FLIGHT VS. INITIAL ION POSITION

FIGURE 4



TIME-LAG ENERGY FOCUSING IN BENDIX T.O.F. MASS SPECTROMETER

FIGURE 5

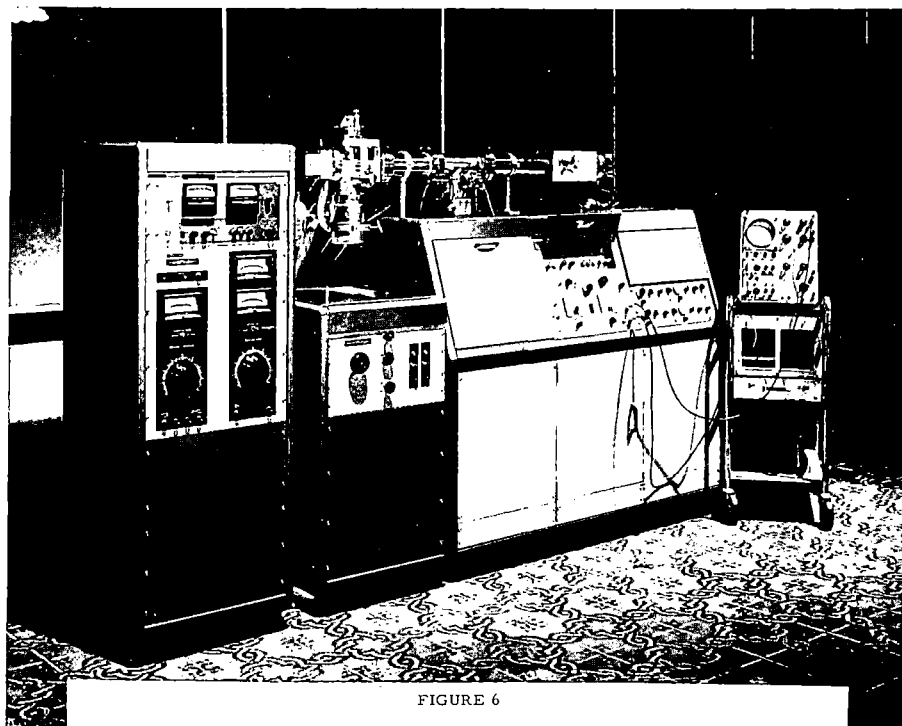
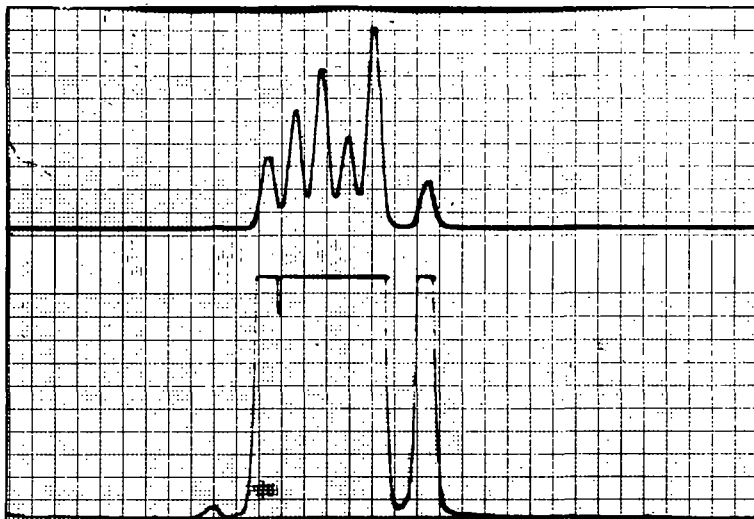


FIGURE 6

Model 12-101 Bendix Mass Spectrometer with 100 cm. flight path



MERCURY ISOTOPES AS SCANNED ON BENDIX TIME OF FLIGHT MASS SPECTROMETER

Bendix

FIGURE 8

Flight path length = 100 cm., lag = 0, energy = 2800 e.v.
Masses, left to right: 196, 198, 199, 200, 201, 202, 204 a.m.u.



FIGURE 7

Model 12-101 Bendix Mass Spectrometer at Dow Eastern
Research Laboratories with 167 cm. flight path.

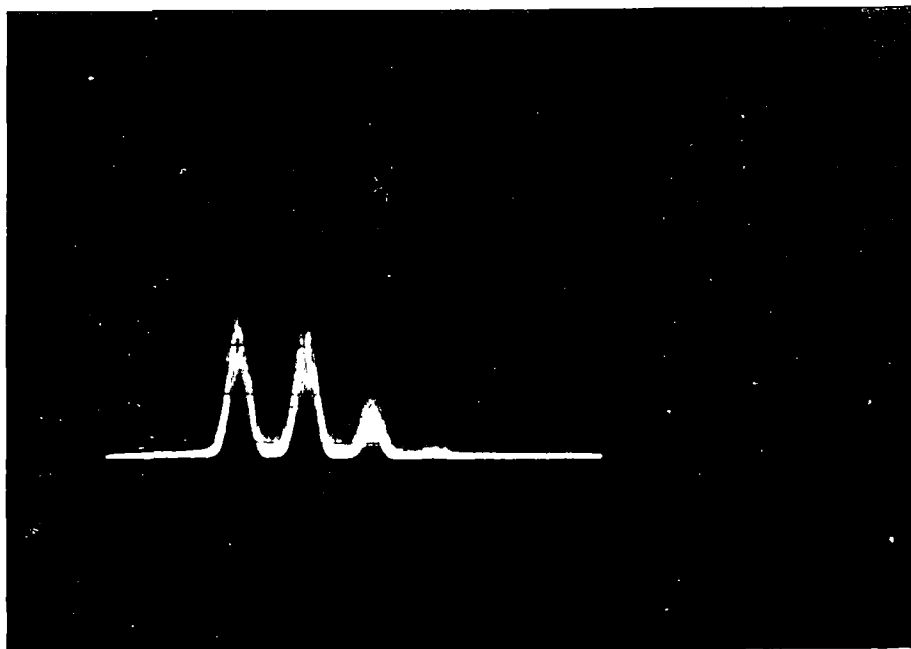


FIGURE 9

CCl_3^+ ions from carbon tetrachloride, oscilloscope presentation.
 Flight path length = 100 cm., lag = 0, energy = 2800 e.v.
 Masses, left to right, 117, 119, 121, 123 a.m.u.

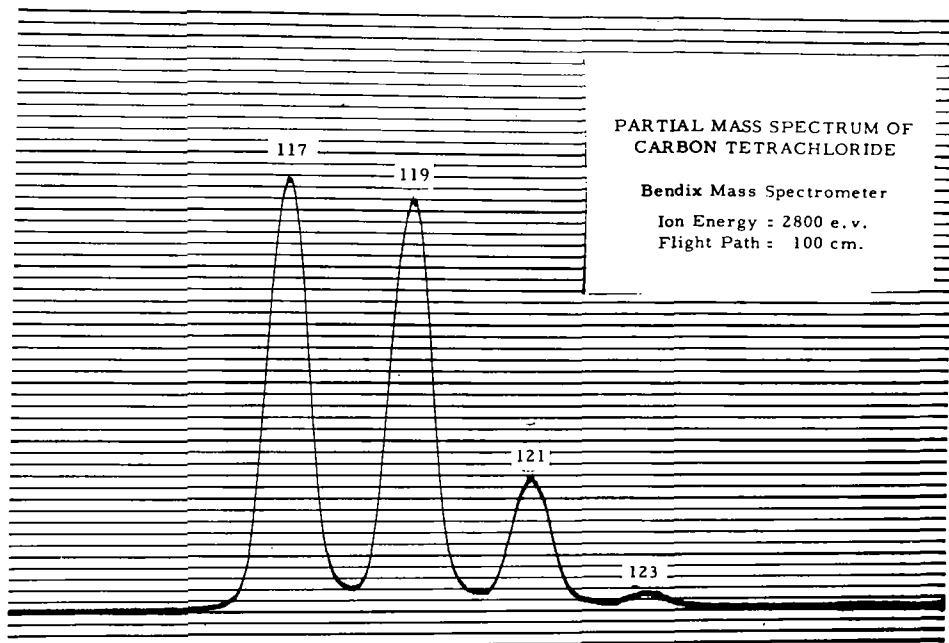


FIGURE 10

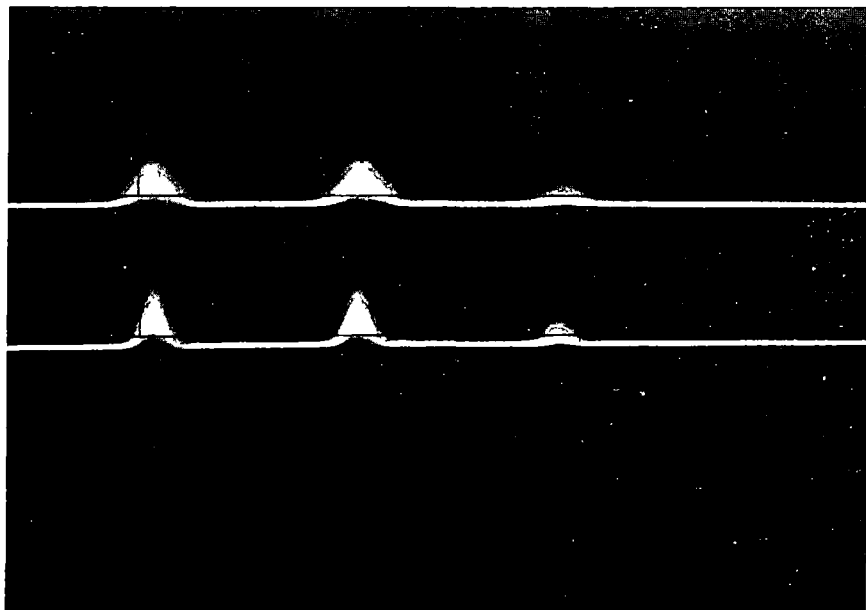


FIGURE 11

CCl_3^+ ions from carbon tetrachloride, oscilloscope presentation.
Flight path = 167 cm., Energy = 3150 e.v. Top Trace, Lag = 0.
bottom trace, lag = 2.6 μ sec. Masses, left to right, 117, 119, 121 a.m.u.

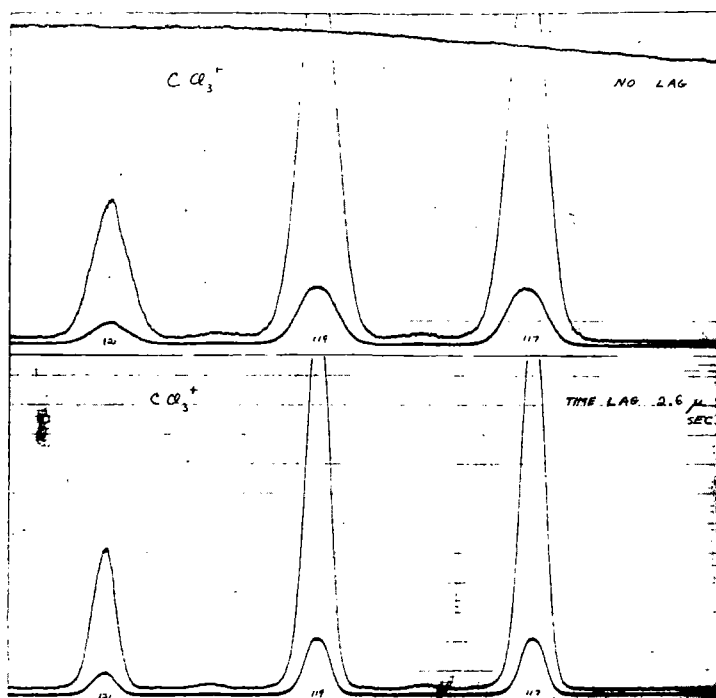


FIGURE 12

CCl_3^+ ions from carbon tetrachloride, oscillograph presentation. Flight path = 167 cm., energy = 3150 e.v.

BENDIX MASS SPECTROMETER

MASS RESOLUTION VS. ION ENERGY AND FLIGHT PATH LENGTH

Ion Energy	Flight Path	Unit Resolution	
		Recorder	Oscilloscope
1600 e.v.	50 cm.	100 a.m.u.	125 a.m.u.
2800	100	200	250
3150	167	290	350
10,000	240	500*	
*Estimated			

FIGURE 13

A CASCADE MASS SPECTROMETER
F. A. White,* J.C. Sheffield, and F.M. Rourke

General Electric Company
Knolls Atomic Power Laboratory**
Schenectady, New York

Introduction

The session this morning is devoted to instrumentation, and I shall describe an apparatus which has been constructed at our laboratory that may have some novel instrumental aspects. However, I should also like to focus attention on the variety of physical investigations which can be pursued with this new tool. Hence, I shall refrain from presenting a detailed description of the spectrometer, in order to indicate several interesting and important phenomena which can be probed with this device.

Physical Description

The first slide is a schematic diagram of the electromagnet. It is basically "C" shaped. You will note that the exciting coils surround a massive cylinder. The cylinder is approximately 2 feet in diameter and 21 inches in height. The exciting coil includes 34,000 turns of copper wire which can produce a field up to 8000 gauss. The top and bottom yoke are trapezoidal shaped slabs, of 8 inches thickness. The dotted lines of the schematic mark the contour of the pole pieces, and suggest why the term "cascade" has been tagged to this spectrometer.

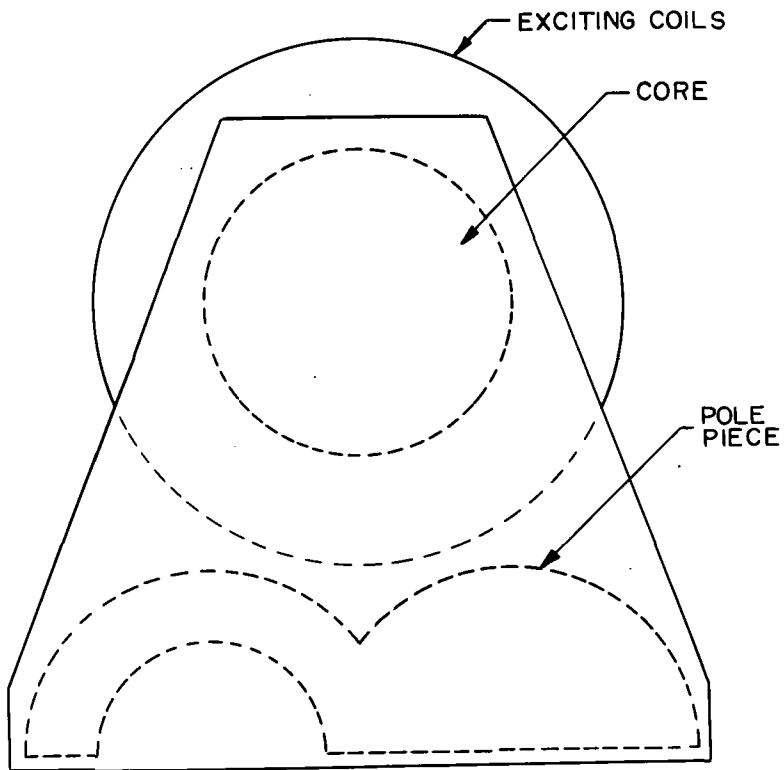
You will note that not one, but two successive 180° trajectories can be accommodated within the pole face boundaries. The pole face is large (over 500 sq. inches) and the mean radius of curvature of the first trajectory is 12 inches. Consider now the second trajectory. You will note that, in principle, there is no lower limit to the radii of curvature---only an upper limit (12 inches $R - 180^\circ$) i.e., we have a continuum of possible ion paths---corresponding to a very wide range of ion energies and masses for a fixed magnetic field strength.

Slide No. 2 shows the complete "cascade" spectrometer. It weighs between 9- and 10-ton. The vacuum chamber is simply a Duraluminum ring, machined to match the contour of the pole pieces that comprise an integral part of the vacuum chamber. Viton "O" rings complete the seal between the Duraluminum ring and top and bottom pole-piece surfaces. The magnet gap is $3/4$ inches and the vacuum chamber is pumped by two diffusion pumps complete with large liquid nitrogen traps. You will note that two mass spectrometer source assemblies, which are attached to the vacuum chamber. The first is a conventional surface ionization source complete with suitable focusing plates. The second is located at the focal point or "detector" position of the first 180° spectrometer. It can be employed for several distinct uses---as a detector, as a surface ionization source, or as a target with which primary ions may interact to produce secondary ions. I shall forego further physical description of the machine except to point out that two detectors (a Faraday cage converting to an electrometer, and a very small "semiconductor" magnetic electron multiplier can be made to "scan" the entire focal plane of the 2nd 180° analyzer. The electron multiplier, in fact, utilizes the fringing field of the magnet for its operation. We have discussed this device at a previous ASTM meeting (1960) and it has also been reported in the literature.¹

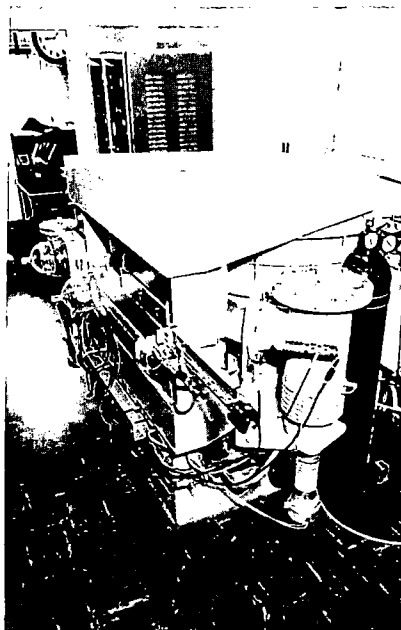
*Present Address: Linear Accelerator Laboratory, Rensselaer Polytechnic Institute, Troy, New York

**Operated for the United States Atomic Energy Commission by the General Electric Company, Contract No. W-31-109 Eng: 52.

¹F. A. White, J. C. Sheffield, and W.D. Davis Nucleonics 19 58 (1961).



Slide 1. Top view of electromagnet indicating the pole piece contour, yoke, and exciting coil.



Slide 2. Assembled cascade spectrometer with oil diffusion pumps and liquid N_2 traps. To the right of the two pyrex caps can be seen the magnetic electron multiplier housing and scanning mechanism.

Slide No. 3 shows the two sources schematically, indicates the trajectories of primary and "cascaded" ion beams, and the "scanning" electron multiplier used to detect the arrival of single ionized atoms along the focal plane of the second 180° analyzing sector. At this point, I should probably state that the instrument was conceived so as to provide some insight into very complex interplay of phenomena that occur in the surface ionization process. It is our opinion that such studies must look at transient as well as equilibrium phenomena. Let me simply indicate the experimental observations which, in principle, can be obtained with this equipment.

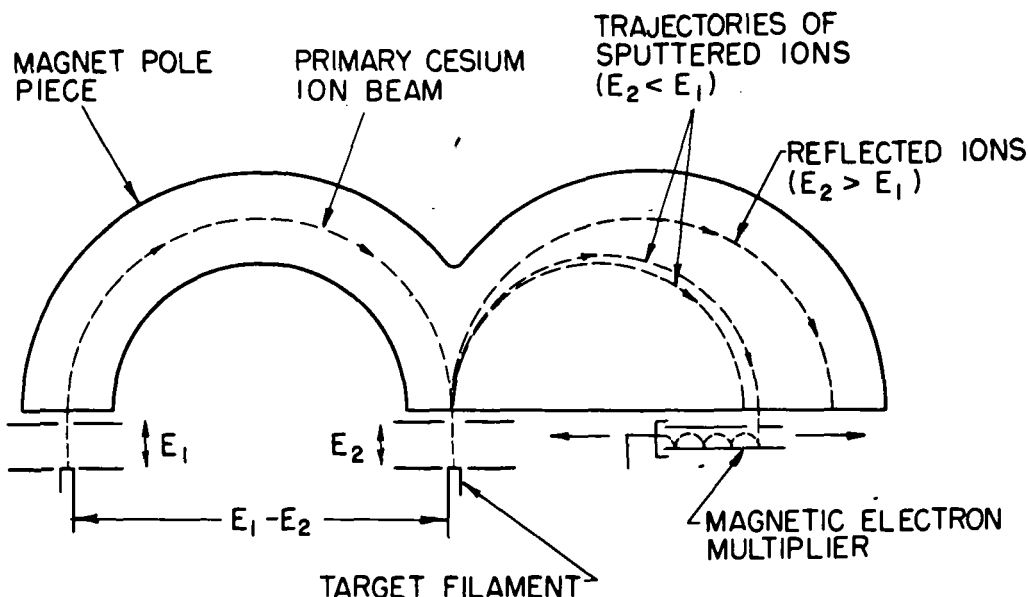
1. Assume $E_2 > E_1$. In this case the primary beam is decelerated, electrostatically reflected, and the "cascaded" trajectory is similar to the primary one. Note that this is a "reflection" two-stage instrument, rather than "transmission" types which we have previously reported.^{2,3} The "abundance sensitivity" we have measured to be about 100 times that of a single stage instrument.
2. Assume $E_2 < E_1$. In this instance the primary beam will be incident on the second surface ionization source filament. We are thus "doping" or loading the 2nd surface ionization filament by ion bombardment. Inasmuch as T_2 is variable (as well as the bombarding energy, $E_1 - E_2$), we can study the re-emission process dynamically.
3. Pulsed Techniques. It is clear that the primary source can be pulsed with variable pulse widths and repetition rates. Our preliminary work indicates that such an approach is necessary in order to clearly differentiate between the primary reflection ions and those which penetrate deeply into the "target" filament, diffuse to the surface, and become re-ionized.
4. Sputtering Phenomena. Sputtering takes place to some extent in every mass spectrometer source, in the conventional analyzing tube, and to an appreciable extent on the cathode of most spectrometer detectors, i.e., electron multipliers of one category or another. Sputtering, in fact, must play some role in changing the work function and hence the secondary electron yield of most mass spectrometer multipliers, at least if high current beams are monitored.

Because my time is limited, I will mention only three specific measurements that should be of academic and instrumental interest to mass spectroscopists.

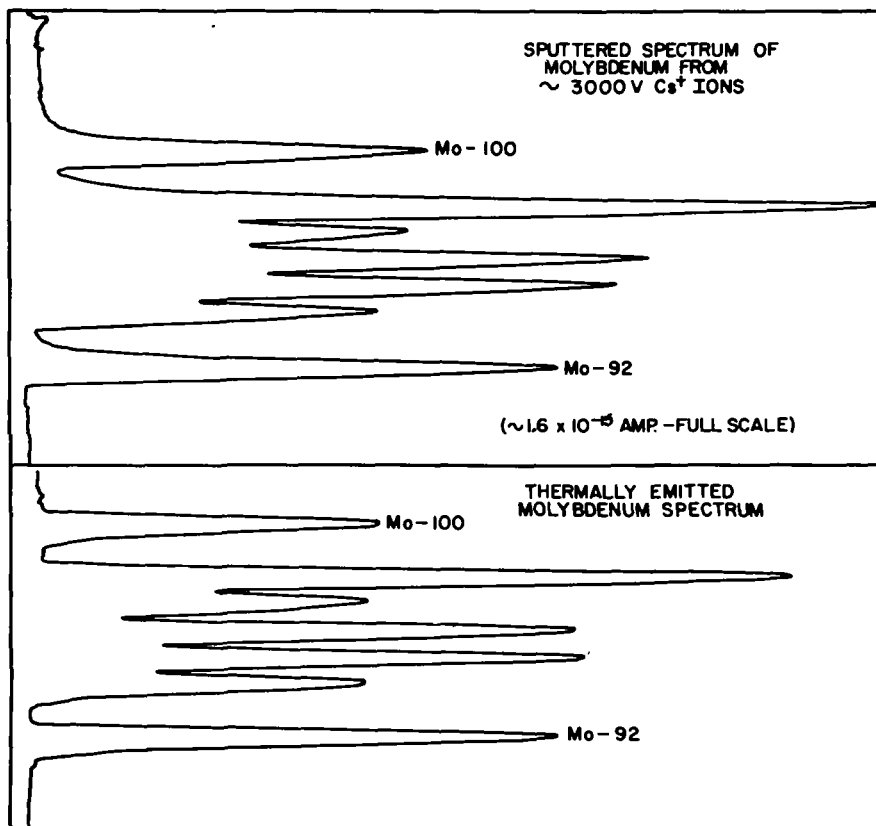
Let us use $Cs^+ - 133$ as the primary ion beam, in all cases let $E_1 > E_2$, and now examine ions which are sputtered from two different "target" filaments, molybdenum and copper. We recall that most atoms sputter off a surface as neutrals, but an appreciable fraction, possibly 1%, will come off as charged particles. The actual percentage is a function of many parameters. First considering the case where E_1 is $\sim 10,000V$, E_2 is $\sim 7000V$ and a thin molybdenum ribbon is used as either a clean surface ionization filament which can be heated, or a sputtering target---where we observe Mo^+ ions and analyze them in the "cascade" or second trajectory.

Slide 4 shows us the qualitative picture we obtain. If we heat the filament to a suitably high temperature, thermally emitted Mo^+ ions from the molybdenum filament may be mass analyzed. The resolution is poor because certain compromises have been made; wide slits, source somewhat out of focus, etc. What is of interest is that we obtain substantially the same spectrum if we do not heat the filament, but bombard the cold molybdenum filament with a beam of Cs^+ ions. Sputtered atoms that leave with a single positive charge are accelerated through a potential E and the similarity of the spectrum to that of the thermally emitted spectrum, clearly indicates that the sputtered ions have a very limited energy distribution (< 10 ev).

It is also now of interest to investigate the sputtering yield, as a function of the energy of the bombarding cesium beam. Slide No. 5 indicates ²F.A.White and T.L.Collins Applied Spectroscopy 8 No. 4, 169 (1954). ³F.A.White, F.M.Rourke, and J.C.Sheffield Applied Spectroscopy 12 No. 2 46 (1958).



Slide 3. Schematic of cascade spectrometer.



Slide 4. Sputtered spectrum of molybdenum produced by ion bombardment compared to a spectrum from a surface ionization source.

our preliminary results and reveals the yield as a monotonically increasing function of bombardment energy. The data was obtained by applying suitable bias potentials, E_2 , and adjusting the magnetic multiplier to the Mo -92 mass position. The assumption is made that the number of sputtered atoms which emerge with a single positive charge is proportional to the total yield (which is predominantly neutral).

Slide No. 6 shows results obtained when a copper filament was bombarded with a cesium beam. It has special interest because copper cannot be analyzed via a surface ionization or thermal ion source. You will note that we obtained a completely resolved spectrum of the two copper isotopes. We were also able to make a reasonably precise ratio determination of Cu-63/Cu-65.

The ratio which we obtained by this technique was 2.25 ± 0.02 , and we believe this is the first precision isotopic ratio determination made by analyzing sputtered species. Our value is in agreement with the accepted values determined by electron bombardment of CuCl_2 vapor by Brown and Inghram⁴ and of Duckworth and Hogg⁵ using a spark source with a copper electrode.

We are not suggesting that a sputtering technique can ever compete in general applicability to surface ionization or electron bombardment sources in mass spectrometry. It will be appreciated, however, that the method is almost non-destructive, requiring in favorable cases, a very small number of sputtered atoms ($\sim 10^{-12}$ grams), and it is possible that isotopic abundance determinations of surface atoms may be useful in diffusion studies, etc., as well as providing a tool for a further understanding of the sputtering phenomenon itself.

I have not had time to review some of the other measurements that can be made with a spectrometer of this type. To date, however, it has proven to be an exceedingly versatile research tool. With the aid of this instrument we hope to make many additional measurements that will allow us to build better analytical spectrometers.

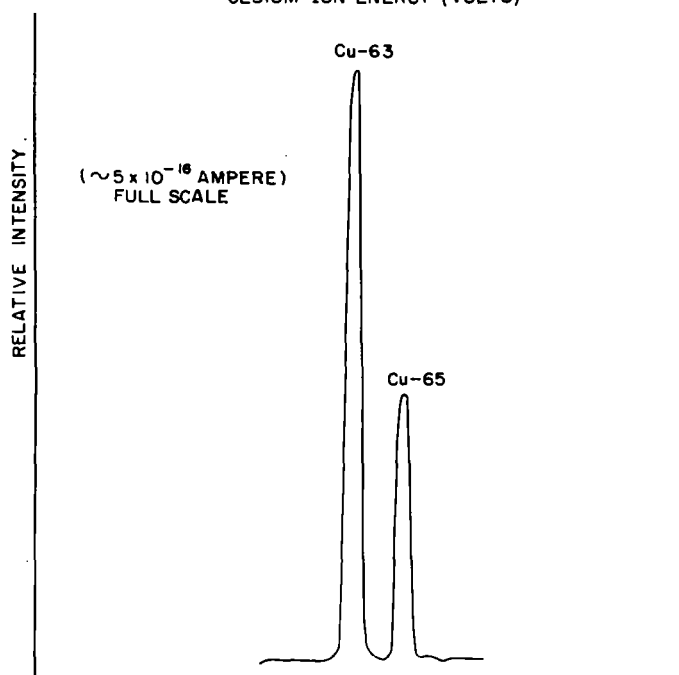
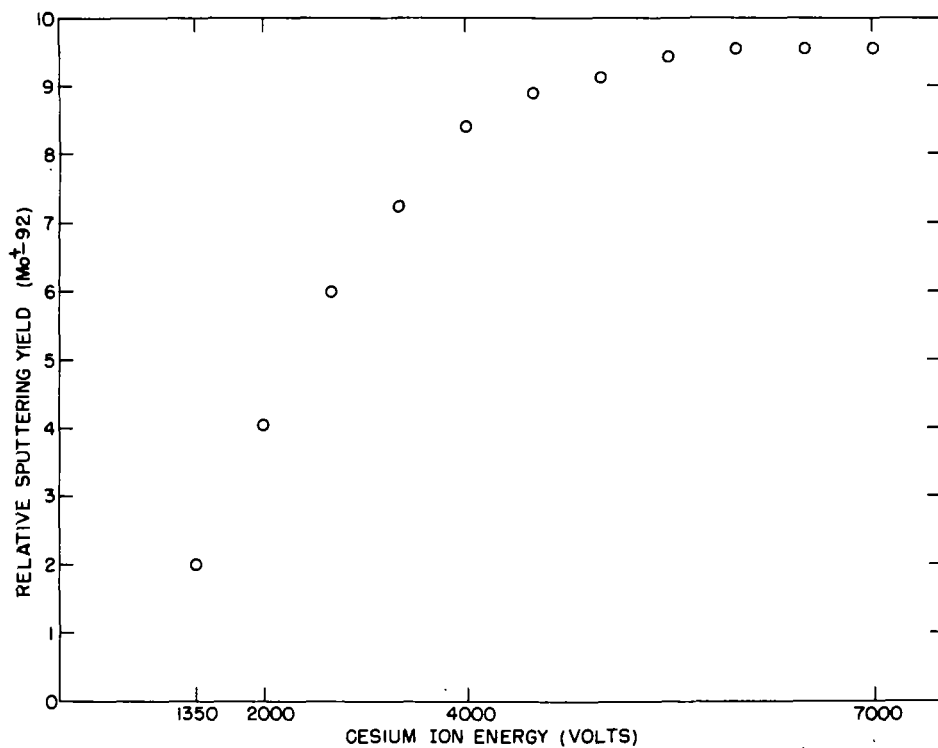
⁴

H. Brown and M. G. Inghram, Physical Review **72**, 347L (1947).

⁵

H. E. Duckworth and B. J. Hogg, Physical Review **71**, 212 (1947).

Slide 5. Relative yield of sputtered Mo^{+92} ions from Cs^{+133} ion bombardment (1350 to 7000 ev range).



Slide 6. Mass spectrum of sputtered copper target (from 600 ev Cs^{+} ions).

AN EXPERIMENT INVOLVING THE NUMERICAL DETERMINATION OF ION PATHS IN NON-HOMOGENEOUS MAGNETIC FIELDS

by A. C. Lilly, Jr., T. J. Weismann and D. A. Lowitz
Gulf Research & Development Co., P. O. Drawer 2038,
Pittsburgh 30, Pennsylvania

INTRODUCTION

In calculating the exact paths of charged particles in inhomogeneous fields, a knowledge of the intensity of the magnetic field at every point is necessary. Presently available empirical methods⁽¹⁻⁴⁾ for the determination of ion paths appear suitable for the design and construction of single collection mass spectrometers. In dealing with the simultaneous collection of more than one ion beam, a knowledge of the exact ion paths becomes important. The need for this information arose in our laboratory in connection with the construction of a double-focusing mass spectrometer employing simultaneous collection of three ion beams. This paper is concerned with the specific method employed in these trajectory calculations and the general applicability of the method in dealing with non-homogeneous, but known, magnetic fields.

Magnetic field matrices were compiled using a Hall device gaussmeter and the procedure of Coggeshall and Muskat⁽⁵⁾ was adapted to enable calculations to be performed on an IBM 7090 computer.⁽⁶⁾

EXPERIMENTAL

In order to adequately measure the magnetic field used in the computations, the apparatus shown in Figure 1 was employed. The field was measured by means of a Radio Frequency Laboratory Model 1295A Gaussmeter equipped with an HB-9338 bismuth Hall-effect probe which was mounted on the carriage of a stepping device (originally designed for a well-logging application) having a variable step length adjustment which permitted the desired interval for measurement to be selected prior to the experiment. In practice, the instrument was so positioned that the interval of the automatic stepping device provided the x interval of an x,y coordinate system. The desired y-value was obtained manually with the aid of a calibrated arm on the carriage and was adjusted before each set of measurements in the x-direction. We have measured the fields of two magnets by this procedure: a permanent magnet with an apparent 60° magnetic sector fabricated from magnetron magnets using soft iron pole pieces and an electromagnet with an apparent 60° magnetic sector in a Nuclide Analysis Associates ratio mass spectrometer. For each of these magnets approximately 3000 field points were measured. Spacings of 0.1 cm in the field of the permanent magnet and 0.1 inch for that of the larger electromagnet were used. The measurements represent the z-component of the field in the central plane of the magnets and are accurate to $\pm 3\%$ or ± 10 gauss with a lower limit of 10 gauss. The matrix of field points thus measured may be transformed into any convenient coordinate system for utilization in the computer program. The format employed in these studies is shown in Figures 2 and 3. The coordinate system for the magnetic field was chosen so that its ordinate, y", was parallel to the bisector of the magnetic sector. The field matrix, defined by the x", y" coordinate system (Figure 2a), was oriented so that the x" axis was parallel to the x', y' coordinate

¹Dempster, A. J., Phys. Rev., 11, 316 (1918).

²Herzog, R., Zeits. f. Physik, 89, 447 (1934).

³Mattauch, J. and Herzog, R., Zeits. f. Physik, 89, 786 (1934).

⁴Nier, A. O., Rev. Sci. Instruments, 11, 212 (1940).

⁵Coggeshall, N. D. and Muskat, M., Phy. Rev., 66, 187 (1944).

⁶The program is available through SHARE.

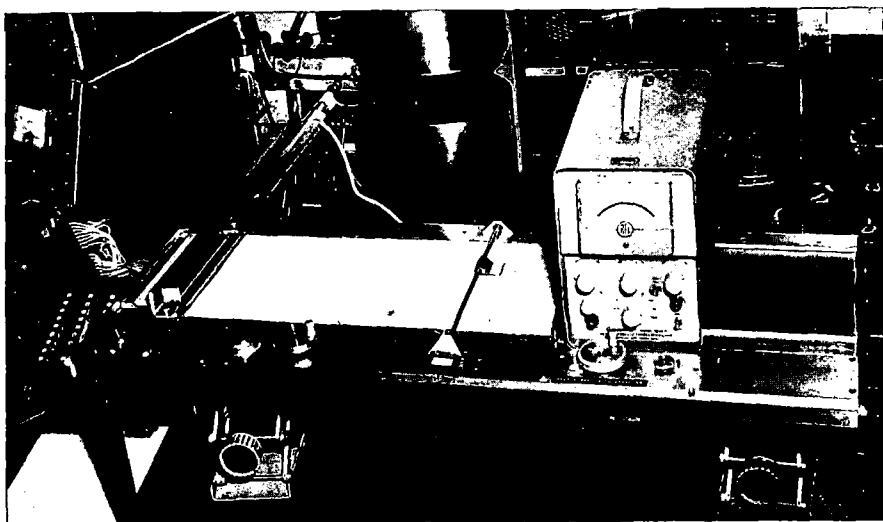


FIGURE 1. Stepping device with Radio Frequency Laboratory Model 1295A Gaussmeter and bismuth Hall-effect probe for magnetic field measurements.

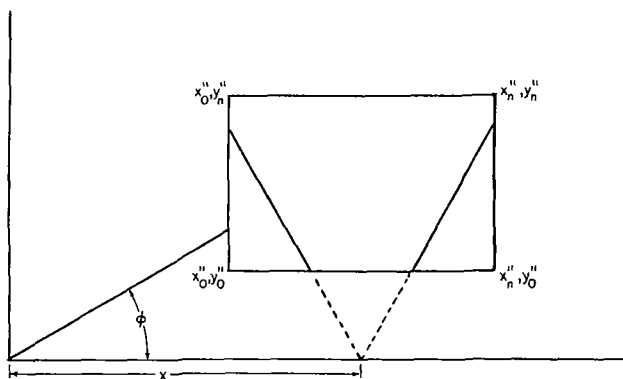


FIGURE 2a. Format showing placement of magnetic field coordinate system within coordinate system of particle's trajectory (fixed instrument coordinate system).

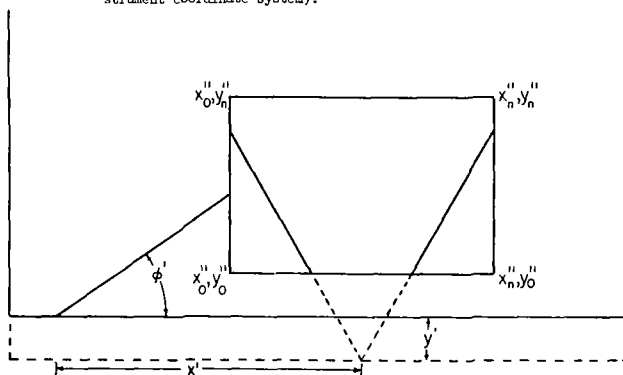


FIGURE 2b. Format showing effective displacement of magnetic field coordinate system.

system of the particle's trajectory. The source was always taken at the origin of the particle's coordinate system. The input data for computing a particle's trajectory then consisted of (i) ϕ_0 , the angle between the particle trajectory and the x' axis at the source; (ii) x_s , the distance of a reference point in the x", y" coordinate system from the y' axis; (iii) y_s , the distance of a reference point in the x", y" coordinate system from the x' axis; (iv) R, the radius of the circular trajectory based on the particle's mass, charge, velocity and on the maximum value of the field, H_0 ; and (v) a dispersion angle, α , at the source, which defines two additional trajectories forming an envelope about the one defined by ϕ_0 and so placed that the trajectory defined by ϕ_0 initially constitutes a central trajectory (Figure 3).

The output data consisted of the x' and y' values for each trajectory and the field value encountered at each "printed out" point for the three trajectories.

In order to reorient the magnet by means of either a rotation or translation, the values of x_s , y_s and ϕ_0 were changed accordingly so that in the next x', y' coordinate system, the x" axis was again parallel to the x' axis, and the source was again at the origin (Figure 2b).

Particle trajectories can, in principle, be calculated for a wide range of particle energies, angles of incidence and source locations.

The procedure used for the calculations was essentially that of Coggeshall and Muskat(5). Starting with the Lorentz force law

$$\vec{F} = \frac{e}{c} (\vec{E} + \vec{v} \times \vec{B}) \quad (1)$$

and letting

$$\vec{E} = 0; \vec{B} = \vec{k}B_z = \vec{k}H_z \quad (2)$$

it follows that

$$\dot{y} = \frac{-eH}{mc} x \quad (3)$$

$$\dot{x} = \frac{eH}{mc} y \quad (4)$$

If the normalized field $h(x,y)$ is defined as follows

$$\frac{H(x,y)}{H_0} = h(x,y) \quad (5)$$

equation (3) yields

$$\frac{y}{v} = -\frac{1}{R} \int h(x,y) dx + \frac{y_0}{v} \quad (6)$$

where $\frac{y_0}{v} = \sin \phi_0$ and H_0 is the maximum field value measured. R is the effective radius in the field H_0 .

Dispersion or aberration effects originating beyond the source slit may be simulated by the appropriate placement of the magnetic field matrix within the instrument coordinate system. The iteration procedure used in carrying out the calculations may be explained as follows. The equation for $\sin \phi_1$ where ϕ_1 is the angle the trajectory makes with the x axis after the first step, is given by

$$\sin \phi_1 = -K \bar{h}_{1,0}(x,y)(x_1 - x_0) + \sin \phi_0 \quad (7)$$

where

$$K = \frac{cmv}{eH_0} \quad \text{and} \quad \sin \phi = \frac{y}{v}$$

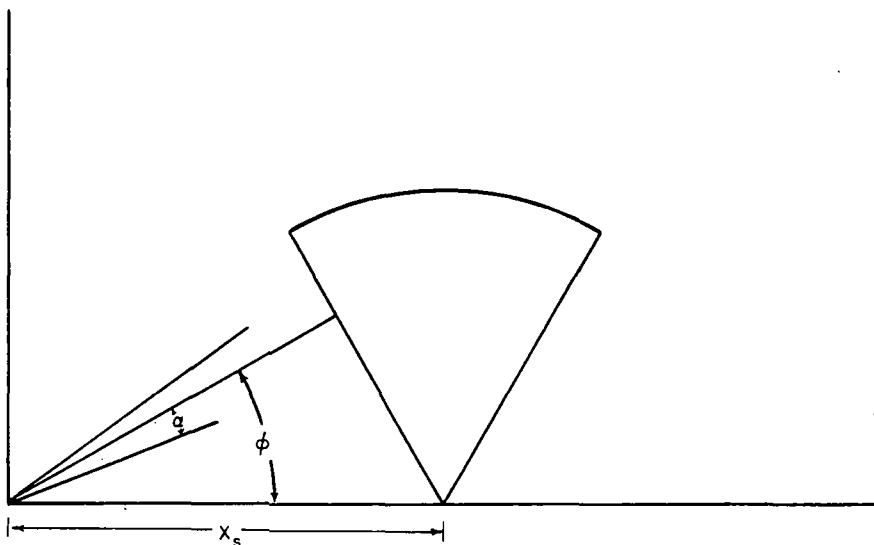


FIGURE 3. General geometry employed in the trajectory calculations.

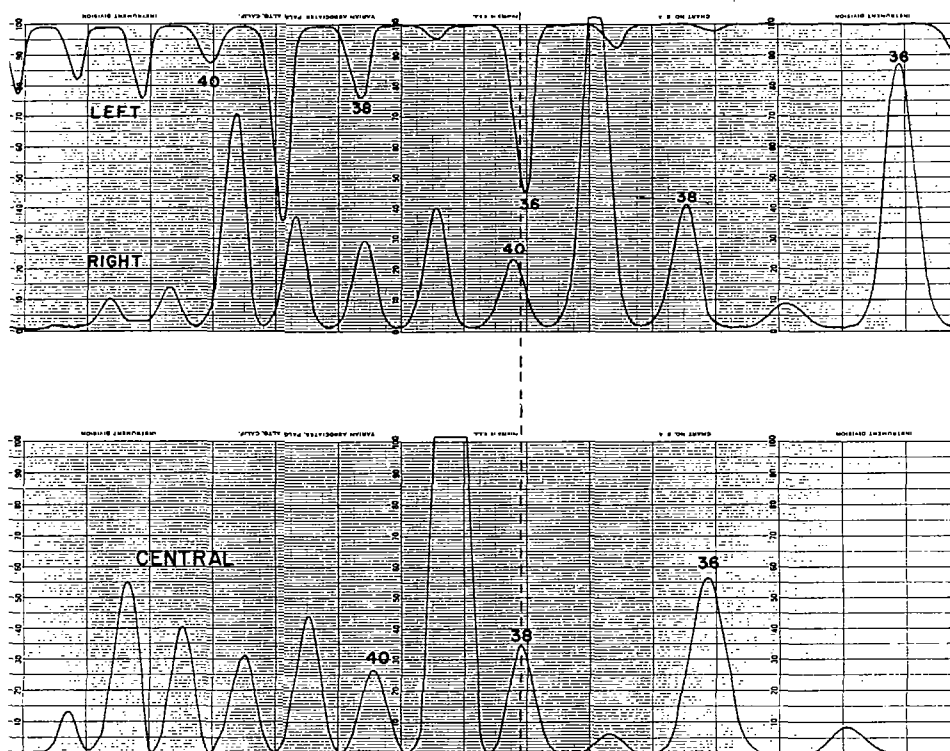


FIGURE 4. Chart traces of mass spectra simultaneously recorded on three channels of multiple collector instrument.

After step 2 (at x_2) the equation for $\sin \phi_2$ is

$$\sin \phi_2 = -K \left(\bar{h}_{2,1}(x,y)(x_2-x_1) + \bar{h}_{1,0}(x,y)(x_1-x_0) \right) + \sin \phi_0 \quad (8)$$

and at step j

$$\sin \phi_j = -K \sum_{n=1}^{n=j} \bar{h}_{n,n-1}(x,y)(x_n-x_{n-1}) + \sin \phi_0 \quad (9)$$

In the limit as the size of the interval approaches zero one obtains

$$\sin \phi_\lambda = -K \int_0^\lambda h(x,y) dx + \sin \phi_0 \quad (10)$$

$$\lim_{x_n - x_{n-1} = 0}$$

or

$$(\lim_{x_n - x_{n-1} = 0}) \frac{\dot{\gamma}_\lambda}{v} = -K \int_0^\lambda h(x,y) dx + \frac{\dot{\gamma}_0}{v} \quad (11)$$

The calculations were repeated for intervals of decreasing length until the value of the integral was stabilized. The calculations described have been used in the design of a small 3.25" radius double-focusing mass spectrometer for potassium-argon geochronometric measurements. The spectrometer measures three focused ion beams simultaneously, i.e., mass 36, 38 and 40. Figure 4 displays chart traces of the three beams obtained simultaneously during a mass scan. By comparison of the peaks in the region of the dashed line, it is evident that mass 36, 38 and 40 occur simultaneously within the width of a single mass peak.

A more quantitative presentation of the results is given in Table I.

TABLE I

Collector	m/e	I/I_{38}	Slit Width
Inner	36	0.84	.040"
Central	38	1.00	.025"
Outer	40	0.56	.040"

$$V_{A(\text{exp.})} = 1365 \pm 40$$

$$\phi_0 = 31.5^\circ$$

$$V_{A(\text{calc.})} = 1290$$

$$x_s = 16.5 \text{ cm}$$

In making these measurements, mass 38 was collected on the central channel and the fraction of masses 36 and 40 entering the designated channels was measured. $V_{A(\text{calc.})}$ is the energy used in the calculations for the total placement of each of the three ion beams in their respective channels. $V_{A(\text{exp.})}$ is the energy required to yield the results shown in Table I, employing the same values of ϕ_0 , x_s and y_s used in the calculations. The observed deviation of $V_{A(\text{exp.})}$ and $V_{A(\text{calc.})}$ of 6% approaches the accuracy of the magnetic field measurements. A detailed measurement of the magnetic field permits other calculations of interest to be made. Figure 5 illustrates the dependence of the focal properties of the 3.25" radius permanent magnet on the angle ϕ . It is seen that as this entry angle is varied from 28° to 33° the image lengths shift along the paths until at 33° the rays diverge completely.

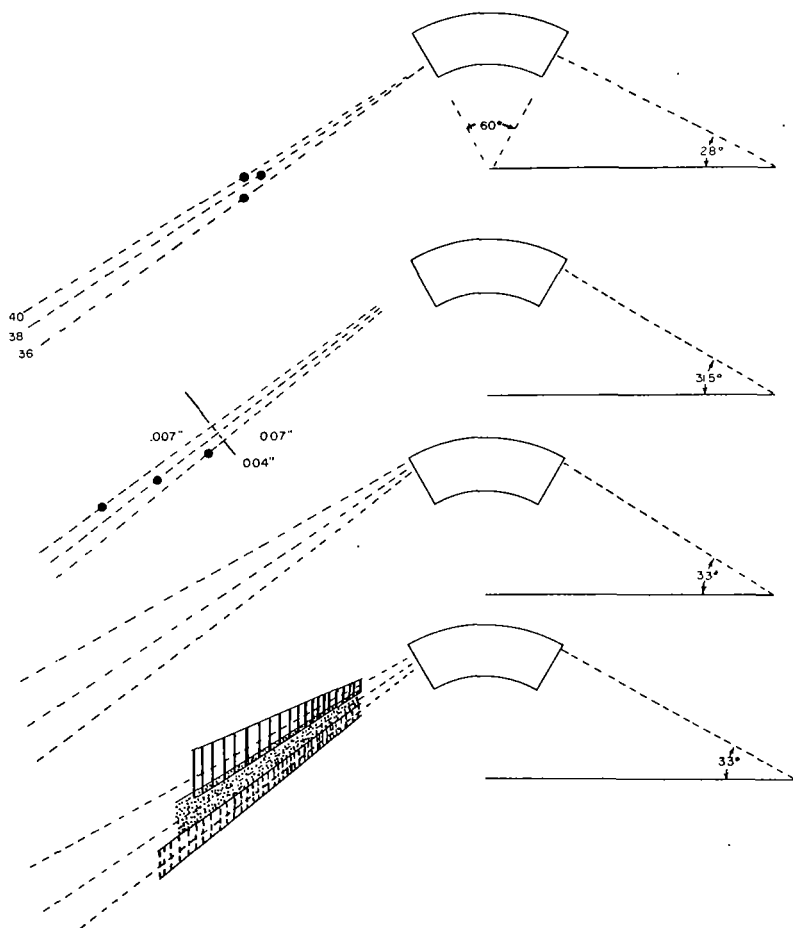


FIGURE 5 . Dependence of focal properties of 3.25" radius permanent magnet on angle ϕ .

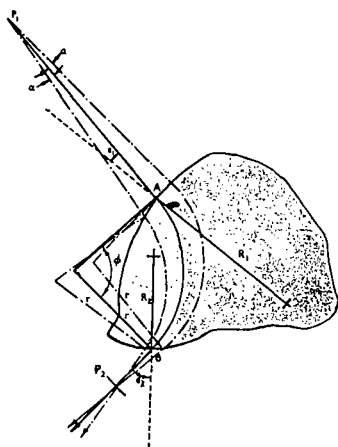


FIGURE 6. General case of first-order focusing of ion beam in homogeneous magnetic field with sharply defined boundaries of any arbitrary shape (after Reference 2).

The symbols in the Herzog equation, which relates the pertinent parameters for focusing by an irregularly contoured field with no fringe effects are defined in Figure 6. Transposed to yield the image distance the Herzog equation is

$$l_2 = - \frac{r \sin \phi + l_1 \frac{\cos(\phi - \epsilon_1)}{\cos \epsilon_1}}{\frac{\cos(\phi - \epsilon_2)}{\cos \epsilon_2} - \frac{l_1}{r} \frac{\sin(\phi - \epsilon_1 - \epsilon_2)}{\cos \epsilon_1 \cos \epsilon_2}} \quad (12)$$

This equation is given in terms of the deviation of the beam ϕ rather than the sector angle. To obtain the equation in terms of the sector angle ϕ' when considering a regular sector, one substitutes $\phi = \phi' + \epsilon_1 + \epsilon_2$. The angle ϵ_1 and ϵ_2 are, respectively, the angle of incidence and the exit angle of the central ray.

Figure 7 illustrates the dependence of l_2 on the position of the sector's apex along the ordinate. Several values of ϵ_1 are considered. The curve predicted by the Herzog equation for a perfect magnet of the same radius and angle is shown for comparison. The differences are probably due to the curvature of the field lines, as shown in Figure 8 for the small permanent magnet.

Figure 9 illustrates the dependence of l_2 on ϵ_1 , the angle of incidence, for the dispersion angles 0.1° and 1.0° for the small permanent magnet. Again the prediction of the Herzog equation for a perfect magnet of the same size is shown for comparison. Figure 10 illustrates this behavior for the NAA 6" radius electro-magnet with α 's of 0.5° and 1.0° .

Coggeshall⁽⁷⁾ has studied the general form of the fringing fields on magnets by assuming the regions of constant magnetic potential are as shown in Figure 11. A Schwarz-Christoffel transformation was then used to transform the upper pole piece surface onto the negative real axis and the median plane onto the positive real axis. The field was calculated between the two planes and again transformed back into the z-plane. The fringing field is then given in normalized form in terms of a parameter n which is the ratio of pole piece thickness to gap width. Using the fringing field curves published by Coggeshall, trajectories were calculated for the permanent and electromagnets described in this paper employing the same technique outlined for the trajectory calculations in the real fringing field. Figures 12 and 13 show the comparisons of the trajectories, for the permanent magnet with $n = 1$ and the electromagnet with $n = 3$, with the trajectories calculated using the real fields. Also shown are the two normalized fields along the beam paths.

CONCLUSIONS

1. Using the measured values of the normal field in the median plane of the magnet of a double focusing mass spectrometer, the simultaneous trajectories for masses 36, 38 and 40 were calculated. Expressions published by Coggeshall and Muskat were used for the calculations. The experimental data for the simultaneous collection of the three masses reproduced the calculated values to a reasonably good degree of accuracy.

2. If the Herzog relationship for image length in terms of object length, incident angle and exit angle is used without considering the actual field contour, large errors can be accumulated due to irregularities in the slope of the contour. Calculated values of the image length based on the actual field deviate greatly from the values calculated by means of Herzog's relationship when the sector is assumed to be regular.

⁷Coggeshall, N. D., Jour. of Applied Physics, 18, 855 (1947).

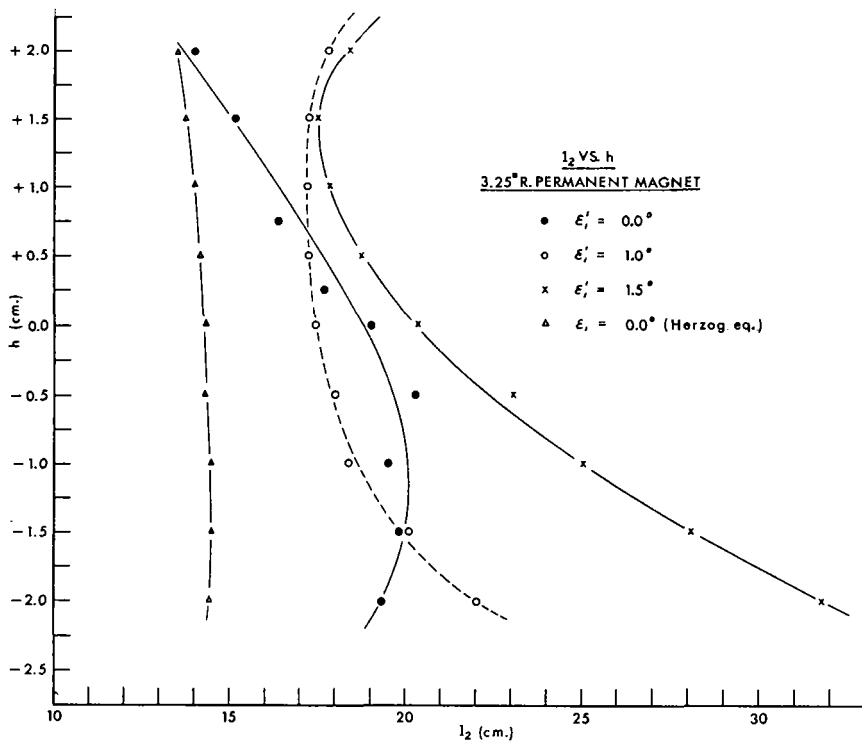


FIGURE 7. Dependence of l_2 on position of apex of magnetic field sector along the ordinate.

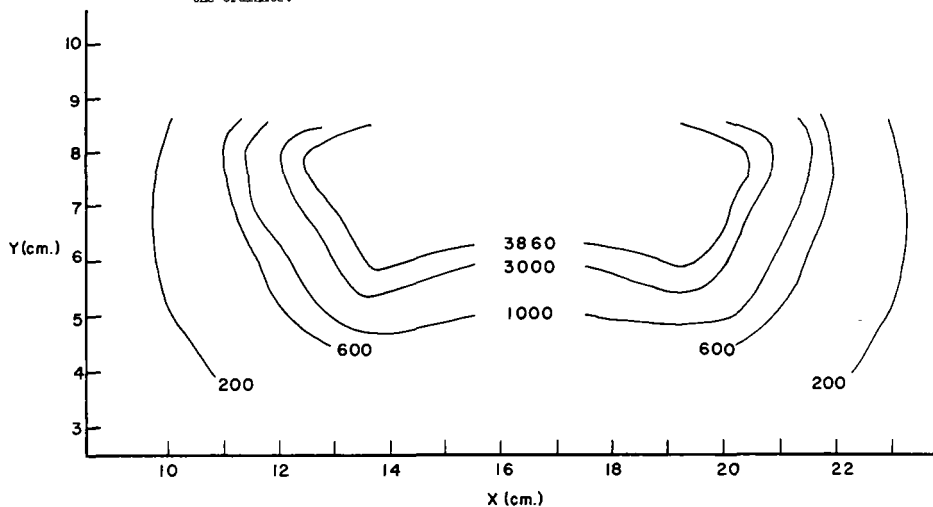


FIGURE 8. Field contour for 3.25" radius permanent magnet sector.

ACKNOWLEDGEMENTS

The authors are indebted to Mr. Emmett B. Shutes for his assistance in design of the experimental apparatus and drawings and to Mr. Nicholas J. Bezak for his work in programming the trajectory problem.

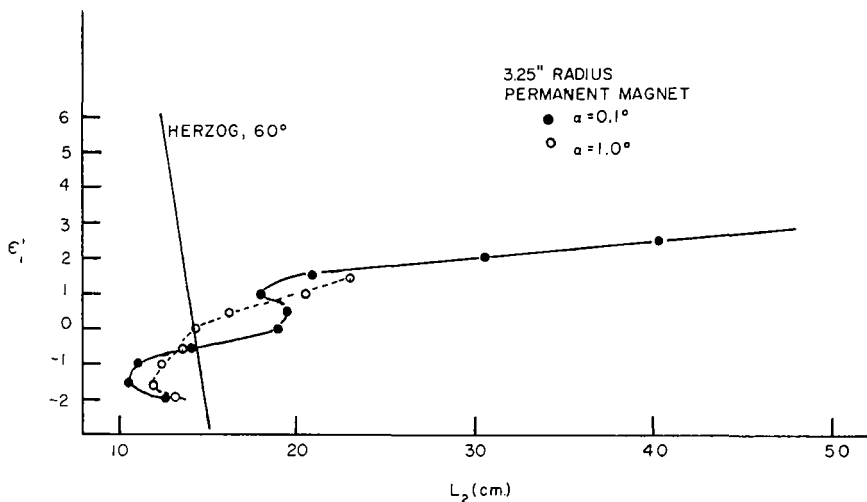


FIGURE 9. Dependence of l_2 on ϵ_1 for 3.25" radius permanent magnet sector.

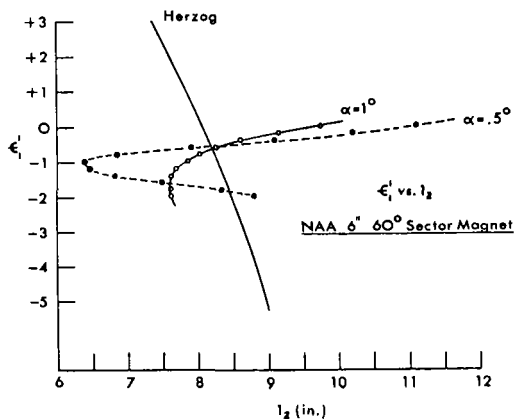


FIGURE 10. Dependence of l_2 on ϵ_1 for 6" radius electromagnet of NAA ratio mass spectrometer.

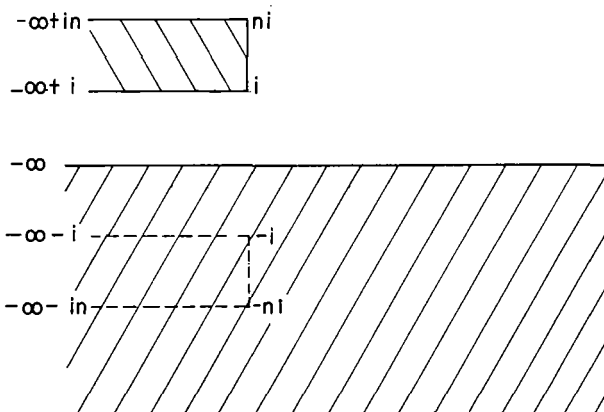


FIGURE 11. Type of magnet pole construction considered in conformal transformation (after Reference 7).

FIGURE 12a. Comparison of trajectory and focal properties of a central ray for 3.25" radius permanent magnet using Coggeshall fringing field(7) with $n = 1$ with those calculated using measured field.

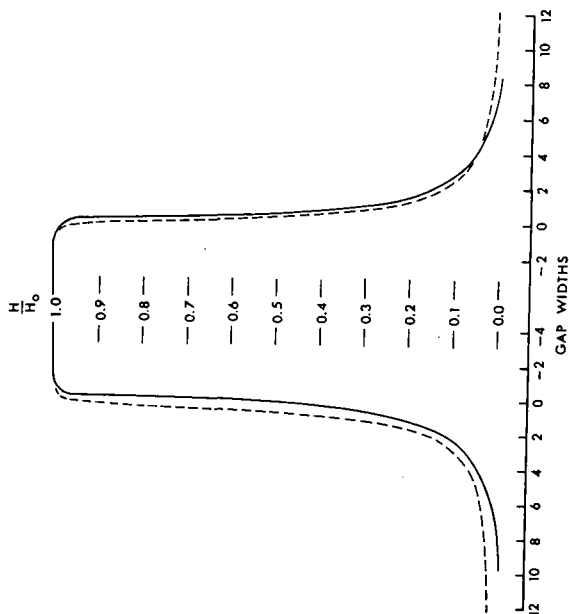
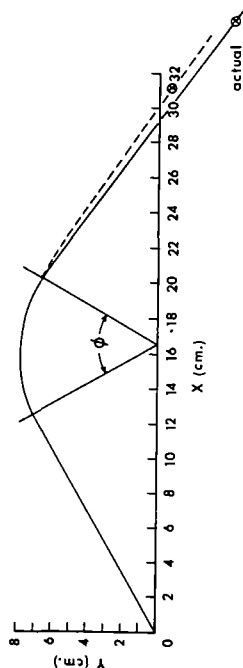


FIGURE 12b. Normalized field plots along path of ray. Dashed line represents field obtained using Coggeshall treatment; solid line represents field calculated by method described in this paper.

FIGURE 13a. Comparison of trajectory and focal properties of a central ray for 6" radius MA electromagnet using Coggeshall fringing field(7) with $n = 3$ with those calculated using measured field.

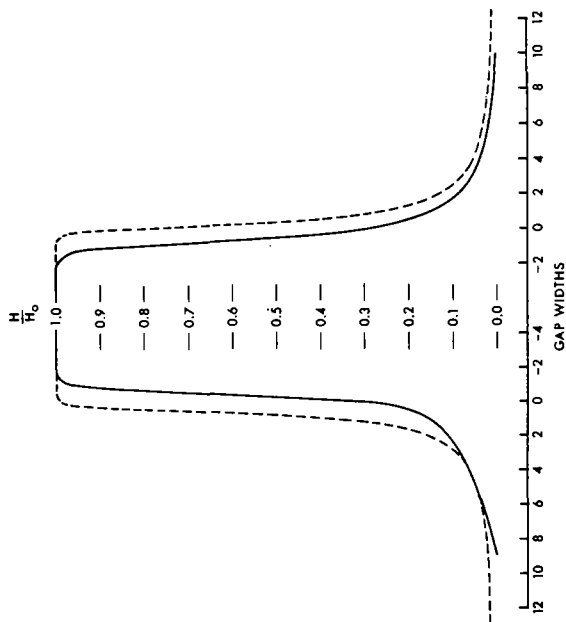
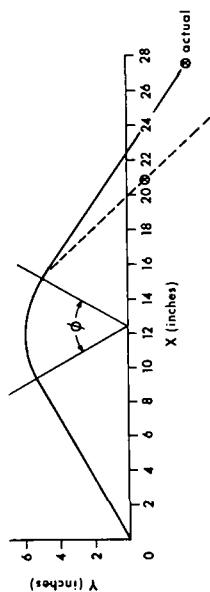


FIGURE 13b. Normalized field plots along path of ray. Dashed line represents field obtained using Coggeshall treatment; solid line represents field calculated by method described in this paper.

A High Sensitivity Mass Spectrometer Ion Source

M. Doctoroff* and S.S. Grossel
Vacuum-Electronics Corp.
Terminal Drive
Plainview, New York

A mass spectrometer ion source¹ capable of producing over 100 times the positive ion output of the conventional Nier-type source² has been developed. The distinguishing feature of this new source is that both ions and electrons move parallel to the axis of the tube. The axial source is similar in concept to the one of Stein and Binns³ but differs in that no magnetic field is required to collimate the electron beam.

Fig. 1 is a schematic diagram of the source. Electrons accelerated from the filament through the grid are brought to a focus in the vicinity of the ion voltage defining slit. Beyond this slit they diverge, some being collected by the ion focusing electrode, and the rest returning to the ion voltage plate and being collected there. As a result, ions are produced in three regions: between the filament and the electron accelerating grid; between the accelerating grid and the voltage defining slit; and between the voltage defining slit and the grounded object slit. Ions formed between the filament and the electron accelerating grid return toward the filament. Ions created beyond the accelerating grid, but not very near the voltage defining slit, are not drawn out. These ions, however, do partially neutralize space charge repulsion in the electron beam,⁴ allowing more effective focusing action. Ions generated in the third region, beyond the voltage defining slit, are not focused, and are only a small percentage of those realized at the collector. Most of the extracted ions originate in a small volume around the voltage defining slit. Stopping potential measurements of the energy distribution in the ion beam, indicate that this volume is bounded by equipotentials separated by only a few volts. Only these ions, created in the immediate neighborhood of the voltage defining slit, are focused onto the object slit, and they constitute nearly all of the emerging beam. In essence, the arrangement is such that the major part of the ions which reach the collector comes from an area where the potential variation is small, though ions with a large range of energies are formed at other points within the source.

The axial source has a partial pressure sensitivity approximately ten times greater than the Veeco-Nier source at the same emission current of 2 milliamperes. Operating at 50 milliamperes the axial source is about 100 times more sensitive than the Veeco-Nier source at 2 milliamperes. The detail available from the axial source is apparent in the inset on Fig. 2 where, at 10 milliamperes, a set of small peaks in the sixties is scanned on a more sensitive scale. Object and image slits were 0.006 and 0.015 inches, respectively, and scans were taken in a Veeco GA-3 gas analyzer tube having a 2 inch radius of curvature and a magnetic field of 4000 gauss. It should be noted that the standard gas analyzer uses the Nier-type source.

In conclusion, the axial source has been found to generate an ion beam with a sufficiently small energy distribution for many mass spectrometry applications, and to be capable of a sensitivity 100 times that of a Nier pattern source.

* Now at Sylvania Research Labs, Waltham, Massachusetts

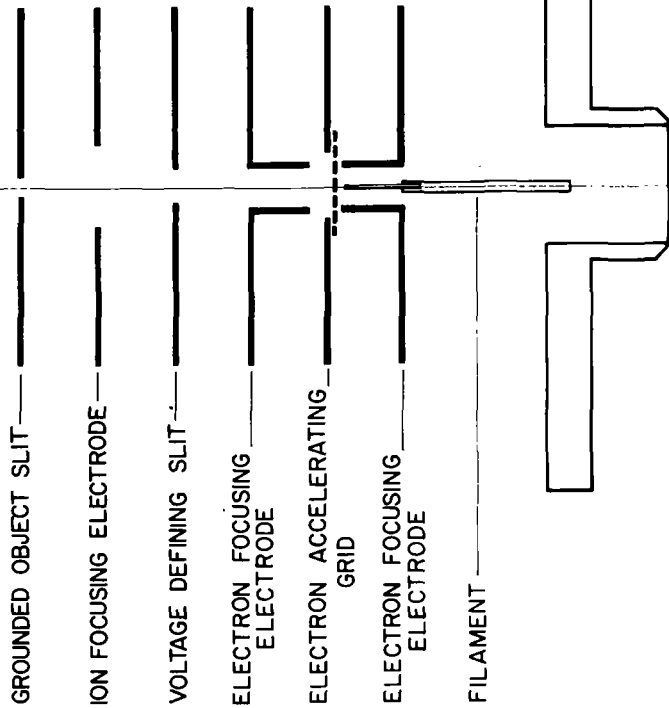
¹ M. Doctoroff, S.S. Grossel, D.W. Oblas, Proceedings of the Second International Congress on Vacuum Techniques, 1961 Pergamon Press (In Print)

² A.O. Nier, Rev. Sci. Inst. 11, 212 (1940)

³ F.S. Stein, J.E. Binns, AEC Document MDC-1670 (1948)

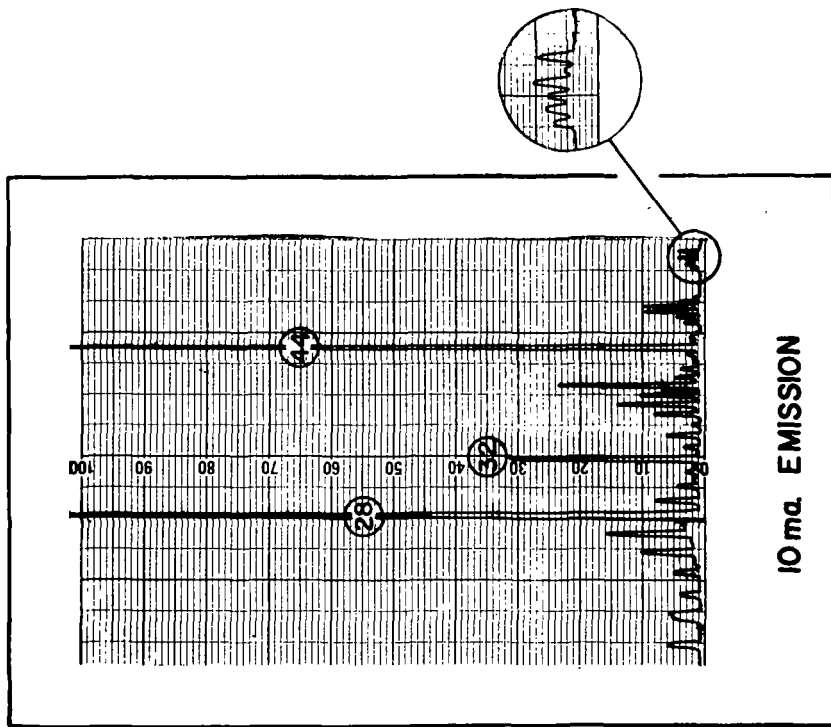
⁴ E.G. Linder, K.G. Hernquist, J. Appl. Phys., 21, 1088 (1955)

Figure 1



SCHEMATIC DIAGRAM OF THE AXIAL SOURCE

Figure 2



AXIAL SOURCE SCAN

SOURCE DESIGN CONSIDERATIONS FOR SECTOR FIELD MASS SPECTROMETERS

George Salser and Yuji Tajima
Department of Chemical Engineering
New York University, New York, New York

In our work with a 60° magnetic deflection rapid scan mass spectrometer, we have been able to observe certain effects which, in all probability, have not been as readily detected in machines with lower sweep speeds. Two of these effects, which I will discuss, originate in the source region and are highly undesirable. They are, namely,

1. The voltage effect described by Nier and others -- it is characterized by a drop in detector ion current when acceleration voltage is decreased; and
2. The instability of detector ion current with time under conditions which should lead to a stable ion current.

A short description of the machine will undoubtedly make the discussion somewhat clearer. The machine, modeled after that of Blanchard and others at Laval University, is a rapid scan 60° magnetic deflection instrument with a 6" radius of curvature. An electron multiplier is used as a detector with its output displayed on an oscilloscope. For slow speed operation and absolute measurement of ion current, provision is made to replace the multiplier with a vibrating reed electrometer. An emission regulator is used and all circuits at high voltage are protected by guard shields. The normal sweep voltage is from 6000 to 1000 volts although the machine will sweep down to 500 volts. The sweep speed may be varied from a sweep taking several seconds to sweeps of about a millisecond. All the units are highly regulated.

The machine as it was originally set up showed great instability and variability. Consequently, a program of rebuilding was started -- all electronic control units were rebuilt to give outputs of high stability. Provisions were also made to supply the source region with all types of voltages which might be useful. Draw-out and repeller voltages, both fixed and variable with sweep, were installed.

The original source and its ion lens are, I am sure, familiar to most of you who have worked with sector machines. This is shown on Fig. 1. The source itself is of the electron bombardment type. The lens consists of plates set upon glass insulators -- the voltages of these plates being derived from the accelerator.

To determine the voltage effect, all variables were maintained constant and the accelerator was allowed to sweep. This results in a panoramic display of mass peaks on the scope. The magnet was then manually swept at very slow speed causing the whole mass peak display to move across the face of the oscilloscope. When the peak of a particular mass was focused at various acceleration voltages, its height was plotted to give a graph such as that shown in Fig. 2. The solid line is one of the better curves drawn from such data. As can be seen, the ion current falls off alarmingly when the acceleration voltage is decreased below 2000 volts. Furthermore, the voltage effect curve was not at all stable -- it varied almost from one minute to the next. The broken lines show some of the other curves which were obtained and indicate the variability which was encountered. Analytical work was, of course, impossible under such conditions.

It was felt that modulation of the beam by the accelerator linked draw-out might cause the drop observed in the ion current. Consequently, the machine was equipped with both repeller and drawout plates, connected in a manner so that their voltages would remain fixed relative to the ionization region, during the period of a sweep. However, the voltage could be set at any desired level. This modification resulted in a rather small improvement indicating that although a modulation did occur, its contribution was small. The instability as well as a major portion of the voltage effect remained unaffected.

Fig. 3 shows one of the many modifications of the ion lens which was tried -- deflector plates of the type shown were installed but again the improvement was small. The instability remained unchanged.

Theoretical considerations show that ions may be lost in a number of ways. One of these is space charge dispersion of the beam. Fig. 4 gives the formula used for calculating this effect and some of the calculated values for our system. We have assumed that the beam consists of ions traveling in parallel paths with a

FIG. 1

TYPICAL SOURCE OF ORIGINAL MACHINE

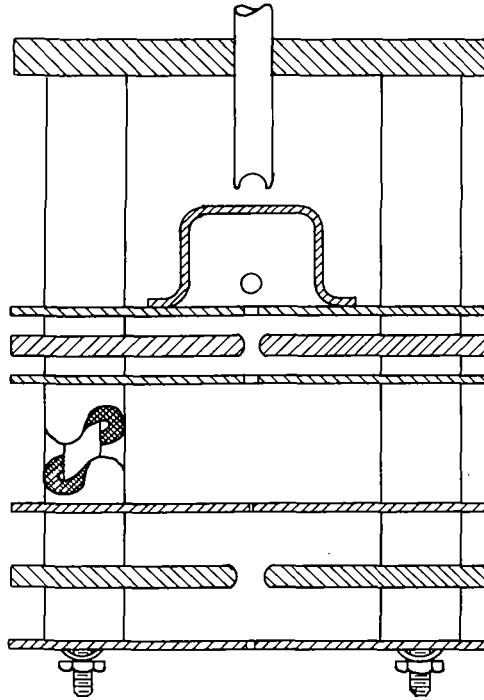
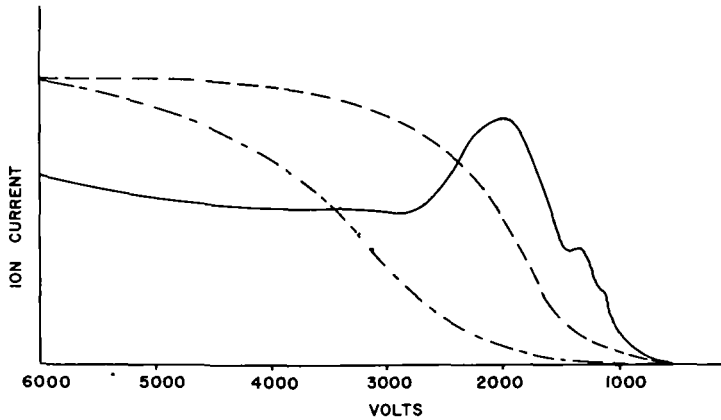


FIG. 2

VARIATION IN ION CURRENT
OF A
SINGLE PEAK FOCUSED AT
VARIOUS ACCELERATION VOLTAGES



cross section equal to that of the exit slit. The values calculated are acceleration voltages required to prevent a widening of the beam by a factor greater than 2 in a length of 100 cm. This effect is mass dependent while our observations have shown that the voltage effect has little if any mass dependence. Furthermore, we do not have a parallel beam of ions -- but one which broadens through the magnet region and is subsequently refocused which lowers the current density, and we do not normally operate with ion currents much in excess of 10^{-9} amperes. On the basis of these considerations, we concluded that this space charge dispersion effect will not be prominent above 1000 volts, the region where we operate. However, in larger machines with longer path lengths, or at higher ion currents, the contribution of this effect might be quite large in the high mass range.

At this point, let us consider a top view of the mass spectrometer. This is shown in Fig. 5 -- one can see the track which ions must take to reach the detector. Along the plane of the tube perpendicular to the vertical plane, there are no deflector plates to correct for deviations in the ion path. Consequently, any side accelerations received in this plane within the source region will irreversibly deflect the beam. If we consider a simple vector diagram of the acceleration voltage and some side acceleration, it can be seen that the effect of side vectors is indeed a voltage effect since the angle changes rapidly as the acceleration voltage is reduced. At 1000 volts, for example, a side vector of only 26 volts will completely eliminate the beam. This is in the order of magnitude of the voltage which would create the effect which has been observed in our machine.

Since such side vectors may arise in the ionization region as a result of penetration of the electron acceleration voltage and anode voltage, efforts have been made to eliminate such fields. After considerable shielding, it was found that the ionization region did indeed contribute a small side vector. This, however, was not enough to explain the voltage effect encountered. In the course of this work, it was found that screens are not permissible in the electron beam since heating by electron bombardment occurred and resulted in surface ionization.

It was noticed that often for brief periods of perhaps 3-4 seconds, the voltage effect would disappear. These were always preceded by a discharge of some kind, suggesting that perhaps arcing over the insulators occurred and effectively wiped them free of charge. Charges upon insulators would cause side acceleration vectors which would be variable with time. In view of the foregoing observations, some method of shielding the beam from the insulators was sought.

The use of a lens to shield a beam has long been known in cathod ray tube work. A detailed description of the two cylinder lens used by Epstein is given in the Proceedings of the Institute of Radio Engineers, Vol. 24, 1936. At the upper right in Fig. 6 is the lens used in cathode ray tube work -- it consists of two metal cylinders forming an optically spherical lens. For our work, an optically cylindrical lens is needed. This configuration is shown in the lower right -- the lens consists of flat plates. The source using this lens is shown on the left half of the slide.

This assembly not only eliminated almost all traces of the voltage effect but also gave extreme stability. Repeller and drawout voltages were held constant with respect to the ionization region. When they are linked to the accelerator power supply, modulation of the beam occurred.

In the present lens design, the voltage ratio used is between 4:1 and 6:1, making the focal point for the main lens lie within the ionization region. A second lens formed between the focus plates and the drawout plate shorten the focal length so that the crossover formed at the drawout plate is refocused as is shown in the slide. An exit slit has been omitted since the resolution is determined by the crossover at the drawout plate and the presence of the slit would probably only cause modulation of the beam.

In conclusion, to eliminate the voltage effect and minimize the instability of the ion current, certain principles must be adhered to in the design and operation of sector field mass spectrometers. Namely,

1. The ion beam must "see" only conductors since insulators tend to collect charges causing highly undesirable electrostatic fields. Insulators may

FIG. 3

A TYPICAL MODIFICATION OF FOCUS PLATES

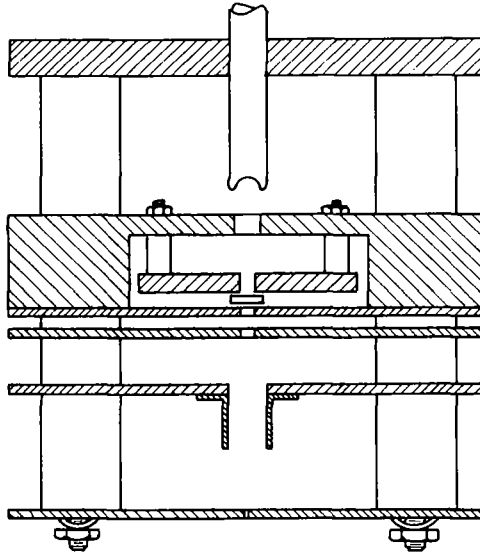


FIG. 4

MUTUAL REPULSION OF IONS

$$Z = \sqrt{\frac{m_e c}{4\pi e}} \left\{ \frac{2e}{c^2 m_e} V + \left(\frac{e}{c^2 m_e} V \right)^2 \right\}^{\frac{3}{2}} \cdot \frac{1}{i} \int_1^R \frac{d(R/r)}{\sqrt{\ln(R/r)}} \text{ cms.}$$

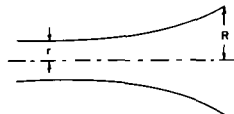
Voltage required for $\frac{R}{r} = 2$

Current - i	AMU			
	200	100	50	25
200×10^{-10}	3200	2460	1950	1550
100×10^{-10}	2010	1590	1260	1000
10×10^{-10}	435	345	274	218
1×10^{-10}	93	74	58	46

Path Length 100 cm

$$\frac{R}{r} = 2$$

Beam Cross Section = 0.25 mm²



* Watson - Watt, R. A. Phil Mag. 3, p 849, 1927

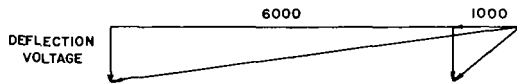
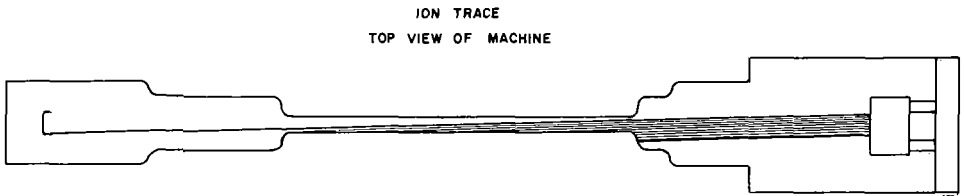
be either physical supports and/or deposits from the back diffusion of pump oil, samples analyzed or residues from improper cleaning.

2. The ion lens and ion ejection system must be designed so that modulation does not occur. Modulation can be produced not only during ion ejection from the ionization region but also by angles produced at crossover so that the ions can no longer be termed paraxial.

3. The ion beam must be shielded from all electrostatic fields crosswise to its path or deflection plates placed in the tube to correct for the effect of such fields.

We would like to take this opportunity to thank the Air Force Office of Scientific Research, Propulsion Division for their support of this work under contract AF 49(638)173 and Dr. C. E. Berry for his invaluable advice at a time when we had run out of answers.

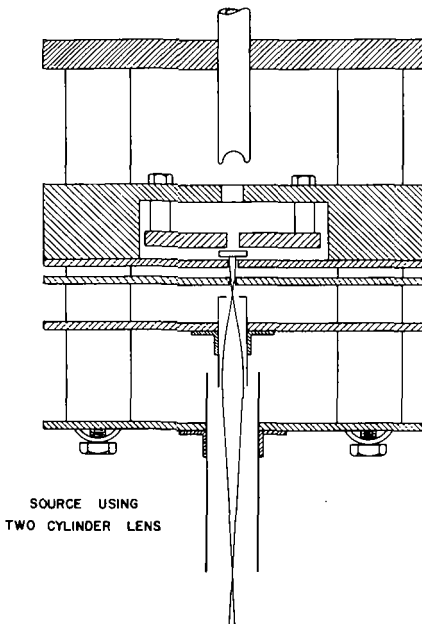
FIG. 5



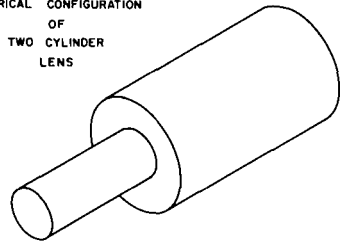
SIDE DEFLECTION VOLTAGE WHICH WILL ELIMINATE BEAM AT COLLECTOR

ACCELERATION VOLTAGE	SIDE DEFLECTION
6000	156
3000	78
1000	26
500	13

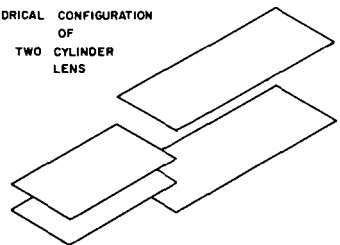
FIG. 6



SPHERICAL CONFIGURATION
OF
TWO CYLINDER
LENS



CYLINDRICAL CONFIGURATION
OF
TWO CYLINDER
LENS



"STUDY OF RESOLVING POWER OF A SINGLE-FOCUSSING, 12 IN. RADIUS, 60°, MASS SPECTROMETER"

Graham G. Wanless and George A. Glock, Jr.

I. INTRODUCTION

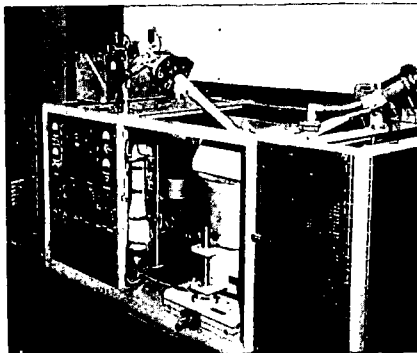
We thought that it would be of interest to describe the performance of our 12 in. radius, 60°, single-focussing mass spectrometer.

This instrument was a joint effort of General Electric Company and Esso Research and Engineering Company. I should give credit to L. A. Dietz of General Electric Company, and to W. H. King, Jr., and to B. E. Hudson, Jr., of Esso Research and Engineering Company.

In the past, this mass spectrometer has been used on a variety of high temperature and high mass range problems up to about mass 900, where the peaks were still individually resolved. With the original 0.008 in. collimating slits, the resolving power was about 500.

More recently its resolving power has been increased to a least 2750. It is the purpose of this paper to describe some experiments made with this problem in mind.

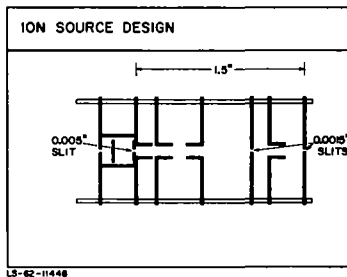
The first slide, if you please, will show a photograph of the mass tube.



Slide 1

The output signals are fed through a Cary vibrating reed amplifier, alternatively, to an oscillographic recorder and to a sensitive high-impedance recorder.

The ion source design is shown schematically in the second slide.

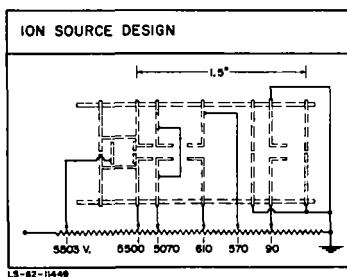


Slide 2

It contains three slits -

- a) 0.005 in. ion-gun slit
- b) Two 0.0015 in. collimating slits.

There is a lot to show on one slide. So let me show slide 2A, which is the same as slide 2 with the voltage divider added.



Slide 2A

II. POTENTIAL RESOLUTION OF A SINGLE-FOCUSSING INSTRUMENT: -

Slide 3

THE POTENTIAL RESOLVING POWER (M_p) IS

$$M_p = \frac{R}{(S + W + A)}$$

LS-62-11450

Slide 3

where R = mass tube radius
 S = collector slit width
 W = width of ion-beam object (not necessarily equal to collimating slit widths)
 A = sum of instrumental aberrations contributed to the refocussed ion beam.

W is the result of the electrostatic focussing in the ion gun, and it is difficult to know. If we assume that W equals the actual collimating slit widths, then we can estimate the sum of the instrumental aberrations.

In our case,

$$M_p = 2750, \text{ MINIMUM}$$

$$R = 12. \text{ IN.}$$

$$S = 0.00025 \text{ IN.}$$

$$W = 0.0015 \text{ IN. [ASSUMED]}$$

LS-62-11451

Slide 4

(a) If there were no instrumental aberrations,

$$M_p = \frac{12.0}{(0.00025 + 0.0015)} = 6857.$$

(b)

FOR AN ASSURED RESOLUTION OF 2750,

$$M_p = 2750 = \frac{12.0}{(0.00025 + 0.0015 + A)}$$

$$\therefore A = 0.0026 \text{ IN.}$$

LS-62-11452

Slide 5

(c) If 0.001 in. collimating slits were used, the resolution could be increased to 3109, or by about 14%.

Thus, it is evident that there is no use in reducing slit widths, unless concurrent progress is made in reducing aberrations.

III. PRACTICAL MEANS OF IMPROVING RESOLVING POWER: -

This subject has been considered carefully by Thorburn and Robbins (1) in relation to a Metropolitan-Vickers M.S. 2 mass spectrometer. Their paper is an excellent guide when studying this problem.

1. In the time available, it has not been possible to make a critical investigation of every variable. The subjects, although important, on which we have not worked are: -

- (a) Spherical aberrations, and aberrations causing image curvature.
- (b) Increasing the field strength of the yoke magnets.
- (c) Space charge effects. These have been avoided. All of the work presented was done with a sample charge of 0.6 mg.

2. We have studied eleven other variables which are discussed below: -

Reduction of slit widths: -

- (a) Ion beam object width (collimating slits):

This instrument had great sensitivity, and it has been possible to trade some of it for increased resolving power. The collimating slits have been reduced gradually from the original 0.008 in. widths to 0.0015 in.

- (b) Collector slit:

At the same time, the collector slit has been reduced to 0.00025 in. Concurrently with these changes, reduction in instrumental aberrations have been made and these will be discussed.

The net result is a single-focussing instrument which can be used for conventional work, and after reducing collector slit width - in high resolution studies. As an example, we may enjoy a sensitivity for n-dodecane parent ion, in a resolved doublet, of 2000 chart divisions per milligram. Later slides will show examples.

INSTRUMENTAL ABERRATIONS	
(a)	<u>STABILITY OF ACCELERATING VOLTAGE.</u>
(b)	<u>PARALLEL ALIGNMENT OF COLLIMATING AND COLLECTOR SLITS.</u>
(c)	<u>REDUCTION OF SLIT LENGTHS.</u>
(d)	<u>MINIMIZE EFFECT OF BACKGROUND SCATTERING BY DIFFERENTIAL PUMPING.</u>

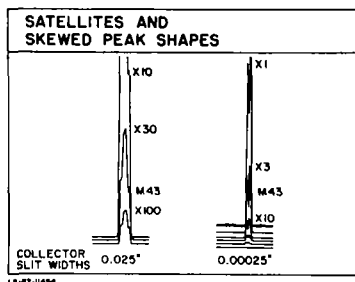
LS-62-11453

Slide 6

- (c) Accelerating voltage:

We have studied this extensively and found that in our case, the stability of the high voltage power supply was not critical. This was established by various filter experiments. (See section 3-(k)). Our problem was shown to be a chromatic aberration.

(d) Parallel alignment of slits is extremely critical. Slide 7 will show the symptoms of this trouble.



Slide 7

- (i) Satellite peaks which can be seen when the collector slit is opened rather widely,
- and (ii) Skewed peak shapes which are observed when the collector slit is closed down.

(These peaks were obtained from a blend of equal volumes of n-nonane and 2-octanone.)

After all of the electrical improvements were made, and which are discussed in this paper, successful twisting of the mass tube removed the peak satellites and increased resolution by 119% (from 1320 to 2900).

(e) Reduction of slit lengths to prevent scattering of the ion beam by impinging on the mass tube, in the region of the analyzer magnet.

Thorburn⁽¹⁾ found a 15% gain in resolution when the second collimating slit was shortened, and a 40% gain when the collector slit was shortened.

So far, we have applied this to the second collimating slit by shortening it from 0.60 in. to 0.31 in. Time did not permit a special investigation of this change, but undoubtedly it helps, since our mass tube is 0.67 in. wide, inside, in the analyzer region.

(f) Differential pumping of the mass tube has been simulated in our instrument, by installing a second diffusion pump at the collector slits, and by inserting a slotted plate between the ion gun region and the analyzer region of the mass tube. The slot in this plate is 17 mm x 5 mm, and it has had no adverse effect on sensitivity. Narrower slots will be tried out.

This change was made to reduce pressure and to reduce ion beam scattering in the analyzer region. It has demonstrated that a mass tube of this size needs a second diffusion pump at the collector end of the tube. During the two years when the instrument was run with one diffusion pump, some accumulation of heavy ends occurred at the far end of the mass tube. This accumulation is being removed gradually since installation of the second pump. The pressure below the leak is now down to 1.8×10^{-7} mm Hg. Although we have not measured the gain in resolution directly, this change is undoubtedly a contributing factor to increased resolution.

Two other changes which contribute to quiet instrument operation include (1) a separate ground from the chassis of the high voltage power supply, and (2) internal grounds in the mercury diffusion pumps.

3. Chromatic Aberrations: -

This is the principal area for research. We will discuss five factors which we have had a chance to study:

CHROMATIC ABERRATIONS	
(p)	<u>MINIMIZE EFFECT OF DRAWING-OUT FIELD.</u>
(q)	<u>OPTIMIZE FILAMENT TO SHIELD POTENTIAL.</u>
(r)	<u>INCREASE ACCELERATING POTENTIAL.</u>
(s)	<u>PROVIDE D.C. CURRENT AROUND ION GUN.</u>
(t)	<u>REMOVE ION GUN OSCILLATION.</u>

LS-62-11455

Slide 8

(g) Any effect of the drawing-out field which may have existed was minimized by reducing the slit width at the ion chamber from 0.008 in. to 0.005 in. We found that this did not decrease sensitivity. It does hurt the cracking pattern somewhat, but we can stand it. With an ionization chamber temperature of 190°C., in our instrument, the M226/M57 peak height ratio for n-cetane is still 0.071.

(h) For our instrument the optimum filament - to - shield potential appears to be 45 volts. This is shown by data in the following table:

<u>Table I</u>	
<u>Filament-to-shield potential</u>	<u>Percent valley in mass 43 doublet</u>
55V	28.5% (1)
50	25.
45	21. ←
40	22.
35	28.
30	30.
25	25.
20	43.
15	42.

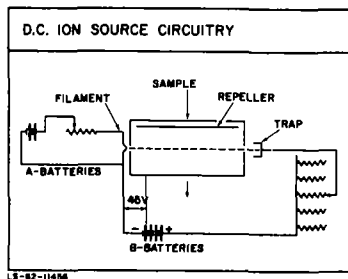
(1) Measured from base-line.

(i) Increasing accelerating potential increases resolving power as shown: -

<u>Table II</u>		
<u>Accelerating Voltage</u>	<u>Percent valley in mass 128 doublet</u>	<u>Approximate Resolving power</u>
5500V.	21%	2780
6600	15	2990

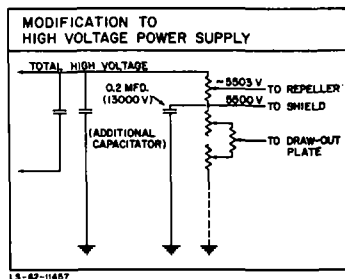
Most of our work has been done at 5500 Volts. Work above 6000 Volts will require redesigning of the clearances in the ion source.

(j) D.C. Circuitry around the ion source is commonly used in appearance potential work. We have been pleased to find that it also contributes to increase resolving power. The arrangement shown in slide 9 gave a 50% gain in resolution compared to that obtained with the conventional AC-regulated filament circuit.



Slide 9

(k) Ion source oscillation. Even with complete D.C. circuitry around it, we have found that there is still an oscillation associated with the ion source. It can be removed or greatly reduced by installing an additional capacitator in the high voltage power supply, as shown in slide 10. This modification produces another gain in resolution of about 45%.



Slide 10

Many additional circuit modifications have established that the effect is not a superimposed AC ripple coming from the high voltage power supply. The ripple is a phenomenon associated with the ion gun itself.

4. Instrument Tuning Parameters: -

INSTRUMENT TUNING PARAMETERS	
0)	DRAWING-OUT POTENTIAL
01)	FOCUSSING POTENTIAL
011)	BEAM CENTERING POTENTIAL
0v)	REPELLER POTENTIAL

LS-62-11458

Slide 11

(i) Drawing out potential: (Referring to Slide 2A, again, please):

In this ion source design, the clearance between the flanges on the ion-gun exit slit plate and the drawing-out plate is only 0.055 in. This makes the drawing out potential non-critical with respect to general tuning of the ion beam. However, it does influence resolution. For a 5500 V. accelerating potential, the drawing-out potential is set at about 430 volts with respect to the shield potential.

(ii) Focussing and (iii) beam centering potentials:

These are extremely critical and require 10-turn Helipot on the fine adjustments.

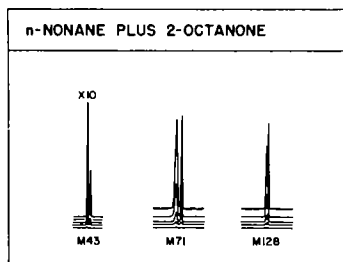
(iv) Repeller potential:

Potentials of +2.2 to +2.9 volts are preferred for optimum resolving power.

IV. RESULTS:

(a) Resolution:

The net result of attention to these details is shown in slide 12.



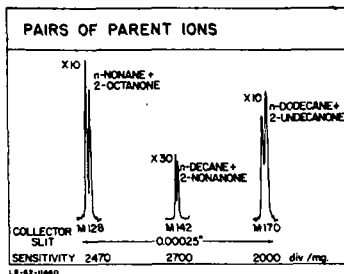
LS-62-11458

Slide 12

We show the separation of the mass 43, 71 and 128 (parent) peaks for the pair n-nonane and 2-octanone. A resolving power of 2750 can be claimed.

Slide 13 shows similar pairs of parent peaks for the pairs

n-nonane and 2-octanone
n-decane and 2-nonanone
n-dodecane and 2-undecanone



Slide 13

(b) Sensitivity:

This is indicated on the previous slide. With a 0.00025 in. collector slit, the sensitivity at mass 170 is 2000 divisions per milligram.

(c) Absolute Mass Measurements:

Finally does the machine give the right answers? Are they as accurate as can be obtained with a double-focussing machine?

To attempt to answer this we have examined the nonane/octanone pair in the CEC-21-110 double-focussing mass spectrograph and in the mass spectrometer which we are describing. Ten sets of measurements were made in each instrument. The absolute values are quite close together as shown in the last slide:

ABSOLUTE MASS MEASUREMENTS			
	CORRECT NUMBER	D.F. MASS SPECTROGRAPH	S.F. MASS SPECTROMETER
M43 Δ	43.0321	43.0318 -0.0005	43.0340 +0.0019
M71 Δ	71.0723	71.0739 +0.0016	71.0729 +0.0006
M128 Δ	128.1610	128.1599 -0.0011	128.1598 -0.0012

LS-62-11461

Slide 14

The 95% confidence limits for the data from the single-focussing mass spectrometer are as follows: -

<u>95% Confidence Limits</u>		
<u>M 43</u>	<u>M 71</u>	<u>M 128</u>
0.0031	0.0018	0.0035

With the single-focussing machine we appear to have a slight systematic error at mass 43. It has not yet been investigated fully. But we can say that it is due neither to errors (a) in peak measuring, nor (b) in chart drive rate, nor (c) in ability of the recorder to keep up with the scanning rate. Probably the error is associated with the analyzer magnet power supply.

We acknowledge the help of E. S. McBride, who provided the spectrographic results.

Reference (1):

R. Thorburn and E. J. Robbins, "Increasing the Resolving Power of a Metropolitan - Vickers M.S.2 Mass Spectrometer with Particular Reference to Analysis of Uranium Hexafluoride." (United Kingdom Atomic Energy Authority, report DEG-94 (CA)).

CORRECTION COILS FOR SECOND ORDER FOCUSING WITH
THE ARGONNE 100 INCH RADIUS MASS SPECTROMETER

C. M. Stevens^{*}
Argonne National Laboratory
Argonne, Illinois

ABSTRACT

The second order coefficients, B_{11} , B_{12} , and B_{22} in the expression

$$y_B = a_m (B_{11} \alpha^2 + B_{12} \alpha\beta + B_{22} \beta^2) ,$$

have been made very small for the Argonne 100 inch radius double focussing instrument by the use of three circular coils placed in the magnet gap at the entrance, middle, and exit regions. The set of currents I_1 , I_2 , and I_3 required in each coil to give complete second order focussing was determined assuming a set of linear first order equations,

$$\underline{K} \underline{I} = \underline{B}$$

Comparison has been made between the measured value of the second order coefficients before correction and the calculations of Hintenberger and Konig.

^{*}This work was supported by the United States Atomic Energy Commission.

MECHANICAL MODIFICATION OF TWO-STAGE,
12-INCH RADIUS MASS SPECTROMETER AT
VALLECITOS ATOMIC LABORATORY

by

W. E. Duffy

I. INTRODUCTION

The instrument discussed in this report evolved from one developed at Knolls Atomic Power Laboratory of General Electric Company. It was described first by White and Collins in 1954 in Applied Spectroscopy, Volume 8, page 169. The instrument originally contained an all-glass vacuum system. Vacuum was maintained by three large glass liquid nitrogen cold traps, three mercury diffusion pumps and one 140 l/min. mechanical pump. Pressure was measured by one thermocouple gage and three ionization gages. In this laboratory a second, 70 l/m mechanical pump and a thermocouple gage were added but otherwise the system remained unchanged. A flow diagram of the system as it existed at our laboratory is shown in the first slide.

Introduction of a solid sample required isolation of the source region by closing valves 3, 4, and 5, venting the source cap to atmosphere, melting the black sealing wax with a torch and removing the cap. The old sample was then removed and replaced with a new one. The source cap was resealed on the system, pumped out with the mechanical pump and then opened to the mercury diffusion pump which pumped upon the source region. This operation usually required ten to fifteen minutes. Subsequent pumpdown necessary to attain an operating pressure of 2 or 3×10^{-7} Torr required 3 to 4 hours. Since a complete isotopic analysis required an hour or more the instrument was limited to two analyses per day, even with overnight pumping on the first sample.

II. PLANNED CHANGES

An increase in the analytical requirements of the laboratory necessitated a modification of the mass spectrometer to permit more capacity. The most obvious improvement was some means to reduce pump-down time between analyses. The rapid sample-changers known personally to the author and reported in the literature did not possess all of the characteristics desired. It was resolved, therefore, to design a changer based upon that built by C. M. Stevens of Argonne National Laboratory but differing enough in detail to fit the particular requirements of this instrument. Since adding a sample changer would mean redesign of the source end of the vacuum system it was decided that a completely new vacuum system would be designed. The idea grew until the system became all metal. The cold traps and diffusion pumps were eliminated and replaced by ion getter pumps. The glass analyzer tubes were replaced by copper wave guide tubing bent to the proper dimensions.

The changes thus contemplated were intended to remove danger of glass breakage, to increase pumping speed and to eliminate cold traps and the attendant dependence upon liquid nitrogen. Also, use of ion getter pumps would provide a clean system free from potential contamination by mercury or oil diffusion pumps.

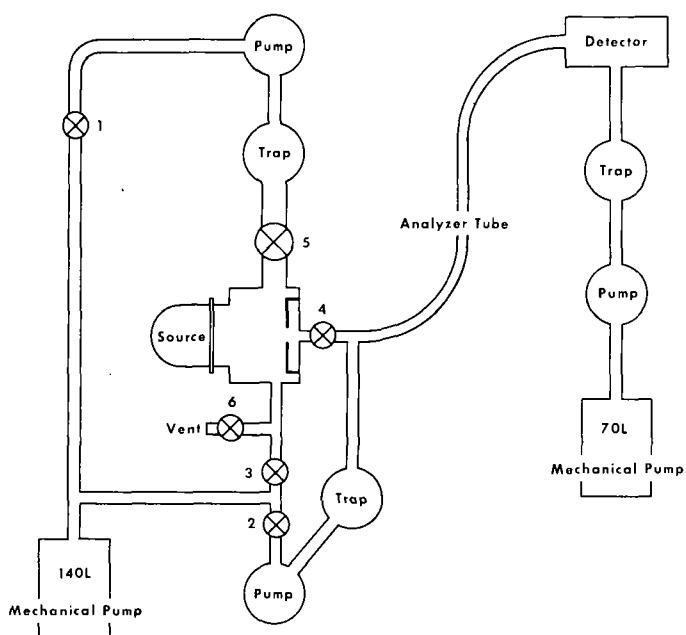


Figure 1. ORIGINAL ALL-GLASS SYSTEM

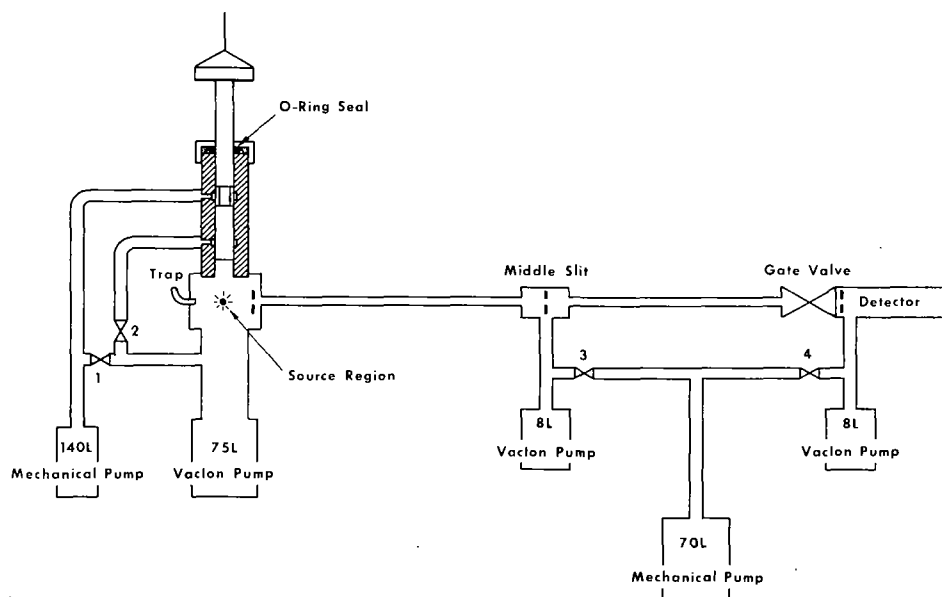


Figure 2. PRESENT ALL-METAL SYSTEM

III. MODIFICATION DESCRIPTION

Using the basic vacuum lock developed by C. M. Stevens of ANL and the high voltage ion source described by L. A. Dietz of KAPL as starting points the system shown in the second slide was designed. (1,2)

The vacuum lock contains essentially two stages of differential pumping. The first stage is mechanical and operates continuously. It roughs out the source assembly after the O-ring seal has been tightened about the sliding piston. After pumping on this stage for a short period the O-ring seal is loosened sufficiently to permit movement of the piston and the source assembly is moved to the second stage. The O-ring is then retightened. Valve No. 2, located between this second stage and the source region is kept closed during this operation. This valve is then opened slightly to permit a small amount of the included air to leak into the large Vac Ion pump. It is now closed until the Vac Ion pump recovers. This is repeated several times until the valve can be opened wide with very little change in the Vac Ion pump current reading. The O-ring is now loosened slightly and the source assembly is moved into the source region. The O-ring is again tightened. The valve is closed and the Vac Ion pump now pumps directly upon the source assembly. Valve No. 1 is kept closed except during initial evacuation of the system.

Extraction of the source assembly is accomplished by loosening the O-ring seal and lifting the piston until the source assembly just clears the O-ring tightening nut. The counter weight stops at this point and holds the piston in this position. The O-ring is tightened and the old sample hat and filament is replaced by a new one. The sample introduction procedure is then repeated.

The sliding piston and cylinder of the vacuum lock are made of 304 SS. Both surfaces are hard chrome plated and machined to a clearance of ± 0.0002 ". The diameter of the piston is 2 inches. The close tolerances maintained minimize in-leakage of air. This is decreased further by the Viton O-ring preceding the first stage of pumping.

The path of the ions in this instrument lies in a horizontal plane. The vacuum lock was designed to operate in a vertical plane along the axis of the source slit assembly. This arrangement permits the movable piston to be of minimum diameter and allows rotational and translational adjustment of the ion source.

The short piston is connected to the long piston directly through the source assembly and acts as a plug when the source is extracted. Furthermore the short piston separates the first stage of pumping from the second when the source is extracted. The source assembly itself is isolated from ground by specially built ceramic spacers. Each piston section is supported at three points. To permit proper alignment of the two sections during the insertion or extraction operations the short piston is supported by screws which hang loosely from the ceramic spacer. This allows a self-centering action during axial movement.

The electrical leads are introduced through a special ceramic seal with a stainless steel sleeve which is heliarc welded inside

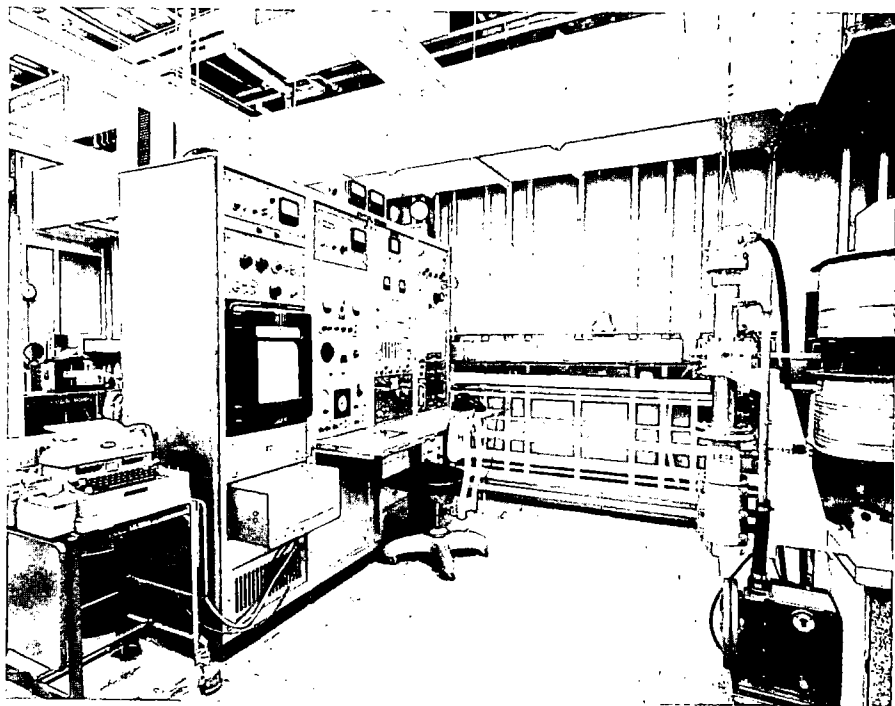


Fig. 3 - Mass Spectrometer and Control

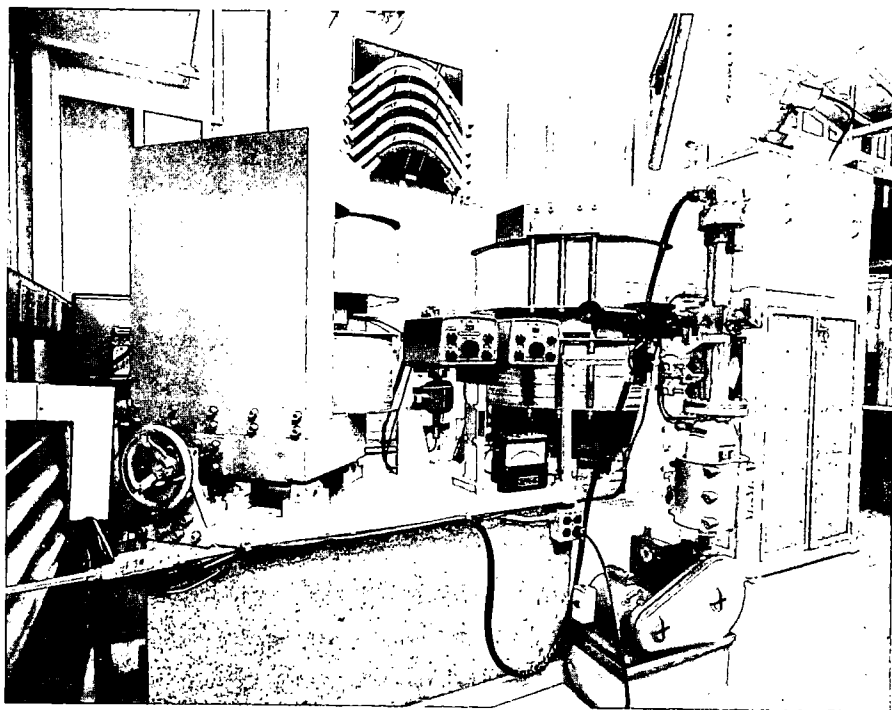


Fig. 4 a - Front View of Vacuum and Magnet Sections

the long piston. The short piston is grounded during source operation to prevent the buildup of a static charge. The two ion beam collimating slits are of fixed dimension and both are at ground potential. This differs from the design of Dietz which specifies a potential upon the first collimating slit. The z-focus plates are located between the two collimating slits and are insulated from them. A battery voltage up to ± 300 volts may be applied to these plates.

The ion source was designed to operate at 15,000 volts. Tests with a megohmmeter show that the source will operate as designed. So far our power supply has limited us to 5000 volts.

A 75 liter per second Vac Ion pump operates continuously upon the source region. This is isolated from the analyzer by the 8-mil beam collimating slit. The first and second stage analyzer tubes are pumped on by an 8 liter per second Vac Ion pump which is located directly beneath the center slit. The detector region is pumped on by a second 8 liter per second Vac Ion pump and is isolated from the analyzer region by the detector slit. The detector, an electron multiplier, may be sealed off from the remainder of the system by a one-inch gate valve which normally remains open. The two eight liter/sec. pumps share a common power supply. The 75 liter per second pump has an independent power supply.

The two analyzer tubes were bent to specifications from oxygen free, high conductivity copper wave guide.

The center slit and detector slit were each made continuously adjustable by using bellows seals and two flat bladed micrometer depth gages to move the slits.

All vacuum seals were made with commercial shear seal flanges and copper gaskets or with Viton O-rings where use of copper gaskets was impractical.

Two sapphire windows were located to observe the source region and permit pyrometer measurement of the sample filament temperature. A small cold-finger liquid nitrogen trap was flanged into the source region to reduce sample background and help reduce pressure. Use of this cold trap was intended only when very high abundance sensitivity was desired. However, it has been found that regular use of the cold trap reduces sample introduction time by about one-half. The trap is kept filled throughout the day and allowed to warm up overnight.

Although the system was constructed entirely of metal, extensive high temperature bakeout was impractical due to the fixed and inflexible connections between the various components. This did not hinder the highly satisfactory performance of the vacuum system, however.

IV. PERFORMANCE

Operating pressure in the source region was generally 1 to 3×10^{-7} Torr. Following an overnight pump-down the pressure was often 2 to 3×10^{-8} Torr. The pressures in the analyzer and detector regions were nearly equal and remained at about 2×10^{-7} Torr, even during sample change. There were no detectable leaks in these parts of the system.

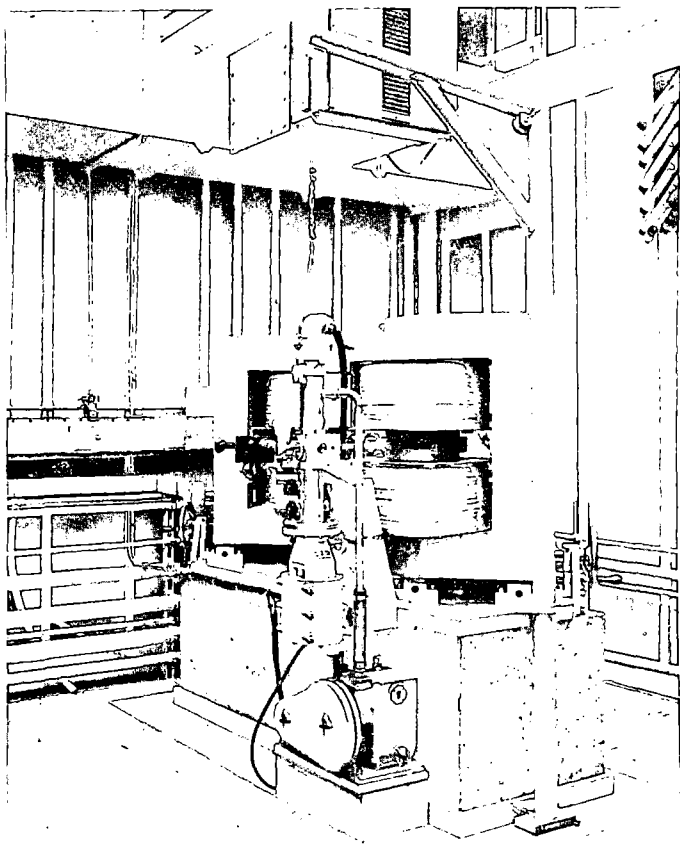


Fig. 4 b - Front View of Vacuum and Magnet Sections

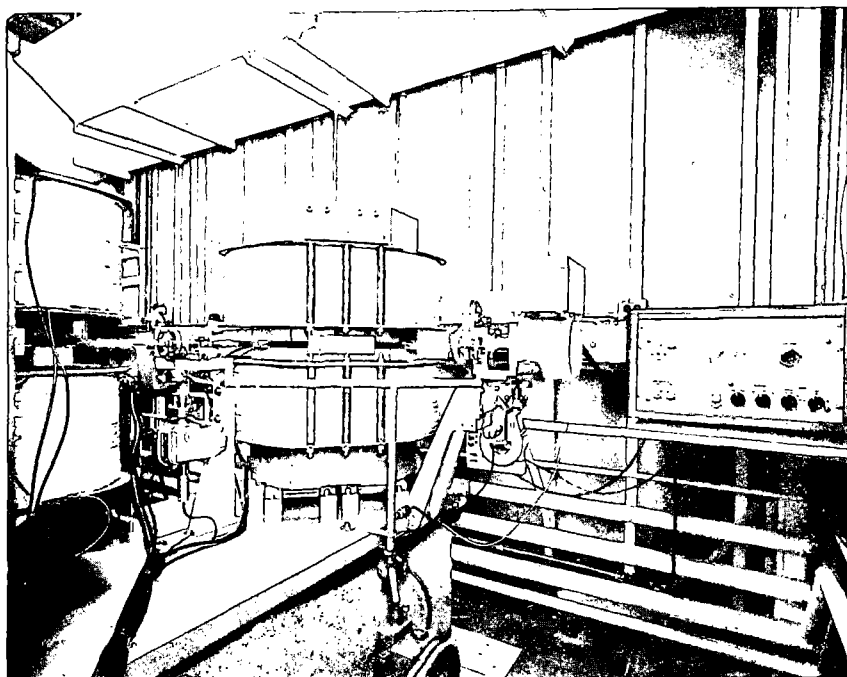


Fig. 5 a - Middle Slit and Detector Assemblies

During routine instrument operation, using the cold finger, sample introduction procedure consisted of three minutes of pumping in the first stage, two minutes pumping in the second stage and ten minutes pumping in the source region before a satisfactory vacuum was obtained and sample analysis commenced. Occasionally additional time was required, but seldom was more than 20 minutes of pumping necessary.

Approximately one hour is required for a complete isotopic analysis. The result is that the instrument easily may run from four to six samples per eight hour day.

Shut down of the instrument for any reason consists simply of switching off the pumps and venting the instrument. In order to protect the electron multiplier during a shutdown the one-inch gate valve in the rear is closed and the rear Vac Ion pump is left on.

Operation of the rapid sample-changer is quite simple. Trouble from galling of the sliding surfaces is eliminated by reasonable attention to cleanliness.

The use of copper sealing gaskets and Viton O-rings has proven very satisfactory. The initial assembly of the system resulted in a practically leak-free unit.

V. COMPARISON OF OLD AND NEW INSTRUMENTS

Prior to modification the instrument was limited to one to two analyses per eight hour day. Since modification the instrument easily may analyze four to six samples in the same period. Elimination of the large cold traps has reduced instrumental requirements for liquid nitrogen from 250 liters to 5 liters per week. Sample size, abundance sensitivity, adjacent mass resolution and counting rates remain essentially the same as before. Use of the z-focus and the mechanical translational and rotational adjustments permits very accurate positioning of the source filament and minimizes physical misalignment. The physical appearance of the instrument is improved and housekeeping simplified.

VI. FIGURES

The attached figures show different views of the instrument.

References:

1. Stevens, C. M., Rev. Sci. Instr. 24 148 (1953).
2. Dietz, L. A., et al, Anal. Chem. 32 1276 (1960).

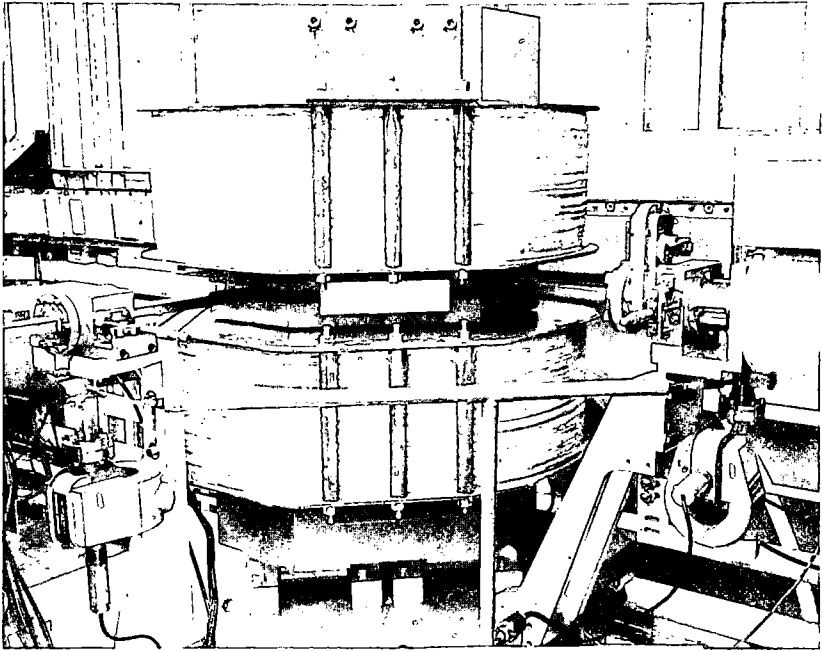


Fig. 5 b - Middle Slit and Detector Assemblies

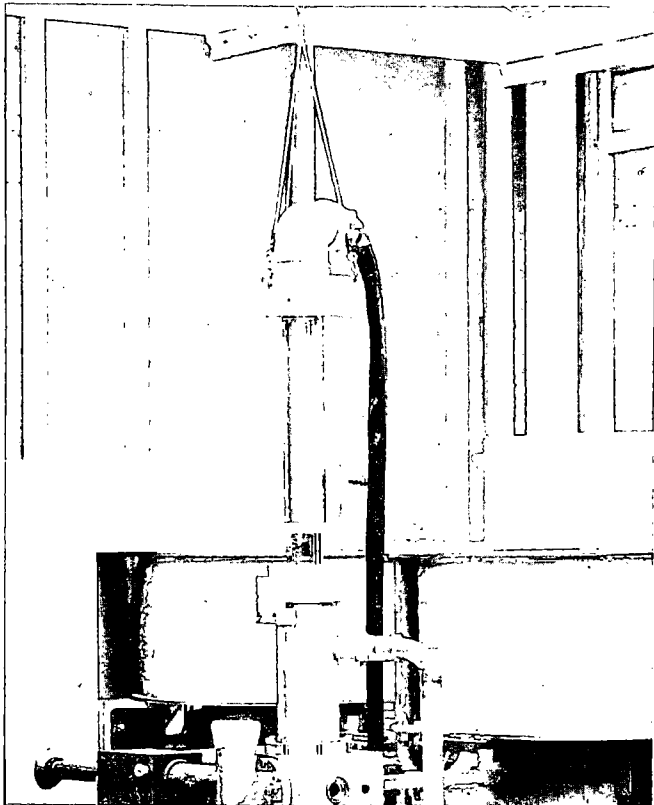


Fig. 6 - Source Piston Fully Withdrawn

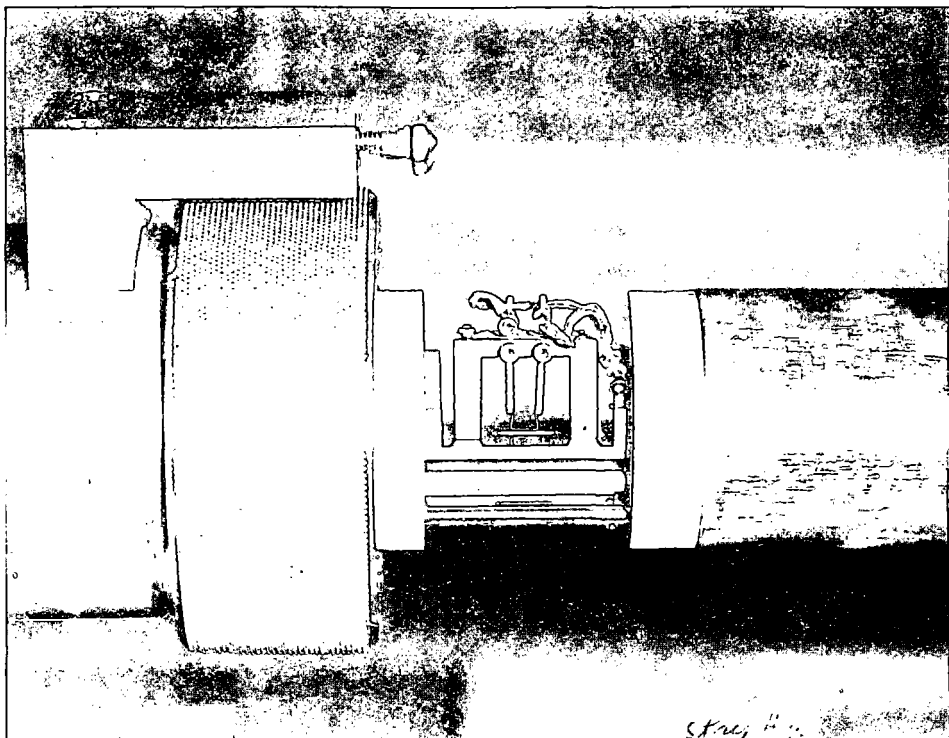


Fig. 7 a - Close-up View of Source Assembly

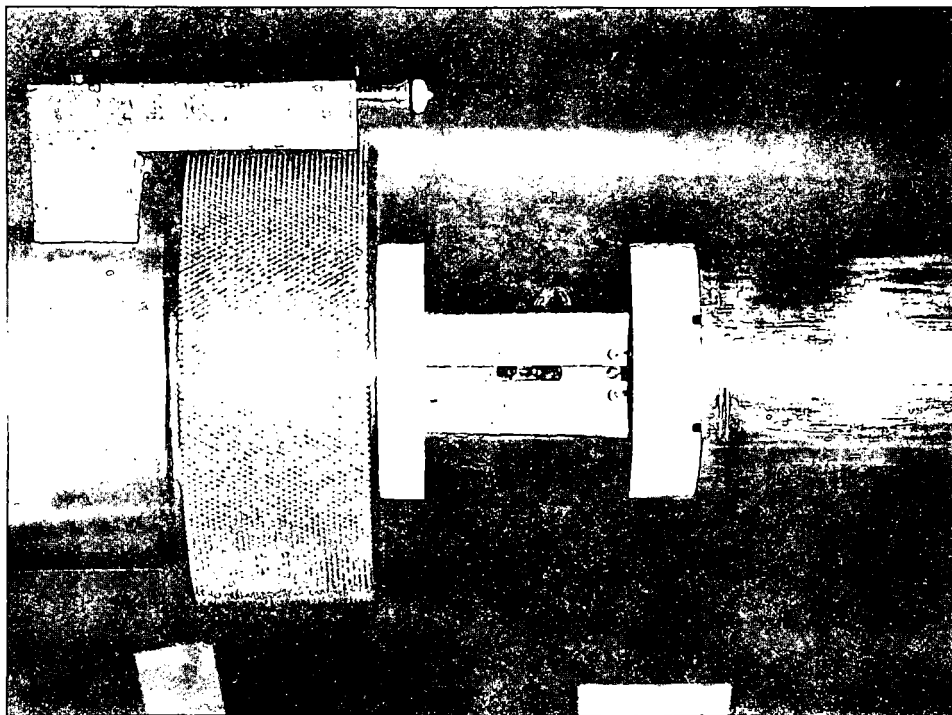


Fig. 7 b - Close-up View of Source Assembly

1. Identification of fractions which have been separated in a gas chromatographic capillary column

a) Instrument

In order to apply the Mass spectrometer CH 4 for this problem, a special inlet device had to be developed. This device can be seen in Fig. 1 as part of the total arrangement.

At the end of the capillary column, the gas stream is split. The one part of the gas stream is directed to the detector of the gas chromatograph, the other part is directed to the inlet connection of the mass spectrometer. This inlet connection consists of a throttle capillary. The gas stream leaving the column flows freely around the throttle capillary without being in direct contact with the wall of the capillary column. In this way the liquid phase is prevented from reaching the inlet line to the ion source. The entire inlet arrangement can be heated up to 350°C.

In addition to this special inlet arrangement, the CH 4 was also equipped with a special ion detection assembly, consisting of a multiplier and a cathode ray oscilloscope or a multiple galvanometer recorder respectively. The performance data which can be attained with such an instrument are listed in Fig. 2 as far as they are of interest for the problem discussed here.

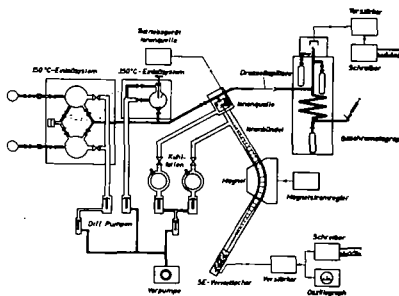


Fig. 1

b) Measuring accuracy under different conditions

The accuracy of the recording of an ion current J belonging to a definite characteristic mass is mainly dependent on the mean statistical fluctuations F which decrease with increasing values of the ion current J and of the time constant T of the recording system, proportional to $1/\sqrt{JT}$; $F = K/\sqrt{JT}$.

The value of JT depends on the necessary resolution and on the necessary scanning speed.

To increase the resolving power requires narrowing the slit widths, which results in a decrease of the ion current J_{\max} . An increase of the resolving power with the scanning speed V remaining constant requires a reduction of the time constant T of the recording system. A reduction of the time constant T is also unavoidable when the scanning speed V is increased.

In summary, it results:

$$F \approx \text{const.} \cdot \sqrt{A^2 \cdot V}$$

where A is the resolving power and V is the number of recorded mass oktaves p.sec.

It depends on the specific problem which resolving power and which scanning speed at a given maximum ion current has to be chosen for the performance of a mass spectrometric analysis. Among many factors the substance quantity and the time period of the appearance of the fractions at the outlet of the column must be considered. In any case, resolving power and scanning speed should be chosen not higher than absolutely necessary.

To retain high readout accuracy we shall reduce the minimum scanning speed required for the exact recording of the mass spectrum in that way that we do not record the absolute ion currents but the proportion of the ion currents to the prevailing partial pressure of the fraction measured, in order to eliminate the influence of the temporary alteration of the partial pressure on the distribution of the peak heights in the mass spectrum

ATLAS Mass Spectrometer CH 4
(Performance Data)

Mass Range:	Mass 1 - 500 Mass 2 - 1000
Resolution:	$\frac{M}{\Delta M} = 200 / 400 / 1500$
Scanning Period:	<p>a) Alteration of the magnet field $T_{\text{ms}} = \frac{0.6 \text{ sec}}{\text{mass octave}}$</p> <p>b) Alteration of the ion energy $T_{\text{ms}} = \frac{0.04 \text{ sec}}{\text{mass octave}}$</p>
Sensitivity:	<p>a) $J_{\text{max}} \approx 1 \cdot 10^{-8} \text{ A}$ for $\frac{M}{\Delta M} = 200$ and gas consumption of $5 \text{ atm} \cdot \text{ml} / \text{min}$</p> <p>b) $J_{\text{min}} \approx 1 \cdot 10^{-16} \text{ A}$ (1000 counts of the recorder 0.1 sec, accuracy 10%)</p> <p>c) concentration range $\frac{J_{\text{min}}}{J_{\text{max}}} \approx 10^{-8}$</p>

Fig. 2

for a larger part of the scanning time of the fraction.

c) Practical examples of measurements

With a cathode ray oscilloscope (Tektronics 545) 10 scans of the mass range $ME = x$ to $ME = 2,5 \cdot x$ per second could be recorded. The time constant in this case was $T = 2 \cdot 10^{-4}$ sec. With this measuring arrangement, continuous mass spectrometric analyses at the output of a gas chromatographic capillary column have been demonstrated consecutively on the AICHEMA 13 Exhibition in Frankfurt/M, Germany, in Summer 1961.

In the meantime, the cathode ray oscilloscope has been replaced by a multiple trace ultraviolet beam galvanometer recorder (ABEM). This type recorder offers the advantage that the mass spectra can be taken and recorded in 7 different sensitivity ranges simultaneously. Measurement results are shown in figures 3 to 6.

Fig. 3 shows the gas chromatogram of a sample obtained with a capillary column. This sample consisted of the following components:

PEAK No.	COMPONENT	CONCENTRATION [%]	PEAK No.	COMPONENT	CONCENTRATION [%]	PEAK No.	COMPONENT	CONCENTRATION [%]
39	2,2-Dimethylhexane	0.50	44	Toluene	28.20	49	n-Octane	2.62
40	2,6-Dimethylhexane	1.09	45	2,3-Dimethylhexane	1.00	50	Ethylbenzene	
41	2,4-Dimethylhexane	2.00	46	2-Methylheptane	3.74	51	p-Xylene	
42	2,2,3-Trimethylpentane		47	4-Methylheptane	1.80	52	m-Xylene	
43	3,3-Dimethylhexane	0.73	48	3-Methylheptane	6.03	53	o-Xylene	

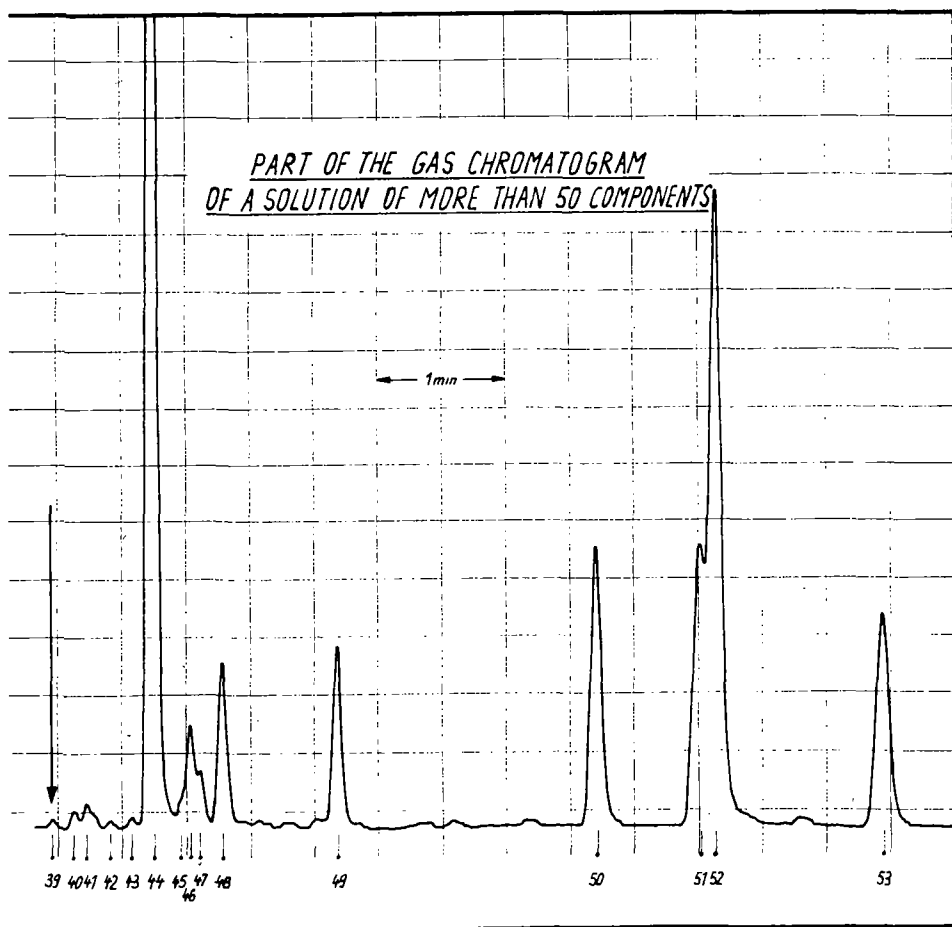


Fig. 3

Of the gas stream leaving the capillary column, mass spectrograms have been recorded continuously with a scanning time of 1/4 second for the mass range ME = x to ME = 2,5x. (ME = 40 - 120)

Fig. 4 shows a cut-out of the mass spectrum of the component No. 39 marked in the gas chromatogram. This cut-out shows that even this component, which is present in the sample to 0,5 % only, can be well analyzed by mass spectrometry. Evaluable mass spectra are still obtained with a concentration of 0,1 % of the component concerned. If only the main peak in the mass spectrum of the component is recorded, considerably smaller concentrations are still detectable.

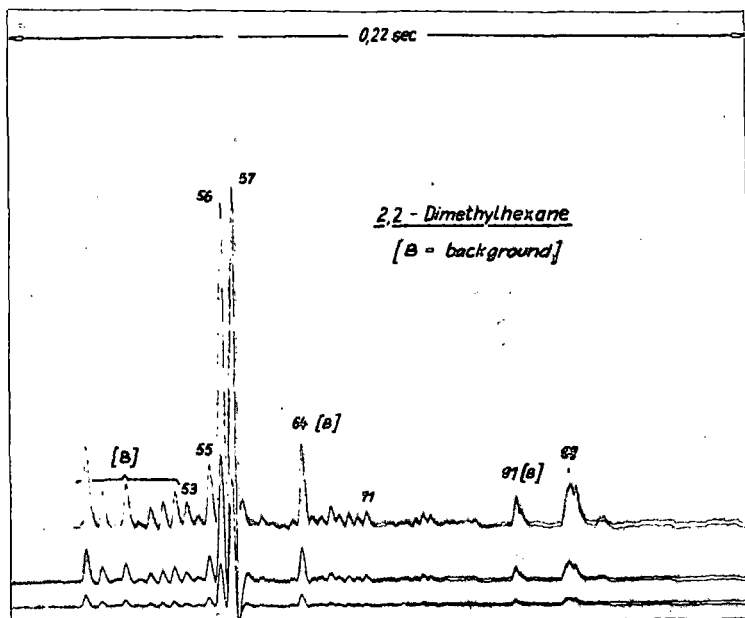


Fig. 4 Spectrum 2,2-Dimethylhexane (Peak No.39 of gas chromatogramm, Fig. 3)

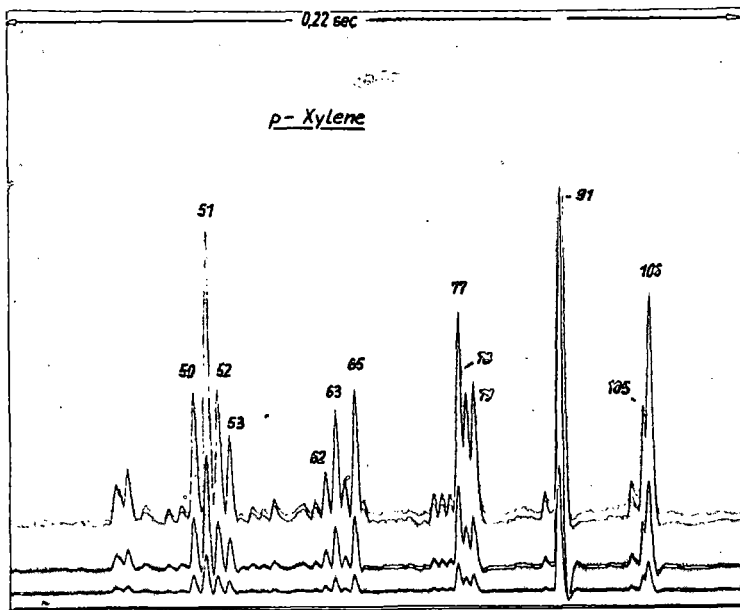


Fig. 5a

Spectrum
p-Xylene
No.4 of
table Fig.6

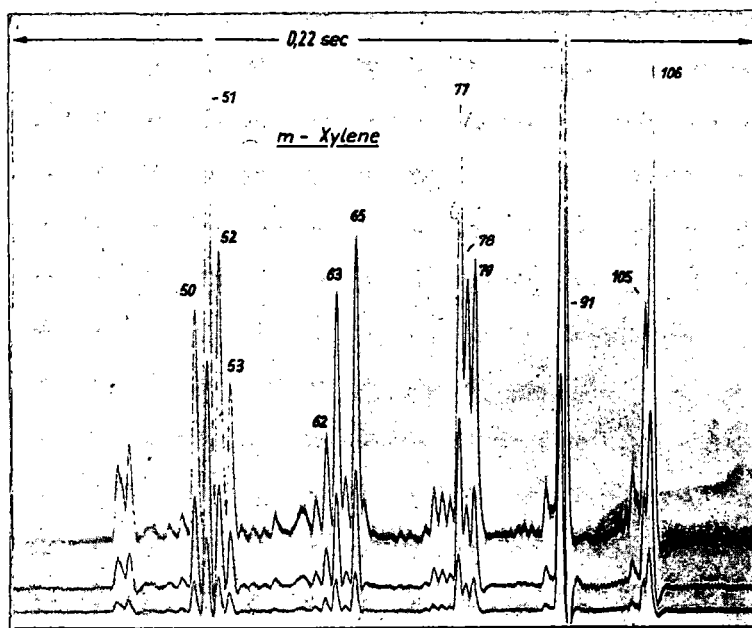


Fig. 5b
Spectrum
m-Xylene
No. 3 of
table Fig. 6

Fig. 5 shows the mass spectra taken of p-Xylene and m-Xylene which were not separated in the gas chromatogram of Fig. 3. The evaluation of these spectra for the ratio $^{152}/^{150}$ is listed in the table of Fig. 6 for 5 different recordings.

Each of the five spectra recorded in 0,22 sec.	1	2	3	4	5	Medium value	API
p-Xylene Ratio of peaks $\frac{52}{50}$	$\frac{29,3}{28,5}=1,03$	$\frac{30,3}{29,8}=1,02$	$\frac{31,5}{30,3}=1,04$	$\frac{31,8}{31,5}=1,01$	$\frac{31,8}{30,1}=1,03$	1,03	$\frac{1,40}{1,02}=1,05$
m-Xylene Ratio of peaks $\frac{52}{50}$	$\frac{73,3}{59,0}=1,24$	$\frac{70,0}{58,3}=1,19$	$\frac{69,0}{55,7}=1,24$	$\frac{69,0}{58,3}=1,18$	$\frac{66,2}{53,0}=1,25$	1,22	$\frac{8,11}{6,24}=1,30$

Fig. 6

2. Measurements with an RPD Ion Source according to Fox and Schiff

For exact AP-measurements an ion source for the Mass Spectrometer CH 4 has been developed and tested with which retarding potential difference measurements can be performed. With an emission current of 250 μ A, an electron current of 6 μ A was measured at the collector. This current was independent from the electron energy down to about 3 volts. A multiplier was used for the measurement of the ions.

Fig. 7 is a schematic outline of the construction of this ion source. Since the impulse periods for electron current and ion current can be chosen independently from each other, it is also possible to measure the lifetime of shortlived ions with the source. The performed measurements had the following result:

- a) With the original arrangement published by Fox, Hickam, Kjeldas and Grove, Rev. Sci. Instr. 26, 1101 (1955) the adjustment of the electron optic proved to be rather critical and not always reproducible. With a somewhat altered arrangement, published on the Joint Conference on Mass Spectrometry in London by Cloutier and Schiff, however, well reproducible ionization efficiency curves could be recorded with a simple ion source alignment. The less favourable result achieved with the arrangement according to Fox can probably be explained by the fact that the critical field of the retarding plate is very easily disturbed by surface charges whereas the space-charge threshold of the arrangement according to Schiff is not subject to such interference.
- b) As has already been observed repeatedly by others the ionization efficiency curves for argon and other rare gases showed breaks. With CO, however, perfectly straight ionization efficiency curves could be taken with our ion source. These curves were very well reproducible. Several times repeated appearance potential measurements on CO coincided within a tolerance of 0,02 volts (Fig. 8).

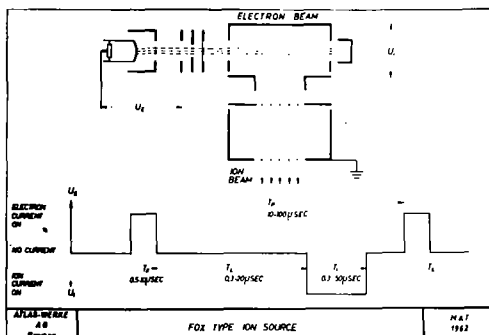


Fig. 7

3. Structure analyses on various alkaloides

Mr. G. Spitteller (Org. Chemical Institute, University of Vienna, Austria) carried out a number of structural investigations on a series of low volatile alkaloides using a CH 4 Mass Spectrometer. As a result of these analyses Fig. 9 shows the mass spectrum and the formula derived therefrom for "Kopsin", an Indian vegetable poison. A detailed description of the measurements and of deliberations with respect to the correct coordinating of the measured ion currents will be published elsewhere.

The samples were vaporized from a small graphite furnace which can be heated under controlled conditions. The graphite furnace is introduced into the ion source by means of the vacuum lock of the CH 4.

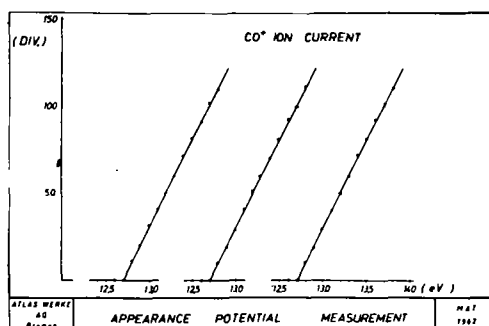


Fig. 8

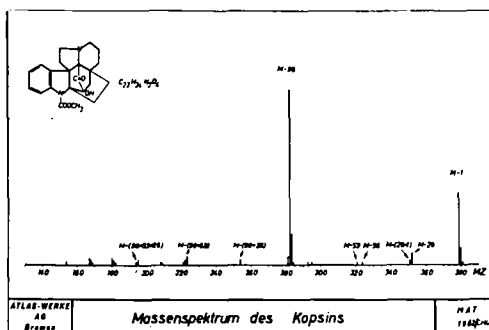


Fig. 9

In Fig. 10 this vacuum lock is shown in a demounted arrangement. A replaceable ionization unit containing the furnace with sample and the ionization chamber can be introduced into the ion source without venting the analyzer. Because the sample enters the ionization chamber directly in vapor phase, an extremely low vapor pressure suffices for taking a spectrum, which is reached by most organic compounds without decomposition. The lowest value to which the temperature of the ion source and like wise the temperature of the vaporization furnace can be set is 150°C.

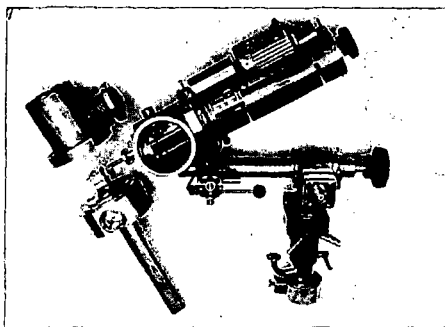


Fig. 10

For measurements of this kind it is desirable to have a high resolving power and to be able to determine the exact masses of unknown ion currents. The latter is possible in the CH 4 with an accuracy of 0,1 % for differences in mass between two peaks. The highest resolution, which can be achieved is demonstrated in Fig. 11. These completely separated peaks represent the ions $C_9H_{20}^+$ and $C_{10}H_{20}^+$ on mass number 128, which have a relative difference in mass of 1/1305. This high resolution was achieved in the Shell Research Institute in Delft (Netherlands) by using slits of 0,01/0,03 mm.

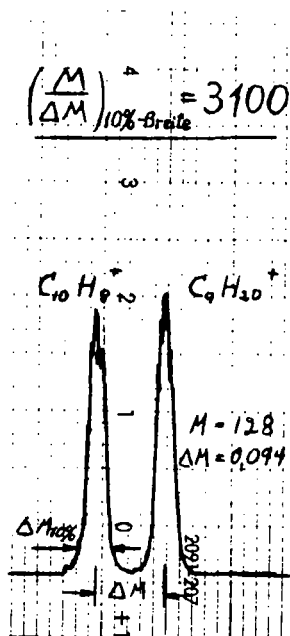


Fig. 11: Maximum Resolution CH 4. Slit Widths 0,01/0,03 mm

APPLICATION OF POLYPHENYL ETHERS AS CONDENSATION PUMP FLUIDS

IN MASS SPECTROMETRY

By

F. C. Maseles

Mass Spectrometry Laboratory

University of Texas

Austin 12, Texas

The exhaust high vacuum system of a large mass spectrometer such as the Consolidated 21-100 series should remain in operation at all times as downtime is usually more costly than pump operation. Until the development of the Penning sorption type high vacuum pumps, most mass spectrometers have used mercury condensation pumps and cascaded dry ice and liquid nitrogen traps with all their attendant evils. Mercury pump fluid possesses some inherent advantages that organic pump fluids quite likely will never surpass. However, mercury's shortcomings in this situation outweigh its advantages.

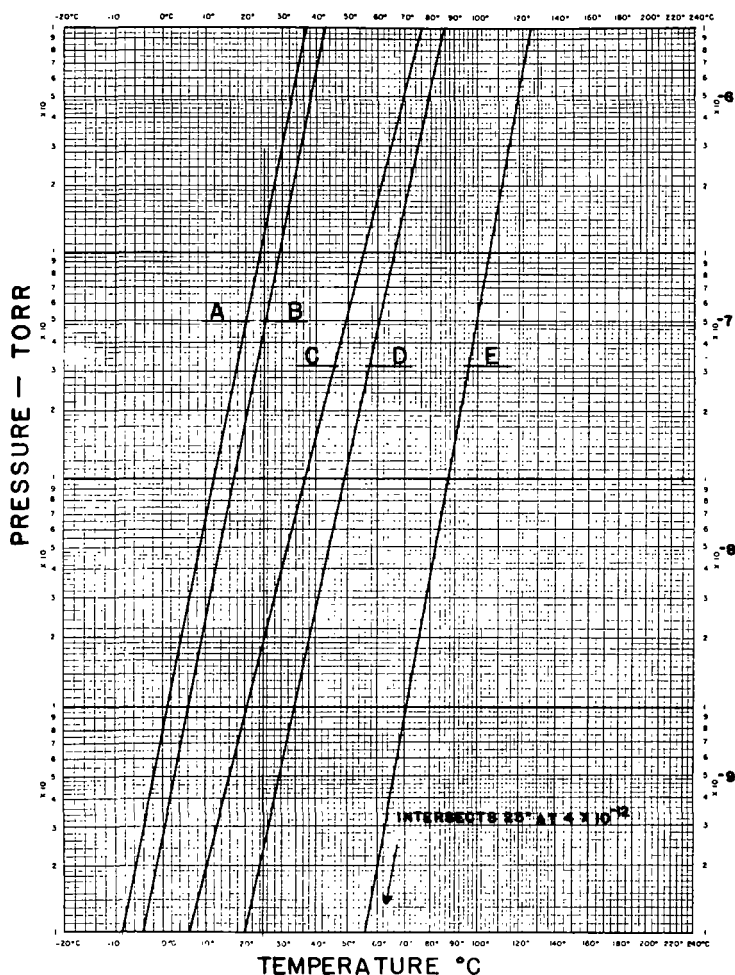
Mercury pumps have been favored for mass spectrometer service, not because oil pumps are incapable of attaining the required low pressure with less elaborate cold trapping, but as long as one must rely on cold traps, cold trap failure on a mercury system is less disastrous than cold trap failure on an oil system. Unlike oils, mercury is not decomposed thermally or chemically with the release of large volumes of volatile decomposition products diffuse into the analyzer and contribute to the background and to the formation of insulating layers in the analyzer that become statically charged and adversely affect the resolution of the instrument. Mercury pumps are cheap; one charge of fluid lasts a lifetime; they are designed to work into a high forepressure lessening the requirement for very high quality forepumps; and, where treated with due respect, constitute little hazard to personnel. Were it not for the requirement of liquid traps to obtain pressures below 10^{-4} torr, one would not be justified in considering the elimination of the mercury pump.

However, a liquid nitrogen trap is required on a mercury system and its apparent pumping speed for C hydrocarbons and some even more readily condensed materials is limited. Maintenance and annoying task and, in spite of the best logistics, the nitrogen supply is too frequently interrupted necessitating shut-down and loss of time.

Introduction of the polypehnyl ethers as condensation pump fluids promises a revolution in vacuum techniques and elimination of liquid nitrogen traps except in the most sophisticated systems.

Qualification as an acceptable pump fluid for mass spectrometer service imposes some very severe requirements on an organic compound. I will dwell briefly on two of these requirements and, for those interested in pursuing the subject further, I recommend Mr. Kenneth Hickman's paper "High Vacuum with the Polyphenyl Ethers", to be published shortly in the Transactions of the American Vacuum Society.

An organic pump fluid should have a vapor pressure below 10^{-8} torr at room temperature and be sufficiently stable that in service its rate of decomposition does not exceed the capacity of the pump to eliminate the volatile decomposition products before they diffuse into the analyzer.



- A. BISIM-PHOXY-PHENYL) ETHER
- B. 2-ETHYL HEXYL SEBACATE (PERRY & WEBBER) - (OCTOIL-S)
- C. BL-10 MIXED FIVE RING ETHERS
- D. M-BISIM-PHOXY-PHOXY) BENZENE
- E. BIS-MIM-PHOXY-PHOXY)PHENYL ETHER (OS 138)

FROM "HIGH VACUUM WITH THE POLYPHENYL ETHERS"
BY K.C. HICKMAN

Fig. 1

Slide #1: Temperature- vapor pressure plot.

This slide, a temperature-vapor pressure plot for several of the polyphenyl ethers and Octoil-S illustrates how the polyphenyl ethers meet the vapor pressure requirement. Because of the extremely large extrapolation used here, ten orders of magnitude in the case of Compound E, there is considerable uncertainty as to the true vapor pressures of these compounds at 25°C; however, if we assume three orders of magnitude as reasonable limits to the uncertainty of this data and combine this with the information that Monsanto Chemical Company, Texas City, operates a mass spectrometer with an oil diffusion pump and double conner chevron baffles cooled to -40 C with Compound B¹⁾, it is not unreasonable to expect Compound E to perform satisfactorily from a vapor pressure standpoint at room temperature.

The second of these criteria is more important and more difficult to determine and, as a first approximation, we distributed information on the polyphenyl ethers around the campus and several of our more venturesome colleagues tested Monsanto OS-138 in their vacuum systems. All tests were made in glass systems, Baird Alphonse structure ion gauges were used to measure pressures. OS 138 performed better than the previously used oils and one man who operates a very clean system for helium purification reported untrapped ultimate pressures in the 10⁻⁹ range. Addition of liquid nitrogen to the traps did not lower this pressure. An unexpected and still not fully explained bonus was an apparent increase in pumping speed as ultimate pressures were attained much more rapidly with OS 138. With this information, we decided to install an untrapped glass pump on our 21-102 and give it a try.

Slide #2: Shot of pump.

This slide shows the present installation and includes a tap-water cooled "D" trap. The first installation was identical except that the trap was not in the line and a VGLA was used in place of the Veeco gauge tube shown here. I will explain why the trap was installed when the next slide is shown. The pump shown here is a two-stage glass fractionating similar to Consolidated's CF20 and was used because it was available. It is backed by a Welch Duo-seal 1400 series. This diffusion pump will eventually be replaced by a three-stage pump of the same type and a magnetically-actuated glass ball isolation valve will be provided to facilitate bakeout of the suction line and trap and to provide overpressure protection for the analyzer. You will notice that the boilers of the pump have been heavily insulated. We have used a coat of high temperature aluminum paint on the glass covered by one inch of asbestos fiber. The operating temperature of OS 138 is about 285°C depending on the forepressure, and adequate insulation is essential in present pumps to attain this temperature without excessive power input to the boilers and to minimize fluctuations with room temperature and drafts. Variac control of the individual boilers is desirable permitting fine adjustment of the power input and operation of the pump in its most efficient range. Oil diffusion pumps are frequently condemned when the real fault is excessive boiler temperature causing decomposition of the oil. The temperature we use is slightly below that temperature at which pumping speed ceases to rise with an increase in boiler temperature and is judged with sufficient accuracy by observing the change in exhaust pressure with boiler temperature while nitrogen is admitted through the sample inlet system. The entire pump is operated at as high a temperature as is possible to facilitate rapid purging of materials of low volatility. The exhaust pressure attained by the untrapped system was below the capacity of the original VGLA vacuum gauge. The background is shown on the next slide.

Slide #3: Spectrum records.

The record marked number one is a typical background of the original installation and except for the peaks shown the record is clean to mass 600.

1) An Oil Diffusion Pump System for Mass Spectrometers, G. L. Roberts, K. Allan Pinkerton, and R. F. Wall, Monsanto Chemical Company, Texas City, Texas.

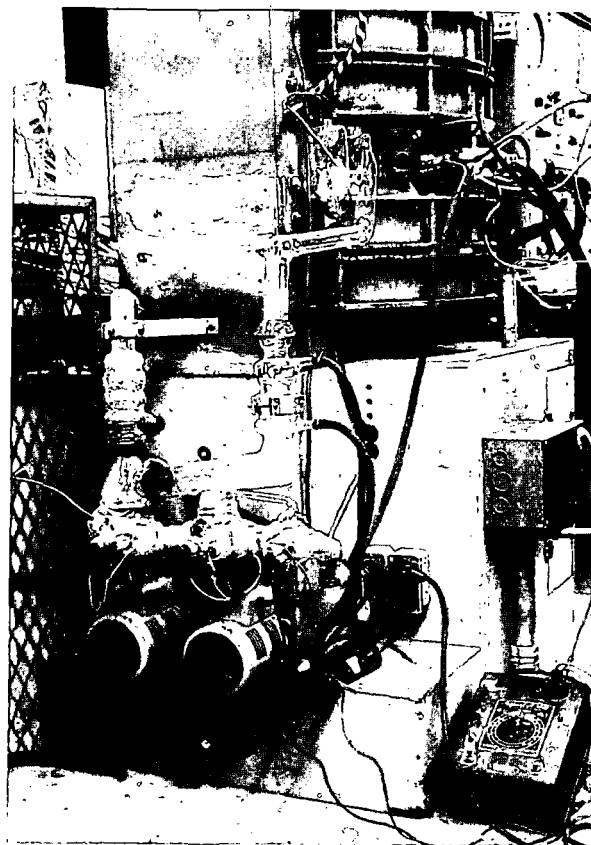


Figure 2

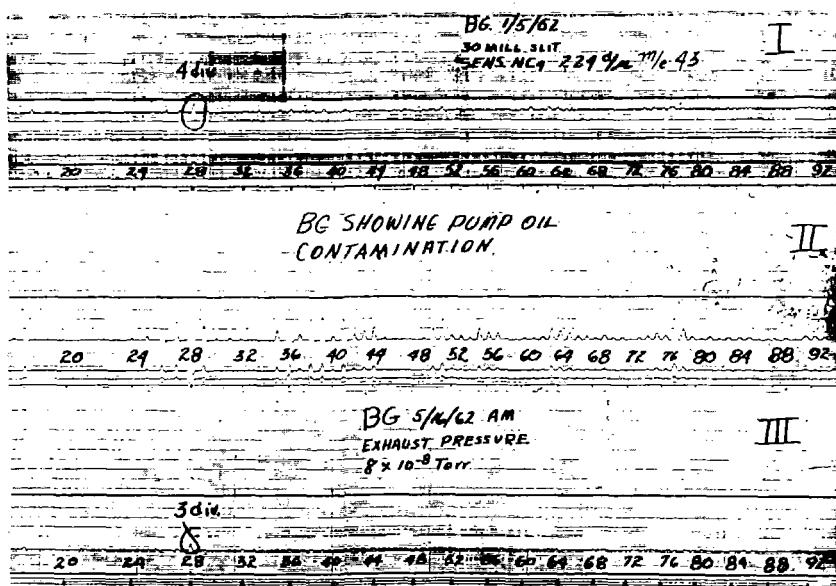


Figure 3

The second record is the type pattern produced by oil backstreaming into the analyzer. The higher mass record shows a few peaks in the 200 and 350 range. The base peak would be 28 as indicated here. We have made no attempt to obtain a mass spectrum of this oil as we are not equipped to properly bake out the inlet system. This record was obtained quite by accident and is the result of leaving the magnet on maximum current over the weekend. Monday morning one could toast bread on the magnet and the pump suction line was hot to the touch. We shut down, cleaned up, installed the trap, the Baird Alhert type gauge, and modified the exhaust vacuum gauge to accommodate the new tube and to extend its range one decade lower to 10^{-7} . A typical background for the present system and the usual exhaust pressure is shown on the third record. We have cooled this trap by filling it with liquid nitrogen and the magnitude of the peaks does not decrease. Filament emission of the new gauge is very sensitive to contamination by a sample so we have no information on the exhaust pressure during a sample run or for half an hour after as it usually takes that long for the gauge to recover; however, all traces of the sample disappear from the record as rapidly as the inlet exhaust system can dispose of the sample. Whereas formerly, with a liquid nitrogen trap, it took from three to five minutes and sometimes longer for all traces of substances such as acetylene and benzene to disappear, pump out time now seldom exceeds one minute.

Needless to say, our liquid nitrogen purchases have dropped to almost zero with a resulting annual saving of approximately \$1500; however, the most gratifying result has been the ability to leave the laboratory overnight or over the weekend without so much as a glance at the filament of the discharge vacuum gauge and speculating about whether one will find it still burning on return.

With our present knowledge and glassblower's time accounted at \$7.00/hr., we can duplicate this entire system for less than \$175.00.

Our use of the 21-620 mass spectrometer is experimental and necessitates frequent opening of the vacuum system to make changes in the analyzer or inlet system. Even when let up with helium, it usually requires 24 hours or more to complete the cycle. In an attempt to shorten this time by elimination of the charcoal trap, we removed the original pump and trap and first replaced it with a water-cooled "D" baffle and an externally heated glass body pump using the jet assembly from the original metal diffusion pump. This system was assembled using Buna S "O" rings coated with OS 138. The pump reduced the pressure to zero on the discharge Penning gauge in two hours, but there remained large peaks at masses 2, 18, 28, and 44. Four days of pumping eliminated the 44 peak but the 28, 18, and 2 peaks were still 40, 80, and 20 divisions respectively. The sensitivity of the instrument at this time was 100 divisions/micron for mass 43 of N-butane. Our first speculation concerning this behavior was that the metal jet assembly was causing catalytic decomposition of our oil, and we have not yet ruled out this possibility. The pump was replaced with a pump similar to the one used on the 21-102. One "O" ring was eliminated in the change. Pump down was again quite rapid and the magnitude of the background peaks were reduced considerably but not to zero. At this time a vessel containing a Buna S "O" ring was opened to the gold leak and the background peaks rose into the thousands range indicating that our background was originating in the "O" rings in spite of their coating of OS 138. The system was again reworked and all but one of the "O" rings were eliminated with a consequent reduction in the background. To eliminate the last ring required machine work not convenient at the time. Vigorous baking of the last remaining "O" ring has reduced the background to less than ten divisions. Sometime in the near future, we will eliminate it also and re-install the glass-metal pump and evaluate pumps that have metal in contact with the oil.

The method we have used for conversion of the 21-620 to this type exhaust system is more difficult and costly than converting the 21-102 as machine work is required and space is limited. The benefits accruing to the usual user are few and, in our opinion, not worth the effort required. In our case, the reduced turnaround time is worth the effort and we will continue to use the system for that reason; and, as we intend to continue our experiments with the polyphenyl ethers, it is a convenient system for that purpose.

Presented at Tenth Annual Meeting of ASTM Committee E-14 on Mass Spectrometry, June 3-June 8, 1962, New Orleans, La.

Simultaneous Measurement of Two Ion Currents by Pulse Counting in a Mass Spectrometer

Leonard A. Dietz
General Electric Company
Knolls Atomic Power Laboratory*
Schenectady, New York

Abstract

Simultaneous measurement by pulse counting two ion beams with a mass separation of $\Delta M/M$ as small as $1/250$ has been accomplished in a 30-in radius double-focusing mass spectrometer of the Dempster type. Positively-charged ions are produced by thermal ionization on a hot filament and are detected by two heavily shielded electrostatic electron multipliers. The disadvantage of multiplier size is overcome by using electrostatic deflecting plates to increase the dispersion between two resolved beams by deflecting each beam in opposite directions from the focal plane of the magnet into its multiplier detector.

Introduction

In certain experiments with low intensity beams of charged particles, it is desirable to detect two or more beams simultaneously in order to improve the precision of comparing small currents. Simultaneous collection of two ion beams was first accomplished in a mass spectrometer used for gas analysis by Nier, Ney, and Inghram.¹ This paper describes a dual pulse counting system for detecting two ion beams which are resolved in a large mass spectrometer. The dual ion beams can be used in special investigations or for precise isotopic analysis. Dual pulse counting has a basic advantage over conventional direct current methods used in measuring the ratio of two small currents, since the instantaneous statistical fluctuations of both beams are summed over time, directly in digital form. This paper is a report of the progress we have made in achieving simultaneous pulse counting at the Knolls Atomic Power Laboratory. A few details of the technique still need to be worked out.

Apparatus

The mass spectrometer used in this investigation is a Dempster type with a 90°, 30-in radius electrostatic analyzer followed by a 180°, 30-in radius magnet. It was constructed by F. A. White,² who first used the magnet to analyze the energies of radioactively-emitted alpha particles.

An all-metal vacuum system has been built to incorporate five 75 liter/sec Varian getter-ion pumps, one on the source chamber, one at each end of the electrostatic analyzer, and two on the magnet chamber. A view of the completed mass spectrometer is shown in Fig. 1. All vacuum joints are copper shear gaskets or are Viton O-rings of 1/8-in cross sectional diameter. The source chamber is machined from a single block of stainless steel and the electrostatic analyzer vacuum chamber is bent from a 5-in diam stainless steel seamless tube with an end flange welded on each end. Each end of the electrostatic analyzer rests on an accurately positioned ball bearing and the middle is supported by a rod which can be raised or lowered by means of a bellows-sealed micrometer drive. This technique was developed by Nier³ and has proved very useful in the alignment of our optics. The electrostatic

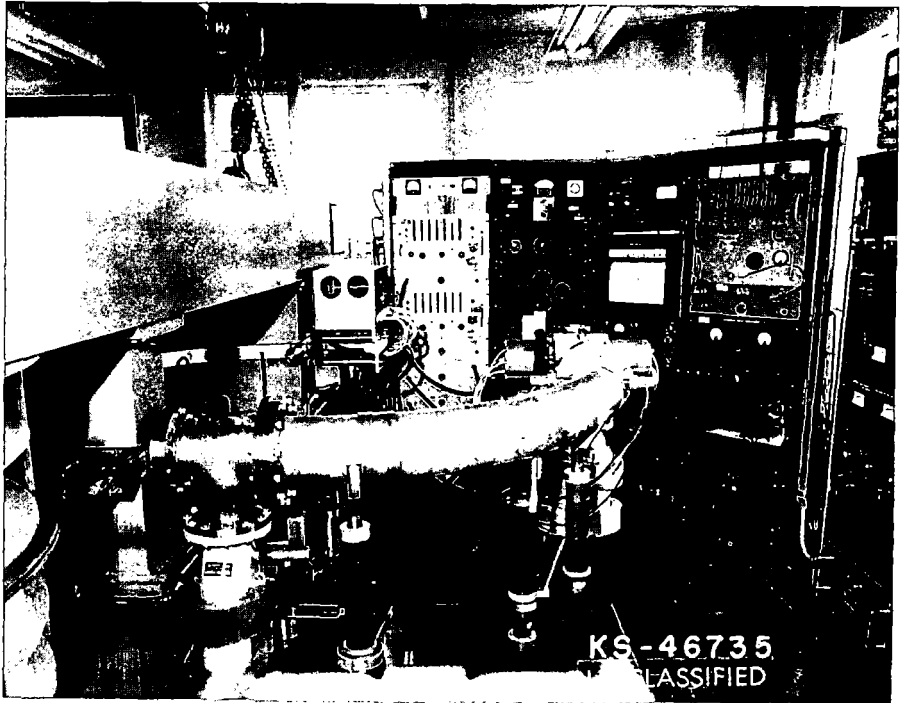
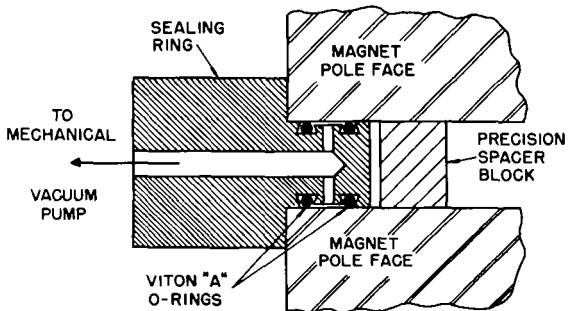


Fig. 1

UNCLASSIFIED



KS- 46892
UNCLASSIFIED

Fig. 2

analyzer plates are mounted between two flat electrically grounded sectors by means of accurately ground pyrex spheres, after the method of Berry.⁴ The magnet pole faces are sealed from atmosphere by two sets of Viton O-rings in a stainless steel ring which extends 1-in inside the entire periphery of the pole faces. Two O-rings are positioned concentrically in dovetailed grooves cut in the top surface of the sealing ring and are in contact with the top pole face and the sealing ring. Two more O-rings are positioned similarly in the bottom surface of the sealing ring. Each of the four O-rings is about 16-in in circumference. Beam access holes on the median plane of the magnet are cut through the ring, between the two pairs of O-rings. The space between each set of O-rings is evacuated to a few microns pressure by a mechanical pump as shown in Fig. 2. Pressures in the unbaked electrostatic and magnetic analyzer portions of the mass spectrometer are less than 1×10^{-8} and approximately 4×10^{-8} Torr, respectively. The higher pressure in the magnet chamber appears to be limited primarily by the vapor pressure of Viton. Differential pumping reduces the contribution of source chamber pressure to the analyzer pressure by a factor of 100. The source chamber contains a small liquid nitrogen cold trap. It is the only cold trap in the entire high vacuum system.

A "ferris wheel" type of sample loader⁵ mounts 6 V-type filaments⁶ and permits 6 samples to be analyzed without breaking vacuum. The sample loader is shown in Fig. 3. It is mounted on a KAPL-type ion gun with z focus.⁷

The dual pulse counting arrangement is shown schematically in Fig. 4. Each beam is deflected from a point slightly beyond the focal plane of the magnet, into its electron multiplier detector, by means of electrostatic deflecting plates. The shape of the electric field between the deflecting plates was optimized by field plotting and ray tracing. The beam deflectors are not shielded from the fringe field of the magnet. The output of each multiplier is fed into a 10-Mc counting system, i.e. the resolving time of the system is 0.1 microsecond. Except for starting and stopping gating pulses, the two counting systems operate independently of each other.

Other types of detectors were considered, i.e. solid state crystal counters and semiconductor magnetic multipliers, but at the time the dual counting system was designed, data were lacking on their response to random counting rates of several megacycles. Therefore, we decided to use a small 14-stage electrostatic electron multiplier and counting system which we are using in the detection of single beams.⁷

Magnetic shielding by means of a hollow circular iron cylinder reduces the stray magnetic field in the region of the electron paths through a multiplier by a factor of about 10^4 . The magnetic shielding of each detector extends approximately 2-in beyond either end of the dynode structure. We have found this type of simple shield far more effective than many layers of high permeability foil or an iron shield of rectangular cross section. For an isotopic analysis, the separation between the center lines of each pair of beam deflector plates is adjusted by means of micrometer drives to equal the dispersion between the two beams for isotopes of masses M_1 and M_2 . Also, the deflection voltages, $\pm V_1$ and $\pm V_2$, are adjusted independently to give maximum counting rate from each electron multiplier. The deflection voltages are obtained from voltage dividers connected across the positive and negative voltages supplied to the electrostatic analyzer.

Experimental Results

For precise ratio determinations, the ratio response must be independent of small fluctuations in magnetic field intensity and accelerating voltage, and in small errors in dial settings. By adjusting the width of the defining

UNCLASSIFIED

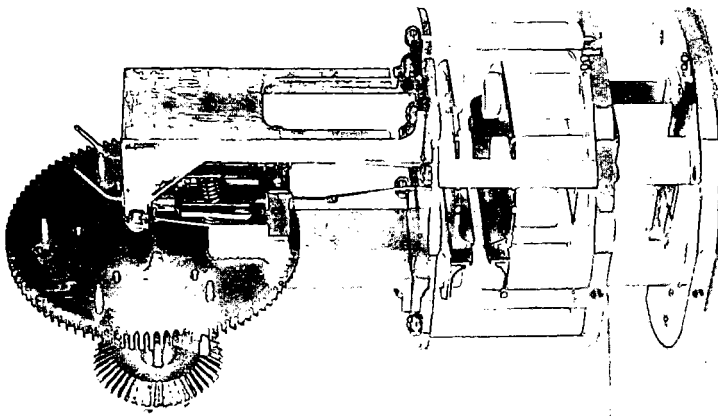


Fig. 3

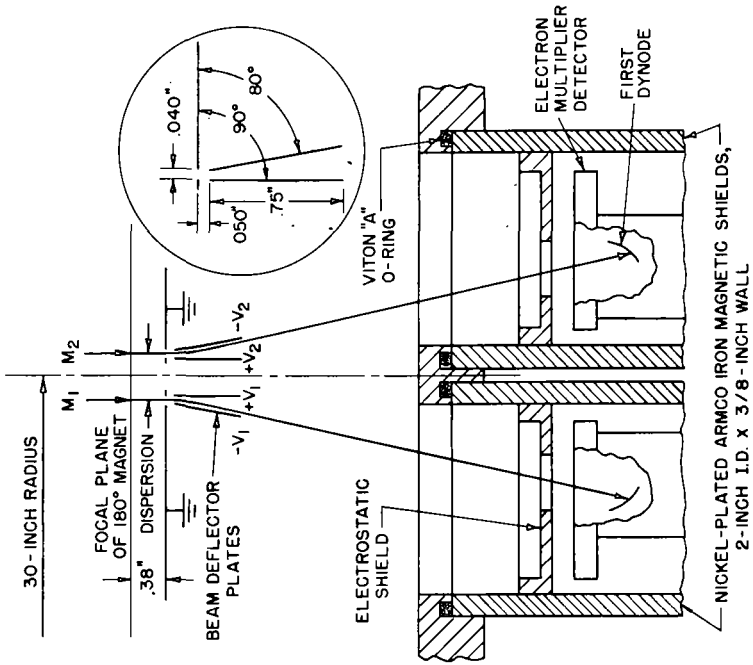


Fig. 4

KS-46893
UNCLASSIFIED

slit at the entrance to the 180° magnet, the beam width at the magnet focal plane can be made much narrower than the smallest separation of the beam deflector plates (0.040-in), so that none of the beam is intercepted by these plates. The ratio response as a function of changes in the accelerating voltage is shown in Fig. 5. That is, both beams are translated simultaneously, stepwise across the beam deflector defining slits. Voltages and focusing conditions for each multiplier were the same. Notice that the value of the observed ratio drops in going from curve B to curve C, even though the ion gun was not refocused. This results from changing the illuminating current density distribution over the sensitive areas of each of the first dynodes. We find that the ratio response is different for different filaments or for different focusing conditions with the same filament. For example, we find no plateau when both beams are deflected along the z (vertical) axes of both first dynodes. Therefore, it appears that the dual pulse-counting technique presented here is limited at this time to comparison measurements only, and cannot be used for absolute abundance measurements.

In applying dual pulse counting to precise isotopic abundance measurements, we have found that alternately measuring a sample and a standard, both on different filaments, does not give the desired precision. As was just mentioned, this is due to the non-uniform sensitivity of the electron multiplier over the length of a dynode. It appears that an ion which strikes the middle of the first dynode has a higher probability of producing a detectable pulse than one striking at either end. For instance, the distribution of ions in the z (vertical) direction is large enough so that ions can strike the first dynode of the RCA electron multiplier at a point only 1/8-in from either end. We believe this can be corrected by proper baffling and multiplier design. However, this limitation currently restricts our application of simultaneous pulse counting to certain measurements which can be accomplished with a newly developed internal standard technique.⁸ In addition to applying this promising new technique to our two-stage instruments, we are currently engaged in extending it to simultaneous collection.

Acknowledgment

It is a pleasure to acknowledge the contributions of the following people: J. W. Owens, F. A. Emmer, C. T. DeGroat, J. H. Thomas, and J. E. Demers during the design and fabrication of parts; L. R. Hanrahan and G. A. Land during the assembly and test of the mass spectrometer; and A. E. Cameron for supplying us parts for the sample loader.

REFERENCES

* The Knolls Atomic Power Laboratory is operated by the General Electric Company for the United States Atomic Energy Commission.

1. A. O. Nier, E. P. Ney, and M. G. Inghram, *Rev. Sci. Instr.* **18**, 294 (1947).
2. F. A. White, F. M. Rourke, J. C. Sheffield, R. P. Schuman, and J. R. Huizenga, *Phys. Rev.* **109**, 437 (1956).
3. A. O. Nier, private communication.
4. O. E. Berry in U. S. Nat'l. Bureau of Stds. Circular 522 (U. S. Govt. Printing Office, 1953), pp. 267-268. Also see L. A. Dietz, *Rev. Sci. Instr.* **32**, 859 (1961).
5. The sample loader was designed by A. E. Cameron's mass spectrometry group at the Oak Ridge National Laboratory, Oak Ridge, Tennessee.
6. L. A. Dietz, *Rev. Sci. Instr.* **30**, 235 (1959).
7. L. A. Dietz, O. F. Pachucki, J. C. Sheffield, A. B. Hance, and L. R. Hanrahan, *Anal. Chem.* **32**, 1276 (1960).
8. L. A. Dietz, O. F. Pachucki, and G. A. Land, *Anal. Chem.* **34**, 709 (1962).

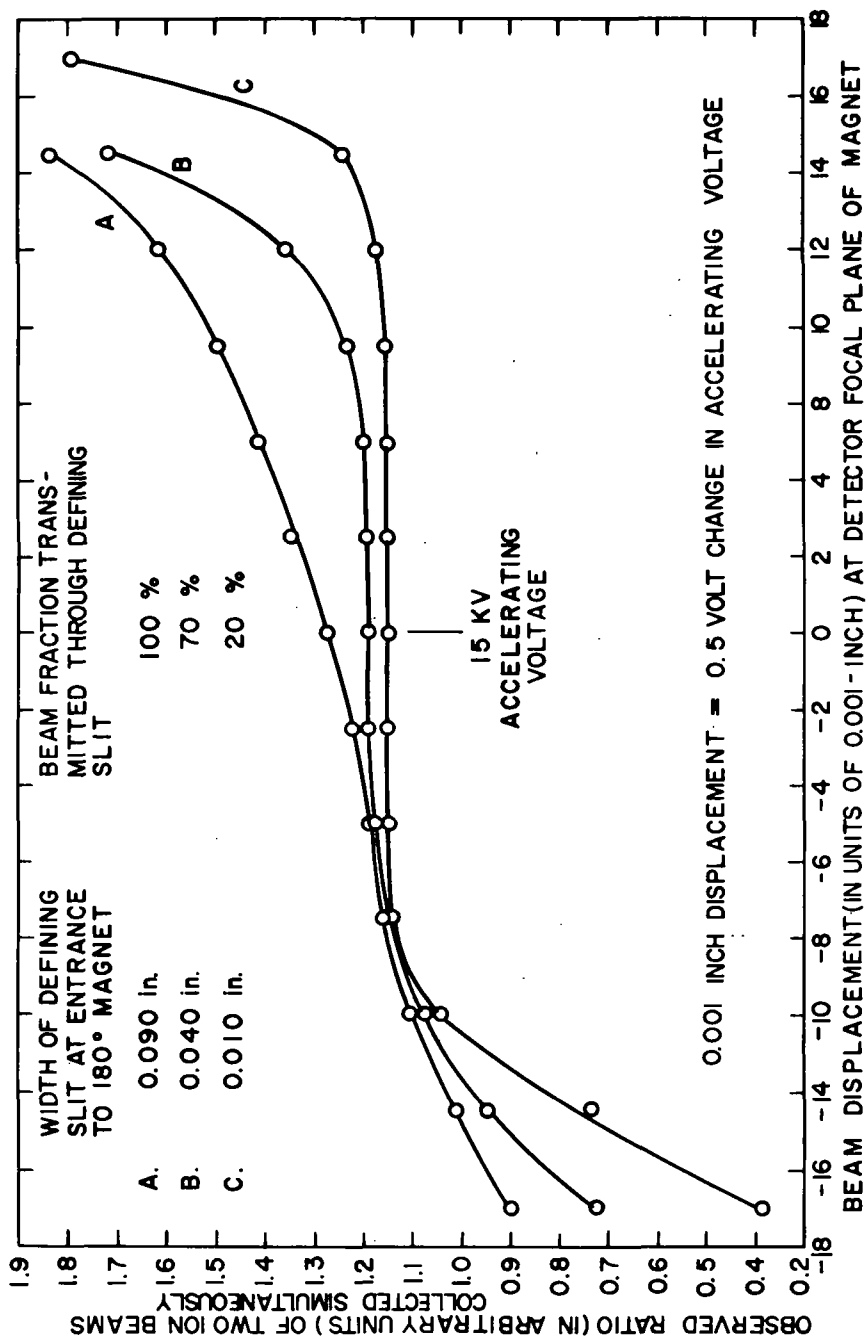


Fig. 5

KS-46891
UNCLASSIFIED

DISPLAY SYSTEM FOR RECORDING RAPID

CHANGES IN GAS COMPOSITION

B. R. F. Kendall

Nuclide Analysis Associates
State College, Penna.

INTRODUCTION

During the past few years, increased attention has been given to the development of fast-scanning mass spectrometers. Many of these instruments are capable of supplying thousands of complete mass spectra during the course of gas reactions lasting for small fractions of a second. In order to record such rapid changes in gas composition, particularly when these changes involve several different gases, special output circuits and display systems are required.

Where all of the information appearing at the output of a fast-scanning mass spectrometer must be recorded, a rotating drum camera can be used¹. Successive spectra are displaced vertically, so that peak heights must be measured and replotted before a detailed study can be made of peak height variations as functions of time.

If changes in the amplitude of a single mass peak are to be recorded, a system described by Damoth² can be used. The mass peak is displayed on an oscilloscope screen and caused to move steadily across the screen in a direction parallel to its baseline. The envelope of such a display indicates variations of peak height with time.

Changes in the amplitudes of particular mass peaks can also be recorded using multi-channel systems. Some of these have been described by Fowler and Hugh-Jones³, Harrington⁴, and Stallard⁵. Systems of this kind are restricted to use at a limited number of preselected mass positions.

Another method of recording changing spectra has been suggested by Levine⁶, as an extension of the usefulness of the linear intensity-modulated oscilloscope display mentioned in a previous paper⁷ by the present author. In this type of display, the positions and brightness of spots along a straight line give the mass numbers and qualitative indications of the peak amplitudes. If this display is moved in a direction at right angles to its length at a suitable rate, peak amplitude changes are seen as intensity variations in the moving spots representing each ionic species. The method is sensitive and makes it possible to record a large amount of information on a single photograph. A disadvantage is the difficulty of obtaining quantitative indications of peak amplitudes from the density-modulated negatives.

This paper describes a new type of display system, developed in the course of a general study of methods of extracting, processing, and displaying data obtained from spectral instruments. The system transforms information contained in repeatedly swept mass spectra directly into simultaneous peak height versus time traces for all peaks in the spectrum. The baselines of these traces are positioned on the vertical axis of the display in such a way as to identify the corresponding mass numbers. The display is normally presented on an oscilloscope screen and can easily be recorded on a single photograph.

PRINCIPLE OF OPERATION

The new system gives a quantitative display of both mass and peak height information along the vertical axis of the oscilloscope screen. The horizontal axis is used as the time axis. Intensity modulation is used to make visible the separate peak height versus time traces for each mass.

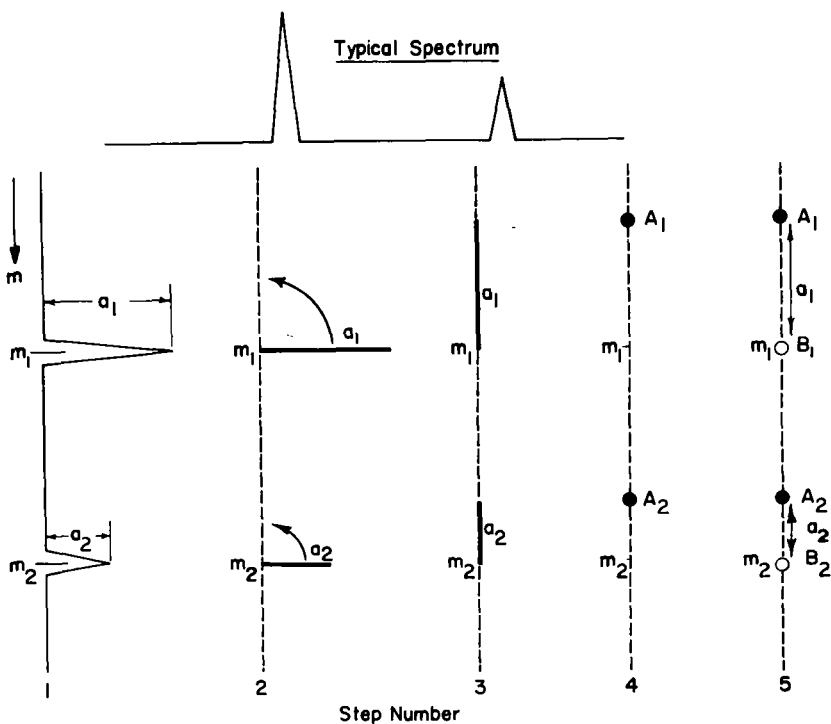


Fig. 1. Example of conversion of two-dimensional spectrum to vertical one-dimensional display.

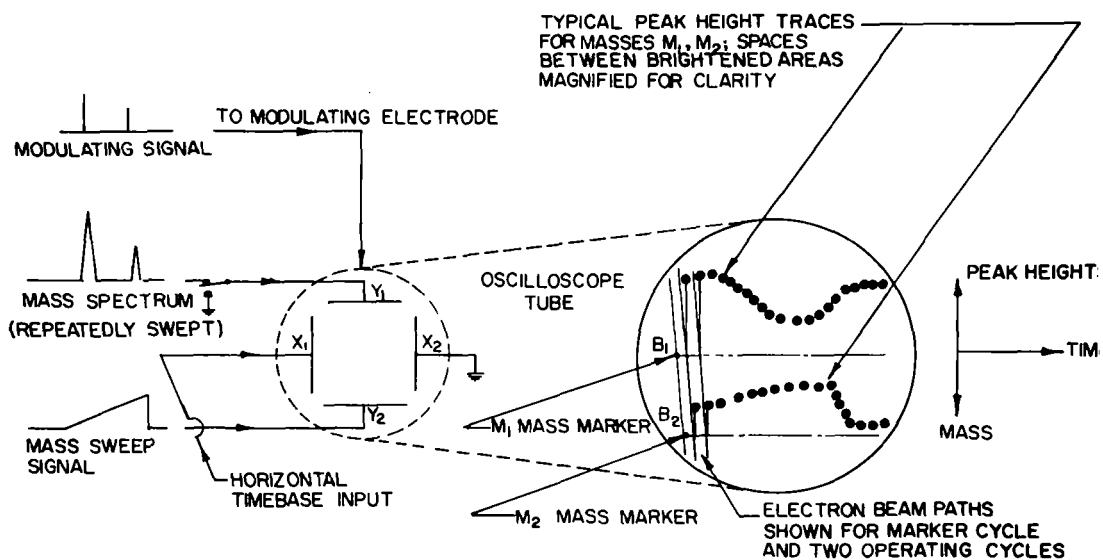


Fig. 2. Principle of display system.

The manner in which mass and amplitude data can be displayed quantitatively along a vertical axis can be explained by reference to Figure 1. A typical two-dimensional mass spectrum is shown at the top of Figure 1. This can be displayed as in Step 1, with mass plotted vertically. In general only the masses m_1 , m_2 and the amplitudes a_1 , a_2 of the peaks will be required; the spectrum can therefore be displayed as in Step 2, without loss of useful information. The idealized mass peaks can be folded along the vertical axis, as in Step 3, without loss of information provided they do not overlap. To allow for peak height indications even in the event of overlapping, the folded idealized peaks can be replaced by markers A_1 , A_2 indicating the positions of the peak tops, as in Step 4. Fluctuations in the peak amplitudes a_1 , a_2 are then represented by corresponding movements of A_1 and A_2 . By reducing the amplitudes of the idealized peaks instantaneously to zero as in Step 5, A_1 and A_2 can be brought to the baseline positions B_1 and B_2 . These positions respectively indicate the mass numbers m_1 and m_2 on the mass scale and the datum positions from which the corresponding peak amplitudes are to be measured.

The simplest of several possible practical arrangements is shown in Figure 2. The mass spectrum (a plot of ion current versus time) is applied to the vertical deflection plate Y_1 via a two-position switch which provides for grounding Y_1 so that the baselines can be marked. The signal representing collected mass number as a function of time is applied to the other vertical deflection plate Y_2 . A modulating signal, proportional to the second differential of the peak amplitude with respect to time, is applied to a suitable modulating electrode in the cathode-ray tube. A normal time-base signal is applied between the horizontal deflection plates X_1 and X_2 .

Suppose the system is put into operation with Y_1 grounded so that the base lines can be marked. The oscilloscope electron beam is set at an intensity too low for it to be visible. The beam is swept downwards by the sawtooth voltage representing the mass sweep of the mass spectrometer. Whenever a mass peak passes through a maximum the trace brightens, giving the two markers B_1 and B_2 which identify the masses and indicate the baseline levels from which peak heights are to be measured.

Suppose that Y_1 is then reconnected to the signal representing the mass spectrum. The oscilloscope electron beam is again swept downwards by the sawtooth voltage, but superimposed on this steady sweep are rapid upward deflections which occur whenever a mass peak is registered by the ion detector. The amplitude of each upward deflection is proportional to the height of the corresponding mass peak. At the limit of each upward deflection the spot is brightened so that it becomes visible. The horizontal time-base voltage is simultaneously deflecting the moving electron beam slowly across the screen so that simultaneous peak height versus time traces are obtained for each peak.

EXPERIMENTAL EQUIPMENT

The prototype display system was developed for use with a special time-of-flight mass spectrometer operating at sweep repetition frequencies of 25-50 Kc. The equipment was intended for use in studying gas evolution processes lasting for times as short as a few milliseconds.

A block diagram of the experimental system is shown in Figure 3. The mass spectrum signal is applied to the Y_1 plate of the oscilloscope tube through a delay line. The press-button switch $Sw 1$ makes it possible to suppress the peak height indications so that the baselines of the peak height versus time traces can be determined. The second differential of the mass spectrum signal, after amplification with phase inversion and removal of negative components of the waveform, is applied to the cathode of the oscilloscope tube. The delay line is adjusted to cancel the delay introduced by the modulating amplifier. A sawtooth voltage representing the mass sweep is applied through an attenuator so that the mass scale of the display can be varied. A

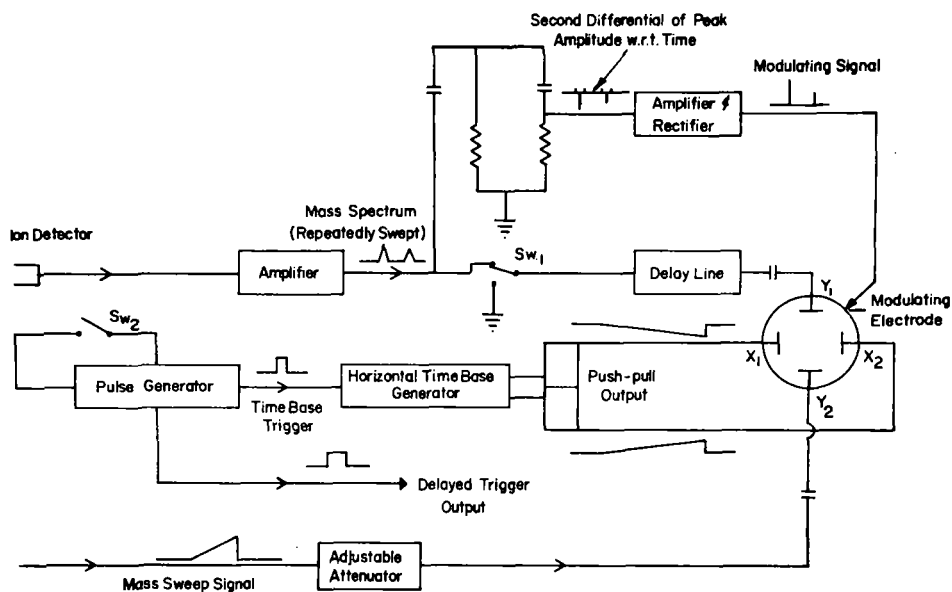


Fig. 3. Block diagram of experimental display system.

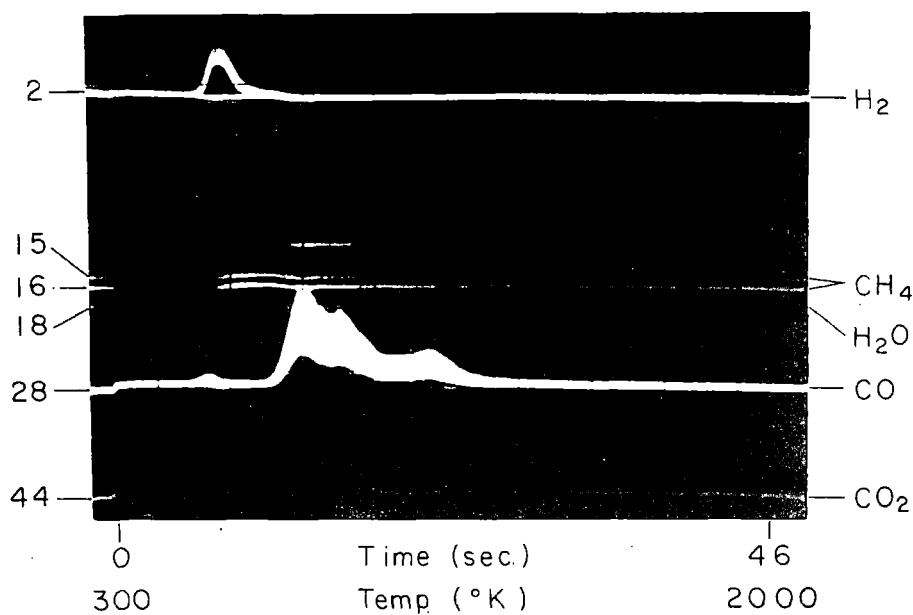


Fig. 4. Changes in gas composition during desorption from tungsten filament. Adsorption time: 4 hours at residual gas pressure of 1.6×10^{-8} torr.

simple pulse generator controlled by the switch Sw 2 triggers a standard oscilloscope time-base circuit and supplies a second triggering pulse at a preselected time thereafter to initiate the phenomenon to be studied.

RESULTS OBTAINED WITH EXPERIMENTAL DISPLAY SYSTEM

A typical photographic record is shown in Figure 4. This shows variations in the partial pressures of gases desorbed from a tungsten filament during heating from 300°K to 2000°K at 38°C/sec. Adsorption time was four hours at a total residual gas pressure of 1.8×10^{-9} torr. The baseline markers down the left side of the photograph identify the gases present and indicate the levels from which the corresponding peak heights are to be measured. The steps following the baseline markers indicate the partial pressures of the residual gases, the major contributions being from hydrogen and carbon monoxide. Smaller amounts of carbon dioxide and methane are also present. The single hydrogen and complex carbon monoxide desorption peaks are clearly indicated. The largest vertical deflection of the carbon monoxide trace corresponds to a partial pressure of approximately 10^{-8} torr. Traces of methane and nitrogen can be detected at approximately 700°K and 1200°K, respectively.

The limited bandwidth of the circuits used to amplify the modulating signal caused some filling-in of the desorption peak contours. This does not affect the accuracy of partial pressure indications, which are measured from the upper edges of the peak contours. It does, however, make it more difficult to interpret traces which cross or overlap. Production versions of the display system will be available with a special nonlinear pulse amplifier in the modulating circuit in order to avoid this effect.

Figure 5 shows a set of results taken under the same conditions as Figure 4, except that the adsorption times were varied from 1 minute in trace 1 to 24 hours in trace 11. The changes in shape and amplitude of the hydrogen and carbon monoxide peaks for different adsorption times (and hence surface coverage) are in general accordance with results obtained by other investigators using pure hydrogen and carbon monoxide in separate experiments.

The experimental display system has also been used to study gas evolution from heated metallic surfaces, cleanup of gases from glass during exposure to intense light, evolution and pumping of gases during flashing of titanium getters, and desorption of adsorbed carbon dioxide from tungsten. The latter experiments showed that carbon monoxide was the only gas desorbed as a result of heating a tungsten filament on which carbon dioxide had been adsorbed. The carbon monoxide desorption spectrum was almost identical with that obtained in experiments in which pure carbon monoxide was adsorbed, except for a very small additional desorption peak between 350°K and 400°K.

Figure 6 shows a record of gas evolution from Pyrex as a result of irradiation for 1 millisecond by a 10^3 watt Xenon lamp. The record was traced from the original photograph because some of the details were too faint for satisfactory reproduction. The glass was in the form of a side tube with a 7cm. line-of-sight path into the ionizing region of the time-of-flight mass spectrometer.

Before the flash, the baseline positions were marked in the usual way. The background gas pressure was 10^{-9} torr, consisting almost entirely of hydrogen, carbon monoxide and a smaller amount of carbon dioxide.

The timebase was then triggered and the flash tube fired at time zero. Maximum flash intensity occurred at the point marked x on the time scale. The rapid increase in hydrogen and carbon monoxide partial pressures is clearly shown. Further experiments with the equipment adjusted for a higher mass range showed that a smaller amount of carbon dioxide (indicated by the dotted line in Figure 6) was also evolved. Each of the three traces reached a maximum after about 1 to 3 milliseconds, the effective time constants increasing with molecular weight.

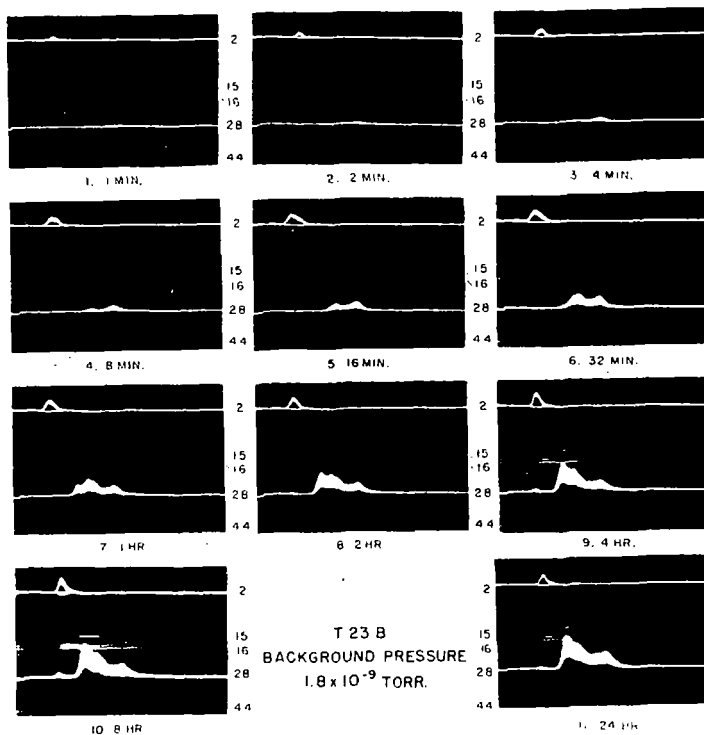


Fig. 5: Set of desorption records for adsorption times ranging from 1 min. to 24 hrs. Other conditions as for Fig. 4.

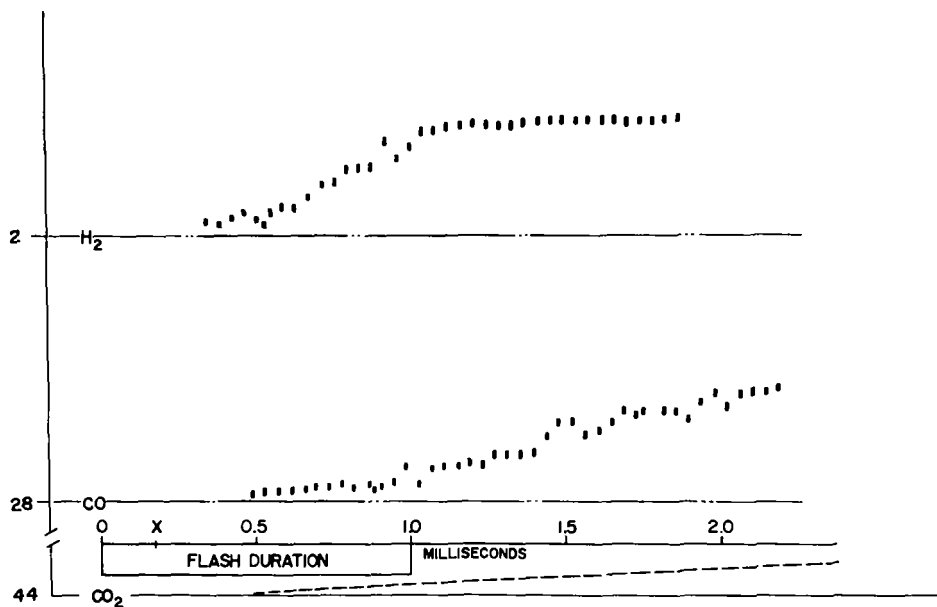


Fig. 6. Desorption of H_2 , CO and CO_2 from glass during exposure to 10^5 watt, 1 millisecond light pulse from Xenon flash tube.

These pressure transients then fell with time constants of several tens of milliseconds as the evolved gases were pumped away. Allowing for the time taken for evolved gases to reach equilibrium in the ionizing region, it appears likely that desorption occurred only during the flash for each of the three gases.

Similar experiments with helium, methane, water vapor and argon present in small quantities in the background gas showed a barely detectable photodesorption of methane, and no detectable photodesorption of the other gases.

The photodesorption effects were found to be reversible if clean glass surfaces were used. After 12 flashes, each lasting one millisecond, the amount of gas desorbed at each flash had fallen by an order of magnitude. After 5 to 10 minutes without flashing, the amount of gas desorbed at the next flash was close to the original value.

DISCUSSION

Results obtained with the display system show that it offers a simple and convenient way of displaying and recording rapidly changing mass spectra. Although the existing equipment was designed for use at the very high sweep frequencies characteristic of time-of-flight mass spectrometers, the principle is equally applicable to other types of mass spectrometers which can be adjusted so that the peak tops are narrow and well-defined.

An important advantage of the display system over a conventional multichannel output system, apart from relative simplicity, is the ability to register peak amplitude changes throughout the mass range instead of only at a limited number of preselected mass positions. There is therefore no possibility of failing to record unexpected but possibly significant changes in the mass spectrum.

The main applications of the system appear to lie in the study of fast gas reactions, such as flash photodesorption, photochemical reactions, and flash thermal desorption. The method is also likely to be useful for studying slower but much more complex reactions, the detailed courses of which would be very tedious to follow by conventional means.

REFERENCES

1. Kistiakowsky, G.B., and Kydd, P.H., J. Amer. Chem. Soc. 79 4825 (1957)
2. Damoth, D.C., paper presented at Eighth Annual Meeting on Mass Spectrometry of A.S.T.M. Committee E-14, Atlantic City, New Jersey (1960)
3. Fowler, K.T., and Hugh-Jones, P., Brit. Med. J., 1 1205 (1957)
4. Harrington, D.B., Encyclopedia of Spectroscopy (C.F. Clark, ED.) p.628 (Reinhold, N.Y. 1960)
5. Stallard, M.J.H., paper presented at Third International Conference on Medical Electronics, London (1960)
6. Levine, L.P., (Honeywell Research Center, Hopkins, Minn.) Private Communication (1961)
7. Kendall, B.R.F., Proceedings of Ninth Annual A.S.T.M. E-14 Meeting on Mass Spectrometry, 1961, p.158 (Published 1962)

MODIFICATIONS TO THE INLET AND RECORDING SYSTEMS OF A C.E.C. 21-103C MASS SPECTROMETER TO ENABLE DIRECT GAS INTRODUCTION FOR DYNAMIC EVOLUTION STUDIES by J. D. Reynolds and P. C. Green. General Dynamics/Fort Worth, A Division of General Dynamics Corporation.

ABSTRACT

The glass inlet system of a Consolidated Electrodynamics Corporation 21-103C Mass Spectrometer was modified to accommodate alternately the direct introduction of evolved gases into the ionizing region or conventional sample analyses utilizing the standard molecular leak.

Relationships between peak height and flow rate through the ionizing region have been established experimentally in order to correlate peak height data with evolution rates from a dynamic system.

An oscillograph recorder drive speed control was designed and installed to facilitate continuous scanning over long periods of time without prohibitive paper usage. Paper feed rates of one, two, four, and eight inches per minute are available.

This work was performed under United States Air Force Contract 33(600)-38946.

INTRODUCTION

Expanding the useful range of mass spectrometric analysis has opened many fields of investigation. Several modifications to allow direct introduction of samples into the ionizing region appear in the literature⁽¹⁾. The modifications described in this study permit the convenient use of the instrument in part-time conjunction with a dynamic gas evolution cell.

Gases may be analyzed quantitatively and qualitatively as they are generated from a sample excited by thermal, electrical, or radiation energy.

The variable speed control on the recorder drive motor opens possibilities of uninterrupted tracings of single m/e evolutions and of spectrum scans compressed to optimum length.

INLET SYSTEM MODIFICATIONS

The modifications incorporated into the glass inlet system of a Consolidated Electrodynamics Corporation 21-103C Mass Spectrometer have wide applicability to dynamic gas evolution studies such as thermal degradation and pyrolysis product analysis. These alterations offer the obvious advantages of being able to take an analytical look at a system at any phase of a reaction in that system without interrupting the progress of the reaction.

At General Dynamics/Fort Worth the apparatus was used to dynamically introduce gases evolved from irradiated polyethylene into the ionizing region of the mass spectrometer, thus allowing the first real look at primary decomposition of the polymer in a radiation field⁽²⁾. The irradiation cell used is shown in Figure 1.

A thermal bath was incorporated in the cell to maintain controlled temperatures during irradiation. A second cold trap between the reaction cell and the mass spectrometer may be used with various thermostat fluids to fractionally freeze out high molecular weight species, thus aiding the analysis of lower molecular weight components of the evolved gases.

Gases evolved from the cell are pumped into the ionizing region through a three-way high-vacuum hollow plug stopcock allowing the reaction cell to be evacuated through the sample inlet cabinet vacuum system or pumped into the isatron. The gold leak is bypassed by means of another high-vacuum hollow stopper stopcock.

Initially, a six-inch section of one-inch O.D. half-inch I.D. Tygon was inserted between the reaction cell and the mass spectrometer to give structural flexibility to the system. A very high rate of water evolution at reduced pressures necessitated the removal of this link and illustrated the advantages of the all-glass system which may be flame degassed.

The stopcocks are lubricated with Dow Corning 11 Compound Silicone High Vacuum Lubricant. After in-place bakeout, the system exhibited a low background entirely suitable for precise measurements.

This configuration allows normal sample introduction through the inlet cabinet and gold leak or direct introduction of evolved gases into

the isatron with or without the molecular leak. The micromanometer may also be fed directly from the reaction cell to check evolution volumes.

INSTRUMENT CALIBRATION

In order to quantitatively correlate data from the gas evolution cell the peak height to molecular flow rate ratio must be established.

The relationship between pressure in the inlet volume as measured by the micromanometer and the observed peak height was determined for hydrogen, methane, ethane, ethylene, propane, and normal butane.

Next, the leak rate was calculated as the change of pressure in the inlet system versus time as the gas escapes through the molecular leak(3).

The exact volume of the system was obtained from C.E.C. furnished inlet block prints and physical measurements of the additional glassware. Using the established gas flow rate out of a known volume at a measured pressure and the peak height associated with this pressure, the number of molecules per unit time flowing through the isatron can readily be correlated with the observed peak height.

In plotting chamber pressure in microns versus the net peak height of various calibrating gases, a slope of 1.02 to 1.14 was observed in all cases. The curves for hydrogen, methane, ethylene, and propane are shown in Figure 2. This variation appears to be real and not a function of micromanometer zero drift, as drift corrections were applied to all curves.

American Petroleum Institute Mass Spectral Data(4) normalized with known normal butane furnished sensitivities and cracking patterns of other gases of interest not available.

RECORDER DRIVE SPEED CONTROL

In observing gas evolutions over long periods of time, the benefits of providing calibrated and synchronized speed reductions in oscillograph recorder chart drive of the mass spectrometer became evident. One of the foremost advantages is that of extending the recording time so that data from protracted tests can be preserved without the necessity of interrupting the procedure for the replenishment of chart paper. Additionally, optimum time scales can be chosen to suit the particular requirement, arranging the data for easy identification of peaks and for convenient comparison. Finally, the time scale compression made recordings with physical sizes which are convenient for reproduction and incorporation into reports.

The use of gear changing to reduce the drive speed is not practical because the fragile nature of the equipment makes it unsuitable for mechanical modification, because the modification would prevent the substitution of similar but unmodified recorders, and because of the inconvenience associated with the gear changing operations. Electronic means of reducing the frequency to the synchronous motor were chosen over mechanical techniques for greater reliability, better synchronization, less electrical noise and for the greater ease of construction brought about by the ready availability of the standard electrical components.

The synchronous motor on the recorder chart drive normally operates with a 60 cps input frequency. Driving this motor with frequencies of 30, 15, or 7.5 cps, respectively, reduces the shaft speed by factors of 2, 4, and 8. A monostable multivibrator triggered by a negative pulse rectified from the 60-cycle power line provides a uniform pulse to drive cascaded binary counters. A selector switch on the inputs to buffer amplifiers which drive the thyratrons grids to allow the chosen number of alternations to be gated through the thyratrons to the motor from the AC anode supply. It is the use of this AC supply on the thyratrons which enables the tubes to be shut off without other turn-off circuitry. Using an oscilloscope to observe the waveform of the voltage appearing across the motor at the normal speed, a 60 cps sine wave could be seen. At half speed, a positive pulse would be observed across the motor for the first 1/60-second period, and a negative pulse on the second period. The waveform at 1/4 speed (or 15 cps) shows positive pulses for the first two periods and negative pulses for the second two. Similarly, the waveform at 1/8 speed shows positive pulses for the first four periods and negative pulses for the successive four periods.

Transistors were used for the frequency dividers because of their ready availability, although glow transfer tubes might accomplish the

same function equally well. Thyratrons were used to drive the motor instead of silicon-controlled-rectifiers on account of the lower cost of tubes.

Power supply requirements for the circuits are very modest. Principally, this is due to the use of alternating current for the thyratrons, the only elements of the circuit with large power demands. Two readily available isolation transformers are used in a series connection to provide the 220-volt anode potential for the thyratrons which drive the recorder motor. A simple, dual-voltage, zener-regulated supply furnishes power for the transistors.

A ten-second time delay relay prevents the application of anode potential to the thyratrons before their cathodes can be brought up to temperature. Other protective features include the use of a 1.6-ampere slow-blow fuse in the main power line to secure the circuit in general and a 1.0-ampere fast-blow fuse in the transistor power circuit for added safety.

The output of the recorder drive speed control unit is connected to the oscillograph motor through the existing motor control switch on the recorder control panel. This simplifies wiring and provides for the simultaneous initiation of recorder drive and other functions within the spectrometer. Due to the nature of the voltage waveforms applied to the motor for the various speeds, the single existing motor phasing condenser is usable under all conditions. This obviates the necessity for any changes in the recorder itself, either mechanical or electrical. Under other circumstances separate phasing condensers would be required for each speed and additional connectors would be needed for interconnections.

The driving circuits were constructed on vertical panels surrounding a central opening which provides cooling through a chimney-like air flow. Consistent with the concept of minimal spectrometer alteration, the equipment was located in a vacant space underneath the clock on an existing panel (see Figure 3).

After installation, checks were made for overheating, excess vibration, and inadequate torque. As seen in Figure 4, motor temperature was actually decreased by 40°C at slower speeds. At the low speeds, inertia does not prevent the obvious movement of the motor with each pulse but the existing shock mounts were found to prevent the transmission of this vibration to the galvanometer assembly. Synchronism, which might be impaired by inadequate torque, was checked satisfactorily by the comparison of the measured length of records to calculated true length.

To make records at normal speed, the speed selector is set at the 60 cps position making the electrical circuit and operating procedures exactly the same as with the unmodified spectrometer. For slow speed operation, either 30, 15 or 7.5 cps operation is selected with the switch, ten seconds warmup time is allowed, and the motor in the recorder is controlled as it was previously. A neon light connected across the motor gives visual indication of the frequency being applied.

As a temporary alternative, the motor can be driven at slow speed with off-the-shelf equipment found in many laboratories. This has been done using a Hewlett-Packard low frequency audio oscillator (function generator) to drive a 60-watt McIntosh Audio Amplifier. The 500-ohm output of the amplifier was coupled directly to the motor leads and two 10-microfarad oil filled condensers were connected in parallel across the existing motor phasing condenser. Although the resulting operating frequency was 7.5 cps for a factor of eight reduction in speed, there was no direct synchronization with the power line using this method. Further, different values of shading capacity are required for the optimum operation at each speed.

Another possible method which was considered but not tried involves the use of clock motor, cam, and interruptor switch to reduce the duty cycle of the power applied to the recorder drive motor. While this method is simple and inexpensive it provides poor synchronization with time, is subject to frailties inherent in mechanical mechanisms, gives discontinuous movement of the chart paper (which may distort data), and may cause electrical noise.

The transistor-thyatron circuit described previously was designed and fabricated in the Nuclear Aerospace Research Facility (NARF) and was installed on the C.E.C. mass spectrometer in the chemical division of the General Dynamics/Fort Worth Environmental Test Laboratory. Since its installation in November of 1961, the electronic speed control has been used in numerous experiments without malfunction.

ACKNOWLEDGEMENTS

The authors wish to gratefully acknowledge the generous aid of O. H. Hill and R. L. Johnston of General Dynamics Nuclear Laboratories in the compilation of this manuscript. Full credit for the detail design, construction, and installation of the Recorder Drive Speed Control belongs to H. W. Blackman of the Development Manufacturing Department of General Dynamics/Fort Worth. This work was performed under contracts with the United States Air Force.

REFERENCES

1. J. B. Farmer and F. P. Lossing Can. J. Chem. 33 (1955) 861.
2. O. H. Hill and R. H. Johnston "Gaseous Yields from X-Irradiated Polyethylenes". Bulletin The American Phy. Soc. Ser. 2, Vol. 7, No. 1, Jan. 1962.
3. "Mass Spectrometer Operation and Maintenance Manual" Consolidated Electrodynamics Corporation.
4. "Mass Spectral Data" American Petroleum Institute Research Project 44, Carnegie Institute of Technology.

IMPROVEMENT IN READOUT ACCURACY OF THE CEC MASGOT

by

H. M. Grubb and R. W. Vander Haar

Research and Development Department, American Oil Company, Whiting, Indiana

The addition of the CEC Mascot peak digitizer to the high mass spectrometer system at Whiting has saved a great deal of time in handling routine spectra. In this area of application, its limitation on minimum readable peak height and non-readout of metastable peaks have been of little concern. An additional shortcoming was discovered recently, however, in connection with the accuracy of the peak digitizer. This problem had not previously been publicized and indeed may not have been recognized, to judge from the tone of the most recent CEC letter to "Mascot Users" (July 25, 1961).

During the course of recent maintenance work, tests were made to see how well the peak digitizer followed small changes in amplitude of simulated peak input, particularly in the regions of range changes. A portion of one of the curves that was obtained is given in Figure 1. Each point represents the average of ten or more measurements. The irregular stepwise shape of the curve is obvious. The location of the ideal response curve is unknown, since no calibration points are located in this area, but errors up to 1% appear likely in this region as a result of peak digitizer non-linearity.

The step curve suggested that the peak digitizer was off calibration. Accordingly, the Digital-to-Analog Converter calibration resistors were reset following CEC's recommended calibration procedure. An E.S.I. Model DV-411 Dekavider was used to obtain the precise voltage ratios needed, and a Tektronix Type 543 Oscilloscope served as the null detector. The calibration points--800, 400, 200, 100, 80, 40, 20, 10, and 8 counts--were set so that the voltage output of the Digital-to-Analog (D-A) Converter was accurate to the equivalent of 0.2 count or better.

Following the calibration, the output of the D-A converter was checked over various ranges of counts between and beyond the calibration points, using the same voltage divider and oscilloscope. The errors found in the range 0-100 counts are presented in Figure 2; here the errors, in counts, are plotted against the number of counts applied to the D-A converter circuit. The maximum absolute error is 3.6 counts at 79 counts, giving a relative error of over 4%. Figure 3 shows a similar plot of the errors found in the range 700-800 counts; here the maximum error is 5.7 counts, but the relative error is less than one per cent because of the greater number of counts involved. These errors are large enough to account for the step curves in Figure 1. It is apparent that nine calibration points are not sufficient to guarantee good peak digitizer linearity.

The error curves in Figures 2 and 3 show repetitive cycles. The pattern of errors for the units repeats at each multiple of ten, shifted upward or downward by the amount of error present at that tens level. Similarly, the pattern for the range 0-100 counts was found to repeat at each multiple of one hundred, with a similar offset due to the error at that hundreds level. These plots indicated immediately that the largest errors were being introduced at the various tens levels.

The output of the D-A converter is a current which is fed back to the input of the peak digitizer. This feedback current should be exactly proportional to the number of counts in register. Figure 4 shows a portion of the D-A conversion circuit, and indicates how the feedback current is developed. The left side of the figure is the "800" adding circuit from the hundreds board; that on the right is the "80" adding circuit from the tens board. When the counter indicates an "800" is needed, transistor Q-607 shorts the negative end of Zener diode CR-604 to ground, transistor Q-608 is effectively an open circuit, and the Zener voltage across CR-604 contributes to the feedback voltage, measured at the feedback summing point. When "800" is not needed, the transistors reverse and the positive end of the Zener diode is shorted to ground;

FIGURE 1
MASCOT NONLINEARITY

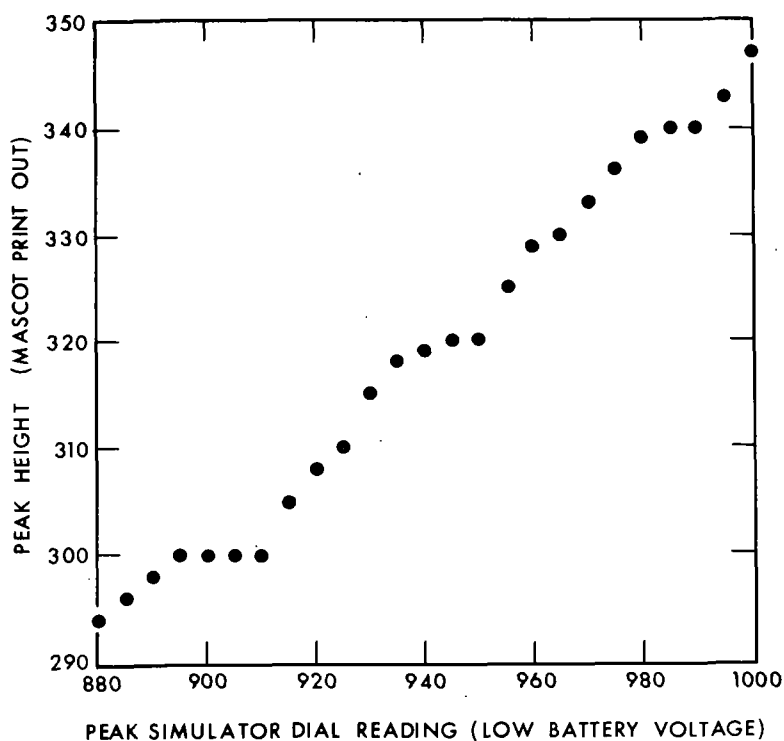
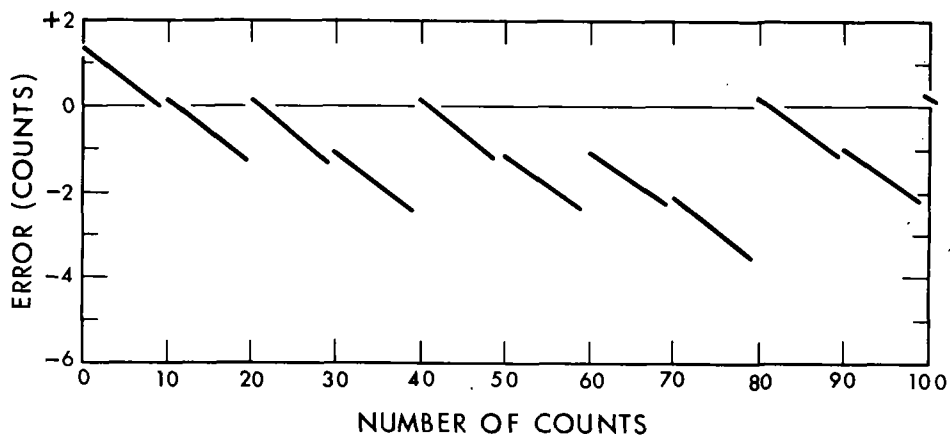


FIGURE 2
D-A CONVERTER ERRORS



however, any D.C. voltage present across Q-608 in its shorted configuration contributes to the feedback voltage. Similarly, when "80" is called for, transistor Q-612 is an open circuit across Zener diode CR-612, and the voltage across this diode adds to the feedback voltage. If "80" is not needed, Q-612 shorts out CR-612, but here also any D.C. voltage across Q-612 still contributes to the feedback voltage.

The CEC manual for the Mascot* indicates that the transistor shorting voltages are quite small, and that in normal operation, they are compensated. The calibration procedure does effect compensation at the calibration points, but it may not do so elsewhere.

The voltages across the shorting transistors on the hundreds board (Q-608 and three others in the same configuration) ranged from 1.2 to 3.0 millivolts. Those on the tens and units boards (in positions similar to that of Q-612) were much larger, however; they ranged from 20 to 55 millivolts. The order of magnitude difference in these voltage drops appears reasonable considering the circuit differences. Referring again to Figure 4, it is seen that Q-612, on the tens board, must pass about 5 milliamperes (250 volts divided by 47K) when it shorts out the Zener diode. On the other hand, the current that Q-608, on the hundreds board, must carry in order to transfer the positive end of the Zener diode to ground potential need not be more than the Zener voltage divided by the series resistance, or about 0.1 milliamperes. Fifty times as much shorting current could easily cause ten or twenty times as much shorting voltage drop.

In order to appraise the effects of these transistor shorting voltages, the D-A conversion circuits were analyzed and circuit equations developed from which errors could be estimated. An example, Figure 5 illustrates the situation that exists on the hundreds board when "800" is called for. The currents in and out of the summing point at the top of the 20K summing resistor, disregarding the tens and units boards, are given by:

$$(1) \quad \frac{E_z - E_{cal}}{R_{800}} = (E_{cal} - V_s) \left(\frac{1}{R_{100}} + \frac{1}{R_{200}} + \frac{1}{R_{400}} \right) + \frac{E_{cal}}{20K}$$

E_{cal} is the feedback voltage at the summing point for 800 counts. E_z is the "800" Zener diode voltage, and V_s represents the voltage drop across the shorted transistors (the transistor voltage drops are all assumed to be equal here). Equation (1) can be rearranged and simplified to:

$$(2) \quad \frac{E_{cal}}{R} = \frac{E_z}{R_{800}} + V_s \left(\frac{1}{R_{100}} + \frac{1}{R_{200}} + \frac{1}{R_{400}} \right)$$

where R is defined by:

$$\frac{1}{R} = \frac{1}{R_{100}} + \frac{1}{R_{200}} + \frac{1}{R_{400}} + \frac{1}{R_{800}} + \frac{1}{20K}$$

Equations similar to (2) can be written for 100, 200, and 400 counts (one-eighth, one-quarter, and one-half of 800 counts, respectively):

$$(3) \quad \frac{1}{8} \frac{E_{cal}}{R} = \frac{E_z}{R_{100}} + V_s \left(\frac{1}{R_{200}} + \frac{1}{R_{400}} + \frac{1}{R_{800}} \right)$$

$$(4) \quad \frac{1}{4} \frac{E_{cal}}{R} = \frac{E_z}{R_{200}} + V_s \left(\frac{1}{R_{100}} + \frac{1}{R_{400}} + \frac{1}{R_{800}} \right)$$

$$(5) \quad \frac{1}{2} \frac{E_{cal}}{R} = \frac{E_z}{R_{400}} + V_s \left(\frac{1}{R_{100}} + \frac{1}{R_{200}} + \frac{1}{R_{800}} \right)$$

*Operation and Maintenance Manual, Mascot Mass Spectrum Digitizer, Type 34-201, Lots 1-4, Consolidated Electrodynamics Corporation, May, 1960.

FIGURE 3
D-A CONVERTER ERRORS

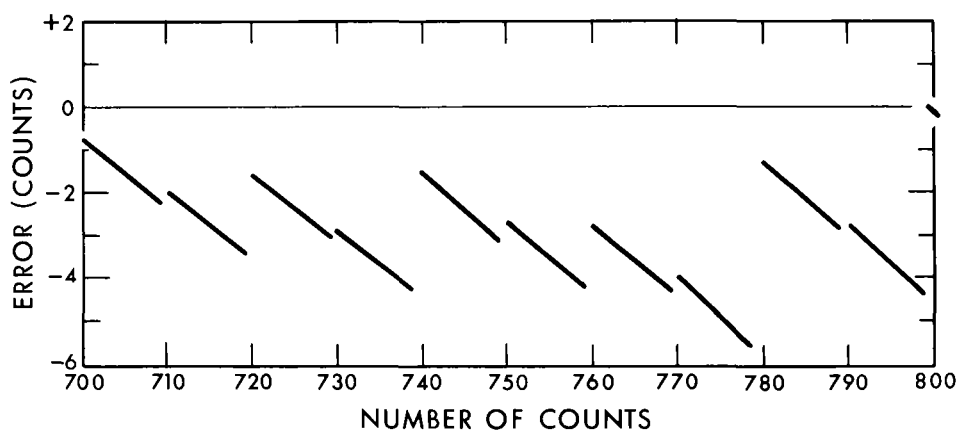
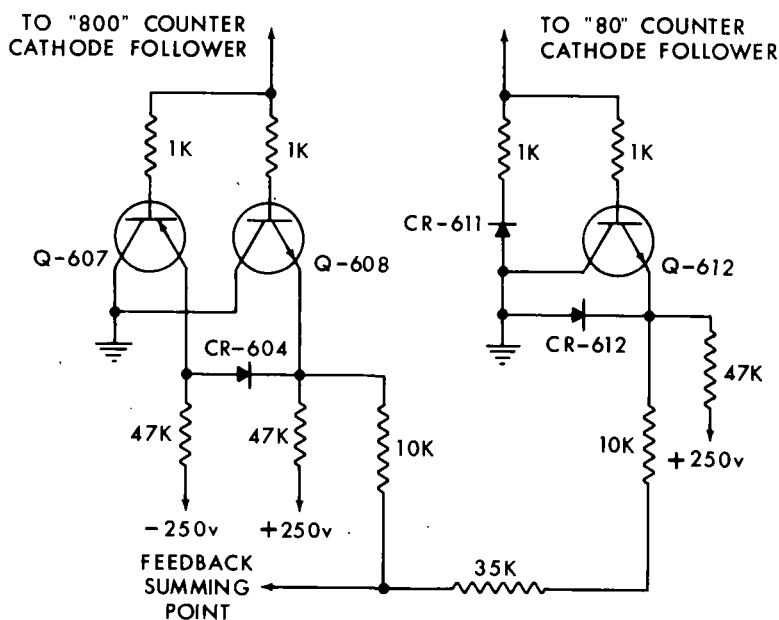


FIGURE 4
D-A CONVERTER CIRCUITRY



In each case, the Zener diode voltage is applied to the proper branch resistance, as called for, and the transistor shorting voltages are applied to the remaining resistances. The Zener diode voltages are also assumed equal.

If now equations (3), (4), and (5) are added, the result will represent the proper feedback for 700 counts:

$$(6) \quad \frac{7}{8} \frac{E_{cal}}{R} = E_z \left(\frac{1}{R_{100}} + \frac{1}{R_{200}} + \frac{1}{R_{400}} \right) + \frac{V_s}{R_{800}} + 2V_s \left(\frac{1}{R_{100}} + \frac{1}{R_{200}} + \frac{1}{R_{400}} + \frac{1}{R_{800}} \right)$$

Equation (6) cannot be realized by the D-A converter, however, because one transistor cannot simultaneously supply E_z and V_s to the same branch resistance. The following equation represents the actual "700" count, where E_z is applied to the 100, 200, and 400 resistances and V_s is applied to the 800 branch:

$$(7) \quad \frac{E_{700}}{R} = \frac{7E_{cal}}{8R} + \frac{E_{error}}{R} = E_z \left(\frac{1}{R_{100}} + \frac{1}{R_{200}} + \frac{1}{R_{400}} \right) + \frac{V_s}{R_{800}}$$

The difference between equations (6) and (7),

$$(8) \quad \frac{E_{error}}{R} = -2V_s \left(\frac{1}{R_{100}} + \frac{1}{R_{200}} + \frac{1}{R_{400}} + \frac{1}{R_{800}} \right)$$

represents the error that must exist at 700 counts if the transistor shorting voltages are not zero, no matter how accurate the calibration at 100, 200, and 400.

An error of not more than one count is desirable. The feedback voltage equivalent of one count was determined to be 3.3 millivolts. Substituting this value for E_{error} in equation (8) leads to a limit of 2.1 millivolts for the transistor shorting voltage drops on the hundreds board. Similarly, the voltage drops across the tens transistors should be less than 16 millivolts; both of these limits apply only if error is being produced by the board in question. Comparison of these limits to the voltage drops actually measured on the hundreds and tens D-A boards led to the conclusion that the 2.1 millivolt limit on the hundreds board was attainable by selection of transistors, but that the 16 millivolt limit for the tens board was not. The shorting voltage characteristics of a dozen locally purchased transistors did not differ markedly from those supplied with the Mascot.

An obvious solution to the problem was the replacement of the tens board with a duplicate hundreds board, with the addition of the series resistors between boards. A new hundreds board was not readily obtainable from CEC, however, so the alternate course was taken; the tens board circuitry was converted to that present on the hundreds board. The physical construction and printed circuitry on the two boards are identical, so that the conversion was relatively simple. The transistors on these boards were placed in the order of their shorted voltage drops, with the lowest one in the "800" spot, the next best in the "400" spot, and so on down through the two circuits. The 2.1 and 16 millivolt limits specified above were met in this way. An accompanying problem was that of obtaining an extra 20 milliamperes from the -250 volt regulated power supply. CEC indicated, in response to an inquiry, that the power supply transformer T-703 did not have the necessary capacity. The problem was solved by replacing T-703 with a UTC Type H-84 transformer.

After these changes were completed, the D-A converter was recalibrated and error measurements in the various count ranges were determined as before. Figure 6 shows a comparison of these latest error measurements with the original errors for the range 0-100 counts. The maximum error in this range is now only 0.9 count, at 74-79 counts. The largest error found on any of the ranges checked was +1.5 counts, at 780 counts.

FIGURE 5

"800" CALIBRATION:

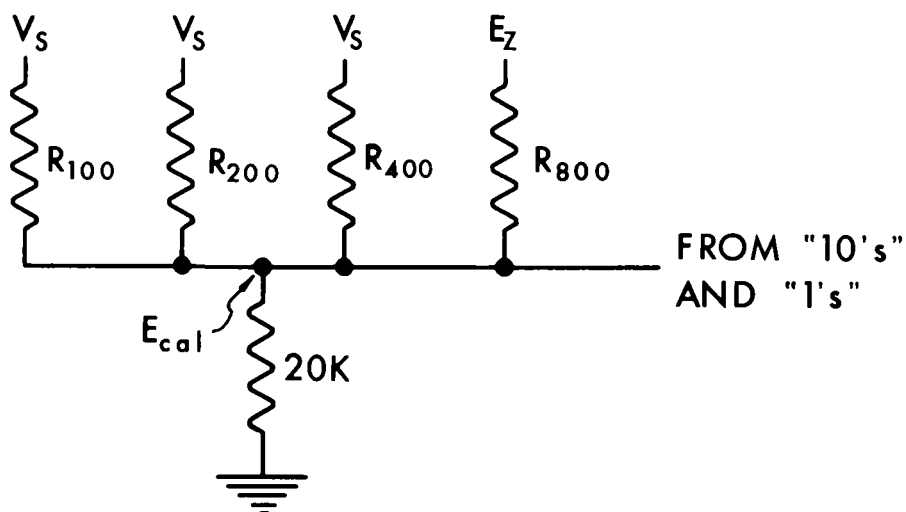
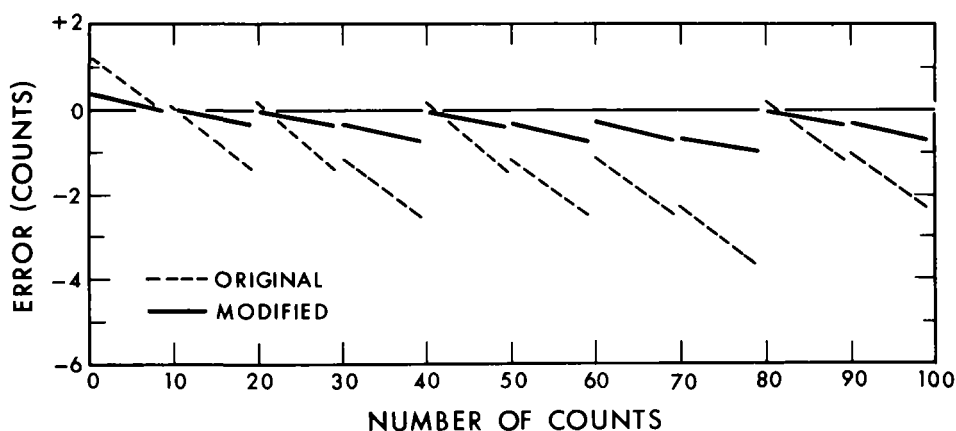


FIGURE 6

D-A CONVERTER ERRORS



The "Mascot User" letter referred to previously states that a linearity of 1 part per 1,000 is inherent in the design of the D-A converter. This is taken to mean a maximum error of 1 count in any part of the 1,000 count range. This specification places limits on transistor shorting voltages which are not readily met in the Mascot circuitry originally supplied by CEC. As a result of the changes described above, however, the linearity of the D-A converter of the Mascot at Whiting appears now to approach 1 part per 1,000.

NEGATIVE ION FORMATION IN VARIOUS GASES AT PRESSURES UP TO .5 mm OF Hg*

R. K. Curran
Westinghouse Research Laboratories, Pittsburgh 35, Pennsylvania

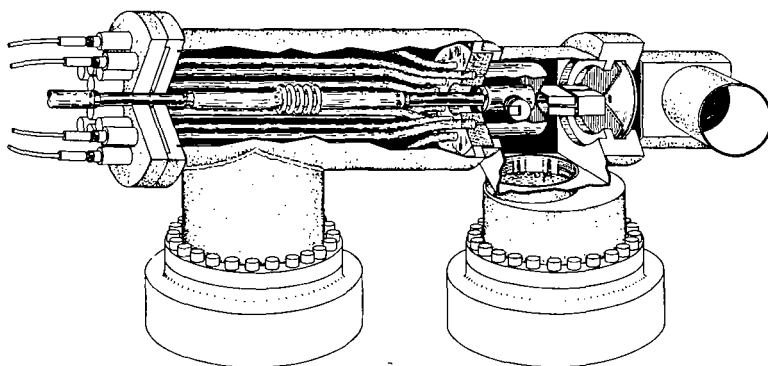
The work that I would like to report on was performed with two different mass spectrometers. Measurements at pressures less than 1μ were made using a mass spectrometer designed by Dr. R. E. Fox, slightly modified to permit some differential pumping and the use of a source with an improved collection efficiency for ions with kinetic energy. The RPD method was used to control the electron beam. The source end of the instrument for the pressure range above a few microns is shown in Fig. 1. The gas sample is introduced through the center glass tube. After passing through the ion source most of the gas exits through the first pump. With the source at 1 mm Hg of He the analyzer region is at less than 10^{-6} mm Hg. To facilitate kinetic energy measurements, the vacuum envelope is run at the acceleration voltage with the source at or near ground potential. This requires that the individual wires leading to the source be enclosed in a glass tube to eliminate corona. The electron beam is controlled with an RPD electron gun. Distribution widths at half maximum of about .1 ev are obtained.

Figure 2 represents the layout of the two mass spectrometers. With the ion collector at ground and the analyzer at the accelerating voltage, the source potential may be varied to trace out the retarding curve for an ion. The ions are retarded at the collector. Both mass spectrometers can be equipped with electron multipliers. The output noise of the multiplier used corresponds to an input current of less than 10^{-18} amp.

The operation of the high pressure mass spectrometer was checked using the He^+ and He_2^+ ions from He. Figure 3 shows the electron energy dependence of the He^+ and He_2^+ ion currents. The electron energy scale was calibrated from the vanishing point of the He^+ ion current. The He_2^+ ion current is formed by a secondary reaction in which the atoms that have been excited by electron impact later collide with unexcited He atoms with the result that the excitation energy is carried off by an ejected electron leaving behind an He_2^+ molecular ion. The He_2^+ ion current may be expected to reflect the excitation functions for the various He excited states that result in its formation. The vertical lines indicate the position of lowest level of the $n = 3, 4, 5$ groups that apparently contribute to He_2^+ formation. The correlation between these and the breaks in the He_2^+ ion current is quite good. Figure 4 shows the pressure dependence of the He_2^+ and He^+ ion currents. The pressure dependences were taken with zero repeller voltage. The solid line through the He_2^+ points has a slope of two up to a pressure of over 1000μ . This is consistent with the forming process discussed above. The He^+ ion current is observed to be linear with pressure to over 500μ after which it bends over. It has been shown that this is due to charge exchange collisions between He^+ and He in the region between the electron beam and the exit slit of the ion source, a distance of about 2 mm. The He_2^+ ion with an apparently smaller charge transfer cross section in He does not depart from its p^2 dependence until pressures in excess of 1000μ are reached. Similar results have been obtained for Ne^+ and Ne_2^+ .

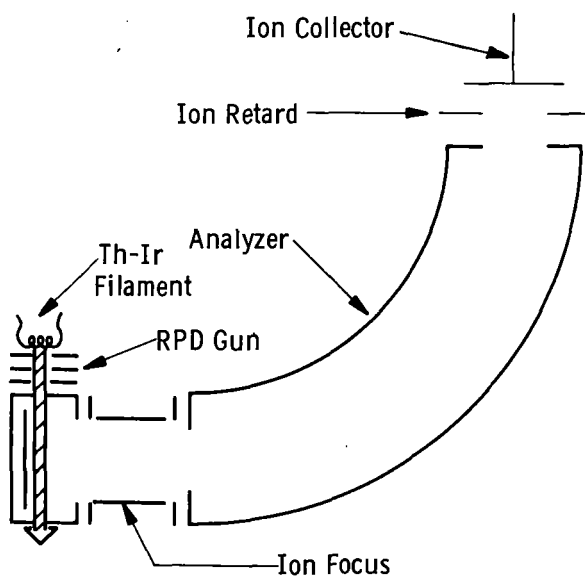
Negative ion formation in O_2 was examined. An O^- ion was observed to arise from two processes. The O^- from dissociative attachment is shown in Fig. 5. The kinetic energy of the O^- fragment was measured as a function of electron energy. The results are shown plotted in Fig. 6. The line of slope 1/2 through the points has an intercept of 3 ev which should be the difference between the dissociation energy of O_2

*This work has been supported in part by the Advanced Research Projects Agency through the Office of Naval Research.



High pressure mass spectrometer tube.

Figure 1



Mass Spectrometer

Figure 2

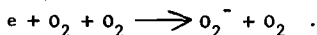
and the electron affinity of O. These results are in agreement with the work of G. J. Schulz using a total tube but do not agree with the value for the electron affinity of O obtained by photodetachment or, as will be noted later, with the value obtained from the study of ion pair formation by electron impact.

An O^- ion onsets at 11.3 ev and its dependence on electron current is not linear but rather appears as though the O^- arises from two processes, one involving one electron and another requiring the excitation of an O_2 molecule by one electron followed by the dissociative attachment of a second electron. At present nothing can be said of the details of these processes.

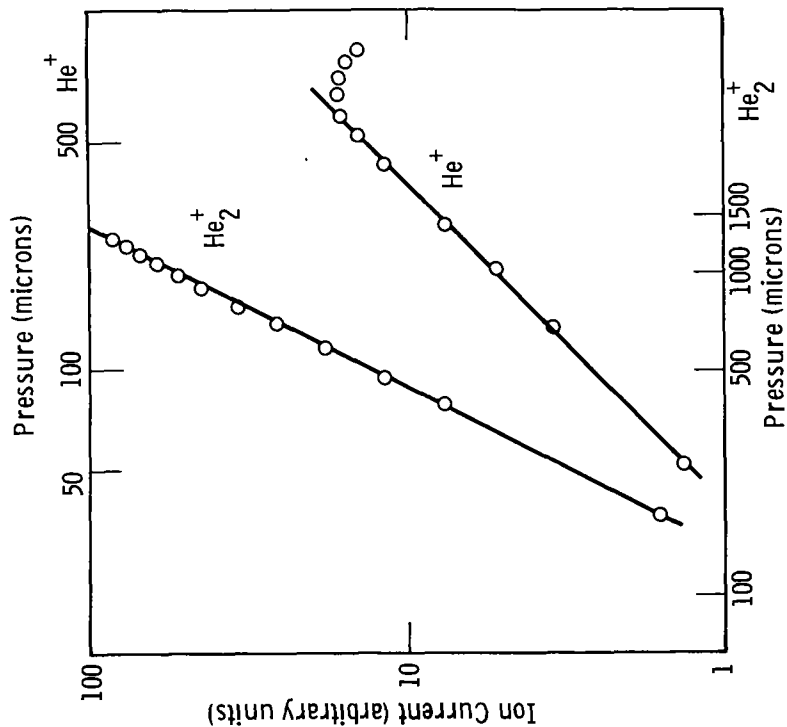
An O_2^- ion was observed in the negative ion spectrum. In order to discuss its mode of formation it is necessary to recall some previous work in O_3 . In O_3 it was observed that O^- and O_2^- ions were formed by low energy electrons. The appearance potentials of these ions, along with their dependence on electron energy, led to the construction of a proposed set of potential energy curves for the O_2^- molecule. These are shown in Fig. 7. Collisions involving O^- and O_2 should be described by these curves. In particular it would appear from the curves that if an O^- ion has sufficient energy to approach an O_2 molecule along the lower O_2^- potential curve, then there will be a possibility that the system will separate along the upper curve to form O_2^- and O. This type of process is proposed to explain the O_2^- ion current observed. The dependence of the O_2^- and O^- ion currents on electron energy is shown in Fig. 5. The O_2^- ion is observed to onset at 1 ev above the O^- ion current threshold. The pressure dependence of the ratio of the O_2^-/O^- currents is linear, but the pressure dependence of the individual ion currents does not depend on pressure in the way one would expect. That is O_2^- and O^- exhibit pressure dependences that are too large. The origin of this difficulty appears to be in the discrimination of the mass spectrometer against ions with kinetic energy. The mass spectrometer apparently collects only those ions with kinetic energy that are initially directed into a very small solid angle determined by the exit slit. (The exit slit is small to allow sufficient differential pumping.) As the pressure is increased, fast ions directed in an unfavorable solid angle undergo collisions and are slowed before they escape the allowable collection region for slow particles and thus are collected with an efficiency depending on the pressure. This effect has been verified by mixing Ne with O_2 and observing the O^- ion current to be linear with O_2 pressure at partial Ne pressures of about 200 μ or more. The ions also exhibit proper pressure dependences when the repeller voltage is large compared to the ion kinetic energy.

Figure 8 shows the equations for energy balance in the proposed reaction for the formation of O_2^- . The first line expresses the fact that to effect the removal of an electron from O^- and reattach it to O_2 , one has to supply energy at least in the amount of the difference between $EA(O)$ and $EA(O_2)$. This energy is supplied through the kinetic energy of the O^- ion which is determined by the kinetic energy of formation plus the effect of the repeller voltage. The 2/3 has its origin in the fact that at most only 2/3 of the O^- kinetic energy can go into potential energy of the collision complex. The second line is the expression for $KE(O^-)$ at O_2^- threshold. Eliminating $KE(O^-)$ between the two equations and substituting the values indicated, one obtains the result $EA(O) \leq 1.5$ ev, which is consistent with the accepted value of $EA(O)$. This is somewhat surprising since the O^- ions come from the dissociative attachment process previously found to give a value of $EA(O) = 2.1$ ev. No convincing argument can be given to resolve this discrepancy.

A very weak O_2^- signal has also been found to onset at 0 ev. The dependence of this ion on electron energy is shown in Fig. 9. Also shown is the electron retarding curve used to calibrate the energy scale. The shape of this curve is consistent with the results of Schulz obtained in a total tube. The process here is probably the three-body attachment process

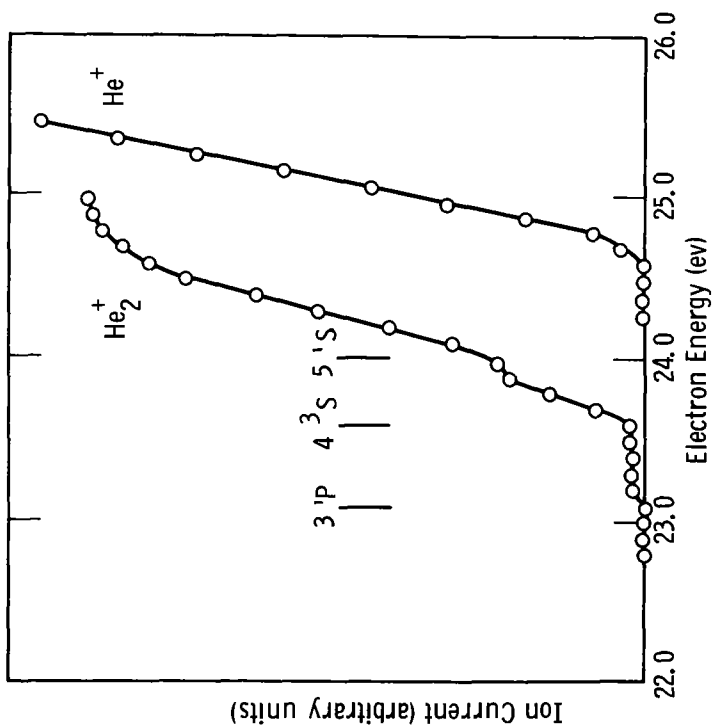


Some investigation has also been done on pair formation processes. The type of measurement made is shown in Fig. 10 where H_2^+ and H^+ from H_2 are plotted vs electron energy. The vanishing point of the H_2^+ ion current is used to calibrate the electron energy scale. Such a plot gives two determinations of the electron affinity of H. First from the onset at 17.3 assuming this to be $H^+ + H^-$, one obtains $EA(H) = .8$ ev using the accepted values of $I(H)$ and $D(H_2)$ and second from the difference between the onset of $H^+ + H^-$ and the second break assuming it to be the onset of $H^+ + H$ gives again $EA(H) = .8$ ev. These are in quite good agreement with the accepted value of $EA(H)$.



Pressure dependence of He^+ and He_2^+

Figure 4



Electron energy dependence of He^+ and He_2^+

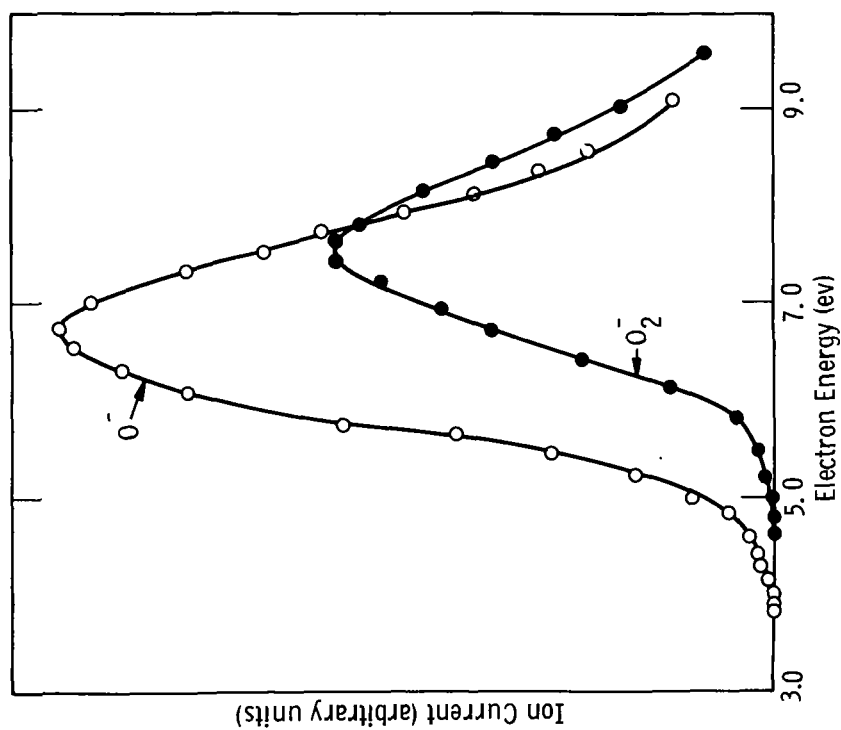
Figure 3

Pair formation processes have been studied previously in O_2 by Randolph and Geballe,¹ in NO by Cloutier and Schiff,² and in CO by Lagergren.³ The work has been repeated to obtain the data from a single instrument. Figure 11 shows data on pair formation taken in O_2 , NO, and CO. In O_2 , the onset 17.2 ev gives $EA(O) = 1.5$ ev while the difference between onsets gives $EA(O) = 1.4$ ev. In NO the onset 19.5 ev gives $EA(O) = 1.5$ ev, while the difference gives $EA(O) = 1.6$ ev. In CO the 20.8 ev onset gives $EA = 1.6$ ev, while the difference gives $EA(O) = 1.5$ ev. It would appear that there is little doubt that the electron affinity of O obtained from pair formation appearance potentials is in agreement with the accepted value of 1.465 ev.⁴

Figure 12 shows the electron energy dependence of O^+/CO . If the AP of O^+ at 23.7 ev is taken as the threshold for $O^+ + C^-$, then $EA(C) = 1.0$ ev and if the 24.8 onset is $O^+ + C$, then the difference gives $EA(C) = 1.1$ ev. It is interesting to note that the O^+ ion current has structure at less than 1 ev above threshold. If this is interpreted as evidence for an excited state of C^- , then from the O^+ data it is .5 ev above the ground state. The recent work of Seman and Branscomb⁵ on photodetachment in C^- indicates an excited state of C^- somewhere below .5 ev above the ground state of C^- . The present results would appear to be consistent with this result.

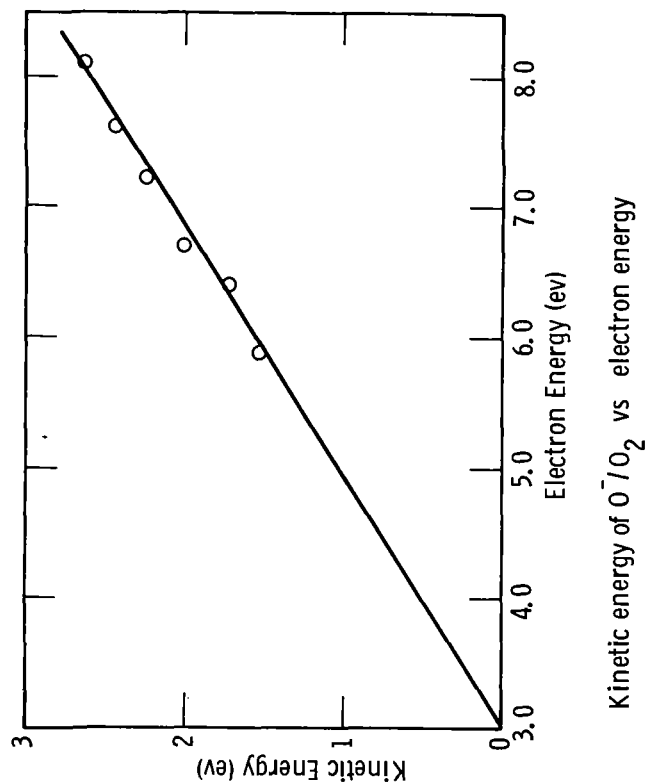
REFERENCES

1. P. L. Randolph and R. Geballe, University of Washington, Thesis, 1958 (unpublished).
2. G. G. Cloutier and H. I. Schiff, J. Chem. Phys. 31, 793 (1959).
3. C. R. Lagergren, University of Minnesota, Thesis, 1955 (unpublished).
4. L. M. Branscomb, J. Chem. Phys. 29, 452 (1958).
5. M. L. Seman and L. M. Branscomb, Phys. Rev. 125, 1602 (1962).



Electron energy dependence of O^- and O_2^-

Figure 5



Kinetic energy of O^-/O_2 vs electron energy

Figure 6

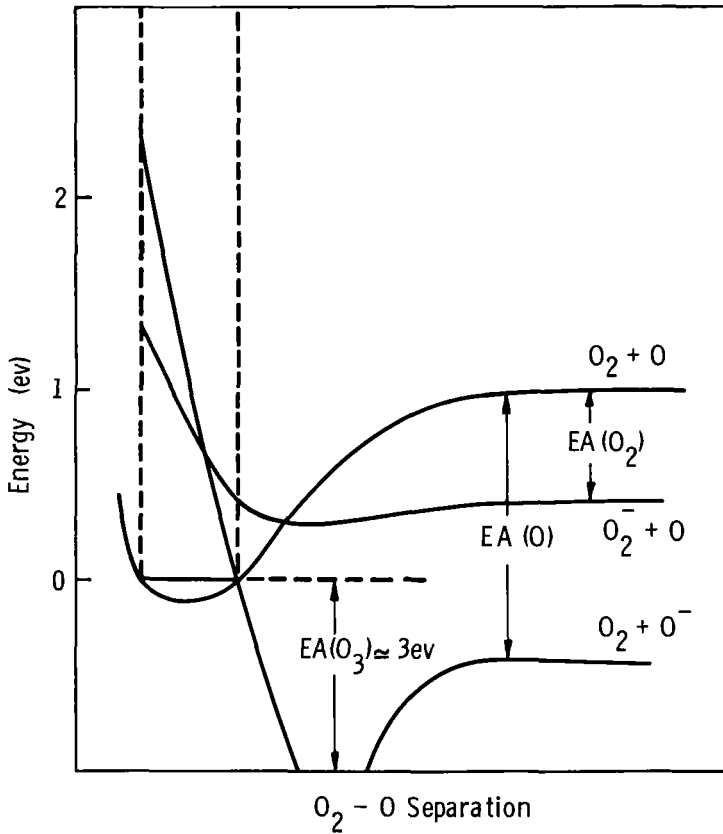


Figure 7

$$EA(O) - EA(O_2) - \frac{2}{3}(KE(O^-) + V_R) \leq 0$$

$$2KE(O^-) + D(O_2) - EA(O) = AP(O_2^-)$$

$$2EA(O) \leq 3EA(O_2) + 2V_R + AP(O_2^-) - D(O_2)$$

$$EA(O_2) = .6 \text{ ev}$$

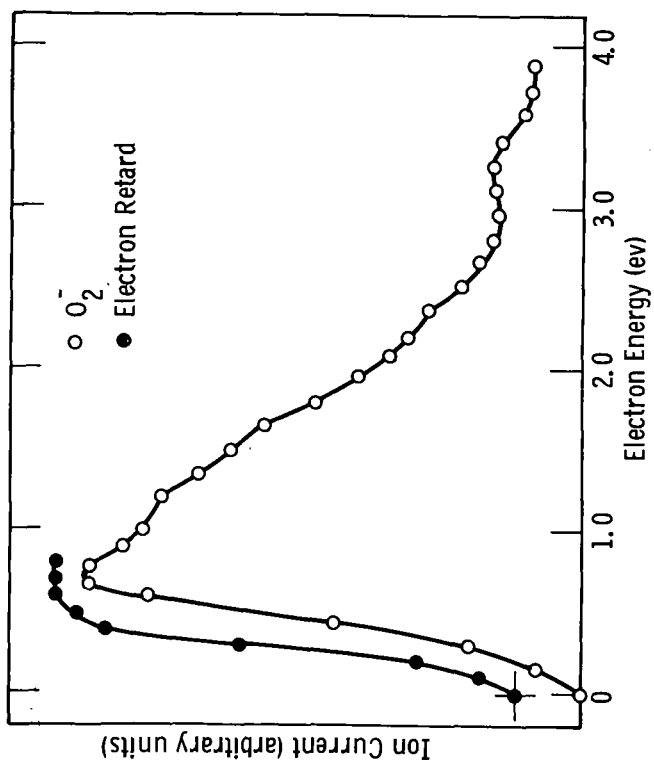
$$V_R = .5 \text{ ev}$$

$$AP(O_2^-) = 5.3 \text{ ev}$$

$$D(O_2) = 5.11 \text{ ev}$$

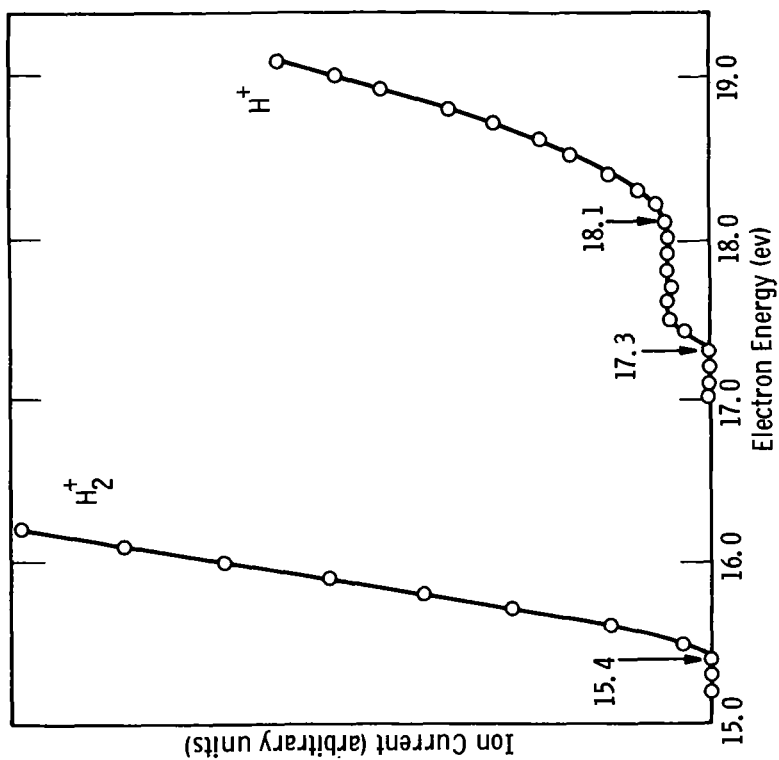
$$EA(O) \leq 1.5 \text{ ev}$$

Figure 8



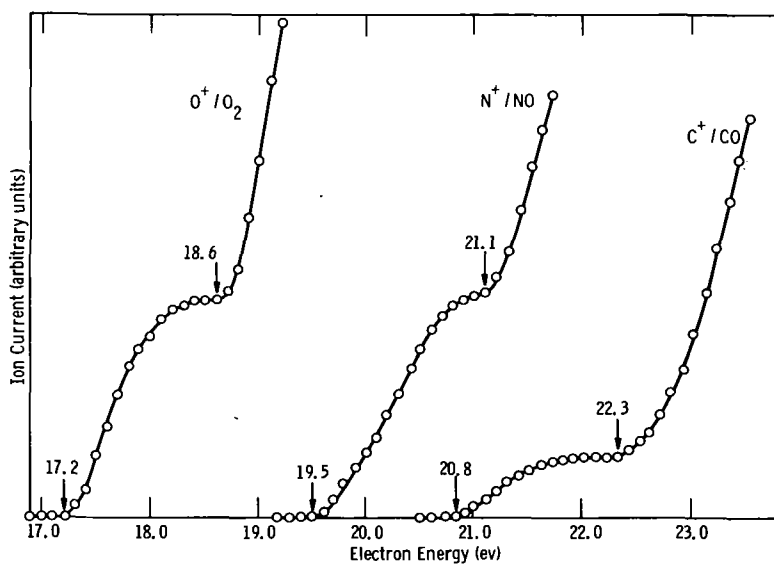
Electron energy dependence of O_2^-

Figure 9



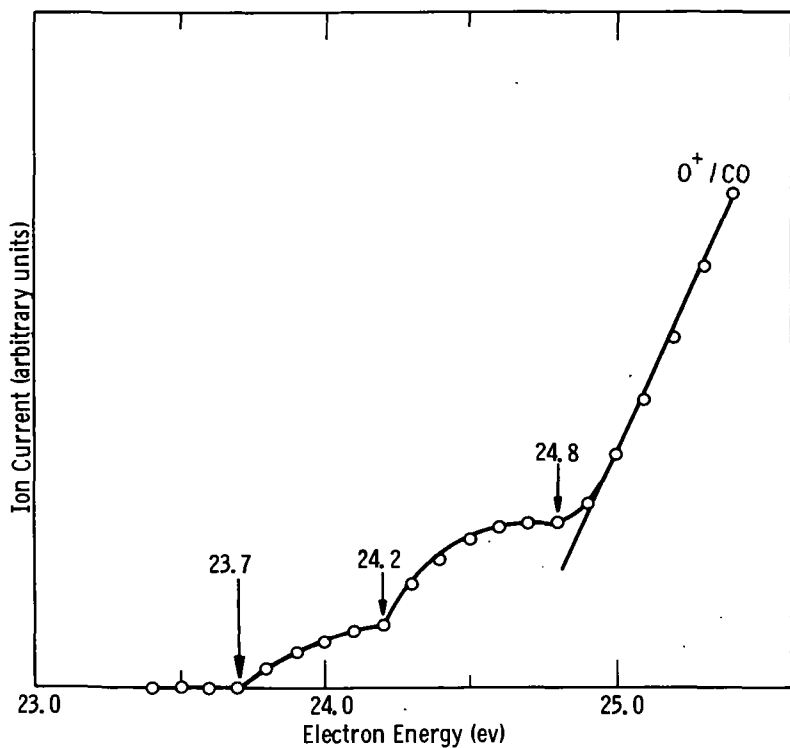
Electron energy dependence of H_2^+ and H^+

Figure 10



Electron energy dependence for M^+ in $M^+ + O^-$ processes

Figure 11



Electron energy dependence of C^- and O^+ from pair formation in CO

Figure 12

ELECTRON TRANSFER IN COLLISIONS OF NEGATIVE IONS WITH O₂ MOLECULES

T. L. Bailey

College of Engineering and Department of Physics
University of Florida, Gainesville, Florida

Cross sections for the production of slow heavy negative ions and for the production of free electrons in collisions of negative ions with O₂ molecules have been measured by an ion beam-gas scattering technique. The experimental method consists of directing a momentum analyzed beam of primary negative ions, of kinetic energy variable over the range 4-350 e.v. through a collision chamber containing gas at low pressures. Slow electrons, produced by detachment processes, and slow heavy negative ions, which arise from simple electron transfer (and perhaps other processes), are extracted from a known length of the primary beam path by a weak electrostatic field. These product species then pass through a region containing a radio-frequency field. When the radio-frequency field is adjusted to the proper frequency and voltage, it sweeps out all electrons, without attenuating the current of slow heavy ions. Thus the currents of product ions and electrons can be measured separately, and are used to calculate separately σ_t , the cross section for production of slow heavy negative ions, and σ_d , the cross section for production of free electrons.

The systems O₂⁻ in O₂, H⁻ in O₂, and O⁻ in O₂ have been studied. The results obtained for O₂⁻ in O₂ and for H⁻ in O₂ show that σ_t is rather large for both systems over the entire energy range of the measurements. In both cases, the dominant contribution to σ_t is attributed to simple charge transfer. For O₂⁻ in O₂, σ_t rises fairly smoothly with decreasing primary ion energy W, from a value $\sigma_t = 7.9 \times 10^{-16}$ cm² at W = 294.3 e.v. to 20.6×10^{-16} cm² at W = 3.6 e.v. The behavior of σ_t versus W is indicative of a process for which the energy defect ΔE is approximately zero. For H⁻ in O₂, σ_t increases from $\sigma_t = 6.4 \times 10^{-16}$ cm² at W = 350 e.v. to a shallow maximum of $\sigma_t = 13.0 \times 10^{-16}$ cm² at W = 70.5 e.v., then drops to $\sigma_t = 9.6 \times 10^{-16}$ cm² at W = 25.0 e.v., and from this minimum again rises to 13.0×10^{-16} cm² at W = 7.7 e.v., the lowest energy of the measurements. If σ_t is due to simple electron transfer alone, its behavior with energy below W = 25.0 e.v. indicates that the electron affinity of O₂ is approximately equal to that of H, and it is estimated that $E(O_2) = 0.75 \pm .24$ e.v. The maximum at W = 70.5 e.v. may arise from the reaction $H^- + O_2 = H + (O_2)^*$, where $(O_2)^*$ is in an excited internal state. σ_t for O⁻ in O₂ was smaller throughout the range of the measurements than σ_t for O₂⁻ in O₂, or H⁻ in O₂. For this system, σ_t versus W shows an unusual double maximum structure: there is a flat maximum at W \approx 100 e.v., where $\sigma_t = 3.4 \times 10^{-16}$ cm². It is nearly certain that σ_t in the region of the W \approx 100 e.v. maximum is due to simple charge transfer alone. An interpretation of this maximum, based on the preceding assumption, and on the adiabatic hypothesis, gives the inequality $E(O_2) > 0.9$ e.v., which is consistent with the estimate deduced from the low energy behavior of σ_t for H⁻ in O₂. The maximum at W \approx 9 e.v. is attributed to contributions from an ion-molecule reaction, such as $O^- + O_2 = (O_2)^* = O^- + O_2$, rather than to simple charge transfer.

The electron detachment cross sections at energies above W \approx 30 e.v. for all three systems are similar in magnitude and in behavior with ion energy to those which have been observed for other colliding systems. The behavior of σ_d versus W for O⁻ and H⁻ at very low ion energies is rather unexpected, however. σ_d for O⁻ in O₂ extrapolates to zero at an ion energy considerably less than the appearance potential for direct collisional detachment, $O^- + O_2 = O + O_2 + e^-$, and the low energy σ_d 's for H⁻ in O₂ extrapolate to a positive value at W = 0. These results suggest that at very low energies the σ_d 's may arise in part from the reactions $O^- + O_2 = O_3 + e^-$, and $H^- + O_2 = HO_2 + e^-$.

Preliminary studies of collisions of O⁻ ions in N₂ show that σ_t for this system is negligible in the range $25 \leq W \leq 350$ e.v., and therefore that the electron transfer reaction $O^- + N_2 = O + N_2$ does not occur. For O⁻ in N₂, abnormally large currents of relatively fast heavy ions, scattered through 30° or more, were observed. This indicates that either (a) there is an unusual amount of large angle elastic scattering, or (b) an ion-molecule reaction, such as $O^- + N_2 = NO^- + N$, is taking place with high probability at fairly elevated energies.

SOME UNIQUE APPLICATIONS OF NEGATIVE ION MASS SPECTRA

Russell Baldock
Chemistry Division, Oak Ridge National Laboratory*
Oak Ridge, Tennessee

Abstract

The negative ion mass spectra of some organic materials stand in contrast to the positive ion mass spectra as being more readily understood in terms of molecular structure and chemical behavior. Spectra of some of the simple hydrocarbons and alcohols are presented to support this viewpoint. Often the negative ion spectra, because of their simplicity and unambiguity, readily lend themselves to quantitative analyses in mixtures such as formic acid, HCOOH , and formic-d acid, DCOOH . It is shown that negative ion spectra are the principal data which made it possible to identify the transient species observed in the reaction of $\text{D}_2 + \text{CO}_2$ on platinum. Evidence for the contribution of negative ions in the polymerization of mixtures of $(\text{CN})_2 + \text{Xe}$ are presented and discussed.

Introduction

Some years ago Melton and Rosenstock^{1,2} employed a commercially built mass spectrometer to investigate metastable and collision induced dissociations. This experience and a number of other considerations led us to design and build a versatile and sensitive instrument which would be suitable for a wide range of applications and investigations in chemical physics.

All of the pertinent³ features of the mass spectrometer have been presented in earlier publications^{3,4} so I will list here only those features which are pertinent to the study of negative ions. They are as follows:

1. A high degree of differential pumping so that the pressure in the ionization chamber may be built up to 1 mm of Hg.
2. A 14 stage electron multiplier plus a vibrating reed electrometer and counting circuitry for high sensitivity of ion detection.
3. A Hutchison type emission regulator for stability of the beam of ionizing electrons, and
4. A thorium iridium filament for inertness.

It has become evident in the past year that other workers have also found that essentially these same instrument features are useful in applying a mass spectrometer to problems in chemical research.

Figure 1 is a drawing of our ion source. With versatility as well as exploratory applications in mind, the ion source was constructed as shown. With differential pumping, the pressure in the ionization chamber can be made about an order of magnitude higher than in the general region of the ion source. Since the final exit slit of the source is the only vacuum connection between the ion source and the analyzer tube, a second pump (not shown) is able to maintain the vacuum in the analyzer tube about three orders of magnitude lower than the vacuum in the ion source region.

By means of relatively simple changes to the ion source, ions may be formed by any one of the following means:

1. Low energy electrons (50-100 ev which were used for the work reported in this paper).

*Operated by Union Carbide Corporation for the U. S. Atomic Energy Commission.

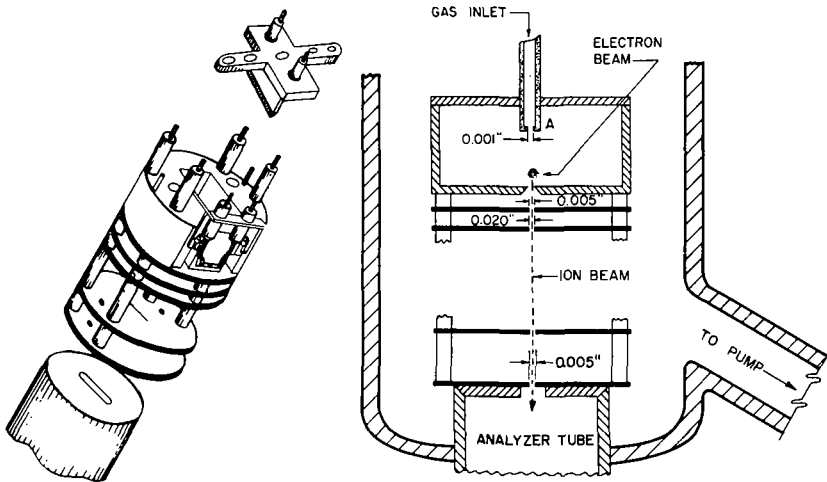


Figure 1 - MASS SPECTROMETER ION SOURCE

Figure 2

NEGATIVE IONS FROM HCOOH, \underline{D} COOH, AND HCOOD

MASS	<u>HCOOH</u>		<u>\underline{D}COOH</u>		<u>HCOOD</u>	
	<u>ION</u>	<u>R.A.</u>	<u>ION</u>	<u>R.A.</u>	<u>ION</u>	<u>R.A.</u>
16	O^-	6.3	O^-	6.6	O^-	6.9
17	OH^-	3.4	OH^-	3.5	OH^-	0.6
18	—	—	OD^-	0.2	OD^-	3.5
44	COO^-	0.1	COO^-	0.1	COO^-	0.1
45	$HCOO^-$	100.0	$COOH^-$	1.2	$HCOO^-$	100.0
46	—	—	$\underline{D}COO^-$	100.0	—	—
91	$HCOOH \cdot HCOO^-$	0.1	—	—	—	—
92	—	—	—	—	$HCOOD \cdot HCOO^-$	0.1
93	—	—	$\underline{D}COOH \cdot \underline{D}COO^-$	0.1	—	—

2. High energy (up to 6 kev) electrons.
3. Alpha particles from Po-210 mounted on a platinum disc and placed in front of the ion repeller.
4. Beta particles from Ni-63 mounted on a platinum disc and placed in front of the ion repeller, or
5. Replace the ion repeller with a coil of platinum wire and use a beam of electrons to ionize species evolved from the surface of the catalyst.

The information reported here on negative ion mass spectra comes from studies in our group by Melton who was assisted from time to time by other interested members of the Chemistry Division as noted in the bibliography.

Acids

The negative ion mass spectra of formic acid, HCOOH, formic acid-d, HCOOD, and formic-d acid, DCOOH were studied rather extensively by Melton and Ropp.⁵ They have shown that negative ion formation in these acids is predominantly by loss of the hydroxyl hydrogen. The formation of negative ions from reactants in the gas phase in these acids by hydroxyl bond cleavage is analogous to liquid phase ionic dissociation of organic acids containing the carboxyl group.

In Figure 2, one can clearly see by examining the data, especially for masses 45 and 46, that in the formic acids the formation of negative ions results almost exclusively from the cleavage of the hydroxyl bond.

It was also found in some additional studies that the trend in sensitivity to negative ion formation in formic acid, acetic acid, and propionic acid is roughly comparable in magnitude to the relative tendencies of these acids to ionize in aqueous solution, as measured by their ionization constants.

We note in passing that the small, but measurable intensities at masses 91, 92 and 93 led to a subsequent investigation of an interesting negative ion-molecule reaction in a mixture of HCOOH and DCOOH.⁶

The tremendous advantage of using the negative ion spectra for quantitative measurements in a mixture such as formic-d acid, DCOOH, and formic acid, HCOOH, is seen from the data in Figure 3. One needs to measure only mass 46 as representative of the unlabelled acid as contrasted with the 28 ionic species in the positive ion spectra.

The power and simplicity of the negative ion spectra of organic acids containing the carboxyl group, especially when one is concerned with a mixture of labelled and unlabelled acids as is sometimes the case in biological studies, has been recognized and is being demonstrated in some studies now in progress.

Hydrocarbons and Alcohol

Two general conclusions can be drawn from the mass spectral data now available for a few of the aliphatic hydrocarbons, methane, the C₂-hydrocarbons and n-butane.⁷ First, ionization and dissociation reactions induced by 50-75 volt electrons yield about 1 negative ion to 10⁴ positive ions. Second, the percent of C₂H⁻ formed from the aliphatics, in the open chain molecules above methane increases with increasing saturation. If one considers acetylene, ethylene, ethane and n-butane in that order, then the percent of C₂H⁻ increases from 23 to 30 to 38 to 59.

Methane, the first in the series of paraffins, has been studied rather extensively by three groups of investigators. Since high energy (~ 75 v) electrons were employed in these studies, the mass spectra were produced predominantly by ion pair production. The relative distribution of both positive and negative ions is shown in Figure 4. The negative ion data is from the work

Figure 3

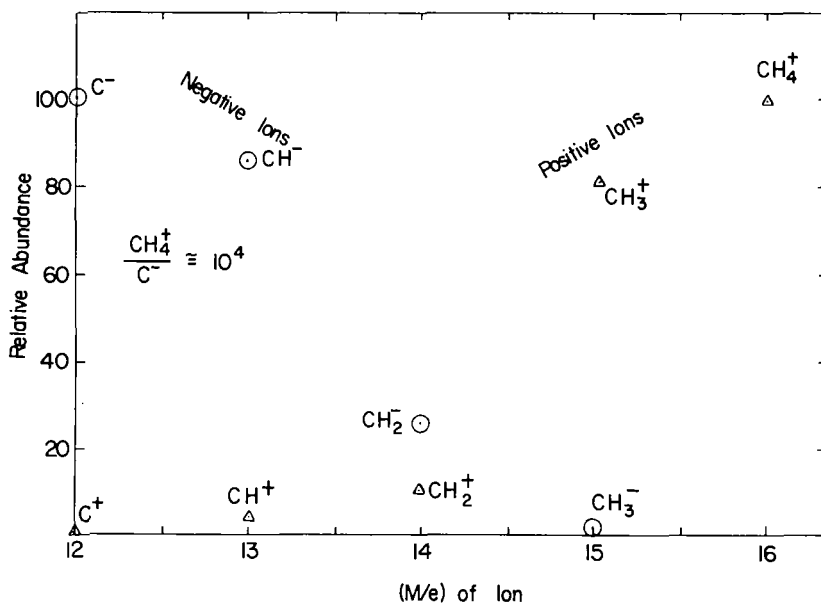
UNCLASSIFIED
ORNL-LR-Dwg. 24919

POSITIVE AND NEGATIVE IONS FROM DCOOH

MASS	ION	RELATIVE ABUNDANCE	RELATIVE ABUNDANCE (OF NEGATIVE IONS ONLY)
12	C ⁺	0.90	
13	CH ⁺	0.10	
14	DC ⁺	0.90	
15	HCD ⁺	0.18	
16	O ⁺	2.04	
17	OH ⁺	3.79	
18	HOH ⁺ OD ⁺	8.03	
19	HOD ⁺	18.67	
20			
28	CO ⁺	15.51	
29	HCO ⁺	12.08	
30	DCO ⁺	88.61	
31	DC ₃ O ⁺	1.35	
44	CO ₂ ⁺	23.09	
45	HCOO ⁺	36.84	
46	DCOO ⁺	38.22	
47	DCOOH ⁺	100.00	
16	O ⁻	0.14	6.6
17	OH ⁻	0.07	3.5
18	OD ⁻	0.004	0.2
44	COO ⁻	0.002	0.1
45	HCOO ⁻	0.02	1.2
46	DCOO ⁻	2.06	100.0
47	DC ₁₃ O ₁₈ O ⁻	0.004	0.2

UNCLASSIFIED
ORNL-LR-Dwg. 56175

Figure 4

RELATIVE ABUNDANCE FOR NEGATIVE AND POSITIVE IONS
INDUCED IN METHANE BY ELECTRON IMPACT

of Melton and Rudolph and the positive ion data is from the work of Melton and Rosenstock. These curves have been normalized by making the most abundant ion in each spectrum equal to 100. The absolute intensity differs by a factor of 10^4 as shown. The relative intensities of the ions as a function of the number of hydrogens remaining on an individual carbon atom are of interest here. The negative ion abundance decreases rapidly with increasing saturation of the carbon atom, which is in accord with the decreasing electron affinity with increasing saturation of the carbon while in the case of the positive ions, just the reverse is true.

The negative ion mass spectra of the alcohols have several general features which have been correlated to molecular structure and chemical properties. Melton and Rudolph have shown that loss of hydrogen by negative ion formation is almost entirely restricted to loss of an odd number of hydrogen atoms. Furthermore, the most predominant negative ion formed by hydrogen extraction in all the alcohols results in the loss of a single hydrogen atom. For example, an examination of methyl alcohol labelled in the hydroxyl position, i.e., CH_3OD , has shown that the CH_2O^- ion is formed almost exclusively as a result of cleavage of the O-D bond. This mode of formation of CH_3O^- is analogous to the previously referred to breakup of formic acid. These observations strongly suggest that negative ions formed by hydrogen extraction are formed in all alcohols predominantly by loss of the hydroxyl hydrogen.

Negative ion formation by electron impact of secondary and tertiary alcohols proceeds almost exclusively by loss of the hydroxyl hydrogen. In primary alcohols, in addition to forming negative ions by loss of the hydroxyl hydrogen, other ions can be formed by the loss of two additional hydrogens, probably the alpha hydrogens. Since it is known that the alpha hydrogens are more active in oxidation reactions than the other aliphatic hydrogens, these observations appear to be in good agreement with the chemical properties of the alcohols.

It can be seen in Figure 5 that the negative ion spectra of n-butane and n-butyl alcohol show remarkable similarity. This agreement is in accord with the fact that the reactivity of an alcohol in an homologous series more closely approaches that of the corresponding alkane as the alkyl radical increases in length. By way of contrast, the negative ion spectra of ethane and ethanol are not nearly so similar to one another, as might well be expected.

We also note that in n-butane, which is the heaviest aliphatic hydrocarbon for which we have negative ion mass spectral data, the C_2^- ion is an order of magnitude more abundant than the other carbon species. Ionic species containing a single hydrogen are generally more abundant than when an even number of hydrogens are present. It has been noted that in positive ion mass spectra, positive ions containing an odd number of hydrogens are usually much more abundant than those containing an even number.

Catalysis

Melton has also used our research mass spectrometer to identify and study the volatile transient species produced by catalytic action.⁶ Several investigators have reported that free radicals are formed on and possibly desorbed from catalysts during heterogeneous reactions but these have not heretofore been identified mass spectrometrically.

The catalyst in the form of a spiral of 0.5 mm platinum wire, 3×13 mm with a surface of $\sim 1 \text{ cm}^2$ was mounted inside the ionization chamber in approximately the position of the ion repeller and parallel to and just behind the electron beam. The catalyst could be self heated by passing a current through it. Gases under investigation were introduced in the usual manner and products evolved from the reaction on the catalyst passed into the electron beam and were ionized. Products of the reactions were studied as a function of catalyst temperature, and the pressure and concentration of each reactant.

Figure 5

Relative abundance of negative ions from some alkanes and corresponding alcohols.

<i>m/e</i>	Ion	Ethane	Ethanol	<i>n</i> -Butane	<i>n</i> -Butanol
12	C ⁻	20	31	3	3
13	CH ⁻	29	51	13	7
14	CH ₂ ⁻	8	18	7	4
15	CH ₃ ⁻		28	2	1
24	C ₂ ⁻	100	61	29	31
25	C ₂ H ⁻	100	100	100	100
26	C ₂ H ₂ ⁻	3	3	5	3
36	C ₃ ⁻			3	6
37	C ₃ H ⁻			2	4
38	C ₃ H ₂ ⁻				2
48	C ₄ ⁻			1	1
49	C ₄ H ⁻			3	2

UNCLASSIFIED
ORNL-LR-Dwg. 50133

Figure 6

**FREE RADICALS AND INTERMEDIATES
DETECTED IN THE REACTION $D_2 + CO_2 \xrightarrow{Pt} D_2O + CO$**

<u>M/e</u>	<u>ION</u>	<u>PROBABLE PRECURSOR</u>	<u>PROBABLE SOURCE</u>
2	D ⁺ , D ⁻	D	D ₂ \xrightarrow{Pt} D + D
30	DCO ⁺	DCO	DCO DESORBED
46	DCOO ⁻	DCOOD; COOD	CO ₂ + D ₂ \xrightarrow{Pt} DCOOD
60	CO ₃ ⁻	D ₂ CO ₃ ; CO ₃	D ₂ O + CO ₂ \xrightarrow{Pt} D ₂ CO ₃
62	DCO ₃ ⁻	D ₂ CO ₃ ; DCO ₃	D ₂ O + CO ₂ \xrightarrow{Pt} D ₂ CO ₃

The reaction of $D_2 + CO_2$ was investigated in an extensive series of experiments. The formation and desorption of species containing D, C, and O was deduced. To determine the configuration of the intermediates, all of the positive and negative ions produced from neutral species during the course of the reaction were identified. The results are given in Figure 6.

The positive and negative ions appeared to be derived from two structural classes of neutral species, namely, a carbonate type giving rise to DCO_3^- and CO_3^- and a formic acid type giving rise to $DCOO^-$ and DCO^+ . Since the behavior of the catalyst with respect to these ionic species had been determined, it seemed reasonable to determine whether or not the catalyst presented the same behavior when exposed to a stable compound having either the formic acid or carbonate type configuration. The test was restricted to the use of formic acid labelled with deuterium on the carbon atom. The behavior of the radicals displaced from the surface of the catalyst was completely analogous to that in the earlier experiments.

We simply wish to emphasize here that the major portion of the information found useful in a study of the transient species desorbed from a platinum catalyst in the course of the heterogeneous reaction of D_2 and CO_2 came from an investigation of the negative ion spectrum.

Mixture of $(CN)_2 + Xe$

Some years ago Lind and Bardwell^{9,10} showed that the rates of radiolytic polymerization are, in general, increased by the admixing of noble gases. In most systems studied the rare gases had higher ionization potentials than the reactant gases and the increased rates of reaction were explained on the basis of charge transfer. In the $(CN)_2 + Xe$ system charge transfer to the reactant is not energetically possible since Xe has the lower ionization potential, 12.1 ev against 13.6 ev for $(CN)_2$. However, Lind and Bardwell found that Xe increased rather than decreased the yield of polymerization of cyanogen.

Melton and Rudolph investigated the transient species produced in the $(CN)_2$ and $(CN)_2 + Xe$ systems and part of their observations are summarized in Figure 7.¹¹ When Xe was admixed with $(CN)_2$ the total intensity of negative ions was markedly increased. For example, in a 9Xe: 1 $(CN)_2$ mixture, the intensity of $(CN)^-$ was increased about twenty fold. This increase in negative ion intensity is attributed to two processes: One, ionization by secondary electrons from Xe, and two, a reaction of metastable Xe^* ($5p^56s$) with $(CN)_2$ to form CN radicals which are subsequently ionized.

The increased intensity of negative-ion polymers plus a reaction addition complex $[Xe(CN)_2]^+$ observed in the positive ion spectrum are believed to be the explanation of the previously observed increased rate of polymerization of $(CN)_2$ upon the admixture of Xe.

References

1. H. M. Rosenstock and C. E. Melton, J. Chem. Phys., 26, 314 (1957).
2. C. E. Melton and H. M. Rosenstock, J. Chem. Phys., 26, 567 (1957).
3. C. E. Melton and G. F. Wells, J. Chem. Phys., 27, 1132 (1957).
4. G. F. Wells and C. E. Melton, Rev. Sci. Instr., 28, 1065 (1957).
5. Gus A. Ropp and C. E. Melton, J. Am. Chem. Soc., 80, 3509 (1958).
6. C. E. Melton, G. A. Ropp and T. W. Martin, J. Phys. Chem., 64, 1577 (1960).
7. C. E. Melton and P. S. Rudolph, J. Chem. Phys., 31, 1485 (1959).
8. C. E. Melton, J. Chem. Phys., 35, 1751 (1961).
9. S. C. Lind, D. C. Bardwell and J. H. Perry, J. Am. Chem. Soc., 48, 1556 (1926).
10. S. C. Lind and D. C. Bardwell, J. Am. Chem. Soc., 48, 1575 (1926).
11. C. E. Melton and P. S. Rudolph, J. Chem. Phys., 32, 1594 (1960).

Figure 7

POLYMER-ION MASS SPECTRA OF (CN) ₂ AT 1 mm				
M/e	FORMULA	INTENSITY		
		+ ion x 10 ⁻³	- ion	
26	CN	2.5 x 10 ⁸	2.4 x 10 ⁸	-
52	(CN) ₂	9.0 x 10 ⁹	1.9 x 10 ⁷	
78	(CN) ₃	1.6 x 10 ⁸	1.3 x 10 ⁶	
104	(CN) ₄	5.2 x 10 ¹⁰	2.0 x 10 ⁶	
130	(CN) ₅	6.0 x 10 ⁵	4.5 x 10 ⁵	
156	(CN) ₆	1.2 x 10 ⁶	3.1 x 10 ⁵	
182	(CN) ₇	4.7 x 10 ³	5.4 x 10 ⁴	
208	(CN) ₈	1.1 x 10 ³	3.7 x 10 ²	
234	(CN) ₉	1.0 x 10 ¹	3	
260	(CN) ₁₀	2.2 x 10 ¹	5	

ELECTRON AFFINITY OF ATOMIC IODINE⁺

Bruce Steiner
Michael L. Seman *
Lewis M. Branscomb

Atomic Physics Division, National Bureau of Standards, Washington 25, D. C.

Photodetachment of I^- ions has been observed in a crossed beam experiment. The apparatus used was essentially similar to that in previous photodetachment experiments. Use of four Sharp Cut filters provided good "effective" resolution close to threshold but did not permit an independent determination of the behavior of the cross section as a function of wavelength. A step function cross section, shown by Berry and co-workers to approximate closely the true cross section behavior, was used to provide an upper energy limit to the electron affinity shown to be close to the actual value. The value of the electron affinity thus determined, $3.076 \pm .005$ ev, is in excellent agreement with the shock wave determination of Berry, $3.075 \pm .003$. The absolute magnitude of the cross section in the region 0.3 ev above threshold was determined to be $2.1 \pm 1.1 \times 10^{-11}$ cm².

INTRODUCTION

Until recently, the electron affinities of the halogen atoms have been regarded as rather well determined¹. Confidence was encouraged by the fact that the various values determined generally agreed with one another within typical uncertainties of 0.10 ev, as listed in Table IV.

However, a recent series of shock wave experiments by R. Stephen Berry and co-workers² has yielded a set of photon absorption thresholds for Cl^- , Br^- and I^- consistently lower by about 0.10 ev than the previously accepted values. These spectra are especially noteworthy in that they are the first absorption spectra of negative ions ever obtained in which the absorption of the light is observed spectroscopically. The chief uncertainty in the experiments of Berry and co-workers is the accuracy with which the lowering of the threshold energy by Debye-Hückel effects in the shock wave plasma can be estimated.

The present crossed-beam experimental study of the photodetachment of electrons from I^- represents an effort (1) to determine the threshold energy for photodetachment of free I^- ions independent of plasma effects, and (2) to determine the absolute magnitude of the cross section in the region of the threshold. The absolute magnitude of the cross section can be used in the shock wave experiment to give directly the negative ion densities in the shock wave. This information can then be used in the calculation of the Debye-Hückel correction to the observed absorption threshold, which is required to convert this threshold energy to the free state electron affinity of iodine.

⁺This research was supported in part by the Office of Naval Research and the Advanced Research Projects Agency, Department of Defense.

* Present address: Joint Institute for Laboratory Astrophysics,
University of Colorado, Boulder, Colorado.

Table I. Filters used in threshold measurement

Filter Identification (M)	Corning Number	Transmission less than 1% for λ greater than: (A)
A	3389 + 3391	4025
B	3391	3997
C	3389	3980
D	3060	3730

Table II. Experimentally determined relative photodetachment probability, P_M

Filter Identification (M)	P_M	Standard Deviation (%)	Total Uncertainty (%)
A	.28	54	55
B	1.36	6	12
C	3.66	14	17
D	43.5	9	13

Table III. Electron affinity* of atomic iodine as determined in this work

	λ (A) ^o	Standard Deviation (A)	Total Uncertainty (A)	$h\nu$ (eV)	Standard Deviation (ev)	Total Uncertainty (ev)
P_C/P_D	4031	+4 -6	+6 -7	3.076	-.003 +.004	-.005 +.005
P_B/P_C	4036	+11 -19	+15 -32	3.072	-.008 +.014	-.012 +.024
P_A/P_B	4057	>+43 -32	>+43 -35	3.056	>-.032 +.024	>-.032 +.027

* Wavelengths (λ_o) and equivalent electron affinities ($h\nu$) corresponding to the threshold for photodetachment determined by ratios of signal (P_M) using various filters (M) and a step function cross section.

EXPERIMENTAL PROCEDURE

The apparatus used was essentially similar to that in previous photodetachment work^{3,4}. I^- ions were formed in a hot cathode arc discharge⁴ through a mixture of iodine vapor and ammonia. The negative ions were extracted from the ion source, accelerated, and mass analyzed by a 90° sector magnetic field. After deceleration, the beam entered the reaction chamber, where it intersected a chopped photon beam which photodetached electrons from the ions. These electrons were detected by an electron multiplier and the signal amplified, synchronously detected, and integrated for periods up to 50 sec. A 1000 watt dc xenon arc discharge lamp replaced the carbon arc of earlier experiments. The consecutive introduction of four Sharp Cut filters, listed in Table I, provided the information concerning the wavelength dependence of the cross section.

When adjusted to transmit I^- , the mass analyzer was capable of full resolution of one part in 15. The most likely possible contaminant in the "resolved" beam is thought to be HI^- . However, the closed shell-plus-one structure of such an ion, analogous to that of noble gas negative ions, is considered to be unstable; almost certainly, HI^- constitutes a negligibly small fraction of the beam, if indeed HI^- exists at all.

The procedure for the measurement of the photon flux differed from that of previous photodetachment experiments. Before performance of the present photodetachment experiments, a section of the reflected arc light was focussed on the slit of a small prism monochromator which was fitted with a thermocouple detector and previously calibrated for response as a function of wavelength by an "NBS Standard of Spectral Radiance"⁵. The average of three wavelength scans, corrected for monochromator-detector sensitivity, was taken to be representative of the relative spectral radiance of the xenon lamp within the 10 percent intensity fluctuation of the source. For the photodetachment experiment, the fixed fraction of the total light reaching the monitoring bolometer³ was filtered so that the bolometer received light only in the region $\lambda < 4850 \text{ \AA}$. The bolometer was then used to measure fluctuations of the light in this wavelength region during the course of the experiment. The light output of the xenon lamp varied no more than 10 percent during a period of several minutes while the current through the lamp was maintained at 41.2 ± 0.2 amperes.

The transmission of each of the various filters was measured independently by the NBS Photometry and Calorimetry Section.

EXPERIMENTAL RESULTS

Threshold Energy

The direct experimental results are listed in Table II as signals in arbitrary units for each of the filters. Each result represents the average of five or six individual determinations. The uncertainties are listed both for the standard deviation assuming random errors only and also as total uncertainties for systematic as well as random errors.

The threshold energy determinations in Table III were made in the following manner. When time-varying factors are removed, the photodetached electron current with filter M in place is given³ by the equation,

$$P_M = k \int \varphi'(\lambda) T_M(\lambda) \lambda \sigma(\lambda) d\lambda. \quad (1)$$

Since the geometrical factor, k , is independent of the particular filter used, the measurement of ratios of P_M 's for the various filters of known transmission, $T_M(\lambda)$, together with measured values for the source radiance, $\varphi'(\lambda)$, permits determination of the threshold energy if the shape of the cross section, $\sigma(\lambda)$, is known. The curves representing $\varphi' \lambda T_M$ as a function of wavelength for the various filters are shown in figure 1. Although the wavelength differences in the transmission limits of the various filters used in these experiments were far less than in previous crossed beam experiments, with a resulting increase in "resolving power" at threshold, the relatively small number of filters did not permit a precise independent determination of this threshold shape.

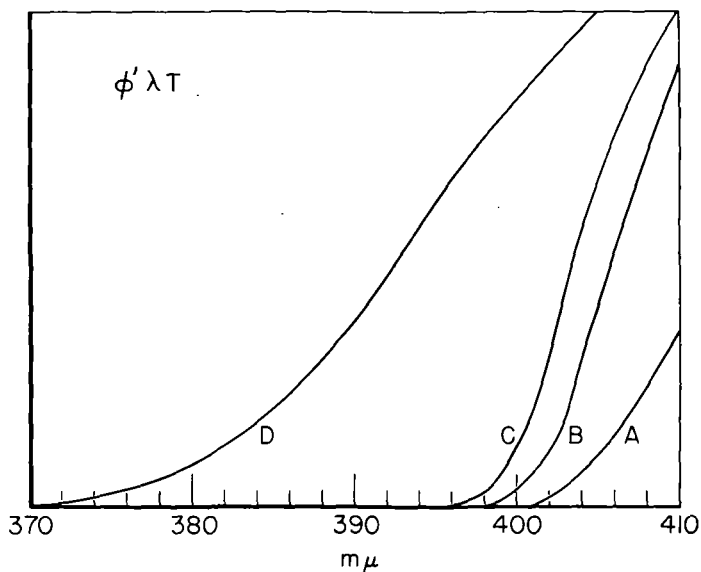


Figure 1. Photon density per angstrom, $\phi' \lambda T$ in arbitrary units, as a function of wavelength, for light from xenon arc lamp with each of four filters used in the determination of the threshold for photodetachment of electrons from I^- .

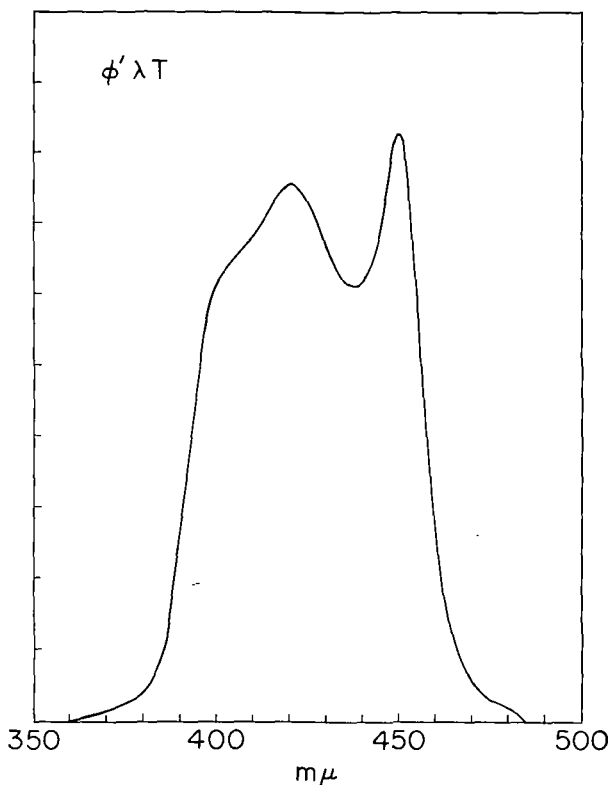


Figure 2. Photon density per angstrom, $\phi' \lambda T$ in arbitrary units, as a function of wavelength, for light from xenon arc lamp with filter combination "E", used in the determination of the absolute cross section for photodetachment of electrons from I^- .

Previous theoretical treatment⁶ has shown the threshold behavior of the cross section to be represented by the series $\sigma = aE^{1/2}(b+cE+dE^2\dots)$ where E is the ejected electron kinetic energy, i.e. $(h\nu - E_0)$ where $h\nu$ is the photon energy and E_0 is the threshold energy. Although the relative magnitude of the higher order terms is not determined by first principles, a fit of previous experimental data for oxygen⁶ and carbon⁴ has proved possible over about 0.3 ev energy range with the predicted infinite slope at threshold and two or three series terms. In contrast to the work on those negative ions, the experiments of Berry et al.² show that the threshold behavior for I^- approximates a step function, infinite slope at threshold and constant cross section above. Thus for I^- , many higher order terms are necessary to describe the cross section as observed by Berry in the above series, even in the first 0.3 ev.

Berry's observations also show that there are no strong absorption lines near threshold due to photoexcitation followed by autodetachment. Although the exact shape of the absorption cross section is obscured by Debye-Hückel effects, the curve is observed by Berry to rise monotonically (and nearly as a step function) within 0.3 ev of the threshold. It follows that the use of a step function, instead of a more slowly rising function in the determination of the threshold energy from our beam experiment, provides an upper limit for the iodine electron affinity. The integration in equation (1) with a step function cross section reduces to an integration of the experimental function shown in Figure 1:

$$P_M = k \int_{T_M=0}^{T_{\sigma=0}} \varphi'(\lambda) T_M(\lambda) \lambda d\lambda$$

The upper limit of this integration is the threshold to be determined. The upper limit in energy we thus obtain is $3.076 \pm .005$ ev. This value is to be compared with Berry's uncorrected experimental value, 3.070 ± 0.003 , which is a lower limit in energy.

The main systematic error in this work is undoubtedly the 10% uncertainty in the spectral radiance, $\varphi'(\lambda)$. Compared to this, other factors can be neglected. Thus, the uncertainties in the last column of Table III include this 10% in each P_M in addition to the standard deviation of the various P_M values of assuming random errors.

Absolute Cross Section

The magnitude of the cross section between threshold and 3600 Å has been measured relative to the absolute magnitude of the cross section for photodetachment of H^- between 4900 Å and 3600 Å⁷. Figure 2 shows $\varphi' T$ as a function of wavelength for filter "E" used in this measurement. The absolute cross section magnitude thus determined for a step function is $(2.1 \pm 0.5) \times 10^{-17} \text{ cm}^2$. This error limit is again the standard deviation assuming random errors.

The difference in area under the true cross section curve from that under a step function from threshold to 3600 Å probably is not more than 10 percent. Systematic errors due to beam inhomogeneity probably are not greater than the range of statistical error. Hence, the total uncertainty may be ± 50 percent.

The absolute cross section, $2.1 \pm 1.1 \times 10^{-17} \text{ cm}^2$ has been used by Berry and co-workers to arrive at an ion density for I^- . This density leads them to a Debye-Hückel correction of 6 Å, or an electron affinity of $3.075 \pm .003$ ev. A summary of this and other determinations of the electron affinity of atomic iodine appear in Table IV.

ACKNOWLEDGMENTS

We are grateful to Professor R. Stephen Berry for his sharing his experimental data with us prior to publication. The careful measurement of the transmissions of the various filters by John Schleter of the Bureau of Standards was essential to this work. Dr. Herbert P. Broida, of the Bureau of Standards, has also been most helpful.

Table IV. Determinations by various workers of the electron affinity of atomic iodine

Method	Value (ev)	Worker
Surface ionization	3.23 ± 0.02 (assuming $A(\text{Br}) = 3.50$)	Bakulina and Ionov ^a
Surface ionization	3.17 ± 0.07	Bailey ^b
Lattice energies	3.19 ± 0.06	Cubiciotti ^c
Photoionization	3.13 ± 0.12	Morrison <u>et al</u> ^d
Shock tube photodetachment (lower bound)	3.070 ± 0.003	Berry, Reiman, Spokes ^e
(corrected)	3.075 ± 0.003	Berry, Reiman, Spokes
Crossed beam photodetachment (upper bound)	3.076 ± 0.005	This work

^aI. N. Bakulina and N. I. Ionov, Dokl. Akad. Nauk SSSR, 105, 680 (1955).

^bT. L. Bailey, J. Chem. Phys., 28, 792 (1958).

^cD. Cubicciotti, J. Chem. Phys. 34, 2189 (1961).

^dJ. D. Morrison, H. Hurzeler, M. G. Inghram, and H. E. Stanton, J. Chem. Phys. 33, 821 (1960).

^eR. S. Berry, C. W. Reiman, and G. N. Spokes, J. Chem. Phys. accompanying paper.

REFERENCES

1. T.L. Bailey, J. Chem. Phys. 28, 792 (1958).
2. R. Stephen Berry, et al, J. Chem. Phys. 35, 2237 (1961); Bull. Am. Phys. Soc. 7, 69 (1962).
3. S. J. Smith and L. M. Branscomb, Rev. Sci. Inst. 31, 733 (1960).
4. M. L. Seman and L. M. Branscomb, Phys. Rev. (March 1, 1962).
5. R. Stair, et al, J. Research Nat'l. Bur. Standards, 64A, 291 (1960).
6. L. M. Branscomb, et al, Phys. Rev. 111, 504 (1958).
7. T. John, Mon. Notices Roy. Astron. Soc. 121, 41 (1960).

Measurement of Electron Capture Cross Sections Using Swarm Methods

G. S. Hurst
Health Physics Division
Oak Ridge National Laboratory*
Oak Ridge, Tennessee

(*Operated by Union Carbide Corporation for the U. S. Atomic Energy Commission)

I. INTRODUCTION

In the experimental studies of the formation of negative ions, electron swarm methods appear to have a definite role. In the swarm method electrons make many collisions with the atomic and molecular gas through which they move under the action of an applied electrical field, and unlike in beam experiments, they have a wide distribution of kinetic energy. This disadvantage concerning the spread of electron energies does not preclude the following applications of swarm experiments: 1) in spite of the wide spread in electron energies, careful analysis of swarm data may give reasonably accurate total cross sections for electron capture; 2) swarm experiments may be performed over a wide range of average electron energies, e.g., thermal to greater than 10 ev, depending on the gas used and the magnitude of E/P (volts cm^{-1} (mm Hg) $^{-1}$); 3) swarm experiments may be done at much higher pressures than beam experiments, hence collision processes may be examined for various atomic and molecular effects.

In the usual swarm method the types of ions formed are not determined, and the investigator must resort to theory or to mass spectrometry for this information. Hence, beam experiments which are not sufficient within themselves to determine all the information which is needed may be combined with mass spectrometer experiments to considerable mutual advantage.

In swarm experiments electrons are set free in a gas by various means, e.g., thermionic emission, UV irradiation, or gas ionization with energetic particles. Regardless of their energy of liberation, they come into an equilibrium energy which is characteristic only of the gas and E/P . This equilibrium distribution of electron energies is established as a balance between the energy gained from the electrical field and the energy lost by atomic or molecular collisions. Several swarm parameters are open to direct experimental measurement; among these are w , the rate of drift of the electron swarm in the field direction, w/D , where D is the electron diffusion coefficient, and α , the probability of electron capture per cm of travel in the field direction at unit pressure. From these measured quantities one may derive other quantities of interest such as the average kinetic energy, $\bar{\epsilon}$, the probability, h , of electron capture in a collision, and σ_c , the capture cross section. The reader is referred to Healey and Reed¹ for a comprehensive treatment of the electron swarm and for a valuable compilation of experimental data.

II. ELECTRON DIFFUSION EXPERIMENTS AND AVERAGE ELECTRON ENERGY

Several investigators have used various versions of the Townsend^{2,3} diffusion apparatus to study the motion of electrons in gases; recent publications^{4,5} contain references to the earlier work. The method is based on a theoretical treatment of electron transport which considers simultaneous diffusion and electron drift due to the applied field. For example, if electrons are transported in the z direction due to an applied field in this direction, the differential equation expressing the time and space dependent density n is given by

$$\frac{1}{D} \frac{\partial n}{\partial t} = \nabla^2 n - \frac{w}{D} \frac{\partial n}{\partial z} \quad (1)$$

where t is the time, and w and D are the drift velocity and diffusion coefficients, respectively. The steady state solution (i.e., $\partial n / \partial t = 0$) of Eq. (1) has been worked out for boundary conditions appropriate to experimentally convenient geometries by Huxley and Bennett⁶ and by Huxley and Crompton.⁷ Having obtained the solution for the electron density, one may write expressions for the current received by concentric collectors, and the experimentally measured ratio, R , of currents received by two collectors may be used to calculate w/D . For example, consider a source located at the point where the z axis makes a normal intersection with one end of an infinite slab of height, h , the other end of which contains two concentric planar regions of inner radius b and outer total radius c (about the z axis). Figure 1 shows a plot⁵ of

Table I. Coefficient k_T for the Druyvesteyn Distribution for Electrons in Nitrogen, Carbon Dioxide, Methane, Ethylene, and Cyclopropane.

E/P $\frac{\text{Volts}}{\text{cm/mm Hg}}$	Nitrogen	Carbon Dioxide	Methane	Ethylene	Cyclopropane
0.2	6.74		2.15		2.48
0.4	11.7		3.30	2.36	2.54
0.6	16.0		4.39	2.53	2.81
0.8	19.3	2.00	5.85	2.82	3.09
1.0	21.3	2.05	7.52	3.11	3.50
1.2	23.0	2.12	9.10	3.50	3.83
1.4	24.4	2.13	11.0	3.82	4.14
1.6	25.6	2.21	13.1	4.29	4.45
1.8	26.6	2.31	15.2	4.73	4.83
2.0	27.5	2.39	17.4	5.03	5.22
2.5	29.9	2.72	22.9	6.34	6.08
3.0	31.0	3.12	29.6	7.99	7.06
3.5	33.1	3.77	35.1	9.48	8.01
4.0	33.8	4.67	42.0	11.3	8.93
4.5	35.0	6.07	46.9	13.1	9.95
5.0	35.8	7.85	53.4	14.8	11.1

Table II. Evaluation of the Ratio $w\alpha_0/f(\epsilon)$ for Various Values of ϵ .
An (E/P) -Independent Ratio Indicates a Solution to Eq. (9).

E/P	α_0 $\text{cm}^{-1}(\text{mm Hg})^{-1}$	$v \cdot \alpha_0 \cdot 10^{-6}$ $\text{sec}^{-1}(\text{mm Hg})^{-1}$	Electron Energy (ev)							
			6.3		6.4		6.5		6.6	
			$f(\epsilon)$	$w\alpha_0/f(\epsilon)$	$f(\epsilon)$	$w\alpha_0/f(\epsilon)$	$f(\epsilon)$	$w\alpha_0/f(\epsilon)$	$f(\epsilon)$	$w\alpha_0/f(\epsilon)$
0.40	0.18	0.058	0.00224	25.9×10^6	0.00161	36.0×10^6	0.00114	50.9×10^6	0.000793	73.1×10^6
0.45	0.57	0.185	0.00615	30.1×10^6	0.00472	39.2×10^6	0.00358	51.7×10^6	0.00269	68.8×10^6
0.50	1.20	0.396	0.0126	31.4×10^6	0.0102	38.8×10^6	0.00813	48.7×10^6	0.00643	61.6×10^6
0.55	2.0	0.670	0.0213	31.5×10^6	0.0179	37.4×10^6	0.0149	45.0×10^6	0.0122	54.9×10^6
0.60	3.0	1.02	0.0317	32.2×10^6	0.0273	37.4×10^6	0.0233	43.8×10^6	0.0198	51.5×10^6
0.65	4.1	1.41	0.0428	32.9×10^6	0.0377	37.4×10^6	0.0330	42.7×10^6	0.0287	49.1×10^6
0.70	5.3	1.86	0.0540	34.4×10^6	0.0484	38.4×10^6	0.0432	43.1×10^6	0.0383	48.6×10^6
0.75	6.6	2.34	0.0647	36.2×10^6	0.0589	39.7×10^6	0.0533	43.9×10^6	0.0481	48.6×10^6

$R = i_b / (i_b + i_c)$ as a function of $E/h/k_1$ for various ratios, b/h , and for a fixed value of $c/h = 1.5$. The coefficient k_1 is related to w/D by the equation,

$$\frac{w}{DP} = \frac{A \cdot 38.92 \cdot E/P}{k_1} = \frac{38.92 \cdot E/P}{k_T} \quad (2)$$

where $A = 1$ for the Maxwellian distribution and $A = 1.14$ for the Druyvesteyn distribution. The Townsend coefficient, k_T , is a convenient measure of the average kinetic energy of the electrons, usually called agitation energy, and is defined as follows:

$$k_T = \frac{\text{Electron Agitation Energy}}{\text{Molecular Agitation Energy at } 25^\circ \text{C}} \quad (3)$$

Clearly, k_T is a function of E/P since the kinetic energy for molecules is unaffected by the electrical field, and the agitation energy for electrons generally increases with E/P . Of the two distribution functions, i.e., Maxwellian or Druyvesteyn, it should be said that the latter is generally more meaningful since it is derived from the Boltzman transport equation and is applicable to electrons under the influence of an electrical field.

The diffusion apparatus used by Cochran and Forester has been described in considerable detail.⁵ Figure 2 is a schematic diagram of the diffusion chamber in which h was held constant at 3 cm, b could be set at 0.3, 0.6, 0.9, or 1.5 cm, and c was held constant at 4.5 cm.

Table I summarizes the Townsend coefficient k_T for electrons in nitrogen, carbon dioxide, methane, ethylene, and cyclopropane. These are based on diffusion measurements of w/DP and Eq. (2). It is noted that the average electron energy corresponding to these k_T values covers the range from about 0.08 eV to 2.0 eV, depending on the gas and E/P .

III. THE DISTRIBUTION OF ELECTRON ENERGIES IN ARGON

Holstein⁸ has shown that the distribution of energies for electrons making elastic collisions in a gas may be obtained from a solution of the Boltzman transport equation. This theory has been applied by Barbieri⁹ to He and Ar and the connection between the energy distribution and drift velocity was shown. Figure 3 shows the drift velocity in Ar as measured by Bowe¹⁰ and by Bortner et al.¹¹ Bowe¹² has shown that measured drift velocity as a function of E/P (P is the pressure normalized to 25°C) gives a basis for estimating the transport cross section for Ar as a function of electron energy. The transport cross sections so obtained are in general agreement with the Ramsauer-Kollath data;¹³ thus, the electron energy distributions derived from transport theory are consistent with the experimental drift velocities. Figure 4 shows some of the distribution functions for Ar at a few values of E/P .¹⁴

IV. MEASUREMENT OF ELECTRON CAPTURE CROSS SECTIONS WITH SWARM EXPERIMENTS

One example of an electron swarm experiment for the measurement of the attachment coefficient, α , is shown schematically in Fig. 5. In the apparatus¹⁵ the motion of free electrons is examined in two chambers having a common atmosphere. In one case the "pulse height" due to the work done by the electrical field in transporting free electrons (liberated by alpha particle ionization) in the field direction is measured with a pulse amplifier. In the other case the drift velocity is measured. From these two quantities, α is calculated.

It has been shown¹⁵ that the time-dependent change in potential $g(t)$ of the collector plate of a plane ionization chamber of separation d cm, due to free electrons moving through the chamber, is given by

$$g(t) = (A/f) [1 - \exp(-ft/\tau_0)] \quad (4)$$

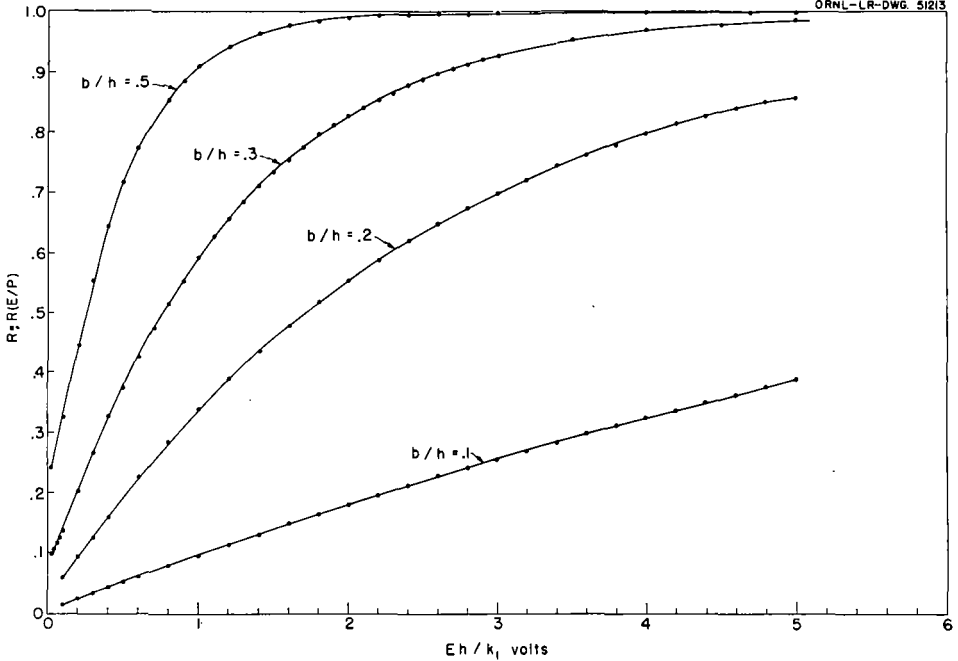


Fig. 1. Curves Showing the Electron Current Ratio R as a Function of Eh/k_1 for Several Values of b/h .

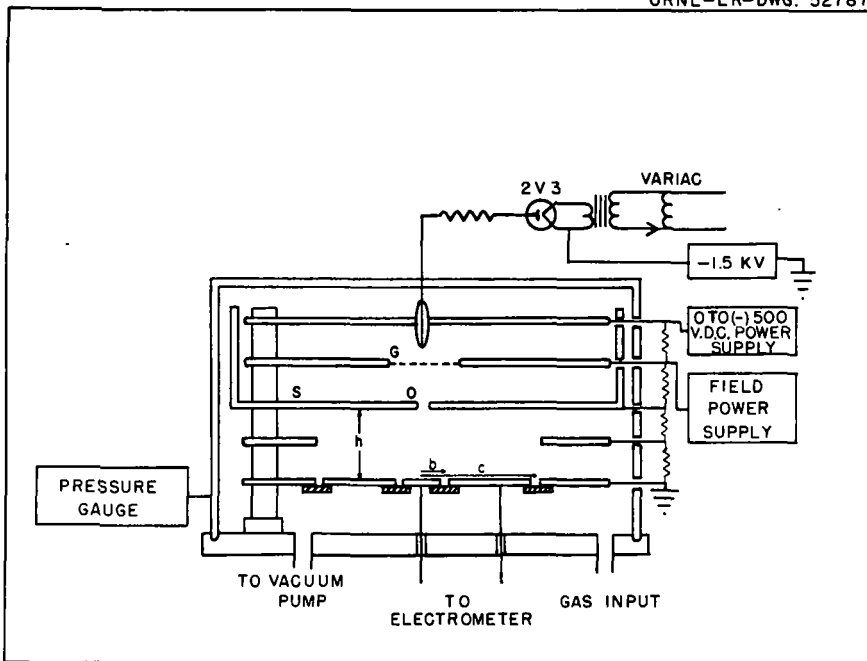


Fig. 2. Schematic Diagram of the Electron Diffusion Chamber

where A is a constant, τ_0 is the collection time of free electrons, and $f = \alpha f_1 P d$. In this expression α is the attachment coefficient for electrons defined by

$$dN = -\alpha N f_1 P dx \quad (5)$$

where $-dN/N$ is the fraction of electrons captured in moving dx in the field direction and $f_1 P$ is the pressure of the attaching gas, referred to a standard temperature of 25°C . If the pulse is examined with a pulse amplifier of equal differentiating and integrating time constants (both equal to t_1), the output pulse of such an amplifier is given by

$$V(\tau) = \int_0^\tau \frac{dq(t)}{dt} \frac{(\tau-t)}{t_1} e^{-(\tau-t)/t_1} dt \quad (6)$$

where $t/t_1 e^{-t/t_1}$ is the response of the amplifier to a step function.

Using Eq. (4) for $g(t)$, the expression given in Eq. (6) for $V(\tau)$ becomes for $\tau \leq \tau_0$

$$V(\tau) = \frac{A e^{-\tau/t_1}}{(\tau_0 - t_1 f)} \left[\frac{\exp(u\tau)}{u} - \tau - \frac{1}{u} \right] \quad (7a)$$

and for $\tau \geq \tau_0$

$$V(\tau) = \frac{A \exp(-\tau/t_1)}{(\tau_0 - t_1 f)} \left[\{ \exp(u\tau_0) - 1 \} \tau - \exp(u\tau_0) \left(\tau_0 - \frac{1}{u} \right) - \frac{1}{u} \right] \quad (7b)$$

where $u = (\tau_0 - t_1 f)/t_1 \tau_0$, and where τ_0 is the collection time for free electrons and is equal to w_0 . Equations (7a) and (7b) have been evaluated to find the "pulse height" i.e., the maximum value of $V(\tau)$ for $\tau/t_1 = 0, 1, 2, 3, 4$, and 5 as a function of f .¹⁶ With experimental values for τ_0 and the pulse height, f and α may then be calculated.

The apparatus illustrated in Fig. 5 has been applied¹⁷ to the study of dissociative electron capture in H_2O vapor. To obtain electrons in the energy range where dissociative capture takes place in many molecules, it is convenient to mix these molecular gases in Ar. Figure 6 shows the pulse-height data obtained when various amounts of water vapor were mixed with Ar at 400 mm Hg. Drift velocity data for mixtures of Ar and water are shown in Fig. 7. From these data the attachment coefficients α were calculated and are shown in Fig. 8. In this figure, α for various E/P values is plotted as a function of the ratio of water pressure, $f_1 P$, to Ar pressure, $f_2 P$.

From Fig. 8 it is seen that α is, within experimental error, independent of total pressure but depends strongly on the ratio $f_1 P/f_2 P$. This suggests that the electron energy distribution in Ar is influenced by water, and that an increase in $f_1 P/f_2 P$ decreases the number of electrons in the range where dissociative capture takes place. It seems reasonable to expect that the limiting values of α as $f_1 P/f_2 P$ approaches zero, α_0 , are to be associated with the electron energy distribution of pure Ar. Thus we can write α_0 in terms of the capture cross section, $\sigma_c(\epsilon)$, at energy ϵ as follows:

$$\alpha_0 \left(\frac{E}{P} \right) = \frac{N_0 (2/m)^{\frac{1}{2}}}{w(E/P)} \int_0^\infty \epsilon^{\frac{1}{2}} \sigma_c(\epsilon) f \left(\epsilon, \frac{E}{P} \right) d\epsilon \quad (8)$$

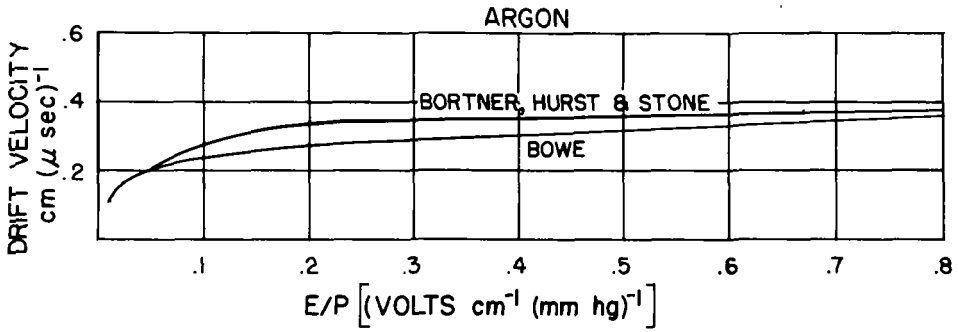


Fig. 3. Drift Velocity in Ar as Measured by Bowe and by Bortner, Hurst, and Stone

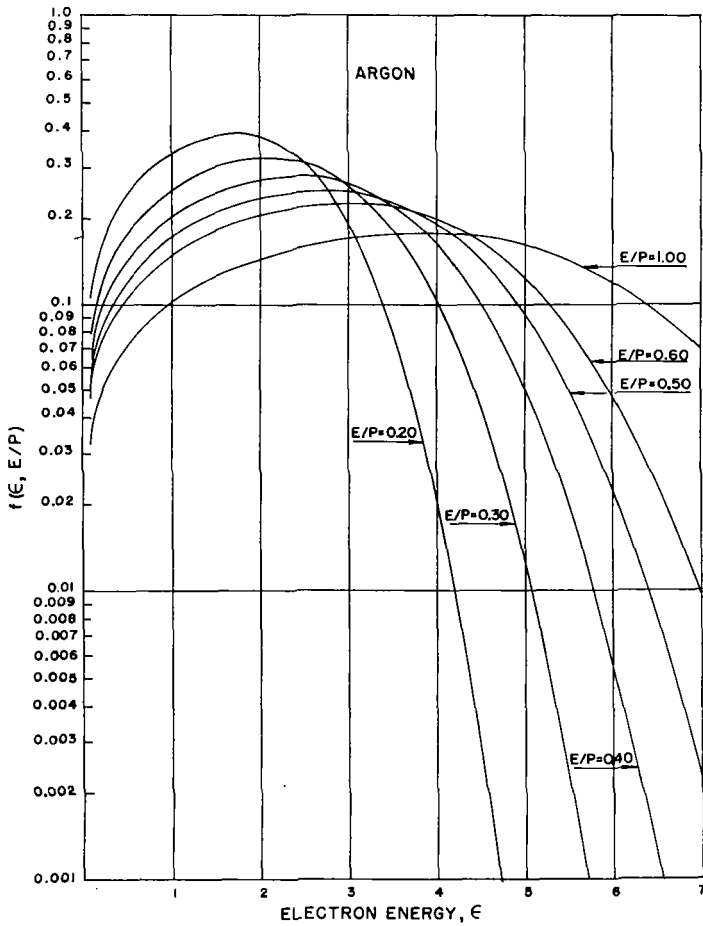


Fig. 4. Distribution Functions for Ar at Various Values of E/P

where $f(\epsilon, E/P)$ is the normalized energy distribution function for electrons in pure Ar, $w(E/P)$ is the electron drift velocity in Ar, m is the electron mass, and N_0 is the number of water molecules per cm^3 at 1 mm Hg.

Considering the fact that the mass spectrograph data¹⁸⁻²⁰ and a beam experiment²¹ show a fairly narrow peak for the formation of H^- and that in all such experiments the electron beam has an appreciable spread in energy, it is reasonable to select a strongly peaked function as a trial solution for $\sigma_c(\epsilon)$ in Eq. (8). Hence,

$$\alpha_0 \left(\frac{E}{P} \right) = \frac{N_0 (2/m)^{\frac{1}{2}}}{w(E/P)} \epsilon_1^{\frac{1}{2}} \sigma_c(\epsilon) f \left(\epsilon_1, \frac{E}{P} \right) \int_0^{\infty} \sigma_c(\epsilon) d\epsilon \quad (9)$$

where ϵ_1 is the energy at which the capture cross section peaks. Since the various observers are not in agreement on the energy at which the cross section peaks, we consider ϵ_1 as a variable and find a value which satisfies Eq. (9) for the experimental range of E/P . Tabulations of $w\alpha_0/f(\epsilon)$ for various electron energies ϵ are shown in Table II. In these tabulations the drift velocity w for Ar was taken from Bortner, Hurst, and Stone.¹¹ The values of the electron energy distribution function for Ar are those given in Section III. It is seen from Table II that if we let $\epsilon_1 = 6.3$ or 6.5, the fit to Eq. (9) is less accurate. The magnitude of the cross section integral

$$A = \int_0^{\infty} \sigma_c(\epsilon) d\epsilon$$

corresponding to $\epsilon_1 = 6.4$ eV is $7.7 \times 10^{-18} \text{ cm}^2 \text{ ev}$. The magnitude of A and the energy where the cross section is a maximum, ϵ_1 , derived in this way compared favorably with the results obtained by Buchel'nikova.²¹ From the curve published by Buchel'nikova, one may estimate $\epsilon_1 = 6.4$ eV and $A = 6.5 \times 10^{-18} \text{ cm}^2 \text{ ev}$.

The above discussions illustrate the use of swarm experiments to obtain absolute cross sections, i.e., application (1) in the introduction. Similarly, good agreement has been found between beam experiments²¹ and swarm measurements^{15,17} for the cross section for electron capture to form O^- due to interaction with O_2 . Finally, let us refer to the applications of electron swarm experiments to (2) and (3) in the introduction. For example, it has been found²² that for mixtures containing small amounts of O_2 in N_2 , α depends both on the pressure of O_2 and of N_2 . In this case the average electron energy ranged from about 0.4 eV to 0.8 eV, corresponding to the E/P range 0.2 to 0.8 (see Table I), and thus unstable O_2^- , i.e., $(\text{O}_2^-)^*$ is formed by direct capture.

It was found that the cross section for stabilization of O_2^{*-} by a collision with O_2 , σ_1 , was $3 \times 10^{-15} \text{ cm}^2$ and with N_2 , σ_2 was $6 \times 10^{-17} \text{ cm}^2$. These widely differing cross sections are consistent with the idea that σ_1 corresponds to the transfer of electronic excitation and that σ_2 corresponds to vibrational transfer, and this in turn suggests that O_2^{*-} is initially the $4\Sigma_{\mu}^-$ level.

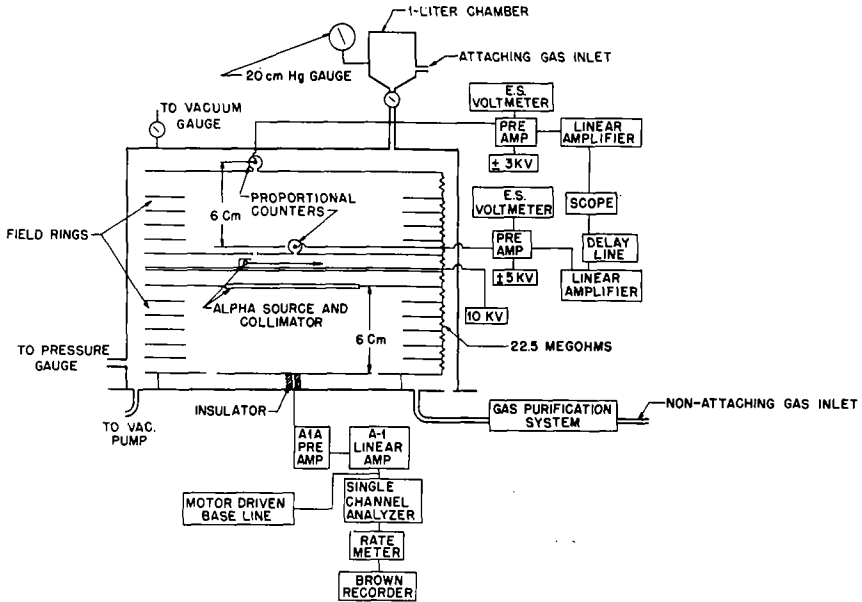


Fig. 5. Electron Attachment Apparatus

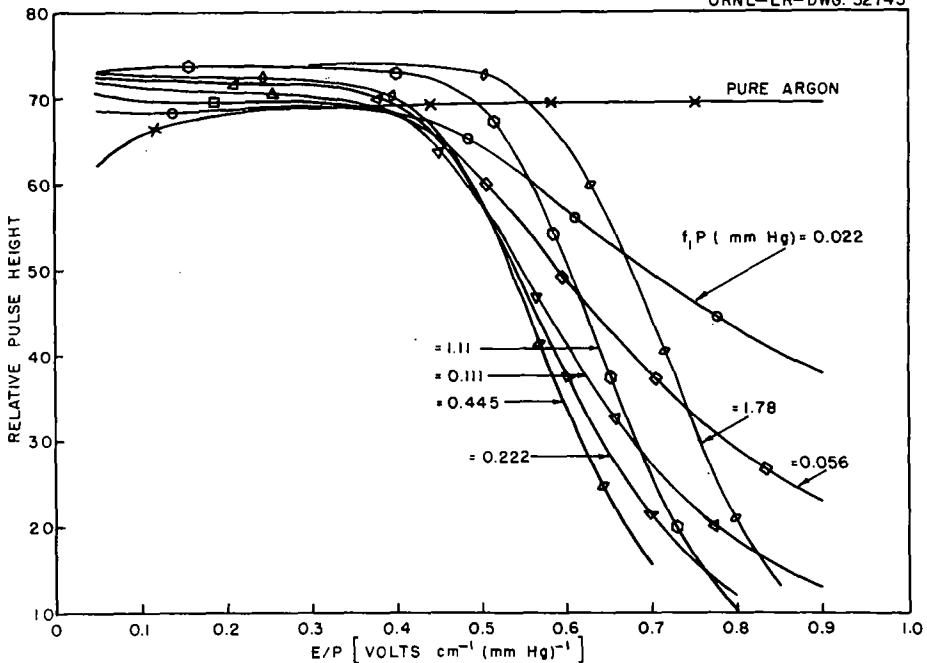


Fig. 6. Pulse Height vs E/P for H_2O -Ar Mixtures (400 mm Hg)

REFERENCES

1. R. H. Healey and J. W. Reed, The Behavior of Slow Electrons in Gases (The Wireless Press for Amalgamated Wireless Ltd., Sydney, Australia, 1941).
2. J. S. Townsend and V. A. Bailey, Phil. Mag. 44, 1033 (1922).
3. J. S. Townsend, in Electrons in Gases (Hutchinson's Scientific and Technical Publications, New York, 1948).
4. L. W. Cochran and D. W. Forester, Phys. Rev. (to be published).
5. D. W. Forester and L. W. Cochran, "Diffusion of Slow Electrons in Gases," ORNL-3091, Sept. 29, 1961.
6. L. G. H. Huxley and F. W. Bennett, Phil. Mag. 30, 396 (1940).
7. L. G. H. Huxley and R. W. Crompton, Proc. Phys. Soc. B68, 381 (1955).
8. T. Holstein, Phys. Rev. 70, 367 (1946).
9. D. Barbieri, Phys. Rev. 84, 653 (1951).
10. J. C. Bowe, Phys. Rev. 117, 1411 (1960).
11. T. E. Bortner, G. S. Hurst, and W. G. Stone, Rev. Sci. Instr. 28, 103 (1957).
12. J. C. Bowe, Phys. Rev. 117, 1416 (1960).
13. C. Ramsauer and R. Kollath, Ann. Physik 12, 837 (1932).
14. For a complete tabulation, see R. H. Ritchie and G. E. Whitesides, "Equilibrium Electron Distributions in Elastically Scattering Gases," ORNL-3081, June 2, 1961.
15. T. E. Bortner and G. S. Hurst, Health Phys. 1, 39 (1958).
16. The original publication (Ref. 15) contained errors for $\tau_0/t_1 \geq 2$ which have subsequently been corrected and reported by H. B. Eldridge, "Pulse Height Calculations for a Parallel Plate Ionization Chamber Containing Electron Attaching Gases," ORNL-3090 (to be printed). This report contains a detailed tabulation of the pulse height as a function of f for various values of τ_0/t_1 .
17. G. S. Hurst, L. B. O'Kelly, and T. E. Bortner, Phys. Rev. 123, 1715 (1961).
18. W. W. Lozier, Phys. Rev. 36, 1417 (1930).
19. M. M. Mann, A. Hustrulid, and J. T. Tate, Phys. Rev. 58, 340 (1940).
20. M. Cottin, J. Chim. Phys. 56, 1024 (1959).
21. I. S. Buchel'nikova, Soviet Phys. JETP 35(8), 783 (1959).
22. G. S. Hurst and T. E. Bortner, Phys. Rev. 114, 116 (1959).

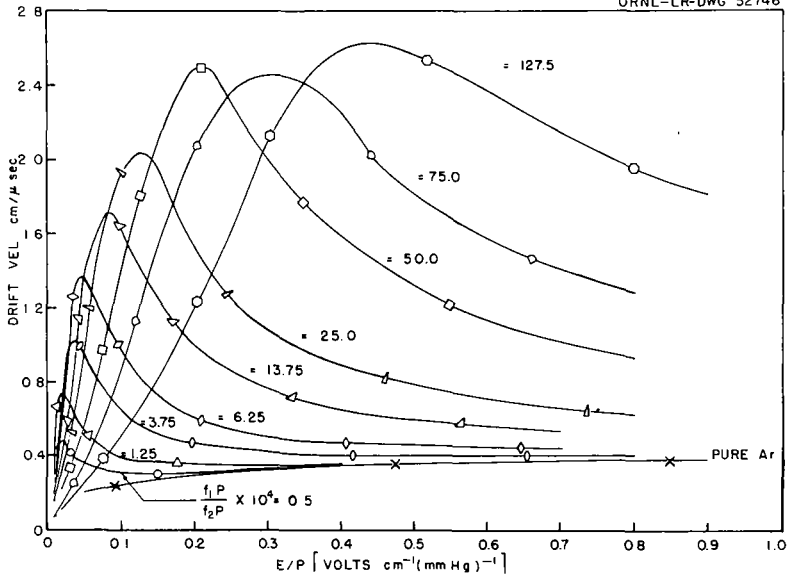


Fig. 7. Electron Drift Velocity in H₂O-Ar Mixtures (400 mm Hg)

UNCLASSIFIED
ORNL-LR-DWG-58155

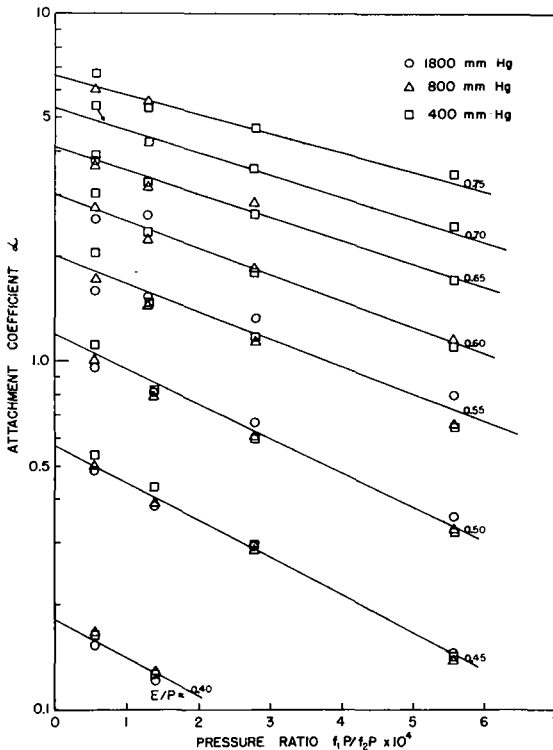


Fig. 8. Attachment Coefficient α as a Function of the Ratio of H₂O Pressure to Ar Pressure for Various Values of E/P.

A Mass Spectrometric Investigation of Secondary Reactions in Mixtures Containing Mercury Vapor.

V. Čermák and Z. Herman

Institute of Physical Chemistry, Czechoslovak Academy of Sciences, Prague

This paper deals with the first results of an investigation of the reactivity of ions and neutral excited particles in mixtures containing vapors of metals. We started this work at the Institute of Physical Chemistry of the Czechoslovak Academy of Sciences in Prague, hoping to obtain valuable data in a field hitherto quite unexplored. The data for such reactions--which occur, for example, in mixtures containing mercury vapor--might be of importance in gaseous electronics, in radiation chemistry (Hg atoms are reported to act in some cases as ion scavengers (Newton and Mains, 1961)), or in the theory of ion-molecule reactions and interactions of excited neutral species.

We have been studying the reactions occurring in mixtures of mercury with the noble gases, O_2 , N_2 , CO_2 , H_2O , NH_3 , CH_4 , C_2H_6 , C_3H_8 , C_2H_2 , and CH_3OH . An ordinary mass spectrometer of the Nier type was used; it was equipped with a sensitive vibrating reed amplifier so that minimum currents of $3 \cdot 10^{-16}$ a could be measured.

The reactions occurring in the mixtures are of two types. To the first type belong reactions between two neutral particles, one of which is in an electronically excited state. In the reaction a charged addition product is formed and an electron is released. This type is analogous to the reactions forming Cs_2^+ ions in vapors of Cs, (Mohler and Boeckner, 1930), Ar_2^+ ions in Ar (Tuxen, 1936), (Arnot and M'Ewen, 1938), or $XeCH_4^+$ ions in mixtures of Xe and methane (Field and Franklin, 1961).

In mixtures of mercury with noble gases (Table I) the reacting excited particle can be identified, by measurement of the appearance

Table I.

Reactions of excited species in mercury vapor

Number	Mixture	Secondary ion	Appearance potential	Reaction ^{a)}
1	Xe + Hg	XeHg ⁺	9.8	Xe* + Hg → XeHg ⁺ + e
2	Kr + Hg	KrHg ⁺	10.6	Kr* + Hg → KrHg ⁺ + e
3	Ar + Hg	ArHg ⁺	11.4	Ar* + Hg → ArHg ⁺ + e
4	Ne + Hg	-		not observed
5	He + Hg	-		not observed
6	N ₂ + Hg	N ₂ Hg ⁺	9.4	N ₂ * + Hg → N ₂ Hg ⁺ + e
7	H ₂ O + Hg	H ₂ OHg ⁺		
8	NH ₃ + Hg	NH ₃ Hg ⁺	8	N ₂ or N ₂ * + Hg* → N ₂ Hg ⁺ + e H ₂ O* + Hg* → H ₂ OH ⁺ + e
9	CH ₄ + Hg	CH ₄ Hg ⁺	8 - 8.5	NH ₃ * + Hg* → NH ₃ Hg ⁺ + e
10	C ₂ H ₂ + Hg	C ₂ H ₂ Hg ⁺	< 10	CH ₄ * + Hg* → CH ₄ Hg ⁺ + e
11	CH ₃ OH + Hg	CH ₃ OHg ⁺	8.8	C ₂ H ₂ * + Hg* → C ₂ H ₂ Hg ⁺ + e
			7.9	CH ₃ OH* + Hg* → CH ₃ OHg ⁺ + e

a) An asterisk denotes an electronically excited atom.

potential of the reaction product, as an excited noble gas atom. This is so even if the excitation energy is higher than the ionization potential of mercury (10.43 V: Table I, reaction No. 3).

In mixtures of mercury with molecules the secondary ions contain, beside the mercury atom, the combined molecule (Table I: reactions 7-11). The appearance potential of these secondary molecular ions is always lower than the ionization potential of both particles. In this case the reacting excited species are probably Hg atoms.

The current of secondary ions depends on the energy of exciting electrons and exhibits a sharp maximum at an electron energy about twice as great as the excitation energy of the primary particle (Fig. 1). These curves resemble the excitation function for optically-forbidden transitions, but the peaks in Fig. 1 are not so sharp and are shifted towards greater excitation energies. We tried to get more information about the nature of the reactive particles using the $i_s E_k - \log E_k$ plot (i_s is the current of the secondary ions, E_k is the energy of the exciting electrons). In these coordinates both the ionization efficiency curves in electron impact spectroscopy and excitation efficiency curves in optical spectroscopy, corresponding to allowed transitions, are (at $E_k \gg 13.6$ eV) straight lines with positive slope (Miller and Platzman, 1956). Deviations occur if the transition violates either total spin or orbital momentum conservation rules.

The $i_s E_k - \log E_k$ plot for ArHg^+ ions is shown in Fig. 2. If the same considerations could be applied in the case of excitation by electron impact as in excitation by photons, then the shape of the curve would indicate the simultaneous participation of long-lived and short-lived excited states formed by optically forbidden and allowed transitions, respectively. However, since very little is known about the shape of electron impact excitation efficiency curves for transitions in which electron exchange occurs, no definite conclusions can yet be drawn from a graph of the type presented in Fig. 2.

Secondary Ion	Appearance Potential	Reaction	Relative Abundance of Secondary Ions
1			
2	$H_2O + Hg$		
3			
4			
5	$O_2 + Hg$	$H_2O^+ + Hg = OHHg^+ + H$	
6	$CO_2 + Hg$	$OH^+ + Hg = OHg^+ + H$	1.0
7	$NH_3 + Hg$		0.2
8		$O_2 + Hg^+ = OHg^+ + O$	
9a		$NH_3^+ + Hg = NH_2Hg^+ + H$	
9b		$NH_2^+ + Hg = NHHg^+ + H$	
10	$CH_3OH + Hg$		1.0
11a		$CH_3OH^+ + Hg = CH_2OHg^+ + H_2$	0.06
11b		$CH_3O^+ + Hg = CH_2OHg^+ + H$	
12		$CH_3O^+ + Hg = CHOHg^+ + H_2$	1.0
13		$CH_3OH^+ + Hg = OHHg^+ + CH_3$	0.2
14		$CH_3O^+ + Hg = OHHg^+ + CH_2$	0.8
15		$CH_3OH^+ + Hg = CH_3Hg^+ + OH$	
16	$CH_4 + Hg$		0.6
		$CH_4^+ + Hg = CH_3Hg^+ + H$	0.4
		$CH_4^+ + Hg = CH_2Hg^+ + (H_2)$	1.0

(Continued on next page)

Table II.
(continued)

Number	Mixture	Secondary Ion	Appearance Potential	Reaction	Relative Abundance of Secondary Ions
17	CHHg^+				< 0.1
18	HHg^+				
19	$\text{C}_2\text{H}_6 + \text{Hg}$	$\text{C}_2\text{H}_4\text{Hg}^+$			~ 0.05
20		C_2HHg^+			~ 0.05
21		C_2Hg^+			~ 0.05
22		CH_3Hg^+	11.6	$\text{C}_2\text{H}_6^+ + \text{Hg} = \text{CH}_3\text{Hg}^+ + \text{CH}_3$	1.0
23		CH_2Hg^+			0.2
24	$\text{C}_3\text{H}_8 + \text{Hg}$	$\text{C}_3\text{H}_7\text{Hg}^+$		$(\text{C}_3\text{H}_8^+ + \text{Hg} = \text{C}_3\text{H}_7\text{Hg}^+ + \text{H})$	0.02
25		$\text{C}_2\text{H}_5\text{Hg}^+$	11.3	$\text{C}_3\text{H}_8^+ + \text{Hg} = \text{C}_2\text{H}_5\text{Hg}^+ + \text{CH}_3$	0.3
26		$\text{C}_2\text{H}_4\text{Hg}^+$			0.1
27		CH_3Hg^+	11.8	$\text{C}_2\text{H}_5^+ + \text{Hg} = \text{CH}_3\text{Hg}^+ + \text{CH}_2$	1.0
28		CH_2Hg^+			0.2
29	$\text{C}_2\text{H}_2 + \text{Hg}$	C_2HHg^+	12.2	$\text{C}_2\text{H}_2^+ + \text{Hg} = \text{C}_2\text{HHg}^+ + \text{H}$	1.0
30		C_2Hg^+	~ 17	$\text{C}_2\text{H}^+ + \text{Hg} = \text{C}_2\text{Hg}^+ + \text{H}$	0.1
31		CHHg^+			0.03
32		CHg^+			0.1

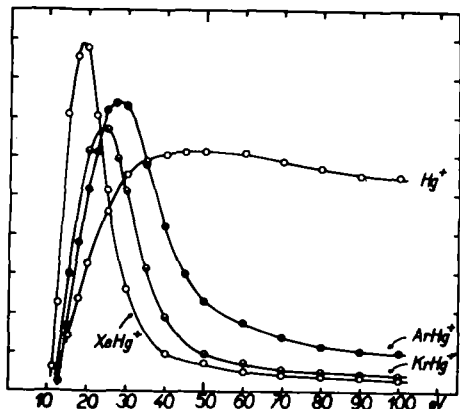


Fig. 1:

Dependence upon electron energy (uncorrected) of ion current of Hg^+ ion and of secondary ions ArHg^+ , KrHg^+ , and XeHg^+ . The current for a particular ion represents the sum of all isotopic contributions. Ordinate heights are extended, for KrHg^+ and XeHg^+ , 4 x and 10 x, respectively. Concentration of atoms in ionization chamber: Hg : $3.8 \cdot 10^{12}$ atoms/cm³, Ar : $1.9 \cdot 10^{13}$ atoms/cm³, Kr : $1.2 \cdot 10^{13}$ atoms/cm³, Xe : $8 \cdot 10^{12}$ atoms/cm³.

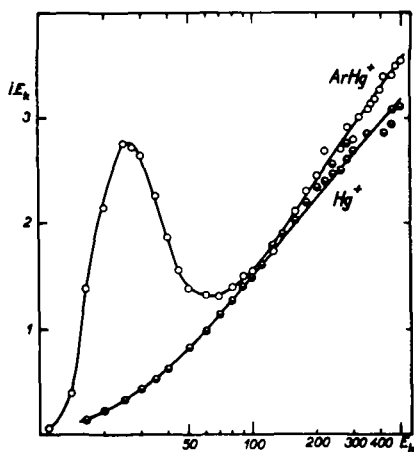


Fig. 2:

Dependence of iE_k upon $\log E_k$ (i - ion current, E_k - electron energy) for Hg^+ ion and secondary ion ArHg^+ .

To the second type of reaction belong those in which ions take part. Secondary ions and neutral particles are formed in these ion-molecule reactions (Table II). In the mixtures containing saturated hydrocarbons, secondary ions with one carbon atom are formed more readily than the ions with two or three carbon atoms (see Table II). In some cases the secondary ion HHg^+ was observed. Its relative abundance is comparable to or greater than the abundance of the most frequent secondary ions in the given mixture. However, it was impossible to identify the primary reacting ions, because the measurement of the appearance potential of HHg^+ ions was very inaccurate due to the great current of primary Hg^+ ions.

Using the equation

$$Q = i_s (i_p n l)^{-1} \quad (1)$$

the reaction cross sections Q were calculated in some of the cases, and the data are summarized in Table III. (In this equation i_s and i_p denote the current of secondary and primary ions, respectively, n the concentration of neutral reacting particles in l cm^3 , and l the distance between the center of the ionizing electron beam and the exit slit of the ionization chamber.) One of the most frequent secondary ions is the CH_3Hg^+ ion. If the value of the heat of formation of the CH_3Hg^+ ion, $\Delta H_f = 160$ kcal/mole, is used (Hobrock and Kiser, 1962), the calculated energy of the $(\text{CH}_3 - \text{Hg})^+$ bond is 102 kcal/mole. The bond is very strong and is comparable to the strength of the $\text{CH}_3\text{-H}$ bond in the methane molecule (102 kcal/mole).

Table III.

Reaction Cross Sections of Several Ion - Molecule Reactions in Mercury Vapor.

Calculated from equation (1). Electron energy 75 eV, extracting potential 154 V, ionizing electron current 30 μA .

Mixture	Reaction	Reaction Cross Section $Q \cdot 10^{16} \text{ cm}^2$
$\text{Ar} + \text{H}_2$	$\text{Ar}^+ + \text{H}_2 = \text{ArH}^+ + \text{H}$	99
H_2O	$\text{H}_2\text{O}^+ + \text{H}_2\text{O} = \text{H}_3\text{O}^+ + \text{OH}$	69
$\text{O}_2 + \text{Hg}$	$\text{Hg}^+ + \text{O}_2 = \text{OHg}^+ + \text{O}$	3.6
$\text{H}_2\text{O} + \text{Hg}$	$\text{H}_2\text{O}^+ + \text{Hg} = \text{OHHg}^+ + \text{H}$	2.1
	$\text{OH}^+ + \text{Hg} = \text{OHg}^+ + \text{H}$	1.6
$\text{CH}_4 + \text{Hg}$	$\text{CH}_4^+ + \text{Hg} = \text{CH}_3\text{Hg}^+ + \text{H}$	2.0
	$\text{CH}_4^+ + \text{Hg} = \text{CH}_2\text{Hg}^+ + (\text{H}_2)$	1.2

Rare Gas Molecule-Ion Formation by Mass Spectrometry.
Kinetics of Ar_2^+ , Ne_2^+ , and He_2^+ Formation by Second and Third Order Processes

J. S. Dahler, J. L. Franklin, M. S. B. Munson, and F. H. Field
Research and Development

Humble Oil & Refining Company
Baytown, Texas

Summary

The ions Ar_2^+ , Ne_2^+ , and He_2^+ , are formed in a mass spectrometer operated at high pressures (up to 300 microns) by the bimolecular excited atom reaction $\text{R}^* + \text{R} = \text{R}_2^+ + \text{e}$, and Ar_2^+ and Ne_2^+ are formed by the termolecular ion-molecule reaction $\text{R}^+ + 2\text{R} = \text{R}_2^+ + \text{R}$. In helium, while He_2^+ is formed by a third order process, there is doubt that an ionic reaction is involved.

Ratios of the rates (cross-sections) for excitation leading to R_2^+ formation and ionization are found to be 5.5×10^{-2} , 1.0×10^{-2} , and 6.4×10^{-2} for argon, neon, and helium. The measurements were made at nominal electron voltages (EV) of 15, 20, and 22 volts, respectively, which correspond to maximum excitation. Values of 1.4×10^{-2} and 0.45×10^{-2} were also obtained at EV = 70 volts for argon and neon.

The experiments yield only the product of the bimolecular rate constant and the lifetime of the R^* reactant atom ($k_r \tau_u$), and the values of this product obtained at EV = 15, 20, and 22 volts are for argon, neon, and helium 3.6×10^{-16} , 11.6×10^{-16} , and 0.58×10^{-16} cc/mol. At EV = 70 volts values of 2.7×10^{-16} and 1.1×10^{-16} cc/mol are obtained for argon and neon. Speculations are given concerning the magnitude of the lifetimes of R^* , and it is concluded that values of about 10^{-8} sec must be considered as possible. The corresponding cross-sections for the reaction forming R_2^+ lie in the range $1000 - 10,000 \times 10^{-16} \text{ cm}^2$.

The rate constants for the formation of Ar_2^+ and Ne_2^+ by the three-body process are, respectively, 2.1×10^{-28} and $2.0 \times 10^{-29} \text{ cc}^2/\text{mol}^2\text{sec}$. It is recognized that values as large as these are in disagreement with values inferred from pulsed discharge ion drift velocity experiments. A possible mode of reconciliation is suggested; namely, at sufficiently high pressures collisional decomposition of R_2^+ ions formed by the termolecular process occur in the drift velocity experiments.

A High Pressure Mass Spectrometric Study of
Reactions of Rare Gases with N_2 and CO

M. S. B. Munson, F. H. Field, and J. L. Franklin
Research and Development
Humble Oil & Refining Company
Baytown, Texas

Summary

Studies have been made in a mass spectrometer at ionization chamber pressures of about $160\ \mu$ on mixtures of rare gases, $R = \text{He, Ne, Ar, Kr, and Xe}$, with N_2 and CO. The ions R_2^+ , ArN_2^+ , KrN_2^+ , XeN_2^+ , ArCO^+ , KrCO^+ , KrCO^+ , XeCO^+ , N_4^+ , and $(\text{CO})_2^+$ were observed as the result of reactions of excited rare gas atoms. Under conditions which maximize the effect of excited state reactions, RN_2^+ , N_4^+ , RCO^+ , and $(\text{CO})_2^+$ are formed by reactions which compete with reactions for the formation of R_2^+ . Three body ion-molecule reactions also form these ions under conditions of higher electron energy and pressure.

At higher electron energies (30 ev compared to 15 ev) and lower field strengths (12.5 v/cm compared to 50 v/cm) and other ions, ArC^+ , KrC^+ , XeC^+ , C_2O^+ , CO_2^+ , C^+ , O^+ , ArN^+ , KrN^+ , XeN^+ , N_3^+ , and N^+ , are formed. N_3^+ and RN^+ appear to be formed from excited nitrogen molecule ions. C_2O^+ appears to be formed from excited carbon monoxide molecule ions, but RC^+ appears to be formed from excited rare gas ions.

No compound ions between He or Ne and N_2 or CO were observed under the normal conditions of these experiments, nor were any RO^+ ions detected.

Observation of the Products of Collision Processes and Ion
Decomposition in a Linear, Pulsed Time-of-Flight Mass Spectrometer

R. E. Ferguson, K. E. McCulloh, and H. M. Rosenstock
National Bureau of Standards
Washington, D.C.

ABSTRACT

The feasibility of detecting neutral species and small fragment ions associated with ion pulses in a linear, pulsed time-of-flight mass spectrometer has been investigated. The fast neutral species may be produced by charge exchange, and both neutrals and fragment ions may result from collision-induced dissociation or spontaneous dissociation (metastable decomposition) of ions in the field-free region of the flight tube after acceleration.

The method used is application of a DC retarding potential a few centimeters before the electron multiplier detector target. Neutral species are unaffected and appear at the original mass position of the parent ion; ions are retarded but can still be focused as sharp pulses arriving after and well separated from the neutral pulses; fragment ions (with the same velocity as the parent ion but with smaller mass) are retarded more and appear after the parent ion peak.

Charge exchange of fast ions (2.8 keV) with gas molecules in the flight tube, single and double charge exchange of doubly charged species, neutrals and small ions from collision-induced dissociation, and neutrals and ions from spontaneous decomposition of a parent ion have been observed and will be illustrated.

The method is a simple and powerful one for surveying mass spectra for peculiarities of current interest. With appropriate improvements in the apparatus, the opportunity exists as well for making quantitative measurements of cross sections for the various collision processes observed.

VELOCITY DEPENDENCE OF ION-MOLECULE REACTION CROSS SECTION

D. A. Kubone and W.H. Hamill

Department of Chemistry and Radiation Laboratory
University of Notre Dame

INTRODUCTION

In general an ion-molecule reaction can be represented by



where P^+ is the reactant or primary ion, M the neutral molecule, S^+ the secondary or product ion and F one or more neutral fragments. Parent-daughter relationships are usually established by the correspondence of their appearance potentials. The choice of the fragment species is dictated by the criterion of $\Delta H_R \leq 0$, since endothermic reactions are not likely to be observed in the mass spectrometer (8,9).

These ion-molecule reactions, as studied by mass spectrometry, have gained wide interest in recent years. Much emphasis has been placed upon the various types of ion-molecule reactions and their implications for radiation chemistry (1,2,3,4). There have been few publications which have dealt directly with the dependence of the reaction cross section, Q , on the primary ion energy, E_0 .

Gioumouisis and Stevenson (5) have presented a treatment based on the rigorous kinetic theory of gases which relates the microscopic cross section, σ , to the cross section, Q , measured by the mass spectrometer. Field et al (13), using averaged quantities instead of distribution functions, have also treated this problem. Both treatments predict that Q varies as the inverse square root of the ion energy, E_0 . A treatment leading to a very useful relation between σ and Q given by Boelrijk and Hamill (6) is reviewed.

The present theory introduces the physical size of the colliding particles, a feature ignored in earlier treatments (5,13), to explain the deviation of Q from the predicted $E_0^{-1/2}$ dependence.

THEORY

Langevin (10) described the interaction of an ion with a molecule in terms of a point charge inducing a dipole moment in a polarizable molecule. The potential function for such a system is given by

$$V = - \frac{e^2 a}{2r^4} \quad (1)$$

where e is the electronic charge, a the polarizability and r the ion-molecule separation.

The calculated orbits for this type of potential show a critical value, b_0 , of the impact parameter, b , which is the distance of closest approach of the colliding pair in the absence of polarization forces such that if $b > b_0$ the interaction results only in scattering and if $b < b_0$ the interaction leads to an intimate spiralling collision. It is assumed that for collisions with $b > b_0$ there is no reaction and all collisions with $b < b_0$ lead to reaction. Hence, b_0 can be used to define a microscopic cross section.

$$\sigma = \pi b_0^2 \quad (2)$$

An expression for σ in terms of reduced mass, μ , molecular polarizability, a and relative velocity, g , can be calculated in a straightforward manner.

$$b_0 = (4e^2 a / \mu g^2)^{1/4} \quad (3)$$

$$\sigma(g) = \pi b_0^2 = 2 \pi e g^{-1} (a/u)^{1/2} \quad (4)$$

where $\mu = m_1 m_2 / (m_1 + m_2)$. The subscripts 1 and 2 refer to the ion and molecule, respectively.

Stevenson and Gioumousis (5) have related the microscopic cross section σ to the cross section measured by the mass spectrometer in the following manner. Neutral molecules with a Maxwellian distribution of velocities are ionized by an electron beam in the ion source. The resulting ions are repelled towards the exit slit of the ion source by a voltage E applied between the repeller electrode and the exit slit, giving the ions a maximum energy E_0 . Between the electron beam and the exit slit these non-Maxwellian ions collide with neutral thermal molecules to form collision complexes. The average cross section must be calculated at each point between the electron beam and the exit slit and then averaged over this reaction path.

The distribution function of velocity component v_z of ions of mass m_1 along the ion path z , in the direction of the exit slit, is given by

$$f(v_z, z) = \nu(v_z, z) \frac{B m_1 \exp [(-1/kT) (1/2 m_1 v_z^2 - ezE)]}{(1/kT) (1/2 m_1 v_z^2 - ezE)} \quad (5)$$

where B is the rate of formation of primary ions and ν has the values

$$\begin{aligned} \nu &= 1 & z < 0 \\ \nu &= 2 & z > 0, v_z > 0, (1/2 m_1 v_z^2 - ezE) > 0 \\ \nu &= 0 & v_z < 0 \\ \nu &= 0 & (1/2 m_1 v_z^2 - ezE) < 0 \end{aligned}$$

The velocity distributions of the ions in the x and y directions and all the components of neutral molecules are one dimensional Maxwellian distributions

$$f(v_x) dx = \left(\frac{m}{2 kT}\right)^{1/2} e^{-\frac{mv_x^2}{2 kT}} dx \quad (6)$$

The rate of reaction R can be expressed in terms of the velocity distributions f_1 and f_2 of the ions and molecules and the microscopic cross section $\sigma(g)$

$$R = N \int_0^{l_0} \left[\int \int f_1(v_1) f_2(v_z) g \sigma(g) dv_1 dv_z \right] dz \quad (7)$$

where N is the concentration of neutral molecules in the ion source and l_0 the distance from the electron beam to the exit slit.

Since $\sigma(g)$ is an inverse function of g the factor $g \sigma(g)$ is a constant and the integral reduces to an integral of the product of the distribution functions. Making the assumption that $E_0 \gg kT$

$$R = 2 \pi B l_0 N \left(\frac{2 m_1 a e^2}{\mu} \right)^{1/2} E_0^{-1/2} \quad (8)$$

E_0 is identified with $el_0 E$.

The number of secondary ions n_s is proportional to the number of primary ions n_p , to N , to l_0 and to the average cross section Q . Thus

$$n_s = n_p N l_0 Q \quad (9)$$

and so

$$Q = 2 \sigma_L / E_0^{1/2} \quad (10)$$

where

$$\sigma_L = 2^{1/2} \pi e \left(\frac{m_1 + m_2}{m_2} a \right)^{1/2} \quad (11)$$

Boelrijk and Hamill have given a more useful relation between σ (g) and Q (6). The number of secondary ions formed in a volume element with 1 cm^2 area parallel to the electron beam and sides z and $z + dz$ from the plane of the beam can be written

$$dn_s = n_p N \sigma(z) dz \quad (12)$$

Here the microscopic cross section is expressed as a function of position along the reaction path.

Integration over the path gives

$$n_s = n_p N \int_0^{l_0} \sigma(z) dz \quad (13)$$

and z can be written in terms of l_0 , E and E_0 . Thus

$$z/l_0 = E/E_0 \quad (14)$$

and making the substitution (11)

$$i_s/i_p = n_s/n_p \quad (15)$$

where the i 's represent the respective measured ion currents,

$$i_s = i_p N l_0 E_0^{-1} \int_0^{E_0} \sigma(E) dE \quad (16)$$

and finally

$$i_s/i_p (N l_0)^{-1} = Q = E_0^{-1} \int_0^{E_0} \sigma(E) dE \quad (17)$$

To a good approximation the relative velocity g can be taken as the velocity of the ion, i.e.,

$$E = 1/2 m_1 g^2 \quad (18)$$

and so equation (4) becomes

$$\sigma(E) = 2^{1/2} \pi e \left(\frac{m_1 + m_2}{m_2} a \right)^{1/2} E^{-1/2} = \sigma_L / E^{1/2} \quad (19)$$

Using (17) and (19)

$$Q = E_0^{-1} \int_0^{E_0} \sigma_L / E^{1/2} dE = 2 \sigma_L / E_0^{1/2} \quad (20)$$

The result is identical to the one obtained by Stevenson.

Equation (10) has been used to describe a number of ion-molecule reactions (5, 12). However, there are many reactions which show a departure from an $E_0^{-1/2}$ dependence indicating that (10) is not an adequate description (6, 7, 13). One fact not taken into account in deriving (10) was the physical size of the colliding particles. In other words it was assumed that πb_0^2 was much larger than σ_K , the hard sphere collision cross section. This assumption appears not to be valid in many cases (6). For some value of E_0 , πb_0^2 will be eclipsed by σ_K , i.e.,

$$E_t = (\sigma_L / \sigma_K)^2 \quad (21)$$

where E_t is the energy at which $\pi b_0^2 = \sigma_K$. Introduction of this σ_K , which is assumed to be energy independent in the present context, into equation (19) will lead to a discontinuity in the functional dependence of Q on E_0 .

Instead of (19) the microscopic cross section is now written

$$\sigma_1(E) = P_L (\sigma_L / E^{1/2} - \sigma_K) + P_K \sigma_K: E < E_t \quad (22)$$

The term in brackets represents the energy dependent area and σ_K the area for head-on or "hard" collisions. The P-factors represent reaction efficiencies and are taken to be energy independent. From (17) and (22) the integrated cross section is

$$Q_1 = 2P_L \sigma_L E_0^{-1/2} + \sigma_K (P_K - P_L) : E < E_t \quad (23)$$

If $E > E_t$ there are only the energy-independent collisions and

$$\sigma_2(E) = P_K \sigma_K : E > E_t \quad (24)$$

Integrating over the reaction path

$$Q_2 = E_0^{-1} \int_0^{E_t} \sigma_1(E) dE + E_0^{-1} \int_{E_t}^{E_0} \sigma_2(E) dE \quad (25)$$

$$= E_0^{-1} (2P_L \sigma_L E_t^{1/2} - P_L \sigma_K E_t) + P_K \sigma_K \quad (26)$$

Using (21) and simplifying

$$Q_2 = P_L \sigma_L E_t^{1/2} E_0^{-1} + P_K \sigma_K : E > E_t \quad (27)$$

Thus, at high ion energies ($E > E_t$) Q will vary as E_0^{-1} . This prediction is the direct consequence of the introduction of the energy independent cross section σ_K .

There is another criterion which will also lead to an E_0^{-1} dependence. At a critical ion energy E_c the ion molecule complex becomes unstable, i.e.,

$$\sigma_3(E) = 0, \quad E > E_c \quad (28)$$

An example of this situation has been reported in the case of "sticky collision" complexes (14) and in the ion-molecule reactions of cyclopropane (7).

The integrated cross section is

$$Q_3 = E_0^{-1} \int_0^{E_t} \sigma_1(E) dE + E_0^{-1} \int_{E_t}^{E_c} \sigma_2(E) dE + E_0^{-1} \int_{E_c}^{E_0} \sigma_3(E) dE \quad (29)$$

Integrating and simplifying

$$Q_3 = E_0^{-1} (P_L \sigma_L E_t^{1/2} + P_K \sigma_K E_c) : E > E_c; E_c > E_t \quad (30)$$

If $E_c < E_t$

$$Q_4 = E_0^{-1} \int_0^{E_c} \sigma_1(E) dE + E_0^{-1} \int_{E_c}^{E_0} \sigma_3(E) dE \quad (31)$$

and

$$Q_4 = E_0^{-1} (2 P_L \sigma_L E_c^{1/2} + \sigma_K (P_K - P_L) E_c) : E > E_c; E_c < E_t \quad (32)$$

EXPERIMENTAL

The instrument used for all measurements is the CEC 21-103A mass spectrometer equipped with a 31-402 ion source. Modification of the ionizing voltage and repeller voltage circuits to facilitate ion-molecule measurements are described elsewhere (6). The detection and recording of ion currents was accomplished with an Applied Physics model 30 vibrating reed electrometer and a Sargent model MR

chart recorder. The range of sensitivity attainable with this combination is 10^{-7} to 10^{-14} amperes. The electrometer has been modified for critical damping and is equipped with a turret switch to expedite rapid changing of the sensitivity of the electrometer over the stated range.

A complete description of the techniques for measuring appearance potentials, cross sections, pressure dependences and other related measurements is given in "Techniques for Studying ion-Molecule Reactions" (15).

Normal gases used in this study were obtained from Matheson and were purified as needed by standard techniques. Heavy hydrogen was obtained from the Stuart Oxygen Co. and methane- d_4 from Merck of Canada; n-butane- d_{10} was prepared by catalytic exchange between n- C_4H_{10} and D_2 (16).

All cross section measurements were made under the following ion source conditions: ion accelerating voltage, 500 v; electron energy, 70 v; electron current, 10.5 microamp; total pressure in the 3-liter bulb of 570 microns Hg which corresponds to a N of 1.2×10^{13} molecules/cm³. l_0 is 1.3 mm.

RESULTS AND DISCUSSION

In the reactions reported here no evidence of E_C was found, i.e., only one discontinuity is observed in the plot of Q against E_0^{-1} . Hence, all results will be interpreted on the basis of equations (23) and (27).

Before presenting the actual experimental results it is instructive to examine a "synthetic" reaction with regard to the plots of Q against $E_0^{-1/2}$ and E_0^{-1} . Such a reaction has been constructed using (23) and (27) with the values $\sigma_L = 50 \times 10^{-16}$ cm² ev^{1/2}, $E_t = 2.0$ ev, $\sigma_K = 35.4 \times 10^{-16}$ cm², and $P_L = P_K = 1$ and is shown in Figure 1. P_K and P_L will not always be unity for actual cases; different values of P_K and P_L will only shift the curves along the ordinate. The arrows indicate the position of E_t on the energy scale. It is evident that E_t cannot be determined accurately by direct observation. However E_t can be determined analytically by the following method. Rearranging (23) and (27),

$$Q_1 - \sigma_K (P_K - P_L) = 2P_L \sigma_L E_0^{-1/2} \quad (33)$$

$$Q_2 - P_K \sigma_K = P_L \sigma_L E_t^{1/2} E_0^{-1} \quad (34)$$

Dividing (33) by (34) and rearranging again

$$E_t^{1/2} = 2E_0^{1/2} \frac{Q_2 - P_K \sigma_K}{Q_1 - \sigma_K (P_K - P_L)} \quad (35)$$

Values of Q_1 (by extrapolation from the low energy region) and Q_2 are read from a plot of Q against $E_0^{-1/2}$ at a value of E_0 above E_t (estimated by direct observation). $P_K \sigma_K$ and $\sigma_K(P_K - P_L)$ are the intercepts of Q against E_0^{-1} and $E_0^{-1/2}$, respectively. Values of E_t , calculated using several different values of E_0 , all above E_t , were found to be essentially independent of E_0 .

An actual reaction which can be compared to the synthetic reaction just described is shown in Figure 2. In this case P_K is zero.

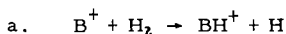
There are several means to test the adequacy of the treatment. First, values of $P_L \sigma_{Lobs}$ obtained from the slope of Q against $E_0^{-1/2}$ can be compared to the value calculated from (11).

$$\sigma_{Lcalc} = 2^{1/2} \pi e \left(\frac{m_1 + m_2}{m_2} a \right)^{1/2} \quad (11)$$

This comparison is shown in Tables I and II. The high values of $P_L \sigma_{Lobs}$ for the mixtures of light and heavy hydrogen with nitrogen, carbon monoxide and argon can be

explained by the following consideration.

Hutchison, et al. (17) and Giese (18) have pointed out that in such systems the secondary ion can arise from the reaction going by



and also by



Consider the following. In general

$$i_s = i_p N l_o E_o^{-1} \int_0^{E_o} \sigma(E) dE \quad (16)$$

$$i_s / (i_p N l_o) = Q = E_o^{-1} \int_0^{E_o} \sigma(E) dE \quad (17)$$

and

$$i_s = i_{sa} + i_{sb} \quad (36)$$

where i_s is the total measured ion current of BH^+ . Then;

$$i_s = i_{pa} N_b l_o E_o^{-1} \int_0^{E_o} \sigma_a(E) dE + i_{pb} N_a l_o E_o^{-1} \int_0^{E_o} \sigma_b(E) dE \quad (37)$$

rearranging

$$\frac{i_s}{i_{pa} N_b l_o} = E_o^{-1} \int_0^{E_o} \sigma_a(E) dE + \frac{i_{pb} N_a}{i_{pa} N_b} E_o^{-1} \int_0^{E_o} \sigma_b(E) dE \quad (38)$$

From (17) and since $i_p = kN$

$$Q'_a = Q_a + (k_b/k_a) Q_b \quad (39)$$

Q'_a is the cross section plotted using the measured i_s and taking B as the reactant ion. Q'_a will of course be larger than either Q_a or Q_b . (39) could also have been written

$$Q'_b = (k_a/k_b) Q_a + Q_b \quad (40)$$

Making the assumption that P_L is unity for reactions a and b, the ratio Q_b/Q_a can be obtained from theory

$$Q_b/Q_a = (m_a \alpha_b / m_b \alpha_a)^{1/2} \quad (41)$$

where m_a is the mass of the neutral molecule and α its polarizability. Calling this ratio β

$$Q'_a = (1 + k_b/k_a \beta) Q_a \quad (42)$$

k_a and k_b can be obtained from plots of i_p against N . For a given E_0 , (41) can be written

$$\sigma'_{La} = (1 + k_b/k_a \beta) \sigma_{La} \quad (43)$$

In Table III values of $\sigma'_{La,calc}$ from equation (43) are compared to observed values of σ_{La} .

$P_L \sigma_{Lobs}$ is $50.5 \times 10^{-16} \text{ cm}^2 \text{ ev}^{1/2}$ compared to $71.6 \times 10^{-16} \text{ cm}^2 \text{ ev}^{1/2}$ for σ_{Lcalc} for the reaction

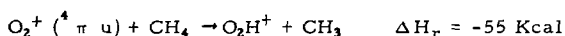


This may be understood qualitatively in terms of a 'steric' factor. If the structure of the CO_2H^+ ion is

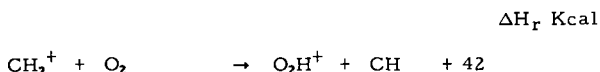
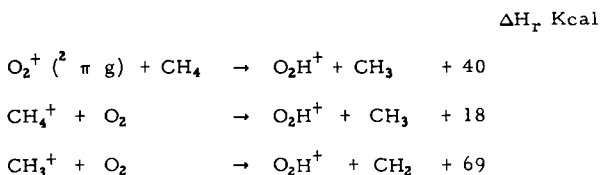


there will be a steric hindrance for the H-atom to get on the carbon atom, making P_L less than unity. Unfortunately, there is no information that the author is aware of which gives any clue as to the structure of this ion. One fact in favor of this structure is that it is a resonant structure.

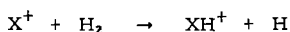
In the case of the $\text{O}_2\text{-H}_2$ (D_2) system, the reactant ion is taken to be O_2^+ in its first excited state. Since the number of O_2^+ in the excited state is less than in the ground state σ_{Lobs} will be less than σ_{Lcalc} . However, other work in the literature lists H_2^+ as the reactant ion (12,21). The present choice of O_2^{*+} is based on the following facts. The appearance potentials of O_2H^+ and H_2^+ coincide with each other. However, the appearance potential of O_2H^+ also coincides, within experimental error, with the first excited state of O_2^+ (19). The observation of O_2H^+ in a mixture of oxygen and methane shows an excited state of O_2^+ is involved. The only reaction energetically allowed in this system is



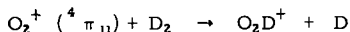
all others are endothermic: (ΔH_f 's obtained from ref. 20).



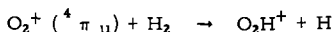
If the reactant ion were H_2^+ this would be the only case where H_2 is not the molecule in reactions of the type (22)



Another fact which strongly supports the choice of O_2^{*+} is that E_t is observed for



but not for



Replacing H_2 by D_2 will lower the value of E_t about a factor of two. This is evident on inspecting equations (11) and (21). Measurements of Q did not extend to sufficiently high values of E_0 to see E_t in the $\text{O}_2\text{-H}_2$ system but was high enough to see it in the $\text{O}_2\text{-D}_2$ system. If the ion were H_2^+ the value of E_t would be the same whether H_2 or D_2 were used.

This feature of being unable to observe E_t also, applies to mixtures of light and heavy hydrogen with argon, nitrogen, carbon monoxide, carbon dioxide and hydrogen cyanide. According to equation (21) the combination of a large σ_L and a small σ_K dictates a high value of E_t . Q for the $\text{N}_2\text{-H}_2$ and $\text{N}_2\text{-D}_2$ systems were examined at higher values of E_0 by use of extra batteries in the repeller circuit. E_t was observed for both H_2 and D_2 mixtures. The calculated ratio $E_{t\text{H}_2}/E_{t\text{D}_2}$ from equations (11) and (21) is 1.875, the observed ratio is 2.1.

Another comparison involves $\sigma_{K_{Obs}}$ obtained from

$$\sigma_{K_{Obs}} = \sigma_L / E_t^{1/2} \quad (44)$$

and values calculated from Van der Waals 'b', gas viscosity and molar refraction. These comparisons are shown in Table IV. The values of $\sigma_{K_{Obs}}$ are very reasonable and in fact appear to reflect the differences between the molecules more faithfully than do the other σ_K 's.

CONCLUSION

The treatment presented here provides an adequate description of the experimental facts. It is a more realistic approach than the point particle treatment used by Stevenson, since Q rapidly decreases with increasing energy.

The general nature of the present treatment, the agreement between predicted and observed quantities, the various correlations between the parameters and the reasonable values of σ_K indicate a direct and so far unique approach to particle mechanics.

TABLE I

ion	molecule	sec. ion	$\sigma_{L_{calc}}$	$\sigma_{L_{obs}}$
D ₂	H ₂	D ₂ H	26 Å ² ev ^{1/2}	31.7 Å ² ev ^{1/2}
O ₂ *	H ₂	O ₂ H	61.6	25
O ₂ *	D ₂	O ₂ D	45	14.6
H ₂ O	D ₂	H ₂ OD	35	28
D ₂ O	H ₂	D ₂ OH	47.4	45
H ₂ O	n-C ₄ D ₁₀	H ₂ OD	55	56.5
CD ₄	CD ₄	CD ₅	38	42
CD ₃	CD ₄	C ₂ D ₅	37	40

TABLE II

ion	molecule	sec. ion	σ_{Lcalc}	σ_{Lobs}
N ₂	H ₂	N ₂ H	58 Å ² ev ^{1/2}	84 Å ² ev ^{1/2}
N ₂	D ₂	N ₂ D	42	66.5
CO	H ₂	COH	58	75
CO	D ₂	COD	42	57
CO ₂	H ₂	CO ₂ H	71.6	50.5
CO ₂	D ₂	CO ₂ D	51.8	36
A	H ₂	AH	68.5	76
A	D ₂	AD	49.6	60.5
HCN	D ₂	HCND	41.6	48.6
D ₂	D ₂	D ₃	21.2	21.5
H ₂	H ₂	H ₃	21.2	23.5

TABLE III

system	sec. ion	σ'_{Lacalc}	σ'_{Laobs}
N ₂ - H ₂	N ₂ H	71 Å ² ev ^{1/2}	84 Å ² ev ^{1/2}
CO - H ₂	COH	71	75
A-H ₂	AH	77	76
N ₂ - D ₂	N ₂ D	53	66
CO - D ₂	COD	53	57
A - D ₂	AD	58	60

TABLE IV

ion	molecule	$E_t^{1/2}$	K _{obs}	K _{gv}	K _{vdw}	K _{mr}
D ₂	D ₂	2.6 ₄ ev ^{1/2}	8 Å ²	18.3 Å ²	24 Å ²	10.8 Å ²
H ₂	H ₂	2.6 ₀	8.1	18.3	24	10.8
D ₂	H ₂	2.4 ₂	10.7	18.3	24	10.8
H ₂ O	D ₂	1.5 ₇	22.2	18.8	25	13.3
D ₂ O	H ₂	2.7 ₆	17.2	18.8	25	13.3
H ₂ O	n-C ₄ D ₁₀	2.0 ₀	27.5	34.8	44	31.6
CD ₄	CD ₄	1.6 ₅	23	31.4	33	24.2
CD ₃	CD ₄	1.7 ₅	21.2	31.4	33	24.2

REFERENCES

1. M. Haissinsky, Ed., "The Chemical and Biological Action of Radiations," Academic Press, Inc., New York, N.Y., Vol. V, 1961, Chapter 4.
2. W.H. Hamill, Ann. Rev. Phys. Chem., 11, 87 (1960).
3. W.H. Johnston, et al., "Ion-Molecule Reactions", No. JLI-650-3-7 UC-23, Isotopes, William H. Johnston Laboratories, 1959.
4. J. Durup, "Les Reactions Entre Ions Positifs et Molecules en Phase Gazeuse", Gauthier-Villars, Paris, 1960.
5. G. Gioumousis and D.P. Stevenson, J. Chem. Phys., 29, 294 (1958).
6. N. Boelrijk and W.H. Hamill, J. Am. Chem. Soc., 84, 730 (1962).
7. R.F. Pottie, A.J. Lorquet and W.H. Hamill, J. Am. Chem. Soc., 84, 529 (1962).
8. F.W. Lampe and F.H. Field, Tetrahedron 7, 189 (1959).
9. V.L. Tallroze and E.L. Frankevitch, Proceedings of the First All-Union conference on Radiation Chemistry, Moscow, 1957, Consultants Bureau, Inc., New York, 1959.
10. P. Langevin, Ann. Chim. Phys., 8, 245 (1905).
11. D.A. Kubose and W.H. Hamill, J. Phys. Chem. 65, 183 (1961).
12. D.P. Stevenson and D.O. Schissler, J. Chem. Phys., 29, 282 (1958).
13. F.H. Field, J.L. Franklin and F.W. Lampe, J. Am. Chem. Soc., 79, 2419 (1957).
14. R.F. Pottie and W.H. Hamill, J. Phys. Chem., 63, 877, (1959).
15. Techniques for Studying Ion-molecule Reactions, on deposit, Science Library, University of Notre Dame.
16. H. Gillis, R. Williams and W.H. Hamill, J. Am. Chem. Soc., 83, 17 (1961).
17. D. Hutchison, A. Kuppermann and L. Pobo, presented at ASTM Committee E-14 on Mass Spectrometry, Chicago, June, 1961.
18. C.F. Giese and W.B. Maier, II, J. Chem. Phys., 35, 1913 (1961).
19. D.C. Frost and C.A. McDowell, J. Am. Chem. Soc., 80, 6183 (1958).
20. F.H. Field and J.L. Franklin, "Electron Impact Phenomena and the Properties of Gaseous Ions", Academic Press, Inc., New York, N.Y., 1957, appendix.
21. P. Dong and M. Cottin, J. Chem. Phys. 57, 557 (1960).
22. H. Gutbier, Zeit. Naturforsch. 12A, 499 (1957).

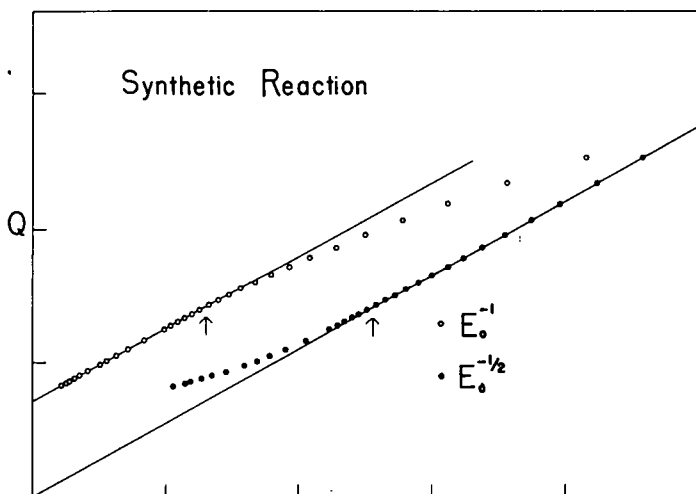


Figure 1. Plot of Q against $E_0^{-1/2}$ and E_0^{-1} for a synthetic reaction. Range of E_0 is 0.5 to 11.5 ev. The arrows indicate E_t .

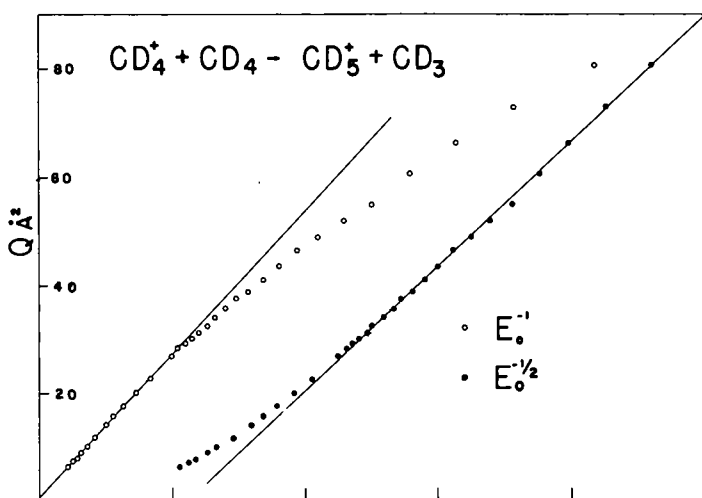


Figure 2. Plot of Q against $E_0^{-1/2}$ and E_0^{-1} for the reaction $CD_4^+ + CD_4 \rightarrow CD_5^+ + CD_3$. Range of E_0 is 0.5 to 11.5 ev.

MASS SPECTROMETRIC OBSERVATION OF ELECTRON AND PROTON TRANSFER
REACTIONS BETWEEN POSITIVE IONS AND NEUTRAL MOLECULES*

A. Henglein and G. A. Muccini

Radiation Research Laboratories, Mellon Institute, Pittsburgh, Pa.

and

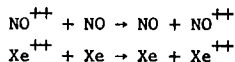
Hahn-Meitner-Institut für Kernforschung, Berlin-Wannsee

* This work was supported, in part, by the U. S. Atomic Energy Commission.

SUMMARY

The method of Cermak and Herman has been applied to mass spectrometric studies of symmetrical electron and proton transfer processes. The characteristics of the ion source used have been investigated both experimentally and theoretically. A new type of ionization efficiency curve is obtained if the current of a secondary ion is plotted as a function of the voltage between ionization chamber and electron trap at constant low voltage between the filament and the chamber. Essentially complete discrimination of primary ions has been achieved.

Electron transfer occurs with rather low cross section in methane but increases with molecular size and with increasing unsaturation. Large cross sections were observed in sulfur and iodine containing compounds. Double charge transfer reactions such as



have also been observed. Proton transfer reactions have been observed in several simple molecules. Some experimental results are presented which indicate that proton transfer may occur via a complex (at low kinetic energies) or as a stripping process (at higher energies).

Fragment ions have also been observed in the secondary mass spectra of several compounds. While part of these may result from the scattering of primary fragment ions, in some cases additional processes have to be postulated such as hydride ion transfer and dissociative charge transfer from vibrationally excited ions.

INTRODUCTION

A simple new method for mass spectrometric studies of the interactions between ions and neutral molecules has recently been described by Cermak and Herman.¹ The electron accelerating voltage between the filament and the ionization chamber of a conventional ion source is kept below the ionization potential of the gas. The electrons traverse the chamber without causing any ionization and are then further accelerated by an electric field between the ionization chamber and the electron trap. The primary ions are accelerated in the direction opposite to the electron beam by this field before entering the ionization chamber. These primary ions are not able to pass the slit system of the mass spectrometer because of a kinetic energy component perpendicular to the direction of analysis. However, secondary ions produced by collisions with gas molecules in the chamber can be extracted into the analyzing section of the instrument if they are formed with negligible amounts of kinetic energy. Cermak and Herman demonstrated this in studies of dissociative charge transfer reactions in cases in which the transfer of mass and therefore of kinetic energy is extremely small.

The methodology of Cermak and Herman has been applied in studies carried out with a Consolidated Electrodynamics Corporation Model 21-103 C mass spectrometer. The sensitivity of the instrument was increased by using a Model 31 Cary (Vibrating Reed) Electrometer for the measurement of the ion currents. Studies of the characteristics of the ion source showed that essentially complete discrimination between primary and secondary ions is obtained. As a result it has been possible to investigate a number of typical resonant charge transfer reactions. In addition, the mass spectra of secondary ions of several simple compounds have been studied. It has been found that these secondary mass spectra contain not only the parent ions (formed by resonant charge transfer) but also protonated molecules as well as ions of lower masses resulting from ion-molecule reactions. It seems noteworthy to emphasize that the high degree of discrimination of primary ions makes it possible to detect certain secondary ions which cannot be observed in the conventional operation of the ion source.

Characteristics of the ion source

a) Experimental

The normal operation of the ion source is demonstrated in Fig. 1 for methane (curve 1). The current of the parent ion is given as a function of the electron

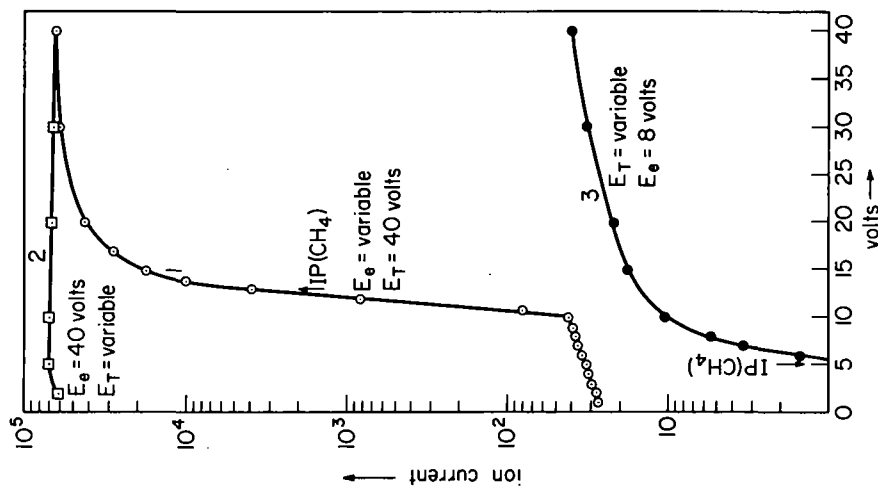


Fig. 1. CH_4^+ current from methane as a function of E_e or E_T , respectively. (E_e : voltage between filament and ionization chamber. E_T : voltage between ionization chamber and electron trap. Methane pressure in the gas inlet system: 0.054. Repeller field: 3.8 volts/cm)

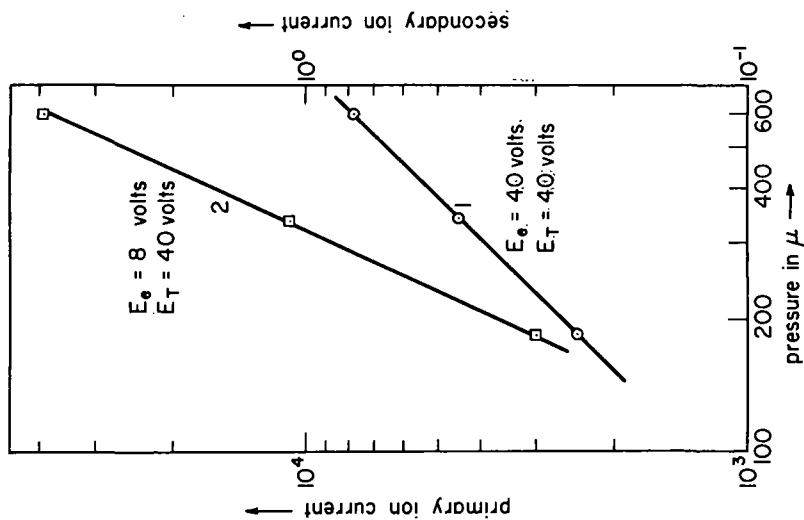


Fig. 2: Dependence of the CH_4^+ current on the pressure of methane in the gas inlet system (Curve 1: left ordinate scale, curve 2: right scale)

accelerating voltage at constant trap voltage. A small current which decreases rapidly with decreasing electron voltage can still be observed below the ionization potential of methane (13.0 volts). Between 11.0 and 13.0 volts this current is attributed to the energy spread of the electron beam. At 11.0 volts the slope of curve 1 changes discontinuously and at lower voltages becomes nearly independent of the electron accelerating voltage. Fig. 2 shows the dependence of the CH_4^+ -current on the pressure in the gas inlet system. Proportionality exists if the ion source is operated in the conventional way, i.e., with incident electron energies above the ionization potential of the methane (curve 1). The current increases with the square of the pressure if the electron accelerating voltage is kept below 11.0 volts (curve 2). In this range only secondary CH_4^+ ions which result from some interaction of primary ions formed between the chamber and trap with gas molecules in the chamber are observed.

The formation of these secondary CH_4^+ ions is described in a more detailed manner by curve 3 in Fig. 1. The electron accelerating voltage E_e has been kept constant at 8.0 volts and the CH_4^+ current has been studied as a function of the trap voltage E_T . Curve 3 represents an "ionization efficiency curve" for the secondary ion. The "appearance potential" here amounts to 5.0 volts. This corresponds exactly to the ionization potential of 13.0 volts of methane since the energy of the electrons is equal to $E_e + E_T = 13.0$ when they reach the electron trap. It can therefore be concluded that the precursor of the secondary CH_4^+ ion is the primary CH_4^+ ion which transfers its charge in a collision with a methane molecule. "Secondary ionization efficiency curves" are therefore helpful in investigations of the nature of the primary ion. However, the meaning of such secondary ionization efficiency curves is somewhat different from that obtained in more conventional ion sources. This will be discussed in detail in the following theoretical part.

The description of the characteristics of the ion source is completed by curve 2 in Fig. 1 where the ion current is plotted versus the trap voltage at constant accelerating voltage above the ionization potential of the gas. As it is well known from conventional operation the ion current is practically independent of E_T over a wide range.

b) Theoretical

The secondary ions cannot reach the collector if they have excessive kinetic energy either parallel to the long axis of the slits (i.e. in the direction of the primary ions) or perpendicular to this axis and to the direction of analysis. Only a beam within the divergence angles α and β (perpendicular to and in the plane of analysis, respectively) will pass through the whole slit system. The angle α is determined by the length l_1 of the exit slit of the ionization chamber and l_2 of the entrance slit of the collector system as well as the distance a between the two slits. The angle β is determined by the widths d_1 and d_2 of the exit slit of the ionization chamber and the exit slit of the ion accelerating system as well as their distance b . In the mass spectrometer employed here l_1 , l_2 and a were 1.0, 1.26 and 40 cm, and d_1 , d_2 and b were 0.15, 0.15 and 7.2 mm, respectively. The values of α and β are calculated to be equal to 0.056 and 0.0415 radians from these data. The maximum kinetic energy components U_α and U_β parallel and perpendicular to the direction of the primary ion beam which will allow analysis are given by

$$U_\alpha = \alpha^2 \cdot V \quad (1)$$

$$U_\beta = \frac{\beta^2 \cdot V}{4} \quad (2)$$

where V is the ion accelerating high voltage of the ion source. In this work V was equal to 800 volts. U_α and U_β are found to amount to

$$U_\alpha = 2.5 \text{ eV} \quad (3)$$

$$U_\beta = 0.34 \text{ eV} \quad (4)$$

Let x_0 be the distance between the ionization chamber and electron trap, x the distance between the chamber and a point between these two electrodes. The total kinetic energy of an electron which ionizes a molecule at this point is equal to $E_{\text{tot}} = E_e + U(x)$ where U is the potential difference between the chamber and this point. If the field gradient between chamber and trap is linear $U = E_T \cdot \frac{x}{x_0}$. The primary ion formed at the distance x is accelerated by the potential U and enters the chamber with the kinetic energy $eU(x)$. At the appearance potential, AP, of the secondary ionization efficiency curve, all ionizations take place immediately in front of the collector, i.e. $x = x_0$ and $E_{\text{tot}} = E_e + E_T$, and all primary ions entering the ionization chamber have the kinetic energy eE_T . However, at higher values of E_T ionization can occur between x_0 and a minimum distance x_1 which is given by the condition $E_e + U(x_1) = \text{AP}$. The primary ion beam therefore will have a distribution in kinetic energy between $eU(x_1)$ and eE_T . Since x_1 decreases with increasing E_T this distribution will become broader and broader.

The number of primary ions which are formed between x and $x + dx$ (or U and $U + dU$) and which will therefore obtain the kinetic energy eU is equal to

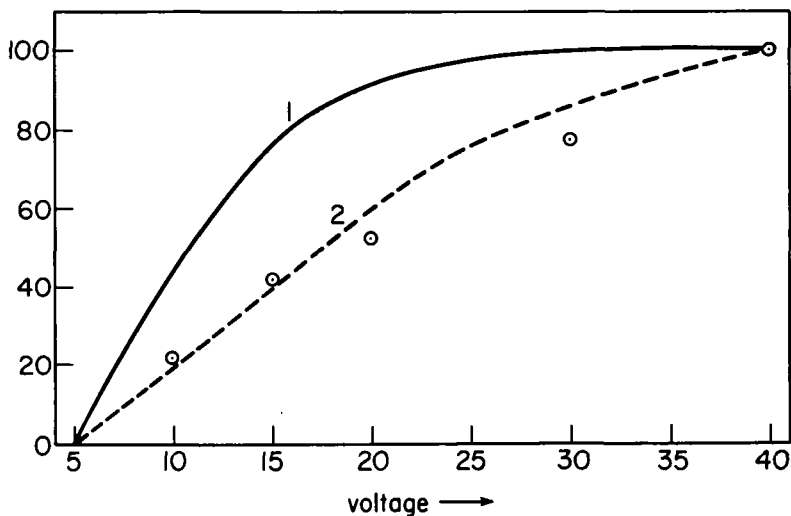


Fig. 3: Curve 1: Ionization efficiency curve of CH_5^+ (E_T constant at 40 volts. E_e variable. Abscissa: E_e -8 volts. Curve 1 is normalized at E_e -8 = 40 volts)
 Curve 2: Total primary CH_4^+ current as function of E_T at E_e = constant at 8 volts. (Curve 2 is calculated from curve 1 according to Eq. 7. Normalization of curve 2 at E_T = 40 volts)
 X: Observed secondary CH_4^+ current at various values of E_T (E_e constant at 8 volts. Normalization at E_T = 40 volts)

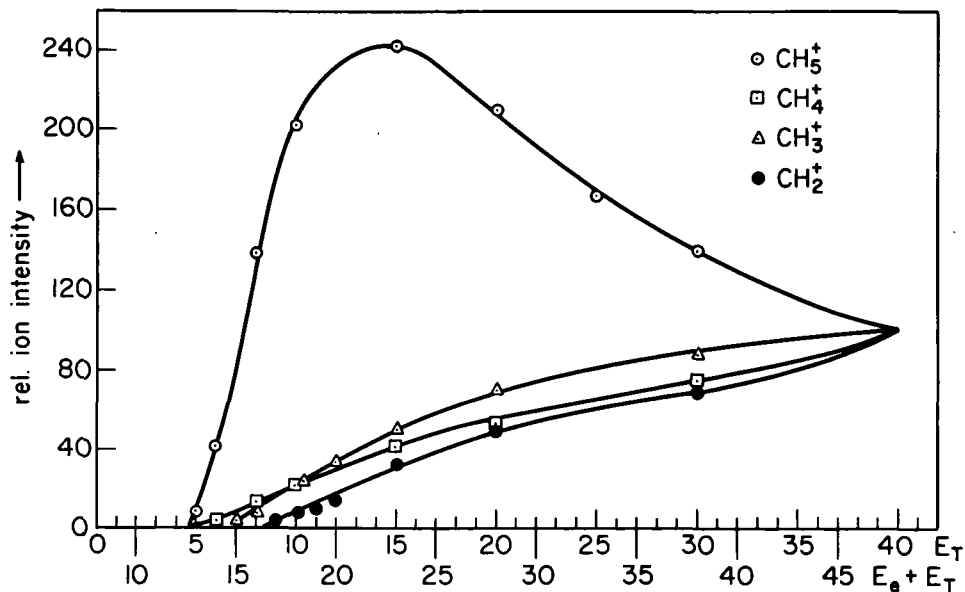


Fig. 4: Ionization efficiency curves of secondary ions in methane (E_e = constant at 8 volts. E_T variable. All curves normalized at E_T = 40 volts)

$$N(U) dU \propto c \cdot \sigma(U) \cdot dx \quad (5)$$

where c is the concentration of gas molecules in the ion source and $\sigma(U)$ the cross section for ionization at the distance x , i.e. at total electron energy $E_e + U$. If $U = E_T \cdot \frac{x}{x_0}$

$$N(U) dU \propto c \cdot \frac{x_0}{E_T} \sigma(U) \cdot dU \quad (6)$$

The total number of primary ions formed between x_0 and x_1 will amount to

$$N_{\text{tot}} \propto c \cdot \frac{x_0}{E_T} \cdot \int_{AP-E_e}^{E_T} \sigma(U) dU \quad (7)$$

$\sigma(U)$ is easily derived from the conventional ionization efficiency curve. For example, curve 1 in Fig. 3 represents $\sigma(U)$ for CH_4^+ if E_e is equal to 8 volts. This curve is the measured primary ionization efficiency curve 1 in Fig. 1 (the scale of the abscissa is just shifted by 8 volts). Curve 2 in Fig. 3 is the integral

$$\frac{1}{E_T} \cdot \int_{AP-8}^{E_T} \sigma(U) dU$$

of curve 1 and represents the total primary CH_4^+ current at different voltages E_T . Both curves are normalized at 40 volts.

The number of secondary ions which are produced by reactions of the primary ions in the ionization chamber is proportional to

$$N'_{\text{tot}} \propto c \cdot \int_{AP-E_e}^{E_T} N(U) \cdot \sigma'(U) dU \quad (8)$$

where $\sigma'(U)$ is the cross section of the ion-molecule reaction. By combining Eq. 6 and 8

$$N'_{\text{tot}} \propto c^2 \cdot \frac{x_0}{E_T} \int_{AP-E_e}^{E_T} \sigma(U) \cdot \sigma'(U) \cdot dU \quad (9)$$

is obtained. If σ' is independent of the kinetic energy of the primary ion, N'_{tot} becomes proportional to N_{tot} , i.e. the shape of the secondary ionization efficiency curve will be identical to that calculated from Eq. 7 (Fig. 3). In these considerations it has been assumed that all secondary ions reach the collector. However, if the secondary ions are formed with kinetic energies perpendicular to the direction of flight only a fraction, f , will be collected. As the kinetic energy of the primary ion increases f will decrease and N' will be described by the relation

$$N'_{\text{tot}}(E_T) \propto c^2 \cdot \frac{x_0}{E_T} \int_{AP-E_e}^{E_T} \sigma(U) \cdot \sigma'(U) \cdot f(U) \cdot dU \quad (10)$$

Symmetrical charge transfer reactions

Symmetrical charge transfer processes have been studied by a number of authors.²⁻⁵ These investigations have mainly been restricted to the noble gases. The reaction $\text{H}_2^+ + \text{H}_2 \rightarrow \text{H}_2 + \text{H}_2^+$ seems to be the only process studied in which molecular species are involved. The cross sections of such resonance processes are expected and have been found to be higher than gas collision cross sections. This arises because the resonance introduces a long range interaction which would otherwise not occur. Relatively little variation of the cross section with the kinetic energy of the ion has been found. At energies above 200 eV in all cases the cross section observed falls very slowly and steadily as the relative kinetic energy of the collision partners increases. At lower kinetic energies, however, a small maximum has been observed in argon and in neon⁶ and a very pronounced one in hydrogen.⁴ These anomalies have been attributed to the occurrence of non-resonant processes in the noble gases due to the spin multiplicity of the lowest state of these ions. In the case of H_2 a side reaction in which a change of vibrational energy is involved has been assumed.⁴ Scattering of ions in the case of exact resonance occurs primarily at small angles, the scattering intensity at 90° being practically zero.⁷ It can therefore be assumed that all secondary parent ions formed in our ion source exclusively result from symmetrical charge transfer.

Fig. 3 contains a few points from curve 3 in Fig. 1. These points fit curve 2 in Fig. 3 fairly well. This curve is calculated on the assumption that both $f(U)$ and $\sigma'(U)$ in Eq. 10 are constant over the range from 5-40 volts. The agreement indicates, as mentioned above, that the transfer of kinetic energy is very small and that the cross section of the observed process is not significantly dependent on the kinetic energy.

TABLE I

Relative cross section of symmetrical charge transfer reactions

ion	relative cross section	ion	relative cross section
CH_4^+ ^a	(1.0) ^a	HCl^+	7.0
C_2H_6^+	3.3	NH_3^+	7.8
C_2H_4^+	10	H_2S^+	15
C_2H_2^+	14	CS_2^+	19
$\text{c-C}_6\text{H}_{12}^+$	5.0	I_2^+	27
$\text{c-C}_6\text{H}_{10}^+$	29	Ne^+	3.7
C_6H_6^+	13	Ar^+	9.3
NO^+	4.1	Kr^+	15
H_2O^+	4.2	Xe^+	23
CO_2^+	4.3		
Ar^{++}	1.1		
Kr^{++}	1.8		
Xe^{++}	3.0		
NO^{++}	0.3		

^a reference reaction: $\text{CH}_4^+ + \text{CH}_4 \rightarrow \text{CH}_4 + \text{CH}_4^+$

Fig. 4 shows the ionization efficiency curves for the secondary ions observed in methane and Figs. 5-7 show similar data for some other simple molecules. The appearance potentials of the parent ions are always identical with those of the primary parent ions. All observed symmetrical charge transfer processes are listed in Table 1. The lowest cross section for transfer of a single electron has been found in methane. This reaction has been selected for reference in Table 1. In order to obtain relative cross sections, the ratio

$$\frac{\text{current of secondary ion at } E_e = 8 \text{ and } E_T = 40 \text{ volts}}{\text{current to primary ion at } E_e = 40 \text{ and } E_T = 40 \text{ volts}} \quad (11)$$

has been measured relative to the similar ratio for methane. This procedure assumes that the primary ion current in the Cermak-Herman operation of the ion source ($E_e = 8$, $E_T = 40$) is proportional to the ion current in the more conventional operation of the source (i.e. $E_e = 40$ volts). Since the primary ion current contained ions of kinetic energies between about 5 and 40 volts, the value of the cross section obtained is an average over this range. An additional complication arises since the primary molecular ions formed by electron impact will have various amounts of vibrational energy. The data obtained by the present method of measuring cross sections can be compared with literature values in the case of the noble gases. Our ratio of the cross sections in argon and neon amounts to $9.3/3.7 = 2.5$ which agrees with the ratio of 2.5-3.0 calculated from the measurements of Rostagni.⁶ Absolute cross sections may be calculated from the data in Table 1 by using the known absolute cross section of the transfer process in argon ($38 \times 10^{-16} \text{ cm}^2$ at 20 eV).

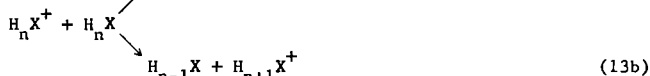
The cross section depends significantly on the nature of the compound. In molecules of similar size (such as ethane, ethylene and acetylene) the cross section increases with increasing unsaturation. A similar increase is observed by going from cyclohexane to cyclohexene. High cross sections have been found in the sulfur containing compounds and in iodine. Table 1 also contains some examples of symmetrical double charge transfer. In these experiments, 110 volts were used instead of 40 to carry out the measurements and Eq. 11 adjusted accordingly. The process



was the only one found for the transfer of two charges in a molecular system.

Proton transfer reactions

The secondary mass spectra of some simple molecules are listed in Table 2. The ionization efficiency curves of these secondary ions are shown by Figs. 4-7. Ions of the form $H_{n+1}X^+$ from parent molecules H_nX have been observed in all cases. The secondary ionization efficiency curves of these ions begin at the same appearance potentials as those of the parent ions H_nX^+ . Primary ions H_nX^+ must therefore be the precursors of the protonated species as well as the secondary parent ions.



In order to compare the competing processes of electron and proton transfer the ratio of the currents of the secondary ions $H_{n+1}X^+$ and H_nX^+ is plotted in Fig. 8 versus the voltage E_T .

The general shape of the secondary ionization efficiency curves of the ions $H_{n+1}X^+$ differs markedly from that of the ions H_nX^+ . A maximum at 10-15 volts above the appearance potential can usually be observed (Figs. 4-7). The decrease in the ratio $H_{n+1}X^+/H_nX^+$ in Fig. 8 indicates that electron transfer predominates more and more at higher kinetic energies. The shape of the $H_{n+1}X^+$ curves in Figs. 4-7 may be explained by the inverse dependencies of σ , σ' and f on the kinetic energy eU of the primary ions (Eq. 10). The increase in $\sigma(U)$ at rather low kinetic energies determines the main features of the shape of the curve while the decrease in $\sigma'(U)$ and in $f(U)$ becomes predominant at higher kinetic energies. The decrease of σ' is well known from conventional studies on ion-molecule reactions.^{3,9} It may be described by the relation

$$\sigma' \propto U^a \quad (14)$$

over a certain range of U . Values for a of -0.5 to -1.4 have been observed for different reactions.¹⁰

The collection efficiency, $f(U)$, can no longer be assumed to be constant as in the electron transfer reactions since the transfer of the mass of the proton will be accompanied by the transfer of kinetic energy. This term is therefore expected to decrease above a certain value of U , but the decrease should depend strongly on the nature of the collision. The reaction may occur via an activated complex which dissociates into the final products after a lifetime much longer than the time of a molecular vibration. The existence of such complexes has been proven indirectly⁹ and directly^{11,12} in several

TABLE 2

Primary and secondary mass spectra of simple molecules

Substance ^a	Ion	ionization potential (volts) ^c	relative intensity	
			primary spectrum ^b	secondary spectrum ^b
water	H ₃ O ⁺		2.4	29
	H ₂ O ⁺	12.61	100	100
	OH ⁺	~12.8	20	-
	O ⁺	13.61	0.7	-
hydrogen sulfide	H ₃ S ⁺		<0.04	2
	H ₂ S ⁺	10.47	100	100
	HS ⁺		38	4
	S ⁺	10.36	41	3
hydrogen chloride	H ₂ Cl ⁺		1.2	7
	HCl ⁺	12.90	100	100
	Cl ⁺	13.01	15	0.7
ammonia	NH ₄ ⁺		0.6	15
	NH ₃ ⁺	10.52 - 11.3	100	100
	NH ₂ ⁺		67	2
	NH ⁺		3.5	-
	N ⁺	14.54	7.8	-
methane	CH ₅ ⁺		2.8	20
	CH ₄ ⁺	13.1	100	100
	CH ₃ ⁺	9.9	78	120
	CH ₂ ⁺	11.9	12	6
	CH ⁺	11.13	5	-
	C ⁺		1	-
ethane	C ₂ H ₇ ⁺		not detectable	0.2
	C ₂ H ₆ ⁺	11.6	100	100
	C ₂ H ₅ ⁺	8.7	82	122
	C ₂ H ₄ ⁺	10.51	410	93
	C ₂ H ₃ ⁺		133	17
	C ₂ H ₂ ⁺	11.41	74	3
	C ₂ H ⁺		6	-
	C ₂ ⁺		0.8	-
ethylene	C ₂ H ₅ ⁺		not detectable	2
	C ₂ H ₄ ⁺	10.51	100	100
	C ₂ H ₃ ⁺		54	9
	C ₂ H ₂ ⁺	11.41	52	5
	C ₂ H ⁺		8	-
	C ₂ ⁺		1	-

^aPressure of the gas inlet system: 600μ. Repeller field: 3.84 volts/cm^bPrimary spectra; E_e = 40 volts, E_T = 40 volts. Secondary spectra; E_e = 8 volts, E_T = 40 volts^cData taken from F. H. Field and J. L. Franklin, "Electron Impact Phenomena", Academic Press, Inc., New York 1957

ion-molecule reactions. Complexes are probably preferentially formed at low kinetic energies. At higher kinetic energies the lifetime of the complex will become shorter than the time required for distribution of the excitation energy in the various degrees of freedom in the complex, i.e. there is practically no real complex formation. Reactions which are observed at higher kinetic energies are more likely to occur as stripping processes. Essentially the cross sections of such processes are not expected to exceed gas kinetic cross sections. In the case of complex formation the intermediate complex will move with half the original kinetic energy (eU) in the direction of the primary ion, the rest of the kinetic energy appearing as internal energy. The reaction product $H_{n+1}X^+$ will have the kinetic energy $\frac{1}{2}(eU) \cdot \frac{A+1}{2A} \sim \frac{1}{4}(eU)$ in the direction of the primary ion (where A is the mass of the molecule H_nX). It will have an additional component of kinetic energy directed at random if part of the excitation energy of the complex and of the exothermicity of the reaction appears as kinetic energy of the final products. At values of U above 10 volts the maximum energy component U_c , at which collection is allowed, will have been reached. The collection efficiency is expected to fall significantly as the kinetic energy of the primary ion exceeds a few electron volts.

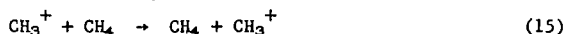
Where the secondary ion results from stripping of a proton from the primary ion the protonated molecule will be formed with the kinetic energy $\frac{1}{A} \cdot \frac{1}{A+1}(eU)$ in the direction of the primary ion. This amount is much less than in the case of complex formation. There $f(U)$ is expected to depend only slightly on the kinetic energy in the range of 5-40 volts. The ratio $H_{n+1}X^+/H_nX^+$ in Fig. 8 is only slightly dependent on E_T in the cases of hydrogen chloride, hydrogen sulfide and ammonia. If we can again assume that σ' and f of the electron transfer are nearly independent of energy it must be concluded that σ' and f of the proton transfer show the same behavior. The stripping model would therefore be more adequate to describe these reactions than the activated complex model (at least for kinetic energies above 5 eV). The very strong decrease in the current ratio CH_5^+/CH_4^+ in Fig. 8 indicates that this reaction occurs via a complex at low kinetic energies while a stripping reaction predominates at higher energies. This may also explain some observations of Field et. al.⁹ who studied the reaction $CH_4^+ + CH_4 \rightarrow CH_5^+ + CH_3$ by operating the ion source in the conventional way. They found the cross section to decrease at repeller field strengths between 10-100 volts/cm but to become constant at higher field strengths.

The $C_2H_7^+$ ion which could not be detected in conventional studies on ion-molecule reactions in ethane¹³ has been observed (Table 2, Fig. 8) with low intensity. Since the appearance potentials of $C_2H_6^+$, $C_2H_5^+$ and $C_2H_4^+$ from ethane do not differ very much, it is difficult to attribute the secondary $C_2H_7^+$ to one of these primary ions. A rough estimate shows that the cross section of the formation of $C_2H_7^+$ in ethane must be 100 times smaller than that of the proton transfer in water. This low cross section explains the failure to detect $C_2H_7^+$ in the conventional operation of an ion source since $C_2H_7^+$ is here masked by the C^{13} isotopic peak of the $C_2H_6^+$ ion.

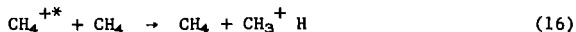
Fragment ions in the secondary mass spectra

The secondary mass spectra in Table 2 contain a number of ions of lower mass numbers. Their secondary appearance potentials are identical with the known appearance potentials of these ions when formed by electron impact. It cannot be ruled out that primary ions are not scattered and pass through the slit system of the mass spectrometer. The collection efficiency of scattered ions is expected to be very small since most will have components of kinetic energy perpendicular to the direction of analysis. Furthermore, the scattering intensity at 90° is very low.¹⁴ This would explain the rather low relative intensities of most of the fragment ions in Table 2. The table, however, contains a few examples which strongly indicate that there must be additional processes of formation of secondary fragment ions.

The ion CH_3^+ is the most abundant in the secondary mass spectrum of methane. Its intensity is even higher than that of CH_4^+ (the abundant ion in the primary mass spectrum). Furthermore, the secondary ionization efficiency curve of CH_3^+ always runs above that of CH_4^+ except for the immediate vicinity of the appearance potential of CH_3^+ (Fig. 4). This is in contrast to the behaviour of the primary ionization efficiency curves of these ions.¹⁵ It must be concluded that CH_3^+ ions are formed by some ion-molecule reactions such as H⁺ transfer from methane



or dissociative electron transfer



If reaction (16) is initiated by a CH_4^+ ion in its ground state the energy deficit $D(CH_3^+-H)$ has to be taken from the kinetic energy of the CH_4^+ ion. The cross section of this process would be very small since the collision occurs adiabatically in the energy range studied. However, if the CH_4^+ ion is formed with an amount of vibrational energy only about one-tenth of an electron volt smaller than $D(CH_3^+-H)$ the rest of the energy deficit may easily be delivered by the kinetic energy. It is at present not possible to distinguish between reactions (15) and (16). Similarly the $C_2H_5^+$ ion occurs with

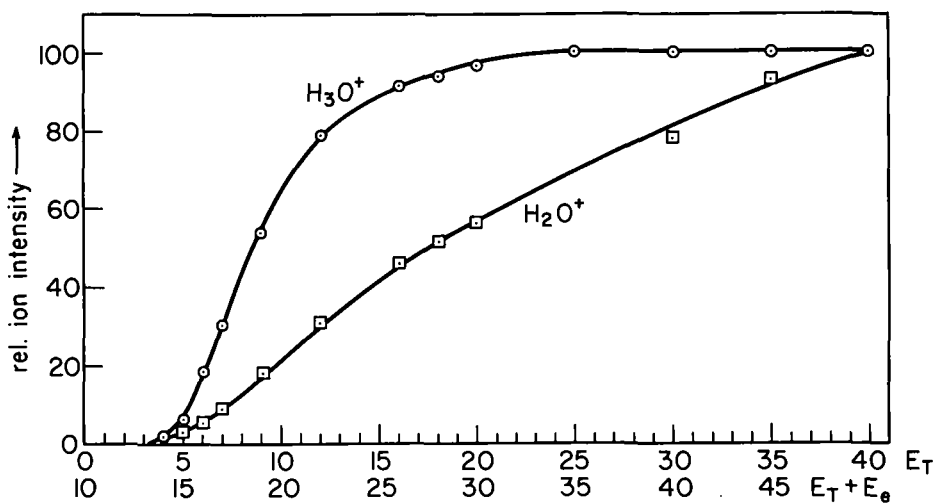


Fig. 5: Ionization efficiency curves of secondary ions in water (E_e = constant at 10 volts, E_T variable)

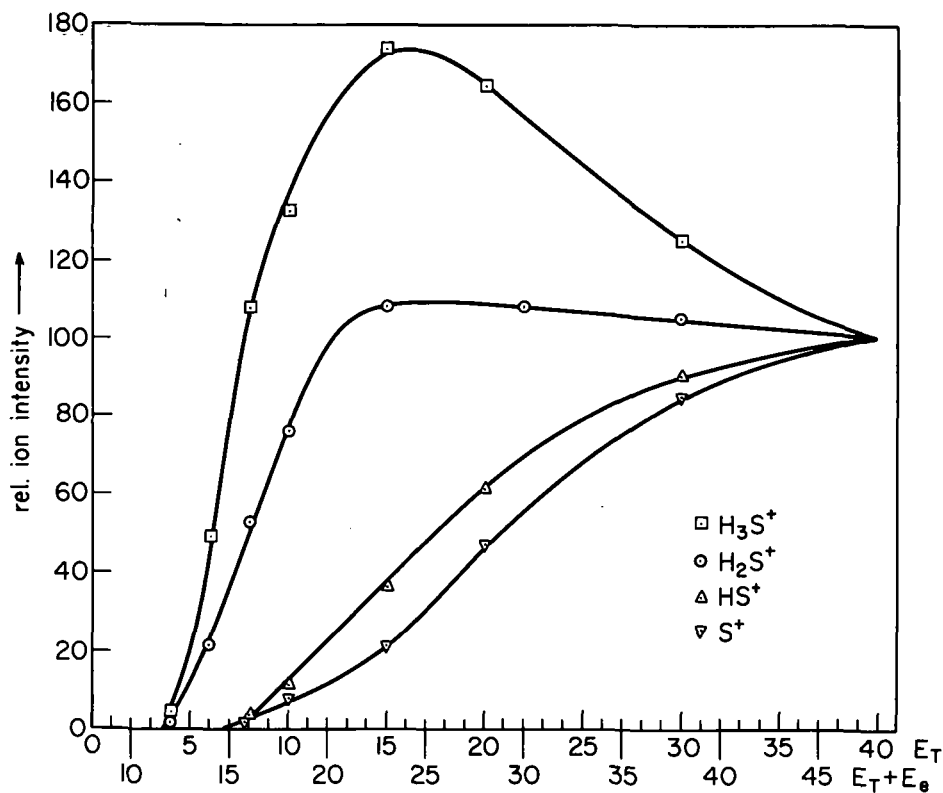


Fig. 6: Ionization efficiency curves of secondary ions in hydrogen sulfide (E_e = 8 volts, E_T variable)

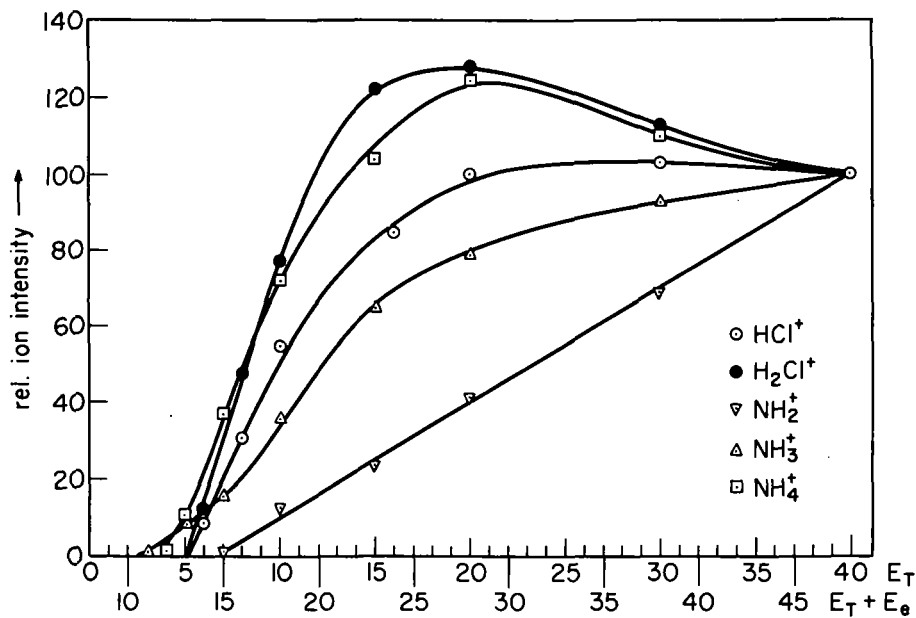


Fig. 7: Ionization efficiency curves of secondary ions in hydrogen chloride and ammonia ($E_e = 8$ volts, E_T variable)

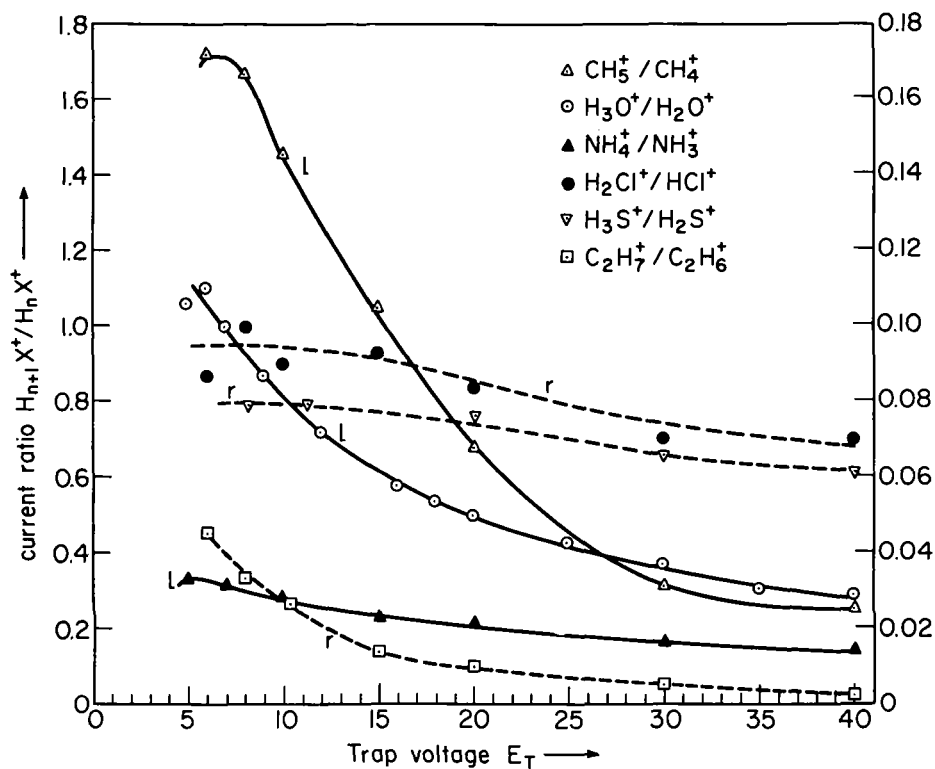
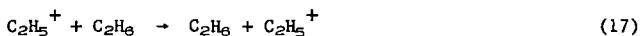
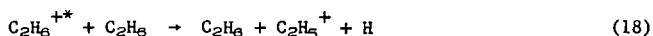


Fig. 8: Current ratio of protonated molecules and secondary parent ions as a function of E_T ($E_e = 8$ volts. l and r: left and right ordinate scale, respectively)

abnormally high intensity in the secondary mass spectrum of ethane. It is therefore attributed to the analogous reactions



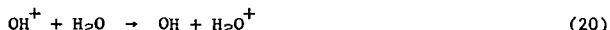
or



The OH^+ ion could not be detected in the secondary spectrum of water although its intensity as primary ion is very high. The absence of this ion as a secondary ion would seem to corroborate the above ideas that the high intensities observed for CH_3^+ and $C_2H_5^+$ cannot be due to scattering of the primary ions. It also indicates that hydride ion transfer (Eq. 19) does not occur. The ionization potential of OH seems to be



slightly higher than that of water while that of CH_3 is much lower than that of methane (Table 2). In the case of water electron transfer



is expected to compete with reaction (19). Reaction 20 is of interest in considerations of the radiation chemistry of water. It explains the fact that there is no chemical evidence of OH^+ although the mass spectrum of water indicates that OH^+ is formed in high yield by high energy radiation. In the case of hydrogen chloride, the fragment Cl also has a slightly higher ionization potential than the molecule. The reaction $Cl^+ + HCl \rightarrow Cl + HCl^+$ may therefore be responsible for the very low relative intensity of Cl^+ in the secondary mass spectrum of hydrogen chloride.

LITERATURE REFERENCES

- 1.) V. Cermak and Z. Herman, *Nucleonics* **19**, 106 (1961)
- 2.) H. S. W. Massey and E. H. S. Burhop, "Electronic and Ionic Impact Phenomena", Oxford, At the Clarendon Press 525 (1952)
- 3.) J. B. Hasted, *Proc. Roy. Soc.* **205 A**, 421 (1951)
- 4.) H. B. Gilbody and J. B. Hasted, *Proc. Roy. Soc.* **238 A**, 334 (1956)
- 5.) J. B. Hasted, *Advances in Electronics and Electron Physics*, **13**, 1 (1960)
- 6.) A. Rostagni, *Nuovo Cimento* **12**, 134 (1935)
- 7.) Reference 2, p. 443
- 8.) D. P. Stevenson and D. O. Schissler, *J. Chem. Phys.* **29**, 282 (1958)
- 9.) F. H. Field, J. L. Franklin and F. W. Lampe, *J. Am. Chem. Soc.* **79**, 2419 (1957)
- 10.) A. Henglein, *Z. Naturforschung*, **17a**, 37 (1962)
- 11.) R. F. Pottier and W. H. Hamill, *J. Phys. Chem.* **63**, 877 (1959)
- 12.) A. Henglein, *Z. Naturforschung*, **17a**, 44 (1962)
- 13.) F. W. Lampe and F. H. Field, *J. Am. Chem. Soc.* **81**, 3242 (1959)
- 14.) Reference 2, p. 496-497
- 15.) A. Henglein and G. A. Muccini, *Z. Naturforschung*, **15a**, 584 (1960)

THE EFFECT OF PRESSURE SCATTERING ON HIGH PRECISION
ISOTOPIC ABUNDANCE MEASUREMENTS*

K. A. Kaiser **
University of Minnesota

ABSTRACT

As part of a study of the present limitations on attainable precision in isotopic abundance measurements, pressure scattering of the mass spectrometer ion beam was calculated using a hard sphere scattering model. For a conventional sector field instrument the calculations predict;

- (1) asymmetric scattering tails which fall off logarithmically from abundant mass peaks,
- (2) that nearly all scattered ions which are collected come from two source regions--one immediately before the collector and the other immediately before the analyzer,
- (3) an apparent change in a null method isotopic abundance ratio when the collected ion beams move with respect to the collector slits. Also in precision isotopic gas analysis, the calculations give a natural explanation of the "Pressure Effect" i.e. the change of a null method isotopic abundance ratio with ion beam intensity. Preliminary experiments gave quantitative agreement with calculated values of the scattering intensities.

* Paper submitted in partial fulfillment of the requirements for the M.S. degree.

** Presently employed at the Argonne National Laboratory.

Ions in the Carbon Dioxide Glow Discharge

P. H. Dawson and A. W. Tickner
Applied Chemistry Division,
National Research Council,
Ottawa, Canada.

This work is part of a study of d.c. glow discharges in which the ions are observed by means of a mass spectrometer. The general significance of the results extends beyond the direct application to discharge physics since ion-molecule reactions will be reflected in the ion abundances that are observed.

The apparatus is shown in Figure 1. The instrument is of a conventional double-focussing type with a variable slit in the plane of the energy spectrum so that any band of ion energies can be selected. Figure 2 shows the discharge tube and ion source in greater detail. The electron gun is electrostatically focussed to avoid interference with the discharge and is used only for setting up and testing the instrument. The discharge tube cathode is movable, and, since the negative glow maintains its position relative to the cathode, movement of the cathode enables the various regions of the discharge to be sampled by the probe. Ions are drawn from the plasma by a potential difference of about twelve volts maintained between the probe and the potential of the plasma in front of the probe.

Figure 3 shows a simple physical picture of a discharge and its principal regions: the cathode dark space, the negative glow and Faraday dark space and the positive column. An important characteristic is the variation of electric field. The cathode dark space has a high field and positive ions from the front of the negative glow are accelerated to the cathode. Electrons from the cathode are accelerated to the glow and a substantial proportion reach it with energies of several hundred volts. The primary ion formation in the negative glow is therefore that caused by relatively high energy electrons. The interior of the glow is a nearly field free region in which ions are lost mainly by diffusion to the walls and it is here that ion-molecule reactions are likely to occur. On the anode side of the negative glow, the field increases and this results in the formation of the positive column. The mean electron energy increases as the positive column is entered but energies only reach values great enough to maintain the necessary ionisation and effects requiring the lowest energies predominate, in contrast with the negative glow.

Figure 4 shows some results for a carbon dioxide discharge at 0.1 mm pressure and a current density of 0.01 mA/cm^2 . The major ion produced in the negative glow is, as expected, CO_2^+ . CO^+ is also found but is much smaller than would be expected from electron impact data. It is relatively larger at the front of the glow. In the interior it probably readily undergoes charge exchange with carbon dioxide since its ionisation potential exceeds that of CO_2 by only 0.2 eV. The O_2^+ ions have two possible origins. They may be formed from reactions between excited CO_2^+ ions and carbon dioxide molecules or by charge exchange between CO_2^+ ions and oxygen molecules formed as products of the discharge. The relative displacement of the O_2^+ maximum into the interior of the glow is consistent with both of these processes. The HCO_2^+ ion closely parallels the behaviour of CO_2^+ and is presumably formed by a reaction of CO_2^+ with hydrogenous impurities, such as water. The concentrations of such impurities are very small but they produce significant effects. The interior of the negative glow seems particularly suitable for the formation of ion clusters and several are observed as shown. Clusters observed in smaller amounts and not shown in the figure were $\text{CO}_2.\text{CO}_2^+$ and $\text{CO}.\text{CO}_2^+$. The clusters must have considerable stability in order to be detected and this may have some application to current theories in radiation chemistry.

Figure 5 gives some results for a discharge at the same pressure but with a fivefold increase in current so that the discharge is more abnormal. CO^+ is about the same relative to the total level of ionisation, but O_2^+ is now the dominant ion except at the front of the glow. This is consistent with its formation from an excited CO_2^+ ion since it is known that in a more strongly abnormal discharge a greater proportion of the electrons reaching the glow have energies equal to the full cathode fall. The increase in O_2^+ relative to CO_2^+ is, however, also consistent with the

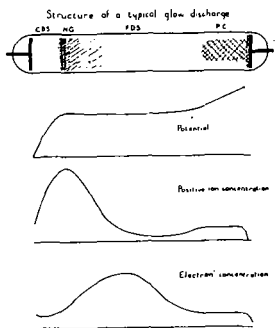


Figure 3

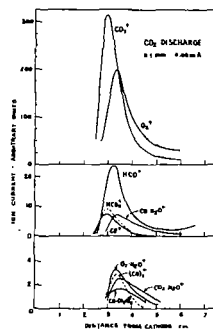


Figure 4

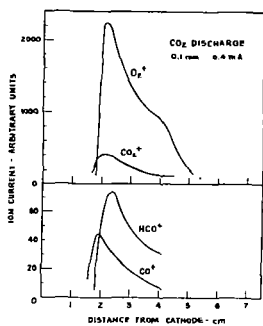


Figure 5

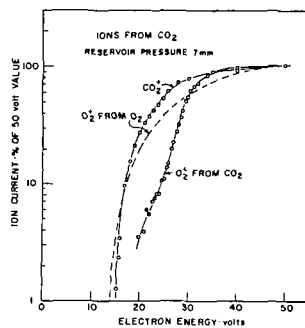


Figure 6

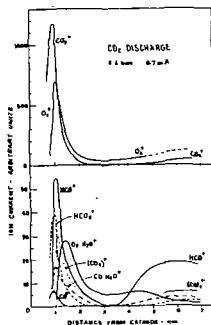


Figure 7

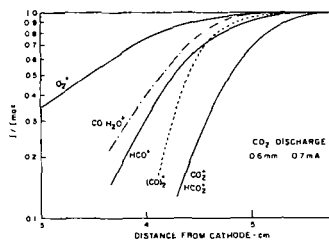


Figure 8

formation of O_2^+ by charge exchange since the percentage of decomposition increases with increasing current density.

We have also studied the mass spectrum of carbon dioxide in an analytical mass spectrometer at higher than usual ion source pressures. The situation is complicated by the apparent occurrence of surface processes producing oxygen but some O_2^+ is found with an appearance potential of about 24 eV. as shown in Figure 6. This is surprisingly high since only 18.2 eV. is required for a thermoneutral reaction and excited states of CO_2^+ are known, from spectroscopic work, to occur at 18.2 and 19.2 eV.

Several experiments have been carried out with the CO_2 discharge using different flow rates to give different overall conversions. Low flow rates and added oxygen increase the proportion of O_2^+ but not as much as would be expected if the increased concentration of O_2 in high current density experiments was due only to charge exchange with the increased amounts of oxygen produced. It seems likely, therefore, that although the charge exchange mechanism does play some part in the occurrence of O_2^+ , formation by an ion-molecule reaction involving an excited CO_2^+ is also important. Further experiments are being carried out in an attempt to assess more exactly the relative importance of the two processes.

Some results at a higher pressure are shown in Figure 7. In the negative glow, CO^+ is now smaller relative to the total ionisation, as might be expected. (The ion marked $(CO_2)^+$ should be $C_2O_2^+$). In the Faraday dark space O_2^+ is the most abundant ion. The relative positions at which the various ions increase in abundance as the field increases at the start of the positive column gives some indication of the mechanisms of formation in this region. Figure 8 shows a logarithmic plot of the ratios of ion currents to their respective constant values in the positive column. For O_2^+ , the increase occurs nearest the cathode where the mean electron energy is lowest showing that the O_2^+ is formed by the ionisation of oxygen produced in the discharge. On the other hand CO_2^+ and HCO_2^+ are formed nearest the anode and show identical behaviour suggesting a common mode of formation requiring higher energy - that is, the ionisation of carbon dioxide. $H_2CO_2^+$ and HCO^+ require an intermediate amount of energy and must form from easily ionised impurities or from excited molecules of carbon dioxide or carbon monoxide. The increase of $C_2O_2^+$ before that of CO_2^+ is in accordance with the recent finding of Field and co-workers that it can be formed by reaction of an excited carbon monoxide molecule (12.8 eV.) with another carbon monoxide molecule. No CO^+ is observed in positive column.

In conclusion, the possible significance of these results to work on the radiation chemistry of carbon dioxide should be noted since one might expect some analogy with the discharge phenomena. Currently accepted mechanisms explaining the radiation chemistry of the gas assume that ions play little part but our results suggest that ion-molecule reactions may be important.

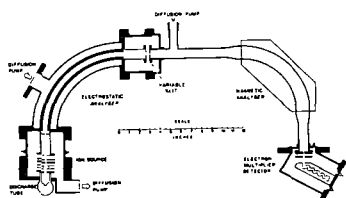


Figure 1

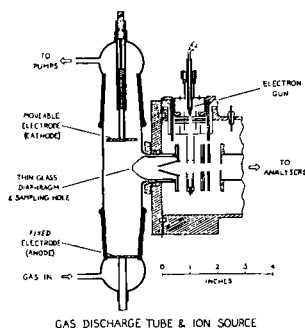


Figure 2

DETERMINATION OF ELECTRONIC ENERGY LEVELS
OF MOLECULES BY LOW ENERGY ELECTRON IMPACT

Aron Kuppermann and Lionel M. Raff
Department of Chemistry
University of Illinois
Urbana, Illinois

Abstract

A method has been devised for determining electronic energy levels of molecules by inelastic scattering of low energy electrons. The method consists in sending a beam of monoenergetic electrons with energy in the range of 25 to 50 eV into a gas at about 10^{-4} mm Hg pressure. The electrons scattered by the gas molecules are energy-analysed by retarding fields produced by cylindrical grids whose axis is the incident non-scattered beam. The energy losses of the electrons furnish the electronic excitation energies. The electronic transitions induced include optically forbidden ones, due to exchange scattering. The method is thus specially suited for the determination of the energies of low lying excited triplet states of molecules. Using the optical ionization potential of helium (24.585 eV) to calibrate the electron beam energy, the determination of the energy of the 2^3S state of helium furnished 19.8 eV. The known optical value is 19.818 eV. Impact spectra were also obtained for argon, ethylene and other molecules. The apparatus will be described and the results obtained so far given.

PHOTOIONIZATION PROCESSES STUDIED BY MASS SPECTROMETRY

D. C. Frost, D. Mak and C. A. McDowell
Department of Chemistry
University of British Columbia
Vancouver 8, B. C.

Manuscript Withdrawn

ANALYSIS OF LOW MELTING METALS BY SPARK SOURCE MASS SPECTROMETRY

by

J. D. Waldron and W. A. Wolstenholme
Associated Electrical Industries Ltd.
Manchester, England

1. INTRODUCTION

The problem in the analysis of low melting metals by spark source mass spectrometry is primarily one of forming suitable electrodes from the sample material. From this point of view gallium (melting point 29.8°C) presents the most difficult problem since it becomes molten under conditions normally existing on the spark.

This paper describes techniques which have been successfully employed to analyse gallium by spark source mass spectrometry and which might be applied with advantage to other low melting metals.

2. GRAPHITE SUPPORT METHOD

The first approach to this problem was made using graphite as a supporting electrode for a globule of gallium⁽¹⁾. During sparking the gallium melts and spreads over the surface of the carbon, as shown in Fig.1, and enables spectra of gallium to be obtained.

The technique has the advantage of simplicity but there is strong evidence that selective distillation of certain impurities occurs and only semi-quantitative results can be given. Also it is difficult to obtain long exposures and therefore high sensitivity with this method. To achieve quantitative determination of impurities and high sensitivity it is therefore essential that the gallium should be in the solid state.

3. COOLED ELECTRODE TECHNIQUE

For this method the gallium samples were prepared by etching three times in transistor grade hydrochloric acid and washing in deionized water. The material was then melted under an infra red lamp and formed into electrodes 1/16" diameter and approximately 3/8" long in P.T.F.E. tubing. The tubing was then cut away and the electrodes placed directly in the ion source of an A.E.I. MS7 mass spectrometer.

The ion source of the instrument was modified for this work so that the electrodes could be cooled to prevent melting while the high voltage spark is passed between them. A glass tube sealed to a metal flange was fitted to the top of the ion source as shown in Fig.2. The tube could be filled with liquid nitrogen and thermal contact between the cooled inner surface of the electrodes made by means of two pieces of copper braid connected to copper strips which were wrapped round the glass tube and clamped to the electrodes as shown. The tube was filled with liquid nitrogen after evacuation of the ion source and the level maintained by topping up approximately every 15 minutes.

Using this method of cooling analyses were carried out with spark conditions typical of those used for materials of higher melting point. The only difficulty encountered in maintaining the spark was the need to adjust the electrode rather more frequently than usual. Typical pressures in the analyser and source regions of the instrument during the analysis were 1×10^{-8} torr and 1×10^{-6} torr respectively.

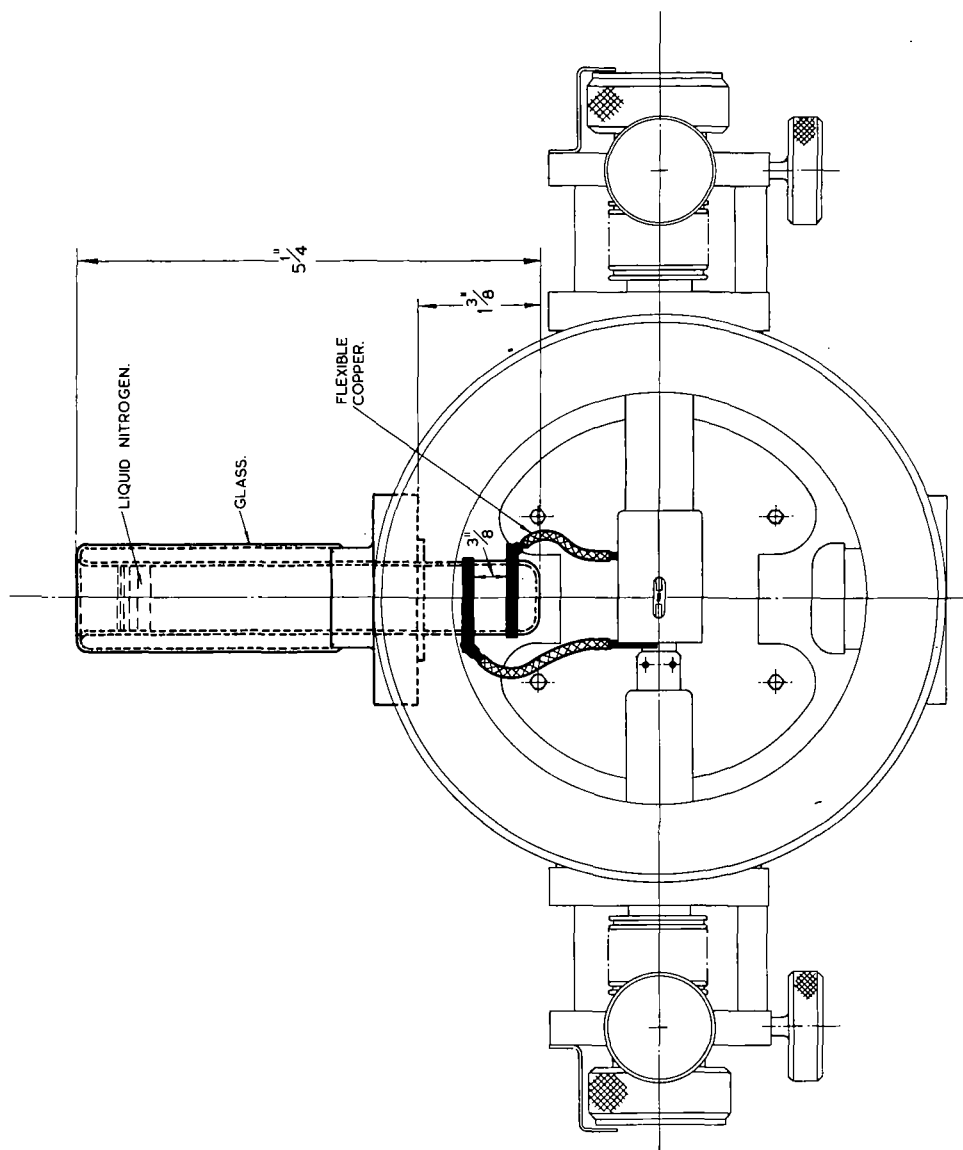


Fig. 2

4. RESULTS OBTAINED BY THE COOLED ELECTRODE TECHNIQUE

Results obtained in the analysis of three different gallium samples are shown in Table 1. For this analysis the concentrations were estimated by the visual method(2) on the assumption that all the elements had the same sensitivity. Significant differences were observed between the samples; the results of zinc and copper were particularly interesting for the use of gallium in semi-conductors.

TABLE 1

<u>Element</u>	<u>Sample 1</u>	<u>Sample 2</u>	<u>Sample 3</u>
Pb	200	200	<0.006
Tl	10	<0.003	<0.003
Hg	3	1	<0.03
Sn	3	1000	0.1
In	1	3	<0.01
Ag	<0.006	2	<0.006
Ge	1	<0.03	<0.1
Zn	0.006	6	0.02
Cu	3	1	<0.03
Fe	1	<0.2	0.03
Ca	0.1	<3	0.3
K	0.1	1	<0.01
Cl	4	1	0.1
S	<0.2	<1	0.6
Si	0.1	1	<0.3
Al	0.1	10	0.1
Mg	<0.1	0.1	<0.1
B	0.03	0.1	<0.01

As with normal samples more accurate determinations of concentration were carried out for certain elements using a microdensitometer. The densities of the impurity and the gallium lines were measured and plotted against the logarithm of the exposure (i.e. the total integrated monitor current). The results obtained for the $^{208}\text{Pb}^+$, $^{205}\text{Tl}^+$, $^{63}\text{Cu}^+$ and $^{71}\text{Ga}^+$ lines are shown in Fig.3. From these plots the exposures required to produce a given density for the gallium and the impurity element were compared and an estimate of the impurity concentration obtained by substituting the values of exposure so calculated in the same expression as that used for the visual method.

Table 2 shows the results obtained for the concentrations of lead, copper and thallium in three analyses of one sample. Although more analyses are required in order to obtain really meaningful statistics the results suggest that the reproducibility of the method is of the order of 25%.

TABLE 2

<u>Plate</u>	<u>Concentration (ppm atomic)</u>		
	<u>Pb</u>	<u>Cu</u>	<u>Tl</u>
1	104	3.4	4.5
2	129	3.4	3.1
3	135	5.6	4.1

ANALYSIS OF GALLIUM USING GRAPHITE SUPPORTING ELECTRODES.

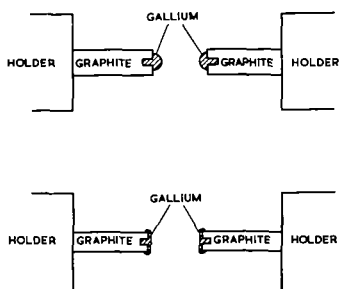


Fig.1.

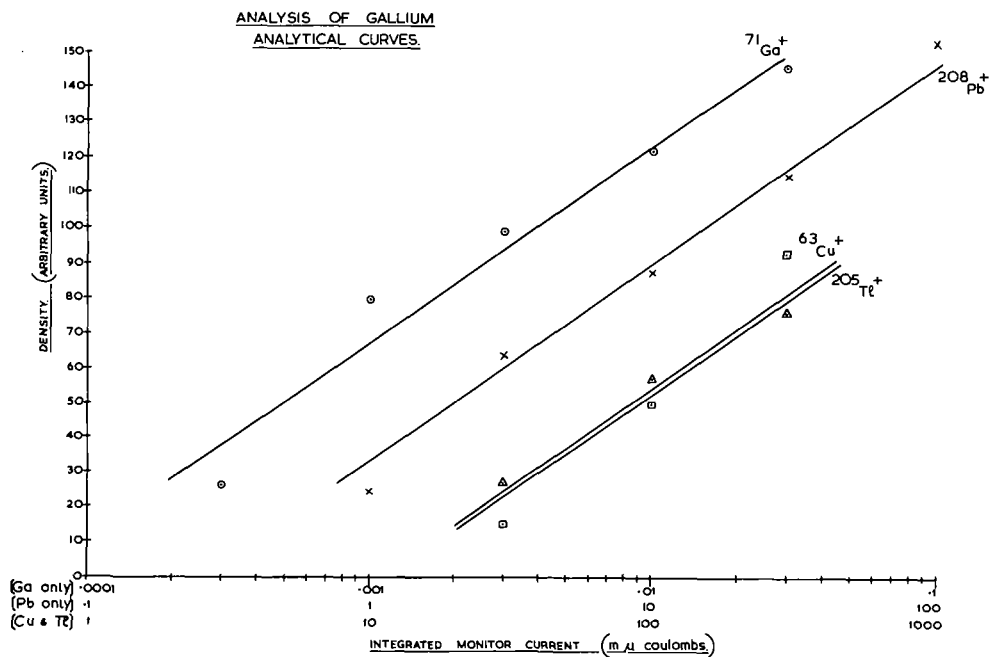


Fig.3.

Table 3 gives the estimated limits of detection of the method for 72 elements in gallium. These limits have been estimated from the photographic plate on the basis of a longest exposure of 10^{-6} coulombs. An exposure of this length can be obtained with gallium in approximately 2½ hours.

TABLE 3

<u>Element</u>	<u>Limit of Detection</u>	<u>Element</u>	<u>Limit of Detection</u>
Uranium	0.003	Palladium	0.01
Thorium	0.003	Rhodium	0.003
Bismuth	0.01	Ruthenium	0.01
Lead	0.006	Molybdenum	0.01
Thallium	0.003	Niobium	0.003
Mercury	0.01	Zirconium	0.006
Gold	0.03	Yttrium	0.003
Platinum	0.01	Strontium	0.1
Iridium	0.006	Rubidium	0.01
Osmium	0.006	Bromine	0.02
Rhenium	0.006	Selenium	0.1
Tungsten	0.01	Arsenic	0.01
Tantalum	0.1	Germanium	0.03
Hafnium	0.01	Zinc	0.006
Lutetium	0.003	Copper	0.01
Ytterbium	0.01	Nickel	0.003
Thulium	0.003	Cobalt	0.003
Erbium	0.01	Iron	0.003
Holmium	0.003	Manganese	0.003
Dysprosium	0.01	Chromium	0.003
Terbium	0.003	Vanadium	0.01
Gadolinium	0.01	Titanium	0.1
Europium	0.006	Scandium	0.01
Samarium	0.01	Calcium	0.03
Neodymium	0.01	Potassium	0.01
Praseodymium	0.03	Chlorine	0.04
Cerium	0.1	Sulphur	0.03
Lanthanum	0.01	Phosphorus	0.01
Barium	0.1	Silicon	0.03
Cesium	0.01	Aluminium	0.01
Iodine	0.003	Magnesium	0.1
Tellurium	0.01	* Sodium	No value
Antimony	0.006	Fluorine	0.01
Tin	0.01	Boron	0.003
Indium	0.003	Beryllium	0.01
Cadmium	0.01	Lithium	0.01
Silver	0.006		

* - overlap by $^{69}\text{Ga}^{3+}$

5. COMPARISON WITH STANDARDS

Two samples doped with approximately 0.8 ppm by weight of copper and zinc respectively were cast into rods in p.v.c. sheathing and then etched in the same way as indicated above before being mounted in the ion source.

In Table 4 the results obtained by mass spectrometry are compared with those obtained by neutron activation analysis.

TABLE 4

	<u>Mass Spectrometry</u>			<u>Neutron Activation</u>
	<u>1</u>	<u>2</u>	<u>Mean</u>	
Cu concentration (ppm wt)	0.90	0.72	0.81	1.3
Zn concentration (ppm wt)	0.66	0.91	0.79	1.0

Bearing in mind that the mass spectrometric results were calculated on the assumption that the elements copper, zinc and gallium all had the same sensitivity, the agreement between the mass spectrometric and neutron activation analyses is encouraging. This is particularly the case with zinc which was observed to give spuriously high results in the graphite support technique due to selective distillation effects.

The difference between the neutron activation and mass spectrometric results should not be taken as indicating an absolute error in one or other method. Accepting the neutron activation figures as correct, the results suggest that copper and zinc have low relative sensitivities in the spark compared with gallium.

6. CONCLUSIONS

Spark source mass spectrometry can be successfully applied to the estimation of impurities in gallium by cooling the electrodes. The cooled electrode technique has a number of advantages over the graphite support method in that firstly, it enables longer exposures and therefore lower limits of detection to be obtained (about a factor of 30), secondly, selective distillation of impurities is prevented and thirdly, the possibility of interference from the graphite support electrode is removed.

It is possible that the technique could be applied with advantage to other low melting metals such as indium (melting point 156.4°C). Although indium does not actually melt during sparking there have been indications that impurity elements such as zinc may give spuriously high results due to selective distillation effects and this might be reduced by using the cooled electrode technique.

ACKNOWLEDGEMENT

The authors wish to thank Mr. J. A. James of Associated Electrical Industries (Rugby) Ltd. for making available the results of the neutron activation analysis.

REFERENCES

1. R. Brown, R.D. Craig, J. A. James and C.M. Wilson "Analysis of Trace Impurities by Spark Source Mass Spectrometry". Proceedings of Boston Conference on Ultra-purification of Semiconductor Materials, 1961 (to be published by Macmillan).
2. R.D. Craig, G.A. Errock and J.D. Waldron "Advances in Mass Spectrometry" Edited by J.D. Waldron, Pergamon Press, 1959, p.143.

ION CHARGE DISTRIBUTION IN AN R. F. SPARK ION SOURCE
AND ITS EFFECT ON QUANTITATIVE ANALYSIS

Edward B. Owens
Lincoln Laboratory,* Massachusetts Institute of Technology
Lexington 73, Massachusetts

SUMMARY

Data are presented showing the ion charge distribution observed from an r. f. spark source with samples of GaAs, GaSb, InAs, InSb and stainless steel. The experiments were performed with source conditions varied to have pulse lengths of 5, 40, 50, and 160 microseconds, repetition rates of 100 and 1000 pulses per second, and spark voltages of 30 and 90 kv. Ilford Q₂ plates were used for the ion detector.

The emulsion was calibrated by the "two line" method to convert the non-linear photographic data to ion density values. The line widths were taken into consideration by multiplying the peak ion density of a line by the width of the line at half peak ion density. Background corrections were made by subtracting the ion densities due to the background from the ion density values of the lines. The validity of this method of handling photographic data was demonstrated with results of two experiments. One experiment was to put constant exposures on a plate while changing the magnet to plate distance to deliberately cause the lines to broaden. With line widths changing by a factor of two, the number of ions determined from the photographic data was constant within 10%. The second verifying experiment was to measure isotope ratios. The relative abundance of Sb and of Ga isotopes determined with this method agreed with the accepted values within 5%.

In all the exposures used in these tests the charge exchange lines, the polymer lines, and the triply charged lines were observed to contribute not more than 1% to the total number of ions striking the plate. Therefore the charge distribution of an element in an exposure was reported as the number of singly charged ions of that element divided by the total of singly charged ions plus doubly charged ions of that element. Detailed examination of the data revealed:

- 1) The charge distribution is not the same for all materials under all conditions. There is no single, universally applicable constant.
- 2) The charge distribution is constant to within about 5% for a given element in a given matrix sparked with constant source conditions, but differs for the same matrix under different source conditions and for different matrices under the same source condition.
- 3) For each material tested the ion charge distributions of the constituent elements fluctuated together. That is, under a given source condition the constituent elements of a sample all have approximately the same ion charge distribution. This is a highly desirable condition because when it exists only a small error will result in the quantitative analysis if the multiply charged ions are neglected and the element concentrations are determined from the ratios of the singly charged ions.
- 4) No consistent pattern was found for the relationship between the ion charge distribution and a change in pulse length, the number of pulses per second, or the sparking voltage.

Additional information was obtained from this investigation by using the data to calculate the composition of the ion beam from each of the III-V semiconductor compounds used. These compounds have a one-to-one ratio (at least to within 1 ppm) for the two elements in the solid sample. The results showed the ion beam from GaAs to be 52 to 53% Ga, from GaSb to be 54 to 64% Ga, from InAs to be 50 to 59% In, and from InSb to be 57 to 63% In. The error terms for these experiments are such that the composition of the beams from GaAs and InAs are probably not significantly different 50 - 50. It was found also that after prolonged sparking the ion beam from GaAs became predominantly Ga (87 to 97% Ga), indicating perhaps a loss of the more volatile As from the area of sparking. No other compound showed this effect.

*Operated with support from the U. S. Army, Navy, and Air Force.

PHOTOGRAPHIC QUANTITATIVE ANALYSIS
WITH A SOLIDS SPARK MASS SPECTROGRAPH

By

C. W. Hull
Consolidated Electrodynamics Corporation
Pasadena, California

ABSTRACT

Any method of quantitative analysis with a mass spectrograph, which uses a photoplate as a detector, must take several factors into consideration.

In the spectrograph, every mass is focused at a different radius. This introduces two quantitative problems.

1. Line width and shape vary across the plate.
2. The ion transmission of the instrument itself varies with path length.

The photoplate as a detector also offers various problems.

3. The emulsion does not darken in a linear manner, and the darkening characteristics change from plate to plate.
4. The sensitivity of the emulsion exhibits ion mass dependence, ion energy dependence, and may have chemical dependence as well.
5. Errors may be introduced in the densitometry.

Also, the problems that exist in any mass focusing instrument are present.

6. Space charge may broaden the ion beam.
7. A substantial background level may exist, due in this case to gas scattering.

And in the spark source, two problems are significant.

8. The ratio of singly charged to multiply and fractionally charged ions may vary, both from element to element and with time.
9. Ionization efficiency changes from element to element.

Each of these effects can contribute an error in a quantitative calculation. A quantitative method has been developed which gives consistent results, which can lead to analysis by comparison with known standards, and gives a more refined method of studying the problems inherent in the system.

I. DISCUSSION OF PROBLEMS

A. Calibration Curve

In photographic quantitative analysis, the first thing that must be determined is the relationship between the number of ions striking the emulsion and the darkening effect they have on the plate.

Such a "calibration curve" is necessary not only for relating densitometer transmission scans to exposure, but is essential for measuring line widths and studying line shapes.

Also, at least with the plates now being used, it is quite essential that some sort of a calibration be done on each plate. Both sensitivity and curve shape change from plate to plate, even under carefully controlled developing conditions.

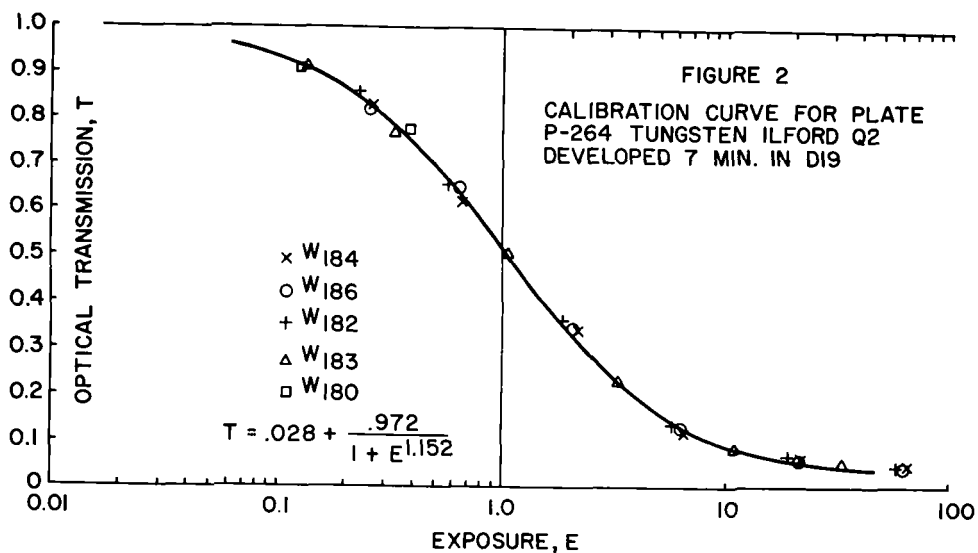
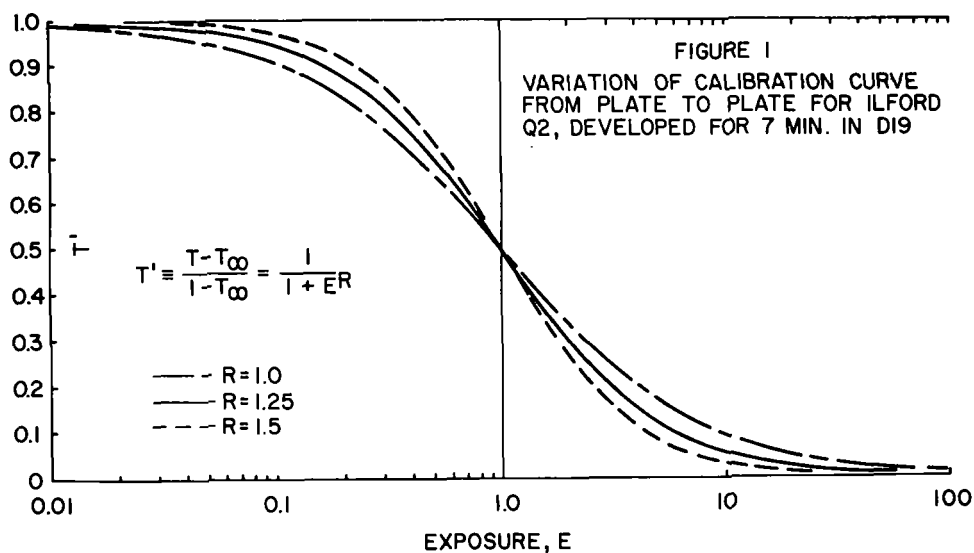


Figure 1 shows how the slope of the calibration curve can change from plate to plate. Using a curve calibrated from some previous plate could lead to an error of several hundred percent, even if normalized for sensitivity.

The variation from plate to plate is not well understood, but is often attributed to changes in the emulsion due to heat and vacuum. The calibration within a plate is relatively consistent.

There are several empirical methods available for calibrating a plate. One method is to make a series of exposures by measuring the total ion beam electrically with a beam monitor and covering the dynamic range of the photoplate. The dependability of this method depends upon the accuracy of the beam monitor and upon the stability of the ratio of singly to multiply and fractionally charged ions.

Also, various methods using known isotope abundances have been used successfully,¹ and are useful when the errors of the beam monitor method are excessive.

A device often found convenient is to "curve match" the experimental data to an empirical equation that is known to match a correct calibration curve. Ilford Q2 plates are found to normalize to within a few percent to the function.

$$T(E) = T_{\infty} + \frac{1 - T_{\infty}}{1 + ER}$$

or, solved for E

$$E(T) = \left(\frac{1 - T}{T - T_{\infty}} \right)^{1/R}$$

Here T is optical transmission, T_{∞} is the saturation transmission, R is an experimental constant between 1 and 1.5, and E is "relative exposure," normalized to unity at

$$T(1) = \frac{1 + T_{\infty}}{2}$$

Figure 1 is this function, solved for

$$T' = \frac{T - T_{\infty}}{1 - T_{\infty}} = \frac{1}{1 + ER}$$

and plotted for several values of R.

Figure 2 is that function, normalized to an experimental calibration curve of tungsten. The curve matching method seems to be the best for interpolation and for extrapolation to small exposures.

B. Line Width And Shape

When using an ion-sensitive plate as a detector, there are two assumptions generally made about its collective properties. The first is that the reciprocity law is not violated, consequently the plate is a perfect integrator over time.

^{1/} E. Owens, "Quantitative Analysis In a Solid State Mass Spectrograph," paper delivered before American Chemical Society, Washington, D.C., March, 1962.

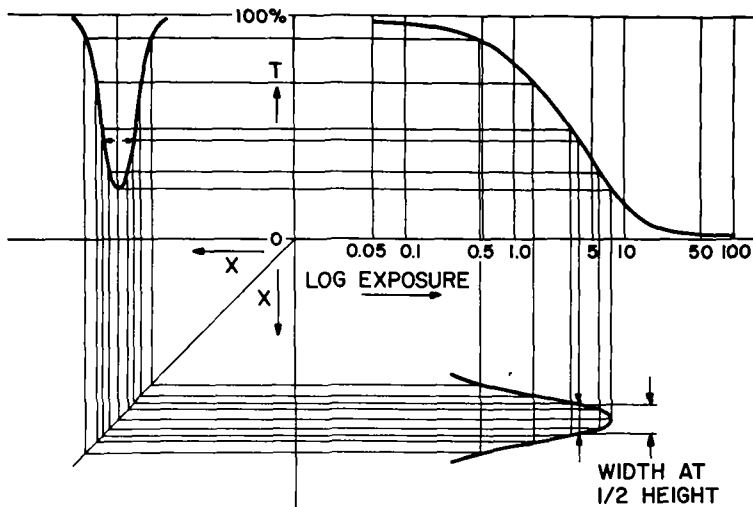
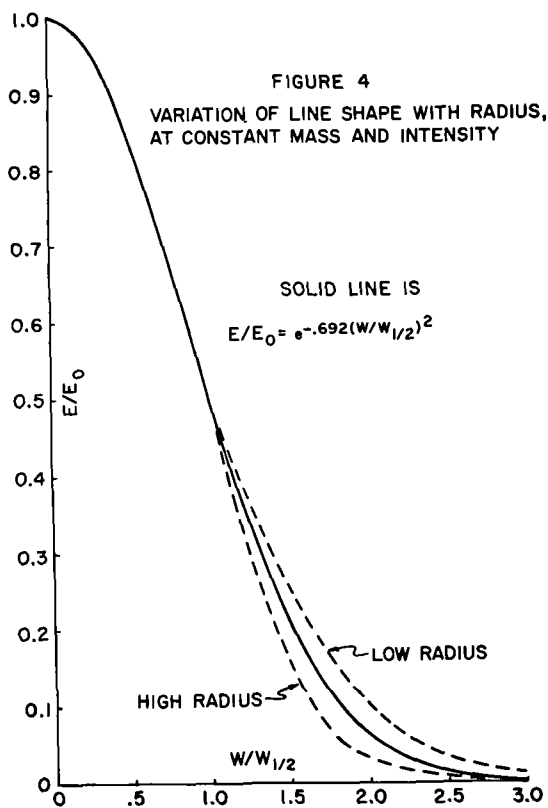


FIGURE 3

GRAPHICAL TRANSFORMATION OF OPTICAL
TRANSMISSION SCAN INTO EXPOSURE
DISTRIBUTION CURVE



The second assumption is that the exposure on the plate is proportional to the charge striking the plate, point for point, and hence the plate is a perfect integrator across the line. Within what limits these assumptions are true is not yet well known.

After the calibration curve has been determined, the integration across the line may be performed. Figure 3 shows how the optical transmission scan, as obtained from the densitometer, could be transformed into an exposure distribution curve.

This curve could be integrated by counting squares or using a planimeter, but it is generally much more convenient to determine only the half exposure height and assume that the integral is the product of the exposure, the width at half exposure height, and a shape factor. As long as the shape factor is constant, area corrections may be made by making width corrections only. Figure 4 shows the variance in peak shape found across the plate. The area under that normalized curve has a maximum change of about 7%.

The width itself, however, may change considerably more than this. Figure 5 shows how line width varies across the plate. This variance is a function of the individual spectrograph, but a factor of two is not uncommon.

Figure 6 shows line broadening due to space charge effects. It is a plot of line width versus isotope ratio for tungsten. Here the change in width is only around 20%. However, analytical errors up to a factor of eight have been observed due to this effect.

C. Ion Transmission

The ion beam is not collimated in the vertical direction, so that the number of ions transmitted through the magnetic analyzer at high radius is less than the number transmitted at low radius. Figure 7 shows this magnetic analyzer efficiency function, as derived from the geometry of the spectrograph. Again an error of up to a factor of two could result if a correction for the effect were not made.

D. Background And Densitometer Errors

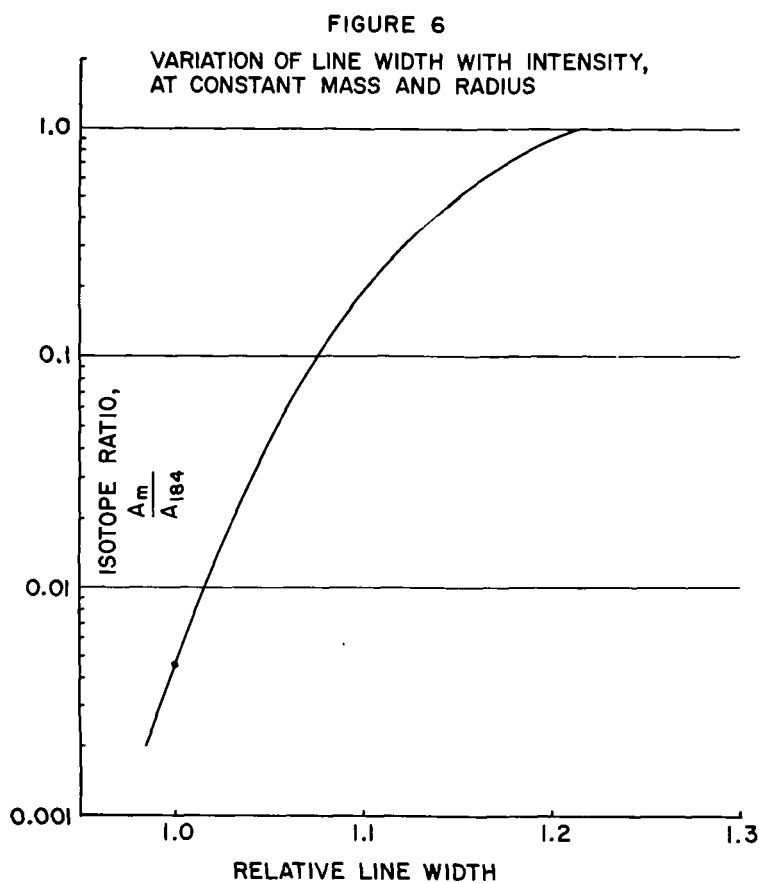
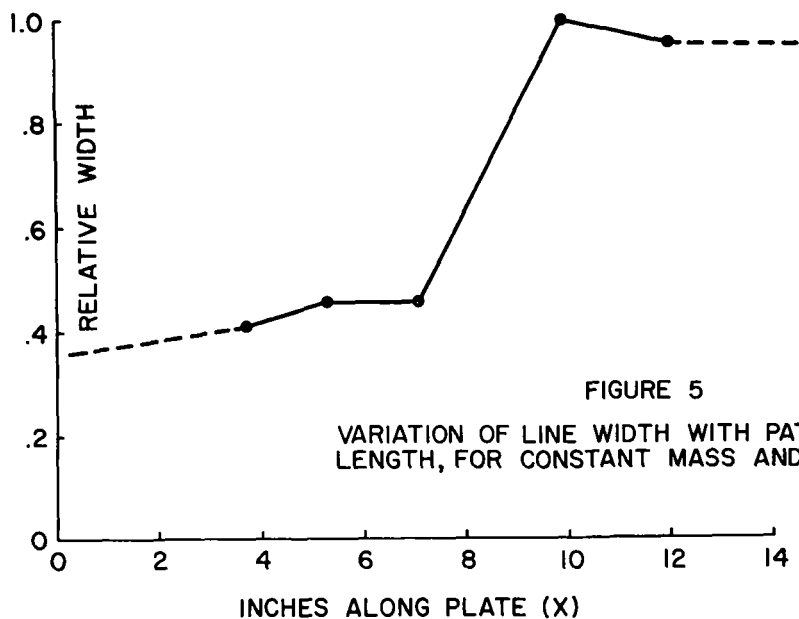
Various types of background effects almost always exist around the low abundance lines. For background due to gas scattering, the densitometer reading for the background should be converted to exposure from the calibration curve, and this exposure should be subtracted from the peak exposure of the line. Quite consistent results have come from this technique.

However, drift in the densitometer cannot be corrected in this manner, nor have good results been obtained where the development fog was inconsistent across the plate.

Another error may result due to the finite width of the densitometer slit. As a close approximation, it can be shown that the error due to slit width averaging is

$$\Delta T = \frac{T_{1/2} - T_{MIN}}{3} \left(\frac{W_d}{W_{1/2}} \right)^2$$

where T_{MIN} is the peak transmission, $T_{1/2}$ is the transmission at half exposure height, $W_{1/2}$ is the width at half exposure, and W_d is the effective width of the densitometer slit. If W_d is near $W_{1/2}$, errors of about 10% in T_{MIN} , or up to 30% in exposure may result. W_d being finite contributes other errors, but in the highly non-linear case of a photoplate the shift in T_{MIN} is the most significant.



E. Example

Figure 8 shows how the measurements just discussed are made on a typical peak. T_{MIN} is 0.288, and is converted to $E_{MAX} = 2.46$ from the calibration curve. $T_{BAK} = 0.692$ is also converted to $E_{BAK} = 0.518$. The half exposure height is then

$$E_{1/2} = \frac{E_{MAX} - E_{BAK}}{2} + E_{BAK} = \frac{E_{MAX} + E_{BAK}}{2} = 1.49$$

Again from the calibration curve $E_{1/2}$ is converted to $T_{1/2} = 0.405$, and the peak width is measured at this $T_{1/2}$ point. $W_{1/2}$ is found to be 0.16.

Next, the ΔT due to densitometer slit averaging is calculated and found to be .015, so that

$$T_{MIN} - \Delta T = .288 - .015 = .273$$

and from the corrected T a corrected E is found

$$E_{MAX} + \Delta E = 2.67$$

Table 1 lists the effects of making the various corrections discussed concerning Figure 8. Here the line width correction and the background correction are the most significant, although this need not be the case.

F. Other Errors

Although the total of these effects is significant, others just as important have not been considered. The sensitivity of the plate is dependent upon ion mass, ion energy, and may have a chemical dependence. These effects have been investigated by Owens,² Ewald,³ and Hintenberger.⁴ The variance experienced is similar to that found in electron multiplier detection of ions.

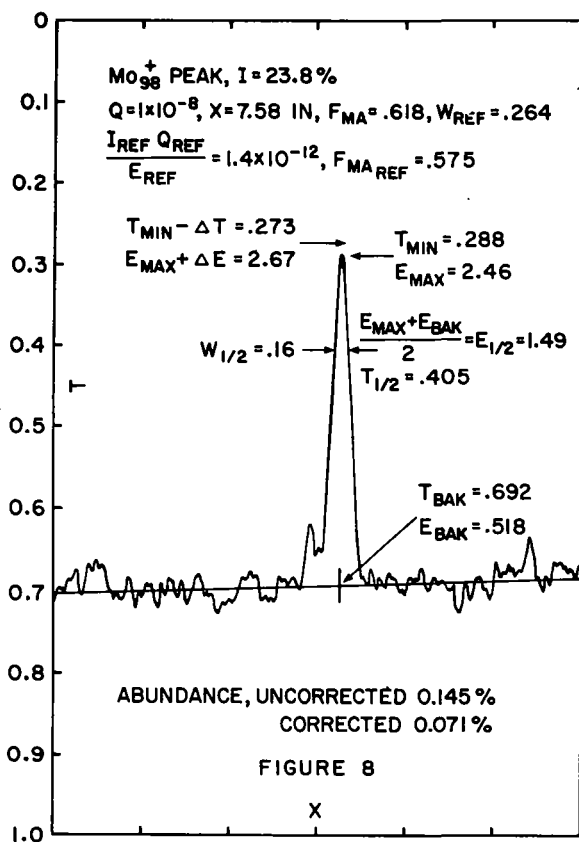
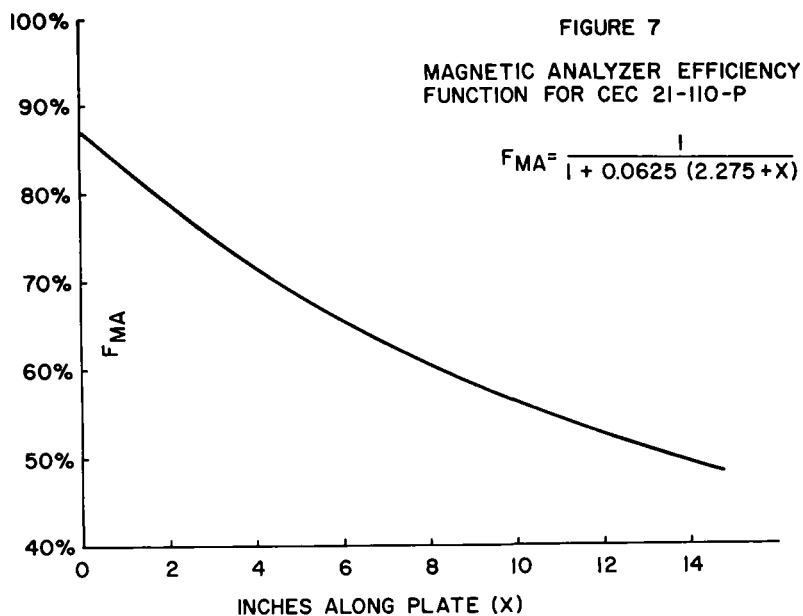
Also, the relationship of the numbers of singly charged ions to multiply and fractionally charged ions clearly affects any analysis. This has been investigated by Owens.⁵

And lastly, due to a lack of analytical tools, the relative ionization efficiencies of the elements in a spark have not yet been determined to any high degree of sophistication.⁶

The latter two problems, however, are not problems introduced by photoplate detection, but come from the spark source itself. The photoplate detector will be most helpful in determining both charge ratio patterns and ionization efficiencies.

Also, the corrections of Table 1 would have to be made, in some manner or another, with any type of detecting system attempting to detect at more than one radius.

-
- 2/ E. Owens, "The Effect of Ion Mass and Ion Energy on the Sensitivity of Ilford Q2 Plates as Ion Detectors in Mass Spectroscopy," Lincoln Laboratory Report JA - 1855.
 - 3/ F. Burlefinger and H. Ewald, Z. Naturforschung, p. 430, April, 1961.
 - 4/ E. Dornenburg and H. Hintenberger, Z. Naturforschung, p. 676, July, 1961.
 - 5/ E. Owens, "Ion Charge Distribution in an R. F. Spark Ion Source and Its Effect on Quantitative Analysis," paper delivered before ASTM Committee E-14 Meeting on Mass Spectrometry, June, 1962.
 - 6/ B. Chakravarty, V. S. Venkatasubramanian, and H. E. Duckworth, "Relative Ionization Efficiencies for Elements in a Spark Source," delivered before symposium on Mass Spectrometry, Oxford, September, 1961.



ABUNDANCE CORRECTIONS

<u>CORRECTION</u>	<u>ABUNDANCE</u>	<u>DEVIATION</u>
NONE	0.145%	0
BACKGROUND	0.114%	-27.2%
LINE WIDTH	0.088%	-64.8%
SLIT WIDTH	0.157%	+ 7.6%
ANALYZER EFFICIENCY	0.135%	- 7.4%
ALL ABOVE	0.071%	-103.0%

TABLE I

II. ANALYTICAL

Under ideal conditions, the basic accuracy of the photoplate is good. The isotope ratios of tungsten, Figure 2, were determined to within 3% of the published values (closer for the major isotopes). A trace impurity of iron in aluminum at 0.8 ppm has been reproduced to within 3.5% from one plate to another. And, in general, when a plate is analyzed and several lines are available for analysis, after proper background and width corrections have been made the concentrations determined vary by less than 20%.

This suggests that an analyst interested in detecting element A in matrix B, by comparison with known standards, should be able to do so with good accuracy to low detection limits.

It also suggests that the photoplate can be a good tool for studying ionizing effects in the spark source. And in the event that these effects are predictable, general analysis should be as accurate as analysis by known standard comparison.

IMPROVED ACCURACY IN SOLIDS MASS SPECTROMETRY

George D. Perkins and Charles F. Robinson
Bell and Howell Research Center
Pasadena, California

Manuscript Withdrawn

THE APPLICATION OF SPARK SOURCE MASS SPECTROMETRY
TO ANALYTICAL PROBLEMS ARISING IN AN ATOMIC ENERGY INDUSTRY

R. G. Fitzsimmons, W. Fletcher and R. Tushingham

An atomic energy programme presents many problems to the analytical chemist and to meet this challenge it is essential to exploit the new instruments and techniques. This paper describes some of the ways in which the newly available spark source mass spectrometer, A.E.I. Type MS.7,⁽¹⁾ has been of value.

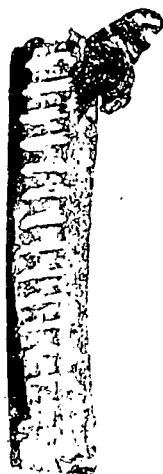
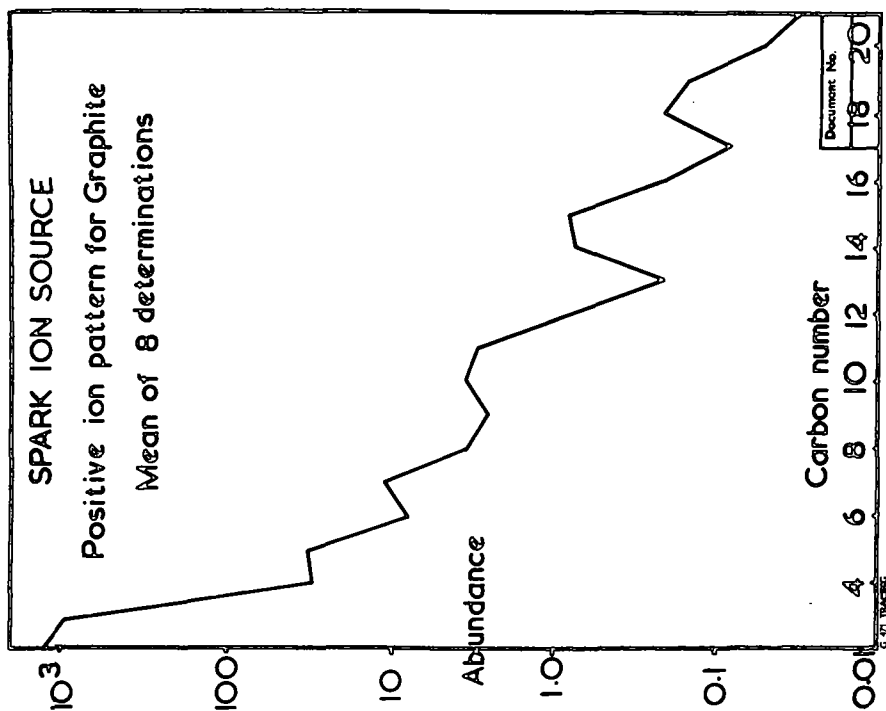
One of the attractive features of this instrument is its ability to yield a great deal of information about essentially pure substances when only a few milligrams of the material are available. This feature has been exploited in the analysis of crystals of natural graphite which have been purified by Dr. J. M. Thomas⁽²⁾ of University College of North Wales, Bangor. These crystals weighed about 2 mg each and were about 3 mm. square by 0.1 mm. thick. Fig. 1 shows the size of such a crystal compared with an electrode of normally accepted size and shape. The problem of introducing the crystals into the spark was solved by supporting them in extension electrodes of high purity indium metal. Indium was chosen because it was readily obtainable in a state of high purity, was very malleable and possessed two isotopes of odd mass numbers (In^{113} , In^{115}). This last property makes the indium readily identifiable and ensures that its multiply charged ions produce negligible interferences at lower masses. No difficulty was experienced in striking a spark between two crystals mounted in this way. The spark, which did not wander from the crystals, could be maintained for several hours when necessary and limits of detection of 0.01 ppm. atomic were readily obtainable. Over forty impurity elements were detected in some of the samples. An example of the results obtained is given in Table I.

Table I
Analyses of Graphite Crystals

Results quoted are as p.p.m. wt/wt with respect to carbon.

ELEMENT	Cu	Ni	Co	Fe	Mn	Cr	V	Ti	Sc	Ca	K
Detn. 1	0.6	0.3	<0.05	9	<0.05	1.2	0.2	<0.7	<0.04	2000	<3
Detn. 2	1.5	3	<0.05	10	0.13	3	<0.1	<0.7	<0.04	20	<3
Detn. 3	0.2	0.05	<0.55	2	0.05	0.4	0.2	1.2	0.04	13	<4
Detn. 4	0.4	1.0	<0.05	4	0.1	1.3	0.1	1.1	0.7	15	0.3
Detn. 5	0.4	0.5	<0.1	12	0.2	1.1	0.2	3	0.07	60	0.6
Detn. 6	0.3	0.6	<0.05	3	0.05	0.9	0.2	0.8	0.04	30	0.2
Coefficient of Variation	50%	100%	-	50%	60%	75%	50%	50%	-	-	-

The large variation in the calcium content is not entirely unexpected since the graphite crystals have been obtained from a marble-like matrix.



1 CM.

Fig. 1.

Fig. 1. Comparison of size of graphite crystal with a sample of normally accepted size and shape.

Carbon is one of the few elements which produce polyatomic ions in significant numbers. Visual examination of the spectra obtained in this work showed that the relative abundance of the polyatomic carbon ions did not fall off uniformly with increasing carbon number.

Fig. 2 shows the variation of relative abundance of the ions with carbon number. Each point on the graph is the mean of eight separate determinations. Up to a carbon number of eight, the abundance falls off with carbon number with even-odd intensity alternations. This positive ion pattern is similar to that obtained by Honig⁽³⁾ and agrees with the prediction of Pitzer and Clementi⁽⁴⁾. Above a carbon number of eight the pattern becomes more confused. This modification at higher carbon numbers may well be due to the high local temperatures in the spark, quoted by Alimov and Malkov⁽⁵⁾ as 5×10^4 K.

The great sensitivity and small sample requirements of spark source mass spectrometry has permitted the examination of small areas and corrosion cavities in alloys and graphite. In this case the technique consists of holding a fine probe of about 0.5 mm. diameter close to the area or cavity to be examined and maintaining the spark between the probe and the area under test. The probe is made of similar material to that of the sample but of higher purity, as shown by previous analysis. For example, in the case of graphite, spectroscopically pure graphite is employed as the probe. Fig. 3 is a photograph showing the probe and sample mounted for insertion in the source. The value of this technique is in comparing the impurities present on small areas of the surface. Using this technique detection limits of about 0.5 p.p.m. atomic were obtained and it was found that the spark could be localised to an area of about 1 sq. mm. The surface was penetrated to about 0.1 mm. during the analysis. At levels above 10 p.p.m. atomic determinations with a coefficient of variation of 70% were obtained without the use of microphotometry of the plates. Fig. 4 shows some corrosion cavities in a commercially available graphite which were examined by this technique. The damage caused by the spark can be clearly seen, indicating the small area examined. Using this method concentrations of impurities in the cavities have been detected and the investigation is continuing.

Surface impurities and variation of impurity content with depth have been studied. In these cases samples were obtained by milling the specimens and segregating the different layers. The millings were then compacted under pressure in a moulding die to produce a suitable electrode form.

During this work difficulty was experienced with the examination of magnesium alloys. The efficiency of ionisation of magnesium in the spark source proved to be about ten times greater than expected. Consequently in order to meet a given detection limit the exposure had to be ten times longer than normal. The high volatility of the magnesium caused electrical leakage in the source, overloading the accelerating voltage power supply. It was therefore necessary to limit the ion current which slowed down the rate of analysis still further.

This technique of milling and recompacting has also been used to investigate the diffusion of metals through other metals. Table II shows some results obtained for a sample which had been held in contact with uranium at 500°C for one week.

Table II

Migration of Uranium in a sample after contact at 500°C for 1 week

Distance from contact surface	Uranium content p.p.m. by weight
0 - 0.005"	9 7
0.005" - 0.010"	0.5 1.4
0.010" - 0.015"	<0.4 <0.5

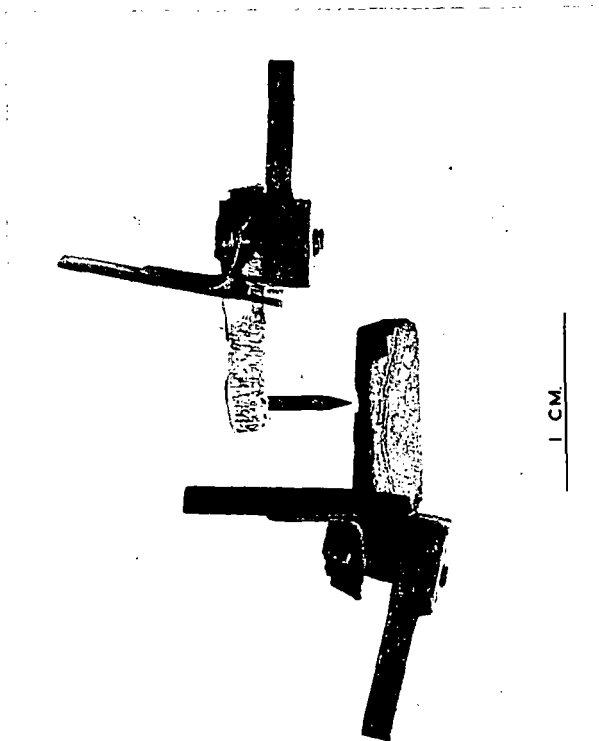


Fig. 3. Photograph showing the probe and sample mounted for insertion in the source.



Fig. 4. Corrosion cavities in a commercially available graphite examined by this technique.

All the studies reported above have employed visual examination of the photographic plates. More accurate results can be obtained using microphotometry. Here it has been found advantageous to calibrate the photographic plate using a polycrystalline element. The relative abundance of its isotopes are known and by plotting the product of isotopic abundance and total integrated charge against density, many points become available for defining the characteristic curve. Curves obtained in this way are shown in Fig. 5 and 6. Using the more usual technique of plotting relative exposure against density only about four points will be on the linear portion of the curve. Adoption of the isotopic method when analysing a standard copper alloy (Johnson Matthey C.40) gave a coefficient of variation of 20% instead of the 25% to 30% using the older technique.

ACKNOWLEDGEMENT

The authors wish to express their thanks to Mr. G. G. Cookson and Mr. W. G. Griffiths who helped with the analytical determinations. The authors also wish to thank the Managing Director, U.K.A.E.A., Production Group for his permission to publish this paper.

REFERENCES

1. Elliott, R. M., Craigh, R. D., and Errock, G. A.
Proc. Fifth International Instruments and Measurement Conference,
Stockholm, 1960.
2. Hughes, E. E. G. and Thomas, J. M.,
Nature, 193, 833 (1962).
3. Honig, R. E., Symposium on Mass Spectrometry, Oxford, 1961.
4. Pitzer, K. S. and Clementi, E.,
J. Am. Chem. Soc. 81, 4477 (1959).
5. Akimov, E. A. and Malkov, E. P., Optics and Spectroscopy, 6, 56 (1959).

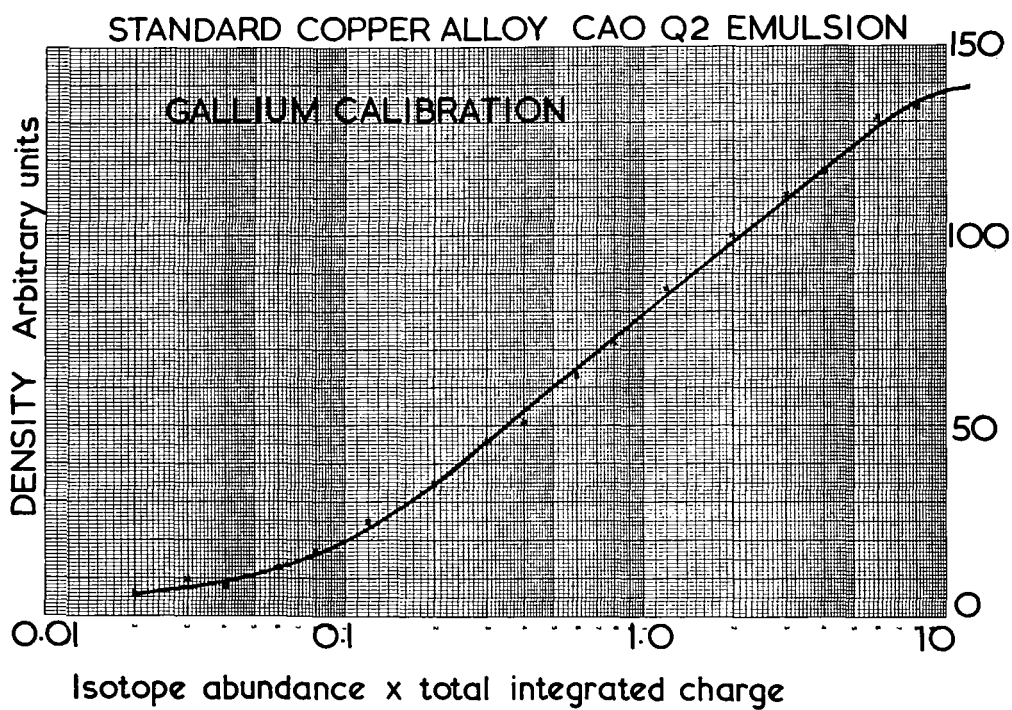
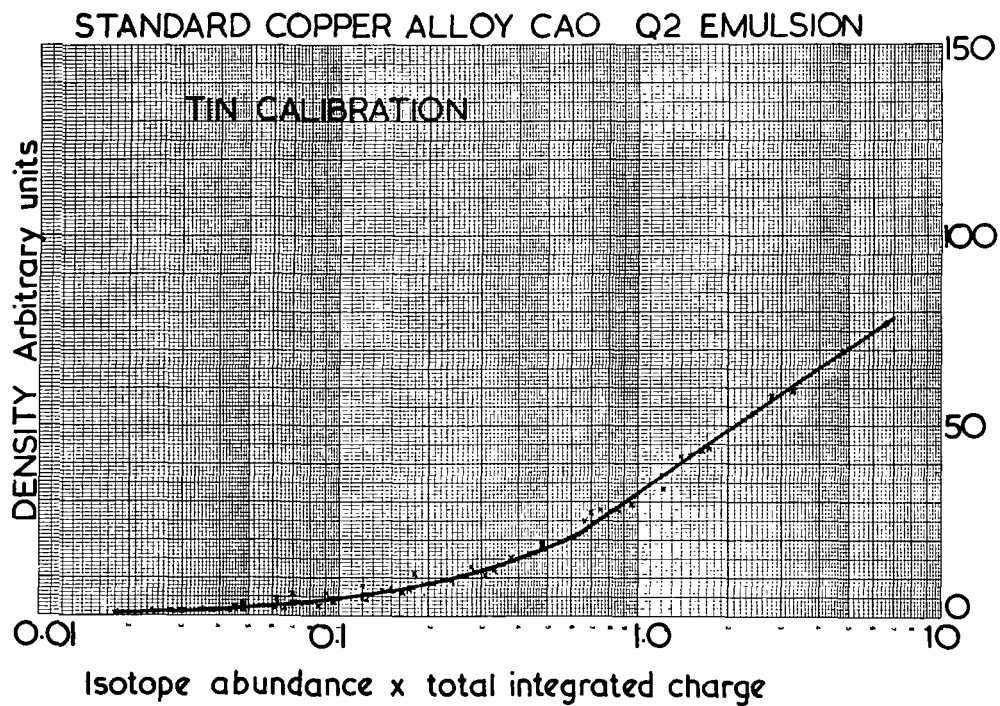


Fig. 5 & 6. Characteristic curves for photographic plates.

High Temperature Vaporization Studies^(*)

J. Drowart.

Laboratoire de Chimie Physique Moléculaire

Université Libre de Bruxelles

Brussels, Belgium

The present report summarizes work done during the past one and a half years at the Laboratoire de Chimie Physique Moléculaire, University of Brussels. It presents definite results for a number of systems and preliminary ones for others still under investigation.

The mass spectrometer^(1,2) and experimental technique have been described previously^(3,4). Briefly, obtaining thermochemical data is based upon the evaporation of the sample from a Knudsen cell of known temperature, formation of a molecular beam, ionization of the neutral species by electron impact with electrons of adjustable energy (5-70 eV) and identification of the parent molecules from the mass, appearance potential and ionization efficiency curves of the ions. Pressures P_i are obtained for the various molecules so identified through pressure calibrations based on quantitative evaporations of known amounts of the sample or of pressure calibrants, or on the observation of known equilibria. The first procedure requires in general knowledge of the relative ionization cross sections of species of minor importance. The second procedure requires this knowledge for all species, including the pressure calibrant. These cross sections are either measured by simultaneous or successive quantitative evaporations of the sample and of a reference element, the study of congruently vaporizing compounds^(5,6) or the use of double oven techniques^(7,10), or derived from calculated values⁽¹¹⁾.

Heats of reaction ΔH_T^0 are calculated from the relations

$$\Delta H_T^0 = \Delta F_T^0 - T \Delta \left\{ (F_T^0 - H_T^0) / T \right\}$$

or
$$\Delta H_T^0 = - R \, d \ln K / d(1/T)$$

where $\Delta F_T^0 = - RT \ln K$ is the change in free energy

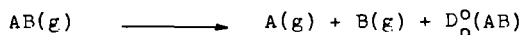
$K = \prod_i P_i^{\nu_i}$ the equilibrium constant,

ν_i the stoichiometric coefficient for each reactant or product in the reaction considered.

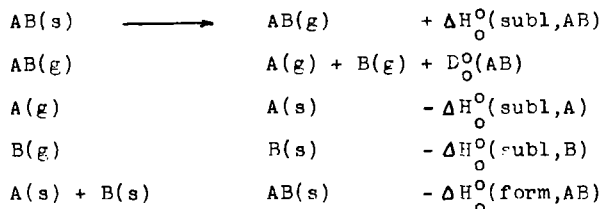
$\Delta(F_T^0 - H_T^0)/T$ the difference in free energy function of products and reactants,

T the absolute temperature.

Dissociation energies D_0^0 given below were obtained either directly from equilibria of the type



or from thermochemical cycles



The systems studied comprise elements, alloys, carbides, oxides, sulfides, selenides and tellurides. The results obtained are as follows.

Reaction		ΔH_0^0 or D_0^0 in kcal/mole	ref.
1. Elements			
$B(s) \longrightarrow$	$B(g)$	128.0 ± 2.5	12
$B_2(g)$	$2 B(g)$	65.5 ± 5.5	12
$S_2(g)$	$2 S(g)$	97.2 ± 5	13, 14
(obtained in the study of CaS, SrS and BaS (see 5))			
$Se_2(g)$	$2 Se(g)$	77.2 ± 5	14
(obtained in the study of ZnSe (see 9))			
2. Alloys.			
$AgSn(g)$	$Ag(g) + Sn(g)$	31.6 ± 5	15
$CuSn(g)$	$Cu(g) + Sn(g)$	41.4 ± 4	15
$AuSn(g)$	$Au(g) + Sn(g)$	57.5 ± 4	15
$AuCr(g)$	$Au(g) + Cr(g)$	50.4 ± 3.5	16



3. Systems Boron-Carbon and Boron-Carbon-Silicon

$1/4 \text{ B}_4\text{C(s)}$	$\text{B(g)} + 1/4 \text{ C(graphite)}$	131.5 ± 2.5	12
BC(g)	$\text{B(g)} + \text{C(g)}$	105 ± 10	17
$\text{B}_2\text{C(g)}$	$2 \text{ B(g)} + \text{C(g)}$	260 ± 10	17
$\text{BC}_2\text{(g)}$	$\text{B(g)} + 2 \text{ C(g)}$	302 ± 10	17
BSi(g)	$\text{B(g)} + \text{Si(g)}$	70 ± 10	17
BCSi(g)	$\text{B(g)} + \text{C(g)} + \text{Si(g)}$	250 ± 10	17

4. Magnesium, Calcium and Strontium oxides (G.Verhaegen and G.Exteen)

(Molybdenum or Tungsten crucibles)

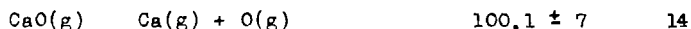
MgO(g)	$\text{Mg(g)} + \text{O(g)}$	77 ± 10	
CaO(g)	$\text{Ca(g)} + \text{O(g)}$	97 ± 6	
SrO(g)	$\text{Sr(g)} + \text{O(g)}$	97 ± 6	
$\text{Sr}_2\text{O(g)}$	$2 \text{ Sr(g)} + \text{O(g)}$	180 ± 12	
$\text{SrMoO}_3\text{(g)}$	$\text{SrO(g)} + \text{MoO}_2\text{(g)}$	150 ± 20	
$\text{SrMoO}_4\text{(g)}$	$\text{SrO(g)} + \text{MoO}_3\text{(g)}$	175 ± 20	
$\text{SrWO}_3\text{(g)}$	$\text{SrO(g)} + \text{WO}_2\text{(g)}$	160 ± 20	
$\text{SrWO}_4\text{(g)}$	$\text{SrO(g)} + \text{WO}_3\text{(g)}$	190 ± 20	

5. Calcium Strontium, Barium and Manganese Sulfides

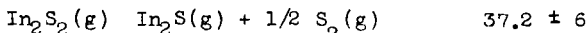
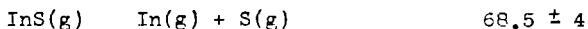
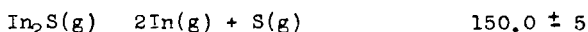
CaS(s)	CaS(g)	$142.8 \pm 5 \text{ (298°K)}$	13,14
CaS(g)	$\text{Ca(g)} + \text{S(g)}$	71.0 ± 5	13,14
SrS(s)	SrS(g)	$136.2 \pm 12 \text{ (298°K)}$	14
SrS(g)	$\text{Sr(g)} + \text{S(g)}$	73.9 ± 5	14
BaS(g)	BaS(g)	$119 \pm 11 \text{ (298°K)}$	14
BaS(g)	$\text{Ba(g)} + \text{S(g)}$	90.2 ± 6	14
2 BaS(s)	$\text{Ba}_2\text{S}_2\text{(g)}$	$154 \pm 16 \text{ (298°K)}$	14
$\text{Ba}_2\text{S}_2\text{(g)}$	2 BaS(g)	84 ± 11	14



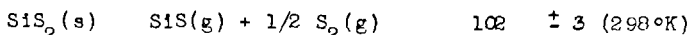
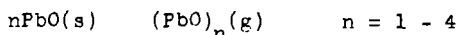
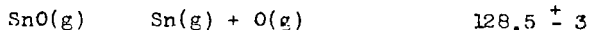
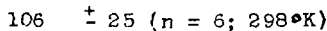
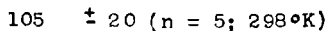
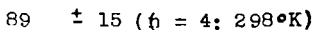
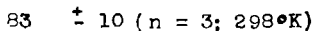
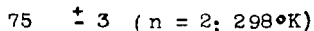
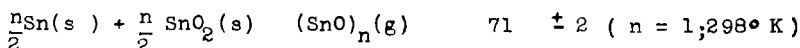
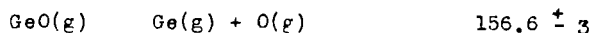
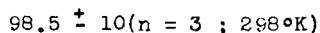
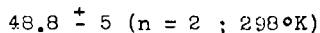
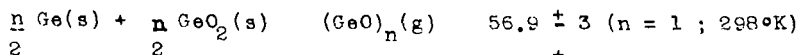
6. Mixtures of Calcium, Strontium and Barium Oxides and Sulfides



7. Indium Sulfide (R.Colin)



8. Group IV - Group VI Compounds (R.Colin, F.Degreve, J.C. Lievin, J.Michelet and G. Verhaegen)



$\text{GeS(s)} \longrightarrow \text{GeS(g)}$			
GeS(g)	$\text{Ge(g)} + \text{S(g)}$	134.1 ± 2.0	
SnS(s)	SnS(g)	52.6 ± 1.6 (298°K)	19
2SnS(s)	$\text{Sn}_2\text{S}_2(\text{g})$	56.5 ± 5.0 (298°K)	
SnS(g)	$\text{Sn(g)} + \text{S(g)}$	110.1 ± 3.0	
PbS(s)	PbS(g)	55.7 ± 1.6 (298°K)	19
2PbS(s)	$\text{Pb}_2\text{S}_2(\text{g})$	66.6 ± 5.0 (298°K)	
PbS(g)	$\text{Pb(g)} + \text{S(g)}$	79.1 ± 2.8	
$\text{SnPbS}_2(\text{g})$	$\text{SnS(g)} + \text{PbS(g)}$	46.5 ± 5.0 (298°K)	19
SnSe(s)	SnSe(g)	47.5 ± 3.0 (298°K)	
2SnSe(s)	$\text{Sn}_2\text{Se}_2(\text{g})$	47.9 ± 5.0 (298°K)	
SnSe(g)	$\text{Sn(g)} + \text{Se(g)}$	95.0 ± 4.0	
SnSe(s)	$\text{Sn(s)} + \text{Se(s)}$	15.6 ± 3.0 (298°K)	
SnTe(s)	SnTe(g)	48.3 ± 3.0 (298°K)	
SnTe(g)	$\text{Sn(g)} + \text{Te(g)}$	80.9 ± 4.0	
SnTe(s)	$\text{Sn(s)} + \text{Te(s)}$	11.0 ± 3.0 (298°K)	

(8,9)
9. Relative Ionization Cross Sections from Double Oven Experiments with ZnSe (R.Colin, D.Detry, P.Goldfinger and M.Jeunhomme).

$$\sigma_{\text{Se}_2} / \sigma_{\text{Se}} / \sigma_{\text{Zn}} = 2.3/1/0.7 \quad (\pm 20 \%) \quad (24 \text{ eV})$$

$$\sigma_{\text{Se}_2} / \sigma_{\text{Se}} / \sigma_{\text{Zn}} = 1.5/1/0.5 \quad (\pm 20 \%) \quad (70 \text{ eV}) \quad 14$$

*

This work was sponsored in part by the Wright Air Division of the Aeronautical System Division, A.F.S.C., U.S. Air Force, through its European Office.

REFERENCES.

1. J.Drowart and R.E.Honig, J.Chem.Phys., 25, 581 (1956)
J.Phys.Chem., 61, 980 (1957)
2. M.Ackerman, F.E.Stafford and J.Drowart, J.Chem.Phys., 33, 1784 (1960).
3. M.G.Inghram and J.Drowart in High Temperature Technology, Mc Graw Hill Book Company, New York 1960.
4. P.Goldfinger, Mass Spectrometry Conference, Atlantic City 1960.
5. P.Goldfinger, M.Ackerman and M.Jeunehomme, Vaporization of Compounds and Alloys at High Temperature, Final Technical Report, Contract AF 61(052)-19 January 1959.
6. A.W.Searcy, S.Williams and P.Schissel, J.Chem.Phys., 32, 957 (1960)
7. T.A.Milne, J.Chem.Phys., 28, 717 (1958).
8. R.Colin, Ind.Chim.Belg., 26, 51 (1961).
9. P.Goldfinger, Mass Spectrometry Conference, Chicago, Ill. 1961.
10. J.Berkowitz, H.A. Tasman and W.A.Chupka, J.Chem.Phys., 36, 2170 (1962).
11. G.W.Otvos and D.P.Stevenson, J.Am.Chem.Soc., 78, 546 (1956).
12. G.Verhaegen and J.Drowart, J.Chem.Phys., in press.
13. R.Colin, P.Goldfinger and M.Jeunehomme, Nature, 187, 408 (1960).
14. M.Jeunehomme, Thesis, University of Brussels (1962).
15. M.Ackerman, J.Drowart, F.E.Stafford and G.Verhaegen, J.Chem. Phys., 36, 1557 (1962).
16. M.Ackerman, F.E.Stafford and G.Verhaegen, J.Chem.Phys., 36 1560 (1962).
17. G.Verhaegen, F.E.Stafford, M.Ackerman and J.Drowart, Nature, 193, 1280 (1962).
18. R.Colin, P.Goldfinger and M.Jeunehomme, Nature, 194, 282 (1962).
19. R.Colin and J.Drowart, J.Chem.Phys., in press.

Thermodynamics of Dilute Solutions by
Knudsen Cell Techniques

J. H. Norman and P. Winchell
General Atomic/Division of General Dynamics
John Jay Hopkins Laboratory for Pure and Applied Science
San Diego 12, California

INTRODUCTION

A program to study the thermodynamic properties of semi-conducting devices is in progress at General Atomic. One portion of this program, which has been reported elsewhere,⁽¹⁾ is concerned with the measurement of the distribution coefficient of a doping agent between a solid semiconductor and a corresponding melt. This coefficient is the ratio of the activity coefficient of the doping agent in the melt to the activity coefficient in the solid. The portion of the program reported here involves mass-spectrometric studies of the activity coefficient of a doping agent in appropriate melts. This work has been done by studying effusates from a Knudsen cell containing the melts by means of mass-spectrometric techniques similar to those originated by W. A. Chupka and M. G. Inghram.⁽²⁾

EXPERIMENTAL PROCEDURE

This investigation was concerned with the antimony-indium system, with zinc used as the doping agent. Vapor-pressure measurements on the liquid metals were found to be tractable. It was possible to make significant, accurate mass-spectrometric observations of intensities of $^{64}\text{Zn}^+$ and Sb^+ .

In the first experiments, with a heat-shielded furnace, the zinc background signal far exceeded the zinc signal from the Knudsen cell. In the next experiments, a water-cooled plate was installed as a first collimating slit and the heat shielding was removed. The background zinc peaks were reduced to a few per cent of the cell signal. However, in this furnace configuration, the Knudsen cell had a large temperature gradient and antimony condensed on the lid of the cell and plugged the orifice. Radiant-energy heating was installed above the Knudsen cell, parallel to and not blocking the collimating slit. This did not appreciably affect the background and allowed the temperature of the top of the cell to be maintained near that of the melt.

During the early investigations, the molybdenum Knudsen cell was found to interact with the sample. Analysis of the cell contents showed that an antimony sample dissolved 5% molybdenum. This problem was circumvented by using a graphite cell liner, so that the melt did not come into contact with the molybdenum.

The furnace and cell used in obtaining the thermodynamic data reported here are shown in Fig. 1. The furnace is of a tantalum-wire, resistance-heated type. Its body is molybdenum, and the tantalum wire is threaded through embedded alumina tubes. The furnace rests on a molybdenum tripod.

The molybdenum Knudsen cell consists of three separate pieces, a cell body, a lid, and a ring. Cell lids are 3/4-in. disks 25 mils thick with 90° "v" slits cut in them; the orifices are approximately 5 mils wide and from 1/8 to 1/2 in. long. The use of a slit affords a greater flux than a circular orifice when the cell pressure is limited by Knudsen conditions. The lid is held tightly to the cell body by six stainless steel screws (graphite lubricated). There is a 3° bevel toward the center, such that considerable pressure can be applied between the body and the lid. The top ring serves to distribute the pressure evenly. Platinum-platinum-10%-rhodium thermocouples are held in wells in the top ring and in the bottom of the cell body. These thermocouples are protected by alumina tubes, since they are attacked by antimony vapors. Above the furnace the grid of 16 strands of 5-mil tungsten wire is held in a nickel-ceramic frame. The furnace is hung from the furnace base—water-cooled plate. There is a beam shutter plate in this base. The ion source is also affixed to the base.

The ion source is similar to that reported by Chupka and Inghram.⁽²⁾ Although repellers are available, field penetration from the focus plates is used to draw out the ions from the source. Using the source in this manner slightly improves the spectrometer's signal-to-noise ratio, since the noise consists mainly of hydrocarbon peaks. It is believed that the velocity of the beam causes this discrimination. A virtual slit is used to keep source contamination low. Electrons of nominally 20-v energy produced the ions for this study.

FIGURE 1

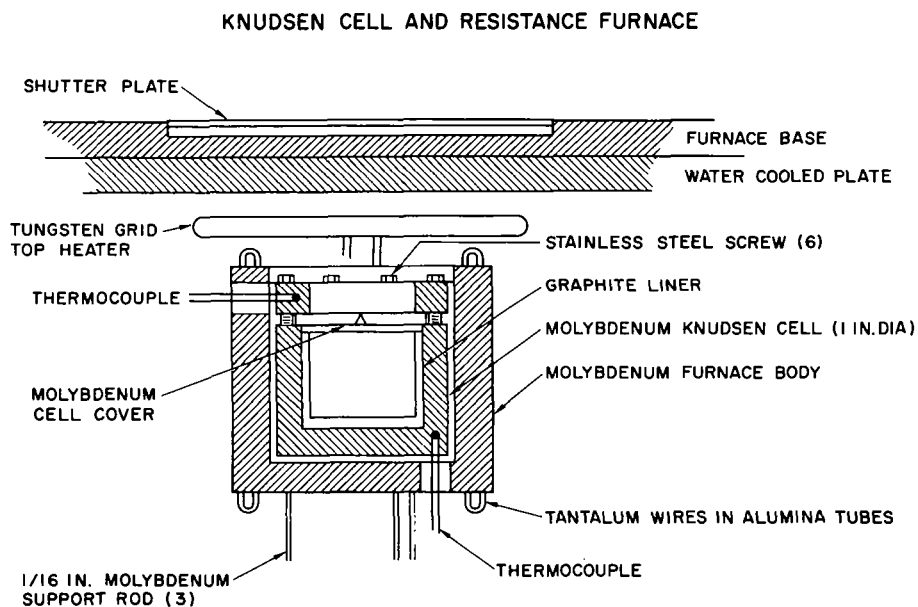
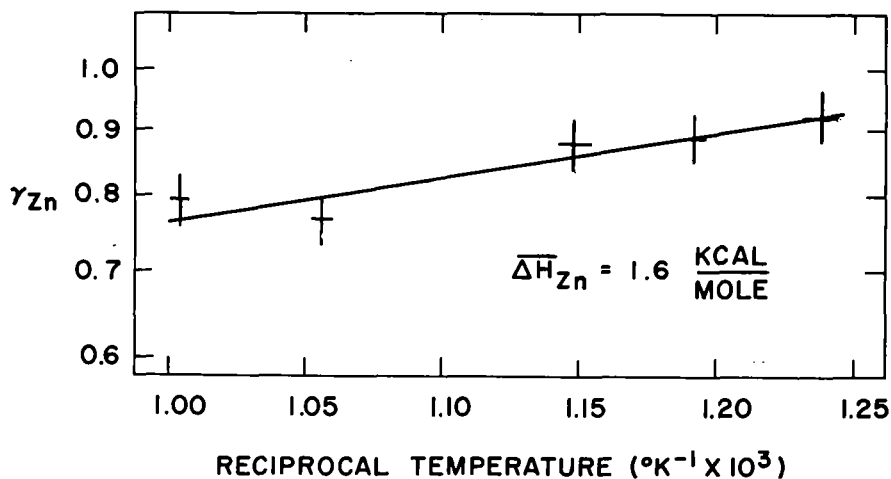


FIGURE 3

**ZINC ACTIVITY COEFFICIENT, γ_{Zn} , AND PARTIAL MOLAR
HEAT OF SOLUTION, $\overline{\Delta H}_{Zn}$, FOR DILUTE ZINC SOLUTIONS
IN ANTIMONY-50% INDIUM MELTS**



A 3-in. radius, 45° sector-magnet serves as the mass analyzer. The resolution of the system is around forty using a 1/2-mm collector slit. The detector is a DuMont FN-SP-181 electron multiplier with 2800 v stepped regularly between its 14 Be-Cu dynodes. The multiplier anode was removed from the ceramic base and mounted separately to reduce noise. The signal is amplified by a Keithley Model 410 micromicroammeter.

An experiment is performed by loading the Knudsen cell with antimony, indium, and 2 at-% of zinc. After assembling the equipment and establishing a vacuum (approximately 10^{-6} torr), the cell is heated and measurements are taken of the cell temperature, zinc-64 ion signal, and tetrantimony ion signal. The cell temperature is maintained essentially constant and these measurements are repeated frequently, the time of each measurement being noted.

DISCUSSION AND RESULTS

When a unique vaporizing species exists for a dilute-solution component, the data obtained in studies such as those described for zinc can be interpreted with the aid of Knudsen flow equations and Henry's law concerning dilute solutions.

At a constant temperature, T , the number of moles of the species leaving the cell per unit time, $-(dn/dt)$, or the change in the number of moles in the cell, dn/dt , is given by

$$-\frac{dn}{dt} = \frac{pA}{K(MT)^{1/2}}, \quad (1)$$

where p is the species partial pressure in the cell, M is the species molecular weight, A is the effective orifice area, and K is a constant.

If one assumes that the evaporating species is the same as the solution component species and that the solution species is dilute, then Henry's law can be used to describe the species partial pressure as follows:

$$p = P\gamma \frac{n}{\sum n_1} \text{ where } n \ll \sum n_1. \quad (2)$$

In Eq. (2), n is the moles of the species in solution, $\sum n_1$ is the total moles of the solution components, γ is the activity coefficient of the species in solution, and P is the pressure of the species when $n = \sum n_1$.

$$\begin{aligned} \gamma &= \frac{-d \ln n}{dt} \cdot \frac{K(MT)^{1/2} \sum n_1}{PA} \\ &= \frac{d \ln \{I_{Zn^+}\}}{dt} \cdot \frac{K(MT)^{1/2} \sum n_1}{PA}, \quad (3) \end{aligned}$$

where $n \ll \sum n_1$.

The significance of Eq. (3) in these studies can be seen in the replacement of $d \ln n / dt$ by $d \ln \{I_{Zn^+}\} / dt$ (because $n \propto p \propto I_{Zn^+}$), where I_{Zn^+} is the intensity of the $^{64}\text{Zn}^+$ peak. This substitution can be made at constant temperature for a Henry's-law solution, in which case the mass spectrometer signal is a linear function of the cell pressure. In Eq. (3) all factors, except the time differential of the logarithm, are known to be constants in dilute solutions; thus, the term $d \ln \{I_{Zn^+}\} / dt$ must also be a constant. The slope of the line produced when $\ln \{I_{Zn^+}\}$ is plotted against time is this constant. The data shown in Fig. 2 illustrates the slope determination. In this figure $\log \{I_{Zn^+} / I_{Sb_4^+}\}$ is plotted in place of the $\ln \{I_{Zn^+}\}$ above. Since the rate of antimony effusion is essentially constant, the use of this ratio tends to cancel furnace shifts, source drifts, and changes in detector sensitivity. The use of the

ratio is unnecessary to demonstrate the method, but tends to give more reproducible results.

According to the derivations, it is necessary to consider only isothermal data. However, this is experimentally impossible. Therefore, methods of correcting the data to an isothermal equivalent have been used. Equation (4) is derived from Eq. (1) and from a statement that the number of ions formed in the source is dependent upon the quantity of material passing through the source in a given time divided by the beam velocity, the latter being a residence time factor $\sqrt{I\alpha(n/T)}$:

$$\frac{I_1 T_1}{P_1} = \frac{I_0 T_0}{P_0} \quad (4)$$

In Eq. (4), the 1 subscripts refer to the existing conditions (temperature, T_1 ; species pressure, P_1 ; and signal intensity, I_1). The conditions that would govern an isothermal experiment are given by 0 subscripts. The use of Eq. (4) involves selecting a T_0 , and calculating I_0 from I_1 , T_1 , T_0 , and P_0/P_1 (the latter term is obtained from the heat of vaporization of the species in an iterative process.) Also, the evaporating time should be corrected according to another modification of Eq. (1) as follows:

$$\frac{n_1 T_1}{P_1 t_1} = \frac{n_0 T_0}{P_0 t_0} \quad (5)$$

Here, one equates the moles, n_1 , leaving the cell for the experimental temperature, T_1 , to the moles, n_0 , that would leave at the isothermal temperature. The isothermal evaporating time, t_0 , is then calculated from knowledge of T_0 , T_1 , t_1 , and P_1/P_0 .

Two thermocouples monitor the cell temperature. The effective cell temperature, T , is then calculated according to the following empirical function of the base temperature of the cell, T_B , and the ring temperature of the cell, T_R (See Fig. 1):

$$T = 0.6T_B + 0.4T_R \quad (6)$$

This equation was developed empirically and can reasonably be applied for small differences in the two measured temperatures (e.g., 10°C).

The temperature corrections serve a purpose other than that of correcting minor temperature fluctuations during an experiment. It is possible by using these temperature corrections to extrapolate with negligible error the value of I_{Zn}/I_{Sb_4} to zero heating time and obtain an initial value for this ratio. This initial value can be assigned to the initial composition of the melt. By properly comparing the initial values of this ratio to values obtained when essentially pure antimony is used, the activity coefficient for antimony can be obtained.

By studying the variations in the activity coefficients of zinc and antimony with temperature, the partial molar heats of solution of these two entities can be determined. The heat of solution of antimony is also available from an experiment in which the temperature is varied and the intensity of the tetrantimony peak is observed. Here the antimony heat of solution equals one quarter of the difference between the heat of vaporization of tetrantimony from pure antimony and from the solution in question. A close study of the antimony activities should allow a calculation of indium values by using the Gibbs-Duhem equation.

Shown in Fig. 3 is an example of these data. Here the measured zinc activity coefficients according to Eq. (3) are shown for a 50-50 at-% melt of indium and antimony with a negligible quantity of zinc present. In Eq. (3), the value of P for zinc that was used in determining the activity coefficients presented in Fig. 3 is given by

the equation published by R. F. Barrow, et al.:⁽³⁾

$$\log P = 9.5672 - 1.274 \log T - \frac{6676.4}{T} \quad (7)$$

An accuracy of 5% is shown for the activity coefficients, and it would appear that the precision of these measurements is approximately this value. For a Knudsen cell method using a mass spectrometer, this precision exceeds that normally reported for similar thermodynamic quantities. It is believed that errors in the effective cell temperature are responsible for most of the uncertainty in these measurements.

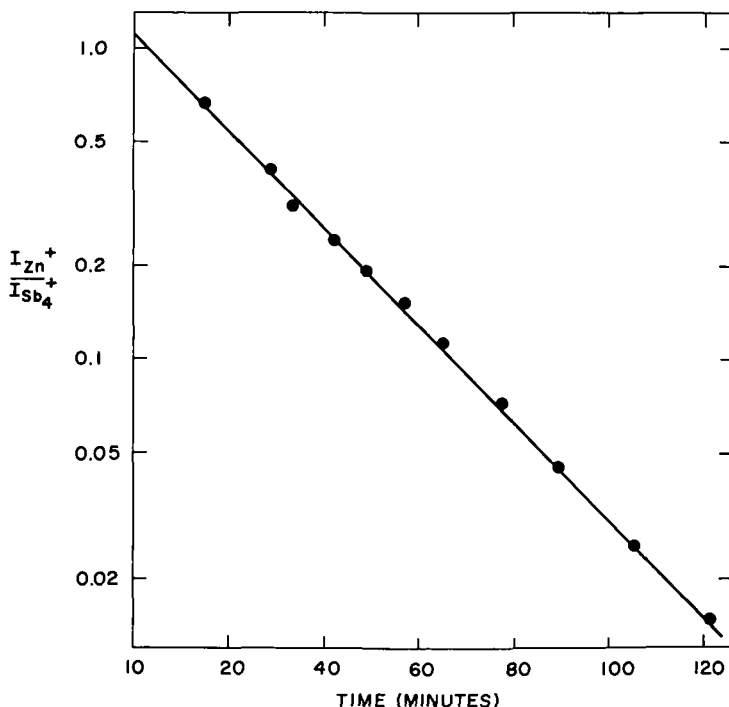
One feature of this method for obtaining thermodynamic data by mass-spectrometric means is of particular interest--only the relative intensities of a time-dependent peak are important. Questions of mass spectrometric sensitivities are eliminated. This method, in fact, may well be used in determining these mass spectrometric sensitivities.

REFERENCES

1. U. Merten and A. P. Hatcher, submitted for publication in J. Phys. Chem. Solids.
2. W. A. Chupka and M. G. Inghram, J. Phys. Chem. **59**, 100 (1955).
3. R. F. Barrow, et al., Trans. Faraday Soc., **51**, 1354 (1955).

FIGURE 2

TIME DEPENDENCE OF THE Zn^+ SIGNAL. (KNUDSEN CELL
CONTENTS: ANTIMONY-INDIUM 20a% INITIALLY WITH
ZINC-2a %)



THE VAPORIZATION OF BERYLLIUM, MAGNESIUM AND ALUMINUM BORATES AND THE PROBLEM OF SECOND-LAW MEASUREMENTS*

Alfred Büchler, J. B. Berkowitz-Mattuck and J. L. Stauffer
Arthur D. Little, Inc., Cambridge 40, Mass.

Introduction

The purpose of this note is to report briefly on the current status of our work on gaseous metaborates and to discuss in detail some points of high-temperature technique which arose in connection with this work. It was shown earlier⁽¹⁾ that the vaporization behavior of alkali metaborates paralleled that of the alkali halides with monomer, dimer and trimer molecules being produced in the vapor. The fragmentation pattern of these molecules corresponded to that of the alkali halides, the ions produced by the higher species having the formula $M_n(BO_2)_{n-1}^+$. It was therefore of interest to investigate the existence of other gaseous metaborates.

Since the ultimate objective of this work is the determination of the heats of formation of gaseous compounds, and since thermodynamic functions for many species of interest are only very imperfectly known, considerable attention was given to the determination of thermochemical data from the slopes of vapor pressure vs temperature curves. It was found that small temperature gradients in effusion crucibles could have a surprisingly large effect on the accuracy of the so-called second-law heats of vaporization. The uniformly heated Knudsen cell source with two thermocouples on the inside, which is described in this paper, provides reliable second-law enthalpies.

Apparatus

The instrument used in these studies was a 12 inch radius, 60° sector mass-spectrometer designed by Inghram and built by Nuclide Analysis Associates. Molecules effusing from Knudsen cells are ionized by 60-volt electrons. Resulting ions are accelerated by a 4000 volt field, deflected by a magnetic analyzer, and collected either on a sample collector plate or on the first dynode of a 16-stage electron multiplier, with a gain of the order of 5×10^5 . The output of either the collector or the electron multiplier is fed to a Vibrating Reed Electrometer and then displayed on a chart recorder.

For the experiments on the metal-oxide boron-oxide systems discussed below, a molybdenum Knudsen cell with platinum liners was used. Temperatures were measured with a platinum-10% rhodium thermocouple placed in a well at the bottom of the crucible. Once the systems of interest have been characterized, the improved Knudsen cells described in this report will be used for determination of accurate second-law data.

Sample Preparation

Samples were prepared by mixing the appropriate metal oxide in the Knudsen cell and heating for at least 8 hours near 1000°. Where necessary, the formation of condensed phase products was demonstrated by obtaining X-ray diffraction patterns of the residue left after the experiment. X-ray patterns were obtained on a Philips-Norelco X-ray diffractometer.

* Supported by the United States Army Bureau of Research under the Advanced Research Projects Agency Program.

FIGURE 4 SILVER CALIBRATION

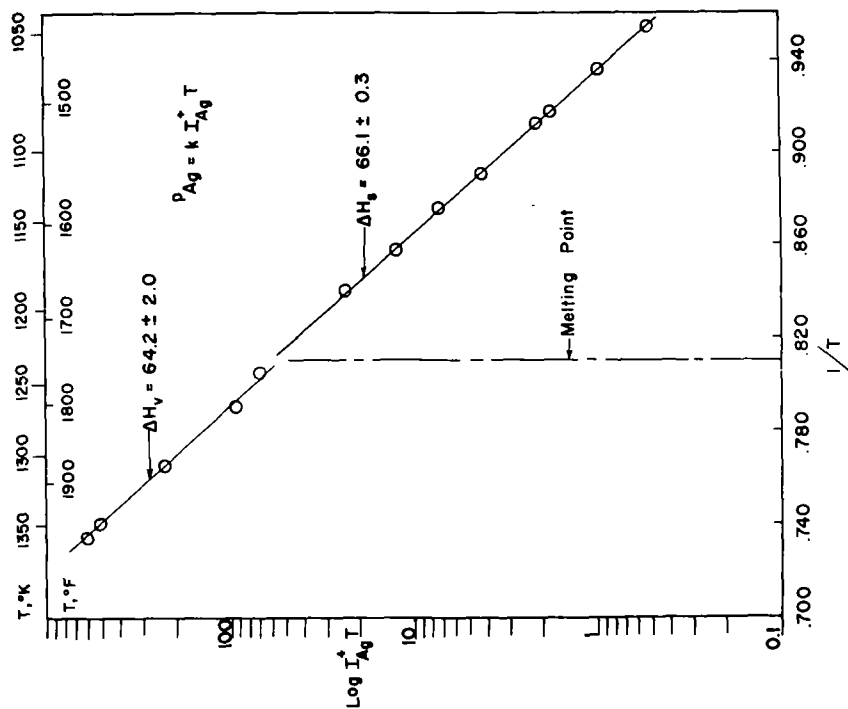
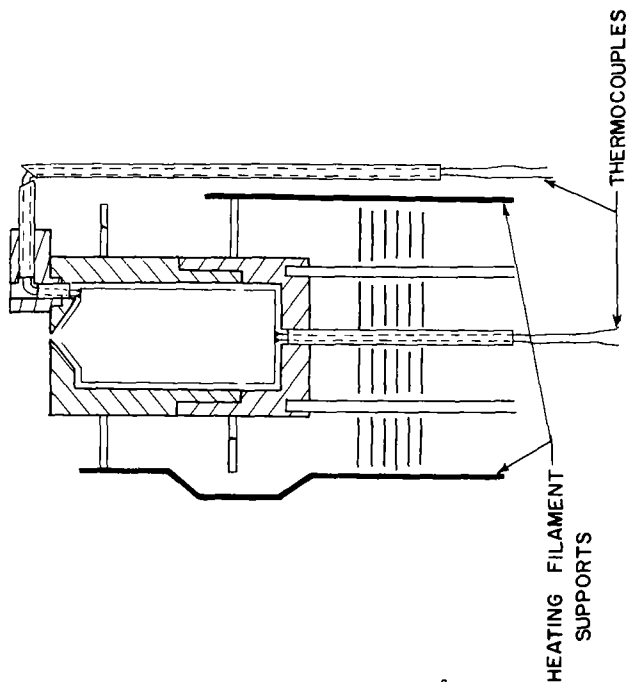


FIGURE 3 CRUCIBLE DESIGN

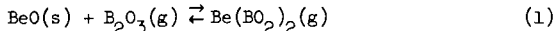
1/8" WALL Mo BODY
 .015" Pt LINER
 1 3/16" X 3/4" OVERALL
 .075" Thermocouple insulators



Results

A. Beryllium Oxide-Boron Oxide

Gaseous beryllium metaborate was observed at temperatures between 1320 and 1520°K. The principal ionic species was $\text{Be}(\text{BO}_2)_2^+$ at mass numbers 93 to 95, the ion-current ratio $\text{Be}(\text{BO}_2)_2^+/\text{B}_2\text{O}_3^+$ being of the order of 1/50. No phase diagram is available for the $\text{BeO-B}_2\text{O}_3$ system. In the course of an extended experiment, however, the ion ratio $\text{Be}(\text{BO}_2)_2^+/\text{B}_2\text{O}_3^+$ was found to be only a function of temperature, although the absolute intensities of both ionic species decreased with time. These observations suggest that the equilibrium



obtained. With this assumption, reaction (1) is found to have an enthalpy of 35 kcal mole⁻¹. The heat of formation of $\text{Be}(\text{BO}_2)_2$ from the elements, which is calculated from this value, is approximately twice that of the heat of formation of gaseous lithium or sodium metaborate, a relation which may be compared to a ratio of approximately 2.5 between the heats of formation of beryllium fluoride and lithium or sodium fluoride. To a limited extent, therefore, the similarity of BO_2^- to halide ions is borne out in the case of the beryllium compounds.

B. Magnesium Oxide-Boron Oxide and Aluminum Oxide-Boron Oxide Systems

In the magnesium oxide-boron oxide system the principal ion species was identified as MgBO_2^+ at mass numbers 65 and 66. Only small ion currents were found at peaks corresponding to $\text{Mg}(\text{BO}_2)_2^+$. The phase diagram in this case is known⁽²⁾ and is very complex. Further experiments are in progress to deduce the molecular species in the vapor from the ion species, and to determine the heat of formation of magnesium metaborate. In the aluminum oxide-boron oxide system no species corresponding to a gaseous aluminum borate were observed at temperatures up to 1400°C. In both the magnesium oxide-boron oxide and aluminum oxide-boron oxide systems X-ray examination of the residue at the termination of the experiment showed the presence of crystalline mixed oxides demonstrating that reaction between the two condensed phases indeed occurred.

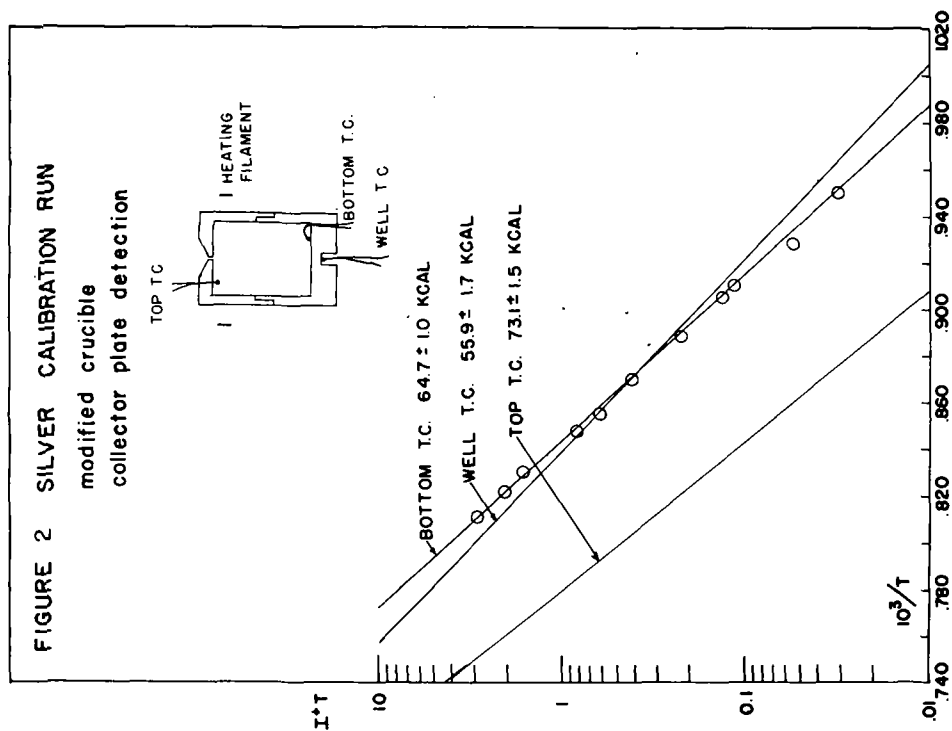
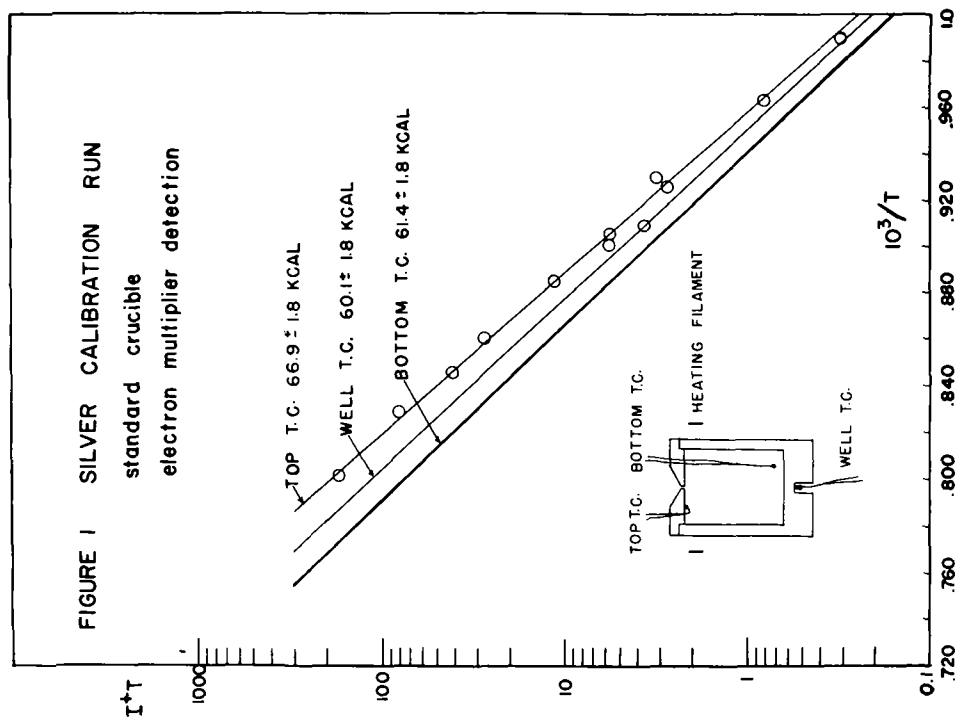
The Determination of Second-Law Heats

A. Second and Third-Law Heats

The procedure which has been used most extensively so far to obtain thermodynamic data by mass-spectrometric techniques has been the third-law method. Thus, in the case of a heat of sublimation, a value of ΔH_s can be obtained from every value of the vapor pressure P measured if the entropies of the condensed phase and the gaseous species are known:

$$\Delta H_s = -RT \ln P + T\Delta S_g \quad (2)$$

Much less emphasis has been placed on the second-law method which in this case would involve the determination of ΔH_s from the slope of a $\log P$ vs $\frac{1}{T}$ plot. It was realized from the beginning of this work, however, that the scarcity of molecular constants for the gaseous metaborates was likely to produce an uncertainty in the third-law heats of formation of these molecules, which would be at least as large as the 5 to 10 kcal mole⁻¹ uncertainty normally associated with second-law determinations.⁽³⁾ Since the precision of any given slope determination was usually of the order of ± 2 kcal per mole, it was felt that considerable improvement of the reliability of second-law measurements should be possible.



The problem was further underlined at the start of the work on the mixed oxide systems discussed in this note. In these systems, gaseous B_2O_3 is, under the conditions of measurement of the experiment, either the major or the only gaseous species formed. It was therefore planned to use gaseous B_2O_3 as a pressure-calibrating substance. A series of runs with pure boron oxide gave heats of vaporization which were consistently about 15 kcal mole⁻¹ higher than the most frequently quoted value in the literature.⁽⁴⁾ A series of silver calibration runs were then carried out. The second-law heats of sublimation of silver determined from these runs showed a scatter of as much as ± 10 kcal mole⁻¹ about the best current value.⁽⁵⁾ Temperature errors provided the most obvious explanation of these results. Traditional analysis of the effect of temperature errors on second-law heats, however, gave values for these errors which appeared excessively large.

Nevertheless, a standard molybdenum crucible was finally equipped with two platinum-rhodium thermocouples, one of which was spot-welded to the inside of the crucible lid while the other projected to the bottom of the crucible. Both thermocouples were led through the lid by means of alundum insulators, with Sauereisen cement used to make the openings tight.

The results of a silver vaporization run carried out with this crucible are shown in Figure 1. Each of the experimental values of I^+T (where I^+ is the intensity of the $^{107}Ag^+$ peak, in arbitrary units) was plotted against the temperatures given respectively by the well, inside-top, and inside-bottom thermocouples. Only the points plotted against the inside-top thermocouple temperature are shown; for the other two sets of points the least square lines are shown. It is clear from Figure 1 that with the type of crucible and heating arrangement illustrated, the lid is the coolest part of the cell and determines the vapor pressure. The second-law heat of sublimation obtained with the lid temperature is 66.9 ± 1.8 kcal mole⁻¹ for a mean temperature of 1110°K, in excellent agreement with the best third-law value available for this temperature, 67.0 ± 0.2 kcal mole⁻¹. The experiment was terminated before all the silver had evaporated, and it was found that the residual silver had indeed been transferred completely to the lid. It should also be pointed out that the temperature distribution implied in Figure 1 will be observed only when the principal source of heating is electron bombardment from a filament. At high temperatures, when electron emission from radiation shields is the principal source of heat, the top of the crucible will always be hotter than the bottom.

B. Analysis of Temperature Errors

Figure 1 also demonstrated the shortcomings of the standard analysis of the effect of temperature errors. In this analysis, the temperature read by thermocouple or pyrometer is assumed to be $T + \delta T$, where T is the "true" temperature in the crucible (i.e. the temperature which represents the vapor pressure), while δT represents the error in temperature reading, which is assumed to be constant over the entire temperature range of the experiments. Under these circumstances the error $\delta(\Delta H)$ in the second-law heat ΔH produced by an error δT is given by

$$\frac{\delta(\Delta H)}{\Delta H} = - \frac{2\delta T}{T} \quad (3)$$

where T is the mean temperature of the experiments. Typically, a temperature error of 60° is then required to produce a 10% error in ΔH if the experimental temperature is near 1200°K.

As can be seen from Figure 1, however, the temperature gradient actually varies over the experimental interval. Thus, instead of the true temperature interval $T_2 - T_1 = \Delta T$, one measures an interval which is in error by an amount of $\delta(\Delta T)$. The error in ΔH is given by

$$\frac{\delta(\Delta H)}{\Delta H} = \frac{\delta(\Delta T)}{\Delta T} \quad (4)$$

If measurements are carried out over a 150° range, a 10% error in ΔH will be produced if the temperature is correct at one end of the range, but is off by only 15° at the other end.

The critical nature of errors in temperature range is illustrated in Figure 2, which shows a silver run made in the course of development of a new crucible design. Here the temperature of the lid was about 100° hotter than that of the bottom. Nevertheless, the inside-bottom thermocouple gave a second-law heat of sublimation which was correct to within 2 kcal, whereas the heat given by the well thermocouple was nearly 10 kcal low. It will be observed that the temperature measured in the thermocouple well actually crosses that of the inside-bottom of the crucible. Hence, in this case, a pressure calibration using total evaporation of a silver sample at temperatures anywhere in the center region of the measurements would have given excellent results from the point of view of third-law measurements, but would have been completely misleading as to the reliability of second-law slopes.

C. Crucible Design

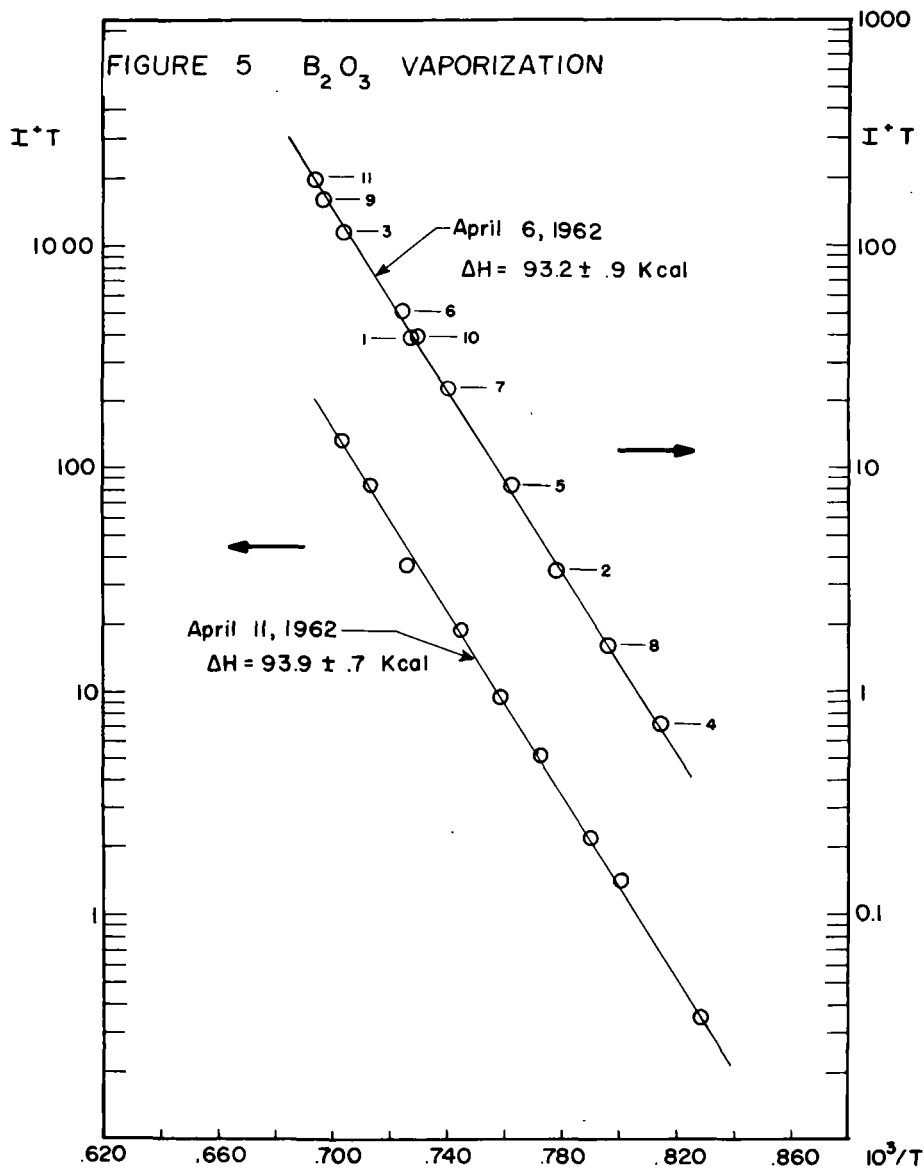
The crucible design finally developed is shown in Figure 3. The over-all configuration resembles closely that used by Panish⁽⁵⁾ with the important addition that two thermocouples are introduced into the inside of the crucible. The two halves of the crucible are heated by independently controlled filaments. It is thus easily possible to keep the top and bottom temperatures identical within two degrees. A further complication is introduced in work involving molten boron oxide since the latter would react with the alumund thermocouple leads. In this case, a thin platinum liner is used with the thermocouples welded to the liner. To perform silver calibration runs with the latter arrangement (Fig. 4), the silver was placed in an alumund liner. Even with this rather complex arrangement, heats obtained from slopes have always been within 3 kcal mole⁻¹ of the accepted value. We therefore believe that the crucible configuration is capable of producing second-law data with an accuracy of ± 3 kcal.

The new crucible design has been used in a redetermination of the heat of sublimation of boron oxide. The experimental data are shown in Figure 5. The two sets of points have been displaced relative to each other by one decade, since otherwise they overlap very closely. The numbers attached to one set of points show the order in which they were obtained and show that there was no trend with time in these experiments. The resulting heat of sublimation of boron oxide at a mean temperature of 1500°K is 93.5 ± 3 kcal/mol.

References

- (1) Blichler, A., and Berkowitz-Mattuck, J. B., The Vaporization of Lithium and Sodium Metaborate, in Chemical and Thermodynamic Properties at High Temperatures, XVIIIth International Congress of Pure and Applied Chemistry, Montreal, Canada, August 1961, p. 76.
- (2) H. M. Davis and M. A. Knight, J. Amer. Ceram. Soc. 28, 97 (1945).

(Continued on next page)



References - Concluded

- (3) Inghram, M. G., and Drowart, J., Mass Spectrometry Applied to High Temperature Chemistry, in Proceedings of an International Symposium on High Temperature Technology, pp. 219-240, McGraw-Hill Book Company, Inc., New York, 1960.
- (4) R. Speiser, S. Naiditch and H. L. Johnston, J. Amer. Chem. Soc. 72, 2578 (1950).
- (5) M. B. Panish, J. Chem. Eng. Data 6, 592 (1961).

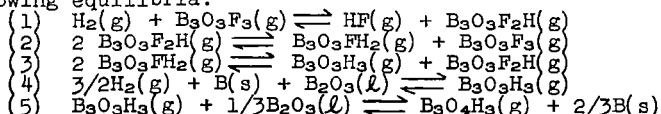
Mass Spectrometric Study of High Temperature Reactions
of $\text{BF}_3(\text{g})$, $\text{H}_2(\text{g})$ and $\text{H}_2\text{O}(\text{g})$ with $\text{B}_2\text{O}_3(\text{l})$ and $\text{B}(\text{s})$.

William P. Sholette and Richard F. Porter
Department of Chemistry, Cornell University, Ithaca, N. Y.

Summary

Low pressure, high temperature reactions of H_2 - BF_3 mixtures with B_2O_3 , of H_2 with B - B_2O_3 mixtures, and of water vapor with elemental boron have been investigated. The experimental technique involves flowing the reactant gas at pressures between 10^{-6} and 10^{-3} atmospheres into a Knudsen-type vessel containing a condensed sample at temperatures in the range 900°K to 1400°K, and observing the gaseous products effusing from the oven mass spectrometrically. (1) Mixtures of H_2 - BF_3 reacted with B_2O_3 to produce a spectrum containing chiefly groupings of $m/e = 80$ -84, 98-102, 116-120, and 135-138, corresponding to ions formed by electron impact of boroxine, $\text{B}_3\text{O}_3\text{H}_3(\text{g})$, and the fluoroboroxines $\text{B}_3\text{O}_3\text{H}_2\text{F}(\text{g})$, $\text{B}_3\text{O}_3\text{HF}_2(\text{g})$, and $\text{B}_3\text{O}_3\text{F}_3(\text{g})$, respectively. In both the reaction of H_2 with $(\text{B} + \text{B}_2\text{O}_3)$ and that of H_2O with B the major product formed is $\text{B}_3\text{O}_3\text{H}_3$, with smaller yields of $\text{B}_3\text{O}_4\text{H}_3(\text{g})$ (hydroxyboroxine) also observed. In the experiments with water vapor and boron, results indicated that H_2O was completely converted to H_2 in the reaction vessel, accompanied by the formation of B_2O_3 . Hence this system was essentially the same as that in which hydrogen was reacted with B - B_2O_3 . In Table I we show a typical mass spectrum obtained in the reaction of $\text{H}_2\text{O}(\text{g})$ on an isotopically enriched sample of ^{10}B .

By means of second law and third law treatments of the data obtained in these studies, heats of reaction were calculated for the following equilibria:



Combining the results for reactions (1)-(3) with a heat of formation for $\text{B}_3\text{O}_3\text{F}_3(\text{g})$ of -567 kcal/mole (2) at 298°K, heats of formation were obtained for $\text{B}_3\text{O}_3\text{F}_2\text{H}$, $\text{B}_3\text{O}_3\text{FH}_2$, and $\text{B}_3\text{O}_3\text{H}_3$. Reactions (4) and (5) led to an independent value of ΔH_{298}° for $\text{B}_3\text{O}_3\text{H}_3$ as well as a value for $\text{B}_3\text{O}_4\text{H}_3$. To complete Table II a value of -541 kcal/mole (2) for ΔH_{298}° of $\text{B}_3\text{O}_5\text{H}_3(\text{g})$ was used to obtain an interpolated heat of formation for $\text{B}_3\text{O}_5\text{H}_3$.

-
- (1) R. F. Porter, D. R. Bidinosti, and K. F. Watterson, *J. Chem. Phys.*, **36**, 2104 (1962).
(2) J.A.N.A.F. Thermochemical Data, Thermal Laboratory, Dow Chemical Company, Midland, Michigan, 1960.

Table I

Mass spectrum of gaseous products in
the reaction of $\text{H}_2\text{O}(\text{g})$ with $^{10}\text{B}(\text{s})$
(enriched).^a
 $T = 1250^\circ\text{K}$, Ionizing electron energy = 75 volts

m/e	Ion	Intensity (relative units)
97		3.7
96	$\text{B}_3\text{O}_4\text{H}_2^+$	12.9
82		6.3
81		40.0
80	$\text{B}_3\text{O}_3\text{H}_2^+$	100.0
79		5.5
70		1.1
69	$\text{B}_2\text{O}_3\text{H}^+$	4.8
68		1.8
54		6.6
53	$\text{B}_2\text{O}_2\text{H}^+$	36.0
52		4.0
27	BOH^+	17.3

a) sample is about 92 percent ^{10}B and 8 percent ^{11}B .

Table II

Heats of Formation of Gaseous Boroxines, Hydroxy-
boroxines, and Fluoroboroxines at 298°K .

Gaseous Molecule	ΔH°_{f298}
$\text{B}_3\text{O}_3\text{H}_3$	-307 ± 8 , -308 ± 6^a
$\text{B}_3\text{O}_3\text{H}_2\text{OH}$	-399 ± 6^a
$\text{B}_3\text{O}_3\text{H}(\text{OH})_2$	-476 ± 10^b
$\text{B}_3\text{O}_3(\text{OH})_3$	-541 ± 10^c
$\text{B}_3\text{O}_3\text{H}_2\text{F}$	-392 ± 6^a
$\text{B}_3\text{O}_3\text{HF}_2$	-479 ± 5^a
$\text{B}_3\text{O}_3\text{F}_3$	-567 ± 3^c

- a) this work
b) interpolated value
c) reference (2).

A NEW METHOD OF INCREASING THE EFFICIENCY OF
SURFACE IONIZATION SOURCES

N. R. Daly and N. C. Fenner
Atomic Weapons Research Establishment
Aldermaston, England

Manuscript Withdrawn

BIBLIOGRAPHY OF PUBLISHED AND UNPUBLISHED PAPERS

on

MASS SPECTROMETRY FOR 1961

The following pages were prepared by subcommittees II, III, V, and VII, as part of the Annual Report of Subcommittees, covering activities in their fields of interest. They are included in the collection of papers in response to many requests for a broader and more useful distribution of such information. In the present effort, no specific attempt was made to avoid multiple references to papers of interest in various fields.

1961 Bibliography

Theoretical and Fundamental Aspects of Mass Spectrometry

Prepared by Sub-Committee II

June, 1962

- I. Mass Spectra - Experimental, Correlations, and General Considerations.
Compiled by W. H. McFadden, USDA, Western Utilization Research and Development Division, Albany, California.
1. Aczel, T., "Correlations of Mass Spectra with Structure in Aromatic Phenols," Anal. Chem., 32, 1819 (1961).
2. Beynon, J. H., "Mass Spectra of Various Quinone and Polycyclic Ketones," App. Spec., 14, 156 (1960).
3. Biemann, K., and Vetter, W., "Separation of Peptide Derivatives by G. C. and Mass Spectral Determination of Sequence," Biochem. Biophys. Res. Commun. 3, 578 (1960).
4. Ryhage, R., and Stenhagen, E., "Mass Spectrometric Studies. Methyl Esters of Normal Chain Oxo-, Hydroxy, Methoxy, and Epoxy Acids," Arkiv Kemi, 15, 545 (1960).
5. Lorquet, J. C., "Electron Molecule Interaction. Electron Transition Induced During Impact," J. Chim. Phys. 57, 1078 (1960).
6. Biemann, K., "Application of Mass Spectrometry in Amino and Peptide Chemistry," Chimia (Switz), 14, 393 (1960).
7. Natalis, P., "Mass Spectra of 6 Cis and Trans Isomers of Dimethyl Cyclohexane," Bull. soc. chim. Belges, 69, 519 (1960).
8. Collin, J., "Dissociation Processes in the Mass Spectra of Oxygen Containing Heterocyclic Derivatives. Furfuryl and Tetrahydrofurfuryl Alcohols," Bull. soc. chim. Belges, 69, 575 (1960).
9. Collin, J., "Dissociation Processes in the Mass Spectra of Oxygen Containing Heterocyclic Derivatives. Dioxolane, 2-methyl-1,3-dioxolane, Dioxane, and 2,4,6-tri methyl- 1,3,5-trioxane," Bull. soc. chim. Belges, 69, 585 (1960).

10. Beynon, J. H., Saunders, R. A., and Williams, A. E., "High Resolution Mass Spectra of Aliphatic Esters," *Anal. Chem.*, 33, 221 (1961).
11. Beynon, J. H., Saunders, R. A., Topham, A., "Fragmentation of Long Chain Paraffins Under Electron Bombardment Using Isotopically Labelled Compounds," *J. Phys. Chem.*, 65, 114 (1961).
12. Steiner, B., Giese, C. F., and Inghram, M. G., "Photoionization of Alkanes. Dissociation of Excited Molecular Ions," *J. Chem. Phys.* 34, 189 (1961).
13. Aczel, T., and Lumpkin, H. E., "Correlation of Mass Spectra with Structure in Aromatic Oxygen Compounds," *Anal. Chem.*, 33, 386 (1961).
14. Hirota, K., *et al.*, "Mass Spectra and Appearance Potentials of Acetic and Deuteroacetic Acid," *Bull. Chem. Soc. Japan*, 34, 226 (1961).
15. Ashima, S., and Katsumata, A., "Qualitative Analysis of Hydrocarbons by Mass Spectrometric Measurement of Rearrangement Ions," *Sekiyu Gakkai Shi*, 4, 24 (1961).
16. Henneberg, D., *et al.*, "Boron Compounds. Mass Spectra of Lower Boron Trialkyls," *Ann. Chem. Liebigs*, 640, 52 (1961).
17. Biemann, K., and Friedmann, S. M., "Mass Spectrometric Evidence for the Structure of Iboxygaine and its Tosylate," *Tetrahedron Letters*, #2, 68 (1961).
18. Levy, E. J., and Stahl, W. A., "Mass Spectra of Aliphatic Thiols and Sulphides," *Anal. Chem.* 33, 707 (1961).
19. Quinn, E. I., and Mohler, F. L., "Mass Spectra of Some Deuteroethanes," *J. Res. Natl. Bur. Stnds.*, 65A, 93 (1961).
20. Cassuto, A., "Variations of Mass Spectra with Temperature Between -195° and +200°C," *Compte Rend.*, 252, 1311 (1961).
21. Meyerson, S., *et al.*, "Organic Ions in the Gas Phase. Bicycloheptadiene," *J. Am. Chem. Soc.* 83, 1401 (1961).
22. Majer, J. R., "Mass Spectra of Cyclic Fluorine Compounds," *J. Appl. Chem.* 11, 141 (1961).

23. Dibeler, V. H., Reese, R. M., and Franklin, J. L., "Mass Spectrometric Study of Cyanogen and Cyano-Acetylenes," J. Am. Chem. Soc. 83, 1813 (1961).
24. Eliel, E. L., et al., "Organic Ions in the Gas Phase. Dissociation of Benzyl Alcohol by Electron Impact," J. Am. Chem. Soc. 83, 2481 (1961).
25. Sporer, A. H., "Photoionization of Triaryl Methyl Leuco Nitriles," Trans. Faraday Soc. 57, 983 (1961).
26. Polyakova, A. A., et al., "Mass Spectra and Structure of Organic Compounds. Mass Spectra of Enin Hydrocarbons with a T-Butyl Radical at the Multiple Bonds," Izvest. Vyskhikh Ucheb. Zavedenii, Khim. I Khim. Tekhnol., 4, #2, 321 (1961).
27. Trent, F. M., and Miller, F. D., "Mass Spectra of Some High Molecular Weight Aliphatic Acids and Their Methyl Esters. Analysis of Nonanoic Acid and 2-Ethyl Heptanoic Acid Mixtures," Appl. Spec., 15, 64 (1961).
28. Saalfeld, F. A., and Svec. H. J., "Mass Spectrum of Stannane," J. Inorg. Nuclear. Chem. 18, 98 (1961).
29. Heyns, K., and Gruetzmacher, H. F., "Mass Spectra of Methyl Esters of n-Formyl- α -Amino Acid," Z. Naturforsch 16B, 293 (1961).
30. Beckey, H. D., "Measurement of Extremely Short Decay Times of Organic Ions with The Field Ionization Mass Spectrometer," Z. Naturforsch 16A, 505 (1961).
31. Vilesov, F. I., et al., "Electron Distribution Over Energies in the Photoionization of Aromatic Amines in the Gaseous Phase," Doklady Akad. Nauk S.S.S.R. 138 1329 (1961).
32. Stenhagen, E., "Mass Spectra as an Aid in the Case of the Determination of the Structure of Organic Compounds, Especially in the Case of Lipides and Peptides," Z. Anal. Chem.. 181, 462 (1961).
33. Biemann, K., et al., "Determination by Mass Spectrometry of the Structure of Proline Derivatives from Apples," Nature 191, 380 (1961).
34. Miller, G. H., and Pritchard, G. O., "Mass Spectra of Pentafluoropropanal and Heptafluorobutanal," Chem. and Ind. (London) 1314 (1961).

35. Berkowitz, J., et al., "Mass Spectrum of Ethyl Lithium Vapor," J. Phys. Chem. 65, 1380 (1961).
36. Mead, W. L., and Wilde, A. J., "Mass Spectrum of Vanadyl Etioporphyrin-I," Chem. and Ind. (London) 1315 (1961).
37. Biemann, K., et al., "Mass Spectra of Organic Molecules. Ethyl Esters of Amino Acids," J. Am. Chem. Soc., 83, 3795 (1961).
38. Omura, I., "Mass Spectra at Low Ionizing Voltages and Bond Dissociation Energies of Molecular Ions from Hydrocarbons," Bull. Chem. Soc. Japan 34, 1227 (1961).
39. Vilesov, F. I., "Photodissociation of Organic Vapors in the Vacuum Region of the Spectrum," Zhur. Fiz. Khim. 35, 2010 (1961).
40. Fritz, G., et al., "Mass Spectral Investigation of Silicon-Methylene Compounds," Z. Anorg. u. Allgem. Chem. 312, 201 (1961).
41. Biemann, K., et al., "Investigation by Mass Spectrometry of the Alkaloids of *Aspidosperma Quebrachoblanco*," Tetrahedron Letters 485 (1961).
42. Akopian, M. E., et al., "Mass Spectrometric Investigation of How the Photoionization Efficiency of Benzene Derivatives is Related to Their Spectra," Doklady Akad. Nauk S.S.S.R. 140, 1037 (1961).
43. Kurbatov, B. L., et al., "Electron Distribution over Kinetic Energies in the Photoionization of Methyl Derivatives of Benzene," Doklady Akad. Nauk S.S.S.R. 140, 797 (1961).
44. Ryha ~~ge~~, R., et al., "Mass Spectral Studies. Methyl Esters of α , β -unsaturated Long-Chain Acids. Structure of 27-Carbon-Phthienoic Acid," Arkiv. Kemi 18, 179 (1961).
45. Kanomata, J., "Mass Spectral Study of Ionization and Dissociation of Di-Ethyl Ether by Electron Impact," Bull. Chem. Soc. Japan 34, 1596 (1961).
46. Biemann, K., and Friedman, S. M., "Application of Mass Spectra to Structure Problems: Iboaga Alkaloids," J. Am. Chem. Soc. 83, 4805 (1961).

47. Biemann, K., "Application of Mass Spectra to Structure Problems: Carbon Skeleton of Sarpagine," J. Am. Chem. Soc. 83, 4801 (1961).
48. McLafferty, F., "Mass Spectral Analysis. Aliphatic Halogenated Compounds," Anal. Chem. 34, 2 (1962).
49. McLafferty, F., "Mass Spectral Analysis. Aromatic Halogenated Compounds," Anal. Chem. 34, 16 (1962).
50. McLafferty, F., "Mass Spectral Analysis. Aliphatic Nitriles," Anal. Chem. 34, 26 (1962).
51. Aczel, T., and Lumpkin, H. E., "Correlation of Mass Spectra with Structure in Aromatic Oxygenated Compounds. Benzoate Type Esters," Anal. Chem. 34, 33 (1962).
52. Polyakova, A. A., and Petrov, A. A., "Mass Spectra and Structure of Organic Compounds. Mass Spectra of Alkenyl Vinyl Acetylene," Zhur. Abshchei Khim. 31, 3515 (1961).
53. Baun, W. L., and Fischer, D. W., "Mass Spectra of Amino Acids Using a Radio Frequency Spark Source," Anal. Chem. 34, 294 (1962).
54. Spiteller, G., "Structural Determination of Ethyl 5,7-Dimethyl-2-aminocumaron-3-carboxylate with the Aid of a Mass Spectrometer," Monatsh. Chem. 92, 1142 (1961).
55. Spiteller, G., "Ortho Effect in the Mass Spectra of Aromatic Compounds," Monatsh. Chem. 92, 1147 (1961).
56. Gallegos, E. J., and Kiser, R. W., "Electron Impact Spectroscopy of the 4 and 5 Membered Saturated Heterocyclic Compounds Containing Nitrogen, Oxygen, and Sulfur," J. Phys. Chem. 66, 136 (1962).
57. Hobrock, B. G., and Kiser, R. W., "Electron Impact Spectroscopy of Tetramethyl Germane, Trimethyl Silane, and Dimethyl Mercury," J. Phys. Chem. 66, 155 (1962).

In addition to the above published works, the following related papers were presented at the ASTM E-14 Mass Spectrometry meeting and at the Mass Spectrometry Conference held at Oxford.

A.S.T.M. E-14 Meeting, Chicago, Illinois, June 1961.

58. Lorquet, J.C., "A Non-Statistical Approach to the Calculation of Mass Spectra."
59. Coggeshall, N. D., "Comparison of Mass Spectral Regularities for n-Paraffins and n-Terminal Olefins."
60. McFadden, W. H., "The Mass Spectra of Three Deuterated Propenes."
61. Finan, P. A., et al., "Correlation Studies on Some Oxygen Containing Compounds."
62. Muccini, G. A., et al., "Metastable Ions in Mass Spectrometry."
63. Harless, H., "Anomalies in the Mass Spectrum of Hexachloropropene and Its Relation to Basic Concepts of the Propene Molecule."
64. Cook, G. L., et al., "Analytically Useful Correlations of Mass Spectra and Molecular Structures of Thiols, Sulfides, and Disulfides."
65. Lange, W. J., "Study of Negative Ions with a Cycloidal Instrument."
66. Hebling, A., and Lightman, D., "Fragment Patterns and Appearance Potentials Using the Omegatron Mass Spectrometer."
67. Crable, G. F., and Kearns, G. L., "Effects of Substituent Groups on the Ionization Potentials of Benzenes."
68. Kennedy, A., and Colburn, C. B., "The Strength of the N-F Bonds in NF_3 and of the N-F Bonds and the N-N Bonds in N_2F_4 ."
69. Foster, N. G., et al., "The Mass Spectra of 2-n-Hexylthiophene and $\alpha\text{-C}^{13}\text{-2-n-Hexylthiophene}$."
70. Bedwell, V. E., et al., "Mass Spectrometric Study of Reactive Materials - I. Chlorine Trifluoride."
71. Bedwell, V. E., et al., "Mass Spectrometric Study of Reactive Materials - II. Pentaborane."

Institute of Petroleum and A.S.T.M. E-14 Joint Conference on Mass Spectrometry, Oxford, 1961.

72. Cassuto, A., "Variations of Mass Spectra with Temperature between -195°C and +200°C."
73. Meyerson, S., et al., "Organic Ions in the Gas Phase. Ionization and Dissociation of Methylcyclopentane and Related Cycloalkanes."
74. Henneberg, D., "Rearrangement in the Spectra of Trialkyl-Boranes."
75. D'Or, L., "Some Factors Affecting the Ionization and Dissociation of Hydrocarbon Molecules (c)."
76. Biemann, K., "Determination of the Structure of Alkaloids by Mass Spectrometry."
77. Reid, K., et al., "The Mass Spectra of Some Flavours and Carbohydrates."
78. Fitches, H. J. M., "The Mass Spectra of Some Steroids."
79. Snedden, W., "The Mass Spectra of Some Borazoles."
80. Botter, R., and Nief, G., "Electron Impact Studies of Carbon Sub-Oxide by Mass Spectrometry."
81. Majer, J. R., and Patrick, C. R., "Electron Impact Studies of Halogenated Benzenes (c)."
- II. Theory of Mass Spectra - Formation of Ions and Dissociation of Ions and Molecules.
Compiled by Morris Krauss, NBS, Washington, D. C.
82. Begun, G. M. and Landau, L., "Mass Spectra and Metastable Transitions in Isotopic Nitrous Oxides," J. Chem. Phys. 35, 547 (1961).
83. Chupka, W. A., and Kaminsky, M., "Energy Distribution and Fragmentation Processes Resulting from Electron Impact on Propane and n-Butane", J. Chem. Phys. 35, 1991 (1961).
84. Cassuto, A., "Variations of Mass Spectra with Temperature Between -195 and 200°C", Compt. rend. 252, 1311 (1961).

85. Dorman, F. H. and Morrison, "Determination of Relative Electronic Transition Probabilities by Impact Methods," J. Chem. Phys. 34, 578 (1961).
86. Dorman, F. H. and Morrison, J. D., "Double and Triple Ionization in Molecules Induced by Electron Impact," J. Chem. Phys. 35, 575 (1961).
87. Eyring, E. M. and Wahrhaftig, A. L., "Dependence of Calculated and Experimental Propane Mass Spectra Upon Electron Voltage," J. Chem. Phys. 34, 23 (1961).
88. Foner, S. N. and Nall, B. H., "Structure in the Ionization Near Threshold of Rare Gases by Electron Impact," Phys. Rev. 122, 512 (1961).
89. Ford, J., "Equipartition of Energy for Non-linear Systems," J. Math. Phys. 2, 387 (1961).
90. Frey, H. M., "New Experimental Tests of the Theories of Unimolecular Reactions," Trans. Faraday Soc. 56, 51 (1960).
91. Harrington, R. E. and Rabinovitch, B. S., "Decomposition of Activated sec-Butyl Radicals from Different Sources and Unimolecular Reaction Theory," J. Chem. Phys. 33, 1271 (1960).
92. Horie, T., Nagura, T., and Otsuka, M., "Radiative Collisions Between Molecular and Electronic Beams. V. Angular Momentum Distribution of CH* Separating from Simple Organic Molecules," J. Phys. Soc. Japan 15, 641 (1960).
93. von Koch, H. and Lindholm, E., "Dissociation of Ethanol Molecule Ions Formed in Charge Exchange Collisions with Positive Ions," Arkiv Fysik 19, 123 (1961).
94. Kurbatov, B. L., Vilesov, F. I., Terenin, A. N., "Electron Distribution over Kinetic Energies in the Photo-ionization of Methyl Derivatives of Benzene," Doklady Akad. Nauk S.S.S.R. 140, 797 (1961).
95. Lavroskaya, K., Markin, M. I. and Talroze, V. L., "Charge Transfer from Ions to Complex Molecules," Kinetika i Kataliz 2, 21 (1961).
96. Monahan, J. E. and Stanton, H. E., "Kinetic-Energy Distribution of Ionic Fragments from Some Hydrocarbons under Electron Impact," Bull. Am. Phys. Soc. II, 6, 356 (1961).

97. Percival, I. C., "Almost Periodicity and the Quantal H-Theorem," J. Math. Phys. 2, 235 (1961).
98. Platzmann, R. L., "Total Ionization in Gases by High-Energy Particles: An Appraisal of our Understanding," Internat. J. Appl. Radiation and Isotopes 10, 116 (1961).
99. Platzmann, R. L., "Probability of Ionization by the Transfer of the Energy of Excited Atoms to Molecules," J. Phys. Radium 21, 853 (1960).
100. Rabinovitch, B. S. and Current, J. H., "On the Classical Approximation in Unimolecular Reactions and Mass Spectra," J. Chem. Phys. 35, 2250 (1961).
101. Rosenstock, H. M., "On the Classical Approximation in the Statistical Theory of Mass Spectra," J. Chem. Phys. 34, 2182 (1961).
102. Schlag, E. W., "Unimolecular Rates Due to Multiple Critical Oscillators," J. Chem. Phys. 35, 2117 (1961).
103. Schug, J. C. and Coggeshall, N. D., "Note on the Statistical Theory of Mass Spectra," J. Chem. Phys. 35, 1146 (1961).
104. Slater, N. B., "Cubic Potential Surfaces in the Transition State Theory of Unimolecular Reactions," J. Chem. Phys. 35, 445 (1961).
105. Tanaka, I., Carrington, T. and Ercida, H. P., "Photon Dissociation of Water: Initial Non-equilibrium Populations of Rotational States of $\text{OH}(\Sigma^+)$," J. Chem. Phys. 35, 750 (1961).
106. Thiele, E. and Wilson, D. J., "Anharmonicity in Unimolecular Reactions," J. Chem. Phys. 35, 1256 (1961).
107. Vestal, M. L. and Rosenstock, H. M., "Oscillator Models in Unimolecular Reactions," J. Chem. Phys. 35, 2008 (1961).
108. Vilesov, F. I., Kurbatov, B. L. and Terenin, A. N., "Electron Energy Distribution During the Photoionization of Aromatic Amines in the Gaseous Phase," Dokl. Akad. Nauk S.S.S.R. 138, 1329 (1961).

109. Wall, F. T., Hiller, L. A. Jr., and Mazur, J., "Statistical Computation of Reaction Probabilities, II," J. Chem. Phys. 35, 1284 (1961).
110. Wallenstein, M. B. and Krauss, M., "Interpretation of the Appearance Potentials of Secondary Ions," J. Chem. Phys. 34, 929 (1961).
111. Watanabe, T., "A Theory of Electron Impact on Some Polyatomic Molecules," J. Phys. Soc. Japan 16, 510 (1961).
- III. Ionization and Appearance Potentials.
Compiled by M. S. B. Munson, Humble Oil & Refining Company, Baytown, Texas.
112. Curran, R. K. and Fox, R. E., "Mass Spectrometer Investigation of Ionization of N₂O by Electron Impact," J. Chem. Phys. 34, 1590 (1961).
113. Fox, R. E. and Curran, R. K., "Ionization Processes in CCl₄ and SF₆ by Electron Beams," J. Chem. Phys. 34, 1595 (1961).
114. Fox, R. E., "Ionization Cross Sections Near Threshold by Electron Impact," J. Chem. Phys. 35, 1379 (1961).
115. Curran, R. K., "Negative Ion Formation in Ozone," J. Chem. Phys. 35, 1849 (1961).
116. Meyerson, Seymour, "Effect of Electron Energy on Some Electron-Impact Processes," J. Chem. Phys. 34, 2046 (1961).
117. Meyerson, Seymour, "Erratum. Effect of Electron Energy on Some Electron-Impact Processes," J. Chem. Phys. 35, 1137 (1961).
118. Momigny, J., "Behaviour of cis- and trans-Dihaloethylenes on Electron Impact," Bull. Soc. Chim. Belges. 70, 241 (1961).
119. Momigny, J., "Erratum. Behaviour of cis- and trans-Ethylenedihalides Under Electron Impact," Bull. Soc. Chim. Belges. 70, 627 (1961).
120. Momigny, J., "The Ionization Potentials of cis- and trans-Dihaloethylenes," Bull. Classe Sci. Acad. Roy. Belg. 46, 686 (1960).

121. Kaneko, Y., "Ionization Efficiency Curves for Ar^+ , Kr^+ , N_2^+ , and CO^+ by Electron Impact," J. Phys. Soc. Japan 16, 1587 (1961).
122. Kaneko, Y., "Single and Double Ionization of Sodium, Potassium and Magnesium by Electron Impact," J. Phys. Soc. Japan 16, 2288 (1961).
123. Herron, J. T. and Dibeler, V. H., "Mass Spectrometric Study of NF_2 , NF_3 , N_2F_2 , and N_2F_4 ," J. Res. Natl. Bureau Stds. 65A, 405 (1961).
124. Schoenheit, E., "Mass Spectrometric Investigation of the Photoionization of Argon," Z. Naturforschg. 16a, 1094 (1961).
125. Kiser, R. W. and Hisatsune, I. C., "Electron Impact Spectroscopy of Nitrogen Dioxide," J. Phys. Chem. 65, 1444 (1961).
126. Gallegos, E. J. and Kiser, R. W., "Electron Impact Spectroscopy of Ethylene Sulfide and Ethyleneimine," J. Phys. Chem. 65, 1177 (1961).
127. Gallegos, E. J. and Kiser, R. W., "Electron-Impact Spectroscopy of Ethylene Oxide and Propylene Oxide," J. Am. Chem. Soc. 83, 773 (1961).
128. Kiser, R. W. and Hobbrook, B. G., "Electron-Impact Spectroscopy of Tetramethyl-Silicon, Tin, and Lead," J. Phys. Chem. 65, 2186 (1961).
129. Dorman, F. H. and Morrison, J. D., "Ionization Potentials of Multiply-Charged Krypton, Xenon, and Mercury," J. Chem. Phys. 34, 1407 (1961).
130. Dorman, F. H. and Morrison, J. D., "Double and Triple Ionization in Molecules Induced by Electron Impact," J. Chem. Phys. 35, 575 (1961).
131. Marmet, P. and Morrison, J. D., "Mass Spectrometer for Ionization Efficiency Studies Using an Electron Velocity Selector," J. Chem. Phys. 35, 746 (1961).
132. Harrison, A. G., Kebarle, P., and Lossing, F. P., "Free Radicals by Mass Spectrometry. XXI. The Ionization Potentials of Some Meta- and Para-Substituted Benzyl Radicals," J. Am. Chem. Soc. 83, 777 (1961).

133. Pottie, R. F., Harrison, A. G., and Lossing, F. P., "Free Radicals by Mass Spectrometry. XXIV. Ionization Potentials of Cycloalkyl Free Radicals and Cycloalkanes," J. Am. Chem. Soc. 83, 3204 (1961).
134. Pottie, R. F. and Lossing, F. P., "Free Radicals by Mass Spectrometry. Ionization Potentials of Cyanoalkyl Radicals," J. Am. Chem. Soc. 83, 4737 (1961).
135. Herzberg, G., "The Ionization Potential of CH_2 ," Can. J. Phys. 39, 1511 (1961).
136. Robertson, E. W. and Barrow, R. F., "Rotational Analysis of the Energy Band Transition System of Diatomic Potassium and the Ionization Potential of Diatomic Potassium," Proc. Chem. Soc. 329 (1961).
137. Kearns, D. R. and Calvin, M., "Solid State Ionization Potentials of Some Aromatic Organic Compounds," J. Chem. Phys. 34, 2026 (1961).
138. Fineman, M. A. and Petrocelli, A. W., "Molecular Studies with a Lozier Electron-Impact Apparatus," Planetary Space Sci. 3, 187 (1961).
139. Hirota, Kozo, Nagoshi, Kazuo, and Hatada, Motoyashi, "Studies on Mass Spectra and Appearance Potentials of Acetic Acid and Deuterioacetic Acid," Bull. Chem. Soc. Japan 35, 226 (1961).
140. Schulz, G. J., "Study of the N_2O Molecule by Using Electron Beams," J. Chem. Phys. 34, 1778 (1961).
141. Klinkenberg, P. F. A., van Kleer, Th. A. M., and Noorman, P. E., "Structure and Ionization Potential of Hf III and Hf IV," Physica 27, 151 (1961).
142. El Sayed, M. F. A., Kasha, M., and Tanaka, Y., "Ionization Potentials of Benzene, Hexadeuteriobenzene, and Pyridine from their Observed Rydberg Series in the Region 600-2000 Å," J. Chem. Phys. 34, 334 (1961).
143. Foner, S. N. and Nall, B. H., "Structure in the Ionization Near Threshold of Rare Gases by Electron Impact," Phys. Rev. 122, 512 (1961).

144. Vainshtein, L. A., "Excitation of Atoms and Ions by Electron Impact," Optika i Spektroskopiya 11, 301 (1961).
145. Dolder, K. T., Harrison, M. F. A., and Thonemann, P. C., "Measurement of the Ionization Cross Section of Helium Ions by Electron Impact," Proc. Roy. Soc. Lon. 264A, 367 (1961).
146. Vilesov, F. I. and Kurbatov, B. L., "Photoionization of Ethers and Carbonyls of Metals in the Gaseous Phase," Doklady Akad. Nauk. S.S.S.R. 140, 1364 (1961).
147. Kanomata, I., "Mass Spectrometric Study on Ionization and Dissociation of Diethyl Ether by Electron Impact," Bull. Chem. Soc. Japan 34, 1596 (1961).
148. Baughan, C. A., "Ionization Potentials, Electron Affinities, and Screening Constants. A Simple Theory," Trans. Far. Soc. 57, 1863 (1961).
149. Omura, I., "Mass Spectra at Low Ionizing Voltage and Bond Dissociation Energies of Molecular Ions from Hydrocarbons," Bull. Chem. Soc. Japan 34, 1227 (1961).
- IV. Free Radicals and Chemical Reactions.
Compiled by P. Kebarle, Dept. of Chemistry, U. of Alberta, Edmonton, Alberta.
150. Barber, M., Cuthbert, J., Farren, J., and Linnett, J. W. , " The Mass Spectrometry of Free Radicals. 2. Some Reactions of Methyl Radicals," Abstract papers. XVIII IUPAC Conference, Montreal 1961.
151. Bidinosti, D. R., and Porter, R. F., "Mass Spectrometric Studies of Low Pressure Pyrolysis Reactions of Chlorinated and Fluorinated C₁ and C₂ Compounds on Graphite," J. Am. Chem. Soc. 83, 3737, (1961).
152. Bornkessel, K. and Pilot, J., "Mass Spectrometric Investigation of the Gas Products on Heating Hydrogen and Silicon Containing Magnesium," (in German), Z. Naturforschung 16a, 432 (1961).
153. Bradley, J. N., and Kistiakowsky, G. B., "Shock Wave Studies by Mass Spectrometry I. Thermal Decomposition of Nitrous Oxide," J. Chem. Phys. 35, 256 (1961).

154. Gutbier, H., "Mass Spectrometric Investigation of Evaporation Processes of Some Compounds with the Zinc Blend Lattice Structure at Temperatures around 1000°K (in German)," Z. Naturforschung 16, 268 (1961).
155. Bradley, J. N., and Kistiakowsky, G. B., "Shock Waves by Mass Spectrometry II: Polymerization and Oxidation of Acetylene," J. Chem. Phys. 35, 264 (1961).
156. Bradley, J. N., "Shock Wave Decomposition of Nitroparaffins. Part I. Mass Spectrometric Study of Nitromethane Decomposition," Trans. Faraday Soc. 57, 1750 (1961).
157. Dong, Pham, and Cottin, Maurice, "Mass Spectrometric Study of the Products of The Thermal Decomposition of Hydrogen, Oxygen and Water Vapour," J. Chim. Phys. 58, 803 (1961) (in French).
158. Goldfinger, P., Huybrechts, G., Verbeke, G., "Mass Spectrometric Studies of Fast Reactions at Atmospheric Pressure," Joint Conference Mass Spectrometry-Oxford - 1961.
159. Harrison, A. G., Kebarle, P., and Lossing, F. P., "Free Radicals by Mass Spectrometry XXI: The Ionization Potentials of Some Meta and Para Substituted Benzyl Radicals," J. Am. Chem. Soc. 83, 777 (1961).
160. Herron, J. T., "Rate of the Reaction of NO + N," J. Chem. Phys. 35, 1138 (1961).
161. Herron, J. T., and Dibeler, V. H., "Mass Spectrometric Study of the Thermal Dissociation of N₂F₄," J. Chem. Phys. 35, 747 (1961).
162. Kebarle, P., "The Mercury Photosensitized Decomposition of Mercury Dimethyl," Joint Meeting Mass Spectrometry - Oxford - 1961.
163. Melton, C.E., "Studies of Transient Species Formed During Catalytic Reactions of CO₂ + D₂ and 1-butene," J. Chem. Phys. 35, 1750 (1961).
164. Pottie, R. F., Harrison, A. G., and Lossing, F. P., "Free Radicals by Mass Spectrometry XXII: Primary Decomposition Steps in the Mercury Photosensitized Decomposition of Methanol and Dimethyl Ether," Canadian J. Chem. 39, 102 (1961).
165. Pottie, R. F. and Lossing, F. P., "Free Radicals by Mass Spectrometry XXIII: Mass Spectra of Benzyl and Benzyl- α -d₂, Free Radicals," J. Am. Chem. Soc. 83, 2634 (1961).

166. Pottie, R. F., Harrison, A. G., and Lossing, F. P., "Free Radicals by Mass Spectrometry XXIV: Ionization of Cycloalkyl Free Radicals and Cycloalkanes," J. Am. Chem. Soc., 83, 3204 (1961).
167. Pottie, R. F., and Lossing, F. P., "Free Radicals by Mass Spectrometry XXV: Ionization Potentials of Cyanoalkyl Radicals," J. Am. Chem. Soc. 83, 4737 (1961).
168. Terenin, A., Vilessov, F., Kurbatov, B., and Dodonova, N., "Mass Spectrometry and Luminescence of Radicals in the Photodissociation and Photoionization of Molecules by Vacuum Ultraviolet Radiation," Abstract Papers XVIII IUPAC Conference, Montreal 1961.
- V. High Temperature Mass Spectrometry.
Compiled by J. Drowart, Service of Chemical Physics, Free University of Brussels, Brussels, Belgium.
169. Ackerman, M., Drowart, J., Stafford, F. E., and Verhaegen, G., Wright Air Development Division, Air Research and Development Command, Contract AF 61(052)225 - Scientific Note No. 5 (1961).
170. Ackerman, M., Stafford, F. E., Verhaegen, G., Wright Air Development Division, Air Research and Development Command, Contract AF 61(052)225 - Scientific Note No. 6 (1961).
171. Ackerman, R. J., and Rauh, E. G., J. Chem. Phys. 36, 448 (1962).
172. Akishin, P. A., Gorokhov, L. N., and Sidorov, L. N., "Mass Spectrometric Study of Cesium Halides," Doklady Akad Nauk SSSR 135, 113 (1960).
173. Akishin, P. A., and Khodееv, Yu. S., "Determination of the Heat of Sublimation of Uranium Tetrafluoride by the Mass Spectroscopic Method," Zhur. Fis. Khim., 35, 1169 (1961).
174. Babeliowsky, T., and Boerboom, A. J. H., "Thermodynamic Study of CaO and Ta," Symposium on Mass Spectrometry Oxford (1961). See also: Mass Spectrometry Conference, ASTM Committee E-14, Chicago (1961).

175. Bascombe, K. N., Greene, J. L., and Sugden, T. M., "The Ionization Produced by Addition of Acetylene to a Hydrogen-Oxygen-Nitrogen Flame," Symposium on Mass Spectrometry, Oxford (1961).
176. Bascombe, K. N., Jenkins, D., Schiff, H. I., and Sugden, T. M., "The Production of NH^+ and NO^+ Ions in Flames," ASTM Committee E-14, Chicago (1961).
177. Berkowitz, J., Tasman, H. A., and Chupka, W. A., "Double Oven Experiment with Lithium Halides," Abstracts, 18th International Congress of Pure and Applied Chemistry, University of Toronto Press, (1961) p. 109.
178. Berkowitz, J., Bafus, D. A., and Brown, T. L., "The Mass Spectrum of Ethyl-lithium Vapor," J. Phys. Chem. 65, 1380 (1961).
179. Berkowitz-Mattuck, J., Buchler, A., and Goldstein, S., "Reaction Between Molybdenum and Oxygen," Contract AF 33 (616)-6154 (1961) (A.D. Little, Inc., Cambridge, Mass.).
180. Bidinosti, D. R., and Porter, R. F., "Mass Spectrometric Studies of Low Pressure Pyrolysis Reactions of Chlorinated and Fluorinated C_1 and C_2 on Graphite," J. Am. Chem. Soc. 83, 3737 (1961).
181. Brackman, R. T., and Fite, W. L., "Condensation of Atomic and Molecular H_2 at Low Temperatures," J. Chem. Phys. 34, 1572 (1961).
182. Buchler, A., and Berkowitz-Mattuck, J. B., "The Vaporization of Lithium and Sodium Metaborate," 18th International Congress of Pure and Applied Chemistry, University of Toronto Press (1961). p. 100.
183. Calcote, H. F., Eight International Symposium on Combustion, Williams and Wilkins Cy., Baltimore, Maryland (1961).
184. Calcote, H. F., and Reuter, J. L., "Mass Spectrometric Studies of Ion Profiles in Low Pressure Flame," Mass Spectrometry Conference, ASTM Committee E-14, Chicago (1961).
185. Cater, E. D., Rauh, E. G., and Thorn, R. J., "Uranium Monosulfide. II. Mass Spectrometric Study of its Vaporization," J. Chem. Phys. 35, 619 (1961).

186. Chupka, W. A., Meschi, D. J., and Berkowitz, J., "Reaction of Graphite with Hydrogen: Heat of Formation of the Methylene Radical," Abstracts, 18th International Congress of Pure and Applied Chemistry, University of Toronto Press (1961) p. 115.
187. Chupka, W. A., Berkowitz, J., Meschi, D. J., and Tasman, H. A., "Mass Spectrometric Studies of High Temperature Systems," Symposium on Mass Spectrometry, Oxford 1961.
188. Colin, R., Goldfinger, P., and Jeunehomme, M., "Mass Spectrometric Investigation of the Vaporization of Sulphides and the Dissociation Energy of S_2 ," Nature 187, 408 (1960).
189. Colin, R., "Ionization Cross-Sections of Te and Te_2 ," Ind. Chim. Belg., 26, 51 (1961).
190. Colin, R., and Drowart, J., "Dissociation Energy of Gaseous SuS , PbS , and Their Dimers," Wright Air Development Division, Office of Aerospace Research, Contract AF 61(052)-225, Scientific Note No. 9 (1962).
191. Colin, R., Goldfinger, P., and Jeunehomme, M., "Dissociation Energy of Gaseous MnS ," Wright Air Development Division, Office of Aerospace Research Contract AF 61(052)-225 Scientific Note No. 10 (1962).
192. DeJaeger, S., Deckers, J., and Van Tiggelen, A., Eighth International Symposium on Combustion. Williams and Wilkins Cy., Baltimore, Maryland 1961.
193. Foster, H. J., "The Adaptation of a Bendix Time-of-Flight Mass Spectrometer for High Temperature Studies," Mass Spectrometry Conference, ASTM Committee E-14, Chicago (1961).
194. Goldfinger, P., "High Temperature Studies at the Brussels Mass Spectrometry Laboratory." ASTM Committee E-14 Chicago (1961).
195. Goldstein, H. W., Walsh, P. N., and White, D., "Rare Earths. I. Vaporization of La_2O_3 and Nd_2O_3 : Dissociation Energies of Gaseous LaO and NdO ," J. Phys. Chem. 65, 1400 (1961).
196. Gorokhov, L. N., Doklady Akad. Nauk. SSSR 142, 113 (1962).

197. Grimley, R. T., Burns, R. P., and Inghram, M. G., "Thermodynamics of the Vaporization of Cr_2O_3 : Dissociation Energies of CrO , CrO_2 & CrO_3 ," J. Chem. Phys. 34, 664 (1961).
198. Grimley, R. T., Burns, R. P., and Inghram, M. G., "Thermodynamics of the Vaporization of Nickel Oxide," J. Chem. Phys. 35, 551 (1961).
199. Grimley, R. T., and Burns, R. P., "Controlled Atmosphere High Temperature Vaporization Studies," Mass Spectrometry Conference, ASTM Committee E-14 Chicago (1961).
200. Honig, R. E., "Mass Spectrometric Studies of Solid Surfaces," Symposium on Mass Spectrometry, Oxford, 1961.
201. Honig, R. E., "The Sputtering of Silicon Carbide by Positive Ion Bombardment," Fifth International Conference on Ionization Phenomena in Gases, Munich (1961).
202. Jeunehomme, M., Thesis, University of Brussels (1962).
203. McKinley, J. D., "A Mass Spectrometric Investigation of the High Temperature Reaction Between Nickel and Chlorine," Abstracts, 136th Meeting, A.C.S., Atlantic City 1959.
204. Moran, T. I., and Trischka, J. W. "New Determinations of the Vibrational Constants of Li^6F and $\text{Li}^6\text{Cl}^{35}$ by the Molecular Beam Electric Resonance Method," J. Chem. Phys. 34, 923 (1961).
205. Nikitin, O. T., and Gorokhov, C. N., Zhurn. Neerg. Khim., 6, 224 (1961).
206. Panish, M. B., "Vaporization of Several Rare Earth Oxides," J. Chem. Phys. 34, 1079 (1961).
207. Panish, M. B., "Vaporization of the Rare Earth Oxides," J. Chem. Phys. 34, 1915 (1961).
208. Panish, M. B., and Reif, L., "Vaporization of Iridium and Rhodium," J. Chem. Phys. 34, 1915 (1961).
209. Porter, R. F., "Stabilities of Gaseous Molecules in the Pb-Te Systems," J. Chem. Phys. 34, 583 (1961).

210. Porter, R. F., "Molecular Association in Sodium Cyanide Vapor," J. Chem. Phys. 35, 318 (1961).
211. Shchukarev, S. A., and Semenov, G. A., Doklady Akad. Nauk. SSSR 141, 652, (1961).
212. Studier, M. H., Sloth, E. N., and Moore, L. P., "The Chemistry of Uranium in Surface Ionization Sources," J. Phys. Chem. 66, 133 (1962). See also Mass Spectrometry Conference, ASTM Committee E-14, Chicago (1961).
213. Studier, M. H., "Gaseous Oxides of Rhenium." J. Phys. Chem. 66, 189 (1962).
214. Tsvetaev, A. A., Glazunov, M. P., Kiselev, V. A., Alekseev, L. A., Chuzhko, R. K., "Activation Energy for Sublimation from Different faces of Zn Monocrystals." Zhurn. Fiz. Khim., 35, 2800 (1961).
215. Verhaegen, G., Stafford, F. E., Ackerman, M., and Drowart, J., Wright Air Development Division, Office of Aerospace Research. Contract AF 61 (062)-225, Scientific Note No. 8 (1962).
216. Walsh, P. N., Dever, D. F., and White, D., "Rare Earths. III. A Mass Spectrometric Investigation of the Isomolecular Oxygen-Exchange Reactions of Lanthanum, Cerium, Praseodymium, and Neodymium with their Monoxides.
217. White, D., Walsh, P. N. Goldstein, H. W., and Dever, D. F., "Rare Earths: II. A Mass Spectrometric Determination of the Heats of Sublimation (or Vaporization) of Neodymium, Praseodymium, Gadolinium, Terbium, Dysprosium, and Neodymium with Their Molecules," J. Phys. Chem. 65, 1405 (1961).
218. White, D., Walsh, P. N., Goldstein, H. W., and Dever, D. F. "The Dissociation Energies of the Gaseous Monoxides of the Rare Earths: Thermodynamic Properties of some Gaseous Oxides," Abstracts, 18th International Congress of Pure and Applied Chemistry, University of Toronto Press (1961) p. 99.
219. White, D., Sommer, A., Walsh, P. N., and Goldstein, H. W., "The Application of The Time-of-Flight Mass Spectrometer to the Study of Inorganic Materials at Elevated Temperatures," Symposium on Mass Spectrometry, Oxford (1961).
220. Akishin, P. A., Gorokhov, L. N., and Khodeev, Yu. S., "Evaporation of Sodium and Lithium Metaborate," Zhurn. Strukt. Khim. 2, 209 (1961).

221. Ryabchikov, L. N., and Tikhinskii, G. F., "Evaporation of Beryllium Chloride," *Fiz. Metall. i Metallov*, 10, 635 (1960).
222. Trulson, O. C., Hudson, D. E., and Spedding, F. H., "Determination of the Heat of Sublimation of Eu, Gd, Ho and Er Using Surface Ionization," *J. Chem. Phys.* 35, 1018 (1961).
- VI. Ion Molecule Reactions
Compiled by J. L. Franklin, Humble Oil and Refining Co., Baytown, Texas
223. Barnes, W. W., Martin, D. W., and McDaniel, E. W., "Mass Spectrographic Identification of the Ion Observed in Hydrogen Mobility Experiments," *Phys. Rev. Letters* 6, 110 (1961).
224. Bates, D. R. and Nicolet, M., "Rate of Ion-Atom Exchange," *J. Atmos. & Terrest. Phys.* 21, 286 (1961).
225. Beynon, J. H., Lester, G. R., Saunders, R. A., and Williams, A. E., "Formation of Ions in Mass Spectrometers by Ion-Molecule Reactions," *Trans. Faraday Soc.* 57, 1259 (1961).
226. Bloch, A., "Mass Spectrum of Ar at an Elevated Pressure in the Ion Beam," *J. Chim Phys.* 58, 289 (1961).
227. Field, F. H., "Reactions of Gaseous Ions. VIII. Multiple Order Ion-Molecule Reactions and the Ultra-High Pressure Mass Spectrum of Ethylene," *J. Am. Chem. Soc.* 83, 1523 (1961).
228. Field, F. H., and Franklin, J. L., "Reactions of Gaseous Ions. X. Ionic Reactions in Xenon-Methane Mixtures," *J. Am. Chem. Soc.* 83, 4509 (1961).
229. Forrestal, L. J., and Hammill, W. H., "Effects of Ionic and Free Radical Processes in the Radiolysis of Organic Liquid Mixtures," *J. Am. Chem. Soc.* 83, 1535 (1961).
230. Franklin, J. L. and Field, F. H., "Reactions of Gaseous Ions. IX. Charge Exchange Reactions of Rare Gas Ions with Ethylene," *J. Am. Chem. Soc.* 83, 3555 (1961).

231. Franzen, J., and Hintenberger, H., "Polyatomic Molecule Ions in a High Frequency Spark between Electrodes of the Elements Be, C, Mg, Ae, Ti, Fe, and Cu," Z. Naturforsch. 16a, 535 (1961).
232. Fuchs, R., "Ion-Molecule Reactions in Paraffins, Olefins, and Acetylene," Z. Naturforsch. 16a, 1026 (1961).
233. Fueno, T., Eyring, H., and Ree, T., "Three-Body Recombination of Gaseous Ions," Can. J. Chem. 38, 1693 (1960).
234. Gatz, C., Smith, F. T., and Wise, H., "Chemi-Ionization in Three Body Gas Phase Reactions," J. Chem. Phys. 35, 1500 (1961).
235. Giese, Clayton F., and Maier, William B., II, "Ion-Molecule Reactions Studied with Mass Analysis of Primary Ion Beam," J. Chem. Phys. 35, 1913 (1961).
236. Gillis, H. A., Williams, R. R., Jr., and Hamill, W. H., "Ionic and Free Radical Processes in the Radiolysis of Liquid Methyl and Ethyl Iodides," J. Am. Chem. Soc. 83, 17 (1961).
237. Hall, R. M. S., " N_2OH Ions from Nitrous Oxide in Mass Spectrometry," Chemistry and Industry 1961, p. 369.
238. Henkes, W., "Ionization and Acceleration of Condensed Molecular Beams," Z. Naturforsch. 16a, 842 (1961).
239. Hertzberg, M., "Ion-Neutral Reactions," J. Atomospheric & Terrest. Phys. 20, 177 (1961).
240. Hertzberg, M., Rapp, D., Ortenburger, I. O., and Briglia, D. D., "Ion-Neutral Reactions in the Helium-Hydrogen System," J. Chem. Phys. 34, 343 (1961).
241. Irsa, A. P., and Friedman, L., "Collision Induced Dissociation of HD^+ ," J. Chem. Phys. 34, 330 (1961).
242. Karachevtsev, G. H., Markin, M. I., and Tal'roze, V. L., "An Investigation of Charge Transfer from the Thermal Ions A^+ , Kr^+ , and Xe^+ to the Molecules CH_4 , C_2H_6 , and C_2H_4 by the Impulse Method," Izvest Akad. Nauk SSSR, Otdel. Khim. Nauk 1961, No. 8, 1528.

243. Kaul, W, Lauterbach, U., and Taubert R., "The Appearance Potentials of HeH^+ , NeH^+ , ArH^+ , KrH^+ , KrD^+ and H_3^+ ," Z. Naturforsch 16a, 624 (1961).
244. King, J. R., "Recombination of Ions in Flames. Effect of Temperature," J. Chem. Phys. 35, 380 (1961).
245. Kondratiev, V. N., and Ptichsin, I. I., "Gas-Phase Interaction Between Carbon Monoxide and Ionized Oxygen," Kinetika & Kataliz, 2, 492 (1961).
246. Kasner, W. H., Rodgers, W. A., and Biondi, M. A., "Electron-Ion Recombination Coefficients in N_2 & O_2 ," Phys. Rev. Letters 7, 321 (1961).
247. Lampe, F. W., Franklin, J. L., and Field, F. H., "Kinetics of the Reactions of Ions with Molecules," Chapter 3 of Progress in Reaction Kinetics. Edited by G. Porter, Pergamon Press, London, 1961.
248. Lavrovskaya, G. K., Maarkin, M. I., & Tal'roze, V. L., "Charge Transfer and Complex Molecules," Kinetika & Kataliz 2, 21 (1961).
249. Libby, W. F., "Chemistry of Positive Ions. I. General Theory Particularly for the Radiation Induced Cross Linkage of Polymers and Polymerization of Saturated Hydrocarbons," J. Chem. Phys. 35, 1714 (1961).
250. Padley, P. J., Page, F. M., and Sugden, T. M., "Effect of Halogen on the Ionization in Alkali-Laden Hydrogen and Acetylene Flames," Trans. Faraday Soc. 57, 1552 (1961).
251. Pratt, T. H., and Wolfgang, R., "The Self Induced Exchange of Tritium Gas with Methane," J. Am. Chem. Soc. 83, 10 (1961).
252. Popescu, I., "Resonant Charge Transfer in Dense Gases," Proc. Phys. Soc. (London) 78, 584 (1961).
253. Smith, C. F., Cornman, B. G., and Lampe, F. W., "Hydrogen Inhibition of the Rare Gas Sensitized Radiolysis of Cyclopropane," J. Am. Chem. Soc. 83, 3559 (1961).
254. Tal'roze, V. L., "Elementary Processes Taking Place Upon Collisions of Slow Ions with Molecules," Izvest. Akad. Nauk SSSR, (Phys Series) 24, 1001 (1960).
255. Von Koch, H., and Lindholm, E., "Dissociation of $\text{C}_2\text{H}_5\text{OH}^+$ Formed in Charge Exchange Collisions with Positive Ions." Arkiv f. Fysik 19, 123 (1961).

256. Wagner, C. D., "Radiolysis of Liquid Propane. Ion-Molecule Condensation," Tetrahedron 14, 164 (1961).

257. Williams, T. F., "Correlation of the Radiation Chemistry of Liquid Hydrocarbons with the Energetics of Molecular-Ion Reactions," Trans. Faraday Soc. 57, 755 (1961).

VIII. Miscellaneous

Compiled by J. Goodings and H. I. Schiff, Department of Chemistry,
McGill University, Montreal, Canada

Solid and Surface Phenomena

258. Moore, G. E., "Dissociation of Adsorbed CO by Slow Electrons," J. Appl. Phys. 32, 1241 (1961).

259. Surplice, N. A., "Emission of Negative Ions of Oxygen from Dispenser Cathodes. I. Cathodes of Barium Oxide in Sintered Nickel," Brit. J. Appl. Physics 12, 214 (1961).

260. Surplice, N. A., "Emission of Negative Ions of Oxygen from Dispenser Cathodes. II Cathodes of Barium Aluminate in Sintered Tungsten," Brit. J. Appl. Phys. 12, 220 (1961).

261. Inguve, H., "Mass Spectrometric Study on Absorption of Water Vapour on a Graphite Surface," Bull. Chem. Soc. Japan 34, 643 (1961).

262. Hannay, N. B., "Mass Spectrographic Analysis of Solids," Science 134, 1220 (1961).

Shock Waves

263. Bradley, J. N., and Kistiakowsky, G. B., "Shock Wave by Mass Spectrometry. I Thermal Decomposition of Nitrous Oxide," J. Chem. Phys. 35, 256 (1961).

264. Bradley, J. N., and Kistiakowsky, G. B., "Shock Wave Studies by Mass Spectrometry. II Polymerization and Oxidation of Acetylene," J. Chem. Phys. 35, 264 (1961).

265. Bradley, J. N., "Shock Wave Decomposition of Nitroparaffins. Part I. Mass Spectrometric Study of Nitromethane Decomposition," Trans. Faraday Soc. 57, 1750 (1961).

Discharges and Plasmas

266. Nastyukha, A. I., Striganov, A. R., Afanas'ev, I. I., Mikhailov, L. N., and Oganov, M. N., "Mass Spectrographic and Spectroscopic Studies of Hydrogen from an Ion Source," *Plasma Phys. - Accelerators - Thermonuclear Res. (English Translation)* 3, 218 (1961).
267. Donahue, T. M., and Hushfar, F., "Formation of Negative Ions in a Gas by Charge Transfer from a Fast Atomic Hydrogen Beam," *Phys. Rev.* 124, 138 (1961).
268. Thompson, J. B., "Electron Energy Distribution in Plasmas. IV Oxygen and Nitrogen," *Proc. Roy. Soc.* A262, 503 (1961).
269. Rose, P. H., Bastide, R. P., and Wittkower, A. B., "High Current Positive Hydrogen Ion Source with Mass Analysis," *Rev. Sci. Instr.* 32, 581 (1961).

Other

270. Reinisch, L., "Radiolysis and Mass Spectrometry," *J. Chem. Phys.* 57, 1064 (1960).
271. Yuasa, T., "Mass Spectrometric Studies of Gaseous Ions. Gaseous Ions of Semi-Conductive, Semi-Metallic and Metallic Elements," *Nippon Kagaku Zasshi*, 81, 1643 (1960).
272. Akishin, P. A., and Khodiev, V. S., "Mass Spectral Determination of the Heats of Sublimation of Uranium Tetrafluoride," *Zhur. Fiz. Chim.* 35, 1169 (1961).
273. Grogerov, I. P., and Turkina, M. J., "Transformation of Phenyl Radicals in Solution, as Investigated by the Isotopic and Mass Spectrometric Method," *Doklady Akad. Nauk., SSSR* 140, 1317 (1961).

Bibliography of High Molecular Weight Mass Spectrometry

Prepared by Subcommittee III

June 1962

1. Aczel, T., and H. E. Lumpkin, "Correlations of Mass Spectra with Structure in Aromatic Oxygenated Compounds, Methyl Substituted Aromatic Acids and Aldehydes", Anal. Chem. 33, 387 (1961).
2. Ardenne, M. von, K. Steinfelder, and R. Tummeler, "Electron Addition Mass Spectrometric Determination of the Number of Carbon Atoms in Oxygenated Molecules from the Ratio C^{13}/C^{12} ", Naturwissenschaften 47, 492 (1960).
3. Ardenne, M. von, K. Steinfelder, and R. Tummles, "Electron Addition Mass Spectrograms of Condensed Aromatic Hydrocarbons", Agnew. Chem. 73, 136 (1961)
4. Bergstroem, S., R. Ryhage, and E. Stenhagen, "Mass Spectrometric Studies on Sterols and Bile Acids", Svensk. Kem. Tidskr. 73, 566 (1961).
5. Beynon, J. H., R. A. Saunders, A. Topham, and A. E. Williams, "Fragmentation of Long-chain Paraffins Under Electron Bombardment Using Isotopically Labeled Compounds", J. Phys. Chem. 65, 114 (1961).
6. Biemann, K., "Determination of the Carbon Skeleton of Sarpagine by Mass Spectrometry", Tetrahedron Letters 1960, 9.
7. Biemann, K., "Application of Mass Spectrometry to Structure Problems. Carbon Skeleton of Sarpagine", J. Am. Chem. Soc. 83, 4801 (1961).
8. Biemann, K., and G. G. J. Deffner, "Determination of N^{15} in Amino Acid Mixtures Without Separation into Individual Components Biochem. and Biophys. Research Commun. 4, 283 (1961).

9. Biemann, K., G. G. J. Deffner, and F. C. Steward, "Determination by Mass Spectrometry of the Structure of Proline Derivatives from Apples", *Nature* 191, 380 (1961).
10. Biemann, K., and M. Friedmann-Spiteller, "Application of Mass Spectrometry to Structure Problems. Iboga Alkaloids", *J. Am. Chem. Soc.* 83, 4805 (1961).
11. Biemann, K., and M. Friedmann-Spiteller, "Mass Spectrometric Evidence for the Structure of Iboxygaine and Its Tosylate", *Tetrahedron Letters* 1961, 68.
12. Biemann, K., M. Friedmann-Spiteller, and G. Spiteller, "Investigation by Mass Spectrometry of the Alkaloids of *Aspidosperma Quebrachoblanco*", *Tetrahedron Letters* 1961, 485.
13. Biemann, K., C. Lioret, J. Asselineau, E. Lederer, and J. Polonsky, "Structure of Lysopine, a New Amino-Acid Isolated from Crown Gall Tissue", *Biochim. et Biophys. Acta* 40, 369 (1960).
14. Biemann, K., and G. Spiteller, "Structure of Quebrach Amine", *Tetrahedron Letters* 1961, 299.
15. Biemann, K., J. Seibl, and F. Gapp, "Mass Spectra of Organic Molecules. I. Ethyl Esters of Amino Acids", *J. Am. Chem. Soc.* 83, 3795 (1961).
16. Bray, E. E., and E. D. Evans, "Distribution of n-Paraffins as a Clue to the Recognition of Source Beds", *Geochim. et Cosmochim. Acta* 22, 2 (1961).
17. Clerc, R. J., and M. J. O'Neal, "Mass Spectrometric Analysis of Asphalt. A Preliminary Investigation", *Anal. Chem.* 33, 380 (1961).
18. Cousins, L. R., D. J. Clancy, and G. F. Crable, "Dehydrogenation as an Aid to the Mass Spectrometric Analysis of Naphthenes", *Anal. Chem.* 33, 1875 (1961).

19. Dink-Nguyen, N., and R. Ryhage, "A Mass Spectrometric Demonstration of Hydrogen-Deuterium Exchange and Hydrogen Redistribution During Catalytic Deuteration of Some Methyl Octadecenoates", J. Research Inst. Catalysis, Hokkaido Univ. 8, 73 (1960).
20. Djerassi, C., B. Gilert, J. N. Shoolery, L. F. Johnston, and K. Biemann, "Alkaloid Studies. XXVI. The Constitution of Pyrrolidine", Experientia 17, 162 (1961).
21. Flinn, R. A., and O. A. Larson, "Effects of Hydrogenation and Catalytic Cracking on Various Molecular Types in Middle Distillates", Preprints, Am. Chem. Soc., Div. Petrol. Chem. 5, No. 3, 19 (1960).
22. Fritz, G., H. Buhl, J. Grobe, F. Aulinger, and W. Reering, "Mass Spectrometric Investigation of Si-Methylene Compounds", Z. Anorg. U. Allgem. Chem. 312, 201 (1961).
23. Gur'eu, M. V., "Mass Spectra and Primary Processes in the Radiation Chemistry of Paraffins", Doklady Akad. Nauk S.S.S.R. 136, 856 (1961).
24. Heyns, K., and H. F. Gruetzmacker, "Mass Spectra of N-Formyl- α -Amino Acid Methyl Esters", Z. Naturforsch. 16B, 293 (1961).
25. Hirt, C. A., "Analysis of Multicomponent Methyl- and Phenyl-chlorosilane Solutions", Anal. Chem. 33, 1786 (1961).
26. Hoene, J. von, and W. M. Hickam, "Electron Attachment in $C_8F_{16}O$ ", J. Chem. Phys. 32, 876 (1960).
27. Holden, H. W., and J. C. Robb, "A Study of Coal by Mass Spectrometry", Fuel 39, 39 (1960).
28. Levy, E. J., R. R. Doyle, R. A. Brown, and F. W. Melpolder, "Identification of Components in Paraffin Wax by High Temperature Gas Chromatography and Mass Spectrometry", Anal. Chem. 33, 698 (1961).

29. Levy, E. J., and W. A. Stahl, "Mass Spectra of Aliphatic Thiols and Sulfides", Anal. Chem. 33, 707 (1961).
30. Lumpkin, H. E., and G. R. Taylor, "A Solids Inlet System for a Mass Spectrometer", Anal. Chem. 33, 476 (1961).
31. Majer, J. R., "Mass Spectra of Cyclic Fluorine Compounds", J. Appl. Chem. 11, 141 (1961).
32. Margrave, J. L., "Ionization Potentials of B₅H₉, B₅H₈I, B₁₀H₁₄, and B₁₀H₁₃C₂H₅ from Electron Impact Studies", J. Chem. Phys. 32, 1889 (1960).
33. Mead, W. L., and A. J. Wilde, "Mass Spectrum of Vanadyl Etioporphyrin", Chem. and Ind. 1961, 1315.
34. Miller, G. H., and G. O. Pritchard, "Mass Spectra of Pentafluoropropanal and Heptafluorobutanal", Chem. and Ind. 1961, 1314.
35. Nagy, B., and G. C. Gagnon, "Geochemistry of the Athabasca Petroleum Deposit", Geochim. et Cosmochim. Acta 23, 155, (1961).
36. Natalis, P., "Behavior of C₃-8-Cycloalkanes and C₄-6-Perfluorocycloalkanes Under the Impact of Electrons", Bull. Soc. Roy. Sci. Liege 29, 94 (1960).
37. Park, R., and H. N. Dunning, "Stable C Isotope Studies of Crude Oils and Their Porphyrin Aggregates", Geochim. et Cosmochim. Acta 22, 99 (1961).
38. Ryhage, R., S. Stallberg-Stenhagen and E. Stenhagen, "Mass Spectrometric Studies. VII. Methyl Esters of α , β - Unsaturated Long Chain Acids. Structure of C₂₇ Phthienoic Acid", Arkiv. Keml 18, 179 (1961).
39. Ryhage, R., and E. Stenhagen, "Mass Spectrometry in Lipid Research", J. Lipid Research 1, 361 (1960).

40. Ryhage, R., and E. Stenhagen, "Mass Spectrometric Studies. IV. Esters of Monomethyl - Substituted Long Chain Carboxylic Acids", Arkiv. Kemi. 15, 291 (1960).
41. Shapiro, I., and H. Landesman, "Fragmentation Patterns of Halogenated Pentaboranes", J. Chem. Phys. 33, 1590 (1960).
42. Sharkey, A. G., J. L. Schultz, and R. A. Friedel, "Comparison of the Mass Spectra of Extracts and Vacuum Pyrolysis Products from Coal", Fuel 40, 423 (1961).
43. Stenhagen, E., "Mass Spectrometry in Determination of Structure of Organic Compounds, Especially Lipids and Peptides", Z. Anal. Chemie 181, 462 (1961).
44. Trent, F. M., F. D. Miller, and G. H. Brown, "Mass Spectrometry of Some High Molecular Weight Aliphatic Acids and Their Methyl Esters. Analysis of Nonanoic and 2-Ethylheptanoic Acid Mixtures", Appl. Spect. 15, 64 (1961).
45. Zimina, K. I., A. A. Polyakova, R. A. Khmel'nitskii, and R. D. Obelentsev, "Mass Spectrometric Study of Some Thiophane Homologs", Zhur. Obschei Khim. 30, 1264 (1960).

BIBLIOGRAPHY of published and unpublished material pertaining to
new instruments and techniques in mass spectrometry for 1961.

Prepared by Subcommittee V
ASTM Committee E-14

1. Ahearn, A. J., "Mass Spectrographic Studies of Impurities on Surfaces," Nat'l Symposium on Vacuum Technology 6, 1-5 (1959).
2. Ahearn, A. J., "Mass Spectrographic Analysis of Insulators using a Vacuum Spark Positive Ion Source," J. Appl. Phys. 32, No. 7, 1195-1196 (1961).
3. Ahearn, A. J., "Mass Spectrographic Detection of Impurities in Liquids," J. Appl. Phys. 32, No. 7, 1197-1201 (1961).
4. Akishin, P. A., Gorokhov, L. N., Nikitin, O. Ti, and Khodeev, Yu. S., "Mass Spectrometer for Vaporization Study of Slightly Volatile Substances," Priory i Tekh. Eksperimenta, No. 4, 98-102 (1960).
5. Akishin, P. A., Gorokhov, L. N., and Sidorov, L. N., "Mass Spectrometric Study of Sodium Chloride and Lithium Fluoride, Using a Double Effusion Chamber," Zhur. Fiz. Khim., 33, 2822-3 (1959).
6. Alekseevskii, N. E., Dubrovin, A. V., Kosourov, G. I., Prudkovskii, G. P., Filimonov, S. E., Chekin, V. I., Shelyapin, V. N., and Shuvalova, T. K., "Inhomogeneous-Field Mass Spectrometer for Analysis of Light-Element Isotopes," Proc. All-Union Sci. Tech. Conf. Appl. Radioactive Isotopes, Moscow, 73-77 (1957).
7. Anbar, M. and Guttman, S., "The Isotopic Exchange of Oxygen Between Iodate Ions and Water," J. Amer. Chem. Soc., 83, 781-783 (1961).
8. Ardenne, M. von, Developments in the Electron-Accumulating Mass Spectrometry of Polyatomic Molecules," Trans. No. MCL-818 of Zeitschrift Fur Angewandte Physik 11, 121-131, (1959).
9. Ardenne, M. V., Seinfeld, K., and Tummler, R., "Mass-Spectrograms of Condensed Aromatic Hydrocarbons, Using Electron Addition," Angew. Chem. 73, 136-42 (1961).
10. Ausloos, P. and Rebbert, R. E., "Intramolecular Rearrangements. III. Formation of 1-Methylcyclobutanol in the Photolysis of 2-Pentanone," J. Amer. Chem. Soc. 83, 4897-4899 (1961).
11. Eader, Michel, Witteborn, Fred C., and Snouse, Thomas W., "Sputtering of Metals by Mass-Analyzed N_2^+ and N^+ ," NASA Tech. Report R-105 (1961).
12. Bafus, D. A. and Brown, T. L., "The Mass Spectrum of Ethyllithium Vapor," J. Phys. Chem., 65-8, 1380-1383.
13. Bainbridge, K. T. and Moreland, P. E. Jr., "The Mass spectrometer at Harvard University," (Contract NONR-186619) Lyman Lab. of Physics, Harvard U., Cambridge, Mass., April 1961.
14. Bakhtin, V. I., and Mikhailin, V. N., "Autocompensated Thermovacuum Meter," Izmeritel'naya Tekh. No. 9, 25-26 (1960).
15. Barnes, W. S., Martin, D. W., and McDaniel, E. W., "Mass Spectrographic Identification of the Ion Observed in Hydrogen Mobility Experiments," Reprint from Phys. Rev. Letters, 6, 110-111 (1961).
16. Beckey, H. D., "Mass Spectrometric Investigation by Means of a Field-Emission Ion Source of Ion-Molecule Reactions and of the Association of Water," Z. Naturforsch., 15a, 822-7 (1960).
17. Begun, G. M. and Landau, L., "Mass Spectra and Metastable Transitions in Isotopic Nitrous Oxides," J. Chem. Phys. 35, 547-551 (1961).
18. Belyakov, Yu. I. and Agishev, E. I., "Application of the Pulse Mass Spectroscope to the Investigation of Gas Evolution from Metals," Zhur. Tekh. Fiz. 29, 796-8 (1959).

19. Benson, B. B. and Parker, P. D. M., Relations Among the Solubilities of Nitrogen, Argon, and Oxygen in Distilled Water and Sea Water," J. Phys. Chem., 65-9, 1489-1496.
20. Bernecker, R. R. and Long, F. A., "Heats of Formation of Some Organic Positive Ions and Their Parent Radicals and Molecules," J. Phys. Chem. 65-9, 1565-1569.
21. Betts, J. F., Fluegge, R. A., O'Halloran, G. J., Narcisi, R. S., "Development of a Balloon-Borne Time-of-Flight Mass Spectrometer," A.S.T.M., Ninth Annual Meeting of Committee E-14, Chicago, Ill., June 4-9, 1961.
22. Bidinosti, D. R. and Porter, R. F., "Mass Spectrometric Studies of Low Pressure Pyrolysis Reactions of Chlorinated and Fluorinated C₁ and C₂ Compounds on Graphite," J. Amer. Chem. Soc., 83, 3737-3743 (1961).
23. Biemann, K., Seibl, J., and Gapp, F., "Mass Spectra of Organic Molecules. I. Ethyl Esters of Amino Acids," J. Amer. Chem. Soc. 83, 3795-3804 (1961).
24. Biemann, K., "Application of Mass Spectrometry to Structure Problems. IV. The Carbon Skeleton of Sarpagine," J. Amer. Chem. Soc., 83, 4801-05 (1961).
25. Biemann, K. and Friedmann-Spitteller, Margot, "Application of Mass Spectrometry to Structure Problems. V. Iboga Alkaloids," J. Amer. Chem. Soc., 83, 4805-10 (1961).
26. Bloch, A., "The Mass Spectrum of Argon at Elevated Pressures in the Ion Source," J. de Chimie Physique 58, 289-91 (1961).
27. Bonnet, Mlle., "Mass Spectrometer for Light Elements," Vide 16, 134-40 (1961).
28. Bradley, J. N. and Kistiakowsky, G. B., "Shock Wave Studies by Mass Spectrometry. I. Thermal Decomposition of Nitrous Oxide," J. Chem. Phys. 35, 256-263 (1961).
29. Bradley, J. N. and Kistiakowsky, G. B., "Shock Wave Studies by Mass Spectrometry. II. Polymerization and Oxidation of Acetylene," J. Chem. Phys. 35, 264-70 (1961).
30. Brown, T. L., Berkowitz, Jr., and Bafus, D. A., "The Mass Spectrum of Ethyl-Lithium Vapor," Contract AF 49 (638) 466 (U. of Illinois in coop. with Argonne Nat'l Labs, Jan. 1961), (AFOSR-220).
31. Bunt, E. A., "Mass Analysis of Flames and Flue Gases," Symposium on Combustion, 7th, London and Oxford, 1958, 325-31 (1959).
32. Burt, R. B., Colligon, J. S., and Leck, J. H., "Sorption and Replacement of Ionized Noble Gases at a Tungsten Surface," British J. of Appl. Phys. 12, 396-400, (1961).
33. Busch, F. V. and Paul, W., "Isotope Separation by the Electrical Mass Filter," Zeitschr. F. Physik, 164, 581-7 (1961).
34. Busch, F. V. and Paul, W., "Non-Linear Resonances in the Electrical Mass Filter due to Irregularities of the Field Distribution," Zeitschr. F. Physik, 164, 588 (1961).
35. Campbell, B. L. and Whitten, K. N., "Isotopic Discrimination Introduced by Electron Multiplier Detection in Mass Spectrometry," Jour. of Sci. Instr. 38, 516, (1961).
36. Cathey, LeConte, "Electron Multiplier as a Detector for a Surface Ionization Mass Spectrometer, Design," U.S. At. Energy Comm. DP-498, 18 pp. (1960).
37. Charles, D., and Warnecke, R. J., Jr., "Experimental Study of an Omegatron-Type Mass Spectrometer," Nat'l Symposium on Vacuum Technol. 6, 34-41 (1959).
38. Chupka, W. A. and Kaminsky, M., "Energy Distribution and Fragmentation Processes Resulting from Electron Impact of Propane and n-Butane," J. Chem. Phys. 35, 1991-1998 (1961).
39. Colin, R., "Measures of Thermodynamic Values by Mass Spectrometer. Study of Sulfur and Zinc," AD-257, 163, Div. 25.17 (1961), Aerospace Tech. Intell. Center, Wright-Patterson AFB, Ohio

40. Colin, R., "Measurement of the Relative Ionization Cross-Sections of Zn, Te, and Te₂, and of the Dissociation Energy of Te by Mass Spectrometry," AD-257-713, Div. 25, Aerospace Tech.Intell. Center, Wright Patterson AFB, Ohio.
41. Cook, G. L., Meyer, R. A., and Earnshaw, D. G., "Dual-Inlet System for a Mass Spectrometer," U.S. Bur. Mines, Rept. Invest. No. 5663, 8 pp. (1960).
42. Cornides, I., Kakuszi, M., Pasztóhy, E., "Mass Spectrometric Investigation of Residual Gases," Ann. Irinyi Tech. School of Chem., 2, 55-63 (1961).
43. Curran, R. K., "Low-Energy Processes for F⁻ Formation in SF₆," J. Chem. Phys. 34, 1069, (1961).
44. Curran, R. K. and Fox, R. E., "Mass Spectrometer Investigation of Ionization of N₂O by Electron Impact," J. Chem. Phys. 34, 1590-1594 (1961).
45. Curran, R. K., "Positive and Negative Ion Formation in CCl₃F," J. Chem. Phys. 34, 2007-10 (1961).
46. Curran, R. K., "Negative Ion Formation in Ozone," J. Chem. Phys. 35, 1849-1851 (1961).
47. Cuthbert, J., "Modifications to an M.S. 2 Mass Spectrometer," J. Sci. Instr., 38, 337 (1961).
48. Daly, N. R., "High Sensitivity Mass Spectrometer Leak Detector," Rev. Sci. Instr. 30, 1093-1095 (1959).
49. Dibeler, V. H., Reese, R. M., and Franklin, J. L., "Mass Spectrometric Study of Cyanogen and Cyanoacetylenes," J. Amer. Chem. Soc., 83, 1813-1817 (1961).
50. Donahue, T. M. and Hushfar, Farid, "Formation of Negative Ions in a Gas by Charge Transfer from a Fast Atomic Hydrogen Beam," Contract DA-36-034-ORD-2912 and NONR-63406, Rept. No. 15, Univ. of Pittsburgh, Unclassified (1961).
51. Dorman, F. H. and Morrison, J. D., "Determination of Relative Electronic Transition Probabilities by Impact Methods," J. Chem. Phys. 34, 578-582 (1961).
52. Dorman, F. H. and Morrison, J. D., "Ionization Potentials of Multiply Charged Krypton, Xenon, and Mercury," J. Chem. Phys. 34, 1407-1410 (1961).
53. Dorman, F. H. and Morrison, J. D., "Double and Triple Ionization in Molecules Induced by Electron Impact," J. Chem. Phys. 35, 575-581 (1961).
54. Doucette, E. I., "Materials for and the Mechanism of Gettering Multiple Component Gases," Ronson Metals Corp, Newark, N. J., Contract AF 19 (604) 8430 (AFCRL-578).
55. Eberhardt, P., "Trochoidal Mass Spectrometer for Small Amounts of Rare Gases," Helv. Phys. Acta. 33, 588-590 (1960).
56. Ehlbeck, H. W., Ruf, J., Schuetze, H. J., "Rapid Scanning R-F Mass Spectrometer," Telefunken, Ulm (Donau), Germany, unpublished material.
57. Ehlbeck, H. W., Loecherev, K. H., Ruf, J., Schuetze, H. J., "The Operation of the R.F. Mass Spectrometer at High r.f. Voltage Levels," Seventh Nat'l Symposium on Vacuum Technology Transaction (1960).
58. Elbert, A. A. Jr., "Use of a Getter-Ion Type Pump with a Mass Spectrometer," Applied Spectroscopy 15, 152 (1961).
59. Eliel, E. L., McCollum, J. D., Meyerson, S., and Rylander, P., "Organic Ions in the Gas Phase. IX. Dissociation of Benzyl Alcohol by Electron Impact," J. Amer. Chem. Soc. 83, 2481-2484 (1961).
60. Ewald, Heinz, "Mass Spectrograph for the Analysis of Particles of High Kinetic Energy," Proc. Intern. Conf. Nuclidic Masses, Hamilton, Ontario, Canada, 491-7.
61. Eyring, E. M. and Wahrhaftig, A. L., "Dependence of Calculated and Experimental Propane Mass Spectra upon Electron Voltage," J. Chem. Phys. 34, 23-28 (1961).

62. Ferguson, L. A., "The Determination of Hydrogen in Uranium by Mass Spectrometry," Nuclear Science and Eng., May 1961.
63. Field, F. H. and Franklin, J. L., "Reactions of Gaseous Ions. X. Ionic Reactions in Xenon-Methane Mixtures," J. Amer. Chem. Soc. 83, 4509-4515 (1961).
64. Field, F. H., "Reactions of Gaseous Ions. VIII. Multiple Order Ion-Molecule Reactions and the Ultra-High Pressure Mass Spectrum of Ethylene," J. Amer. Chem. Soc., 83, 1523-1534 (1961).
65. Fiks, V. B. and Pikus, G. E., "The Analysis of Trace Impurities by the Magnetic Resonance Mass Spectrometer," Fiz. Tverdago Tela 2, 716-727 (1960).
66. Florescu, N. A., "New Thermionic Ionization Gage," Vide 16, 10-17 (1961).
67. Flournoy, J. M. and Wilmarth, W. K., "The Base Catalyzed Exchange of Hydrogen Gas and Protonic Solvents. III. The Catalytic Efficiency of Concentrated Aqueous Alkali," J. Amer. Chem. Soc., 83, 2257-2262 (1961).
68. Fluegge, R. A., "The Use of the Spark Source-Time-of-Flight Mass Spectrometer," Ninth Annual Meeting of Committee E-14, A.S.T.A., Chicago, Ill., June 4-9, 1961.
69. Fogen', Ya. M., Koval', A. G., Leuchenko, Yu. Z., "Formation of Slow Negative Ions in Single Collisions between Fast Negative Hydrogen and Oxygen Ions and Gas Molecules," JETP (USSR) 40, 13-22 (1961); JETP 13, 8-14, (1961).
70. Forrestal, L. J. and Hamill, W. H., "Effects of Ionic and Free Radical Processes in the Radiolysis of Organic Liquid Mixtures," J. Amer. Chem. Soc. 83, 1535-1541 (1961).
71. Fox, R. E. and Curran, R. K., "Ionization Processes in CCl_4 and SF_6 by Electron Beams," J. Chem. Phys. 34, 1595-1601 (1961).
72. Fox, R. E., "Ionization Cross Sections Near Threshold by Electron Impact," J. Chem. Phys., 35, 1379-1382 (1961).
73. Fridirkhov, S. A., "Vacuum Gage for an Ultrahigh Vacuum," Nauch.-Tekh. Inform. Byull. Leningrad. Politekh. Inst. No. 1, 45-49 (1959).
74. Fristrom, R. M., Grunfelder, C., and Favin, S., "Methane-Oxygen Flame Structure. III. Characteristic Profiles and Matter and Energy Conservation in a One-Twentieth Atmosphere Flame," J. Phys. Chem., 65-4, 580-601.
75. Frost, D. C. and McDowell, C. A., "The Determination of Ionization and Dissociation Potentials of Molecules by Radiation of Electrons," Contracts AF-19 (604) 2275, Proj. 7635, Univ. of British Columbia, Canada (1960).
76. Putrell, J. H., "Use of Mass Spectral Data in Radiation Chemistry," J. Chem. Phys., 35, 353-356 (1961).
77. Gabor, D., "A New Thermionic Generator," Nature 189, 868-872 (1961).
78. Gallegos, E. and Kiser, R. W., "Electron Impact Spectroscopy of Ethylene Sulfide and Ethylenimine," J. Phys. Chem., 65-7, 1177-1182.
79. Gallegos, E. J. and Kiser, R. W., "Electron Impact Spectroscopy of Ethylene Oxide and Propylene Oxide," J. Amer. Chem. Soc. 83, 773-777 (1961).
80. Gatz, C. R., Rosser, W. A., Smith, F. T., "Study of Radar Beam Attenuation in Rocket Exhaust Gases. Part 2. The Chemistry of Ionization in Rocket Exhausts," Contract AF-04 (647) 221 AFPM Tr. 61-39 Pt. 2 (1961).
81. Genge, C. A., "Innovations in Heated Inlet System for Mass Spectrometer," Anal. Chem. 31, 1747-1748 (1959).
82. Ghosh, S. N. and Srivastava, B. N., "Sensitivity of UG-1A Ionization Gauge Calculated from the Probability of Ionization of Gases," Can. J. of Phys. 39 (2), 1961.
83. Giedd, G. K. and Roberts, G. C., "Emission Control for the Omegatron-type Mass Spectrometer," J. Sci. Instr. 38, 361-362 (1961).

84. Giese, C. F. and Maier, W. B.II, "Ion-Molecule Reactions Studied with Mass Analysis of Primary Ion Beam," Jr. Chem. Phys. 35, 1913-1914 (1961).
85. Goldstein, H. W., Walsh, P. N., White, D., "Rare Earths. II. Vaporization of La_2O_3 and Nd_2O_3 : Dissociation Energies of Gaseous LaO and NdO ," J. Phys. Chem. 65-8, 1401-1404.
86. Grimley, R. T., Burns, R. P., and Inghram, M. G., "Thermodynamics of the Vaporization of Nickel Oxide," J. Chem. Phys. 35, 551-554 (1961).
87. Grimley, R. T., Burns, R. P., and Inghram, M. G., "Thermodynamics of the Vaporization of Cr_2O_3 : Dissociation Energies of CrO , CrO_2 , and CrO_3 ," J. Chem. Phys. 34, 664-667 (1961)
88. Halloran, G. J., "A Rapid Response Mass Spectrometer for Respiratory Function Analysis," Paper presented at the clinic on Instrumentation Requirements for Psychophysiological Research held at Lafayette Clinic, Detroit, Mich., May 16-17, 1961.
89. Harrison, A. G., Kebarle, P., Lossing, F. P., "Free Radicals by Mass Spectrometry. XXI. The Ionization Potentials of Some Meta- and Para-Substituted Benzyl Radicals," J. Amer. Chem. Soc., 83, 777-780 (1961).
90. Harvey, C. E. and Mellichamp, J. W., "Spectrochemical Detection of Nonmetallic Elements," Contract DA 36-039-SC-78267, In coop. with Army Signal Res. and Devel. Lab., Fort Monmouth, N. J. (1961).
91. Herlan, Albert, "Evaluation of Mass-Spectrometric Analyses by Using a Digital Computer," Z. anal. Chem. 180, 321-330 (1961).
92. Herron, J. T. and Dibeler, V. H., "Mass Spectrometric Study of NF_2 , NF_3 , N_2F_2 , and N_2F_4 ," Jour. of Research, Nat'l Bureau of Standards, 65a, Sept-Oct. 1961, 405-409.
93. Herron, J. T., "Rate of the Reaction $\text{NO} + \text{N}$ and Some Heterogeneous Reactions Observed in the Ion Source of a Mass Spectrometer," Jour. of Research, Nat'l Bureau of Standards, 65a, Sept.-Oct. 1961, 411-413.
94. Hertzberg, M., Rapp, D., Ortenburger, I. B., and Briglia, D. D., "Ion-Neutral Reactions in the Helium-Hydrogen System," J. Chem. Phys. 34, 343- 344 (1961).
95. Hirota, K, Nagoshi, K., Hatada, M., "Studies on Mass Spectra and Appearance Potentials of Acetic and Deuteroacetic Acid, CD_3COOH ," Bull. Chem. Soc., Japan, 34, 226 (1961).
96. Hobrock, B. G. and Kiser, R. W., "Electron Impact Spectroscopy of Tetra Methyl Silicon - Tin and Lead -," J. Phys. Chem. 65-12, 2186-2189.
97. Hoering, T. C. and Parker, P. L., "The Geochemistry of the Stable Isotopes of Chlorine," Geochim. et Cosmochim. Acta, 23, 186 (1961).
98. Holroyd, R. A., "Radiation Chemistry of Neopentane," J. Phys. Chem., 65-8, 1352-1357.
99. Honig, R. E., "Ultra-High Vacuum Studies with a Small Bakeable Mass Spectrometer," Nat'l Symposium on Vacuum Technol. 6, 20-26 (1959).
100. Ingalls, R. B., "Hydrogen Formation in the Radiolysis of Toluene," J. Phys. Chem. 65-9, 1605-1608.
101. Inghram, Mark G., "Thermodynamics of Refractory Materials as Determined with a Mass Spectrometer," Univ. of Chicago, Ill., Proj. TB2-0001 (1543) (Contract DA 11-022-ORD-1993).
102. Inouye, H., "Mass Spectrometric Study on Adsorption of Water Vapor," Bull. Chem. Soc., Japan, 34, 643 (1961).
103. Irsa, A. P. and Friedman, L., "Collision-Induced Dissociation of HD ," J. Chem. Phys. 34, 330-331 (1961).

104. Istomin, V. G., "Mass-Spectrometric Measurements of the Ionic Composition of the Upper Atmosphere by the Third Artificial Earth Satellite," *Doklady Akad. Nauk. S.S.S.R.* 129, 81-84 (1959).
105. Istomin, V. G., "Radio-Frequency Mass Spectrometer for the Investigation of the Ionic Composition of the Upper Atmosphere." *Trans. from Iskusstvennyye Sputniki Zemli (Artificial Earth Satellites, Ac. of Sci., U.S.S.R.)* Jan. 1961.
106. Istomin, V. G., "Variation in the Positive Ion Concentration with Altitude from Data of Mass Spectrometry on the Third Satellite," *Planetary & Space Sci.*, 8, Dec. 1961, Pergamon Press.
107. Janatka, Miroslav, and Urgosik, Bohus, "Analysis of Residual Gases in Vacuum System by Means of the Omegatron," *Ceskolov. Casopis fys.* 10, 461-464 (1960).
108. Kanomata, I., Kaneko, Y., Oguri, T., "Mass Spectrometer for Appearance Potential Study," *Oyo Butsuri (Jour. of Applied Physics, Japan)*, 30, 502 (1961).
109. Karmohapatro, S. B., "Two-Directional, Focusing, High-Intensity Mass-Spectrometer," *Indian J. Phys.* 34, 407-415 (1960).
110. Kauder, L. N., Spindel, W., Monse, E. U., "Fractionation of Oxygen Isotopes by the Distillation of Azeotropic Solutions," *J. Phys. Chem.* 65-8, 1435-1438.
111. Kenezovic, Z. V., "Mass Spectrometric Determination of the Self-Diffusion Coefficient of Boron Trifluoride," *Bull. of the Institute of Nuclear Sciences, "Boris Kidrich,"* 11, 141-144, (1961).
112. Ridley, K. G. and Silver, D. E. P., "Mass Spectrometer for the Isotopic Analysis of Lithium," *Jour. Sci. Instr.* 38, 1961, 47-51.
113. Kirchner, Fritz, "Geiger Counters for Achieving High Sensitivity and Fast Readings in Mass Spectroscopic Investigation," *Z. angew. Phys.* 13, 53-6 (1961).
114. Kiser, R. W. and Hisatsune, I. C., "Electron Impact Spectroscopy of Nitrogen Dioxide," *J. Phys. Chem.* 65-8, 1445-1446.
115. Klopfer, A. and Schmidt, W., "Omegatron Mass Spectrometer and Its Characteristics," *Vacuum* 10, 363-372 (1960).
116. Klopfer, A. and Schmidt, W., "An Omegatron for the Quantitative Analysis of Gases," *Phillips Tech. Rev.* 22, 195-203 (1961).
117. Knox, B. E. and Palmer, H. B., "Bond Dissociation Energies in Small Hydrocarbon Molecules," *Chemical Review* 61, 247-255 (1961).
118. Kohler, R., Paul, W., Schmidt, K., and von Zahn, U., "Preliminary Report on a Quadrupole Spectrometer of High Resolution," *Proc. Intern. Conf. Nuclidic Masses, Hamilton, Ont., Can.*, 507-13.
119. Kokubu, N., Mayeda, I., Urey, H. C., "Deuterium Content of Minerals, Rocks, and Liquid Inclusion from Rocks," *Geochim. et Cosmochim. Acta.*, 21, 247 (1961).
120. Konig, L. A., "Influence of Second-Order Aberrations on the Line Shape in Mass Spectrometers with First-Order Double Focusing," *Proc. Intern. Conf. Nuclidic Masses, Hamilton, Ont., Can.*, 498-506.
121. Kubose, Don A., and Hamill, William H., "Mass-Dependent Ion Collection Efficiencies in a Mass Spectrometer," *J. Phys. Chem.* 65, 183-184, (1961).
122. Kuchkov, E. M., "The Shape of the Mass Spectrum Lines and the Role of the Pulse Ion Source in the Radio-Frequency Mass Spectrometer," *Zhur. Tekh. Fiz.* 30, 568-572 (1960).
123. Kupriyanov, S. E., "Adaptation of the MS-1 Mass Spectrometer for Analysis of Inert Gases and Determination of Small Amounts of Impurities," *Trudy, Postoyan. Mezhist. Kollok. po Tverd. Fazam Peremennogo Sostava, Fiz.-Khim. Inst. im L. Ua. Karpova* 1957-8, No. 8-30, 104-7 (Pub. 1959).
124. Lafferty, J. M., "Hot-Cathode Magnetron Ionization Gage for the Measurement of Ultrahigh Vacuums," *J. Appl. Phys.* 32, 424-434 (1961).

125. Landahl, Charles E. and Merryman, Roy G., "Modifications to CEC 21-620 Mass Spectrometer for Increased Sensitivity," U.S. At. Energy Comm. LAMS-2491 (1961).
126. Levina L. E., "Possible Use of Mass Spectrometry to Study the Thermodynamics of Evaporation," Zhur. Fiz. Khim. 34, 456-459 (1960).
127. Linner, L. R., George, R. I., and McQuistan, R. B., "Automatic Vacuum Control in the $760\text{-}1\times 10^{-8}$ mm Range," Rev. Sci. Str. 31, 650-652 (1960).
128. Locherer, K. H., "Non-Linear Theory for the High Frequency, Redhead type, Mass Spectrometer," Vakuum Technik, Sept. 6, 1961, Rudolf A. Lang, Verlag, Berlin-Charlottenburg, 2.
129. Lumpkin, H. E. and Taylor, G. R., "Solids Inlet Systems for a Mass Spectrometer," Anal. Chem. 33, 476-7 (1961).
130. Lynn, K. R. and Yankwich, P. E., "Cyanide Carbon Isotope Fractionation in the Reaction of Cyanide Ion and Methyl Iodide. Carbon Isotope Effect in the Hydrolysis of Methyl Iodide," J. Amer. Chem. Soc. 83, 53-57 (1961).
131. McDaniel, E. W. and Martin, D. W., "Mobility and Clustering of Negative Ions and Mass Spectrographic Study of Ion-Molecule Reactions Occurring at Thermal Energies Under Gas Kinetic Conditions," Georgia Inst. of Tech., Eng. Exper. Sta., Atlanta, Ga., Final summary report, Mar. 31, 1961.
132. McMullen, C. C., Cragg, C. B., Thode, H. G., "Absolute Ratio of B^{11}/B^{10} in Seearles Lake Borax," Geochim. et Cosmochim. Acta. 23, 147 (1961).
133. Maass, I., The Exchange of O-18 between water and glass," Kernenergie 3, 843-6, 1960.
134. Margrave, J. L., "High Temperature and Plasma Chemistry," Chem. Engin. 68, 168-172 (1961).
135. Marshall, R. R. and Hess, D. C., "Lead from Troilite of the Toluca Iron Meteorite," Geochim. et Cosmochim. Acts 21, 161 (1961).
136. Martynkevich, G. M., "Mass Spectra and Structure of Metal Vapors," Izvest. Akad. Nauk S.S.S.R. Otdel. Tekh. Nauk, Met. i Toplivo, No. 6, 145-7 (1960).
137. Melton C. E., "Studies of Transient Species Formed During Catalytic Reactions of $CO_2 + D_2$ and of 1-Butene," J. Chem. Phys. 35, 1751-1757 (1961).
138. Meyerson, S., McCollum, J. D., Rylander, P. N., "Organic Ions in the Gas Phase. VIII. Bicycloheptadiene," J. Amer. Chem. Soc. 83, 1401-1403 (1961).
139. Meyerson, S., "Effect of Electron Energy on Some Electron Impact Processes," J. Chem. Phys. 34, 2046-2049 (1961).
140. Milne, T. A., Klein, H. M., Cubicciotti, D., "Mass Spectrometer Analysis of the Vapor in Equilibrium with the Alkali-Metal Chlorides," J. Chem. Phys., 28, 718-719 (1958).
141. Milne, T. A., Determination of Relative Partial Pressures from Mass Spectrometer Ion Intensity Measurements," J. Chem. Phys. 28, 717-718 (1958).
142. Morris, J. M., "Spectrographic Analysis of Semiconductor and Related Materials," Metal Hydrides, Inc., Beverly, Mass., Final report, March 1961, contract AF-19 (604) 3469.
143. Muller, Gunter, "Sampling Apparatus for Small Gas Quantities," Chem. Tech. (Berlin) 13, 237 (1961).
144. Mumbach, Norbert R., "Liquid-Sampling Devise for the Mass Spectrometer," Anal. Chem. 33, 318-319 (1961).
145. Narten, A. and Taylor, T. I., "Separation of Nitrogen and Oxygen Isotopes by Exchange of Nitric Oxide Complexes," J. Phys. Chem., 65-10, 1877-1880.
146. Nief, G. and Severin, M., "Mass-Spectrometric Analysis of Trace Oxygen in Carbon Dioxide," Comm. energie at. (France), Rappt. CEA 1941 (1961).

147. Nier, A. O., "Small General Purpose Double Focusing Mass Spectrometer," reprint from Rev. Sci. Instr. 31 1127-1132, (1960).
148. Nikolaev, V. S., Dmitriev, I. S., Fateeva, L. N., and Tepcova, Ya. A. "Investigation of the Equilibrium Charge Distribution in a Fast Ion Beam," J.E.T.P. 12, 627-633 (1961).
149. Nishino, Y., "Studies on the Characteristic Peak and the Sensitivity for the Analysis of the Micro-Component by the Mass Spectrometry," Bunseki Kagaku, 10, 591 (1961).
150. Okano, J., "An Analysis of Residual Gases," Shinku, Jour. of the Vacuum Society of Japan, 4, 154 (1961).
151. Palchak, R. J. F., Norman, J. H., Williams, R. E., "Decaborane, "6-Benzyl" $B_{10}H_{13}$ Chemistry," J. Amer. Chem. Soc. 83, 3380-3384 (1961).
152. Panish, M. B., "Vaporization of Several Rare Earth Oxides," J. Chem. Phys. 34, 1079-1080 (1961).
153. Papazian, H. A., "The Decomposition of Solid H_4N_2 Induced by Charged Particle Bombardment," J. Phys. Chem., 65-1, 53-55.
154. Park, R. and Dunning, H. N., "Stable Carbon Isotope Studies of Crude Oils and Their Porphyrin Aggregates," Geochim. et Cosmochim. Acta 22, 99 (1961).
155. Pavlenko, V. A., Rafal'son, A. E., Slutskii, M. E., Tsveiman, G. A., and Shutov, M. D., "Radiofrequency Mass Spectrometer for Analysis of the Ionic and Molecular Composition of the Upper Atmosphere Layers," Priroda i Tekh. Ekspt. No. 6, 89-95 (1960).
156. Pikus, G. E. and Fiks, V. B., "Analysis of Microimpurities by Magnetic Resonance Mass Spectrometry. II. Calculation of the Background Current," Fiz. Tverdogo Tela 2, 3120-3128 (1960).
157. Pines, H. and Ravoire, J., "Alumina; Catalyst and Support. XII. The Effect of Intrinsic Acidity of Aluminas upon Hydrogen-Deuterium Exchange," J. Phys. Chem. 65-10, 1859-1861.
158. Plyutto, A. A., "Acceleration of Positive Ions in Expansion of the Plasma in a Vacuum," J.E.T.P. (U.S.S.R) 32, 1589-1592 (1960); J.E.T.P. 12, 1106-1108 (1961).
159. Porter, R. F., "Molecular Association in Sodium Cyanide Vapor," J. Chem. Phys. 35, 318-322 (1961).
160. Porter, R. F., Stabilities of Gaseous Molecules in the Pb-Se and Pb-Te Systems," J. Chem. Phys. 34, 583-587 (1961).
161. Porter, R. F., "Mass Spectra of Vapors in the Al-AlF₃ and Al-LiF-AlF₃ Systems," Cornell Univ., Ithaca, N. Y., reprint from J. Chem. Phys. 33, 951-952 (1960).
162. Porter, R. F. and Zeller, E. E., "Mass Spectra of Aluminum (III) Halides and the Heats of Dissociation of Al₂F₆(g) and LiF·AlF₃(g)," Cornell Univ., Ithaca, N. Y., Contract AF-18 (603)1 (AFOSR TN 60-340) Nov. 1960.
163. Potapov, V. K., Vasil'yev, V. G., and Tunitskiy, N. N., "Ionization and Dissociation of Molecules of n-Octane and n-Nonane by Monoenergetic Electrons," Trans. No. MCL-587 from Doklady Akademii Nauk S.S.S.R. Izdatel'stvo Akad. Nauk S.S.S.R. 126, 612-615 (1959).
164. Pottier, R. F. and Lossing, F. P., "Free Radicals by Mass Spectrometry. XXV. Ionization Potentials of Cyano-alkyl Radicals," J. Amer. Chem. Soc. 83, 4737-4739 (1961).
165. Pottier, R. F. and Lossing, F. P., "Free Radicals by Mass Spectrometry. XXIII. Mass Spectra of Benzyl and Alpha-d₂-Benzyl Free Radicals," J. Amer. Chem. Soc. 83, 2634-2636 (1961).
166. Pottier, R. F., Harrison, A. G., Lossing, F. P., "Free Radicals by Mass Spectrometry. XXIV. Ionization Potentials of Cycloalkyl Free Radicals and Cycloalkanes," J. Amer. Chem. Soc. 83, 3204-3206, (1961).

167. Quinn, E. I. and Mohler, F. L., "Mass Spectra of Some Deuteroethanes," Jour. of Research, Natl. Bur. Stds. 65a Mar-April 1961, 93-95.
168. Rauh, E. G. and Thorn, R. J., "Uranium Monosulfide. II. Mass Spectrometric Study of Its Vaporization," J. Chem. Phys. 35, 619-24 (1961).
169. Rohwedder, William Kenneth, "Spark-Source Mass Spectrometer Intended for Major-Component Analysis," Univ. Microfilms (Ann Arbor, Mich.), L.C. Card No. Mic 60-6517, 107 pp.
170. Ropp, G. A. and Guillory, W. A., "Isotopic Studies Involving Formic Acid, and its Derivatives. VII. Oxygen-18 Isotope Effect in the Photochemical Reaction of Formic Acid and Chlorine," J. Phys. Chem. 65-9, 1496-1498.
171. Ropp, G. A., Melton, C. E., and Rudolph, P. S., "Mass Spectrometric Test for an Intermediate in a Photochemical Reaction Involving Chlorine," J. Chem. Phys. 34, 688-689 (1961).
172. Safronov, B. G. Azovskii, Yu. S., and Aseev, G. G., "A Mass Spectroscopic Source of Ions with Surface Ionization," Priboiy i Tekh. Eksperimenta, 70-82 (1957).
173. Saito, Y. and Hino, T., "Thermal Deterioration of Enameled Wires by the Mass Spectrometer Method," Power Appl. and Systems, 653-657 (1960).
174. Schoenheit, E., "Mass Spectrometric Detection of Ions with the Ion Transformer Detector," *f.Naturforsch* 15a, 839-841 (1960).
175. Schoenheit, E., "Mass Spectrometric Examination of the Photoionization of Hydrogen," Feltman Research Lab., Picatinny Arsenal, Dover, N. J., 5 p. (1960), trans. from Zeitschrift fur Naturforschung by Palinkas, A.
176. Schuchhardt, G., "Ion Motion in an Omegatron," Vacuum 10, 373-381 (1960).
177. Schulek, E., Pais, I., and Cornides, I., "Investigation of the Changes in the Oxidation Number by the Use of O-18 Tracer Techniques," J. Inorg. Nucl. Chem. 21, 187-188 (1961).
178. Schulz, G. J., "Study of the N₂O Molecule Using Electron Beams," J. Chem. Phys. 34, 1778-1781 (1961).
179. Shreeve, J. M. and Cady, G. H., "Some Reactions of Peroxydisulfuryl Difluoride," J. Amer. Chem. Soc., 83, 4521-4525 (1961).
180. Shyuttse, V., Demirkhanov, R. A. Gutkin, T. I., Samadashvili, O. A., and Karpenko, I. K., "Mass-Spectrograph with Dual Focusing Along the Total Scale for Measuring Mass Isotopes," Priboiy i Tekh. Eksperimenta No. 4, 92-98 (1960).
181. Smith, Lincoln G., "Design of a New RF Mass Spectrometer," Proc. Intern. Conf. Nuclidic Masses, Hamilton, Ont., Can., 418-431.
182. Spicyn, V. I. and Finikov, F. G., "Application of the O-18 Isotope to Determine the Bond Strength of Oxygen in the Crystal Lattice of Solids," Kernenergie, 3, 834-836, (1960)
183. Stakhovskii, R. I., "Causes of Instability of Ion Currents in the Analytical Mass Spectrometer and a Periodic Calibration Method," Automat. i Telemekh, 91-108 (1958).
184. Steiner, B., Giese, C. F., and Inghram, M. G., "Photoionization of Alkanes - Dissociation of Excited Molecular Ions," J. Chem. Phys. 34, 189-220 (1961).
185. Stevens, C., Terandy, J., Lobell, G., Wolfe, J., Beyer, N., and Lewis, R., "Argonne 100-inch Radius Double-Focusing Mass Spectrometer," Proc. Intern. Conf. Nuclidic Masses, Hamilton, Ont., Can., 403-417.
186. Stief, L. J. and Ausloos, P., "Vapor Phase Radiolysis of Azomethane," J. Phys. Chem., 65-5, 877-881.
187. Sujiura, Toshio, and Hayakawa, Teruo, "Secondary Electron Emission From a Copper-Beryllium (4%) Surface by Bombardment of Various Positive Ions," Bull. Chem. Soc. Japan 34, 58-63 (1961).

188. Sullivan, R. F., Egan, C. J., Langlois, G. E., Seig, R. P., "A New Reaction that Occurs in the Hydro-cracking of Certain Aromatic Hydrocarbons," *J. Amer. Chem. Soc.*, 83, 1156-1160 (1961).
189. Surplice, N. A., "Emission of Negative Ions of Oxygen from Dispenser Cathodes," (Part 1 - Cathodes of Barium Oxide in Sintered Nickel). Physics Dept., Univ. College of North Staffordshire, Keele, Staffordshire, England. *Brit. J. of Appl. Phys.* 12, 214-219 (1961).
190. Beynon, J. H., Saunders, R. A., Topham, A., and Williams, A. E., "The Study of the Fragmentation of Long-Chain Paraffins under Electron Bombardment using Isotopically Labelled Compound," *J. Phys. Chem.*, 65-1, 114-118.
191. Trent, F. M., Miller, F. D., Brown, G. H., "Mass Spectrometry of Some High Molecular Weight Aliphatic Acids and Their Methyl Esters. Analysis of Nonanoic and 2-Ethylheptanoic Acid Mixtures," *Applied Spectroscopy* 15, 64-67 (1961).
192. Trulson, O. C., Hudson, D. E., and Spedding, F. H., "Cohesive Energies of Europium, Gadolinium, Holmium, and Erbium," *J. Chem. Phys.* 35, 1018-1026 (1961).
193. Tumerman, L. A., "New Optical Method of Mass Spectroscopy," *Fiz. Sbornik L'vov. Univ. No. 3*, 81-83 (1957).
194. Tuul, J. and Farnsworth, H. E., "Dependence of Activity and Activation Energy on Surface Treatment of Nickel and Copper-Nickel Catalysts," *J. Amer. Chem. Soc.* 83, 2247-2253 (1961).
195. Vanderwaal, J. and Francken, J. C., "Analysis of Residual Gases in Television Picture Tubes with the Aid of the Omegatron," *Phillips Tech. Rev.* 23, 122-131, (1961/62).
196. Verhaegen, G., "On the Stability of Symmetrical Biatomic Molecules of the Transition Elements," AD-257, 710, Div. 25, June 15, 1961, Aerospace Tech. Intelligence Center, Wright-Patterson AFB, Ohio.
197. Wallenstein, M. B. and Krauss, M., Interpretation of the Appearance Potentials of Secondary Ions," *J. Chem. Phys.* 34, 929-936 (1961).
198. Walsh, P. N., Dever, D. F., White, D., "Rare Earths. III. A Mass Spectrometric Investigation of the Isomolecular Oxygen-Exchange Reactions of Lanthanum, Cerium, Praseodymium, and Neodymium with their Monoxides," *J. Phys. Chem.* 65-8, 1410-13.
199. Webster, R. K., Dance, D. F., Slee, L. J., "Some Possible Applications of Mass Spectrometry to Accounting Problems in Chemical Processing Plants," *Anal. Chim. Acta* 24, 509-525, (1961).
200. Webster, R. K., Smales, A. A., Dance, D. F., and Slee, L. J., "Determination of Plutonium by Mass Spectrometry Using a Plutonium-242 Tracer," *Anal. Chim. Acta* 24, 371-380, (1961).
201. Weininger, J. L., "The Reaction of Active Nitrogen with Liquid Siloxane Heptamer, D7," *J. Amer. Chem. Soc.*, 83, 3388-3390 (1961).
202. Weisz, P. B. and Kern, W. P., "Hydrocarbon Synthesis on Pure Irons", *J. Phys. Chem.* 65-3, 417-419.
203. White, D., Walsh, P. N., Goldstein, H. W., Dever, D. F., "Rare Earths. II. A Mass Spectrometric Determination of the Heats of Sublimation (or Vaporization) of Neodymium, Praseodymium, Gadolinium, Terbium, Dysprosium, Holmium, Erbium, and Lutetium," *J. Phys. Chem.* 65-8, 1404-1409.
204. Williams, W. S., "The Heats of Formation of Titanium Diboride; Experimental and Analytical Resolution of Literature Conflict," *J. Phys. Chem.*, 65-12, 2213-2216.
205. Wolsky, S., "Research Study for Improved Omegatron Tubes," Contract AF-19 (604)-7409, AFCL-76, Final Report Feb. 1961, Raytheon Mfg. Co., Waltham, Mass.
206. Zahn, H. "Mass Spectrometric Analysis of the Lead Isotopes," *Kernenergie* 3, 913-914 (1960).
207. Zdanuk, E. J., Bierig, R., Rubin, L. G., and Wolsky, S. P., "An Omegatron Spectrometer, Its Characteristics and Application," *Vacuum* 10, 382-389 (1960).

208. Zlotowski, J. and Vincel, H., "Mass Spectrometric Studies of Chemical Processes Occurring in a Self-Quenching G. M. Counter-Filled with Long-Chain Saturated Hydrocarbons," *Kernenergie*, 3, 870-879, (1960).
209. Zmbov, K. F. and Ribnikar, S. V., "Note on the Mass Spectra and Structure of the Alcoxydifluoroboranes," *Bull. of Institute of Nuclear Sciences, "Boris Kidrich,"* Vol. II, No. 236, 145-153 (1961).
210. "New Logarithmic Transistorized Electrometer of 10^{+5} Dynamic Range Permits more Convenient Scanning of Mass Spectrum," An Electronic System for Time-of Flight Mass Spectrometer; unpublished material of Bendix Corporation Research Laboratories Division.
211. Geophysics Corporation, "New Instrument, Fundamental Study of Time of Flight," December 1961 (Contract NASW-25).
212. Kuchkov, E. M., "The Connection Between the Energy Distribution of Electrons and the Line Shape of the Mass Spectrum for a Radio-Frequency Mass Spectrometer," *Zhur. Tekh. Fiz.* 30, 948-953 (1960).

MASS SPECTROMETRY OF SOLIDS

A BIBLIOGRAPHY FOR 1961

Sub-Committee VII

Richard E. Honig
RCA Laboratories
Princeton, New Jersey

1. M. Ackerman, J. Drowart, F. Stafford and G. Verhaegen, "Mass Spectrometric Study of Gaseous Molecules Above the AgSn, AuSn and CuSn Alloys," Scientific Note No. 5, Contract No. 61(052)-225, Brussels (1961).
2. A. J. Ahearn, "Mass Spectrographic Analysis of Insulators Using a Vacuum Spark Positive Ion Source," J. Appl. Phys. 32, 1195-7 (1961).
3. A. J. Ahearn, "Mass Spectrographic Detection of Impurities in Liquids," J. Appl. Phys. 32, 1197-1201 (1961).
4. P. A. Akishin and Yu. S. Khodeev, "Determination of Heat of Sublimation of Uranium Tetrafluoride by the Mass-Spectrometric Method," Zhur. Fiz. Khim. 35, 1169-70 (1961).
5. T. Babeliowsky and A. J. H. Boerboom, "Thermodynamic Study of CaO and Ta," Joint Conf. on Mass Spectrometry, Oxford (1961).
6. R. Bradley and E. Ruedl, "Positive Ion Emission from Surfaces," Proceedings of Fifth International Conference on Ionization Phenomena in Gases, H. Maecker, Ed. (North-Holland Publ. Co., Amsterdam 1961).
7. R. Brown, R. D. Craig and R. M. Elliott, "Current Status of Spark Source Mass Spectrometry," Joint Conf. on Mass Spectrometry, Oxford (1961).
8. J. D. Carette and L. Kerwin, "Study of Red Phosphorus by Mass Spectrometry," Can. J. Phys. 39, 1300-19 (1961).
9. E. D. Cater, E. G. Rauh and R. J. Thorn, "Uranium Monosulfide. II. Mass Spectrometric Study of its Vaporization," J. Chem. Phys. 35, 619-24 (1961).
10. B. Chakravarty, V. S. Ventasubramanian and H. E. Duckworth, "The Relative Ionization Efficiency for Elements in a Spark Source," Joint Conf. on Mass Spectrometry, Oxford (1961).
11. W. A. Chupka, J. Berkowitz, D. J. Meschi and H. A. Tasman, "Mass Spectrometric Studies of High Temperature Systems," Joint Conf. on Mass Spectrometry, Oxford (1961).
12. E. A. C. Crouch, "On the Thermal Ionization of Elements of High Ionization Potential," Joint Conf. on Mass Spectrometry, Oxford (1961).
13. E. Doernenburg, H. Hintenberger and J. Franzen, "Structure of Polyatomic C Molecules Formed in HF Sparks," Z. Naturf. 16A 532-4 (1961).
14. J. M. Fluit, L. Friedman, A. J. H. Boerboom and J. Kistemaker, "Isotopic Fractionation of Lithium in Sputtering," J. Chem. Phys. 35, 1143-4 (1961).
15. J. M. Fluit, L. Friedman, J. van Eck, C. Snoek and J. Kistemaker, "Photons and Metastable Atoms Produced in Sputtering Experiments (5-20 kev)," Proceedings of Fifth International Conference on Ionization Phenomena in Gases, H. Maecker, Ed. (North-Holland Publ. Co., Amsterdam 1961).
16. J. Franzen and H. Hintenberger, "Multiatomic Molecular Ions in the High Frequency Spark Between Electrodes from Be, C, Mg, Al, Ti, Fe and Cu," Z. Naturf. 16A, 535-9 (1961).

17. H. W. Goldstein, P. N. Walsh and D. White, "Rare Earths. I. Vaporization of La_2O_3 and Nd_2O_3 : Dissociation Energies of Gaseous LaO and NdO ," J. Chem. Phys. 65, 1400-4 (1961).
18. E. F. Greene, "Reduction of K^+ Ion Background in W Surface Ionization Detectors for Molecular Beams," Rev. Sci. Instr. 32, 860-1 (1961).
19. R. T. Grimley, R. P. Burns and M. G. Inghram, "Thermodynamics of the Vaporization of NiO ," J. Chem. Phys. 35, 551-4 (1961).
20. R. T. Grimley, R. P. Burns and M. G. Inghram, "Thermodynamics of the Vaporization of Cr_2O_3 : Dissociation Energies of CrO , CrO_2 and CrO_3 ," J. Chem. Phys. 34, 664-7 (1961).
21. H. Gutbier, "Mass Spectrometric Investigation of Vaporization of Simple Compounds Having a Zinc Blende Structure at Near 1000°K ," Z. Naturf. 16A, 268-79 (1961).
22. N. B. Hannay, "Mass Spectrographic Analysis of Solids," Science 134, 1220-5 (1961).
23. A. A. Hasapis, A. J. Melveger, M. B. Panish, L. Reif and C. L. Rosen, "The Vaporization and Physical Properties of Certain Refractories," Quarterly Technical Summary Report No. 4, Contract AF33(616)-6840 (1961).
24. R. E. Honig, "The Sputtering of Silicon Carbide by Positive Ion Bombardment," Proceedings of Fifth International Conference on Ionization Phenomena in Gases, H. Maecker, Ed. (North-Holland Publ. Co., Amsterdam 1961).
25. R. E. Honig, "Mass Spectrometric Studies of Solid Surfaces," Joint Conference on Mass Spectrometry, Oxford (1961).
26. G. E. Moore, "Dissociation of Absorbed CO by Slow Electrons," J. Appl. Phys. 32, 1241-51 (1961).
27. H. E. Lumpkin and G. R. Taylor, "Solids Inlet System for a Mass Spectrometer," An. Chem. 33, 476 (1961).
28. M. B. Panish, "Vaporization of the Rare Earth Oxides," J. Chem. Phys. 34, 2197-8 (1961).
29. M. B. Panish, "Vapor Pressure of Silver," J. Chem. Eng. Data 6, 592-4 (1961).
30. M. B. Panish and L. Reif, "Vaporization of Iridium and Rhenium," J. Chem. Phys. 34, 1915-18 (1961).
31. R. F. Porter, "Molecular Association in Sodium Cyanide Vapor," J. Chem. Phys. 35, 318-22 (1961).
32. R. F. Porter, "Stabilities of Gaseous Molecules in the Pb-Se and Pb-Te Systems," J. Chem. Phys. 34, 583-7 (1961).
33. V. I. Raiko, M. S. Ioffe and V. S. Zolotarev, "An Ion Source with Surface Ionization for the Separation of Isotopes of Alkali Metals," (Soviet) Instr. and Exp. Techniques #1, 25-27 (1961).
34. R. G. Ridley and D. E. P. Silver, "Mass Spectrometer for the Isotopic Analysis of Li ," J. Sci. Instr. 38, 47-50 (1961).
35. W. K. Rohwedder, "A Spark Source Mass Spectrometer Intended for Major Component Analysis," Diss. Abstr. 21, 2094 (1961).
36. C. M. Stevens, J. Terandy, G. Lobell, J. Wolfe, R. Lewis and N. Beyer, "High Sensitivity Isotopic Analysis Using the Argonne 100-inch Radius Double Focusing Mass Spectrometer," Joint Conf. on Mass Spectrometry, Oxford (1961).
37. N. A. Surplice, "Emission of Negative Ions from Dispenser Cathodes. I. Cathodes of BaO in Sintered Ni . II. Cathodes of BaAl_2O_3 in Sintered W ," Brit. J. Appl. Phys. 12, 214-19, 20-1 (1961).

38. G. Verhaegen, F. E. Stafford and M. Ackerman, "Mass Spectrometric Studies of the Molecule BC_2 in the Vapor Above the System Boron-Carbon," Scientific Note No. 3, Contract No. AF61(052)-225 (1961).
39. E. Z. Vintaykin, P. L. Gruzin and S. N. Fedovov, "The Use of Isotopes in the Study of Atomic Mobility and Interatomic Interaction in Metals," pp. 278-84 in "Metallurgy and Metallography."
40. P. N. Walsh, D. F. Dever and D. White, "III. A Mass-spectrometric Investigation of the Isomolecular Oxygen-Exchange Reactions of Lanthanum, Cerium, Praseodymium and Neodymium with Their Monoxides," J. Chem. Phys. 65, 1410-3 (1961).
41. D. White, A. Sommer, P. N. Walsh and H. W. Goldstein, "The Application of the Time of Flight Mass Spectrometer to the Study of Inorganic Materials at Elevated Temperatures," Joint Conf. on Mass Spectrometry, Oxford (1961).
42. D. White, P. N. Walsh, H. W. Goldstein and D. F. Dever, "Rare Earths. II. A Mass Spectrometric Determination of the Heats of Sublimation (or Vaporization) of Neodymium, Praseodymium, Gadolinium, Terbium, Dysprosium, Holmium, Erbium and Lutetium," J. Phys. Chem. 65, 1404-9 (1961).
43. J. P. Zingermann and V. A. Morozovsky, "Ionization Method for the Investigation of the Kinetics of Adsorption on the Surface of Solids," Fiz. Tverdogo Tela 3, 123-31 (1961).

